BIODEGRADATION OF FLUORANTHENE AND ANTHRACENE BY INDIGENOUS FUNGI ISOLATED FROM WASTEWATER ACTIVATED SLUDGE

BY

OLUFEMI SAMSON EGBEWALE

UNIVERSITY OF
KWAZULU-NATAL

INYUVESI
YAKWAZULU-NATALI

Submitted in fulfilment of the academic requirement for the degree of Doctor of Philosophy (PhD) in Microbiology; Discipline of Microbiology, School of Life Sciences; College of Agriculture, Engineering and Science at the University of KwaZulu-Natal, Westville campus, Durban, South Africa.

PREFACE

The experimental work described in this thesis was carried out in the School of Life Sciences, University of KwaZulu-Natal (Westville Campus), Durban, South Africa from January 2018 to January 2024, under the supervision of Professor A. O. Olaniran.

These studies represent the original work by the authors and have not otherwise been submitted in any form for any degree or diploma to any tertiary institution. Where use has been made of the work of others, it is duly acknowledged in the text.

… [redacted] …..

Olufemi Samson Egbewale (Student)

Date: 17 July 2024

[redacted] ……...

Professor Ademola O. Olaniran (Supervisor)

Date: 17 July 2024

DECLARATION 1 - PLAGIARISM

I, **Olufemi Samson Egbewale** declare that:

1. The research reported in this thesis, except where otherwise indicated, is my original research.
2. This thesis has not been submitted for any degree or examination at any other university.
3. This thesis does not contain other persons' data, pictures, graphs or other information, unless specifically acknowledged as being sourced from other persons.
4. This thesis does not contain other persons' writing, unless specifically acknowledged as being sourced from other researchers. Where other written sources have been quoted, then:

a. Their words have been re-written but the general information attributed to them has been referenced

b. Where their exact words have been used, then their writing has been placed in italics and inside quotation marks, and referenced.

5. This thesis does not contain text, graphics or tables copied and pasted from the Internet, unless specifically acknowledged, and the source being detailed in the thesis and in the References sections.

Signed ……  ……

DECLARATION 2 - PUBLICATIONS

Details of contributions to publications that form part and/or include research presented in this thesis (include publications in preparation, submitted, *in press* and published and give details of the contributions of each author to the experimental work and writing of each publication)

Published manuscripts

Publication 1: Egbewale, S. O., Kumar, A., Mokoena, M. P. and Olaniran, A. O. (2023). Metabolic biodegradation pathway of fluoranthene by indigenous *Trichoderma lixii* and *Talaromyces pinophilus* spp. *Catalysts*, 13(5), 791. https://doi.org/10.3390/catal13050791.

Authors Contribution:

O. S. Egbewale – Conceptualization, methodology, laboratory work, data curation, formal data analysis, software, validation, visualization, writing (original draft), review and editing of manuscript.

A. Kumar– Conceptualization, methodology, formal analysis, software, supervision review and editing of manuscript.

P. O. Mokoena – Conceptualization, funding acquisition, project administration, resources, review and editing of manuscript.

A. O. Olaniran – Conceptualization, funding acquisition, project administration, resources, supervision, review and editing of manuscript.

Publication 2: Egbewale, S. O., Kumar, A., Olasehinde, T. A., Mokoena, M. P. and Olaniran, A. O. (2024). Anthracene detoxification by Laccases from indigenous fungal strains *Trichoderma lixii* FLU1 and *Talaromyces pinophilus* FLU12. *Biodegradation*. 1 -19. https://doi.org/10.1007/s10532-024-10084-3.

Authors Contribution:

O. S. Egbewale – Conceptualization, methodology, laboratory work, data curation, formal data analysis, software, validation, visualization, writing (original draft), review and editing of manuscript

A. Kumar – Conceptualization, methodology, formal analysis, software, supervision review and editing of manuscript.

T. A. Olasehinde – Conceptualization, methodology, formal analysis, software, supervision review and editing of manuscript.

P. O. Mokoena – Conceptualization, funding acquisition, project administration, resources,

review and editing of manuscript.

A. O. Olaniran – Conceptualization, funding acquisition, project administration, resources, supervision, review and editing of manuscript.

Publication 3: Egbewale, S. O., Kumar, A., Mokoena, M. P. and Olaniran, A. O. (2024). Purification, characterization and three-dimensional structure prediction of multicopper oxidase Laccases from *Trichoderma lixii* FLU1 and *Talaromyces pinophilus* FLU12. *Scientific Reports*, 14(1), 13371. https://doi.org/10.1038/s41598-024-63959-z.

Authors Contribution:

O. S. Egbewale – Conceptualization, methodology, laboratory work, data curation, formal data analysis, software, validation, visualization, writing (original draft), review and editing of manuscript.

A. Kumar– Conceptualization, methodology, formal analysis, software, supervision review and editing of manuscript.

P. O. Mokoena – Conceptualization, funding acquisition, project administration, resources, review and editing of manuscript.

A. O. Olaniran – Conceptualization, funding acquisition, project administration, resources, supervision, review and editing of manuscript.

Publication 4: Egbewale, S. O., Kumar, A., Mokoena, M. P. and Olaniran, A. O. (2024). Mycotransformation of anthracene by indigenous *Trichoderma lixii* and *Talaromyces pinophilus* isolates: insights into the metabolic pathways, enzyme profiles and acute toxicity. ***Journal of fungi (Under Review)***

Authors Contribution:

O. S. Egbewale – Conceptualization, methodology, laboratory work, data curation, formal data analysis, software, validation, visualization, writing (original draft), review and editing of manuscript.

A. Kumar– Conceptualization, methodology, formal analysis, software, supervision review and editing of manuscript.

P. O. Mokoena – Conceptualization, funding acquisition, project administration, resources, review and editing of manuscript.

A. O. Olaniran – Conceptualization, funding acquisition, project administration, resources, supervision, review and editing of manuscript.

Publication 5: Egbewale, S. O., Kumar, A., Mokoena, M. P. and Olaniran, A. O. (2024). Optimization of anthracene biodegradation by indigenous *Trichoderma lixii* and *Talaromyces pinophilus* strains using response surface methodology. ***Ecotoxicology and Environmental Safety*** **(Under Review)**

Authors Contribution:

O. S. Egbewale – Conceptualization, methodology, laboratory work, data curation, formal data analysis, software, validation, visualization, writing (original draft), review and editing of manuscript.

A. Kumar– Conceptualization, methodology, formal analysis, software, supervision review and editing of manuscript.

P. O. Mokoena – Conceptualization, funding acquisition, project administration, resources, review and editing of manuscript.

A. O. Olaniran – Conceptualization, funding acquisition, project administration, resources, supervision, review and editing of manuscript.

Publication 6: Egbewale, S. O., Kumar, A., Olasehinde, T. A., Mokoena, M. P. and Olaniran, A. O. (2024). Synergistic biotransformation of fluoranthene by fungal laccases from indigenous fungal strains *Trichoderma lixii* FLU1 and *Talaromyces pinophilus* FLU12. ***International Biodeterioration and Biodegradation*** **(Under Review).**

Authors Contribution:

O. S. Egbewale – Conceptualization, methodology, laboratory work, data curation, formal data analysis, software, validation, visualization, writing (original draft), review and editing of manuscript

A. Kumar – Conceptualization, methodology, formal analysis, software, supervision review and editing of manuscript.

T. A. Olasehinde – Conceptualization, methodology, formal analysis, software, supervision review and editing of manuscript.

P. O. Mokoena – Conceptualization, funding acquisition, project administration, resources, review and editing of manuscript.

A. O. Olaniran – Conceptualization, funding acquisition, project administration, resources, supervision, review and editing of manuscript.

Signed: [redacted] Name……..……..……Date……

ABSTRACT

Environmental pollution by polycyclic aromatic hydrocarbons (PAHs) poses a significant threat owing to their persistence and toxicity. This thesis investigates the potential of indigenous fungi isolated from wastewater-activated sludge to biodegrade PAHs fluoranthene and anthracene. This study also advances the understanding of the degradation mechanisms, enzymatic pathways, optimization strategies, and catalytic efficiency of purified Laccases as the predominant enzymes utilized by these fungi. Empirical information regarding the characterization, structures, catalytic efficiency, and biological process functions of the purified Laccases is also presented. Two indigenous ascomycete fungi, *Trichoderma lixii* strain FLU1 (*Tl*FLU1) and *Talaromyces pinophilus* strain FLU12 (*Tp*FLU12), were isolated from benzo(b)fluoranthene-enriched activated sludge and tested for their ability to degrade fluoranthene and anthracene as sole carbon sources. *Tl*FLU1 and *Tp*FLU12 degraded 98% and 99% of 400 mg/L fluoranthene, respectively, after 16 and 12 d of incubation. This degradation was associated with the upregulation of ligninolytic enzymes (Laccase, Lignin peroxidase, and Manganese peroxidase). GC-MS and FTIR analyses of the degradation products indicated that degradation was initiated at the C1-C2 position via oxygenation and ring cleavage to form 9-oxo-9H-fluorene-1-carboxylic acid before progressing through the β-ketoadipate pathway via benzene-1,2,3-tricarboxylic acid. The degradation kinetics followed first order and zero-order models for *Tl*FLU1 and *Tp*FLU12. Metabolites from *Tl*FLU1 degradation media showed toxicity to *Vibrio parahaemolyticus* after 6 h of exposure, with effective concentration (EC_{50}) and toxicity unit (TU) values of 14.25 mg/L and 7.018%, respectively. In contrast, *Tp*FLU12 degradation media was non-toxic, with EC_{50} and TU values of 197.1 mg/L and 0.507% respectively. For anthracene, both isolates tolerated exposure of up to 1000 mg/L, with increased ligninolytic enzyme expression (Laccase, Lignin peroxidase, and Manganese peroxidase). The degradation of anthracene was growth-linked and mediated by ligninolytic and intracellular enzymes, resulting in 56% and 38% degradation of 400 mg/L by *Tl*FLU1 and *Tp*FLU12, respectively, after a 24 d incubation period, with pH changes from 5 to 4 (*Tl*FLU1) and 6.2 (*Tp*FLU12). GC-MS and FTIR analyses indicated the formation of 9,10-anthracenedione and benzoic acid as the metabolic products in the *Tl*FLU1 medium and anthrone and 9,10-anthracenedione in the *Tp*FLU12 medium. The degradation by *Tl*FLU1 and *Tp*FLU12 followed a first order kinetic model, with both degradation media metabolites showing no toxicity to *V. parahaemolyticus* after 6 h of exposure, with EC_{50} and TU values of 266.1 mg/L and 0.4% respectively, for *Tl*FLU1 and 262.3 mg/L and 0.4% for *Tp*FLU12. Under optimized conditions using response surface methodology (RSM) for anthracene degradation, 100% degradation efficiency was achieved for *Tl*FLU1 and *Tp*FLU12 on days 8 and 12, respectively, at pH 4 and 5 and temperatures of 30°C and 25°C, with 20 mm biomass and 200 mg/L anthracene. Acute toxicity tests revealed reduced media toxicity, as evidenced by the increased survival rate (log CFU/mL) of *V. parahaemolyticus* after 6 h of exposure. Despite reduced toxicity, both strains degradation

media were classified as harmful based on EC_{50} and TU values of 20.92 ± 1.32 mg/L and 4.78% for *Tl*FLU1, and 35.29 ± 1.55 mg/L and 2.83% for *Tp*FLU12. However, the biocatalytic potential of purified laccases from *Tl*FLU1 and *Tp*FLU12 revealed a reduction in residual fluoranthene concentrations by 46.1% and 38.6% respectively, at 3 U/mL after 96 h. Higher enzyme concentrations (8 U/mL) further reduced the fluoranthene levels to 33.1% and 37.4%, with complete degradation observed at 10 U/mL of either enzyme. The addition of a mediator ABTS (2,2'-azino-bis(3-ethylbenzothiazoline-6-sulfonic acid) significantly enhanced the degradation with a degradation kinetics of v_{max} values, 7.73 ± 0.23 mg/L/h and 7.97 ± 0.18 mg/L/h and K_m value of 54.8 ± 0.27 mg/L and 26.6 ± 0.21 mg/L for *Tl*FLU1 and *Tp*FLU12 respectively. Without ABTS, v_{max} values of 1.35 ± 0.02 mg/L/h and 1.29 ± 0.02 mg/L/h with higher K_m values of 119.2 ± 0.02 mg/L and 170.8 ± 0.03 mg/L for *Tl*FLU-1 and *Tp*FLU-12. GC-MS analysis of the degradation products identified a distinct degradation pathway different from that of whole fungal cell with *Tl*FLU1 generated products such as 9-oxo-fluorene-1-carboxylic acid, 9H-fluoren-9-one, and phthalic acid through dioxygenation at the C1-C2 bond. In contrast, *Tp*FLU12 produces 9,10-phenanthrenedione and benzene-1,2,3-tricarboxylic acid *via* C2-C3 bond cleavage. Ecotoxicity assessments of the degradation products using *V. parahaemolyticus* and cytotoxicity using the HT-22 cell line indicated potential toxicity of *Tl*FLU1 products to *V. parahaemolyticus*, whereas *Tp*FLU12 products were primarily non-toxic. However, complete detoxification was achieved with the degradation products containing ABTS. Also, for anthracene, purified Laccases from *Tl*FLU1 and *Tp*FLU12 degrade anthracene with v_{max} values of 3.51 ± 0.06 mg/L/h and 3.44 ± 0.06 mg/L/h respectively, and K_m values of 173.2 ± 0.06 mg/L and 73.3 ± 0.07 mg/L respectively. The addition of ABTS as a mediator increased degradation by up to 2.9-fold in v_{max} values and reduced K_m values by up to threefold. GC-MS analysis suggested a unique pathway involving hydroxylation and carboxylation at C-1 and C-2 to form 3-hydroxy-2-naphthoic acid, leading to the formation of chromone and subsequent benzoic acid and CO_2. This pathway is in contrast with the dioxygenation route observed in whole fungal cells. Furthermore, toxicity tests using *V. parahaemolyticus* and HT-22 cells demonstrated the nontoxic nature of laccase-ABTS-mediated metabolites. Intriguingly, analysis of the expression level of Alzheimer's-related genes in HT-22 cells exposed to degradation products revealed no induction of neurotoxicity, unlike untreated cells. Furthermore, characterization of *Tl*FLU1 and *Tp*FLU12 laccases revealed that they have molecular masses of 44 kDa and 68.7 kDa, respectively. These enzymes differ in their optimum pH and temperature, with one laccase being more active at a lower pH (*Tl*FLU1) and the other being more active at a higher pH (*Tp*FLU12). Their activity was enhanced by a broad range of metal ions and organic solvents, and sodium azide was a potent inhibitor of its activity. Both laccases have similar kinetic properties, with a better affinity for ABTS as a substrate compared to other phenolic substrates. Based on structural predictions, the difference in the optimum pH is likely due to the different arrangements of copper atoms in the active site. In addition, oxidation-

reduction, lignin metabolism, phenylpropanoid catabolism, biological adhesion, cellular metabolism, cellular metal ion homeostasis, aromatic compound metabolism, and cellulose metabolism have been linked to laccase biological functions. The catalytic efficiency of laccases has been observed to depend primarily on their structural conformation and stability. The Laccase-amino acid conjugates were predicted to be stable, with an instability index ranging from 33.43 to 39.45, thermophilic, with an aliphatic index of 76.58 to 77.50, and hydrophilic, with a grand average of hydropathicity between -0.508 and -0.578. The predicted biological functions of the protein include oxidation-reduction, lignin metabolism, cellular metal ion homeostasis, phenylpropanoid catabolism, aromatic compound metabolism, cellulose metabolism, and biological adhesion. These insights into the enzyme structure-function relationship enhance our understanding of its catalytic mechanism, paving the way for improved bioremediation strategies.

ACKNOWLEDGEMENTS

I would like to express my deepest gratitude to my supervisor, Prof. Ademola O. Olaniran, for his unwavering guidance and support throughout my PhD journey. His mentorship has been invaluable, and I am profoundly grateful for his expertise, encouragement, and dynamic cooperation at every stage of this study. His enthusiasm for research, insightful feedback, vision, support, integrity and motivation have greatly inspired me to continue and advance my academic and research pursuits. Without his help, this thesis would not have been possible.

I extend my heartfelt thanks to my siblings, Mr. Oluwasegun Egbewale, Deborah Egbewale, and Mary Egbewale, for their continuous love and support. Your belief in me has been a source of strength and motivation.

I am immensely grateful to the National Research Foundation of South Africa and the University of KwaZulu-Natal for providing the research grant that made this study possible.

Special acknowledgment goes to my senior colleagues, Dr. Ajit Kumar and Dr. Tosin Olasehinde, for their insightful advice and significant contributions to this research.

I wish to express my sincere gratitude to my laboratory colleagues, Keri Ramessar, Folasade Adu, and Folasade Onisile, as well as the staff and postgraduate students of the Discipline of Microbiology at the Westville campus, for their kind support and camaraderie.

My sincere appreciation also goes to Dr. Ejovwokoghene Collins Odjadjare, Dr. Oladipupo Aregbesola and Abubakar Falaki for their moral support during the course of this study.

Lastly, I would like to thank everyone who, in one way or another, contributed to the success of this study. Though their names are not mentioned here, their contributions are deeply appreciated.

DEDICATION

This Thesis is dedicated to my parents Mr Hassan Ezekiel Egbewale and Mrs Aina Adefunke Egbewale.

TABLE OF CONTENTS **page**

PREFACE **ii**

DECLARATIONS 1: PLAGIARISM **iii**

DECLARATIONS 2: PUBLICATIONS **iv**

ABSTRACT **vii**

ACKNOWLEDGEMENTS **x**

DEDICATION **xi**

LIST OF TABLES **xv**

LIST OF FIGURES **xvi**

CHAPTER ONE: General introduction **1**

1.0 General introduction **2**

1.1 Justification for the study **4**

1.2 Scope of the study **4**

1.3 Hypotheses **5**

1.4 Research questions **5**

1.5 Objectives of the study **6**

1.6 Thesis Outline **6**

1.7 References **9**

CHAPTER TWO: Literature Review **15**

2.0 Summary **16**

2.1 Introduction **16**

2.2 Polycyclic Aromatic Hydrocarbons (PAHs) and their fate in the environment **19**

2.3 Ecotoxicity of PAHs **20**

2.4 The untapped potential of micro-fungi in the bioremediation of Polycyclic Aromatic Hydrocarbons 24

2.5 Current Status of micro-fungi-based bioremediation of PAHs **31**

2.6 Metabolism of low molecular weight PAHs by micro-fungi **33**

2.7 Metabolism of high molecular weight PAHs by micro-fungi **35**

2.8 Mechanism of PAHs metabolism by micro-fungi **38**

2.8.1 Intracellular enzymes **38**

2.8.1.1 Cytochrome P450 monooxygenase **38**

2.8.1.2 Phenol 2-monooxygenase **39**

2.8.1.3 Catechol 1,2-dioxygenase **39**

2.8.1.4 Catechol 2,3-dioxygenase **39**

2.8.2 Extracellular enzymes **39**

2.8.2.1 Peroxidases **40**

2.8.2.2 Laccase **40**

2.9 Kinetics and Modelling of PAHs Bioremediation by micro-fungi **45**

2.9.1 Zero-order bioremediation kinetics **45**

2.9.2 First-order bioremediation kinetics **46**

2.9.3 Second-order bioremediation kinetics **46**

2.9.3.1 Langmuir model **46**

2.9.3.2 Temkin model **46**

2.9.3.3 Freundlich model **47**

2.10 Limitations and challenges of micro-fungi bioremediation PAHs **47**

2.10.1 Bioavailability **47**

2.10.2 pH **48**

2.10.3 Temperature **48**

2.10.4 Inoculum Size **49**

2.10.5 PAHs concentration **49**

2.10.6 Diversity of slow-growing micro-fungi **50**

2.11 Potential Applications of micro-fungi in the bioremediation of PAHs **50**

2.11.1 Soil bioremediation **50**

2.11.2 Water bioremediation **51**

2.11.3 Bio-stimulation **51**

2.11.4 Phytoremediation 51

2.12 Future Perspectives on Micro-Fungi-based Bioremediation of PAHs 51

2.13 Concluding remarks 52

2.14 References 53

CHAPTER THREE: Metabolic biodegradation pathway of fluoranthene by indigenous *Trichoderma lixii* and *Talaromyces pinophilus* spp. 69

CHAPTER FOUR: Mycotransformation of anthracene by indigenous *Trichoderma lixii* and *Talaromyces pinophilus* isolates: insights into the metabolic pathways, enzyme profiles and acute toxicity 98

CHAPTER FIVE: Optimization of anthracene biodegradation by indigenous *Trichoderma lixii* and *Talaromyces pinophilus* strains using response surface methodology 125

CHAPTER SIX: Anthracene detoxification by Laccases from indigenous fungal strains *Trichoderma lixii* FLU1 and *Talaromyces pinophilus* FLU12 190

CHAPTER SEVEN: Synergistic biotransformation of fluoranthene by Laccases from indigenous fungal strains *Trichoderma lixii* FLU1 and *Talaromyces pinophilus* FLU12 and ABTS mediator 214

CHAPTER EIGTH: Purification, characterization and three-dimensional structure prediction of multicopper oxidase Laccases from *Trichoderma lixii* FLU1 and *Talaromyces pinophilus* FLU12 245

CHAPTER NINE: General discussion and conclusion 270

9.1 The research in perspective 271

9.2 Limitations of the Current Study 276

9.3 Potential for future development of the study 276

9.4 References 278

LIST OF TABLES

Page

CHAPTER TWO

Table 2.1: Physiochemical properties of the sixteen priority PAHs by USEPA **22**

Table 2.2: Characteristics of fungal Phyla **26**

Table 2.3: Summary of recent studies on the biodegradation of different low and high-molecular-weight PAHs by non - mushroom-forming fungi **28**

Table 2.4: Summary of the activities of the intracellular and extracellular enzymes during PAHs metabolisms. **42**

LIST OF FIGURES

Page

CHAPTER TWO

Figure 2.1: The environmental matrix response to PAHs toxicity. **21**

Figure 2.2: Publication trends in bioremediation of polycyclic aromatic hydrocarbons. **25**

Figure 2.3: The generalized PAHs metabolism pathways by fungi. **32**

Figure 2.4: Naphthalene and Anthracene metabolic pathways by *Aspergillus glaucus* **33**

Figure 2.5: Fluorene metabolic pathways by *Mucor irregularis*. **34**

Figure 2.6: Pyrene metabolism by Micro-fungi. **36**

Figure 2.7: Fluoranthene metabolism by Micro-fungi. **37**

CHAPTER ONE

General introduction

1.0: General introduction

Our ecosystem has become a reservoir of xenobiotic pollution due to the rapid industrialization and urbanization, worldwide (Hubeny et al., 2021). Among the ubiquitous group of organic xenobiotics found in various matrices of the ecosystem, polycyclic aromatic hydrocarbons (PAHs) are of major environmental priority owing to their carcinogenicity, genotoxicity, cytotoxicity and mutagenic effects which are characterized by low solubility and high lipophilicity to biological functions (Srogi, 2007; Zafra et al., 2015; Ping et al., 2017; Monteiro et al., 2024; Nilén et al., 2024). The increase in bioaccumulation, biomagnification and persistent toxicity of this pollutant made the United States Environmental Protection Agency (USEPA), the United Nations Environmental Programme (UNEP) and the Canadian Council of Ministers of the Environment to create a list of sixteen priority PAH compounds needed to be eradicated from the environment (Ping et al., 2017; Kottuparambil and Park, 2019). Sources of PAHs include incomplete fossil fuel combustion, ship traffic, oil spilling/leakages from corroded tanks at petrol stations, urban runoff and industrial activities (Moghadam et al., 2014; Aranda et al., 2017). Anthracene and Fluoranthene are considered as model compounds for PAHs remediation study owing to their relative abundance in contaminated sites (He et al., 2018; Bankole et al., 2020; 2022).

Although PAHs can naturally be disintegrated from the environment via chemical oxidation, photolysis, volatilization and adsorption, chemical stabilities of PAHs make these methods inefficient for their total removal coupled with formation of many derivatives which are more toxic than their parent compounds (Zeng et al., 2010; Zafra et al., 2014; Mohd Radzi et al., 2015; de Lima Souza et al., 2016; Smol and Włodarczyk-Makuła, 2017). Physical, chemical and biological techniques have been established, optimized and utilized in the amelioration PAH contaminated sites but momentous hitches such as technological complexity, high cost and a general lack of acceptance are some of the drawbacks encountered with these treatment techniques (Alegbeleye et al., 2017; Sakshi et al., 2019). Biological treatment techniques (bioremediation) has recently been of interest for the clean-up of sites contaminated with PAHs because it is considered as safe, least disruptive and cost-effective, compared to the conventional physico-chemical method (Tiso et al., 2016; Elshafie et al., 2020). The role of native microbes isolated from a PAH-contaminated environment during PAHs degradation has been well documented, but degradation rates in microbes like bacteria are often not proportional to the contaminant released into an environment thus leading to accumulation of

PAHs in the contaminated sites that can remain for decades (Aranda et al., 2017; Premnath et al., 2021). Fungi have been appraised as one of the predominant biodegrading agents found in the environment, which are free-living and ubiquitous (Nasrawi, 2012; Ipeaiyeda et al., 2015; Bankole et al., 2021). They employ their metabolic versatility through the induction of non-specific, non-selective extracellular enzymes such as laccases, manganese peroxidases and lignin peroxidases and resilience to utilize PAHs as a carbon and energy source, and thereby mineralize them to simpler compounds, carbon dioxide and water, or transformed them to other non-toxic molecules under harsh environmental conditions like low moisture and high concentrations of PAHs (Ye et al., 2011; Deshmukh et al., 2016). Many non-basidomycetes (non-mushroom forming fungi) like *Aspergillus sp.* strain HJ1, *Aspergillus terricolavar Americanus* (MTCC 2739), *Trichoderma reesei* FS10-C, *Aspergillus ochraceus*, *Cunninghamella elegans*, and *Cunninghamella echinulata* indigenous to contaminated sites has been reported for efficient degradation of anthracene, benzo (k) fluoranthene, benzo(a)anthracene and fluoranthene (Kilikian et al., 2014; Yao et al., 2015; Sharma et al., 2016; Lahkar and Deka, 2017). Conversely, Basidiomycetes (mushroom-forming fungi) like *Phanerochaete chrysosporium, Pleurotus ostreatus, Armillaria sp., Bjerkandere adusta*, *Trametes versicolor* and *Coriolopsis byrsina* strain APC 5 have been well documented for their effective degradation of PAHs (Sack et al., 1997); (Rigas et al., 2009); (Hadibarata et al., 2013); (Balesteros et al., 2014); (Agrawal and Shahi, 2017).

The remarkable progress in the ongoing regulation concerning PAH residues with its derivatives was necessitated by an increasing ecotoxicological risks preoccupation (Adekunle et al., 2018). A few of the risk includes alteration in the taxonomic composition of the macroinvertebrate communities such as DNA integrity reduction, infection prevalence increments and calcification impairment (Gan et al., 2021). Similarly, in *in vitro* study, PAHs derivatives have been linked with more potent mortalities and developmental toxicities in zebrafish embryos (Kim et al., 2020). Also, the effect of PAHs on plants includes photosynthetic activities reduction, lipid peroxidation reduction, DNA damage and plant growth reduction (Urana et al., 2019). Since PAHs' toxicity comes from the intermediates formed during their breakdown process, the European Union legislation recommends acute toxicity for registering, evaluating, authorizing, and restricting chemicals/products before under-studying the long-term effects (Barrantes et al., 2018).

1.1: Justification for the study

The persistence and toxicity of polycyclic aromatic hydrocarbons (PAHs) in the environment demand the development of effective remediation strategies (Venkatraman et al., 2024). While traditional methods have been shown to be effective, they often come with drawbacks such as high costs, significant energy consumption, and the risk of secondary pollution (Patel et al., 2020)). In contrast, bioremediation presents an eco-friendly and potentially more cost-efficient alternative (Akhtar and Mannan, 2020; Gupta and Pathak, 2020). Nonetheless, several challenges must be addressed to fully harness its potential. The primary obstacle lies in the slow degradation rates of PAHs by fungi, attributed to the hydrophobic and recalcitrant nature of these compounds (Shankhwar and Paliwal, 2021). This study seeks to overcome this hurdle by selecting highly tolerant fungal strains and optimizing degradation conditions to boost efficiency. Another critical consideration is the evaluation of potential risks posed by fungal-PAH metabolites to ensure the safety of the remediation process (Bokade and Bajaj, 2023). To this end, a comprehensive toxicity assessment is integrated into the study. Moreover, the diversity of fungi present in activated sludge is an underexplored reservoir for biodegradation efforts (Alao and Adebayo, 2022). By isolating and characterizing these fungi, this study aims to identify novel fungal strains with enhanced degradative capabilities. Additionally, gaining insights into the metabolic pathways and enzymatic mechanisms involved in PAH degradation will provide valuable information for refining and expanding the applicability of the bioremediation techniques.

1.2: Scope of the study

The scope of this research includes the isolation, identification, and characterization of fungal strains from activated sludge that exhibit high tolerance and degradative capabilities for PAHs. The study encompasses several key areas:

i. **Fungal isolation and characterization:** Using PAH-enrichment techniques to isolate fungi from activated sludge, followed by morphological and molecular identification techniques to characterize the isolated strains.
ii. **Metabolic pathway analysis:** Investigating the metabolic pathways employed by the fungi in the degradation of LMW and HMW PAHs, comparing these pathways to those used by other organisms such as bacteria and mushroom-forming fungi.
iii. **Optimization of degradation conditions:** Utilizing response surface methodology (RSM) to optimize the conditions (pH, temperature, biomass size, and PAH concentration) for maximum degradation efficiency.

iv. **Enzymatic degradation study:** Assessing the role of ligninolytic enzymes, particularly laccases, in the degradation of PAHs and characterizing their catalytic properties through purification, enzyme kinetics and in vitro studies.

v. **Toxicity assessment:** Evaluating the acute toxicity of PAH degradation metabolites on marine bacterium and mammalian cell lines to understand the potential environmental and health impacts of the degradation process.

1.3: Hypotheses

It is hypothesized that activated sludges from wastewater treatment plants in Durban, KwaZulu-Natal Province of South Africa, contain indigenous fungi with potential to biodegrade PAHs, such as fluoranthene and anthracene and use the compounds as sole carbon and energy sources.

1.4: Research questions

i. What are the degradation capabilities of indigenous fungi strains isolated from activated sludge for PAHs?

ii. How do the metabolic pathways of these fungi differ when degrading low molecular weight (anthracene) and high molecular weight (fluoranthene) PAHs?

iii. What are the optimum environmental conditions (pH, temperature, biomass size, and PAH concentration) for maximizing PAH degradation by these fungi?

iv. How do ligninolytic enzymes (Laccase, Lignin peroxidase, and Manganese peroxidase) contribute to the degradation process?

v. What are the major characteristics and molecular structures of the ligninolytic enzymes from the isolated fungi? Are they different from the previously reported enzymes from other habitats? Can these enzymes be used for in vitro cell-free degradation of PAHs?

vi. What is the ecotoxicological impact of the PAH degradation products on marine bacterium *Vibrio parahaemolyticus* and mouse hippocampal neuronal (HT-22) cell lines?

1.5: Objectives of the study

The following objectives were pursued in order to answer the research questions:

i. Isolation and identification of indigenous fungi capable of degrading low and high molecular weight PAHs from activated sludge samples.
ii. Evaluation of the degradation efficiency of identified fungi for anthracene and fluoranthene.
iii. Elucidation of the metabolic pathways and enzyme activities involved in the degradation of anthracene and fluoranthene by these fungi.
iv. Optimization of the physico-chemical parameters and culture constituents for enhancing PAH degradation using response surface methodology (RSM).
v. Purification and characterization of the most abundantly produced ligninolytic enzyme from the fungi and evaluation of its efficiency in a cell-free system.
vi. Assessment of the acute toxicity of PAH degradation products on marine bacterium *Vibrio parahaemolyticus* and mouse hippocampal neuronal (HT-22) cell lines.

1.6: Thesis Outline

This thesis is presented in 9 chapters:

1. **Chapter 1:** described the general overview and scope of the research. It also provides a comprehensive introduction to PAHs, elucidating their toxicity levels and existing removal techniques. It emphasizes the pivotal roles played by ascomycetes and ligninolytic enzymes in PAH degradation and addresses the ecotoxicological concerns associated with these hazardous compounds.
2. **Chapter 2:** Titled "The Untapped Potential of Micro-fungi in Bioremediation of Polycyclic Aromatic Hydrocarbons: Current Status and Future Perspectives," this chapter consolidates existing literature and outlines the status and prospects in utilizing micro-fungi for PAH bioremediation.
3. **Chapters 3:** Intricately investigates the metabolic biodegradation pathways of fluoranthene by by two indigenous fungi: *Trichoderma lixii* FLU1 and *Talaromyces pinophilus* isolated from activated sludge. This chapter provides insights into the enrichment process leading to the isolation of indigenous fungi strains capable of

degrading PAHs, their biodegradation efficiency, metabolic pathways, enzyme profiles, and acute toxicity associated with the degradation process.

4. **Chapter 4:** Provides an insight into the myco-transformation of anthracene and its transformation mechanisms by *Trichoderma lixii* FLU1 and *Talaromyces pinophilus* isolates FLU12. Metabolic pathways, myco-transformation kinetics and transformation-related enzymes production during the myco-transformation process of anthracene was also investigated. Further, the acute toxicity of the degradation products was assessed using bacterial survival, EC_{50} (effective concentration) and toxicity unit (TU) determination.
5. **Chapter 5:** Explores the optimization of physico-chemical parameters and culture constituents using Response Surface Methodology for anthracene biodegradation. It delves into the influence of optimized conditions on extracellular enzyme activities during the degradation process, offering insights into sustainable remediation strategies.
6. **Chapter 6:** This chapter examines the detoxification of anthracene by laccases from indigenous fungal strains; *Trichoderma lixii* FLU1 and *Talaromyces pinophilus* FLU12. It evaluates the influence of laccase-mediators on anthracene biotransformation and the ecotoxicity of degradation products on marine bacterium survival, HT-22 cell line viability and analysis of the expression level of Alzheimer's related genes in HT-22 with an insight to neurotoxicity of these degradation products. This approach addresses the overall toxicological issues caused by anthracene and its metabolites in the environment, providing insight into the novel properties of laccases for bioremediation and their broader biotechnological applications.
7. **Chapter 7:** Reports on the investigation of the synergistic biotransformation of fluoranthene by fungal laccases from indigenous fungal strains, *Trichoderma lixii* FLU1 and *Talaromyces pinophilus* FLU12 and ABTS Mediator. The toxicity of the resulting degradation products was evaluated through bacterial survival assays and HT-22 cell line viability tests. This investigation offers a thorough understanding of the environmental effects of fluoranthene and its breakdown products by emphasizing the potential of these fungal laccases in myco-remediation and their broader biotechnological applications.
8. **Chapters 8:** Focus on the purification, characterization, and utilization of multicopper oxidase laccases from the indigenous fungal strains. It provides extensive information about the structural and dynamic of the purified laccase through bioinformatics

analysis. The binding mode and biological functions of the purified laccase were equally elucidated.

9. Finally, **Chapter 9** synthesizes the findings from previous chapters, drawing overarching conclusions and proposing suggestions for future research endeavours. This provides significant advancements in understanding the potential of indigenous fungi for PAH remediation and highlights the novel properties of ligninolytic proteins for myco-remediation and broader biotechnological applications.

1.5: References

Adekunle, A.S., Oyedele Oyekunle, J.A., Ola, I.J., Obisesan, O.R., Maxakato, N.W., 2018. Determination of polycyclic aromatic hydrocarbons (PAHs) and organochlorine pesticides (OCPs) in some personal care products in Nigeria. *Toxicology Reports* 5, 994–1001. https://doi.org/10.1016/j.toxrep.2018.10.003

Agrawal, N., Shahi, S.K., 2017. Degradation of polycyclic aromatic hydrocarbon (pyrene) using novel fungal strain *Coriolopsis byrsina* strain APC5. *International Biodeterioration & Biodegradation* 122, 69–81. https://doi.org/10.1016/j.ibiod.2017.04.024

Akhtar, N., Mannan, M.A., 2020. Mycoremediation: Expunging environmental pollutants. *Biotechnology Reports* 26, e00452–e00452. https://doi.org/10.1016/j.btre.2020.e00452

Alao, M.B., Adebayo, E.A., 2022. Fungi as veritable tool in bioremediation of polycyclic aromatic hydrocarbons-polluted wastewater. *Journal of Basic Microbiology* 62 (3-4), 223–244. https://doi.org/10.1002/jobm.202100376

Alegbeleye, O.O., Opeolu, B.O., Jackson, V., 2017. Bioremediation of polycyclic aromatic hydrocarbon (PAH) compounds: (acenaphthene and fluorene) in water using indigenous bacterial species isolated from the Diep and Plankenburg rivers, Western Cape, South Africa. *Brazilian Journal of Microbiology* 48, 314–325. https://doi.org/10.1016/j.bjm.2016.07.027

Aranda, E., Godoy, P., Reina, R., Badia-Fabregat, M., Rosell, M., Marco-Urrea, E., García-Romera, I., 2017. Isolation of Ascomycota fungi with capability to transform PAHs: Insights into the biodegradation mechanisms of *Penicillium oxalicum*. *International Biodeterioration and Biodegradation* 122, 141–150. https://doi.org/10.1016/j.ibiod.2017.05.015

Balesteros, M.R., de Sa, L.R.V., Pereira, P.M., da Silva, M., de Oliveira, M.A.L., Ferreira-Leitao, V.S., 2014. Monitoring of atrazine biodegradation by *Pleurotus ostreatus* INCQS 40310 through the simultaneous analysis of atrazine and its derivatives by HPLC. *Biocatalysis and Biotransformation* 32 (1), 23–33.

Bankole, P.O., Semple, K.T., Jeon, B.H., Govindwar, S.P., 2021. Biodegradation of fluorene by the newly isolated marine-derived fungus, *Mucor irregularis* strain bpo1 using response surface methodology. *Ecotoxicology and Environmental Safety* 208, 111619. https://doi.org/10.1016/j.ecoenv.2020.111619

Bankole, P.O., Semple, K.T., Jeon, B.H., Govindwar, S.P., 2020. Enhanced enzymatic removal of anthracene by the mangrove soil-derived fungus, *Aspergillus sydowii* BPOI. *Frontiers*

of Environmental Science and Engineering 14. https://doi.org/10.1007/s11783-020-1292-3

Bankole, P.O., Taghoghor Omoni, V., Mulla, S.I., Adebajo, S.O., Adekunle, A.A., 2022. Co-biomass degradation of fluoranthene by marine-derived fungi; *Aspergillus aculeatus* and *Mucor irregularis*: Comprehensive process optimization, enzyme induction and metabolic analyses. *Arabian Journal of Chemistry* 15(2), 104036. https://doi.org/10.1016/j.arabjc.2022.104036

Barrantes, V., Deim, S., Domagalski, S., Grabner, A., Khamidula, K., Krueger, J., Rick, U., Rubbiani, M., Zupanc, A., Shrestha, M., 2018. National chemicals registers and inventories: benefits and approaches to development.

Bokade, P., Bajaj, A., 2023. Molecular advances in mycoremediation of polycyclic aromatic hydrocarbons: Exploring fungal bacterial interactions. *Journal of Basic Microbiology* 63 (3-4), 239–256. https://doi.org/10.1002/jobm.202200499

de Lima Souza, H.M., Sette, L.D., da Mota, A.J., do Nascimento Neto, J.F., Rodrigues, A., de Oliveira, T.B., de Oliveira, F.M., de Oliveira, L.A., dos Santos Barroso, H., Zanotto, S.P., 2016. Filamentous Fungi Isolates of Contaminated Sediment in the Amazon Region with the Potential for Benzo(a)pyrene Degradation. *Water, Air, and Soil Pollution* 227, 1–13. https://doi.org/10.1007/s11270-016-3101-y

Deshmukh, R., Khardenavis, A.A., Purohit, H.J., 2016. Diverse Metabolic Capacities of Fungi for Bioremediation. *Indian Journal of Microbiology* 56, 247–264. https://doi.org/10.1007/s12088-016-0584-6

Elshafie, H.S., Camele, I., Sofo, A., Mazzone, G., Caivano, M., Masi, S., Caniani, D., 2020. Mycoremediation effect of *Trichoderma harzianum* strain T22 combined with ozonation in diesel-contaminated sand. *Chemosphere* 252. https://doi.org/10.1016/j.chemosphere.2020.126597

Gan, N., Martin, L., Xu, W., 2021. Impact of Polycyclic Aromatic Hydrocarbon Accumulation on Oyster Health. *Frontiers in Physiology* 12, 1–19. https://doi.org/10.3389/fphys.2021.734463

Gupta, S., Pathak, B., 2020. Mycoremediation of polycyclic aromatic hydrocarbons, in: Abatement of Environmental Pollutants. Elsevier, pp. 127–149. https://doi.org/10.1016/B978-0-12-818095-2.00006-0

Hadibarata, T., Zubir, M.M., Rubiyatno, F.A., Chuang, T.Z., Yusoff, A.R.M., Salim, M.R., Fulazzaky, M.A., Seng, B., Nugroho, A.E., 2013. Degradation and transformation of anthracene by white rot fungus Armillaria sp. F022. *Folia Microbiol* 58, 385–391.

He, C., Li, Y., Huang, C., Chen, F., Ma, Y., 2018. Genome Sequence and Metabolic Analysis of a Fluoranthene-Degrading Strain *Pseudomonas aeruginosa* DN1. *Frontiers in Microbiology* 9, 1–10. https://doi.org/10.3389/fmicb.2018.02595

Hubeny, J., Harnisz, M., Korzeniewska, E., Buta, M., Zieliński, W., Rolbiecki, D., Giebułtowicz, J., Nałęcz-Jawecki, G., Płaza, G., 2021. Industrialization as a source of heavy metals and antibiotics which can enhance the antibiotic resistance in wastewater, sewage sludge and river water. *PLoS ONE* 16, 1–24. https://doi.org/10.1371/journal.pone.0252691

Ipeaiyeda, A.R., Nwauzor, G.O., Akporido, S.O., 2015. Biodegradation of Polycyclic Aromatic Hydrocarbons in Agricultural Soil Contaminated with Crude Oil from Nigeria Refinery using *Pleurotus sajor-caju* 301.

Kilikian, B. V, Afonso, L.C., Souza, T.F.C., Ferreira, R.G., Pinheiro, I.R., Química, D.D.E., Paulo, U.D.S., Paulo, S., 2014. Filamentous fungi and media for cellulase production in solid state cultures *Brazilian Journal of Microbiology* 45, 279–286.

Kim, Y.C., Lee, S.R., Jeon, H.J., Kim, K., Kim, M.J., Choi, S.D., Lee, S.E., 2020. Acute toxicities of fluorene, fluorene-1-carboxylic acid, and fluorene-9-carboxylic acid on zebrafish embryos (Danio rerio): Molecular mechanisms of developmental toxicities of fluorene-1-carboxylic acid. *Chemosphere* 260, 127622. https://doi.org/10.1016/j.chemosphere.2020.127622

Kottuparambil, S., Park, J., 2019. Anthracene phytotoxicity in the freshwater flagellate alga Euglena agilis Carter. *Scientific Reports* 9, 1–11. https://doi.org/10.1038/s41598-019-51451-y

Lahkar, J., Deka, H., 2017. Isolation of Polycyclic Aromatic Hydrocarbons (PAHs) Degrading Fungal Candidate from Oil-Contaminated Soil and Degradation Potentiality Study on Anthracene. *Polycyclic Aromatic Compounds* 37, 141–147. https://doi.org/10.1080/10406638.2016.1220957

Moghadam, S., Ebrahimipour, M., Abtahi, G., Ghassempour, B., Hashtroudi, A., Seyed, M., 2014. Biodegradation of polycyclic aromatic hydrocarbons by a bacterial consortium enriched from mangrove sediments. *Journal of Environmental Health Science and Engineering* 12, 114. https://doi.org/10.1186/s40201-014-0114-6

Mohd Radzi, N.A.S., Tay, K.S., Abu Bakar, N.K., Uche Emenike, C., Krishnan, S., Shahul Hamid, F., Abas, M.R., 2015. Degradation of polycyclic aromatic hydrocarbons (pyrene and fluoranthene) by bacterial consortium isolated from contaminated road side soil and

soil termite fungal comb. *Environmental Earth Sciences* 74, 5383–5391. https://doi.org/10.1007/s12665-015-4552-y

Monteiro, V., Dias Da Silva, D., Martins, M., Guedes De Pinho, P., Pinto, J., 2024. Metabolomics perspectives of the ecotoxicological risks of polycyclic aromatic hydrocarbons: A scoping review. *Environmental Research* 249, 118394. https://doi.org/10.1016/j.envres.2024.118394

Nasrawi, H. Al, 2012. Biodegradation of crude oil by fungi isolated from gulf of Mexico. *Journal of Bioremediation & Biodegradation* 03. https://doi.org/10.4172/2155-6199.1000147

Nilén, G., Larsson, M., Hyötyläinen, T., Keiter, S.H., 2024. A complex mixture of polycyclic aromatic compounds causes embryotoxic, behavioral, and molecular effects in zebrafish larvae (*Danio rerio*), and in vitro bioassays. *Science of The Total Environment* 906, 167307. https://doi.org/10.1016/j.scitotenv.2023.167307

Patel, A.B., Shaikh, S., Jain, K.R., Desai, C., Madamwar, D., 2020. Polycyclic aromatic hydrocarbons: sources, toxicity, and remediation approaches. *Frontiers in Microbiology* 11, 562813. https://doi.org/10.3389/fmicb.2020.562813

Ping, L., Guo, Q., Chen, X., Yuan, X., Zhang, C., Zhao, H., 2017. Biodegradation of pyrene and benzo[a]pyrene in the liquid matrix and soil by a newly identified *Raoultella planticola* strain. 3 *Biotech* 7. https://doi.org/10.1007/s13205-017-0704-y

Premnath, N., Mohanrasu, K., Guru, R., Rao, R., Dinesh, G.H., Siva Prakash, G., Ananthi, V., Ponnuchamy, K., Muthusamy, G., Arun, A., 2021. A crucial review on polycyclic aromatic hydrocarbons-environmental occurrence and strategies for microbial degradation. *Chemosphere* 280, 130608–130608. https://doi.org/10.1016/j.chemosphere.2021.130608

Rigas, F., Papadopoulou, K., Philippoussis, A., Papadopoulou, M., Chatzipavlidis, J., 2009. Bioremediation of lindane contaminated soil by *Pleurotus ostreatus* in non-sterile conditions using multilevel factorial design. *Water Air Soil Pollut.* 197, 121–129.

Sack, U., Heinze, T.M., Deck, J., Cerniglia, C.E., Martens, R., Zadrazil, F., Fritsche, W., 1997. Comparison of phenanthrene and pyrene degradation by different wood decaying fungi. *Applied and Environmental Microbiology* 63 (10), 3919–3925.

Sakshi, Singh, S.K., Haritash, A.K., 2019. Polycyclic aromatic hydrocarbons: soil pollution and remediation. *International Journal of Environmental Science and Technology* 16, 6489–6512. https://doi.org/10.1007/s13762-019-02414-3

Shankhwar, A.K., Paliwal, R., 2021. Fungi in bioremediation of soil: Mycoremediation of PAHs compounds, in: fungi bio-prospects in sustainable agriculture, environment and

nanotechnology. Elsevier, pp. 157–170. https://doi.org/10.1016/B978-0-12-821925-6.00008-3

Sharma, A., Singh, S.B., Sharma, R., Chaudhary, P., Pandey, A.K., Ansari, R., Vasudevan, V., Arora, A., Singh, S., Saha, S., Nain, L., 2016. Enhanced biodegradation of PAHs by microbial consortium with different amendment and their fate in in-situ condition. *Journal of Environmental Management* 181, 728–736. https://doi.org/10.1016/j.jenvman.2016.08.024

Smol, M., Włodarczyk-Makuła, M., 2017. The effectiveness in the removal of pahs from aqueous solutions in physical and chemical processes: a review. *Polycyclic Aromatic Compounds* 37, 292–313. https://doi.org/10.1080/10406638.2015.1105828

Srogi, K., 2007. Monitoring of environmental exposure to polycyclic aromatic hydrocarbons: a review. *Environmental Chemistry Letters* 5, 169–195. https://doi.org/10.1007/s10311-007-0095-0

Tiso, N., Mikašauskaitė, J., Stankevičius, M., Snieškienė, V., Stankevičienė, A., Polcaro, C., Galli, E., Donati, E., Zacchini, M., Levišauskas, D., Tekorius, T., Ragažinskienė, O., Drevinskas, T., Bartkuvienė, V., Kornyšova, O., Kaškonienė, V., Maruška, A., 2016. Isolation and identification of fungi tolerant to polycyclic aromatic hydrocarbons and coal tar from different habitats in Lithuania. *Toxicological and Environmental Chemistry* 98, 77–89. https://doi.org/10.1080/02772248.2015.1101111

Urana, R., Singh, N., Sharma, P., 2019. Effects of PGPR on growth and photosynthetic pigment of *Trigonella foenum-graceum* and *Brassica juncea* in PAH-contaminated soil. *SN Applied Sciences* 1, 1–9. https://doi.org/10.1007/s42452-019-0780-1

Venkatraman, G., Giribabu, N., Mohan, P.S., Muttiah, B., Govindarajan, V.K., Alagiri, M., Abdul Rahman, P.S., Karsani, S.A., 2024. Environmental impact and human health effects of polycyclic aromatic hydrocarbons and remedial strategies: A detailed review. *Chemosphere* 351, 141227. https://doi.org/10.1016/j.chemosphere.2024.141227

Yao, L., Teng, Y., Luo, Yongming, Christie, P., Ma, W., Liu, F., Wu, Y., Luo, Yang, Li, Z., 2015. Biodegradation of polycyclic aromatic hydrocarbons (PAHs) by *Trichoderma reesei* FS10-C and effect of bioaugmentation on an aged PAH-contaminated soil. *Bioremediation Journal* 19, 9–17. https://doi.org/10.1080/10889868.2014.939137

Ye, J., Yin, H., Qiang, J., Peng, H., Qin, H., 2011. Biodegradation of anthracene by *Aspergillus fumigatus*. *Journal of Hazardous Materials* 185, 174–181. https://doi.org/10.1016/j.jhazmat.2010.09.015

Zafra, G., Absalón, Á.E., Cuevas, M.D.C., Cortés-Espinosa, D. V., 2014. Isolation and selection of a highly tolerant microbial consortium with potential for PAH biodegradation from heavy crude oil-contaminated soils. *Water, Air, and Soil Pollution* 225. https://doi.org/10.1007/s11270-013-1826-4

Zafra, G., Moreno-montaño, A., Absalón, Á.E., Cortés-espinosa, D. V, 2015. Degradation of polycyclic aromatic hydrocarbons in soil by a tolerant strain of *Trichoderma asperellum*. *Environmental Science and Pollution Research* 22, 1034–1042. https://doi.org/10.1007/s11356-014-3357-y

Zeng, J., Lin, X., Zhang, J., Li, X., 2010. Isolation of polycyclic aromatic hydrocarbons (PAHs)-degrading *Mycobacterium* spp. and the degradation in soil. *Journal of Hazardous Materials* 183, 718–723. https://doi.org/10.1016/j.jhazmat.2010.07.085

CHAPTER TWO

Literature Review

2.0: Summary

Polycyclic aromatic hydrocarbons (PAHs) are toxic compounds that are widely present in the environment due to human activities such as industrial processes and combustion. Bioremediation, the use of microorganisms to break down pollutants in the environment, has been identified as a promising approach for removing PAHs. Micro-fungi, a diverse group of organisms that includes yeasts and moulds, have been shown to have the potential to degrade PAHs through a range of metabolic pathways effectively. Despite this potential, micro-fungi use in the bioremediation of PAHs is still in its infancy. More research is needed to understand and harness these organisms' capabilities fully. This review provides an overview of the current state of research on using micro-fungi in the bioremediation of PAHs, focusing on their properties, metabolic pathways, and ability to degrade a wide range of pollutants. Current research on using micro-fungi for the bioremediation of PAHs and the limitations of current studies are also discussed. The future perspectives on the potential of micro-fungi for the bioremediation of PAHs, including the potential for the use of mixed cultures and the potential for commercialization of this approach, are highlighted. However, several challenges must be addressed before micro-fungi can be used for this purpose. These challenges include: (1) the lack of knowledge about the diversity of micro-fungi that can degrade PAHs; (2) the need for more effective methods for isolating and culturing these microorganisms; and (3) the need for more information about the mechanisms by which micro-fungi degrade PAHs. With more research, the potential of micro-fungi in the bioremediation of PAHs could be fully realized.

2.1: Introduction

Contamination of soils, groundwater, sediments, surface water and air with a massive amount of toxic xenobiotics is a critical issue confronting today's world (Li et al., 2021). The release of toxic substances from manufacturing industries, mine tailings, dumping of large metallic wastes, paints, electronic waste, use of natural composts, organic fertilizers, municipal solid waste, sewage spill, pesticides, wastewater irrigation, coal-burning build-ups and petrochemicals spillage remains the significant source of environmental contaminations (Sampaio et al., 2021). Over time, the organic and inorganic contaminants resulting from such activities accumulate, posing a significant hazard to public health, imperils drinking water, devastates natural resources, and disrupts the economy (Rani et al., 2021). Of noteworthy, approximately 10% of the enormous quantities of harmful organo-pollutants produced during the aforementioned human and industrial activities are incessantly disposed (Dhruv Patel and Bhatt, 2022), raising the need for regulation of toxic pollutants including PAHs as their

environmental persistence has been credited to the deleterious, mutagenic and carcinogenic effects on the environment by the United States Environmental Protection Agency (USEPA) (Gaur et al., 2018).

Polycyclic aromatic compounds have become a significant environmental concern globally in the last three decades owing to their chemical stability, low volatility, low solubility in water and low bioavailability coupled with their deleterious effect and environmental ubiquity (Sharma et al., 2022). PAHs originate mainly from incomplete combustion of fossil fuels, volcanic eruptions, and forest fires and are released into the environment through exhausts and solid residues (Kumar et al., 2021). In nature, PAHs cause adverse health and ecological consequences. Health damage associated with PAH exposure has been evaluated repeatedly by different health and environmental protection agencies, such as the International Agency for Research on Cancer (IARC) (Moazzen et al., 2022), the USEPA (ben Ameur et al., 2021), the Scientific Committee on Food (SCF), the International Programme on Chemical Safety (IPCS) (Taghizadeh et al., 2021), the Joint FAO/WHO Expert Committee on Food Additives (JECFA) (Shariatifar et al., 2022), the European Food Safety Authority (EFSA) (Nougadère et al., 2020), the National Toxicology Program (NTP) (Dach et al., 2019) and the Agency for Toxic Substances and Disease Registry (Rohlman et al., 2019). Seven high molecular weight PAHs compounds namely benzo(a)anthracene, benzo(b)fluoranthene, benzo(j)fluoranthene, benzo(k)fluoranthene, benzo(a)pyrene, dibenzo(a,h)anthracene, and indeno(1,2,3-c,d)pyrene, are considered by several agencies as human carcinogens (Adeyeye, 2020), While, low molecular weight-polycyclic aromatic hydrocarbons has been linked with the induction of oxidative damage and inflammation (Guo et al., 2021).

Remediating PAH-contaminated sites is challenging and requires a sustainable and effective approach. Researchers have recently employed different treatment techniques, such as conventional, physical, chemical and biological, during the clean-up of PAHs contaminated sites to an innocuous state (Zhang et al., 2020). Among these techniques, only the biological approach (bioremediation) has witnessed great enthusiasm in the past few decades owing to its contribution to an eco-friendly and low-cost remediation technique which is a natural process that does not produce toxic by-products and provides a permanent solution as a result of complete mineralization of the contaminants in the environment compared with other environmental clean-up techniques (Sharma et al., 2021). While bacteria are typically the primary focus in bioremediation efforts, there is increasing interest in the potential of micro-

fungi for PAHs bioremediation due to their ability to degrade these compounds through enzymatic processes (Bankole et al., 2022). Micro-fungi, besides the extracellular enzymes mediated degradation, displays stronger degradative capabilities than other microorganisms due to their ability to form a hyphal network which facilitates easy penetration of PAHs contaminated sediments (Dell' Anno et al., 2021; Ma et al., 2022). Micro-fungi are ubiquitous and diverse groups of fungi in the environment whose wide range of metabolic capabilities makes them ideal candidates for bioremediation (Álvarez-Barragán et al., 2021). Several studies have investigated their potential in the bioremediation of PAHs, and the results have been promising. One of the major advantages of micro-fungi is their ability to degrade a broad range of PAHs, including high molecular weight compounds (Cao et al., 2020). They achieve this by producing a range of enzymes, including ligninolytic enzymes (peroxidases and laccases), Catechol 1,2-dioxygenase and Catechol 2,3-dioxygenase which can oxidize, hydroxylate, and cleave PAHs into less toxic forms (Vasconcelos et al., 2019; Cao et al., 2020). Another advantage of micro-fungi is their ability to thrive in diverse environments, including harsh and contaminated sites (Stoyanova et al., 2022). They can colonize contaminated soil and water, and the presence of other contaminants does not limit their growth (Álvarez-Barragán et al., 2021). Micro-fungi have also been shown to adapt to PAH-contaminated sites by developing mechanisms to cope with the toxic effects of these compounds (Bankole et al., 2022).

Several studies on PAH degradation *in vitro* and *in vivo* have shown the efficiency of microfungi such as *Aspergillus ochraceus, Bjerkandera sp., Cunninghamella echinulata, Cunninghamella elegans, Phanerochaete chrysosporium* and *Saccharomyces cerevisiae* in the complete degradation of PAHs compounds (Rathore et al., 2021). Yet a major challenge in using micro-fungi for bioremediation is optimizing environmental conditions for fungal growth and activity, including factors like temperature, pH, oxygen availability, and nutrient availability (Agrawal et al., 2021). Another challenge is identifying and isolating micro-fungi with specific PAH degradation capabilities. While many micro-fungi have been shown to have the potential for PAH degradation, there is still a need to identify those with the most efficient degradation capabilities. Also, the ability of fungi to grow and degrade PAHs may vary depending on the type, and chemical structure of PAH compounds needs to be understand (Bankole et al., 2021). Despite these challenges, micro-fungi have the potential for significant ecological roles in PAH bioremediation, especially in harsh environments. Again, their adaptability to different conditions may open up possibilities for use in situ. Thus, this review

describes the untapped potential of micro-fungi in PAHs bioremediation and the different enzymes involved in bioremediation processes. Further, we discussed the new findings on the bioremediation kinetics, focusing on this little-studied group of fungi (micro-fungi) to provide new insights into their use for PAH bioremediation.

2.2: Polycyclic Aromatic Hydrocarbons (PAHs) and their fate in the environment

Polycyclic aromatic hydrocarbons are a group of complex environmental pollutants composed of carbon and hydrogen with fused aromatic rings in linear, angular, and clustered arrangements (Hesham et al., 2017). They are classified according to their molecular weight as low molecular weight PAHs (LMW PAHs), which consist of two or three aromatic rings and high molecular weight PAHs (HMW PAHs), which consist of more than three aromatic rings (Table 1). The Low-molecular-weight (LMW) PAHs are relatively soluble, volatile, and more degradable than the high molecular-weight compounds which are hydrophobic, highly resistant to microbial degradation and relatively sorb strongly to soils and sediments (Hoang et al., 2021). Many PAHs contain bay- and K-region epoxides, which often formed metabolically and are reactive both chemically and biologically (Schut, 2020).

PAHs are ubiquitous environmental pollutants which are often generated primarily during the incomplete combustion of organic materials such as coal, petroleum products, fossil fuels and wood (Szatyłowicz and Hawrylik, 2022). The natural sources of PAHs include open burning, petroleum seeps, coal deposits, volcanic activities and municipal seeps while anthropogenic activities such as residential heating, coal gasification, coal-tar pitch and asphalt production, coke and aluminium manufacturing, catalytic cracking towers and other related activities in petroleum refineries (Gaurav et al., 2021). However, some PAHs are commonly used as intermediaries in pharmaceutical products, agricultural products, photographic products, thermosetting plastics, lubricating substances, and different chemical products (Abdel-shafy and Mansour, 2016).

The fate of PAHs in the environment includes volatilization, photo-oxidation, chemical oxidation, adsorption on soil particles and leaching with consequent release into the food chain (Li et al., 2020). Once exposed to the environment, they do not degrade quickly due to their antagonistic effects on native microbes in contaminated sites and may thus reside in the soil for a prolonged period of time (Espinosa-Ortiz et al., 2022). Also, the persistence of PAHs in the environment could be linked with their low water solubility, coupled with an increased

hydrophobicity (Ding et al., 2021). PAHs persistence and distribution in soils have been extensively detected at a progressive depth of 10 - 15 cm up to distances 10 to 150 m from its contamination source (Revitt et al., 2014; Ding et al., 2021). Half-life in soil ranged from 152 to 313 days for 3 rings PAHs and from 117 to 492 days for 4 and 5ring PAHs respectively (Oleszczuk and Baran, 2003; Li et al., 2009).

2.3: Ecotoxicity of PAHs

The ubiquitous nature of PAHs has become a serious environmental concern owing to their resistance to biodegradation, their potential to be bio-accumulated coupled with their mutagenic and carcinogenic effects which occur through breathing air containing PAHs in the workplace, or by encountering air, water, or soil near hazardous waste sites (Kaushal et al., 2021). Reports have shown that a large percentage of PAHs and their metabolite contamination in the human body is *via* the oral route, while just a little percentage is absorbed through the skin (Sousa et al., 2022). PAHs metabolites (epoxides and dihydrodiols) can interact with cellular proteins and DNA to produce further biochemical alterations and cell damage, which may lead to mutations, tumours, and cancer (Soni et al., 2018; Zhang et al., 2021). However, in humans, exposure to PAHs can be acute or chronic (Shen et al., 2018; Wu et al., 2022). Acute effects of excessive human exposure to PAHs are short-term and could result in skin irritation, nausea, diarrhoea, vomiting, inflammation, convulsion and eye irritation whereas, the chronic health effects of PAHs include cancer of different degrees, cataracts, asthma-like symptoms, decreased immune function, and kidney and liver damage (Soni et al., 2018; Singh et al., 2019; Kuppusamy et al., 2020; Cong et al., 2021; Turaki Usman et al., 2021).

In plants, PAHs induce oxidative stress, cause direct damage of photosynthetic pigments, disruption of proteins and lipids synthesis, chloroplasts, microtubules, cell walls, membranes, and nucleic acid damage leading to cell death (Ahammed et al., 2015; Mo et al., 2021). In the rat, the effect of exposure to PAHs has been linked to induced anxiety, birth defect, neurotoxicity and neurodegeneration while in worms, exposure to PAHs has been attributed to decreasing in alkaline phosphatase activity and increasing in mortality (Shi et al., 2020; Zeb et al., 2020; Calderón-Garcidueñas and Ayala, 2022; Olasehinde and Olaniran, 2022). In aquatic species, exposure to PAHs has been linked to changes in morphological features, defence ability reduction and inhibitory effects on hatching rates and developmental processes such as yolk sac and spinal deformities (Cherr et al., 2017; Kim et al., 2020).

Thus, PAHs toxicity response at different environmental strata could be grouped into three namely: mechanism of toxic action, mode of action and environmental matrix response (Figure 2.1).

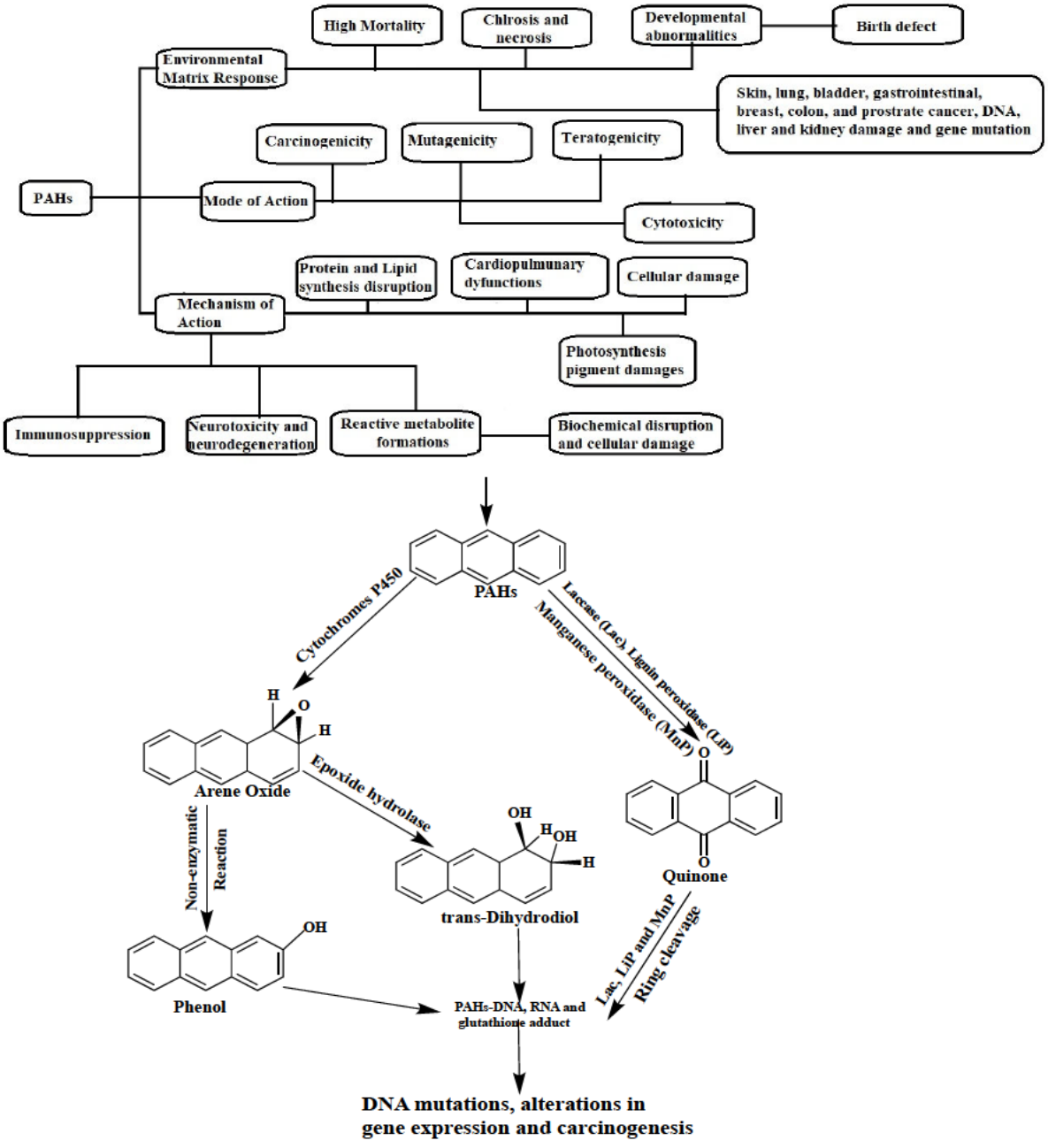

Figure 2.1. The environmental matrix response to PAHs toxicity summarized from (Ahammed et al. (2015); Kim et al. (2020); Kuppusamy et al. (2020); Mo et al. (2021); Turaki Usman et al. (2021); Calderón-Garcidueñas and Ayala, (2022)

Table 2.1. Physiochemical properties of the sixteen priority PAHs by USEPA

PAHs	Structure	Number of Aromatic of Rings	Molecular Formula	Molecular weight (g/mol)	Boiling Point (^{0}C)	Melting Point (^{0}C)	Solubility mg/L at 25 ^{0}C	B. Half-Life in (Days)	USEPA Toxicology Profile
Naphthalene	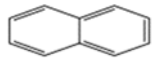	2	$C_{10}H_8$	128.174	218	80.2	31	28.7	
Acenaphthene	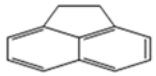	3	$C_{12}H_{10}$	154.212	279	93	3.90	10-102	Haematoxicity (effects on the blood), reproductive, developmental toxicity immunotoxic
Acenaphthylene		3	$C_{12}H_8$	152.196	280	89.4	3.93	12-121	
Anthracene	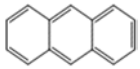	3	$C_{14}H_{10}$	178.234	341.3	216	1.29	108-139	
Phenanthrene	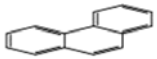	3	$C_{14}H_{10}$	178.234	340	100	1.15	128	
Fluorene	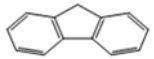	3	$C_{13}H_{10}$	166.223	294	114.76	1.69	2-64	
Fluoranthene	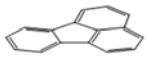	3	$C_{16}H_{10}$	202.256	384	110.2	0.20 - 0.26	152-730	
Benzo(a)anthracene	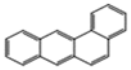	4	$C_{18}H12$	228.294	437.6	155-157	$9.4X10^{-3}$	365	Human carcinogen
Chrysene	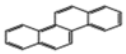	4	$C_{18}H_{12}$	228.294	448	255	$2.0X10^{-3}$	343.8	
Pyrene	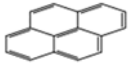	4	$C_{16}H_{10}$	202.256	394	150.62	0.135	283.4	Not Human carcinogen

Table 2.1. Physiochemical properties of the sixteen priority PAHs by USEPA contd's

PAHs	Structure	Number of Aromatic of Rings	Molecular Formula	Molecular weight (g/mol)	Boiling Point (^{0}C)	Melting Point (^{0}C)	Solubility mg/L at 25 ^{0}C	B. Half-Life in (Days)	USEPA Toxicology Profile
Benzo(a)pyrene	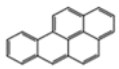	5	$C_{20}H_{12}$	252.316	496	179	$1.62X10^{-3}$	2-693.5	
Benzo(b)fluoranthene	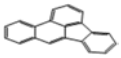	5	$C_{20}H_{12}$	252.316	481	168.4	0.0015 *	1280	
Benzo(k)fluoranthene	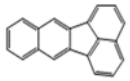	5	$C_{20}H_{12}$	252.316	480	217	$8.0X10^{-4}$	1277.5	Human carcinogen
Dibenzo(a,h)anthracene	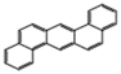	5	$C_{22}H_{14}$	278.354	524	269	$2.49X10^{-3}$	18-21	
Benzo(ghi)perylene	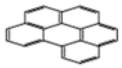	6	$C_{22}H_{12}$	276.338	550	278.3	$2.6X10^{-4}$	600-650	
Indeno(1,2,3-cd)pyrene	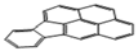	6	$C_{22}H_{12}$	276.338	536	164	$1.9X10^{-4}$	349.2	

The table was formed from the PubChem database which was assessed 19/11,2022. The structures were drawn with ChemDraw ultra 12.0 while the data with an asterisk(*)indicate that the temperature was not recorded. B= Biodegradation half-lives in soil

2.4: The Untapped Potential of Microfungi in the Bioremediation of Polycyclic Aromatic Hydrocarbons

Fungi belong to the kingdom of eukaryotes which come in various sizes and shapes. Some are single cells, like yeast, while others are long chains of cells that can stretch for miles (St. Leger and Wang, 2020; Nuñez Otaño et al., 2021). Typically, fungal cells are oblong, with trichomes that contain organelles and large intracellular granules and structures (Park et al., 2020). They are primary decomposers, meaning they break down dead organic matter into simpler compounds that can be reused by other organisms (López-Mondéjar et al., 2018). In doing so, fungi help to recycle nutrients and contribute to the global carbon cycle (Finlay and Thorn, 2019; Naylor et al., 2020). Fungi are broadly classified into macro-fungi (mushroom-forming fungi) and micro-fungi (non-mushroom-forming fungi) owing to the varying sizes of their fruiting bodies (Karaman et al., 2012). Mushroom-forming fungi have fruiting bodies that are readily visible to the naked eye, with a diameter which is always less than 2mm while non-mushroom-forming fungi are microscopic whose spores range from 2 to 20 μm in size and are of different shapes and colours (Dayarathne et al., 2020; Senanayake et al., 2020).

Fungi play an important role in the bioremediation of organo-pollution, such as PAHs into non-harmful molecules (CO_2 and H_2O) through the secretion of ligninolytic enzymes (laccase, lignin peroxidase and manganese peroxidase) (Agrawal et al., 2019; Chattopadhyay et al., 2020). Unlike bacteria that undergo co-metabolism before metabolising PAHs, fungi can utilize PAHs as a sole source of carbon and energy (Aziz et al., 2018). Also, the advantages of myco-remediation (fungi bioremediation) over other PAHs treatment methods (Physico-chemical treatments) include tolerance to harsh operating conditions such as high contaminant concentrations and extreme pH, temperature, and salinity (Meer et al., 2020). The significant increase in the reports on the bioremediation of PAHs by fungi in the last decades has always focused on macro-fungi compared with micro-fungi with the potential to be very effective at degrading PAHs at the different environmental matrices (Figure 2).

Reports have shown the efficiency of micro-fungi from several habitats in the bioremediation of PAHs (Yakop et al., 2019). In one study, two micro-fungi, namely, *Aspergillus sydowii* and *Aspergillus destruens* were able to degrade over 90% of benzo-α-pyrene and phenanthrene in 8 days (González-Abradelo et al., 2019), while macro-fungus, *Ganoderma lucidum* strain CCG1 could degrade 20 mg/L of phenanthrene (99.65%) and pyrene (99.58%) respectively

just in 30th day (Agrawal et al., 2018). This is a very promising result, and further research is needed to see if micro-fungi can be used on a larger scale to bioremediate PAH-contaminated sites. Thus, the potential benefits of using micro-fungi for PAHs bioremediation include their easy isolation and maintenance, application in various settings, relatively inexpensive, and application to large areas of contaminated land (Nevalainen et al., 2014; Kadri et al., 2017). Also, their metabolic products are non-toxic and pose no risk to human health or the environment (Enyiukwu et al., 2021). In addition, they do not suffer major setbacks such as slow growth rate, mycelia ageing, and the need for relatively high concentrations of oxygen to increase their enzymatic activities, as often observed in macro-fungi (mushroom-forming fungi) (Chatterjee et al., 2016).

The characteristics of the most studied diverse group of fungi involved in the degradation of PAHs include mushroom-forming fungi (basidiomycetes) and non - mushroom-forming fungi (zygomycetes, ascomycetes, hyphomycetes, and Deuteromycetes) (Table 2.2). However, a common characteristic observed among those studies is the high tolerance to PAHs and the capability to sustain their growth in the presence of other pollutants. Interestingly, PAHs degradation efficiencies among these fungi phyla depend on PAH compound's chemical structure. A summary of recent studies on the biodegradation of different low and high-molecular-weight PAHs by non - mushroom-forming fungi is shown in Table 2.3.

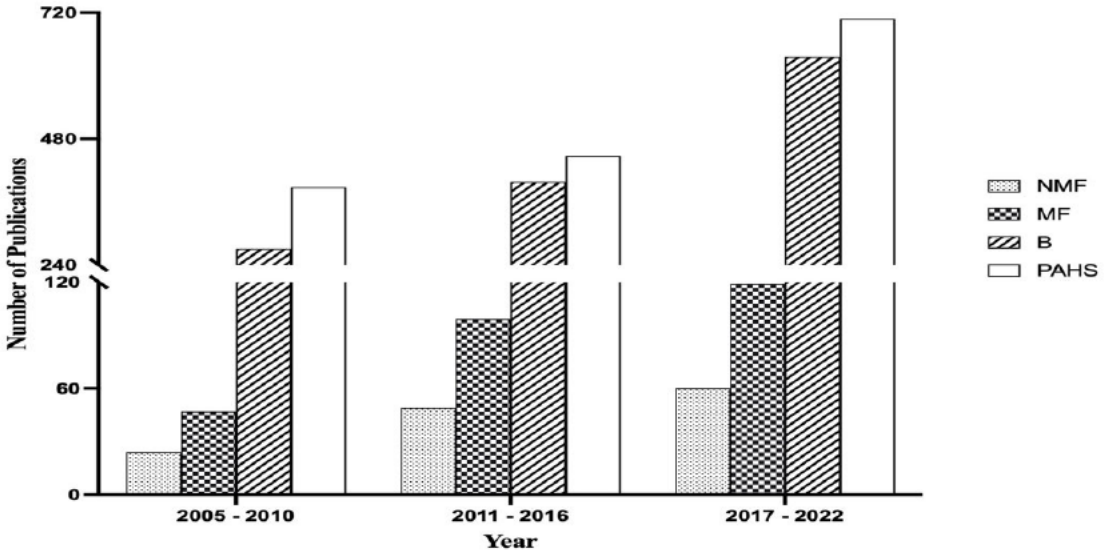

Figure 2.2. Publication trends in bioremediation of polycyclic aromatic hydrocarbons (Based on the ISI Web of Science™ with keywords ''PAHs + non - mushroom-forming fungi", ''PAHs + mushroom-forming fungi", "PAHs +Bacteria" and "PAHs" from 2000 to 2022). Key: PAHs + NMF: Bioremediation of PAHs by non - mushroom-forming fungi, PAHs + MF: Bioremediation of PAHs by mushroom-forming fungi, PAHs + B: Bioremediation of PAHs +Bacteria and PAHs: Monitoring and Risk Analysis of PAHs in the Environment

Table 2.2. Characteristics of fungal Phyla

Phyla	Characteristics	References
Chytridiomycota	They are characterized by the possession of motile spores (called zoospores) that are propelled by Flagella. This group also includes the myxomycetes, or slime molds, which are characterized by their acellular (lacking cells) stage in their life cycle.	Money, (2016)
Zygomycota	They are characterized by having zygospores, which are thick-walled sexual spores that are produced by the fusion of two different gametangia. Also, these fungi are also characterized by a lack of septa between their cells.	Naranjo-Ortiz and Gabaldón, (2019)
Ascomycota	Fungi come in many shapes and sizes, from single-celled yeasts to complex multicellular organisms. More than 110,000 species have been identified in this Phyla. This phyla is characterized by the production of ascocarps, which are fruiting bodies that contain the spores of the fungi during sexual reproduction. Also, they are capable of asexual reproduction by producing conidiophores, which are specialized structures that produce spores	Wijayawardene et al. (2021)

Table 2.2. Characteristics of fungal Phyla Cont'd

Phyla	Characteristics	References
Basidiomycota	They are a large group of fungi that includes mushrooms, stinkhorns, toadstools and puffballs. These fungi are characterized by the presence of basidia, club-shaped cells on which basidiospores are produced. They undergo sexual reproduction by the formation of basidiospores on basidia. Most basidiomycetes are terrestrial, and many are wood-rotting fungi.	Kamil, (2020)
Deuteromycota	A class of fungi that lack a known sexual stage. Many of the fungi in this group are plant pathogens. They are often referred to as *"imperfect"* fungi because of their lack of a sexual stage. Some of the more well-known fungi in this group include the bread mold (*Rhizopus stolonifera*) and the plant pathogen *Verticillium alboatrum*	Nieuwenhuis and James, (2016); Dyer and Kueck, (2017)

Table 2.3. Summary of recent studies on the biodegradation of different low and high-molecular-weight PAHs by non - mushroom-forming fungi.

Organism	Culture Type	PAHs	Initial Concentration (mg/L)	Incubation Period (Days)	Degradation (%)	References
Aspergillus glaucus	Pure	Naphthalene	300	15	66	Stoyanova et al. (2022)
		Anthracene			44	
A. sydowii strain bpo1	Pure	Anthracene	100	3	98.7	Bankole et al. (2020)
Mucor irregularis strain bpo1		Fluorene	100	5	81.5	Bankole et al (2021)
A. aculeatus and *M. irregularis*	Consortium	Fluoranthene	50	7	98.4	Bankole et al. (2022)
Lasiodiplodia theobromae	Pure	Benzo(a)pyrene	100	10	53	Cao et al. (2020)
A. niger	Pure	Naphthalene	100	21	100	Obire et al. (2020)
		Chrysene			100	
A. sydowii	Pure	Acenaphthylene			73.4	
Fusarium lichenicola		Acenaphthene			73.1	
A. niger, A. sydowii and	Consortium	All 16 priority			85.2	
F. lichenicola		PAHs				

Table 2.3. Summary of recent studies on the biodegradation of different low and high-molecular-weight PAHs by non - mushroom-forming fungi Cont'd.

Organism	Culture Type	PAHs	Initial Concentration (mg/L)	Incubation Period (Days)	Degradation (%)	References
Tolypocladium sp. (CBMAI 1346) *Xylaria* sp. (CBMAI 1464)	Pure	Pyrene Benzo(a)pyrene	21	7	95	Vasconcelos et al. (2019)
Aspergillus sp. RFC1	Pure	Naphthalene Phenanthrene Pyrene	50 20 20	7	97.4 84.9 90.7	Al-Hawash et al. (2019)
A. niger (ATC 16404)	Pure	Phenanthrene	100	5	97	Hamzah et al. (2018)
Cadophora sp. TS2	Pure	Phanenthrene	10	7	74.3	Batista-garcía et al. (2017)
A. caesiellus H1		Anthracene Phanenthrene Anthracene			99.4 80.5 99.8	
Candida sp. S1	Pure	Pyrene	20	15	75	Hadibarata et al. (2017)

Table 2.3. Summary of recent studies on the biodegradation of different low and high-molecular-weight PAHs by non - mushroom-forming fungi Cont'd.

Organism	Culture Type	PAHs	Initial Concentration (mg/L)	Incubation Period (Days)	Degradation (%)	References
Penicillium sp.	Pure	Naphthalene	100	28	15	Govarthanan and Fuzisawa, (2017)
		Acenaphthene			10	
		Benzo(a)pyrene			2	
Paecilomyces sp. (SF-8)	Pure	Anthracene	50	7	88	Velmurugan et al. (2017)
		Phenanthrene		7	75	
		Benz(a)anthracene		15	67.5	
		Benzo(b)fluoranthene		15	99.3	
Aspergillus sp. strain HJ1	Pure	Anthracene	20	18	55	Lahkar and Deka, (2017)
Scopulariopsis brevicaulis	Pure	Phenanthrene	100	30	60	Mao and Guan, (2016)
		Fluoranthene			62	
		Pyrene			64	
		Benzo[a]pyrene	20		82	
Trichoderma reesei FS10-C	Pure	Benzo(a)pyrene	20	12	54	Yao et al. (2015)
Candida albicans, A. flavus, Fusarium sp., and *Pseudomonas aeruginosa*	Consortium	Benzo(a)pyrene	3.74 mg/kg	42	65.5	Waszak et al. (2015)

2.5: Current Status of Micro-fungi-Based Bioremediation of PAHs

The primary goal of bioremediation is to break down organic pollutants like PAHs into harmless substances (CO_2 and H_2O) (Agrawal and Shahi, 2017). However, some intermediate metabolites such as dihydrodiols, phenolic compounds, and arena oxides produced during the process, especially in bacteria and some macro-fungi, can be deleterious to the ecosystem with some carcinogenic, mutagenic, and teratogenic effects if not properly managed (Sakshi and Haritash, 2020). Hence, it becomes imperative to track the metabolic pathways employed by microbes to identify any potential obstacles that could arise in the future.

PAHs metabolism by non - mushroom-forming fungi is quite similar to other well-established metabolic pathways by bacteria with a competitive advantage of no toxic end-product and their capability of utilizing PAHs as their carbon and energy sources (Al Farraj et al., 2020). It metabolises PAHs through the oxidation by an enzyme known as cytochrome P450 monooxygenase, which causes ring epoxidation leading to an unstable arene oxide which is further converted into trans-dihydrodiol by another enzyme called epoxide-hydrolase or rearranges itself non-enzymatically to produce phenol which forms conjugates as glucuronides, sulfates, methylated, xylosides and glucosides (Figure 3) (Sakshi and Haritash, 2020). This metabolism pathway has been reported in indigenous non-mushroom-forming fungi (*Aspergillus glaucus*), which were able to metabolise Naphthalene through salicylic acid, catechol, and ketoadipic acid as an intermediate while anthracene metabolism by the same fungal strain proceeded with catabolism into 2-hydroxy-1-naphthoic acid, o-phthalic acid, and protocatechuic acid as intermediate (Stoyanova et al., 2022). Similarly, a result study has shown that *Trametes polyzona* PBURU 12 could metabolise Phenanthrene through hydroxylation into 9,10-Dihydroxyphenanthrene which further undergo ring cleavage with the formation of protocatechuic acid products like pentadecane, hexadecanoic acid, octadecanoic acid, hexadecane, and nonacosane as an intermediate (Wulandari et al., 2021).

Recently, studies have shown that micro-fungi (non-mushroom forming fungi) could degrade PAHs through a second metabolic pathway used by the mushroom-forming fungi. The metabolic pathway is imitated through oxidation/ring cleavage of the parent PAHs leading to the formation of quinone compounds as their primary intermediate before further conversion into water and CO_2 as the dead-end metabolic product (Figure 3). The report of Aranda et al. (Aranda et al., 2017), lends credence to this metabolic route where the metabolism of anthracene by *Penicillium oxalicum* was initiated through the oxidation of the compounds leading to the formation of quinone product (anthraquinone) before undergoing another

oxidation process to form anthrone. Birolli et al. (2018) similarly report the same route in a micro-fungi, *Cladosporium* sp., which was catalyzed by laccase through oxidation to form anthrone and anthraquinone. Also, a more recent study by Bankole et al. (2020), identified three quinone compounds distinct metabolites namely anthracene-1,8,9 (2H,8aH,9aH)-trione, 2,4a-dihydro naphthalene-1,5-dione and 1,3,3a,7a-tetrahydro-2-benzofuran-4,7-dione with 2-hydroxybenzoic acid as a dead-end product which can be easily mineralized by the fungal enzymes.

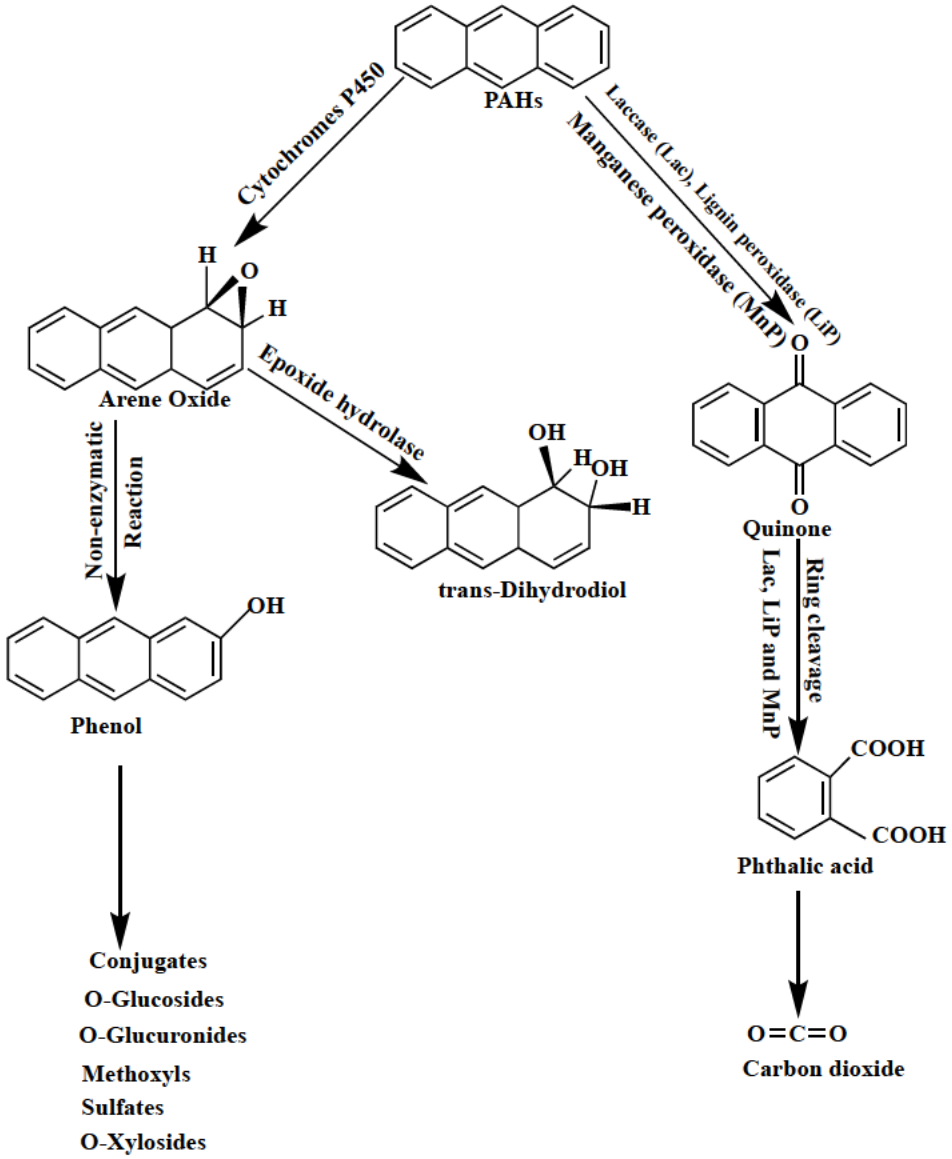

Figure 2.3. The generalized PAHs metabolism pathways by fungi (Modified from Cerniglia, 1997)

2.6: Metabolism of low Molecular weight PAHs by micro-fungi

Organic compounds containing three or fewer aromatic rings are known as low Molecular weight (LMW) PAHs. The available report has shown that micro-fungi are capable of metabolising LMW PAHs into an innocuous state due to the high solubility of these compounds, the degradation enzymes stimulating effects, fast uptake into the fungi cells for onward metabolism and high energy yield for fungal cell growth in comparison with their bacteria and the mushroom-forming fungi counterparts (Greco et al., 2019; Shankhwar and Paliwal, 2021). However, LMW PAHs such as Naphthalene, anthracene, fluorene, acenaphthene and acenaphthylene could be metabolized individually as sole carbon and energy sources into an innocuous state through some metabolic pathways identified in some micro-fungi and bacteria. For instance, Stoyanova et al. (2022) reported the metabolism of Naphthalene and anthracene by a non-mushroom forming fungus (*Aspergillus glaucus*) isolated from Antarctic Soil when used individually as sole carbon and energy sources. In their study, the fungal isolate was found to degrade naphthalene into salicylic acid, catechol, and ketoadipic (TCA cycle intermediates) while that anthracene followed the 2-hydroxy-1-naphthoic acid, o-phthalic acid, and protocatechuic acid metabolic pathways (Figure 2.4). In a recent study, the biodegradation of fluorene by a marine-derived micro-fungus (*Mucor irregularis)* yielded four metabolites, namely; 9H-fluoren-9-one, benzene-1,2-dicarboxylic acid, 2-hydroxybenzoic acid and phenol as the metabolic pathway products (Figure 2.5). It is noteworthy that this was the first study to demonstrate the complete degradation of fluorene to a lower molecular weight compound (Phenol) compared to other documented fluorene degradation pathway products by bacteria and mushroom-

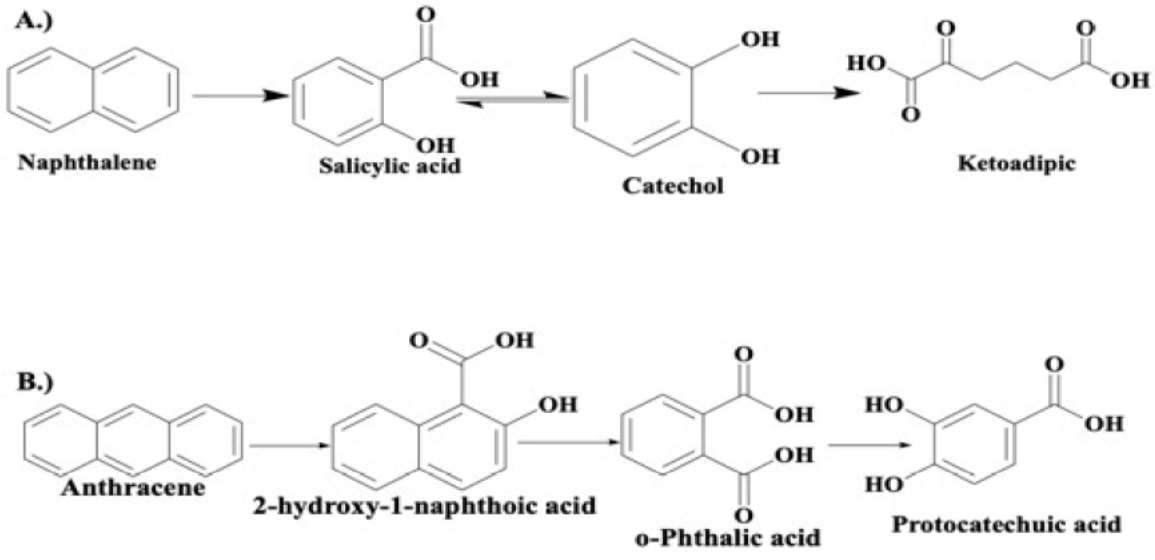

Figure 2.4. Naphthalene and Anthracene metabolic pathways by *Aspergillus glaucus*

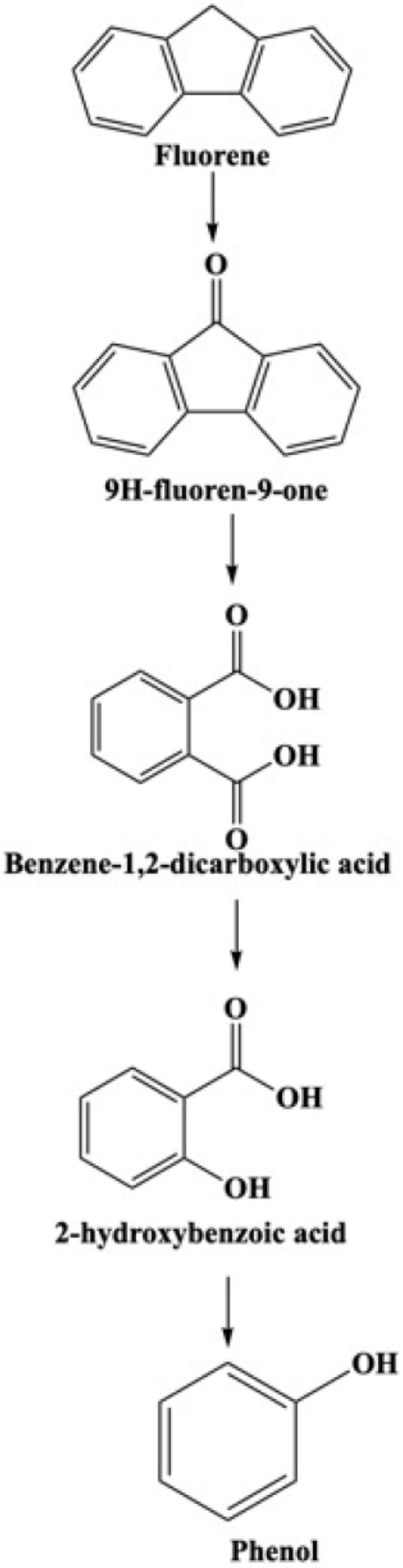

Figure 2.5. Fluorene metabolic pathways by *Mucor irregularis*

2.7: Metabolism of high Molecular weight PAHs by micro-fungi

PAHs having greater than three aromatic rings are known as high Molecular weight HMW PAHs. The available report showed that HMW PAHs such as pyrene, fluoranthene and benzo[a] pyrene (Bap) are the main compound used in assessing the metabolism of HMW PAHs by micro-fungi in the past five years. Hadibarata et al. (2017) demonstrated the potential of a micro-fungus (*Candida* sp. S1) isolated from the tropical rainforest in metabolising pyrene through a cascade of reactions involving hydroxylation to 4,5- dihydroxyphenanthrene, decarboxylation to 1-hydroxy-2-naphthoic acid, and finally to benzoic acid as the dead-end metabolic product (Figure 2.6). The report of Al Farraj et al. (2020) further showed that micro-fungus *Trichoderma* sp. F03 could metabolise pyrene through another route via oxygenation to form pyrene-1,6-quinone, oxidative cleavage and decarboxylation to phenanthrene 4,5-dicarboxylic acid and phenanthrene-4-carboxylic acid before subsequent conversion into benzoic acid, 3-hydroxybenzoic acid, and acetic acid in a chronological manner (Figure 2.6). A recent study by Bankole et al. (2022) showed the potential of micro-fungi (*Aspergillus aculeatus* and *Mucor irregularis)* in the degradation of fluoranthene into an innocuous state.

However, this study provides empirical information about the three possible metabolic pathways employed by these fungi during compound metabolism. Fluoranthene metabolism by *A. aculeatus* was observed to be initiated through the compound's ring cleavage leading to the formation of 2-formylacenaphthylene-1-carboxylic acid, which was further converted into 1,2-dihydroacenaphthylen-1-ol through hydroxylating dioxygenase reactions to form 1,2- dihydroacenaphthylene as the dead-end product. Also, under *M. irregularis* inoculation, the metabolic pathway of fluoranthene was initiated through the extra-diol ring cleavage to form 1,2-dihydroacenaphthylen-1-ol, which was further broken down into 1,2-dihydroacenaphthylene which is similar to the final metabolite (1,2- dihydroacenaphthylene) obtained after degradation by *A. aculeatus*. Conversely, the co-biomass of the two micro-fungi suggests that fluoranthene could be degraded through hydroxylation and ring cleavage to form 1,2- dihydroxyfluoranthene which is further broken down into 9H-fluorene-1,9-dicarboxylic acid, benzene-1,2,4-tricarboxylic acid, benzene-1,3-dicarboxylic acid and benzoic consecutively (Figure 2.7).

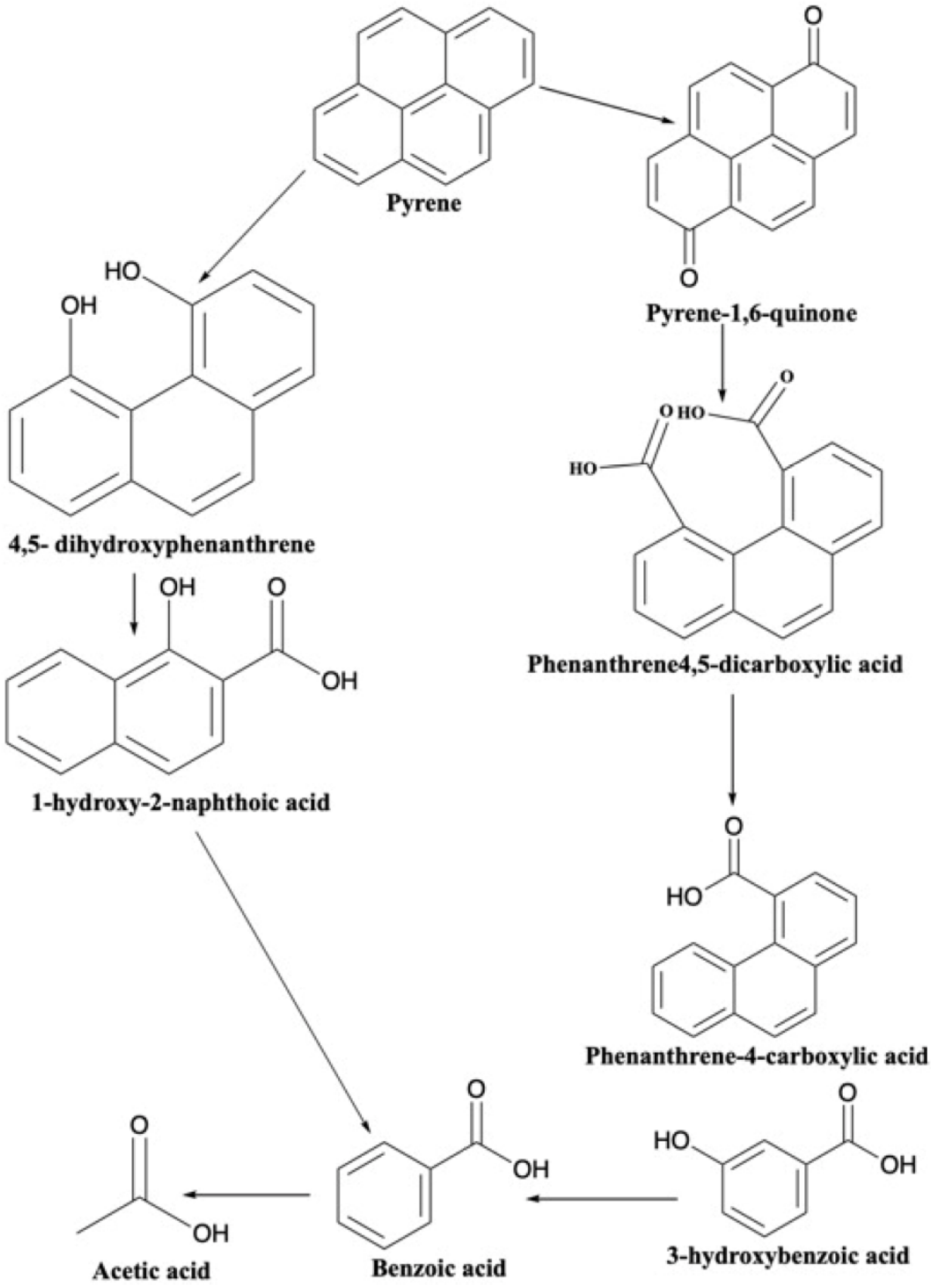

Figure 2.6. Pyrene metabolism by Micro-fungi

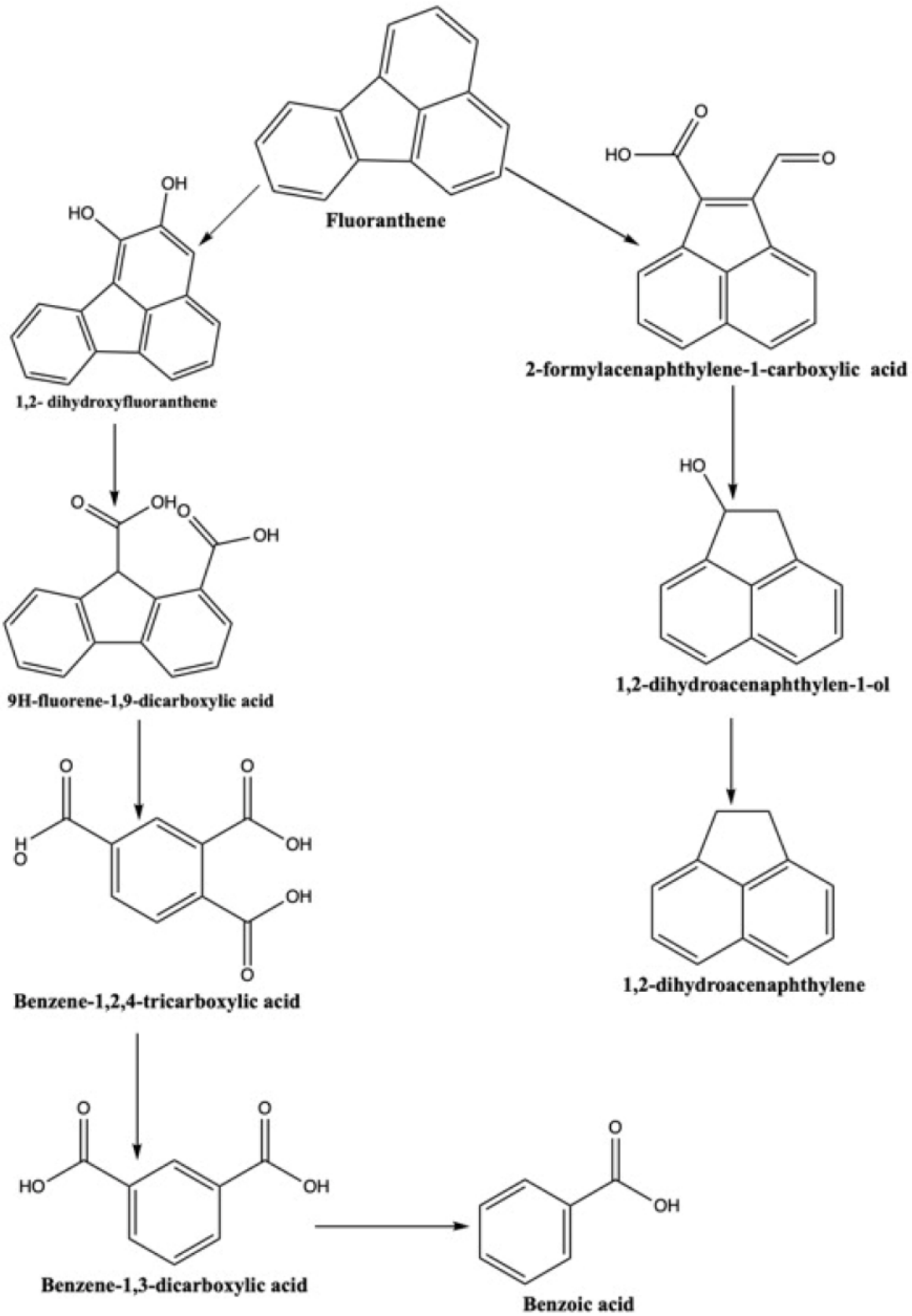

Figure 2.7. Fluoranthene metabolism by Micro-fungi

2.8: Mechanism of PAHs metabolism by micro-fungi

In the last decades, several studies on the mechanisms used by fungi during PAHs degradation have continuously been focused on laccase (Lac), lignin peroxidase (LiP), and manganese peroxidase (MnP) produced by macro-fungi (white-rot fungi) owing to their degradation efficiency (Hadibarata et al., 2022). Yet, the mechanisms of PAH degradation by fungi are not well understood, though several different pathways have been proposed. One possibility is that PAHs are first converted to more water-soluble compounds by intracellular enzymes produced in the case of micro-fungi. These water-soluble compounds are transported across the cell membrane and degraded within the fungal cells using the intracellular enzymes (cytochrome P450 oxidoreductases, Phenol 2-monooxygenase, Catechol 1,2-dioxygenase, and Catechol 2,3-dioxygenase) (Peidro-Guzmán et al., 2021). Another possibility is that PAHs are first converted to other organic compounds, such as benzoic acid, by extracellular enzymes Lac, LiP, and MnP, which can be transported across the cell membrane and degraded within the fungal cells (Agrawal et al., 2021). It is also possible that PAHs are not degraded by fungi but are instead adsorbed to the surface of the fungal cells and then secreted into the environment (Al-Hawash et al., 2019b). A summary of the activities of the intracellular and extracellular enzymes during PAHs metabolisms is shown in Table 2.4.

2.8.1: Intracellular enzymes

Intracellular fungal enzymes are a type of enzymes produced by micro-fungi which can break down organic compounds, such as benzoic acid, which are transported across the cell membrane and degraded within the fungal cells (Abo Nouh et al., 2021). The intracellular enzymes employed by microfungi includes Cytochrome P450 monooxygenase, Phenol 2-monooxygenase, Catechol 1,2-dioxygenase and Catechol 2,3-dioxygenase.

2.8.1.1: Cytochrome P450 monooxygenase, an intracellular enzyme, has been implicated in the primary initiation of PAHs oxidation into an unstable arene-oxide form which is further converted to trans-dihydrodiol through epoxide hydrolase catalyzed reaction (Al-Hawash et al., 2018) (Figure 2.3). These intermediates then undergo non-enzymatic rearrangement to form derivatives such as dihydroxy, hydroxy, dihydrodiol and quinone, which could possibly conjugate to form glucosides, sulfate, xylosides and glucuronides metabolites (Figure 2.3) as

observed in *Trichoderma* species such as *T. atroviride, T. harzianum,* and *T. asperellum* (Zafra et al., 2014b).

2.8.1.2: Phenol 2-monooxygenase (EC 1.14.13.7) belongs to a member of the monooxygenase family, which contains enzymes that use oxygen to oxidize substrates (Wang et al., 2018). The phenol 2-monooxygenase enzyme contains a heme prosthetic group, which is necessary for its function and its responsible for oxidizing phenol to catechol during PAHs metabolic pathway in micro-fungi (Stoyanova et al., 2022).

2.8.1.3: Catechol 1,2-dioxygenase (EC 1.13.11.1) is an intradiol dioxygenase that cleaves the bond between the phenolic hydroxyl groups of catechol using a Fe^{3+} cofactor (Kałduńska et al., 2021). This enzyme catalyzes the oxidative ring cleavage of catechol to form cis,cis-muconic acid (Soal et al., 2022). For example, catechol 1,2-dioxygenase activity in a micro-fungus, *Aspergillus glaucus* has been reported in the breakdown of naphthalene with the formation of catechol and cis,cis-muconic acid in the naphthalene metabolic pathway (Stoyanova et al., 2022).

2.8.1.4: Catechol 2,3-dioxygenase (EC 1.13.11.2), an intracellular enzyme which belongs to the family dioxygenase (Agrawal and Shahi, 2017). Its role in the early stages of PAHs metabolism by microfungi has been well documented. It aids in the catalytic conversion of catechol to 3-keto-catechol (Zafra et al., 2014b).

2.8.2: Extracellular enzymes

Extracellular enzyme activities from the macro-fungi have been significantly studied in the last decade due to their arsenal of mass destruction of different groups of PAHs leading to mineralization (Ferreira-Silva et al., 2022). PAHs metabolism are being catalyzed by the extracellular enzymes (peroxidases and laccase) through aromatic ring oxidation to form PAHs quinone whose rings undergo fission and produce carbon dioxide as end products in the absence of cis-trans dihydrodiol (Bankole et al., 2021, 2022). However, contrary to the popular hypothesis that extracellular enzyme activities during PAHs metabolism are limited to the mushroom-forming fungi (macro-fungi), recent studies on PAHs metabolism have shown that micro-fungi, especially from genera Ascomycetes also employ extracellular enzyme which they use in complementing intracellular enzymes after ring oxidation to complete PAHs metabolism into an innocuous state (Bankole et al., 2020). Few studies have shown that the

purified extracellular enzymes (peroxidases and laccase) from micro-fungi are capable of degrading PAHs individually at extreme conditions by implementing an electron radical oxidation to produce cation radicals from PAHs through the formation of quinones which is further reduced into H_2O and CO_2 (Wu et al., 2010; Vipotnik et al., 2019).

2.8.2.1: Peroxidases

Peroxidases (oxidoreductases, EC 1.11.1.x) are a diverse group of versatile heme-containing enzymes, which use hydrogen peroxide (R-OOH) an electron acceptor, to catalyze the oxidation of numerous substrates like PAHs (Yang et al., 2017). The peroxidase superfamily consists of three classes of peroxidase families. Class I includes intracellular prokaryotic peroxidases; class II secretory fungal peroxidases, that is, lignin peroxidase (LiP), manganese peroxidase (MnP) and versatile peroxidases (VPs) (Riley et al., 2014) while class III includes secretory plant peroxidases (Lüthje and Martinez-Cortes, 2018). Of all, peroxidase families, the class II secretory fungal peroxidases have been of interest to scientists over the past decades owing to their environmental applications in context to this review (Wong, 2009; Simarro et al., 2013; Torres-Farradá et al., 2019). Peroxidases from micro-fungi have been reported to catalyze the oxidation process and can break down the aromatic ring of PAHs, making them more water-soluble and easier to degrade by hydrogen peroxide (Veignie et al., 2004).

2.8.2.2: Laccase

Laccases (E.C. 1.10.3.2 benzenediol: oxygen oxidoreductase) are metalloenzymes that belong to the diverse superfamily of multi-copper oxidases which catalyze the one-electron oxidation of diphenols, polyphenols, diamines, aromatic amines and other electron-rich compound using molecular O_2 (Shrestha et al., 2016). Laccases have been continuously studied over the past decades due to their broad substrate specificity. They use molecular oxygen as the final electron acceptor instead of hydrogen peroxide compared to peroxidases (Shrestha et al., 2016). Their broad substrate specificity has made them an enzyme of high interest in polycyclic aromatic hydrocarbon degradation (Liu and Hua, 2014). However, the production of laccases and other phenol oxidases is also widely distributed among Ascomycota and Basidiomycota fields(Liu and Hua, 2014; Aranda, 2016). The main mechanism of PAHs bioremediation by laccase is through the oxidation of its aromatic ring into quinone compounds whose rings undergo fission and produce carbon dioxide as end products in the absence of cis-trans dihydrodiol (Agrawal

and Shahi, 2017). Thus the efficiency of laccase from microfungi in the oxidation of wide range of PAHs are summarized in Table 2.4.

Table 2.4. Summary of the activities of the intracellular and extracellular enzymes during PAHs metabolisms

PAHs	Enzyme	Source	Metabolites	References
Naphthalene	C12O and Phenol-2-mono	*Aspergillus glaucus* AL1	Salicylic acid Ketoadipic Catechol	Stoyanova et al. (2022)
Anthracene	C12O and Phenol 2-mono		2-hydroxy-1naphtoic acid o-phtalic acid protocatechuic acid	
Anthracene	Lac, LiP, MnP and CAT	*Aspergillus sydowii* BPOI	Anthracene-1,8,9 (2H,8aH,9aH)-trione 2,4a-Dihydronaphthalene-1,5-dione, 1,3,3a,7a-Tetrahydro-2-benzofuran-4,7-dione	Bankole et al. (2020)
Phenanthrene	C23O,P450 mono, Epoxide H and Dehyd	*Phomopsis liquidambari*	Phenanthrene 9,10-oxide Phenanthrol 9,10-Dihydroxyphenanthrene Phenanthrene trans-9,10-dihydrodiol 9,10-Phenanthrenequinone	Fu et al. (2018)

Key. ND: Not determined, Lac: Laccase, LiP: Lignin Peroxidase, MnP: Manganese Peroxidase, CAT: Catalase, C12O: P450 mono: Cytochrome P450 monooxygenase, C23O: Catechol 2,3-dioxygenase,Phenol-2-mono: Phenol 2-monooxygenase, Epoxide H: Epoxide Hydrolase, Dehyd: Dehydrogenase, Intradiol DO: Intradiol dioxygenase and Extradiol DO: Extradiol dioxygenase

Table 2.4. Summary of the activities of the intracellular and extracellular enzymes during PAHs metabolisms Cont'd

PAHs	Enzyme	Source	Metabolites	References
Fluorene	Lac, LiP and MnP	*Mucor irregularis*	9H-fluoren-9-one Benzene-1,2- dicarboxylic acid 2-hydrox-ybenzoic acid Phenol	Bankole et al. (2021)
Fluorene	Lac, LiP and MnP	*Trichoderma viride*	ND	Vipotnik et al. (2021)
Chrysene	Lac and LiP	*Penicillium chrysogenum*		
Pyrene	Lac, LiP and MnP	*T. viride* + *P. chrysogenum*		
Pyrene	Lac, C12O, Epoxide H, Phenol- 2-mono, Intradiol DO and Extradiol DO	*Tolypocladium* sp.	Pyrene dihydrodiol 4,5-Trans-dihydroxy-pyrene 4-Hydroxyphenenthrene Hexadecane Behenic alcohol 5-Eicosane Cetene Lactone	Vasconcelos et al. (2019)
Benzo(a)pyrene	Lac, LiP and MnP	*Lasiodiplodia theobromae*	ND	Cao et al. (2020)

Key: ND: Not determined, Lac: Laccase, LiP: Lignin Peroxidase, MnP: Manganese Peroxidase, CAT: Catalase, C12O: P450 mono: Cytochrome P450 monooxygenase, C23O: Catechol 2,3-dioxygenase,Phenol-2-mono: Phenol 2-monooxygenase, Epoxide H: Epoxide Hydrolase, Dehyd: Dehydrogenase, Intradiol DO: Intradiol dioxygenase and Extradiol DO: Extradiol dioxygenase

Table 2.4. Summary of the activities of the intracellular and extracellular enzymes during PAHs metabolisms Cont'd

PAHs	Enzyme	Source	Metabolites	References
Benzo(a)pyrene	P450 mono and Peroxidase	*Aspergillus fumigatus* *Aspergillus oryzae* *Aspergillus flavus* *Aspergillus nidulans*	ND	Ostrem Loss et al. (2018)
Fluoranthene	Lac, LiP and MnP	*Aspergillus aculeatus*	2-formylacenaphthylene-1-carboxylic acid 9*H*-fluoren-9-ol 1,2-dihydroacenaphthylen-1-ol 1,2-dihydroacenaphthylene	Bankole et al. (2022)
		Mucor irregularis	1,2-dihydroacenaphthylene 1,2-dihydroacenaphthylen-1-ol 9*H*-fluoren-9-one	
		A. aculeatus + *M. irregularis*	1,2- dihydroxyfluoranthene 9H-fluorene-1,9-dicarboxylic acid Benzene-1,2,4-tricarboxylic acid Benzene-1,3-dicarboxylic acid Benzoic acid	

Key. ND: Not determined, Lac: Laccase, LiP: Lignin Peroxidase, MnP: Manganese Peroxidase, CAT: Catalase, C12O: P450 mono: Cytochrome P450 monooxygenase, C23O: Catechol 2,3-dioxygenase,Phenol-2-mono: Phenol 2-monooxygenase, Epoxide H: Epoxide Hydrolase, Dehyd: Dehydrogenase, Intradiol DO: Intradiol dioxygenase and Extradiol DO: Extradiol dioxygenase

2.9: Kinetics and modelling of PAHs bioremediation by micro-fungi

kinetics and modelling of PAHs bioremediation by microfungi is vital in understanding the effects of different environmental factors on the rate of bioremediation and the efficiency of the process so that more efficient bioremediation strategies can be developed (Wang et al., 2010). The bioremediation kinetics thus specifically focuses on understanding the underlying physical and chemical processes that govern the rate of chemical degradation. In contrast, bioremediation modelling uses mathematical models to represent the degradation data and predict future degradation behaviour (Ayub et al., 2020). Three orders of bioremediation kinetics are commonly used to describe the bioremediation process of PAHs, including Zero order, first order and second order (Mandal and Das, 2018), while the Langmuir, Temkin and Freundlich models are often used to describe the bioremediation of polycyclic aromatic hydrocarbons (PAHs) by microfungi (Bankole et al., 2020).

2.9.1: Zero-order bioremediation kinetics

Zero-order degradation kinetics is a valuable tool for evaluating the fate of contaminants such as PAHs, analyzing the effects of pollutants such as PAHs on ecosystems, and formulating strategies to mitigate them (Muthukumaran, 2022). It describes a constant rate at which PAHs are broken down independent of its concentration, which implies that increasing or decreasing the reactant concentration does not affect the rate of the reaction, which is constant and equals the rate coefficient (Reddy et al., 2020). This process is typically observed in reactions involving multiple steps, such as the oxidation of PAHs by laccase and reduction by lignin and manganese (Mandal and Das, 2018).

2.9.2: First-order bioremediation kinetics

This assumes that the degradation rate of PAHs is proportional to the concentration of the parent compound (Abd Manan et al., 2019). In other words, the PAH concentration change rate over time is constant and directly proportional to the concentration. In a study by Mandal et al. (Mandal and Das, 2018), First-order kinetics revealed how the removal of perylene and benzo[ghi]perylene by yeast consortia was time-dependent process and degradation rate was directly proportional to substrate (PAHs) concentration.

2.9.3: Second-order bioremediation kinetics

In the context of PAH degradation by micro-fungi, the concept of second-order bioremediation kinetics involves the interaction between the concentration of PAHs and the biomass of micro-fungi to determine the rate of PAH degradation (Dutta and Laha, 2022; Pozdnyakova et al., 2023). While the Langmuir, Temkin, and Freundlich models are commonly used to describe second order kinetics of PAH degradation, they focus is on the synergistic, binding and adsorption capacity fungi biomass, PAHs concentration and environmental factors (Bankole et al., 2020).

2.9.3.1: Langmuir model

The Langmuir model describes the binding of PAHs to the fungal biomass as a process that follows a simple, reversible, and saturable binding mechanism (Aryal, 2020). The model assumes a maximum binding capacity for PAHs on the fungal biomass and that PAHs' binding affinity decreases as the PAHs concentration in the environment increases (Bankole et al., 2020).

2.9.3.2: Temkin model

The Temkin model describes the biodegradation of PAHs by microfungi as a process that follows a multi-step mechanism. The biodegradation rate is affected by temperature and other environmental factors. The model considers that PAHs are often present in complex mixtures and that the biodegradation rate can be affected by the presence of other compounds in the environment (Bankole et al., 2020).

2.9.3.3: Freundlich model

The Freundlich model is commonly used to describe the bioremediation of PAHs by microfungi, as it can predict the efficiency of bioremediation treatments under different conditions (De-Wet and Brink, 2021). The model can determine fungal biomass's maximum adsorption capacity and pollutants' adsorption intensity on fungal biomass (Bankole et al., 2020). It is important to note that the applicability of this model is limited, as it assumes that adsorption is a reversible process. It does not consider that the biodegradation rate can be affected by other environmental factors or the presence of other compounds in the environment (Oberoi et al., 2019). Also, the Freundlich model is unsuitable for the adsorption of pollutants (PAHs) in high concentrations and is not valid for all fungal species and specific PAH compounds (Bankole et al., 2020). Therefore, it's recommended to use this model with caution and to consider other models, such as Langmuir and Temkin.

2.10: Limitations and challenges of micro-fungi bioremediation PAHs

Although, micro-fungi are more efficient in the bioremediation of PAHs into an innocuous state. Yet, there are several limitations and challenges facing this bioremediation method, including many environmental and biological factors such as the PAHs molecular weight and concentration, type and structure of the soil, biomass concentration, growth medium composition and the survival of PAHs-degrading microorganisms (Magan et al., 2010). Environmental conditions such as the pH of the soil, oxygen availability and nutrient content that affect the growth of microorganisms can restrict PAHs degradation process and further reduce the bioavailability of pollutants to microbial attack (Maiti et al., 2012). It is noteworthy that soil organic matter is a major dominating factor determining the relationship between soil and the organic pollutant because the ratio of soil organic matter controls the partitioning of PAHs into the organic fraction of soil and the extent to which it is determined could affect degradation rate (Datta et al., 2017).

2.10.1: Bioavailability

The bioavailability of PAHs during bioremediation by micro-fungi is limited due to their low biodegradability, adsorption onto soil particles, and ability to form stable complexes with soil organic matter (Chowdhury et al., 2023). Moreover, optimal environmental conditions are needed for the micro-fungi to grow and access the PAHs (Sharma, 2022). Additionally, the presence of other contaminants, high levels of organic matter, inorganic contaminants, and microbial activity in the soil can all reduce the effectiveness of the fungi in degrading PAHs

(Ceci et al., 2018). Optimizing environmental conditions and reducing the presence of other contaminants can improve the effectiveness of micro-fungi in degrading PAHs (Bankole et al., 2021). Ultimately, environmental, chemical, and microbial factors all play a role in determining the bioavailability of PAHs in bioremediation by micro-fungi (Sachaniya et al., 2020).

2.10.2. pH

Micro-fungi have been extensively studied for reducing PAHs through bioremediation. However, there are still some limitations and challenges that must be overcome. The primary challenge is the optimal pH range for bioremediation. The ideal pH range for the bioremediation of PAHs is 6-7, which is slightly acidic (Bankole et al., 2022). However, this range may be too narrow for some micro-fungi, as they may not be able to survive or function in such an acidic environment (González-Abradelo et al., 2019). Also, other environmental pollutants, such as metals, can affect the pH level, making it difficult to maintain the optimal pH range (El-Bondkly and El-Gendy, 2022). Another challenge is that some species of micro-fungi may be more efficient at degrading one type of PAHs over another, limiting their effectiveness at bioremediation (Álvarez-Barragán et al., 2021). Also, some species may be more efficient at degrading a specific PAHs group at a specific pH range but inefficient at degrading other types of PAHs (Álvarez-Barragán et al., 2021). This can make it difficult to achieve effective bioremediation of all types of PAHs in a single environment.

2.10.3: Temperature

Temperature plays a key role in the bioremediation of polycyclic aromatic hydrocarbons (PAHs) using micro-fungi, as it affects the growth, diversity and metabolism of the microbial community (Bankole et al., 2022). Low temperatures can reduce the micro-fungi's metabolic activity and the target PAHs' degradation (Bankole et al., 2020). High temperatures can cause thermotolerance of the micro-fungi and decreased metabolic activity, leading to a decrease in the effectiveness of the bioremediation process (Mandal and Das, 2018). Additionally, fluctuations in temperature can lead to changes in the type of micro-fungi present in the environment and the diversity of the microbial community, resulting in decreased degradation of the target PAHs (Mandal et al., 2018). Temperature gradients in the environment can further lead to increased competition among the different micro-fungi species, reducing the efficiency of the bioremediation process (Hadibarata et al., 2017). Therefore, it is crucial to consider the dynamics of microbial communities in different temperature regimes to ensure successful bioremediation of PAHs using micro-fungi.

2.10.4: Inoculum Size

Inoculum size is a critical factor in the success of the bioremediation of polycyclic aromatic hydrocarbons (PAHs) by micro-fungi. The size of the inoculum, or the number of micro-fungi in the environment, determines the biodegradation rate of pollutants such as PAHs and the ultimate success of the bioremediation process (Bankole et al., 2021). However, there are several limitations and challenges associated with the inoculum size. Firstly, the diversity of the micro-fungi in the environment affects the size of the inoculum (Álvarez-Barragán et al., 2021). As PAHs are toxic pollutants, it is often difficult to introduce large numbers of micro-fungi into the environment. Secondly, competition with other microorganisms for nutrients and space can reduce the size of the inoculum (Zafra et al., 2014b). Finally, the degradation rate of the PAHs can also affect the size of the inoculum. If the PAHs are degraded too quickly, the number of micro-fungi in the environment can decrease, reducing the size of the inoculum (Fu et al., 2018). Therefore, it is crucial to consider the size of the inoculum when implementing bioremediation processes to ensure optimal results (Bankole et al., 2021).

2.10.5: PAHs concentration

The concentration of the targeted contaminant is a significant factor which affects microbial biomass production and degradation efficiency. A low concentration of contaminants might not be able to aid the secretion of degradation enzymes needed for PAHs degradation by micro-fungi, while high contaminant levels might be toxic to the microorganisms (Awasthi et al., 2017; Fu et al., 2018). For instance, a thermotolerant white rot fungus *Trametes polyzona* RYNF13 could yield 100 % of the low concentration of phenanthrene (100 mg/ L). Still, it could only degrade 52% of pyrene of the same concentration in a mineral glucose salt medium culture after 18 days of incubation (Teerapatsakul et al., 2016). Similarly, a microbial consortium consisting of 12 fungal and bacterial PAH-tolerant isolates could only degrade 87.76 % phenanthrene, 48.18 % Pyrene, and 56.55 % Benzo (a)Pyrene of 6,000 mg/L after 14 days (Zafra et al., 2014a).

2.10.6: Diversity of slow-growing micro-fungi

Studies have shown the promising efficiencies of several diversities of slow-growing micro-fungi during the bioremediation of polycyclic aromatic hydrocarbons (PAHs) in contaminated soils and sediments in recent years. However, this process has limitations and challenges, such as its slow growth rate, inability to break down certain PAHs, unsuitable environments for fungi to thrive, and high maintenance cost (Al-Hawash et al., 2019, 2021; Shourie and Vijayalakshmi, 2022). These issues can all lead to reduced effectiveness and perplexity in the bioremediation process, as well as increased costs, making it difficult to achieve the desired outcomes in a timely and cost-effective manner.

2.11: Potential Applications of micro-fungi in the bioremediation of PAHs

Micro-fungi have shown great potential as a bioremediation tool for removing polycyclic aromatic hydrocarbons (PAHs) from contaminated soil and water. These group of micro-organisms can degrade PAHs through a variety of metabolic pathways, making them a versatile solution for addressing PAH pollution. Some of the potential applications of micro-fungi in the bioremediation of PAHs include:

2:11.1: Soil bioremediation: Micro-fungi can degrade PAHs in contaminated soil, breaking down the pollutants and making the soil safe for use. This method is relatively low-cost and can be applied on-site, making it an attractive solution for remediating PAH-contaminated sites (Myazin et al., 2021). Wang et al. [2009] showed that phenanthrene, pyrene, and benzo[a]pyrene in contaminated soils are degraded in the presence of *P. chrysosporium,* with LiP and MnP activity as high as 1.92 U/g. In a Brazilian study, *Mucor racemosus* CBMAI 847 and *Aspergillus sclerotiorum* CBMAI 849 derived from marine environment were found to degrade between 50% and 90% of pyrene and benzo[a]pyrene in a PAH-polluted soil [Passarini et al., 2011]. In another study, three marine-derived basidiomycetes: *Peniophora sp*. CBMAI106, *Tinctoporellus sp*. CBMAI1061, and *Marasmiellus sp.* CBMAI 1062 was shown to be very efficient in degrading PAHs in environmental samples [Vieira et al., 2018]. The latter species (*Marasmiellus sp.* CBMAI 1062) especially, produced nearly 100% of pyrene degradation after 48 h of incubation, an observation highlighting its practicability and the potential bioremediation applications. Further, the analysis of the pyrene metabolic intermediates indicated that the mycoremediation of PAHs could follow the cytochrome P450 system and epoxide hydrolases pathways.

2.11.2: Water bioremediation: Micro-fungi can also be used to remove PAHs from contaminated water, either through fungal-based biofilters or by introducing the micro-fungi directly into the water (Greco et al., 2019). This approach can effectively remove PAHs from surface water, groundwater, and wastewater.

2.11.3: Biostimulation: Introducing micro-fungi can stimulate the activities of native microorganisms' activity and degrade PAHs, enhancing the bioremediation process (Zafra et al., 2015; Myazin et al., 2021). This approach can be helpful in cases where the native microflora of the site is not capable of effectively degrading PAHs (Myazin et al., 2021).

2.11.4: Phytoremediation: Micro-fungi can be used to enhance the ability of plants to remove PAHs from the soil. This approach can be helpful in cases where the plants can take up PAHs but cannot degrade them and adding micro-fungi to the rhizosphere (soil around roots) can help their degradation.

2.12: Future Perspectives on Micro-Fungi-based Bioremediation of PAHs

Although, the efficiency of micro-fungi in the bioremediation of polycyclic aromatic hydrocarbons (PAHs) from contaminated soil and water has been established. However, there are still several areas where research is needed to realize the full potential of micro-fungi in bioremediation. One area of extensive research is the identification and characterization of new micro-fungi strains that can degrade PAHs. Available information has shown that only a limited number of micro-fungi strains have been studied for their ability to remove PAHs. According to Álvarez-Barragán et al. (2021), identifying new strains that are more effective at degrading PAHs is an added advantage as it may further promote the bioremediation efficiency. Furthermore, studying the genetic and enzymatic basis of micro-fungi degradation will enable the development of new strains that can degrade PAHs more efficiently and specifically (Zafra et al., 2017).

Another area of future research is the development of new techniques for enhancing the ability of micro-fungi to remove PAHs. For example, using genetic engineering to introduce new metabolic pathways into micro-fungi strains could increase their ability to degrade PAHs (Zafra et al., 2016). Additionally, the use of chemical and physical techniques to enhance the bioavailability of PAHs to micro-fungi could also lead to an improvement in bioremediation efficiency (Undugoda et al., 2022).

A third area of future research is the exploration of potential applications of micro-fungi bioremediation in other types of pollutants. While micro-fungi have been primarily studied for their ability to remove PAHs, they may also have the ability to remove other types of pollutants such as heavy metals and persistent organic pollutants (Al-Hawash et al., 2019c; Greco et al., 2019; Daccò et al., 2020; Undugoda et al., 2022). By investigating the potential of micro-fungi to remove these other pollutants, the range of applications for bioremediation can be expanded.

2.13: Concluding remarks

Micro-fungi have shown great potential as a bioremediation tool for removing polycyclic aromatic hydrocarbons (PAHs) from contaminated soil and water in an eco-friendly way. In addition to the efficient enzyme-mediated mycoremediation processes, the penetrative ability of the micro-fungi mycelia through PAHs contaminated soil and the spread afterward through the solid matrix to degrade it represent an advantage over the most explored bacterial-based PAHs degradation. In several micro-fungi-based mycoremediation applications, the same set of micro-fungal enzymes or taxa is frequently employed as substitutes for traditional pollution mitigation strategies. Nonetheless, the wealth of micro-fungal taxa and several important enzymes remain to be tapped maximally as natural bioremediating mediators. While there has been a significant amount of research conducted on the use of micro-fungi for PAH bioremediation, there are still many areas where improvement is needed in order to realize the potential of this approach fully. Some areas where future research is needed include identifying and characterising new micro-fungi strains that can degrade PAHs, developing new techniques for enhancing the ability of micro-fungi to remove PAHs, and exploring potential applications of micro-fungi bioremediation in other types of pollutants. As research in these areas progresses, micro-fungi use for bioremediation will likely become an increasingly effective and sustainable solution for addressing PAH pollution.

2.14 References:

Abd Manan, T.S.B., Khan, T., Sivapalan, S., Jusoh, H., Sapari, N., Sarwono, A., Ramli, R.M., Harimurti, S., Beddu, S., Sadon, S.N., Kamal, N.L.M., Malakahmad, A., 2019. Application of response surface methodology for the optimization of polycyclic aromatic hydrocarbons degradation from potable water using photo-Fenton oxidation process. *Science of The Total Environment* 665, 196–212. https://doi.org/10.1016/J.SCITOTENV.2019.02.060

Abdel-shafy, H.I., Mansour, M.S.M.M., 2016. A review on polycyclic aromatic hydrocarbons: Source, environmental impact, effect on human health and remediation. *Egyptian Journal of Petroleum* 25, 107–123. https://doi.org/10.1016/j.ejpe.2015.03.011

Abo Nouh, F.A., Gezaf, S.A., Abo Nahas, H.H., Abo Nahas, Y.H., Vargas-De-La-Cruz, C., Solorzano Acosta, R.A., Landa-Acuña, D., Luis-Alaya, B., Abdel-Azeem, A.M., 2021. Bioprospecting for Biomolecules from Different Fungal Communities: An Introduction 1–71. https://doi.org/10.1007/978-3-030-85603-8_1

Adeyeye, S.A.O., 2020. Heterocyclic amines and polycyclic aromatic hydrocarbons in cooked meat products: A review. *Polycycl Aromat Compd* 40, 1557–1567.

Agrawal, N., Kumar, V., Shahi, S.K., 2021. Biodegradation and detoxification of phenanthrene in in vitro and in vivo conditions by a newly isolated ligninolytic fungus *Coriolopsis byrsina* strain APC5 and characterization of their metabolites for environmental safety. *Environmental Science and Pollution Research* 2021 29:41 29, 61767–61782. https://doi.org/10.1007/S11356-021-15271-W

Agrawal, N., Shahi, S.K., 2017. Degradation of polycyclic aromatic hydrocarbon (pyrene) using novel fungal strain *Coriolopsis byrsina* strain APC5. *Int Biodeterior Biodegradation* 122, 69–81. https://doi.org/10.1016/j.ibiod.2017.04.024

Agrawal, N., Verma, P., Shahi, S.K., 2018. Degradation of polycyclic aromatic hydrocarbons (phenanthrene and pyrene) by the ligninolytic fungi *Ganoderma lucidum* isolated from the hardwood stump. *Bioresour Bioprocess* 5, 11. https://doi.org/10.1186/s40643-018-0197-5

Agrawal, P.K., Shrivastava, R., Verma, J., 2019. Bioremediation approaches for degradation and detoxification of polycyclic aromatic hydrocarbons, in: *Emerging and Eco-Friendly Approaches for Waste Management*. Springer, pp. 99–119.

Ahammed, G.J., Li, X., Xia, X.-J., Shi, K., Zhou, Y.-H., Yu, J.-Q., 2015. Enhanced photosynthetic capacity and antioxidant potential mediate brass in osteriod-induced phenanthrene stress tolerance in tomato. *Environmental Pollution* 201, 58–66.

Al Farraj, D.A., Hadibarata, T., Elshikh, M.S., Al Khulaifi, M.M., Kristanti, R.A., 2020. Biotransformation and degradation pathway of pyrene by filamentous soil fungus *Trichoderma*

sp. F03. *Water Air Soil Pollut* 231, 1–9. https://doi.org/10.1007/S11270-020-04514-0/FIGURES/6

Al-Hawash, A.B., Alkooranee, J.T., Zhang, X., Ma, F., 2018. Fungal degradation of polycyclic aromatic hydrocarbons. *Int J Pure App Biosci* 6, 8–24.

Al-Hawash, A.B., Al-Qurnawi, W.S., Abbood, H.A., Hillo, N.A., Ghalib, H.B., Zhang, X., Ma, F., 2021. Pyrene-degrading fungus *Ceriporia lacerata* RF-7 from contaminated soil in Iraq. *Polycycl Aromat Compd* 42, 40–48. https://doi.org/10.1080/10406638.2020.1713183

Al-Hawash, A.B., Zhang, X., Ma, F., 2019. Removal and biodegradation of different petroleum hydrocarbons using the filamentous fungus *Aspergillus* sp. RFC-1. *Microbiologyopen* 8, e00619. https://doi.org/10.1002/MBO3.619

Álvarez-Barragán, J., Cravo-Laureau, C., Wick, L.Y., Duran, R., 2021. Fungi in PAH-contaminated marine sediments: Cultivable diversity and tolerance capacity towards PAH. *Mar Pollut Bull* 164. https://doi.org/10.1016/j.marpolbul.2021.112082

Aranda, E., 2016. Promising approaches towards biotransformation of polycyclic aromatic hydrocarbons with Ascomycota fungi. *Curr Opin Biotechnol* 38, 1–8. https://doi.org/10.1016/j.copbio.2015.12.002

Aranda, E., Godoy, P., Reina, R., Badia-Fabregat, M., Rosell, M., Marco-Urrea, E., García-Romera, I., 2017. Isolation of Ascomycota fungi with capability to transform PAHs: Insights into the biodegradation mechanisms of *Penicillium oxalicum*. *Int Biodeterior Biodegradation* 122, 141–150. https://doi.org/10.1016/j.ibiod.2017.05.015

Aryal, M., 2020. Advances in biosorption of polycyclic aromatic hydrocarbons from aqueous solutions using natural biosorbents. *Journal of Environmental Engineering* 147, 03120013. https://doi.org/10.1061/(ASCE)EE.1943-7870.0001853

Awasthi, S., Srivastava, N., Singh, T., 2017. Biodegradation of thermally treated low density polyethylene by fungus *Rhizopus oryzae* NS 5. 3 *Biotech*. https://doi.org/10.1007/s13205-017-0699-4

Ayub, A., Raza, Z.A., Majeed, M.I., Tariq, M.R., Irfan, A., 2020. Development of sustainable magnetic chitosan biosorbent beads for kinetic remediation of arsenic contaminated water. *Int J Biol Macromol* 163, 603–617. https://doi.org/10.1016/j.ijbiomac.2020.06.287

Aziz, A., Agamuthu, P., Alaribe, F.O., Fauziah, S.H., 2018. Biodegradation of benzo [a] pyrene by bacterial consortium isolated from mangrove sediment. *Environ Technol* 39, 527–535.

Bankole, P.O., Semple, K.T., Jeon, B.H., Govindwar, S.P., 2021. Biodegradation of fluorene by the newly isolated marine-derived fungus, *Mucor irregularis* strain bpo1 using response surface

methodology. *Ecotoxicol Environ Saf* 208, 111619. https://doi.org/10.1016/j.ecoenv.2020.111619

Bankole, P.O., Semple, K.T., Jeon, B.H., Govindwar, S.P., 2020. Enhanced enzymatic removal of anthracene by the mangrove soil-derived fungus, *Aspergillus sydowii* BPOI. *Front Environ Sci Eng* 14. https://doi.org/10.1007/s11783-020-1292-3

Bankole, P.O., Taghoghor Omoni, V., Mulla, S.I., Adebajo, S.O., Adekunle, A.A., 2022. Co-biomass degradation of fluoranthene by marine-derived fungi; *Aspergillus aculeatus* and *Mucor irregularis*: Comprehensive process optimization, enzyme induction and metabolic analyses. *Arabian Journal of Chemistry* 15, 104036. https://doi.org/10.1016/J.ARABJC.2022.104036

Batista-garcía, A., Vinoth, V., Ariste, A., Tovar-herrera, O.E., Savary, O., Peidro-guzm, H., Jackson, S.A., Dobson, A.D.W., Gonz, D., Folch-mallol, J.L., Leduc, R., Rayo, S., Cabana, H., 2017. Simple screening protocol for identification of potential mycoremediation tools for the elimination of polycyclic aromatic hydrocarbons and phenols from hyperalkalophile industrial effluents 198. https://doi.org/10.1016/j.jenvman.2017.05.010

ben Ameur, W., Hanen, G., ben Hassine, S., Safouen, G., el Megdiche, Y., Mhadhbi, T., Annabi, A., Touil, S., Driss, M.R., 2021. Bioaccumulation of polycyclic aromatic hydrocarbons in Solea solea from Bizerte and Ghar El Melh Lagoons (Tunisia) and human health risk assessment. *Journal of Environmental Science and Health*, Part A 56, 1030–1040.

Calderón-Garcidueñas, L., Ayala, A., 2022. Air pollution, ultrafine particles, and your brain: are combustion nanoparticle emissions and engineered nanoparticles causing preventable fatal neurodegenerative diseases and common neuropsychiatric outcomes? *Environ Sci Technol* 56, 6847–6856.

Cao, H., Wang, C., Liu, H., Jia, W., Sun, H., 2020. Enzyme activities during benzo[a]pyrene degradation by the fungus *Lasiodiplodia theobromae* isolated from a polluted soil. *Scientific Reports* 2020 10:1 10, 1–11. https://doi.org/10.1038/s41598-020-57692-6

Ceci, A., Pinzari, F., Russo, F., Persiani, A.M., Gadd, G.M., 2018. Roles of saprotrophic fungi in biodegradation or transformation of organic and inorganic pollutants in co-contaminated sites. *Applied Microbiology and Biotechnology* 2018 103:1 103, 53–68. https://doi.org/10.1007/S00253-018-9451-1

Chatterjee, S., Kuang, Y., Splivallo, R., Chatterjee, P., Karlovsky, P., 2016. Interactions among filamentous fungi *Aspergillus niger , Fusarium verticillioides* and *Clonostachys rosea* : fungal biomass , diversity of secreted metabolites and fumonisin production. *BMC Microbiol* 1–13. https://doi.org/10.1186/s12866-016-0698-3

Chattopadhyay, Pinaki, Chattopadhyay, Pallavi, Palit, D., 2020. Innovative approach to sustainable development and biodiversity conservation, in: *Environmental and Sustainable Development through Forestry and Other Resources*. Apple Academic Press, pp. 267–304.

Cherr, G.N., Fairbairn, E., Whitehead, A., 2017. Impacts of petroleum-derived pollutants on fish development. *Annu. Rev. Anim. Biosci* 5, 185–203.

Chowdhury, A., Roy, A., Mandal, M., Das, S., Agrawal, G.K., Rakwal, R., Sarkar, A., 2023. Dynamics of biological contaminants along with microbial community during vermicomposting. *Fate of Biological Contaminants During Recycling of Organic Wastes* 101–122. https://doi.org/10.1016/B978-0-323-95998-8.00016-9

Cong, Y., Wang, Y., Zhang, M., Jin, F., Mu, J., Li, Z., Wang, J., 2021. Lethal, behavioral, growth and developmental toxicities of alkyl-PAHs and non-alkyl PAHs to early-life stage of brine shrimp, *Artemia parthenogenetica. Ecotoxicol Environ Saf* 220, 112302.

Daccò, C., Nicola, L., Temporiti, M.E.E., Mannucci, B., Corana, F., Carpani, G., Tosi, S., 2020. Trichoderma: evaluation of its degrading abilities for the bioremediation of hydrocarbon complex mixtures. *Applied Sciences* 2020, Vol. 10, Page 3152 10, 3152. https://doi.org/10.3390/APP10093152

Dach, K., Yaghoobi, B., Schmuck, M.R., Carty, D.R., Morales, K.M., Lein, P.J., 2019. Teratological and behavioral screening of the national toxicology program 91-compound library in zebrafish (*Danio rerio*). *Toxicological Sciences* 167, 77–91.

Datta, R., Kelkar, A., Baraniya, D., Molaei, A., Moulick, A., Meena, R.S., Formanek, P., 2017. Enzymatic degradation of lignin in soil: a review. *Sustainability* (Switzerland) 9. https://doi.org/10.3390/su9071163

Dayarathne, M.C., Jones, E.B.G., Maharachchikumbura, S.S.N., Devadatha, B., Sarma, V. V, Khongphinitbunjong, K., Chomnunti, P., Hyde, K.D., 2020. Morpho-molecular characterization of microfungi associated with marine based habitats. *Mycosphere* 11, 1–188.

Dell' Anno, F., Rastelli, E., Sansone, C., Brunet, C., Ianora, A., Dell' Anno, A., 2021. Microorganisms bacteria, fungi and microalgae for the bioremediation of marine sediments contaminated by petroleum hydrocarbons in the omics era. https://doi.org/10.3390/microorganisms9081695

Dhruv Patel, D., Bhatt, S., 2022. Environmental pollution, toxicity profile, and physico-chemical and biotechnological approaches for treatment of textile wastewater. *Biotechnol Genet Eng Rev* 38, 33–86.

Ding, Q., Gong, X., Jin, M., Yao, X., Zhang, L., Zhao, Z., 2021. The biological pump effects of phytoplankton on the occurrence and benthic bioaccumulation of hydrophobic organic contaminants (HOCs) in a hypereutrophic lake. *Ecotoxicol Environ Saf* 213, 112017.

Dutta, S., Laha, S., 2022. An approach toward the biodegradation of PAHs by microbial consortia. Development in Wastewater Treatment Research and Processes: Microbial Degradation of Xenobiotics through Bacterial and Fungal Approach 383–406. https://doi.org/10.1016/B978-0-323-85839-7.00004-9

Dyer, P.S., Kueck, U., 2017. Sex and the imperfect fungi. *Microbiol Spectr* 5, 3–5.

El-Bondkly, A.M.A., El-Gendy, M.M.A.A., 2022. Bioremoval of some heavy metals from aqueous solutions by two different indigenous fungi *Aspergillus* sp. AHM69 and *Penicillium* sp. AHM96 isolated from petroleum refining wastewater. *Heliyon* 8. https://doi.org/10.1016/J.HELIYON.2022.E09854

Enyiukwu, D.N., Bassey, I.N., Nwaogu, G.A., Asamudo, N.U., Chukwu, L.A., Monday, E.A., MARANZU, J.O., 2021. Pig (*Sus scrofa domesticus*) dung and their associated fungi: Potential candidates for bio-remediation and nutrients improvement of crude oil contaminated soils. *Biodiversitas* 22.

Espinosa-Ortiz, E.J., Rene, E.R., Gerlach, R., 2022. Potential use of fungal-bacterial co-cultures for the removal of organic pollutants. *Crit Rev Biotechnol* 42, 361–383.

Ferreira-Silva, V., de Gusmão, N.B., Gibertoni, T.B., da Silva, L.A. de O., 2022. *Trametes lactinea* and *T. villosa* collected in Brazil are able to discolor indigo carmine. *Acta Bot Brasilica* 36. https://doi.org/10.1590/0102-33062021ABB0356

Finlay, R.D., Thorn, R.G., 2019. The fungi in soil. Modern soil microbiology 65–90.

Fu, W., Xu, M., Sun, K., Hu, L., Cao, W., Dai, C., Jia, Y., 2018. Biodegradation of phenanthrene by endophytic fungus *Phomopsis liquidambari in vitro* and *in vivo*. *Chemosphere* 203, 160–169. https://doi.org/10.1016/J.CHEMOSPHERE.2018.03.164

Gaur, N., Narasimhulu, K., PydiSetty, Y., 2018. Recent advances in the bio-remediation of persistent organic pollutants and its effect on environment. *J Clean Prod* 198, 1602–1631.

Gaurav, G.K., Mehmood, T., Kumar, M., Cheng, L., Sathishkumar, K., Kumar, A., Yadav, D., 2021. Review on polycyclic aromatic hydrocarbons (PAHs) migration from wastewater. *J Contam Hydrol* 236, 103715.

González-Abradelo, D., Pérez-Llano, Y., Peidro-Guzmán, H., del Rayo Sánchez-Carbente, M., Folch-Mallol, J.L., Aranda, E., Vaidyanathan, V.K., Cabana, H., Gunde-Cimerman, N., Batista-García, R.A., 2019. First demonstration that ascomycetous halophilic fungi

(*Aspergillus sydowii* and *Aspergillus destruens*) are useful in xenobiotic mycoremediation under high salinity conditions. *Bioresour Technol* 279, 287–296.

Govarthanan, M., Fuzisawa, S., 2017. RSC Advances Biodegradation of aliphatic and aromatic hydrocarbons using the filamentous fungus *Penicillium* sp . CHY-2 and characterization of its. RSC Adv 7, 20716–20723. https://doi.org/10.1039/C6RA28687A

Greco, G., Di Piazza, S., Cecchi, G., Cutroneo, L., Capello, M., Zotti, M., 2019. Mycoremediation of oily slime containing a polycyclic aromatic hydrocarbon mixture. *Waste Biomass Valorization* 10, 3821–3831. https://doi.org/10.1007/S12649-019-00802-X/FIGURES/5

Guo, H., Zhang, Z., Wang, H., Ma, H., Hu, F., Zhang, W., Liu, Y., Huang, Y., Zeng, Y., Li, C., 2021. Oxidative stress and inflammatory effects in human lung epithelial A549 cells induced by phenanthrene, fluorene, and their binary mixture. *Environ Toxicol* 36, 95–104.

Hadibarata, T., Khudhair, A.B., Kristanti, R.A., Kamyab, H., 2017. Biodegradation of pyrene by Candida sp. S1 under high salinity conditions. *Bioprocess Biosyst Eng* 40, 1411–1418. https://doi.org/10.1007/S00449-017-1798-7/FIGURES/6

Hadibarata, T., Kristanti, R.A., Bilal, M., Al-Mohaimeed, A.M., Chen, T.W., Lam, M.K., 2022. Microbial degradation and transformation of benzo[a]pyrene by using a white-rot fungus *Pleurotus eryngii* F032. *Chemosphere* 307, 136014. https://doi.org/10.1016/J.CHEMOSPHERE.2022.136014

Hamzah, N., Kamil, N., Singhal, N., Padhye, L., Swift, S., 2018. Comparison of phenanthrene removal by *Aspergillus niger* ATC 16404 (filamentous fungi) and *Pseudomonas putida* KT2442 (bacteria) in enriched nutrient-liquid medium, in: IOP Conference Series: *Earth and Environmental Science.* IOP Publishing, p. 012047.

Hesham, A.E.-L., Mohamed, E.A., Mawad, A.M.M., Elfarash, A., Abd El-Fattah, B.S., El-Rawy, M.A., 2017. Molecular characterization of degrades a mixture of low and high molecular weight polycyclic aromatic hydrocarbons. *Open Biotechnol J* 11, 27–35. https://doi.org/10.2174/1874070701711010027

Hoang, S.A., Sarkar, B., Seshadri, B., Lamb, D., Wijesekara, H., Vithanage, M., Liyanage, C., Kolivabandara, P.A., Rinklebe, J., Lam, S.S., 2021. Mitigation of petroleum-hydrocarbon-contaminated hazardous soils using organic amendments: A review. *J Hazard Mater* 416, 125702.

Kadri, T., Rouissi, T., Kaur Brar, S., Cledon, M., Sarma, S., Verma, M., 2017. Biodegradation of polycyclic aromatic hydrocarbons (PAHs) by fungal enzymes: a review. *Journal of Environmental Sciences* 51, 52–74. https://doi.org/10.1016/J.JES.2016.08.023

Kałduńska, K., Kozakiewicz, A., Wujak, M., Wojtczak, A., 2021. Biological inspirations: iron complexes mimicking the Catechol dioxygenases. *Materials* 2021, Vol. 14, Page 3250 14, 3250. https://doi.org/10.3390/MA14123250

Kamil, D., 2020. Genera of rust fungi in India-taxonomy and preservation. pathophenotyping and genome guided characterization of rust fungi infecting wheat and other cereals-a Training manual 29, NAHEP-CAAST, Indian Agricultural Research Institute.

Karaman, M., Novakovic, M., Matavuly, M., 2012. Fundamental fungal strategies in restoration of natural environment. Fungi: *Types, environmental impact and role in disease*. New York: Nova Science Publishers Inc.

Kaushal, D., Bamotra, S., Yadav, S., Chatterjee, S., Tandon, A., 2021. Particulate bound polycyclic aromatic hydrocarbons over Dhauladhar region of the north-western Himalayas. *Chemosphere* 263, 128298.

Kim, Y.-C., Lee, S.-R., Jeon, H.-J., Kim, K., Kim, M.-J., Choi, S.-D., Lee, S.-E., 2020. Acute toxicities of fluorene, fluorene-1-carboxylic acid, and fluorene-9-carboxylic acid on zebrafish embryos (*Danio rerio*): Molecular mechanisms of developmental toxicities of fluorene-1-carboxylic acid. *Chemosphere* 260, 127622.

Kumar, M., Bolan, N.S., Hoang, S.A., Sawarkar, A.D., Jasemizad, T., Gao, B., Keerthanan, S., Padhye, L.P., Singh, L., Kumar, S., 2021. Remediation of soils and sediments polluted with polycyclic aromatic hydrocarbons: To immobilize, mobilize, or degrade? *J Hazard Mater* 420, 126534.

Kuppusamy, S., Maddela, N.R., Megharaj, M., Venkateswarlu, K., 2020. Impact of total petroleum hydrocarbons on human health, in: *Total Petroleum Hydrocarbons*. Springer, pp. 139–165.

Lahkar, J., Deka, H., 2017. Isolation of polycyclic aromatic hydrocarbons (PAHs) degrading fungal candidate from oil-contaminated soil and degradation potentiality study on anthracene. *Polycycl Aromat Compd* 37, 141–147. https://doi.org/10.1080/10406638.2016.1220957

Li, P., Karunanidhi, D., Subramani, T., Srinivasamoorthy, K., 2021. Sources and consequences of groundwater contamination. *Arch Environ Contam Toxicol* 80, 1–10. https://doi.org/10.1007/S00244-020-00805-Z/FIGURES/2

Li, X., Lin, X., Li, P., Liu, W., Wang, L., Ma, F., Chukwuka, K.S., 2009. Biodegradation of the low concentration of polycyclic aromatic hydrocarbons in soil by microbial consortium during incubation. *J Hazard Mater* 172, 601–605.

Li, X., Peng, D., Zhang, Y., Ju, D., Guan, C., 2020. Klebsiella sp. PD3, a phenanthrene (PHE)-degrading strain with plant growth promoting properties enhances the PHE degradation and stress tolerance in rice plants. *Ecotoxicol Environ Saf* 201, 110804.

Liu, Y., Hua, X., 2014. Degradation of acenaphthylene and anthracene by chemically modified laccase from *Trametes versicolor*. *RSC Adv*. 4, 31120–31122. https://doi.org/10.1039/C4RA02807D

López-Mondéjar, R., Brabcová, V., Štursová, M., Davidová, A., Jansa, J., Cajthaml, T., Baldrian, P., 2018. Decomposer food web in a deciduous forest shows high share of generalist microorganisms and importance of microbial biomass recycling. ISME J 12, 1768–1778.

Lüthje, S., Martinez-Cortes, T., 2018. Membrane-bound Class III Peroxidases: unexpected enzymes with exciting functions. *International Journal of Molecular Sciences* 2018, Vol. 19, Page 2876 19, 2876. https://doi.org/10.3390/IJMS19102876

M. De Wet, M.M., G. Brink, H., 2021. Fungi in the bioremediation of toxic effluents. Fungi Bio-prospects in Sustainable Agriculture, Environment and Nano-technology: Volume 2: *Extremophilic Fungi and Myco-mediated Environmental Management* 407–431. https://doi.org/10.1016/B978-0-12-821925-6.00018-6

Ma, Y., Ankit, Tiwari, J., Bauddh, K., 2022. Plant-mycorrhizal fungi interactions in phytoremediation of geogenic contaminated soils. *Front Microbiol* 13, 843415. https://doi.org/10.3389/FMICB.2022.843415/BIBTEX

Magan, N., Fragoeiro, S., Bastos, C., 2010. Environmental factors and bioremediation of xenobiotics using white rot fungi. *Mycobiology* 38, 238. https://doi.org/10.4489/MYCO.2010.38.4.238

Maiti, A., Das, S., Bhattacharyya, N., 2012. Bioremediation of high molecular weight polycyclic aromatic hydrocarbons by *Bacillus thuringiensis* strain NA2. *Journal of Science* 1, 72-75.

Mandal, S.K., Das, N., 2018. Biodegradation of perylene and benzo [ghi] perylene (5-6 rings) using yeast consortium : Kinetic study, enzyme analysis and degradation pathway. *J Environ Biol* 39, 5–15. https://doi.org/10.22438/jeb/39/1/MRN-540

Mandal, S.K., Ojha, N., Das, N., 2018. Optimization of process parameters for the yeast mediated degradation of benzo[a]pyrene in presence of ZnO nanoparticles and produced biosurfactant using 3-level Box-Behnken design. *Ecol Eng* 120, 497–503. https://doi.org/10.1016/j.ecoleng.2018.07.006

Mao, J., Guan, W., 2016. Fungal degradation of polycyclic aromatic hydrocarbons (PAHs) by *Scopulariopsis brevicaulis* and its application in bioremediation of PAH-contaminated soil. *Acta Agric Scand B Soil Plant Sci* 66, 399–405. https://doi.org/10.1080/09064710.2015.1137629

Meer, B.B., Dishan, E.E., Ikima, D., Ateh, G.O., 2020. Ecological implications of environmental contaminants on biodiversity and ecosystem services: The Nigerian experience. *Basic Research Journal of Soil and Environmental Science* 2(1), 001-009.

Mo, F., Wang, M., Li, H., Li, Y., Li, Z., Deng, N., Chai, R., Wang, H., 2021. Biological effects of silver ions to Trifolium pratense L. revealed by analysis of biochemical indexes, morphological alteration and genetic damage possibility with special reference to hormesis. *Environ Exp Bot* 186, 104458.

Moazzen, M., Shariatifar, N., Arabameri, M., Hosseini, H., Ahmadloo, M., 2022. Measurement of polycyclic aromatic hydrocarbons in baby food samples in Tehran, Iran with magnetic-solid-phase-extraction and gas-chromatography/mass-spectrometry method: A Health Risk Assessment. *Front Nutr* 17(9), 833158.

Money, N.P., 2016. Fungal Diversity. The Fungi: Third Edition 1–36. https://doi.org/10.1016/B978-0-12-382034-1.00001-3

Muthukumaran, M., 2022. Advances in bioremediation of nonaqueous phase liquid pollution in soil and water. *Biological Approaches to Controlling Pollutants* 191–231. https://doi.org/10.1016/B978-0-12-824316-9.00006-9

Myazin, V.A., Korneykova, M. V., Chaporgina, A.A., Fokina, N. V., Vasilyeva, G.K., 2021. The effectiveness of biostimulation, bioaugmentation and sorption-biological treatment of soil contaminated with petroleum products in the Russian subarctic. *Microorganisms* 2021, Vol. 9, Page 1722 9, 1722. https://doi.org/10.3390/MICROORGANISMS9081722

Naranjo-Ortiz, M.A., Gabaldón, T., 2019. Fungal evolution: diversity, taxonomy and phylogeny of the Fungi. *Biological Reviews* 94, 2101–2137.

Naylor, D., Sadler, N., Bhattacharjee, A., Graham, E.B., Anderton, C.R., McClure, R., Lipton, M., Hofmockel, K.S., Jansson, J.K., 2020. Soil microbiomes under climate change and implications for carbon cycling. *Annu Rev Environ Resour* 45, 29–59.

Nevalainen, H., Kautto, L., Te'o, J., 2014. Methods for isolation and cultivation of filamentous fungi, in: *Environmental Microbiology*. Springer, pp. 3–16.

Nieuwenhuis, B.P.S., James, T.Y., 2016. The frequency of sex in fungi. Philosophical Transactions of the Royal Society B: *Biological Sciences* 371, 20150540.

Nougadère, A., Sirot, V., Cravedi, J.-P., Vasseur, P., Feidt, C., Fussell, R.J., Hu, R., Leblanc, J.-C., Jean, J., Rivière, G., 2020. Dietary exposure to pesticide residues and associated health risks in infants and young children–results of the French infant total diet study. *Environ Int* 137, 105529.

Nuñez Otaño, N.B., Bianchinotti, M.V., Saparrat, M.C.N., 2021. Palaeomycology: a modern mycological view of fungal palynomorphs. *Geological Society*, London, Special Publications 511, 91–120.

Oberoi, A.S., Jia, Y., Zhang, H., Khanal, S.K., Lu, H., 2019. Insights into the fate and removal of antibiotics in engineered biological treatment systems: a critical review. *Environ Sci Technol* 53, 7234–7264. https://doi.org/10.1021/ACS.EST.9B01131/SUPPL_FILE/ES9B01131_SI_001.PDF

Obire, O., Aleruchi, O., Wemedo, S., 2020. Fungi in biodegradation of polycyclic aromatic hydrocarbons in oilfield wastewater. *Acta Sci. Microbiol* 3, 220–224.

Olasehinde, T.A., Olaniran, A.O., 2022. Neurotoxicity of polycyclic aromatic hydrocarbons: a systematic mapping and review of neuropathological mechanisms. Toxics 10, 417.

Oleszczuk, P., Baran, S., 2003. Degradation of individual polycyclic aromatic hydrocarbons (PAHs) in soil polluted with aircraft fuel. *Pol J Environ Stud* 12.

Ostrem Loss, E.M., Yu, J.H., 2018. Bioremediation and microbial metabolism of benzo(a)pyrene. *Mol Microbiol* 109, 433–444. https://doi.org/10.1111/mmi.14062

Park, J., An, H., Kim, K.W., 2020. Visualization of fungal hyphae in the trichomes of sawtooth oak leaves. *Eur J Plant Pathol* 156, 1119–1133.

Peidro-Guzmán, H., Pérez-Llano, Y., González-Abradelo, D., Fernández-López, M.G., Dávila-Ramos, S., Aranda, E., Hernández, D.R.O., García, A.O., Lira-Ruan, V., Pliego, O.R., Santana, M.A., Schnabel, D., Jiménez-Gómez, I., Mouriño-Pérez, R.R., Aréchiga-Carvajal, E.T., del Rayo Sánchez-Carbente, M., Folch-Mallol, J.L., Sánchez-Reyes, A., Vaidyanathan, V.K., Cabana, H., Gunde-Cimerman, N., Batista-García, R.A., 2021. Transcriptomic analysis of polyaromatic hydrocarbon degradation by the halophilic fungus Aspergillus sydowii at hypersaline conditions. *Environ Microbiol* 23, 3435–3459. https://doi.org/10.1111/1462-2920.15166

Pozdnyakova, N., Muratova, A., Bondarenkova, A., Turkovskaya, O., 2023. Degradation of a Model Mixture of PAHs by Bacterial-Fungal Co-Cultures. Frontiers in Bioscience – Elite 15, 26. https://doi.org/10.31083/J.FBE1504026/F627B4BEFEF9DFF890E247088FBD1A01.PDF

Rani, M., Yadav, J., Chaudhary, S., Shanker, U., 2021. An updated review on synthetic approaches of green nanomaterials and their application for removal of water pollutants: Current challenges, assessment and future perspectives. *J Environ Chem Eng* 9, 106763.

Rathore, D., Dubey, R., Dwivedi, A., 2021. Advances in mycoremediation of emerging potential toxic effluents, in: *Fungi Bio-Prospects in Sustainable Agriculture, Environment and Nano-Technology*. Elsevier, pp. 301–329.

Reddy, K.R., Dastgheibi, S., Cameselle, C., 2020. Removal kinetics of heavy metals and nutrients from stormwater by different filter materials. *Water Air Soil Pollut* 231. https://doi.org/10.1007/S11270-020-04906-2

Revitt, D.M., Balogh, T., Jones, H., 2014. Soil mobility of surface applied polyaromatic hydrocarbons in response to simulated rainfall. *Environmental Science and Pollution Research* 21, 4209–4219.

Riley, R., Salamov, A.A., Brown, W., Nagy, L.G., Floudas, D., Held, B.W., Levasseur, A., Lombard, V., Morin, E., Lindquist, E.A., Sun, H., Labutti, K.M., Jabbour, D., Luo, H., Baker, S.E., Antonio, G., Walton, J.D., Blanchette, R.A., Martin, F., Cullen, D., Hibbett, D.S., Riley, R., Salamov, A.A., Brown, D.W., Nagy, L.G., Floudas, D., Held, B.W., 2014. Correction for Riley et al., Extensive sampling of basidiomycete genomes demonstrates inadequacy of the white-rot/brown-rot paradigm for wood decay fungi. *Proceedings of the National Academy of Sciences* 111, 14959–14959. https://doi.org/10.1073/pnas.1418116111

Rohlman, D., Donatuto, J., Heidt, M., Barton, M., Campbell, L., Anderson, K.A., Kile, M.L., 2019. A case study describing a community-engaged approach for evaluating polycyclic aromatic hydrocarbon exposure in a native American community. *Int J Environ Res Public Health* 16, 327.

Sachaniya, B.K., Gosai, H.B., Panseriya, H.Z., Dave, B.P., 2020. Bioengineering for multiple PAHs degradation for contaminated sediments: Response surface methodology (RSM) and artificial neural network (ANN). *Chemometrics and Intelligent Laboratory Systems* 202. https://doi.org/10.1016/j.chemolab.2020.104033

Sakshi, Haritash, A.K., 2020. A comprehensive review of metabolic and genomic aspects of PAH-degradation. *Arch Microbiol* 202, 2033–2058. https://doi.org/10.1007/s00203-020-01929-5

Sampaio, G.R., Guizellini, G.M., da Silva, S.A., de Almeida, A.P., Pinaffi-Langley, A.C.C., Rogero, M.M., de Camargo, A.C., Torres, E.A.F.S., 2021. Polycyclic aromatic hydrocarbons in foods: biological effects, legislation, occurrence, analytical methods, and strategies to reduce their formation. *International Journal of Molecular Sciences* 2021, Vol. 22, Page 6010 22, 6010. https://doi.org/10.3390/IJMS22116010

Schut, H.A.J., 2020. Biotransformation of Occupational Carcinogens, in: *Chemical Exposure and Toxic Responses*. CRC Press, pp. 221–236.

Senanayake, I.C., Rathnayaka, A.R., Marasinghe, D.S., Calabon, M.S., Gentekaki, E., Lee, H.B., Hurdeal, V.G., Pem, D., Dissanayake, L.S., Wijesinghe, S.N., 2020. Morphological approaches in studying fungi: collection, examination, isolation, sporulation and preservation. *Mycosphere* 11, 2678–2754.

Shankhwar, A.K., Paliwal, R., 2021. Fungi in bioremediation of soil: Mycoremediation of PAHs compounds. Fungi Bio-prospects in Sustainable Agriculture, Environment and Nano-technology: Volume 2: *Extremophilic Fungi and Myco-mediated Environmental Management* 157–170. https://doi.org/10.1016/B978-0-12-821925-6.00008-3

Shariatifar, N., Sharifiarab, G., Kargarghomsheh, P., Moazzen, M., Arabameri, M., Seddighi, M., Tooryan, F., Pirhadi, M., 2022. Polycyclic aromatic hydrocarbons (PAHs) in potato and related products in Tehran: a health risk assessment study. *Int J Environ Anal Chem* 1–14.

Sharma, J., Goutam, J., Dhuriya, Y.K., Sharma, D., 2021. Bioremediation of Industrial pollutants, in: *Microbial Rejuvenation of Polluted Environment*. Springer, pp. 1–31.

Sharma, P., 2022. Microbial communication during bioremediation of polyaromatic hydrocarbons. *Systems Microbiology and Biomanufacturing* 2, 430–444. https://doi.org/10.1007/S43393-021-00072-6/FIGURES/5

Sharma, P., Bano, A., Singh, S.P., Sharma, S., Xia, C., Nadda, A.K., Lam, S.S., Tong, Y.W., 2022. Engineered microbes as effective tools for the remediation of polyaromatic aromatic hydrocarbons and heavy metals. *Chemosphere* 306, 135538. https://doi.org/10.1016/J.CHEMOSPHERE.2022.135538

Shen, M., Xing, J., Ji, Q., Li, Z., Wang, Y., Zhao, H., Wang, Q., Wang, T., Yu, L., Zhang, X., 2018. Declining pulmonary function in populations with long-term exposure to polycyclic aromatic hydrocarbons-enriched PM2. 5. *Environ Sci Technol* 52, 6610–6616.

Shi, Z., Wen, M., Zhang, J., Tang, Z., Wang, C., 2020. Effect of phenanthrene on the biological characteristics of earthworm casts and their relationships with digestive and anti-oxidative systems. *Ecotoxicol Environ Saf* 193, 110359.

Shourie, A., Vijayalakshmi, U., 2022. Fungal diversity and its role in mycoremediation. https://doi.org/10.1080/01490451.2022.2032883 39, 426–444.

Shrestha, P., Joshi, B., Joshi, J., Malla, R., Sreerama, L., 2016. Isolation and physicochemical characterization of Laccase from *Ganoderma lucidum*-CDBT1 isolated from its native habitat in Nepal. *Biomed Res Int* 2016. https://doi.org/10.1155/2016/3238909

Simarro, R., González, N., Bautista, L.F., Molina, M.C., 2013. Biodegradation of high-molecular-weight polycyclic aromatic hydrocarbons by a wood-degrading consortium at low temperatures. *FEMS Microbiol Ecol* 83, 438–449. https://doi.org/10.1111/1574-6941.12006

Singh, P.K., Singh, R.P., Singh, P., Singh, R.L., 2019. Food hazards: Physical, chemical, and biological, in: *Food Safety and Human Health*. Elsevier, pp. 15–65.

Soal, N.C., Coetzee, M.P.A., van der Nest, M.A., Hammerbacher, A., Wingfield, B.D., 2022. Phenolic degradation by catechol dioxygenases is associated with pathogenic fungi with a

necrotrophic lifestyle in the Ceratocystidaceae. G3 *Genes|Genomes|Genetics* 12. https://doi.org/10.1093/G3JOURNAL/JKAC008

Soni, V., Singh, P., Shree, V., Goel, V., 2018. Effects of VOCs on human health, in: Air Pollution and Control. Springer, pp. 119–142.

Sousa, G., Teixeira, J., Delerue-Matos, C., Sarmento, B., Morais, S., Wang, X., Rodrigues, F., Oliveira, M., 2022. Exposure to PAHs during firefighting activities: a review on skin levels, In vitro/in vivo bioavailability, and health risks. *International Journal of Environmental Research and Public Health* 2022, Vol. 19, Page 12677 19, 12677. https://doi.org/10.3390/IJERPH191912677

St. Leger, R.J., Wang, J.B., 2020. Metarhizium: jack of all trades, master of many. *Open Biol* 10, 200307.

Stoyanova, K., Gerginova, M., Dincheva, I., Peneva, N., Alexieva, Z., 2022. Biodegradation of naphthalene and anthracene by *Aspergillus glaucus* strain isolated from Antarctic soil. *Processes 2*022, Vol. 10, Page 873 10, 873. https://doi.org/10.3390/PR10050873

Szatyłowicz, E., Hawrylik, E., 2022. Assessment of migration of PAHs contained in soot of solid fuel combustion into the aquatic environment. *Water* (Basel) 14, 3079.

Taghizadeh, S.F., Azizi, M., Rezaee, R., Giesy, J.P., Karimi, G., 2021. Polycyclic aromatic hydrocarbons, pesticides, and metals in olive: analysis and probabilistic risk assessment. *Environmental Science and Pollution Research* 28, 39723–39741.

Teerapatsakul, C., Pothiratana, C., Chitradon, L., Thachepan, S., 2016. Biodegradation of polycyclic aromatic hydrocarbons by a thermotolerant white rot fungus *Trametes polyzona* RYNF13. *Journal of General and Applied Microbiology* 62, 303–312. https://doi.org/10.2323/jgam.2016.06.001

Torres-Farradá, G., Manzano-León, A.M., Rineau, F., Ramos Leal, M., Thijs, S., Jambon, I., Put, J., Czech, J., Guerra Rivera, G., Carleer, R., 2019. Biodegradation of polycyclic aromatic hydrocarbons by native *Ganoderma* sp. strains: identification of metabolites and proposed degradation pathways. *Appl Microbiol Biotechnol* 103, 7203–7215.

Turaki Usman, A., Abugu, H.O., Okoye, C.O.B., 2021. Environmental impact and human health risk assessment of polycyclic aromatic hydrocarbons (PAHs) in raw milk from free-ranging cattles in northwest Nigeria. *J Environ Health Sci Eng* 19, 1523–1534.

Undugoda, L.J.S., Dharmasiri, R.B.N., Udayanga, D., Nugara, N.N.R.N., 2022. Screening of phyllosphere fungi inhabiting in urbanized areas for phylloremediation capabilities of polyaromatic hydrocarbon pollutants. In *Mycoremediation Protocols*. New York, N.Y; Springer 55–70. https://doi.org/10.1007/978-1-0716-2006-9_6

Vasconcelos, M.R.S., Vieira, G.A.L., Otero, I.V.R., Bonugli-Santos, R.C., Rodrigues, M.V.N., Rehder, V.L.G., Ferro, M., Boaventura, S., Bacci, M., Sette, L.D., 2019. Pyrene degradation by marine-derived ascomycete: process optimization, toxicity, and metabolic analyses. *Environmental Science and Pollution Research* 26, 12412–12424. https://doi.org/10.1007/S11356-019-04518-2

Veignie, E., Rafin, C., Woisel, P., Cazier, F., 2004. Preliminary evidence of the role of hydrogen peroxide in the degradation of benzo[a]pyrene by a non-white rot fungus *Fusarium solani*. *Environmental Pollution* 129, 1–4. https://doi.org/10.1016/J.ENVPOL.2003.11.007

Velmurugan, N., Lee, H.M., Cha, H.J., Lee, Y.S., 2017. Proteomic analysis of the marine-derived fungus *Paecilomyces* sp. Strain SF-8 in response to polycyclic aromatic hydrocarbons. Botanica Marina 60, 381–392. https://doi.org/10.1515/BOT-2016-0101/DOWNLOADASSET/SUPPL/BOT-2016-0101_SUPPL.DOCX

Vipotnik, Z., Michelin, M., Tavares, T., 2021. Ligninolytic enzymes production during polycyclic aromatic hydrocarbons degradation: effect of soil pH, soil amendments and fungal co-cultivation. *Biodegradation* 32, 193–215. https://doi.org/10.1007/S10532-021-09933-2/METRICS

Vipotnik, Z., Michelin, M., Tavares, T., 2019. Degradation of selected PAHs by laccase-mediator system in soil. *Proceedings of the World Congress on New Technologies*. Avestia Publishing 0, 11159. https://doi.org/10.11159/icepr19.133

Wang, C., Wang, F., Wang, T., Bian, Y., Yang, X., Jiang, X., 2010. PAHs biodegradation potential of indigenous consortia from agricultural soil and contaminated soil in two-liquid-phase bioreactor (TLPB). *Journal of Hazardous Materials* 176, 41–47. https://doi.org/10.1016/j.jhazmat.2009.10.123

Wang, Jia, Shen, X., Wang, Jian, Yang, Y., Yuan, Q., Yan, Y., 2018. Exploring the promiscuity of phenol hydroxylase from *Pseudomonas stutzeri* OX1 for the biosynthesis of phenolic compounds. *ACS Synth Biol* 7, 1238–1243. https://doi.org/10.1021/ACSSYNBIO.8B00067/ASSET/IMAGES/MEDIUM/SB-2018-00067S_0005.GIF

Waszak, D.Q., Da Cunha, A.C.B., Agarrallua, M.R.A., Goebel, C.S., Sampaio, C.H., 2015. Bioremediation of a benzo[a]pyrene-contaminated soil using a microbial consortium with *Pseudomonas aeruginosa*, *Candida albicans*, *Aspergillus flavus,* and *Fusarium* sp. *Water Air Soil Pollut* 226. https://doi.org/10.1007/s11270-015-2582-4

Wijayawardene, N.N., Hyde, K.D., Dai, D.Q., 2021. Outline of Ascomycota. *Encyclopedia of Mycology* 246–254. https://doi.org/10.1016/B978-0-12-819990-9.00064-0

Wong, W.S.D., 2009. Structure and action of ligninolytic enzymes. *Appl Biochem Biotechnol* 157, 174–209.

Wu, X., Cao, X., Lintelmann, J., Peters, Annette, Koenig, W., Zimmermann, R., Schneider, A., Wolf, K., Peters, A, Schwettmann, L., 2022. Assessment of the association of exposure to polycyclic aromatic hydrocarbons, oxidative stress, and inflammation: *A cross-sectional study in Augsburg*, Germany. *Int J Hyg Environ Health* 244, 113993.

Wu, Y.R., Luo, Z.H., Kwok-Kei Chow, R., Vrijmoed, L.L.P., 2010. Purification and characterization of an extracellular laccase from the anthracene-degrading fungus *Fusarium solani* MAS2. *Bioresour Technol* 101, 9772–9777. https://doi.org/10.1016/j.biortech.2010.07.091

Wulandari, R., Lotrakul, P., Punnapayak, H., Amirta, R., Kim, S.W., Prasongsuk, S., 2021. Toxicity evaluation and biodegradation of phenanthrene by laccase from *Trametes polyzona* PBURU 12. 3 *Biotech* 2021 11:1 11, 1–11. https://doi.org/10.1007/S13205-020-02556-Z

Yakop, F., Taha, H., Shivanand, P., 2019. Isolation of fungi from various habitats and their possible bioremediation. *Curr Sci* 116, 733.

Yang, Y., Shen, D., Long, Y., Xie, Z., Zheng, H., 2017. Intrinsic Peroxidase-like activity of Ficin. *Sci Rep* 7, 43141. https://doi.org/10.1038/srep43141

Yao, L., Teng, Y., Luo, Yongming, Christie, P., Ma, W., Liu, F., Wu, Y., Luo, Yang, Li, Z., 2015. Biodegradation of polycyclic aromatic hydrocarbons (PAHs) by *Trichoderma reesei* FS10-C and effect of bioaugmentation on an aged PAH-contaminated soil. *Bioremediat J* 19, 9–17.

Zafra, G., Absalón, Á.E., Anducho-Reyes, M.Á., Fernandez, F.J., Cortés-Espinosa, D. V., 2017. Construction of PAH-degrading mixed microbial consortia by induced selection in soil. *Chemosphere* 172, 120–126. https://doi.org/10.1016/j.chemosphere.2016.12.038

Zafra, G., Absalón, Á.E., Cuevas, M.D.C., Cortés-Espinosa, D. V., 2014a. Isolation and selection of a highly tolerant microbial consortium with potential for PAH biodegradation from heavy crude oil-contaminated soils. *Water Air Soil Pollut* 225. https://doi.org/10.1007/s11270-013-1826-4

Zafra, G., Moreno-montaño, A., Absalón, Á.E., Cortés-espinosa, D. V, 2015. Degradation of polycyclic aromatic hydrocarbons in soil by a tolerant strain of *Trichoderma asperellum*. *Environ Sci Pollut Res* 22, 1034–1042. https://doi.org/10.1007/s11356-014-3357-y

Zafra, G., Taylor, T.D., Absalón, A.E., Cortés-Espinosa, D. V, 2016. Comparative metagenomic analysis of PAH degradation in soil by a mixed microbial consortium. *J Hazard Mater* 318, 702–710. https://doi.org/10.1016/j.jhazmat.2016.07.060

Zeb, A., Li, S., Wu, J., Lian, J., Liu, W., Sun, Y., 2020. Insights into the mechanisms underlying the remediation potential of earthworms in contaminated soil: A critical review of research progress and prospects. *Science of the Total Environment* 740, 140145.

Zhang, H., Yuan, X., Xiong, T., Wang, H., Jiang, L., 2020. Bioremediation of co-contaminated soil with heavy metals and pesticides: Influence factors, mechanisms and evaluation methods. *Chemical Engineering Journal* 398, 125657.

Zhang, Yiju, Chen, X., Zhang, Yu, 2021. Analytical chemistry, formation, mitigation, and risk assessment of polycyclic aromatic hydrocarbons: From food processing to in vivo metabolic transformation. *Compr Rev Food Sci Food Saf* 20, 1422–1456.

CHAPTER THREE

Metabolic Biodegradation Pathway of Fluoranthene by Indigenous *Trichoderma lixii* and *Talaromyces pinophilus* spp

This chapter has been published in current format in the journal: *Catalysts, 13: 791. https://doi.org/10.3390/catal13050791.*

The published paper is presented in the following pages.

catalysts

MDPI

Article

Metabolic Biodegradation Pathway of Fluoranthene by Indigenous *Trichoderma lixii* and *Talaromyces pinophilus* spp.

Samson O. Egbewale [1], Ajit Kumar [1], Mduduzi P. Mokoena [1,2] and Ademola O. Olaniran [1,*]

[1] Discipline of Microbiology, Westville Campus, University of KwaZulu-Natal, Durban 4001, South Africa
[2] Department of Pathology, School of Medicine, University of Limpopo, Private Bag X1106, Sovenga 0727, South Africa
* Correspondence: olanirana@ukzn.ac.za; Tel.: +27-31-260-7400 or +27-31-260-7401

Abstract: Two indigenous ascomycetes fungi, *Trichoderma lixii* strain FLU1 (*Tl*FLU1) and *Talaromyces pinophilus* strain FLU12 (*Tp*FLU12), were isolated from benzo(b)fluoranthene-enriched activated sludge and tested for bio-catalytically degrade fluoranthene as a sole carbon source. *Tl*FLU1 and *Tp*FLU12 degraded 98 and 99% of 400 mg/L of fluoranthene after 16 and 12 d incubation period, respectively. Degradation correlated with the upregulation of expression of ligninolytic enzymes. The GC-MS and FTIR analysis of the degradation products suggest that the degradation is initiated at the C1-C2 position of the compound ring via oxygenation and ring cleavage to form 9-oxo-9H-fluorene-1-carboxylic acid before undergoing ring cleavage to yield fluorenone, which then proceeds through the ß-Ketoadipate pathway via benzene-1,2,3-tricarboxylic acid. The degradation rate is better fitted in the first-order and zero-order kinetic model for *Tl*FLU1 and *Tp*FLU12, respectively. The metabolites from the *Tl*FLU1 degradation media are shown to be toxic in *Vibryo parahaemolyticus* after 6 h of exposure with effective concentration (EC_{50}) and toxicity unit (TU) values of 14.25 mg/L and 7.018%, respectively, while also being observed as non-toxic from *Tp*FLU12 degradation media with an EC_{50} and TU values of 197.1 mg/L and 0.507%, respectively. Results from this study show efficient metabolism of fluoranthene into an innocuous state by *Tl*FLU1 and *Tp*FLU12.

Keywords: fluoranthene metabolism; biodegradation; ß-ketoadipate pathway; *Trichoderma lixii*; *Talaromyces pinophilus*

Citation: Egbewale, S.O.; Kumar, A.; Mokoena, M.P.; Olaniran, A.O. Metabolic Biodegradation Pathway of Fluoranthene by Indigenous *Trichoderma lixii* and *Talaromyces pinophilus* spp. *Catalysts* **2023**, *13*, 791. https://doi.org/10.3390/catal13050791

Academic Editors: Rosa María Oliart-Ros and María Guadalupe Sánchez-Otero

Received: 27 February 2023
Revised: 6 April 2023
Accepted: 20 April 2023
Published: 23 April 2023

1. Introduction

Among the ubiquitous group of organic xenobiotics found in the various matrices of the ecosystem, polycyclic aromatic hydrocarbons (PAHs) have become a major environmental priority owing to the carcinogenicity, size-dependent genotoxicity of graphene nanoplatelets in human stem cells, and toxicity of graphene and graphene oxide nanowalls against bacteria and mutagenic effects [1], which are characterized by low aqueous solubility and high lipophilicity to biological functions [2]. Due to the increase in bioaccumulation, biomagnification, and persistent toxicity of this pollutant, the United State Environmental Protection Agency (USEPA) and the United Nations Environmental Program (UNEP) created a list of 16 priority PAH compounds that needed to be eradicated from the environment [3,4]. Sources of PAHs include the incomplete combustion of fossil fuel, ship traffic, oil spilling/leakages from corroded tanks at petrol stations, urban runoff, and industrial activities [5,6]. Some PAHs exhibit carbocatalytic activity as they can act as catalysts to break down hazardous aromatic molecules due to their unique electronic structure and reactivity [7]. PAHs have multiple fused aromatic rings with pi-electrons that make them highly reactive and able to act as electron donors or acceptors when exposed to hazardous aromatic molecules, they undergo redox reactions, breaking them into less toxic compounds [8].

Fluoranthene is a model compound for a PAH degradation study due to its relative abundance in the environment, resistance to degradation, and the fact that it can accumulate

in the soil, water, and air [9]. In plants, it causes some serious biochemical and physiological changes, such as photosynthetic pigments alteration, metabolic activity reduction, and cell membranes disruption leading to defoliation, chlorosis, necrosis, and oxidative stress defense compromise [10,11]. Acute and chronic toxicity of fluoranthene with varied orders of magnitude has been well documented among a diverse group of freshwater and saltwater organisms [12,13]. Additionally, its acute toxicity in animals such as rats includes dysfunction processes, including ataxia, decreased grip strengths, increased landing foot splay, loss of aerial righting, increased urination and defecation, and decreased responses to sensory stimuli in both sexes with server neurological deficits [14]. Its long exposure in humans through pathways, such as inhalation, dermal touch, and ingestion, has been linked to an increased risk of lung cancer, as well as cardiovascular disease (CVD), including atherosclerosis, thrombosis, hypertension, and myocardial infarction (MI) [15]. Apart from its carcinogenicity, mutagenicity, and teratogenicity, preclinical studies have shown a direct link between PAH exposure, oxidative stress, CVD illness, mortality development, and endocrine disruption [16,17].

Although PAHs can naturally disintegrate from the environment via chemical oxidation, photolysis, volatilization, and adsorption, the chemical stabilities of PAHs make these methods inefficient for their total removal coupled with many toxic derivatives which are more toxic than their parent compounds [18]. In addition, techniques such as physical, chemical, and biological techniques have been established, optimized, and utilized in the amelioration of PAH contaminated sites, but significant problems, such as technological complexity, high cost, and a general lack of acceptance are the drawbacks encountered with the physical and chemical treatment techniques [19]. Biological treatment techniques (Biodegradation) using biocatalysts have recently attracted a great deal of interest in the PAHs contaminated site clean-up owing to its safe clean-up means, least disruptive nature, complete degradation, and cost-effective method compared with the conventional physicochemical method, which often leaves behind toxic derivatives which are more toxic than the parent compounds [20]. The role of microbes in PAH degradation has been documented, but degradation rates in some microbes (bacteria) are often not proportional to the contaminant released into an environment and, thus, leading to the accumulation of PAHs in the contaminated sites that can remain for decades [5].

Fungi have been appraised as one of the pre-dominant biodegrading agents found in the environment, which are free-living and ubiquitous [21,22]. They employ their metabolic versatility and resilience to utilize PAHs as a carbon and energy source, and thereby mineralize them to simpler compounds, carbon dioxide, and water, or transformed them into other non-toxic molecules under harsh environmental conditions, such as low moisture and high concentrations of PAHs [23,24]. However, fungi belonging to the Ascomycota family, such as *Aspergillus* sp., *Aspergillus terricola*, *Trichoderma reesei*, *Aspergillus ochraceus*, *Cunninghamella elegans*, and *Cunninghamella echinulata*, indigenous to contaminated sites have been reported to have efficiently degraded PAH compounds, such as Anthracene, Benzo (k) fluoranthene, Benzo(a)anthracene, and Fluoranthene [25–27]. In addition, ligninolytic fungi, including *Nematoloma frowardii*, *Coriolopsis byrsina*, *Pleurotus eryngii*, and *Ganoderma lucidum*, have been well documented for their effective degradation of PAHs [28–30]. Although the biodegradation pathways of two- and three-ring PAHs by fungi are well documented while information regarding the routes and reactions by which the oxidization of higher molecular weight especially four-ring PAHs (fluoranthene) is still limited. Based on the available literature and based on metabolites identified over the last 10 years during fluoranthene degradation, only two biodegradation pathways routes have been reported in fungi belonging to the mushroom-forming fungi (basidiomycetes). The first route is initiated by deoxygenation at C-7 and C-8 position via extra and intra-diol ring cleavage to form acenaphthylene-type metabolites before entering into the ß-ketoadipate pathway via benzene-1,2,3-tricarboxylic acid while the second route involves deoxygenation at C-2 and C-3 position via ortho-cleavage to form a product known as 9-fluorenone-1-carboxylic acid, which is further degraded to yield benzene-1,2,3-tricarboxylic acid and phthalic acid [31].

Thus, in the present study, two indigenous fungal isolates, *Trichoderma lixii* strain FLU1 and *Talaromyces pinophilus* strain FLU12, were investigated for their ability to biocatalytically degrade fluoranthene. The biodegradation kinetics and metabolic pathways were also established via profiling of metabolites produced and enzymes involved in the degradation process. Furthermore, empirical data on the acute toxicity of fluoranthene and its transient metabolic products were elucidated.

2. Results

2.1. Fungal Cultural Morphological Characteristics and Molecular Analyses

The fungal cultural morphological characteristics and the sequence analysis of the ITS rDNA gene were used to identify the strains. Isolate one, grown on a PDA plate, exhibited concentric green conidial production rings. The center of the plate had denser conidiation, while an irregular yellow zone devoid of conidia surrounded the inoculum. Green conidia were distributed throughout the bit granular plate, with white pustules on the green mat. White mycelia without conidial formation were also present. A single green and yellowish concentric ring with a cluster of yellow conidia was observed around the point of inoculation. Light green and yellowish conidia were present throughout the plate, with more conidia towards the margins and the inoculum, except for the white mycelia covering the Petri dish. A single cottony concentric ring with dark green conidiation was found around the inoculum (Figure S1A). Additionally, its microscopic morphology reveals that it has septate hyphae, its conidiophores and conidia are green to yellow green in colour and are produced in chains that measure around 2.5 × 1.5 µm, ellipsoidal to oblong in shape, and typically measure 3 × 2 µm (Figure S1B). ITS gene sequence (submitted as NCBI accession number: MK208694) analysis of the isolate showed that it has 100% genetic similarity with *Trichoderma lixii* and is named as *Trichoderma lixii* strain FLU1 (*Tl*FLU1). Isolate two, grown on PDA plate, forms concentric rings with whitish yellow conidial production, and the conidia production is denser in the center than towards the margins. An irregular white pustule zone without conidia is also present around the inoculum. The density of conidia production is higher towards the center than the margins, and some white pustules are present (Figure S2A). Additionally, its microscopic morphology reveals that the mycelium consists of long, smooth branching hyphae that are septate, and around 2 µm in diameter, it has unbranched conidiophores around 4 µm in diameter with a spherical to oval shape. It has smooth-walled with a greenish grey colour. It has spherical vesicles containing phialides at the tip. These phialides look like flask-shaped acerose phialides that produce asexual spores, along with elongated sausage-shaped cells (Figure S2B). ITS rDNA sequence (submitted as NCBI accession number: MK208704) analysis of the isolate showed that it has 100% similarity with *Talaromyces pinophilus* and named as *Talaromyces pinophilus* strain FLU12 (*Tp*FLU12). FLU is abbreviated for fluoranthene for both strains. Additionally, the phylogenetic typing of these fungal strains with other fungal nucleotide sequences obtained from the NCBI database through the neighbor-joining tree method revealed that *Tl*FLU1 and *Hypocrea lixii* with NCBI accession number JF923807 fall within the same clade and shared a 32% evolutionary relationship (Figure S3A) while *Tp*FLU12 and *Talaromyces pinophilus* with NCBI accession number MN006617 fall within the same clade and shared a 70% evolutionary relationship (Figure S3B).

2.2. Degradation Efficiency, Biomass Production, Protein Content and Change in pH Condition

As shown in Figure 1A, degradation of fluoranthene increases with an increased incubation period in the flask inoculated with strains *Tl*FLU1 and *Tp*FLU12. After 10 d incubation period, *Tl*FLU1 degraded 90.9% of the fluoranthene while *Tp*FLU12 could degrade 92.5% after 16 d incubation period. The dry biomass production and protein content of these fungal strains also increased with an increase in the incubation period, except for some slight decrease observed after reaching their maximum production days. The maximum dry biomass production of 736.8 mg/L was observed at 12 d after the incubation period for *Tl*FLU1, while 564.4 mg/L was recorded for *Tp*FLU12 at 16 d after

the incubation period (Figure 1B). The pH of the inoculation media decreases, from pH 5 to 3.87 (*Tl*FLU1) and 3.66 (*Tp*FLU12) with an increased incubation period. The pH of the control (no inoculum) remains unchanged at the end of the incubation period (Figure 1C); however, the total protein content of about 643.4 µg/mL at 16 d and 566.5 µg/mL at 14 d was recorded for *Tl*FLU1 and *Tp*FLU12, respectively (Figure 1D).

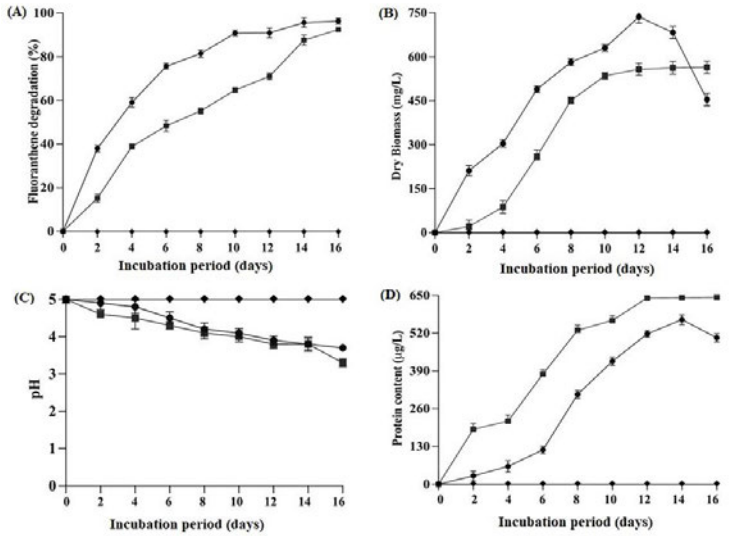

Figure 1. (**A**) Percentage degradation of fluoranthene in BSM by *Tl*FLU1 and *Tp*FLU12, (**B**) dry biomass of individual fungi strains, (**C**) change in pH medium during fluoranthene degradation, and (**D**) total protein content of each fungus. Control (♦), *Tl*FLU1 (•), *Tp*FLU12 (■).

2.3. Degradation Kinetics Study

The kinetic model for the degradation of fluoranthene by *Tl*FLU1 and *Tp*FLU12 is shown in Table 1 and Figure S4. Overall, the degradation kinetics best fitted first-order with the regression coefficient (R^2) values of 0.987 and 0.919 for *Tl*FLU1 and *Tp*FLU12, respectively. *Tp*FLU12 was also shown to degrade the compound following zero-order degradation kinetics with a regression coefficient (R^2) values of 0.968. The first-order degradation kinetics was characterized by a degradation rate constant (k) and half-life (DT_{50}) values of 0.210 d^{-1} and 2.254 d^{-1} for *Tl*FLU1, while 0.15 d^{-1} and 2.588 d^{-1} are for *Tp*FLU12, respectively. In addition, a degradation rate constant (k = 22.280 d^{-1}) and half-life ($D_{1/2}$ = 2.254 d^{-1}) was obtained for *Tp*FLU12 while following the zero-order degradation kinetics.

Table 1. Kinetic parameters for the degradation of fluoranthene by *Tl*FLU1 and *Tp*FLU12.

Kinetic Model	Parameter	Strains	
		***Tl*FLU1**	***Tp*FLU12**
Zero order	Regression Equation	$C_d = -21.24\ d + 290.7$	$C_d = -22.28\ d + 367.7$
$C_d - C_0 = Kd$	K (d^{-1})	21.24	22.28
$D_{1/2} = C_0/2K_0$	$D_{1/2}$	9.412	8.969
	R^2	0.802	0.968
First order	Regression Equation	$lnC_d = -0.2100\ d + 5.924$	$lnC_d = -0.1503\ d + 6.184$
$lnC_d = K_1d + lnC_d$	K (d^{-1})	0.210	0.1503
$D_{1/2} = ln2/K_d$	DT_{50}	2.254	2.588
	R^2	0.987	0.919
Second order	Regression Equation	$1/C_d = 0.0040\ d - 0.008$	$1/C_d = 0.0109\ d - 0.03229$
$1/C_t = 1/C_0 + K_2d$	K (d^{-1})	0.0040	0.0109
$D_{1/2} = 1/C_0K_2$	DT_{50}	0.625	0.229
	R^2	0.849	0.749

R^2: Regression coefficient; K: Degradation rate constant; $D_{1/2}$ and DT_{50}: Half-life.

2.4. Fluoranthene Degradation Metabolites with Its Pathway

The different metabolites formed during the degradation of fluoranthene by *Tl*FLU1 and *Tp*FLU12 are presented in Figure 2 and Table S1, respectively. Two metabolites, namely 9-oxo-9H-fluorene-1-carboxylic acid, with a retention time (RT) of 14.2 min at molecular ion (M^+) m/z: 224, and benzene-1,2,3-tricarboxylic acid (RT: 12.3 and m/z: 148), were observed in the *Tl*FLU1 inoculated flasks while three metabolites, namely fluorenone (RT: 23.9, molecular ion (M^+) at m/z 180), was observed in the *Tp*FLU12 inoculated flask at a varying retention times (RT), such as 18.4 min, 12.3 min, and 7.9 min, respectively, for 2,3-dihydro-1*H*-inden-1-one with molecular ion (M^+) at m/z 104, benzene-1,2,3-tricarboxylic acid with molecular ion (M^+) at m/z 148, and benzoic acid with molecular ion (M^+) at m/z 105. However, the parent compound (control: fluoranthene) was detected at 28.4 min. The theoretical arrangement of these degradation products pathways indicates that parent compound fluoranthene degradation is initiated at the C1–C2 position via oxygenation and ring cleavage to form 9-oxo-9*H*-fluorene-1-carboxylic acid before undergoing ring cleavage to yield fluorenone, which then proceeds through oxygenation and side-chain removal into ß-ketoadipate pathway via benzene-1,2,3-tricarboxylic acid and ring cleavage to form 2,3-dihydro-1H-inden-1-one before undergoing side-chain removal to yield benzoic acid and CO_2 release, respectively, as a dead-end product.

2.5. Analysis of the Transformed Fluoranthene Functional Groups

The FTIR spectra of the changes in the functional group of fluoranthene metabolites are presented in Table 2 and Figure S5. The parent compound (control, fluoranthene) showed an intense peak at 3202 cm^{-1} due to O-H stretching of the alcohol rings, an adsorption peak at 1610 cm^{-1} is an attribution of –C=C aromatic ring stretch, while an adsorption peak at 622 cm^{-1} with attribution of –C-H bending of the substituted benzene ring. However, in the *Tl*FLU1 degradation product spectra, a significant shift in the control sample functional groups was observed with four intense adsorption peaks. An observed adsorption peak at 3284 cm^{-1}, with the attribution of broad O–H stretching of the alcohol rings, was followed by an adsorption peak at 1650 cm^{-1}, which has an attribution of –C=O stretching of the carbonyl/carboxylic. Additionally, a peak at 1385 cm^{-1} was linkable to the bending of aliphatic CH and CH_2 groups was observed to be followed by the intense peak at 600 cm^{-1}, which has an attribution of the –C≡C–H: C–H bend in alkynes. In the *Tp*FLU12 inoculated flask sample, apart from the shift in absorption peaks of control samples which was an attribute of O–H stretching of the alcohol rings observed, seven more adsorption peaks were observed, namely peak at 1730 cm^{-1}, linkable to the presence of C=O rings of the quinone compounds, followed by high adsorption intensity peak at 1421 cm^{-1} with an attribute of aromatic ring vibrations, and plane bending of C–O–H. Additionally, the observed adsorption intensity at 1385 cm^{-1} is linkable to the bending of aliphatic CH and CH_2 groups, followed by a high peak intensity at 1280 cm^{-1}, which corresponds with the C-O functional group due to carboxylic acid stretch. Furthermore, the observed high-intensity peak at 1030 cm^{-1} corresponds with the C-OH and O-CH_3 stretch, while the adsorption intensity at 610 cm^{-1} could be linked with the –C≡C–H: C–H bend in alkynes.

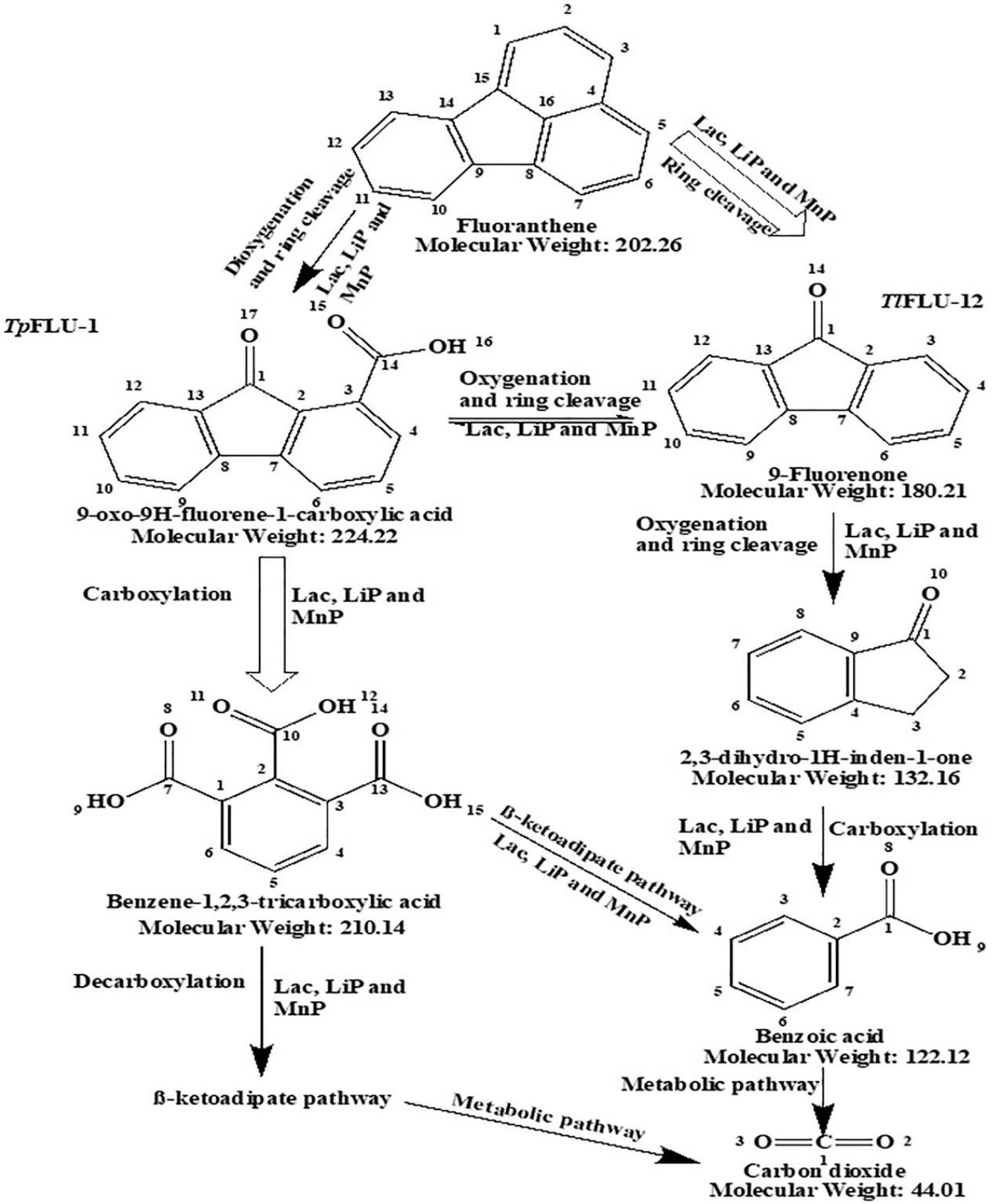

Figure 2. The proposed fluoranthene metabolic pathway by *Tl*FLU1 and *Tp*FLU12. The un-bold arrows denote an unknown transient product which were not detected by GCMS analysis.

Table 2. Assignment of the infrared spectra absorbance bands of fluoranthene degradation metabolites.

Functional Group	Frequency (cm^{-1})			Assignment
	Control	*Tl*FLU1	*Tp*FLU12	
i		3202–3340		O–H stretch of the alcohol rings
ii		1610–1730		C=C and C=O asymmetric vibration stretching of the aromatic, carbonyl and quinone compounds
iii	ND	ND	1421	Plane bending of C–O–H and aromatic ring vibrations
iv	ND	ND	1385	Aliphatic bending of CH and CH_2
v	ND	1030	ND	C–C, C–OH and O–CH_3 stretching
vi		600–610		–C≡C–H: C–H bend in alkynes

ND: Not detected.

2.6. Ligninolytic Activities in the Presence of Fluoranthene

The ligninolytic activities of *Tl*FLU1 and *Tp*FLU12 during fluoranthene degradation are presented in Figure 3. Overall, the production of ligninolytic enzyme activities was dependent on the incubation period. Laccase enzyme showed superior activity in the flask inoculated with *Tp*FLU12 in comparison to *Tl*FLU1. The maximum laccase activity of 8310.4 U/L at 14 d after the incubation period was observed in *Tl*FLU1 inoculated flask, while a maximum laccase activity of 8910.5 U/L was recorded for *Tp*FLU12 at 2 d after the incubation period (Figure 3A). Conversely, Lignin peroxidase activity was observed to be a maximum with 561.2 U/L at 16 d after the incubation period in *Tl*FLU1 inoculated flask while a maximum activity of 431.7 U/L was documented at 4 d after the incubation period in *Tp*FLU12 inoculated flask (Figure 3B). In addition, Manganese peroxidase activity was observed to be maximum with 219.2 U/L at 8 d after the incubation period in the *Tl*FLU1 inoculated flask, while Manganese peroxidase activity of 252.3 U/L was recorded at 12 d after the incubation period (Figure 3C). However, no significant production of laccase, Lignin peroxidase, and Manganese peroxidase was recorded in BSM + *Tl*FLU1 and BSM + *Tp*FLU12 inoculated flask.

2.7. Ecotoxicity Test

The time-course changes in toxicity of fluoranthene degradation products were assessed by survival, EC_{50} and TU (toxicity unit) of *Vibrio parahaemolyticus* after 6 h of exposure time (Figure 4 and Table 3). Toxicity was at its peak at 0 d (parent compound) with 0 Log (CFU/mL) of the marine bacterium. The bacterium survival (Log CFU/mL) on each degradation product of *Tl*FLU1 (Figure 4A) and *Tp*FLU12 (Figure 4B) was dependent on degradation product concentration. Additionally, the bacterium survival was observed to be increasing, with an increase in the degradation product per day for *Tl*FLU1 and *Tp*FLU12. Maximum survival of 7.68 Log (CFU/mL) was observed in the 16 d degradation product of *Tl*FLU1, followed by 14 d product with 6.50 while the least survival of 5.25 Log (CFU/mL) which remains constant on degradation products of 2 to 12 d. However, the 16 d degradation product and the CN (No degradation product/PAHs) with 7.90 Log (CFU/mL), are statistically not significant ($p \leq 0.05$) (Figure 4A). Conversely, the marine bacterium survival was significantly high in every degradation product of *Tp*FLU12 with the maximum survival of 7.85 Log (CFU/mL) at 16 d and least survival of 7.32 Log (CFU/mL). Additionally, the degradation products of 10 d, 12 d, 14 d, 16 d, and the CN (No degradation product/PAHs) with 7.90 Log (CFU/mL) were statistically not significant ($p \leq 0.05$) (Figure 4B). However, the effective concentration (EC_{50}) and toxicity unit (TU) of 14.25 mg/L and 7.018% with toxicity class of harmful was obtained for *Tl*FLU1 degradation products, while that of *Tp*FLU12 was classified as non-toxic with effective concentration (EC_{50}) and toxicity unit (TU) of 197.1 mg/L and 0.507%. It is noteworthy that

significant differences are observed in EC_{50} and TU in the degradation products of *Tl*FLU1 and *Tp*FLU12 (Table 3).

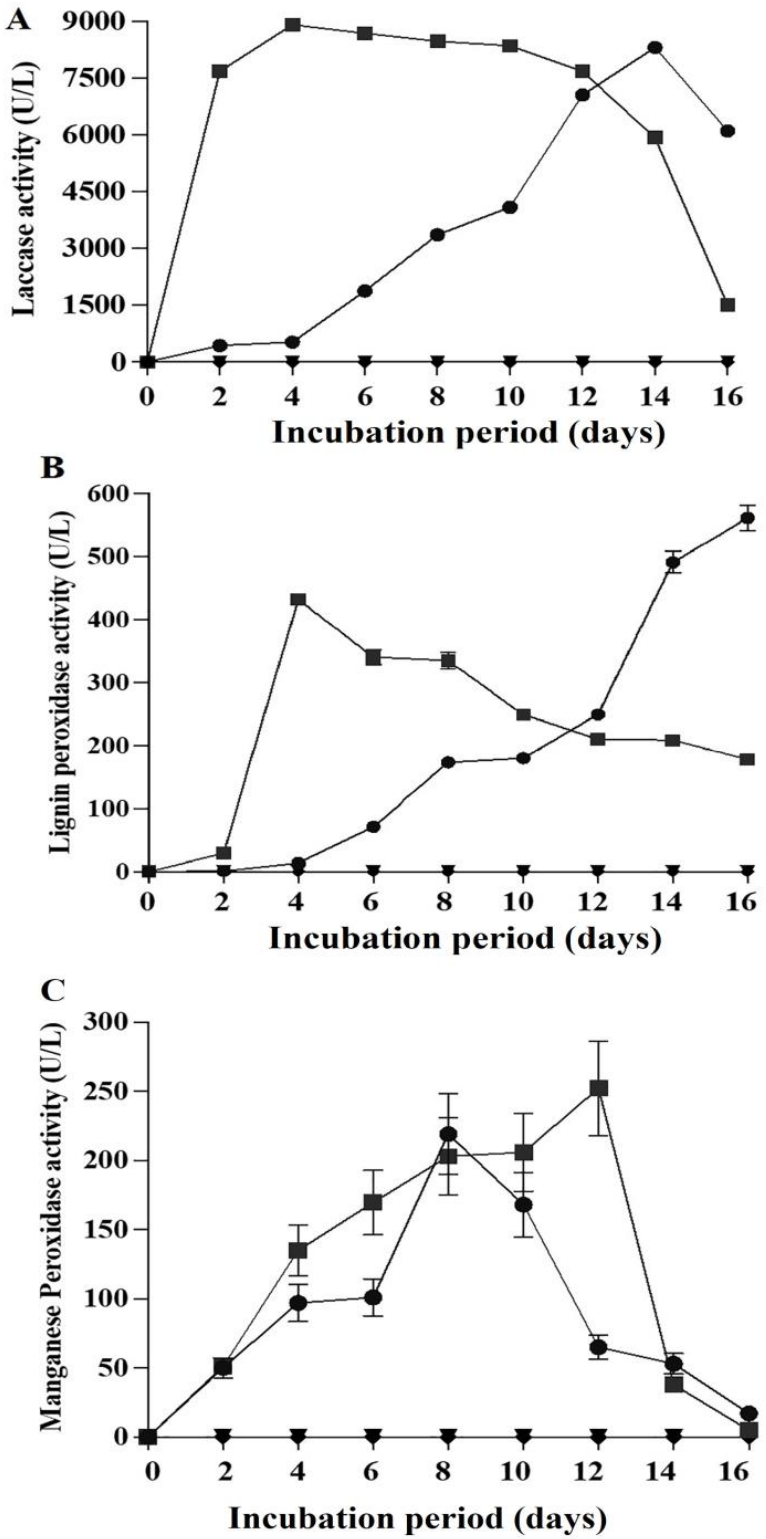

Figure 3. Extracellular ligninolytic enzyme activities response to fluoranthene degradation. (**A**) Laccase activity, (**B**) lignin peroxidase activity, and (**C**) manganese peroxidase activity. Control (♦), Fluoranthene + *Tl*FLU1 (●), Fluoranthene + *Tp*FLU12 (■), BSM + *Tl*FLU1 (▼), BSM + *Tp*FLU12 (▲).

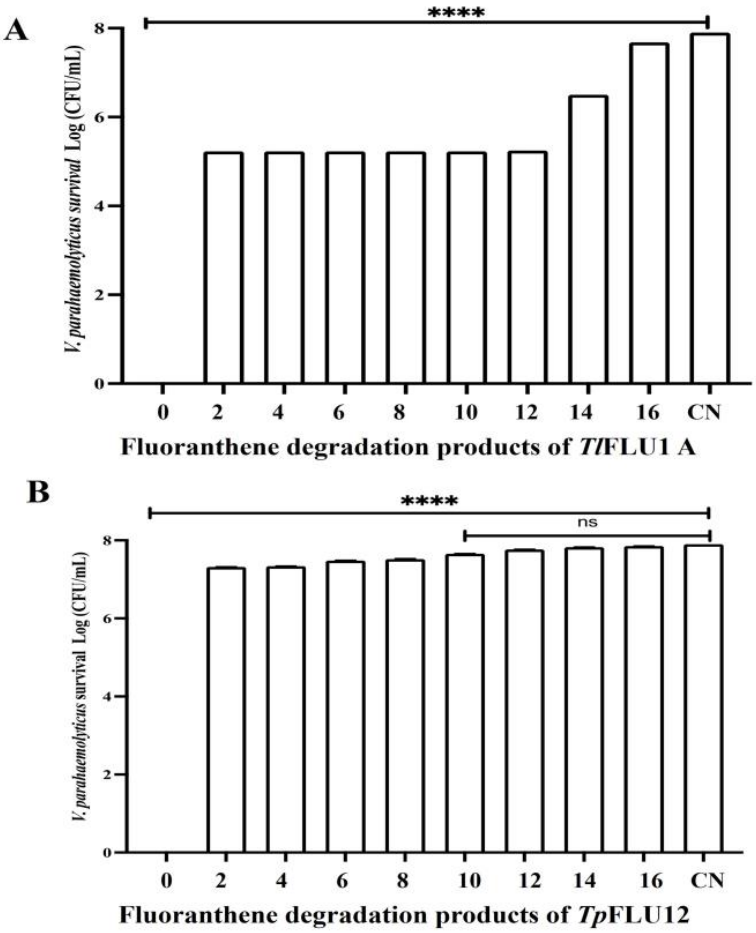

Figure 4. *V. parahaemolyticus* survival after 6 h exposure to fluoranthene degradation products of (**A**) *Tl*FLU1 and (**B**) *Tp*FLU12. CN (Negative Control (no fluoranthene in the growth medium)) and ****: significant difference at $p < 0.001$.

Table 3. Acute toxicity (EC_{50}) of daily fluoranthene biodegradation products of *Tl*FLU1 and *Tp*FLU12.

Acute Toxicity	Strains	
Profile	*Tl*FLU1	*Tp*FLU12
EC_{50} (mg/L)	14.25 ^{b}	197.1 ^{a}
TU (%)	7.018 ^{a}	0.05 ^{b}
Class	Harmful	non-toxic

Key: Very toxic ($EC_{50} < 1$ mg/L); Toxic (1 mg/L < $EC_{50} \leq 10$ mg/L); Harmful (10 mg/L < $EC_{50} \leq 100$ mg/L); Non-toxic (≥100 mg/L) [32]. Values with the same alphabet as superscripts are not statistically different ($p \leq 0.05$).

3. Discussion

The use of high PAHs tolerant fungi indigenous to a heavily PAHs contaminated site should be the preliminary attribute for selecting desirable PAH-degrading fungal species during any biodegradation procedures [33]. Although few studies have shown the ability of two of the most arguably diverse groups of fungi (*Trichoderma* and *Talaromyces*) in the degradation of different classes of hydrocarbons, such as alicyclic, heterocyclics, and some PAH compounds [34,35]. There are no available reports that account for the degradation of fluoranthene by these bio-catalytically fungi either as an individual strain or in a consortium.

In this study, *Trichoderma lixii* strain FLU1 (*Tl*FLU1) and *Talaromyces pinophilus* strain FLU12 (*Tp*FLU12), with a remarkably high degree of physiological and genetic PAHs tolerance were identified. This observation is not surprising because high evolutionary

relationships are common characteristics of fungi with diverse substrate ranges with high tolerance to them [36]. Additionally, fungi from the genus *Trichoderma* and *Talaromyces* have been linked to high PAHs tolerance capability, consistent with their phylogenetic relationship [35,37]. Similarly, the high evolutionary relationships and high PAHs tolerance can be attributed to the extreme metabolic diversity of these fungi [35].

The capability of *Tl*FLU1 and *Tp*FLU12 to effectively metabolize fluoranthene as a sole carbon source could be linked to their extensive substrate affinity for different classes of PAHs when used as a carbon source [38]. The increment in fluoranthene degradation rate by the fungi with an increase in incubation period is comparable to other reports where PAH compounds degradation is proportional to the incubation period [27,39]. Similarly, the ability of the tested fungi to exhibit higher and faster fluoranthene degradation (99%) at 12 d of incubation period compared to earlier reported white-rot fungus (*Pleurotus eryngii*), where 80% of fluoranthene was degraded at 30 d after incubation period under agitated conditions [31]. The efficiency of PAHs degradation can decrease at higher concentrations, possibly due to mass transfer limitations or adsorbent material saturation. Other factors, such as pH, temperature, and the type and concentration of enzymes, can also affect the efficiency of PAH removal. For example, during the biodegradation of anthracene by *Aspergillus sydowii* strain bpo1, high concentration of anthracene, extracellular enzymes activities (laccase, lignin, and manganese peroxidase), pH, and temperature individually have significant impact on the biodegradation efficiency [40]. The significant increase in the dry weight biomass observed is directly correlated with fluoranthene degradation [41]. Furthermore, the pH reduction observed could be explained by the accumulation of certain acidic metabolites formed during PAH metabolic processes [24]. Additionally, the reduction in pH during degradation suggests the production of CO_2 during the aromatic ring decarboxylation [3].

Despite the existence of copious studies on the biodegradation of PAHs by fungi belonging to the family Ascomycota, little is known about fluoranthene persistence through degradation kinetics. It was evident from the study that the high degradation rate constant K (0.150–0.210 d^{-1}) is directly proportional to low half-life time (2.254–2.588 T_{50}), which implies less persistence of fluoranthene due to the fast degradation rate by *Tl*FLU1 and *Tp*FLU12 (Table 1). This result agrees with the previous report [42], where the high degradation constant rate (0.164–0.204 d^{-1}) was, consequently, proportional to low half-life (3.397–4.218 T_{50}) leading to the fast degradation of benzo(ghi)perylene and perylene by yeast consortium YC02 and YC04. Similarly, previous study [40] demonstrated the less persistence of a PAH compound (anthracene) with a low half-life time ($t_{1/2}$) = 3.2 and 5.5 days for concentrations of 400 and 500 mg/L, respectively, which corroborate the result in this study. Additionally, the perceived high biodegradation kinetic constant rates could also be linked to the production of ligninolytic enzymes which non-specifically oxidize fluoranthene through the removal of an electron or a hydrogen atom [43]. In addition, the degradation kinetics model which best fitted first-order kinetics for *Tl*FLU1 and better fitted first-order kinetics for *Tp*FLU12 are not unusual observations but significant in gaining an insight into the rate at which fluoranthene concentration is reduced by half and the most popular model for assessing any biodegradation kinetics [44]. Contrary to the ideal case of first-order kinetics, which is often employed in evaluating degradation kinetics, the ability of *Tp*FLU12 to best fit zero-order kinetics with the highest R^2 = 0.968 is an indication of a linear rate of degradation with a finite persistence half-life of fluoranthene. The most probable explanation for such an observation could be attributed to the PAH compound ring number since the persistence of four four-ring PAHs (fluoranthene and pyrene) in the environment often obey zero-order biodegradation kinetics, which is a time-dependent process with a degradation rate constant directly proportional to PAHs concentration compared to the first-order kinetic model [45].

The result of the GC-MS analysis suggests that the fluoranthene degradation pathway by fungi belonging to the Ascomycota family (*Tl*FLU1 and *Tp*FLU12) is principally initiated at the C1–C2 position of the compound ring via oxygenation and ring cleavage to form

9-oxo-9*H*-fluorene-1-carboxylic acid before undergoing ring cleavage to yield fluorenone, which then proceeds through oxygenation and side-chain removal into ß-Ketoadipate via benzene-1,2,3-tricarboxylic acid (Table 2 and Figure 2). This same metabolic pathway has been reported previously [46], as one of the routes by which a white rot-fungi, *Armillaria* sp. F022 degrades fluoranthene into major products, such as 9-fluorenone-1-carboxylic acid, benzene-1,2,3-tricarboxylic acid, and phthalic acid. Similarly, this same route has been documented as a major route through which fluoranthene metabolism proceeds via dioxygenation and meta cleavage at C-1 and C-2 positions to form 9-fluorenone-1-carboxylic acid which later undergoes decarboxylation to form 9-fluorenone in *Pasteurella* sp. IFA and *Mycobacterium* sp. PYR-1 [12]. Additionally, another study [47] attributed the conversion of 9-fluorenone-1-carboxylic acid to 9-fluorenone as a result of decarboxylation. Unfortunately, phthalic acid was not picked up during the GC-MS analysis of both *Tl*FLU1 and *Tp*FLU12 inoculated flask which could be attributed to the instability of this product or probably it was used by the fungi for its metabolism. Additionally, the oxidation of 9-fluorenone aromatic ring to 2,3-dihydro-1*H*-Inden-1-ol, which was later converted to benzoic acid via ring cleavage, could be linked to the production of laccase, lignin peroxidase, and manganese peroxidase. This observation aligned with another findings [48], where laccase and peroxidase enzymes mediated the oxidation of fluorene to benzoic acid by a marine-derived fungus, *Mucor irregularis* strain bpo1. In addition, the formation of 2,3-dihydro-1*H*-Inden-1-ol was a result of carboxyl ring oxidation in 9-fluorenone, which then yielded in the loss of aldehyde substituent before undergoing decarboxylation of its resulting β-keto acid [49]. It is noteworthy that 9-oxo-9*H*-fluorene-1-carboxylic acid and 9-fluorenone are not stable products due to their absence in chronological order in both the *Tl*FLU1 and *Tp*FLU12 inoculated flasks.

The use of FTIR as a sensitive, high throughput and non-destructive mechanism for monitoring the vibrational frequency changes in functional groups of PAHs during biodegradation pathway mapping has been well documented [28]. The observed spectral absorption peaks at 3202 cm^{-1}–3340 cm^{-1} in both the control sample and fungal inoculated flasks could attribute to the O–H broad stretching of the alcohol rings due to the presence of ethyl-acetate used in during the extraction process [50,51]. The shift in adsorption peak of the control sample at wavelength 1610 cm^{-1} to 1650–1730 cm^{-1} is linkable to the presence of C=O rings of the quinone compounds [52]. Similarly, a previous study opined that a peak at 1650 cm^{-1} is attributable to C=C and C=O asymmetric vibration stretching of the aromatic and carbonyl compound [53]. The high adsorption intensity peak at 1421 cm^{-1} in the *Tp*FLU12 sample, is an attribute of aromatic ring vibrations and plane bending of C–O–H [54]. Additionally, the adsorption intensity at 1385 cm^{-1} in the fungi inoculated flasks could be a result of the bending of aliphatic CH and CH_2 groups [52]. A previous report [55], analogously attributed a close peek at 1380 cm^{-1} to a planar bending of the CH ring. Furthermore, the high peak intensity observed at 1280 cm^{-1} of the *Tp*FLU12 degradation sample corresponds with C–O functional group due to the carboxylic acid stretch [56]. The observed high-intensity peak at 1030 cm^{-1} of the *Tp*FLU12 sample corresponds with the C–OH and O–CH_3 stretch [54]. Likewise, the peak intensity could be linked with the vibration of C–C, C–OH, C–H ring and side group [55]. The adsorption intensity of the fungi inoculated flasks at 600–610 cm^{-1} could be linked with –C≡C–H: C–H bend in alkynes [28].

The high production of extracellular enzymes (Lac, LiP, and MnP) in the presence of fluoranthene suggests that they are PAH inducible and played a crucial role in the oxidation of the aromatic rings [57,58]. Similarly, ligninolytic enzymes have been implicated in the mechanistic and oxidative activities involving oxygenation, ring cleavage, carboxylation, and decarboxylation in the metabolic pathway of fluorene to various intermediate products [48]. In addition, the high laccase observed in strain *Tp*FLU12, in comparison to strain *Tl*FLU1, is not an unusual occurrence, since previous studies have shown that these extracellular enzymes are not always produced at the same rate during the oxidation of fluoranthene, anthracene, naphthalene, and phenanthrene [31]. A preliminary study

for a tolerance test (Table S3, Figure S6A–C) using a solid plate method revealed that the fungi could produce only the extracellular enzyme in the presence of PAHs (low molecular weight and high molecular weight). Additionally, in the first 8 days of the degradation assay, intracellular enzymatic activities were not detectable.

Knowledge about the mechanism and metabolic pathways for fluoranthene degradation by fungi belonging to the Ascomycota cannot be completed without assessing the toxicity of degradation intermediate products formed for a proper environmental impact assessment. It was evident that the formation of one or more metabolites could induce acute toxicity, despite the increase in bacterium survival (log CFU/mL) on degradation product after day 0 in comparison to the non-degradation product treated assay (Figure 4). A similar observation was reported previously [59], where biodegradation of bisphenol A by some thermos-tolerant ascomycetes produces metabolites of higher toxicity than the parent compound. Additionally, the low bacterium survival (log CFU/mL) in the degradation product of the *Tl*FLU1 treated assay in comparison to *Tp*FLU12 could be linked to the occurrence of carboxylation on the C1- position of PAHs and its metabolic products which have been established in lowered defensing mechanism and altered the normal biological functions of the test organism [60]. The presence of aromatic structures with *ortho-substituted* carbonyl and hydroxyl groups metabolic product could have accounted for the low bacterium survival (log CFU/mL) [61]. Additionally, the low EC_{50} and high percentage TU recorded for *Tl*FLU1 treated assay further corroborates the observed low bacterium survival (Log CFU/mL) and the general notion that PAHs metabolites could be more toxic than the parent PAHs. A review [62] further attests that PAHs biodegradation often yielded toxic metabolites which covalently bound to the fish cellular macromolecules (proteins, DNA and RNA) which later resulted in cell damage, mutagenesis, teratogenesis, and carcinogenesis. Similarly, a report [63] demonstrated how high molecular weight PAHs with their derivatives, such as NO_x, O_3, and OH radicals, significantly invoke more developmentally toxic and CYP1A expression in five distinct tissues, including vasculature, liver, skin, neuromasts, and yolk of zebrafish. Additionally, PAHs toxicity increases due to an increase in solubility and/or inherent toxicity of metabolites [63]. Conversely, the high EC_{50} and low TU values of the degradation process by *Tp*FLU12 confirm the efficiency of the fungal strain in biodegradation and detoxifying toxic metabolic products into an innocuous state, especially with compounds with the dimer OH auras as the dead-end degradation product [64]. Additionally, high EC_{50} and low TU values further confirmed the use of marine bacterium as an efficient and cheap bioassay protocol in the environmental risk assessment of organo-pollutants, such as fluoranthene and its metabolites, due to their sensitivity to chemical toxicants [65].

4. Materials and Methods

4.1. Chemicals and Media

Fluoranthene, ethyl acetate, acetone, n-hexane, 2,2- azino-bis-3-ethyl-benzthiozoline-6-sulphonic acid (ABTS), 2, 6-dimethoxy phenol (DMP), azure B, $(NH_4)_2SO_4$, K_2HPO_4, $NaH_2PO_4{\cdot}2H_2O$, NaCl, $MgSO_4{\cdot}7H_2O$, nitrilotriacetic acid, $CaCl_2{\cdot}2H_2O$, $MnCl_2{\cdot}2H_2O$, $FeSO_4{\cdot}7H_2O$, $Co(NO_3){\cdot}6H_2O$, $ZnSO_4$, $CuSO_4$, H_3BO_3, Na_2MoO_4, $Al_2(SO_4)_3$ H_2O, potato dextrose agar, and thiosulphate-citrate-bile salts-sucrose (TCBS) agar were procured from Merck (Burlington, MA, USA). All solvents and reagents are of HPLC grade with ≥98% purity.

4.2. Preparation of Standard Solutions

Fluoranthene stock solution was prepared by dissolving 500 mg of fluoranthene in 10 mL acetone, sterilized by membrane filtration (0.22 µm, Millipore, Merck, Burlington, MA, USA) and stored at 4 °C. Basal salt medium (BSM) was prepared, as described previously [41], and contain (in g/L): $(NH_4)_2SO_4$ 2.4; K_2HPO_4 1.55; $NaH_2PO_4{\cdot}2H_2O$ 0.85; NaCl 0.5; $MgSO_4{\cdot}7H_2O$ 0.26 and 1mL of Trace Elements (mg/L): Nitrilotriacetic acid 15; $CaCl_2{\cdot}2H_2O$ 15; $MnCl_2{\cdot}2H_2O$ 6; $FeSO_4{\cdot}7H_2O$ 1; $Co(NO_3){\cdot}6H_2O$ 1; $ZnSO_4$ 1; $CuSO_4$ 0.1;

H_3BO_3 0.1; Na_2MoO_4 0.1; $Al_2(SO_4)_3{\cdot}H_2O$ 0.1. The pH of the medium was adjusted to 5 with 1 N hydrochloric acid (HCl).

4.3. Fungal Strains and Molecular Identification

Two indigenous fungal strains namely, *Trichoderma lixii* strain FLU1(*Tl*FLU1) and *Talaromyces pinophilus* FLU12 (*Tp*FLU12) previously isolated from a benzo (b) fluoranthene enriched wastewater-activated sludge with tolerance to 3, 4, and 5-ring PAH compounds and with ability to use them as sole carbon sources (Unpublished data). *Tl*FLU1 and *Tp*FLU12 cultures were grown separately on potato dextrose agar plates and incubated at 30 °C for 96 h. DNA was extracted from each fungal strain using the ZR Fungal/Bacterial DNA MiniPrep™ kit (Zymo Research) according to the manufacturer's instructions and used in amplifying, sequencing, and analyzing the fungi intergenic ITS1-5.8S-ITS2 region of the ribosomal DNA (rDNA). The ITS region of the fungal strains were amplified from the extracted DNA using the primers, ITS 4 (5′-TCCTCCGCTTATTGATATGC-3′) and ITS 5 (5′-GGAAGTAAAAGTCGTAACAAGG-3′), in a PCR assay. The PCR mixtures consisted of 10 ng/µL DNA, 5 µL of 10 X reaction buffer, 2 µL 25 mM $MgCl_2$, 2.5 µL of each primer (0.5 µM), 0.25 µL of Taq DNA polymerase, 1 µL of 10 mM dNTPs and volume made up to 50 µL with ultrapure water (MilliQ H_2O). A T100 Thermal Cycler (BioRad, Hercules, CA, USA) was used for amplification with the initial denaturation at 95 °C for 2 min followed by 30 cycles of denaturation at 95 °C for 30s, then annealing at 53 °C for 45 s and elongation at 72 °C for 45 s, with a final extension at 75 °C for 10 min. The PCR products were resolved on 1.0% (*w*/*v*) agarose gels (Seakem, Thermo Fisher Scientific, Arendalsvägen, Göteborg, Sweden) and visualized after staining with ethidium bromide (0.5 µg/mL) using the Chemigenius Bio-imaging System (Syngene, Cambridge, UK). Positive amplicons (~600 bp) were excised and sequenced at Inqaba Biotechnogical Industries, Pretoria, South Africa, and the sequences were compared against the GenBank database. Homologs were identified using the BLASTn program at the National Center for Biotechnology Information (NCBI) (https://blast.ncbi.nlm.nih.gov/Blast.cgi (accessed on: 21 April 2023)). A phylogenetic approach was used for alignment. The evolutionary relationship between the fungi nucleotide sequence and other sequences was matched on NCBI database using muscle (multiple sequence comparison by UMPGA) implanted in MEGA 11. Alignments were examined manually, and a phylogenetic tree was constructed with a neighbor-joining likelihood approach and bootstrap resampling of 1000 replicates using MEGA 11 [66].

4.4. Degradation of Fluoranthene

The potential of the fungal strains to utilize fluoranthene (400 mg/L) as the sole carbon and energy source was carried out in a 250 mL Erlenmeyer flask containing 100 mL BSM broth. BSM broth added with fluoranthene was separately inoculated with two mycelium discs of 10 mm diameter from the edge of an active growing 5 days old culture of each fungal strain from potato dextrose agar plate. The flasks were incubated in the dark at 30 °C on a rotary shaker at 180 rpm for 16 days. Sterile BSM broth containing only fluoranthene (400 mg/L) was set up as a negative control sample to monitor the effect of abiotic factors. Samples were periodically drawn at 2 day intervals for the quantification of residual fluoranthene, metabolite formation, ligninolytic enzyme activity determination, and ecotoxicity test. The initial concentration of 400 mg/L was used based on its zero fungal growth inhibition on both selected strains (Table S2). The pH of the culture broth was also monitored periodically using a pH/temperature bench meter fitted with a digital probe 230 VAC (HANNA instruments, Romania).

4.5. Fungal Strains Biomass Estimation

The fungal biomass was estimated as described previously [31]. The periodically collected culture broth (4 mL) was centrifuged at 10,000 rpm for 15 min. The supernatant was collected for residual fluoranthene quantifications while the pellets were removed

and washed thrice with ethyl acetate to recover any absorbed fluoranthene before passing through a pre-dried and pre-weighed Whatman filter paper no. 1. Thereafter, the Whatman filter paper was dried to a constant weight at 80 °C, and the dry weight of the biomass was determined. It is worthwhile to note that washing the pellet with ethyl acetate (1:10 w/v, 5 times) was necessitated so as not to underestimate the residual fluoranthene concentration since fluoranthene is known to be hydrophobic and to limit biosorption of the PAH by the fungi mycelia pellets.

4.6. Extraction, Quantification of Residual Fluoranthene and Kinetics of Degradation

The residual fluoranthene in the culture medium was extracted and quantified using a UV-Vis spectrometer, as described previously [57], with slight modifications. For brevity, the culture broth (supernatant) obtained during the biomass estimation was mixed with ethyl-acetate (1:4 v/v) in a separating funnel. The mixture was then vigorously shaken for 5 min and allowed to stand for 20 min to enhance the separation of aqueous and organic phases using the standard extraction method. The organic phase was collected, dried over 10 g anhydrous Na_2SO_4, and evaporated to dryness at 40 °C under reduced pressure. The dried fractions were then dissolved with the same extraction solvent and diluted 10-fold with ethyl acetate before quantifying the residual fluoranthene in a scanning spectrum mode of Agilent Cary 60 UV-Vis spectrophotometer (Agilent, Santa Clara, CA, USA) from a wavelength of 400 to 200 nm. The absorption spectrum of fluoranthene showed peak maxima at a wavelength of 265 nm using a quartz cuvette with an optical path length of 10 mm. The fluoranthene residual concentration of the medium was determined by using a standard curve derived from known concentrations of fluoranthene (R^2 value of 0.958). Additionally, a recovery study was carried out in a sterile BSM broth (uninoculated with fungi) with an appropriate volume of known fluoranthene concentrations under a static condition before analytical quantification. This set-up was replicated with an average fluoranthene recovery of 97.9 $\pm$ 7.17%. The Kinetic models of the fluoranthene degradation by the fungi were plotted following the methods, as described previously [67].

4.7. Determination of Intermediates Compounds by GC-MS Analysis

The periodically extracted residual fluoranthene fractions were pooled together and dried at 40 °C under reduced pressure. The dried fractions were then re-dissolved to a final volume of 1 mL in ethyl acetate before analyzing the intermediate compounds using GC–MS as follows, one microliter of the extracted fractions was injected into an Elite-5MS capillary GC column with a length of 30.0 m; ID 0.25 mm; film thickness 250 µm, split injection (injector temperature 280 °C, split 1/8 for samples and 1/20 for standard samples); oven temperature programmed from 60 °C (held for 2 min) to 300 °C (15 min) at 10 °C/min. The carrier gas used was helium at a flow rate of 1 mL/min. The ion trap detector and NIST (National Institute of standard technology) and USA library was used for intermediate compound analysis at a full scan at 10–220 m/z [30].

4.8. Fourier-Transform Infrared Spectroscopy (FTIR) Analysis

The structural changes in the functional group of intermediate compounds were monitored with FTIR spectroscopy in a scanning absorbance mode of PerkinElmer spectrum 100 fitted with a universal attenuated total reflectance (ATR) accessory (PerkinElmer, Waltham, MA, USA). Hundred microliters of sample used for the intermediate compound detection were scanned between wavenumber 4000–400 cm^{-1}. All obtained data were corrected for the background spectrum.

4.9. Quantitative Estimation of Ligninolytic Enzymes Activities

4.9.1. Laccase Assay

Laccase activity was carried out by measuring the increase in absorbance during the oxidation of 2,2- Azino-bis-3-ethyl-benzthiozoline-6-sulphonic acid (ABTS) [68]. The reaction mixture contained 100 µL of 50 mM ABTS and 800 µL of 20 mM Na-Acetate buffer

(pH 4.5), and 100 µL of appropriately diluted enzyme extract. The reaction mixture was incubated at 30 °C for 15 min and thereafter stopped by adding 40 µL of 20% trichloroacetic acid. The absorbance was measured at 420 nm using an Agilent Cary 60 UV-Vis spectrophotometer (Agilent, Santa Clara, CA, USA). The enzyme activity was expressed in unit L^{-1} of the culture filtrate. A unit of laccase activity was defined as 1 µmol of ABTS oxidized per min.

4.9.2. Lignin Peroxidase Assay

Lignin peroxidase assay was performed by measuring the reduction in the substrate (Azure B), as described previously [28]. The reaction mixture contained 749.5 µL of 125 mM sodium tartrate buffer (pH 3.0), 83.5 µL of enzyme extract, and 0.16 mM of substrate Azure B. The enzymatic reaction was also catalyzed with pure 83.5 µL of 2 mM Hydrogen peroxide (pH 3.0) before incubating at 30 °C for 15 min. The color change was measured using Agilent Cary 60 UV-Vis spectrophotometer at 651 nm and expressed in unit L^{-1} of the culture filtrate. One unit of the lignin peroxidase activity was defined as 1 µmol of Azure B reduced per min.

4.9.3. Manganese Peroxidase Assay

Manganese peroxidase activity was determined by monitoring the oxidation of 2, 6-DMP at 469 nm [68]. Briefly, the reaction mixture contained 749.5 µL of sodium tartrate buffer (50 mM, pH 4.0), 83.5 µL of enzyme extract and 2 mM of 2, 6-DMP. The enzymatic reaction was also catalyzed with pure 83.5 µL of 0.4 mM hydrogen peroxide (pH 4.0) before incubating at 30 °C for 15 min. The enzyme activities were expressed as unit L^{-1} of the culture filtrate. One unit of the manganese peroxidase activity was defined as 1 µmol of the substrate oxidized per min.

4.10. Ecotoxicity Test

The ecotoxicity test of the culture medium (undergoing degradation) was evaluated at different incubation periods based on bacterial survival using a modified liquid-to-plate micro-counting method [69]. Briefly, 100 µL of diluted standardized overnight culture broth of *Vibrio parahaemolyticus* (ATCC 17802) with an absorbance value of 0.14 at λ_{max} 600 nm (corresponding to a final inoculum of 1.0×10^8 CFU/mL) was exposed to each degradation product in marine broth (9:1 v/v) to a final volume of 1 mL in 15 mL centrifuge tube. To avoid sedimentation, each toxicant was incubated at 30 °C in a 15 mL centrifuge tube and mixed on MRC Lab suspension mixer SM-3600 (MRC laboratory equipment, Essex, UK) at 180 rpm for 6 h. The suspensions from each exposed toxicant at the initial and final exposure time were serially diluted before spread plating 10 µL on 45 mm TCBS agar plates and incubated at 30 °C for 96 h in triplicates. Bacterium survival for each degradation product was calculated by log transformation of the colony-forming unit (CFU/mL) using GraphPad Prism software (v. 7.05). Additionally, a control (CN) and no degradation product/PAHs was also set up to compare the bacterium survival without stress. The toxicity unit (TU) of the 50% effect endpoint of the toxicant was calculated as the reciprocal of EC_{50} multiplied by 100 [70]. It is noteworthy to state that the EC_{50} toxicity classification was interpreted based on Directive 79/831/EEC [32]. Briefly, the metabolites were classified as very toxic ($EC_{50} \leq 1$ mg/L), toxic (1 mg/L $\leq EC_{50} \leq 10$ mg/L), harmful (10 mg/L $\leq EC_{50} \leq 100$ mg/L), and non-toxic ($EC_{50} \geq 100$ mg/L).

4.11. Data Analysis

The experiments were set up in a completely randomized design (CRD). Data obtained were presented graphically as mean values and error bars using GraphPad prism statistical analysis package version 8.4.3 (471) (San Diego, CA, USA). The effective concentration (EC_{50}) and toxicity unit (TU) of transformation product resulting in 50% reduction in active bacterial replicating/forming colonies after 6 h exposure was evaluated using non-linear regression (log (agonist) vs. response model) of colony-forming unit (CFU/mL).

Additionally, the bacterium survival data (log CFU/mL) was subjected to analysis of variance (ANOVA) while its means were ranked with Bonferroni's multiple comparisons test (BMCT) at $p \leq 0.05$.

5. Conclusions

This study reveals that two indigenous fungal strains, *Tl*FLU1 and *Tp*FLU12, can effectively degrade fluoranthene. The fungi can metabolize fluoranthene as a sole source of carbon and energy through the ß-Ketoadipate pathway via benzene-1,2,3-tricarboxylic acid. The ability of these strains to completely metabolize fluoranthene is linked to their production of ligninolytic enzymes (Lac, LiP, and MnP) and their growth. The study also found that the time-course changes in toxicity of degradation products accumulated during the metabolism process by *Tl*FLU1 are toxic to marine bacterium survival and classified as harmful due to the recorded EC_{50} (14.25 mg/L) and toxicity unit (7.000%) while that of *Tp*FLU12 were non-toxic with EC_{50} (197.1 mg/L) and toxicity unit (0.507%), suggesting it as a proficient strain in metabolizing fluoranthene into an innocuous state and the enzymes reported may be used as biocatalysts in the biotechnology industries.

Supplementary Materials: The following supporting information can be downloaded at: https://www.mdpi.com/article/10.3390/catal13050791/s1, Figure S1: morphological characteristics of *Tl*FLU1 grown on a PDA plate; Figure S2: morphological characteristics of *Tp*FLU12 grown on a PDA plate; Figure S3: neighbor-joining phylogenetic tree for *Tl*FLU1 and *Tp*FLU12 with other fungal strains. Figure S4: Fluoranthene degradation kinetic modelling (A) Zero Order, (B) First Order, and (C) Second Order. *Tl*FLU1 (●), *Tp*FLU12 (■), d = days; Figure S5: FTIR spectra of fluoranthene biodegradation metabolites; Figure S6: Preliminary assay for Ligninolytic enzyme production on solid media. Keys: - flouranthene + no-fungus; + flouranthene + fungus; laccase (oxidation of ABTs to Green colour zones); LiP (Oxi-dation of Azure B to Green colour zones); MnP (oxidation of phenol red to form yellow colour zones); Table S1: GC-MS profile of the metabolite formed during fluoranthene degradation; Table S2: The average fungal growth and growth inhibition after 10 days of exposure to varying fluoranthene concentrations; Table S3: Preliminary assay for extracellular enzyme production on solid media.

Author Contributions: Conceptualization, S.O.E. and A.O.O.; methodology, S.O.E. and A.K.; validation, S.O.E., A.K. and A.O.O.; formal analysis, S.O.E. and A.K.; investigation, S.O.E. and A.O.O.; resources, M.P.M. and A.O.O.; data curation, S.O.E. and A.K.; writing—S.O.E.; writing—A.K. and A.O.O.; visualization, S.O.E.; supervision, M.P.M. and A.O.O.; project administration, A.O.O.; funding acquisition, A.O.O. and M.P.M. All authors have read and agreed to the published version of the manuscript.

Funding: National Research Foundation, South Africa (Grant No: 94036 and 92803).

Data Availability Statement: Data are contained within the article or Supplementary Material.

Acknowledgments: Authors thank University of KwaZulu Natal for fellowship to Samson O. Egbewale.

Conflicts of Interest: The authors declare no conflict of interest.

References

1. Masiol, M.; Hofer, A.; Squizzato, S.; Piazza, R.; Rampazzo, G.; Pavoni, B. Carcinogenic and mutagenic risk associated to airborne particle-phase polycyclic aromatic hydrocarbons: A source apportionment. *Atmos. Environ.* **2012**, *60*, 375–382. [CrossRef]
2. Zafra, G.; Cortés-Espinosa, D.V. Biodegradation of polycyclic aromatic hydrocarbons by *Trichoderma species*: A mini review. *Environ. Sci. Pollut. Res.* **2015**, *22*, 19426–19433. [CrossRef] [PubMed]
3. Ping, L.; Zhang, C.; Zhang, C.; Zhu, Y.; He, H.; Wu, M.; Tang, T.; Li, Z.; Zhao, H. Isolation and characterization of pyrene and benzo[a]pyrene-degrading *Klebsiella pneumonia* PL1 and its potential use in bioremediation. *Appl. Microbiol. Biotechnol.* **2014**, *98*, 3819–3828. [CrossRef]
4. Haneef, T.; Ul Mustafa, M.R.; Yusof, K.W.; Isa, M.H.; Bashir, M.J.K.; Ahmad, M.; Zafar, M. Removal of polycyclic aromatic hydrocarbons (PAHs) from produced water by Ferrate (VI) oxidation. *Water* **2020**, *12*, 3132. [CrossRef]
5. Aranda, E.; Godoy, P.; Reina, R.; Badia-Fabregat, M.; Rosell, M.; Marco-Urrea, E.; García-Romera, I. Isolation of Ascomycota fungi with capability to transform PAHs: Insights into the biodegradation mechanisms of *Penicillium oxalicum*. *Int. Biodeterior. Biodegrad.* **2017**, *122*, 141–150. [CrossRef]

6. Moghadam, S.; Ebrahimipour, M.; Abtahi, G.; Ghassempour, B.; Hashtroudi, A.; Seyed, M. Biodegradation of polycyclic aromatic hydrocarbons by a bacterial consortium enriched from mangrove sediments. *J. Environ. Health Sci. Eng.* **2014**, *12*, 114. [CrossRef] [PubMed]
7. Hung, C.-M.; Chen, C.-W.; Huang, C.-P.; Tsai, M.-L.; Dong, C.-D. Metal-free carbocatalysts derived from macroalga biomass (*Ulva lactuca*) for the activation of peroxymonosulfate toward the remediation of polycyclic aromatic hydrocarbons laden marine sediments and its impacts on microbial community. *Environ. Res.* **2022**, *208*, 112782. [CrossRef] [PubMed]
8. Maharaj Kumari, K.; Lakhani, A. PAHs in gas and particulate phases: Measurement and control. In *Environmental Contaminants: Measurement, Modelling and Control*; Gupta, T., Agarwal, A.K., Agarwal, R.A., Labhsetwar, N.K., Eds.; Springer: Singapore, 2018; pp. 43–75. [CrossRef]
9. Kumar, S.; Upadhayay, S.K.; Kumari, B.; Tiwari, S.; Singh, S.N.; Singh, P.K. In vitro degradation of fluoranthene by bacteria isolated from petroleum sludge. *Bioresour. Technol.* **2011**, *102*, 3709–3715. [CrossRef]
10. Bhushan, K.; Chouhan, S.; Tandey, R.; Mandal, V. Central effect of polycyclic aromatic hydrocarbons liberated from thermal power units on the metabolic and oxidative status of *Raphanus sativus*. *JSM Environ. Sci. Ecol.* **2020**, *8*, 1071.
11. Tomar, R.S.; Jajoo, A. PSI becomes more tolerant to fluoranthene through the initiation of cyclic electron flow. *Funct. Plant Biol.* **2017**, *44*, 978–984. [CrossRef]
12. Šepič, E.; Bricelj, M.; Leskovšek, H. Degradation of fluoranthene by *Pasteurella* sp. IFA and *Mycobacterium* sp. PYR-1: Isolation and identification of metabolites. *J. Appl. Microbiol.* **1998**, *85*, 746–754. [CrossRef] [PubMed]
13. Spehar, R.L.; Poucher, S.; Brooke, L.T.; Hansen, D.J.; Champlin, D.; Cox, D.A. Comparative toxicity of fluoranthene to freshwater and saltwater species under fluorescent and ultraviolet light. *Arch. Environ. Contam. Toxicol.* **1999**, *37*, 496–502. [CrossRef]
14. Saunders, C.R.; Shockley, D.C.; Knuckles, M.E. Fluoranthene-induced neurobehavioral toxicity in F-344 rats. *Int. J. Toxicol.* **2003**, *22*, 263–276. [CrossRef]
15. Mallah, M.A.; Changxing, L.; Mallah, M.A.; Noreen, S.; Liu, Y.; Saeed, M.; Xi, H.; Ahmed, B.; Feng, F.; Mirjat, A.A.; et al. Polycyclic aromatic hydrocarbon and its effects on human health: An overeview. *Chemosphere* **2022**, *296*, 133948. [CrossRef] [PubMed]
16. Hao, G.; Liu, F.; Zhang, Q.; Ali Mallah, M.; Ali Mallah, M.; Liu, Y.; Xi, H.; Wang, W.; Feng, F. Relationship between polycyclic aromatic hydrocarbons and cardiovascular diseases: A systematic review. *Front. Public Health* **2021**, *9*, 763706. [CrossRef]
17. Kubincová, P.; Sychrová, E.; Raška, J.; Basu, A.; Yawer, A.; Dydowiczová, A.; Babica, P.; Sovadinová, I. Polycyclic aromatic hydrocarbons and endocrine disruption: Role of testicular gap junctional intercellular communication and connexins. *Toxicol. Sci.* **2019**, *169*, 70–83. [CrossRef]
18. Nur-Aainaa-Syafini, M.R.; Tay, K.S.; Abu Bakar, N.K.; Uche Emenike, C.; Krishnan, S.; Shahul Hamid, F.; Abas, M.R. Degradation of polycyclic aromatic hydrocarbons (pyrene and fluoranthene) by bacterial consortium isolated from contaminated road side soil and soil termite fungal comb. *Environ. Earth Sci.* **2015**, *74*, 5383–5391. [CrossRef]
19. Alegbeleye, O.O.; Opeolu, B.O.; Jackson, V. Bioremediation of polycyclic aromatic hydrocarbon (PAH) compounds: (acenaphthene and fluorene) in water using indigenous bacterial species isolated from the Diep and Plankenburg rivers, Western Cape, South Africa. *Braz. J. Microbiol.* **2017**, *48*, 314–325. [CrossRef]
20. Jain, P.K.; Gupta, V.K.; Gaur, R.K.; Lowry, M.; Jaroli, D.P.; Chauhan, U.K. Bioremediation of petroleum oil contaminated soil and water. *Res. J. Environ. Toxicol.* **2011**, *5*, 1–26. [CrossRef]
21. Ipeaiyeda, A.R.; Nwauzor, G.O.; Akporido, S.O. Biodegradation of polycyclic aromatic hydrocarbons in agricultural soil contaminated with crude oil from Nigeria refinery using *Pleurotus sajor-caju*. *J. Bioremediat. Biodegrad.* **2015**, *6*, 1000301. [CrossRef]
22. Nasrawi, H.A. Biodegradation of crude oil by fungi isolated from Gulf of Mexico. *J. Bioremediat. Biodegrad.* **2012**, *3*, 1000147. [CrossRef]
23. Deshmukh, R.; Khardenavis, A.A.; Purohit, H.J. Diverse metabolic capacities of fungi for bioremediation. *Indian J. Microbiol.* **2016**, *56*, 247–264. [CrossRef] [PubMed]
24. Ye, J.-S.; Yin, H.; Qiang, J.; Peng, H.; Qin, H.-M. Biodegradation of anthracene by *Aspergillus fumigatus*. *J. Hazard. Mater.* **2011**, *185*, 174–181. [CrossRef] [PubMed]
25. Lahkar, J.; Deka, H. Isolation of polycyclic aromatic hydrocarbons (PAHs) degrading fungal candidate from oil-contaminated soil and degradation potentiality study on anthracene. *Polycycl. Aromat. Comp.* **2017**, *37*, 141–147. [CrossRef]
26. Sharma, A.; Singh, S.B.; Sharma, R.; Chaudhary, P.; Pandey, A.K.; Ansari, R.; Vasudevan, V.; Arora, A.; Singh, S.; Saha, S.; et al. Enhanced biodegradation of PAHs by microbial consortium with different amendment and their fate in in-situ condition. *J. Environ. Manag.* **2016**, *181*, 728–736. [CrossRef] [PubMed]
27. Yao, L.; Teng, Y.; Luo, Y.; Christie, P.; Ma, W.; Liu, F.; Wu, Y.; Luo, Y.; Li, Z. Biodegradation of polycyclic aromatic hydrocarbons (PAHs) by *Trichoderma reesei* FS10-C and effect of bioaugmentation on an aged PAH-contaminated soil. *Bioremediat. J.* **2015**, *19*, 9–17. [CrossRef]
28. Agrawal, N.; Shahi, S.K. Degradation of polycyclic aromatic hydrocarbon (pyrene) using novel fungal strain *Coriolopsis byrsina* strain APC5. *Int. Biodeterior. Biodegrad.* **2017**, *122*, 69–81. [CrossRef]
29. Sack, U.; Hofrichter, M.; Fritsche, W. Degradation of polycyclic aromatic hydrocarbons by Manganese peroxidase of *Nematoloma frowardii*. *FEMS Microbiol. Lett.* **1997**, *152*, 227–234. [CrossRef] [PubMed]
30. Teh, Z.C.; Hadibarata, T. Enhanced degradation of pyrene and metabolite identification by *Pleurotus eryngii* F032. *Water Air Soil Pollut.* **2014**, *225*, 1–8. [CrossRef]

31. Hadibarata, T.; Kristanti, R.A.; Hamdzah, M. Biosorption and biotransformation of fluoranthene by the white-rot fungus *Pleurotus eryngii* F032. *Biotechnol. Appl. Biochem.* **2014**, *61*, 126–133. [CrossRef]
32. Lin, Z.; Du, J.; Yin, K.; Wang, L.; Yu, H. Mechanism of concentration addition toxicity: They are different for nonpolar narcotic chemicals, polar narcotic chemicals and reactive chemicals. *Chemosphere* **2004**, *54*, 1691–1701. [CrossRef] [PubMed]
33. Hesham, A.E.-L.; Mohamed, E.A.; Mawad, A.M.M.; Elfarash, A.; Abd El-Fattah, B.S.; El-Rawy, M.A. Molecular characterization of *Fusarium Solani* degrades a mixture of low and high molecular weight polycyclic aromatic hydrocarbons. *Open Biotechnol. J.* **2017**, *11*, 27–35. [CrossRef]
34. Govarthanan, M.; Fuzisawa, S. Biodegradation of aliphatic and aromatic hydrocarbons using the filamentous fungus *Penicillium* sp. CHY-2 and characterization of its manganese peroxidase activity. *RSC Adv.* **2017**, *7*, 20716–20723. [CrossRef]
35. Zafra, G.; Absalon, A.E.; Cuevas, M.D.C.; Cortes-Espinosa, D.V. Isolation and selection of a highly tolerant microbial consortium with potential for PAH biodegradation from heavy crude oil-contaminated soils. *Water Air Soil Pollut.* **2014**, *225*, 1–18. [CrossRef]
36. Asemoloye, M.D.; Ahmad, R.; Jonathan, S.G. Transcriptomic responses of catalase, peroxidase and laccase encoding genes and enzymatic activities of oil spill inhabiting rhizospheric fungal strains. *Environ. Pollut.* **2018**, *235*, 55–64. [CrossRef]
37. Álvarez-Barragán, J.; Cravo-Laureau, C.; Wick, L.Y.; Duran, R. Fungi in PAH-contaminated marine sediments: Cultivable diversity and tolerance capacity towards PAH. *Mar. Pollut. Bull.* **2021**, *164*, 112082. [CrossRef]
38. Reyes-César, A.; Absalón, Á.E.; Fernández, F.J.; González, J.M.; Cortés-Espinosa, D.V. Biodegradation of a mixture of PAHs by non-ligninolytic fungal strains isolated from crude oil-contaminated soil. *World J. Microbiol. Biotechnol.* **2014**, *30*, 999–1009. [CrossRef] [PubMed]
39. Memić, M.; Vrtačnik, M.; Boh, B.; Pohleven, F.; Mahmutović, O. Biodegradation of PAHs by ligninolytic fungi *Hypoxylon Fragiforme* and *Coniophora Puteana*. *Polycycl. Aromat. Compd.* **2017**, *6638*, 1–8. [CrossRef]
40. Bankole, P.O.; Semple, K.T.; Jeon, B.H.; Govindwar, S.P. Enhanced enzymatic removal of anthracene by the mangrove soil-derived fungus, *Aspergillus sydowii* BPOI. *Front. Environ. Sci. Eng.* **2020**, *14*, 113. [CrossRef]
41. Saraswathy, A.; Hallberg, R. Degradation of pyrene by indigenous fungi from a former gasworks site. *FEMS Microbiol. Lett.* **2002**, *210*, 227–232. [CrossRef]
42. Mandal, S.K.; Das, N. Biodegradation of perylene and benzo [ghi] perylene (5-6 rings) using yeast consortium: Kinetic study, enzyme analysis and degradation pathway. *J. Environ. Biol.* **2018**, *39*, 5–15. [CrossRef]
43. Lee, H.; Jang, Y.; Lee, Y.M.; Lee, H.; Kim, G.H.; Kim, J.J. Enhanced removal of PAHs by *Peniophora incarnata* and ascertainment of its novel ligninolytic enzyme genes. *J. Environ. Manag.* **2015**, *164*, 10–18. [CrossRef] [PubMed]
44. Asemoloye, M.D.; Ahmad, R.; Jonathan, S.G. Synergistic action of rhizospheric fungi with *Megathyrsus maximus* root speeds up hydrocarbon degradation kinetics in oil polluted soil. *Chemosphere* **2017**, *187*, 1–10. [CrossRef]
45. Lu, X.Y.; Li, B.; Zhang, T.; Fang, H.H.P. Enhanced anoxic bioremediation of PAHs-contaminated sediment. *Bioresour. Technol.* **2012**, *104*, 51–58. [CrossRef] [PubMed]
46. Hadibarata, T.; Kristanti, R.A. Biotransformation studies on fluoranthene, a four-ring polycylic aromatic hydrocarbon, by white-rot fungus *Armillaria* sp. F022. *Agric. Agric. Sci. Procedia* **2015**, *3*, 45–50. [CrossRef]
47. Jin, J.; Yao, J.; Liu, W.; Zhang, Q.; Liu, J. Fluoranthene degradation and binding mechanism study based on the active-site structure of ring-hydroxylating dioxygenase in *Microbacterium paraoxydans* JPM1. *Environ. Sci. Pollut. Res.* **2017**, *24*, 363–371. [CrossRef]
48. Bankole, P.O.; Semple, K.T.; Jeon, B.H.; Govindwar, S.P. Biodegradation of fluorene by the newly isolated marine-derived fungus, *Mucor irregularis strain* bpo1 using response surface methodology. *Ecotoxicol. Environ. Saf.* **2021**, *208*, 111619. [CrossRef]
49. Casellas, M.; Grifoll, M.; Bayona, J.M.; Solanas, A.M. New metabolites in the degradation of fluorene by *Arthrobacter* sp. strain F101. *Appl. Environ. Microbiol.* **1997**, *63*, 819–826. [CrossRef]
50. Oliveira, R.N.; Mancini, M.C.; de Oliveira, F.C.S.; Passos, T.M.; Quilty, B.; Thiré, R.M.d.S.M.; McGuinness, G.B. FTIR analysis and quantification of phenols and flavonoids of five commercially available plants extracts used in wound healing. *Rev. Mater.* **2016**, *21*, 767–779. [CrossRef]
51. Sharma, M.; Kumar, S.; Pandey, O.P. Study of energy transfer from capping agents to intrinsic vacancies/defects in passivated ZnS nanoparticles. *J. Nanopart. Res.* **2010**, *12*, 2655–2666. [CrossRef]
52. Mecozzi, M.; Sturchio, E. Computer assisted examination of infrared and near infrared spectra to assess structural and molecular changes in biological samples exposed to pollutants: A case of study. *J. Imaging* **2017**, *3*, 11. [CrossRef]
53. Boguta, P.; Sokołowska, Z.; Skic, K. Use of thermal analysis coupled with differential scanning calorimetry, quadrupole mass spectrometry and infrared spectroscopy (TG-DSC-QMS-FTIR) to monitor chemical properties and thermal stability of fulvic and humic acids. *PLoS ONE* **2017**, *12*, e0189653. [CrossRef] [PubMed]
54. Balogun, A.O.; Lasode, O.A.; Li, H.; McDonald, A.G. Fourier transform infrared (FTIR) study and thermal decomposition kinetics of *Sorghum bicolour* glume and *Albizia pedicellaris* residues. *Waste Biomass Valorization* **2015**, *6*, 109–116. [CrossRef]
55. Auta, R.; Adamus, G.; Kwiecien, M.; Radecka, I.; Hooley, P. Production and characterization of bacterial cellulose before and after enzymatic hydrolysis. *Afr. J. Biotechnol.* **2017**, *16*, 470–482.
56. Mostafa, Y.S.; Alrumman, S.A.; Alamri, S.A.; Otaif, K.A.; Mostafa, M.S.; Alfaify, A.M. Bioplastic (poly-3-hydroxybutyrate) production by the marine bacterium *Pseudodonghicola xiamenensis* through date syrup valorization and structural assessment of the biopolymer. *Sci. Rep.* **2020**, *10*, 1–14. [CrossRef] [PubMed]
57. Teerapatsakul, C.; Pothiratana, C.; Chitradon, L.; Thachepan, S. Biodegradation of polycyclic aromatic hydrocarbons by a thermotolerant white rot fungus *Trametes polyzona* RYNF13. *J. Gen. Appl. Microbiol.* **2016**, *62*, 303–312. [CrossRef] [PubMed]

58. Zafra, G.; Moreno-montaño, A.; Absalón, Á.E.; Cortés-espinosa, D.V. Degradation of polycyclic aromatic hydrocarbons in soil by a tolerant strain of *Trichoderma asperellum*. *Environ. Sci. Pollut. Res.* **2015**, *22*, 1034–1042. [CrossRef]
59. Mtibaà, R.; Olicón-Hernández, D.R.; Pozo, C.; Nasri, M.; Mechichi, T.; González, J.; Aranda, E. Degradation of bisphenol A and acute toxicity reduction by different thermo-tolerant ascomycete strains isolated from arid soils. *Ecotoxicol. Environ. Saf.* **2018**, *156*, 87–96. [CrossRef]
60. Kim, Y.C.; Lee, S.R.; Jeon, H.J.; Kim, K.; Kim, M.J.; Choi, S.D.; Lee, S.E. Acute toxicities of fluorene, fluorene-1-carboxylic acid, and fluorene-9-carboxylic acid on zebrafish embryos (*Danio rerio*): Molecular mechanisms of developmental toxicities of fluorene-1-carboxylic acid. *Chemosphere* **2020**, *260*, 127622. [CrossRef]
61. Kamaya, Y.; Fukaya, Y.; Suzuki, K. Acute toxicity of benzoic acids to the crustacean *Daphnia magna*. *Chemosphere* **2005**, *59*, 255–261. [CrossRef] [PubMed]
62. Tuvikene, A. Aquatic ecotoxicology-study of freshwater systems stressed by toxic chemical. *Ann. Zool. Fenn.* **1995**, *32*, 295–309.
63. So-Young, L.; Kwon, J.-H. Enhancement of toxic efficacy of alkylated polycyclic aromatic hydrocarbons transformed by *Sphingobium quisquiliarum*. *Int. J. Environ. Res. Public Health* **2020**, *17*, 6416. [CrossRef]
64. Arunprasath, T.; Sudalai, S.; Meenatchi, R.; Jeyavishnu, K.; Arumugam, A. Biodegradation of triphenylmethane dye malachite green by a newly isolated fungus strain. *Biocatal. Agric. Biotechnol.* **2019**, *17*, 672–679. [CrossRef]
65. Strotmann, U.; Flores, D.P.; Konrad, O.; Gendig, C. Bacterial toxicity testing: Modification and evaluation of the luminescent bacteria test and the respiration inhibition test. *Processes* **2020**, *8*, 1349. [CrossRef]
66. Tamura, K.; Stecher, G.; Kumar, S. MEGA11: Molecular Evolutionary Genetics Analysis Version 11. *Mol. Bio. Evol.* **2021**, *38*, 3022–3027. [CrossRef]
67. Ortega-González, D.K.; Cristiani-Urbina, E.; Flores-Ortíz, C.M.; Cruz-Maya, J.A.; Cancino-Díaz, J.C.; Jan-Roblero, J. Evaluation of the removal of pyrene and fluoranthene by *Ochrobactrum anthropi*, fusarium sp. and their coculture. *Appl. Biochem. Biotechnol.* **2015**, *175*, 1123–1138. [CrossRef]
68. Patel, H.; Gupte, A.; Gupte, S. Effect of different culture conditions and inducers on production of laccase by a basidiomycete fungal isolate *Pleurotus ostreatus* HP-1 under solid state fermentation. *BioResour* **2009**, *4*, 268–284.
69. Rotini, A.; Tornambè, A.; Cossi, R.; Iamunno, F.; Benvenuto, G.; Berducci, M.T.; Maggi, C.; Thaller, M.C.; Cicero, A.M.; Manfra, L.; et al. Salinity-based toxicity of CuO nanoparticles, CuO-bulk and Cu ion to *Vibrio anguillarum*. *Front. Microbiol.* **2017**, *8*, 2076. [CrossRef]
70. Czech, B.; Jośko, I.; Oleszczuk, P. Ecotoxicological evaluation of selected pharmaceuticals to *Vibrio fischeri* and *Daphnia magna* before and after photooxidation process. *Ecotoxicol. Environ. Saf.* **2014**, *104*, 247–253. [CrossRef]

Supplementary Materials

Metabolic Biodegradation of fluoranthene by indigenous *Trichoderma lixii* and *Talaromyces pinophilus* spp.: Deciphering pathway and determining acute toxicity of metabolites

Samson O. Egbewale, Ajit Kumar, Mduduzi P. Mokena and Ademola O. Olaniran

A

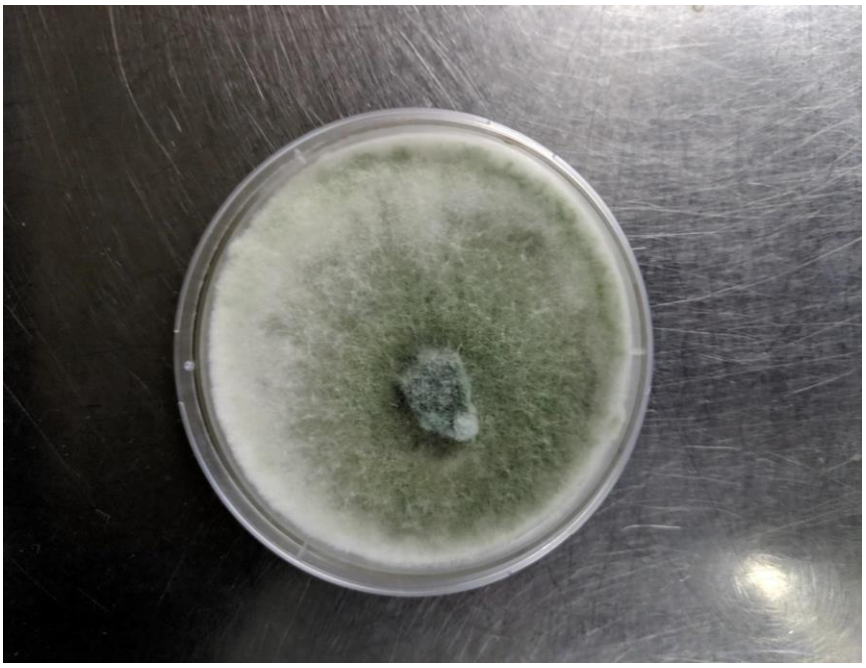

B

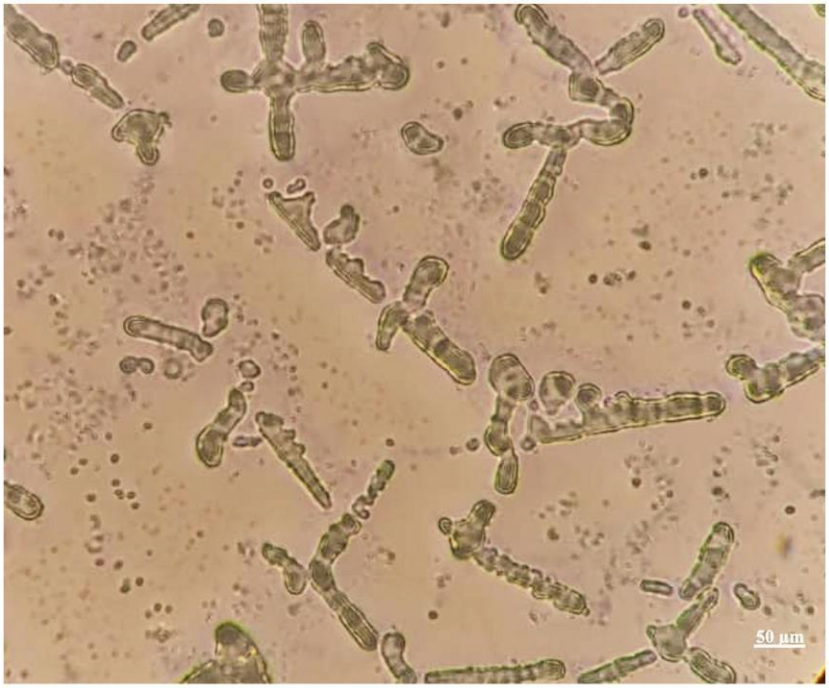

Figure S1. (**A**) Morphological characteristics of *Tl*FLU1 grown on a PDA plate. (B) Microscopic morphology of TlFLU1.

A

B

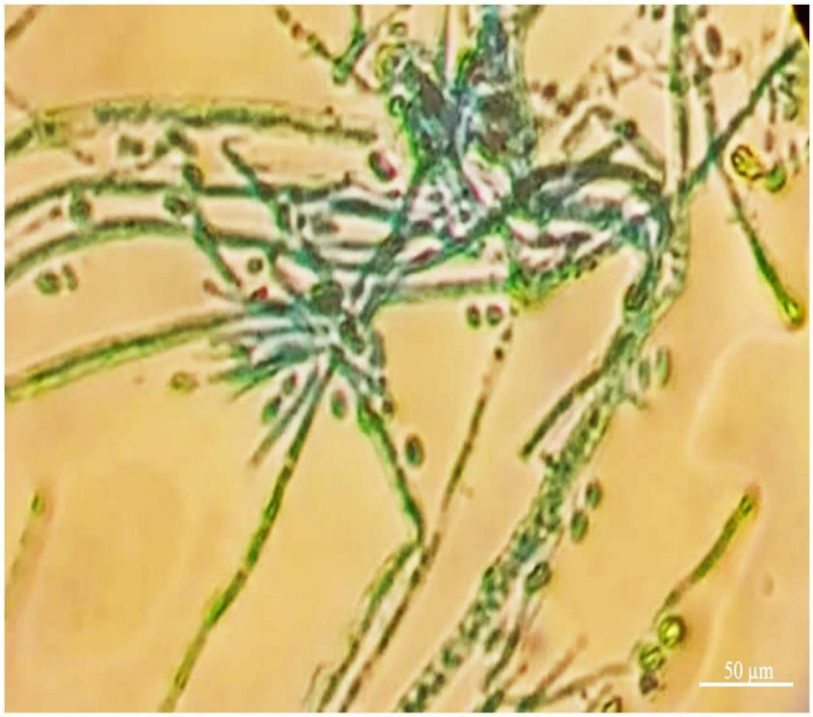

Figure S2. (A) morphological characteristics of *Tp*FLU12 grown on a PDA plate. (**B**) Microscopic morphology of *Tp*FLU12.

A

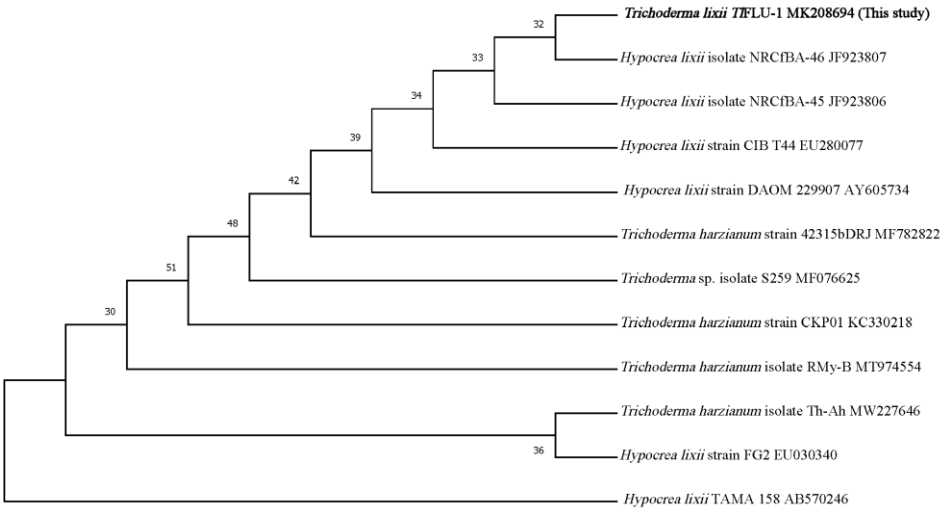

B

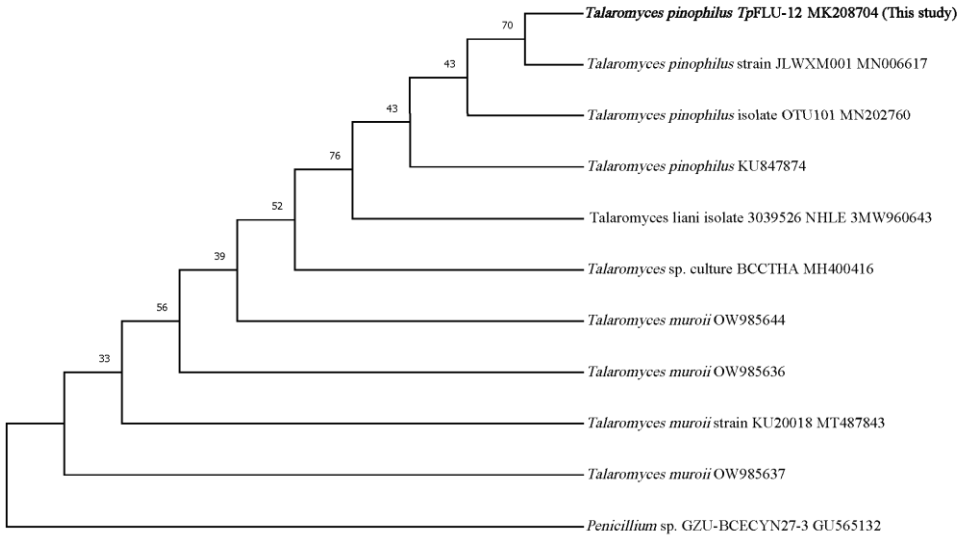

Figure S3. (A) Neighbor-joining phylogenetic tree for *Tl*FLU1. (**B**) Neighbor-joining phylogenetic tree for *Tp*FLU12.

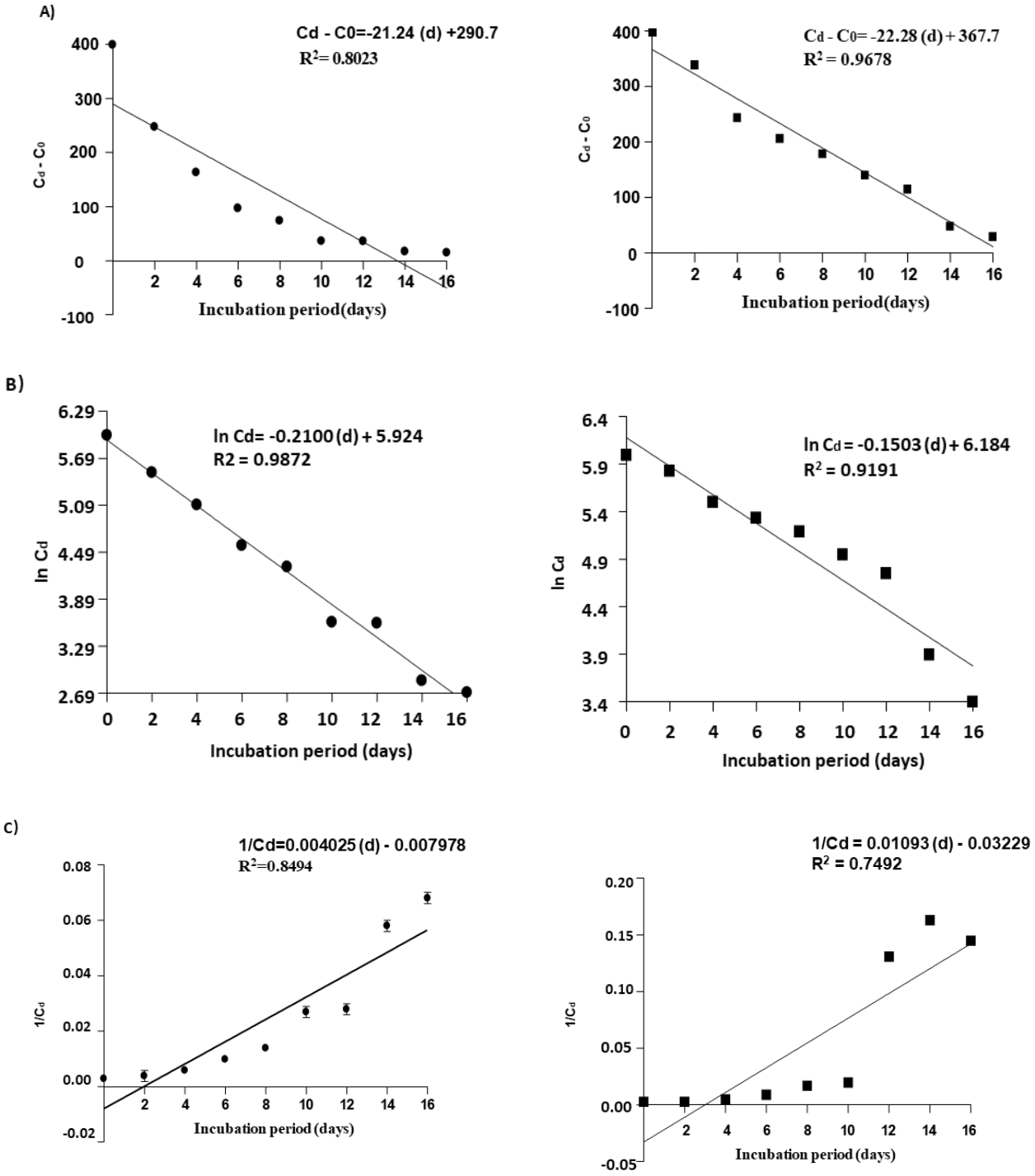

Figure S4. Fluoranthene degradation kinetic modelling (**A**) Zero Order, (**B**) First Order, (**C**) Second Order. *Tl*FLU1 (●), *Tp*FLU12 (■), d = days.

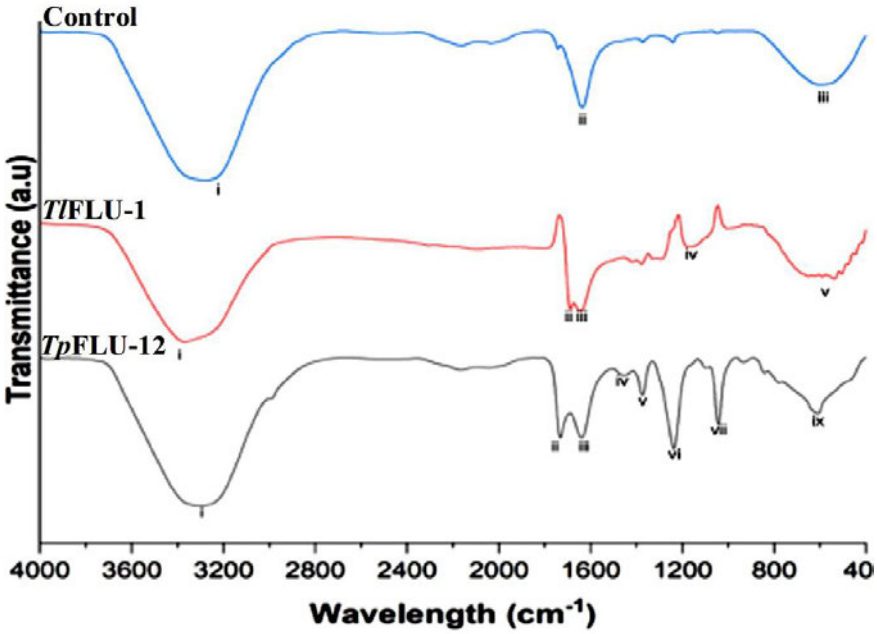

Figure S5. FTIR spectra of fluoranthene biodegradation metabolites.

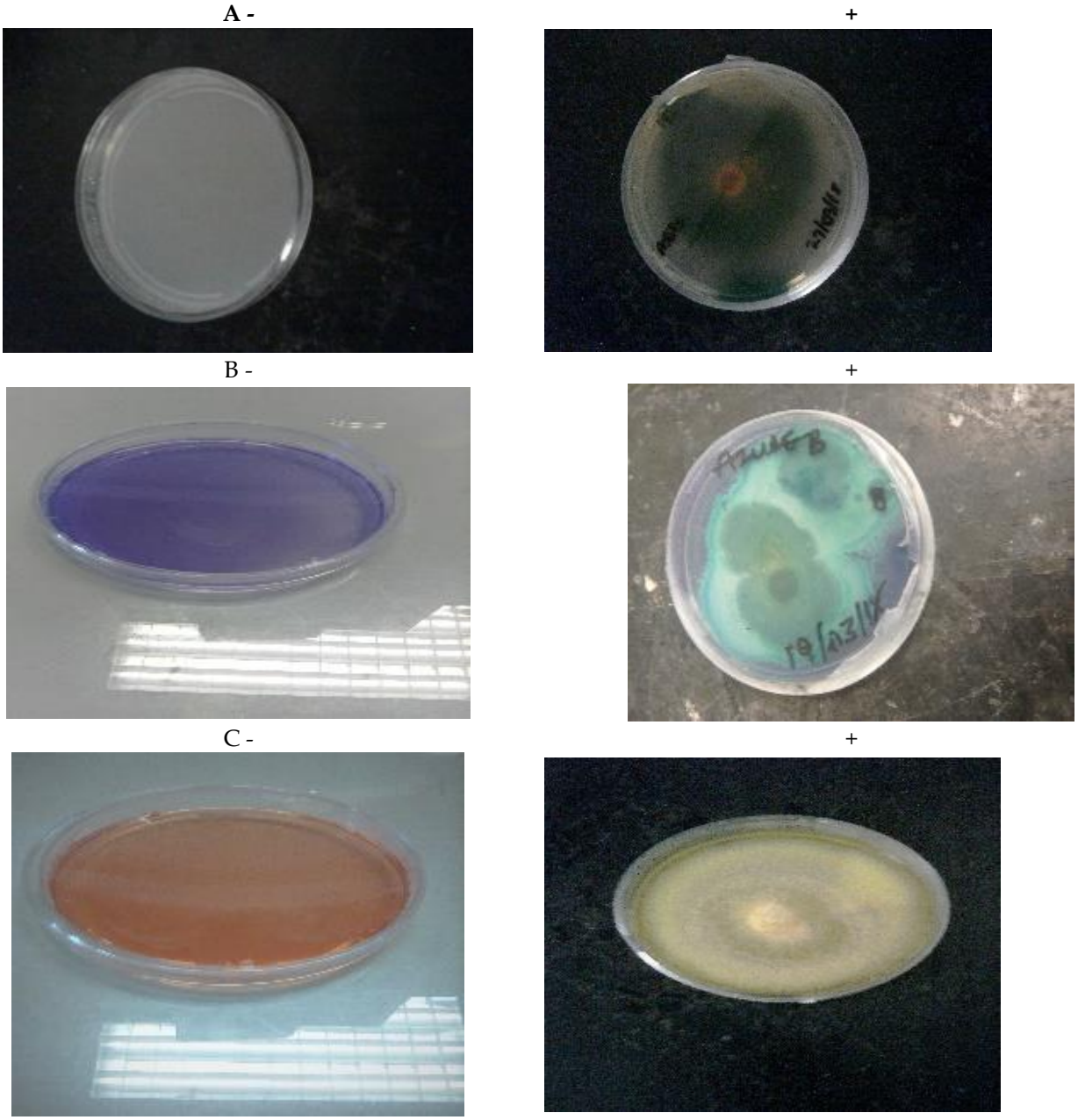

Figure S6. Preliminary assay for Ligninolytic enzyme production on solid media. **Keys**: - flouranthene + no-fungus; + flouranthene + fungus**;** laccase (oxidation of ABTs to Green colour zones); LiP (Oxidation of Azure B to Green colour zones); MnP (oxidation of phenol red to form yellow colour zones).

Table S1. GC-MS profile of the metabolite formed during fluoranthene degradation.

Metabolites	Retention time (min) *Tl*FLU-1	Retention time (min) *Tp*FLU-12	Major m/z of fragment ions (% relative abundance)	Tentative identification	GC-MS spectral
1	**28.4**		88 (3, $\mathbf{M^+}$), 100 (5), 101 (9), 174 (2), 175 (2), 199 (2), 200 (15), 201 (12), **202** (100), 203 (17)	Fluoranthene	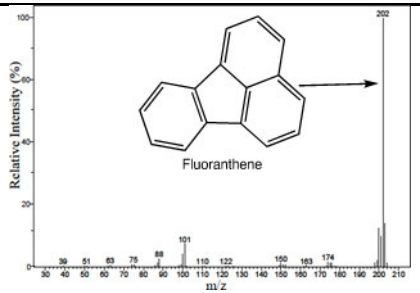
2	ND	23.9	63 (6, $\mathbf{M^+}$), 75 (5), 76 (13), 126 (5), 150 (7), 151 (13), 152 (29), 153 (4), **180** (100), 181 (15)	9-Fluorenone	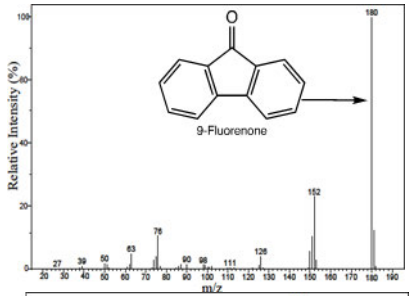
3	ND	18.4	50 (12, $\mathbf{M^+}$), 51 (21), 76 (14), 77 (24), 78 (30), 103 (42), **104** (100), 105 (10), 131 (23), 132 (98)	2,3-dihydro-1*H*-inden-1-one	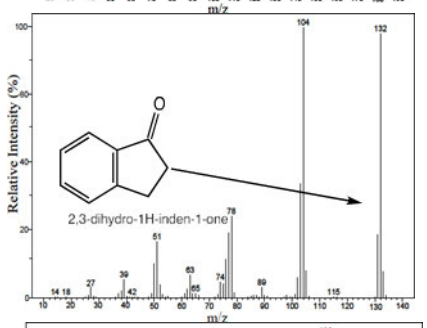
4	14.2	ND	75 (6, $\mathbf{M^+}$), 76 (5), 126 (5), 150 (15), 151 (22), 152 (37), 153 (5), **180** (100), 181 (14), 224 (18)	9-oxo-9*H*-fluorene-1- car-boxylic acid	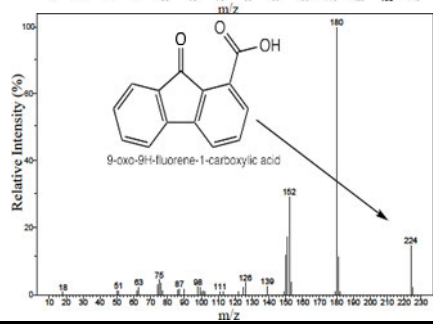

1

5	12.3	ND	18 (15, **M**$^{+}$), 44 (11), 50 (15), 64 (13), 74 (19), 75 (23), 76 (31), 92 (25), 104 (44), **148** (100)	Benzene-1,2,3-tricarboxylic acid	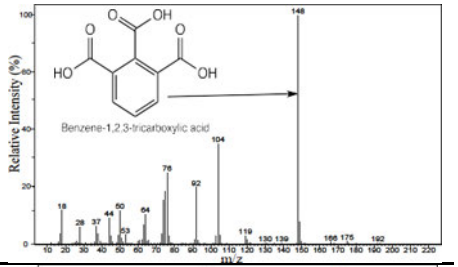
6	ND	7.9	50(19, **M**$^{+}$), 51 (3), 74 (8), 76 (6), 77 (66), 78(6), **105**(100), 106 (7),122 (83), 123 (7)	Benzoic acid	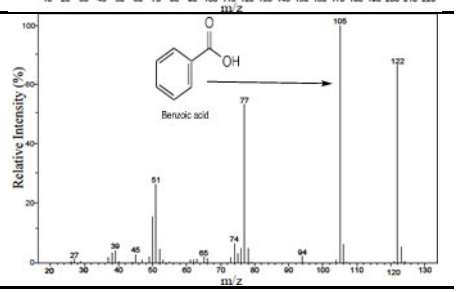

ND: Not detected

Table S2. The average fungal growth and growth inhibition after 10 days of exposure to varying. fluoranthene concentrations.

Concentration (mg/L)	Fungal growth (mm)		Growth Inhibition (%)	
	*Tl*FLU1	*TP*FLU12	*Tl*FLU1	*TP*FLU12
50	9.0 [a]	9.0 [a]	0.0	0.0
100	9.0 [a]	9.0 [a]	0.0	0.0
200	9.0 [a]	9.0 [a]	0.0	0.0
400	9.0 [a]	9.0 [a]	0.0	0.0
600	8.6 [a]	7.9 [b]	4.4 [b]	12.2 [a]
800	7.7 [a]	6.6 [b]	14.4 [b]	26.7 [a]
1000	6.8 [a]	6.1 [b]	24.4 [b]	32.2 [a]

Values with the same superscript alphabet in the same row under the same parameter are statistically non-significant ($p \leq 0.05$).

Table S3. Preliminary assay for extracellular enzyme production on solid media.

Extracellular enzyme	Fungal Colony Diameter (mm)		Colour diameter (mm)		Oxidation Scale at Day 10	
	FLU1	FLU12	FLU1	FLU12	FLU1	FLU12
Laccase	90	80	60	80	+++	++++
LiP	90	68	70	65	++++	++++
MnP	89	87	90	90	+++++	+++++

+ diameter of the oxidized zone 0-20mm, ++ zone diameter 21-40mm, +++ zone diameter 41-60mm, ++++ 61-80 mm,+++++ 81- 100mm

CHAPTER FOUR

Mycotransformation of anthracene by indigenous *Trichoderma lixii* and *Talaromyces pinophilus* isolates: insights into the metabolic pathways, enzyme profiles and acute toxicity

This chapter is currently under final revision in the journal: *Journal of fungi.*

The manuscript is presented in the following pages.

Type of the Paper: Article

Title: Mycotransformation of Anthracene by Indigenous *Trichoderma lixii* and *Talaromyces pinophilus* isolates: Insights into the Metabolic Pathways, Enzyme Profiles and Acute Toxicity

Samson O. Egbewale[1], Ajit Kumar[1], Mduduzi P. Mokoena[2] and Ademola O. Olaniran[1*]

Citation: To be added by editorial staff during production.

Academic Editor: Firstname Lastname

Received: date
Revised: date
Accepted: date
Published: date

[1] Discipline of Microbiology, University of KwaZulu-Natal (Westville Campus), Durban 4000, South Africa; Email: egbewaleprinces@yahoo.com; ajitkanwal@yahoo.com, olanirana@ukzn.ac.za
[2] Department of Pathology, School of Medicine, University of Limpopo, Private Bag X1106, Sovenga-0727, South Africa.; mduduzi.mokoena@ul.ac.za
* Correspondence: Email address: olanirana@ukzn.ac.za, Tel. +27 31 260 7400, Fax: +27 31 260 7809.

Abstract: This study focused on the mycotransformation of a very prominent PAH, anthracene, and its acute toxicity reduction by Ascomycete fungi: *Trichoderma lixii* strain FLU1 (*Tl*FLU1) and *Talaromyces pinophilus* strain FLU12 (*Tp*FLU12) indigenously isolated from benzo[b]fluoranthene enriched activated sludge. The results indicate that both the isolates *Tl*FLU1 and *Tp*FLU12 could tolerate anthracene exposure up to 1000 mg/L, with increased expression of ligninolytic enzymes: Laccase, Lignin peroxidase and Manganese peroxidase. The mycotransformation of anthracene was observed to be growth-linked and mediated by the expression of the intracellular enzymes as the initial mechanism use by these strains followed by the ligninolytic enzymes with up to 56% and 38% anthracene degradation by *Tl*FLU1 and *Tp*FLU12, respectively, after a 24-day period with a concomitant change in pH from 5 to 4 (*Tl*FLU1) and 6.2 (*Tp*FLU12). The GC-MS and FTIR analysis of the samples indicate the appearance of metabolic intermediates: 9,10 anthracenedione and benzoic acid in *Tl*FLU1 grown medium, while anthrone and 9,10 anthracenedione were detected in *Tp*FLU12 grown medium. The mycotransformation of the compound followed first-order kinetic model with an effective concentration (EC50) of 262.3-266.1 mg/L with toxicity unit (TU) of 0.4% in *Vibrio parahaemolyticus* (6 h exposure) to each intermediate. Results show efficient mycotransformation of anthracene into a non-toxic state by *Tl*FLU1 and *Tp*FLU12.

Keywords: Anthracene, mycotransformation, toxicity, Trichoderma lixii, Talaromyces pinophilus.

1. Introduction

Polycyclic aromatic hydrocarbons (PAHs) are a group of recalcitrant and ubiquitous contaminants released into the environment through natural and anthropogenic processes [1]. They exist as derivatives of biogenic, petrogenic and pyrolytic compounds [2]. Due to the recalcitrant characteristics, hydrophobicity, toxicity, carcinogenic effects; and non-bioavailability to biological

agents for degradation; USEPA listed PAHs among priority pollutants need to be expunged from ecosystems [3].

Anthracene, a PAH, is found in various environmental compartments, with its levels varying significantly. In urban air, its concentration ranges from 0.1 to 10 ng/m^3, while in rural areas, it is lower, at 0.01 to 1 ng/m^3. However, in cigarette smoke, its levels can be much higher, at 100 to 1000 ng/m^3. In soil, its concentrations can reach up to 10,000 μg/kg in areas near industrial zones or coal tar deposits [4]. The distribution of PAHs in aquatic ecosystems is influenced by particle size and organic matter content [5]. Gas-particle partitioning of PAHs in urban, coastal, and continental sites is influenced by their subcooled liquid vapor pressure [6]. The concentrations of PAHs in soils are affected by soil properties and climate, with lighter OPAHs being more prevalent in the south, suggesting biological sources [7].

Anthracene is the active ingredient in various products, including dyes, synthetic fibers, wood preservatives, and the chemotherapeutic drug, amsacrine [8]. They pose significant environmental hazards as immunosuppressants, teratogens, and respiratory irritants, with various degrees of toxicity, mutagenicity, and carcinogenicity [9,10]. In plants, anthracene accounts for low yields in crops through the interference with carbon fixation inhibition, enzymatic dysfunction, membrane permeability and reduction in net photosynthesis [11]. Researchers and environmental agencies have been the techniques like chemical oxidation, flocculation, activated carbon, electro-oxidation and photolysis to mitigate the harmful effects of anthracene [12]. However, these techniques are not as efficient as microbial-mediated detoxification/biotransformation methods, which are also deemed to be eco-friendly and low-cost process [13].

Mycotransformation by mushroom-forming fungi (Basidiomycetes) has received tremendous attention over the past decades owing to their effective biotransformation potentials through aggressive growth and ligninolytic enzyme production [14]. Mycotransformation of PAHs is primarily mediated *via* oxidation by forming quinones intermediates involving three enzymes namely, Laccase (Lac, p-Diphenol: dioxygen oxidoreductases; EC 1.10.3.2), Manganese peroxidase (MnP; EC 1.11.1.13) and Lignin peroxidase (LiP; EC 1.11.1.14) [15]. These enzymes have been reportedly induced by PAHs during myco-degradation processes [16,17]. However, PAHs mycotransformation products, such as dihydrodiol (quinones) and epoxides are of great environmental concern due to their deleterious effect compared to their parent compounds [18,19]. The transcriptomic responses of catalase, peroxidase, and laccase encoding genes and enzymatic activities of oil spill inhabiting rhizospheric fungal strains, *Talaromyces purpurogenum* and *Trichoderma harzianum* showed overexpression of genes encoding lignin peroxidase (LiP) and manganese peroxidase (MnP) in response to crude oil contamination [20]. The Ascomycete fungi could contain other types of Class II peroxidases like AA, AB and AC type peroxidases along with DyP type peroxidases and some other intracellular Class II peroxidases [21-25].

Ecotoxicity is a crucial tool for environmental safety and protection assessment. Although, most ecotoxicity bioassays comprises of using representatives from all trophic levels namely, bacteria whose role is the decomposer, algae (producer), invertebrates and vertebrate as the consumers [26]. Yet, the choice of conventional bacteria bioluminescence inhibition tests on toxicants from elutriates samples has a lot of drawbacks ranging from bacterial adsorption on surfaces, interference by sulfur or sulfides, ammonia, interference of bioluminescence due to pH variations, color or particles [27]. Bacteria survival assay using marine bacterium (*Vibrio spp.*) as a bioindicator for ecotoxicity assessment is simple, fast and cheap, corroborate the other toxicity assay responses [28].

Despite the overwhelming reports on the potentials of basidiomycete in the mycotransformation of PAHs, few literatures are available on the mycotransformation of PAHs by non-mushroom forming fungi from the ascomycetes, mechanisms, and pathways for their mycotransformation and ecotoxicity testing of PAHs/metabolites. Thus, this study seeks to bridge the knowledge gaps by determining the tolerance level of indigenous *Trichoderma lixii* strain FLU1 and *Talaromyces pinophilus* strain FLU12 to a varying concentration of anthracene. Metabolites profiling and characterization of enzymes established the biodegradation pathway. The mycotransformation efficiency, mycotransformation kinetics, and acute toxicity of anthracene on the fungal strains as well as the transient mycotransformation products were also elucidated in this study.

2. Materials and Methods

2.1. Materials:

All reagents used are of HPLC grade with ≥ 98 % purity. Anthracene, ethyl acetate, ABTS, DMP, azure B, catechol, $CaCl_2{\cdot}2H_2O$, $(NH_4)_2SO_4$, K_2HPO_4, $MnCl_2{\cdot}2H_2O$, $NaH_2PO_4{\cdot}2H_2O$, NaCl, $MgSO_4{\cdot}7H_2O$, Nitrilotriacetic acid, $FeSO_4{\cdot}7H_2O$, $ZnSO_4$, $CuSO_4$, H_3BO_3, Na_2MoO_4, $Co(NO_3){\cdot}6H_2O$, $Al_2(SO_4)_3{\cdot}H_2O$, PDA and TCBS agar were bought from Merck (NJ, USA). 500 mg of anthracene stock solution prepared in 10 mL methanol and sterilized 0.22 μm filter (Millipore, Merck, New Jersey, USA). BSM was prepared as described previously [29] and pH adjusted to 5 with 1 N HCl. *Tl*FLU1 and *Tp*FLU12 were isolated from BbP-enriched wastewater-activated sludge and the characteristics with identification have been reported previously [30].

2.2. Evaluation of anthracene tolerance on PDA plates.

Anthracene concentrations of 0, 50, 100, 200, 400, 600, 800, and 1000 mg/L were applied to PDA plates with corresponding concentrations using a sterile rod and left in the laminar hood for 2 hours to allow the solvent to evaporate and the anthracene to adhere to the agar surface. Thereafter, mycelia agar plugs (5 mm diameter) from 7 d old actively growing *Tl*FLU1 and *Tp*FLU12 were separately inoculated at the center of Petri dishes containing anthracene-contaminated PDA plates incubated at 30°C for 10 d in four replications under a total darkness condition. Control plates (no anthracene addition)

were also included. Radial growth rate was measured for each fungus every 24 h to the end of the incubation period to assert the tolerance of each fungus to varying anthracene concentrations.

The fungal inhibition percentage due to the anthracene exposure was calculated using the following equations:

$FG\ (\%) = D_{ANT} / D_C \times 100$ ……. Equation 1

$FI\ (\%) = 100 - FG$ ……. Equation 2

Where FG = Fungal growth rate (FG) was calculated from the radial

mycelial growth record

D_{ANT} = Diameter of fungal colony exposed to anthracene,

DC = diameter of the control fungal colony (no anthracene addition).

FI = Fungal growth inhibition of the colonies after anthracene exposure at varying concentrations [31].

2.3. Qualitative screening of isolated fungi for ligninolytic enzymes

Enzymatic assays for strains *Tl*FLU1 and *Tp*FLU12 were conducted using laccase (Lac), lignin peroxidase (LiP), and manganese peroxidase (MnP) as the target enzymes, as they are commonly employed by fungi during biodegradation. Lac activity was screened on each anthracene-contaminated PDA plate by adding ABTS (0.1 % w/v) as a substrate, and the final pH was adjusted to 5.5. The plates were inoculated at the center with 5 mm mycelial agar plugs from 7-day-old actively growing strains and incubated at 30°C for 10 days in four replications under total darkness conditions. Lac activity was evaluated based on green colour development in the presence of ABTS. LiP activity was screened by adding Azure B (0.001% w/v) to the anthracene-contaminated PDA plates and incubating them for 10 days. The reduction in blue/purple colour to sky blue indicated LiP activity. MnP activity was screened on Czapek-Dox agar medium containing phenol red (0.0025% w/v). After 10 days of incubation at 30°C, the reduction in red colour to yellow zones indicated MnP activity.

2.4. Anthracene mycotransformation study and fungal strains biomass estimation:

The anthracene degradation and fungal biomass estimation studies were conducted as described previously [16,30]. Briefly, 400 mg/L anthracene in 100 mL BSM broth was open in laminar hood for 20 mins to allow the solvent used for anthracene preparation to evaporate to yield superficial desire concentration before inoculation with mycelium discs of an actively growing cultures of each fungal strain. Incubation was allowed for 24 days at 30 °C. Only 400 mg/L anthracene in BSM was used as negative control. The aliquots at 4 days intervals were withdrawn to quantify residual anthracene,

intermediates formed, ligninolytic enzymes activity and to perform ecotoxicity test. The initial concentration of 400 mg/L was used based on low fungal growth inhibition in comparison with higher concentration on both selected strains (Table S1, S2). For fungal biomass estimation, 4 mL culture broth was collected by centrifugation and the pellets dry biomass was determined. Also, the residual anthracene was quantified in the supernatant. Washing the pellet with ethyl acetate (1:10 w/v, 5 times) was necessary to remove the residual anthracene from the pellets as it could limit biosorption by the fungi mycelia pellets due to its hydrophobic nature.

2.5. Extraction and quantification of residual anthracene:

Extraction and quantification of residual anthracene culture medium was done as previously described [32] with some modifications [30]. Briefly, the culture broth supernatant mixed with 1:4 v/v ethyl acetate, vigorously shaken and allowed to stand for 20 minutes. The organic phase was dried and quantified for the residual anthracene. The experiments were triplicated with an average anthracene recovery of 98.7 ± 2.53%. The kinetic models of anthracene mycotransformation were plotted as described previously [33]. A composite sample from the tetrad days collections of the residual anthracene and intermediates formed during the mycotransformation were also analyzed by GC-MS and FTIR [30,34].

2.6. Intracellular and Extracellular ligninolytic activity assays:

The preparation of cell lysate for intracellular activity of catechol 1,2 dioxygenase (C12D, ortho-cleaving) and catechol 2,3 dioxygenase (C23D, meta-cleaving) were carried out as described previously [35]. Extracellular activity of Lac [36], LiP-like [37] and MnP-like was carried out as described previously [30]. For determination of the intracellular activity for Lac, LiP-like and MnP-like, the fungal biomass was collected after 4 days interval, filtered, and washed once with BSM. The mycelia were resuspended in 50 mM Na-phosphate buffer (pH 5) and sonicated to get cell free lysate. The enzyme activities for Lac, LiP -like and MnP-like in cell lysate were carried out as described previously [30,36,37]. One unit of respective enzyme activity was defined as 1 µmol of cis,cis-muconic acid (product) for catechol 1,2 dioxygenase, 1 µmol of 2-hydroxymuconic semialdehyde (product) for catechol 2,3 dioxygenase, 1 µmol of ABTS oxidized, 1 µmol of Azure B reduced and 1 µmol of 2, 6-DMP oxidized per min at 30 °C, pH 7.

2.7. Ecotoxicity Test:

The ecotoxicity test were conducted on *Vibrio parahaemolyticus* (ATCC 17802) as described previously [30]. Directive 79/831/EEC [38] was used to classify (very toxic, $EC_{50} \leq 1$ mg/L; toxic, 1 mg/L $\leq EC_{50} < 10$ mg/L; harmful, 10 mg/L $\leq EC_{50} \leq 100$ mg/L and non-toxic, $EC_{50} \geq 100$ mg/L).

2.8. Data Analysis:

A completely randomized design approach was used to were set experiments. Mean values and error bars were shown graphically as GraphPad

Prism version 8.4.3 (v.471, San Diego, CA, USA). The statistics details on EC_{50} and TU can be seen in figure 5 legend.

3. Results:

3.1. Anthracene mycotransformation, biomass yield, and extracellular protein content and pH in liquid media:

The results of anthracene mycotransformation, fungal growth and extracellular protein content indicate that *Tp*FLU12 transforms anthracene more efficiently than *Tl*FLU1 (Fig. 1). A significant decrease in percentage residual anthracene concentration was observed over time for both fungal strains. In *Tl*FLU1 inoculated flasks, 38% anthracene degradation was observed with dry fungal biomass of 710.3 mg/L at the end of the incubation period of 24 days, while maximum extracellular protein content of 666.2 mg/L was measured on day 12 of the incubation period (Fig. 1a). However, 56% anthracene degradation was observed in *Tp*FLU12 with the dry biomass production of 645.6 mg/L, while the extracellular protein of 760 mg/L was measured at day 24 of the incubation period (Fig. 1b). Furthermore, after the incubation period of 24 days, the flask inoculated with *Tl*FLU1 showed a notable decrease in pH from the initial value of 5.0 to 4.2 (Fig. 2, curve A), while the flask inoculated with *Tp*FLU12 displayed an intriguing increase in pH from the initial 5.0 to 6.25 over the same incubation period (Fig. 2, curve B).

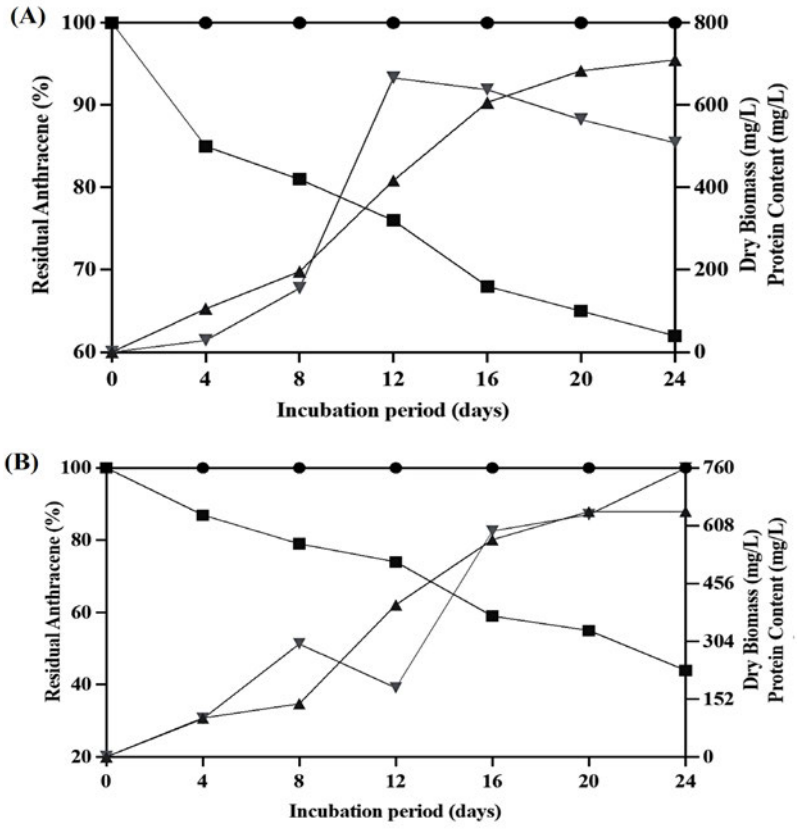

Figure 1. Degradation of anthracene by *Tl*FLU1 (A) and *Tp*FLU12 (B). Curves shown are BSM + anthracene (●), residual anthracene (■), dry biomass (▲) and total protein content (▼).

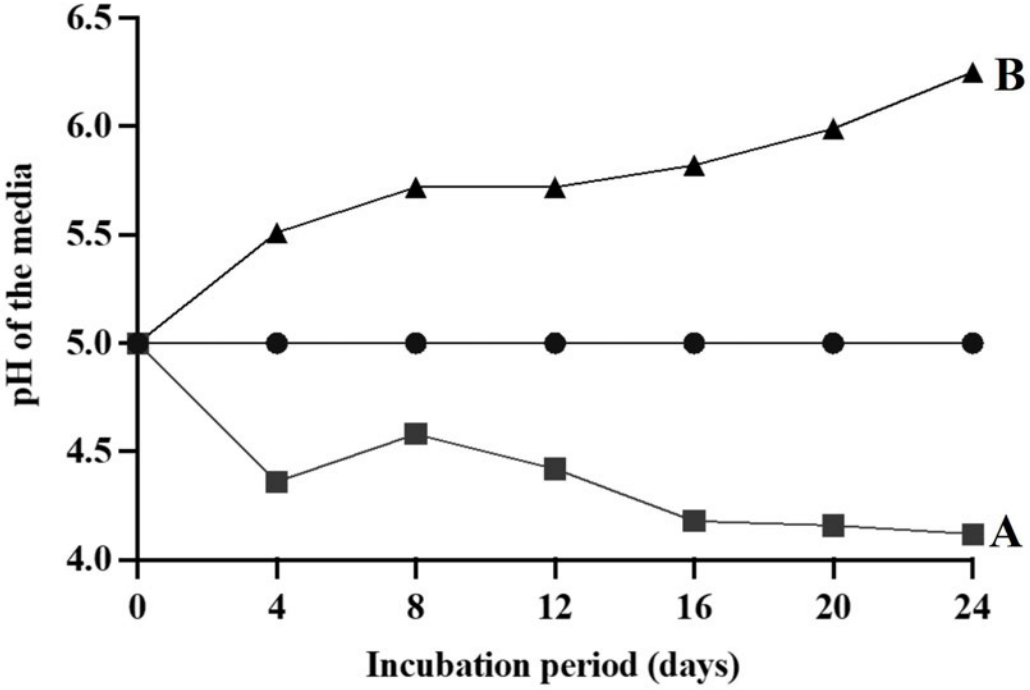

Figure 2. Change in pH of media while anthracene degradation by *Tl*FLU1 (■) and *Tp*FLU12 (▲). BSM+anthracene used as control (●).

The kinetic parameters of the mycotransformation of anthracene are shown in Table 1 and Fig. S1. The anthracene mycotransformation by strains *Tl*FLU1 and *Tp*FLU12 best fitted the zero-order and first-order kinetics. Under the zero-order kinetics, a rate constant of 5.964 and a half-life of 33.54 with a R^2 value of 0.9402 was obtained for isolate *Tl*FLU1 while isolate *Tp*FLU12 inoculated flask has a ate constant of 9.000 and half-life of 22.222 with a R^2 value of 0.9866. However, under the first-order kinetics, *Tp*FLU12 showed a superior rate constant of 0.0328 and a half-life of 21.15 with a R^2 value of 0.9769 while in *Tl*FLU1 inoculated flask, a rate constant of 0.0192, half-life of 36.101 and R^2 value of 0.9670 were obtained. Also, it was observed that both *Tl*FLU1 and *Tp*FLU12 did not obey the second order kinetics. A constant of 0.0001 and a half-life of 46.668 with R^2 value of 0.7500 was obtained for *Tl*FLU1 while, a constant of 0.0001 and a half-life of 20.000 with R^2 value of 0.7903 was obtained for *Tp*FLU12.

Table 1: Kinetic parameters for the degradation of anthracene by *Tl*FLU1 and *Tp*FLU12

Kinetic model	Parameter	Strains	
		*Tl*FLU1	*Tp*FLU12
Zero order	Regression Equation	C_d= - 5.964d + 378.4	C_d = -9.000d + 392.6
$C_t - C_0 = Kt$	K(d^{-1})	5.964	9.0000
$t_{1/2} = C_0/2K_0$	$t_{1/2}$	33.535	22.222
	R^2	0.9402	0.9866
First order	Regression Equation	$\ln C_d$ = - 0.0192d + 5.944	$\ln C_d$ = - 0.0328d + 6.010
$\ln C_t = K_1t + \ln C_0$	K(d^{-1})	0.0192	0.0328
$t_{1/2} = \ln 2 / K_t$	$t_{1/2}$	36.196	21.145
	R^2	0.9670	0.9769
Second order	Regression Equation	$1/C_d = 5.35X10^{-5} + 0.003$	$1/C_d$ = 0.0001d+ 0.002
$1/C_t = 1/C_0 + K_2t$	K(d^{-1})	0.0001	0.0001
$T_{1/2} = 1/C_0K_2$	$t_{1/2}$	46.668	20.000
	R^2	0.7500	0.7903

R^2: Regression coefficient; K: Degradation rate constant; $t_{1/2}$: Half-life period (d); C_0: Initial concentration; C_t: Final concentration.

3.2. Profiles of anthracene mycotransformation metabolic products:

The metabolic products and pathways identified in *Tl*FLU1 and *Tp*FLU12 using GC-MS are shown in Fig. 3, Table 2 and Fig. 4. Two metabolites, 9,10 anthracenedione (molecular ion [M^+] at m/z 180 and benzoic acid (molecular ion [M^+] at m/z 105) were observed in the *Tl*FLU1 inoculated flasks with a varying retention time; 15.6 mins and 9.1 mins, respectively while that of *Tp*FLU-12 inoculated flask were anthrone at a retention time of 11.3 mins with molecular ion (M^+) at m/z 195 and 9,10 anthracenedione (RT: 15.2 mins) with molecular ion (M^+) at m/z 180. However, the parent compound (control: anthracene) was detected at a retention time of 21.8 mins. Furthermore, the identified metabolic intermediates were used to propose possible anthracene metabolic pathways for each of the fungal strains, as shown in Fig. 4. The theoretical arrangement of the metabolic intermediates suggests that an initial attack at the C-9 and C-10 position of anthracene occurred *via* oxygenation to form either anthrone or 9,10-anthracenedione before undergoing a spontaneous tautomeric benzoic acid formation as the dead-end product due to the hydroxylation and ring cleavage at the C-9 and C-10 position.

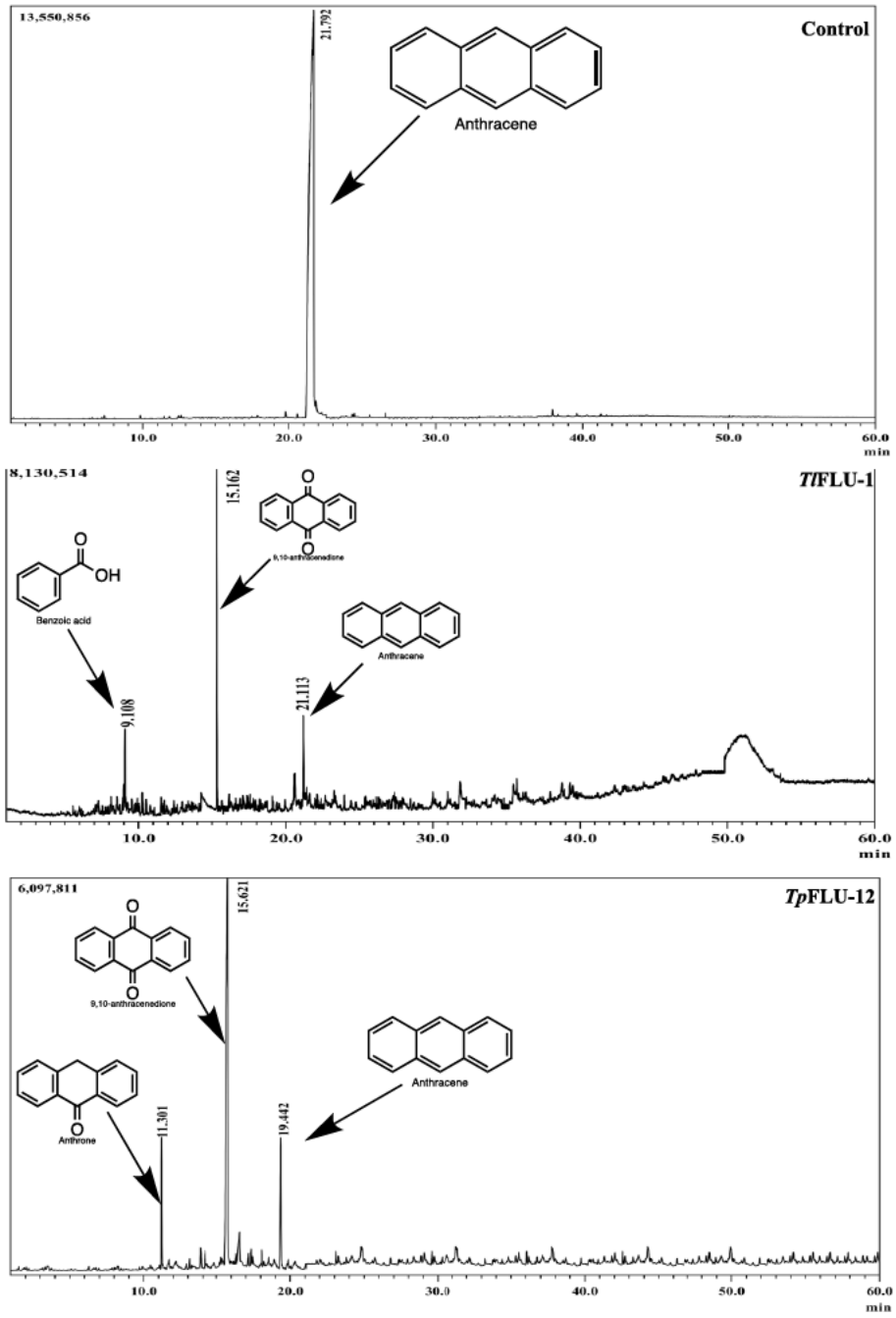

Figure 3. The GC-MS chromatogram of the anthracene mycotransformation peaks identification through the NIST (National Institute of standard technology) library search for control sample (anthracene; 21.792 min), composite sample of *Tl*FLU-1 with retention time (9.108 min for Benzoic acid, 15.162 min for 9,10-anthracenedione and 21.113 min for anthracene) and composite sample of *Tp*FLU-12 (retention time 11.301 min for anthrone, 15.562 for 9,10-anthracenedione and 19.442 min for anthracene)

Table 2: GC-MS profile of the metabolite formed during anthracene degradation.

Metabolites	Retention time (min)		Major m/z of fragment ions (% relative abundance)	Tentative identification
	*Tl*FLU-1	*Tp*FLU-12		
1	21.8		76 (6, M^+), 88 (4), 89 (8), 150 (4), 151 (6) 152 (7), 176 (14),177 (8), 178 (100), 179 (16)	Anthracene
2	15.6	15.2	50 (19, M^+), 75 (17), 76 (44), 150 (15), 151 (78), 152 (78), 180 (100), 181 (14), 208 (98), 209 (15)	9,10 anthracenedione
3	11.3	ND	63 (3, M^+), 82 (7), 139 (4), 163 (7), 164 (6), 165 (53), 166 (10), 193 (9), 194 (100), 195 (15),	Anthrone
4	9.1	ND	50(19, M^+), 51 (3), 74 (8), 76 (6), 77 (66), 78(6), 105(100), 106 (7),122 (83), 123 (7)	Benzoic acid

ND:Not detected

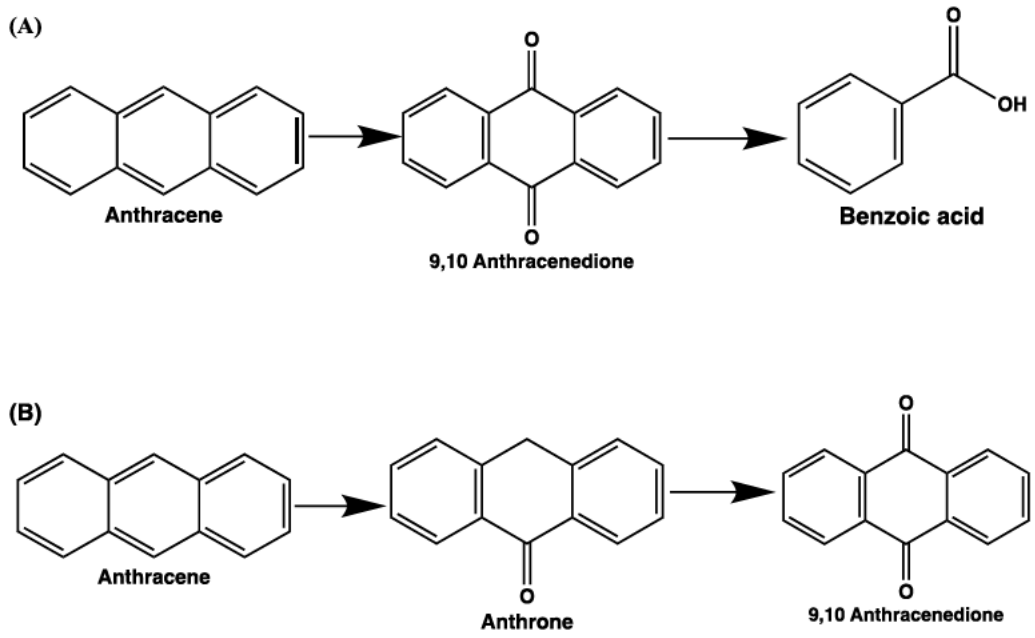

Figure 4: Proposed metabolic pathways for anthracene degradation by *Tl*FLU1(A) and *Tp*FLU12 (B).

3.3. Analysis of the transformed anthracene functional groups:

The FTIR spectra of the changes in the functional group of anthracene metabolites observed in the GC-MS analysis are presented in Table 3, Fig. S2. The parent compound (control; anthracene) showed an intense peak at 3020 cm^{-1} and 1275 cm^{-1} due to the C-H stretch and bending of the aromatic ring while strain *Tl*FLU1 products showed a significant shift in peaks compared to the control set-up. An intense peak was observed at 3170 cm^{-1} due to the C-H vibration stretch of the aromatic rings followed by O-H stretching of the carboxylic acid at 2800 $cm^{-1,}$ while C-H bending of the overtone aromatic ring was recorded at 2000 cm^{-1}. An intense peak at 1740 cm^{-1} is linkable to the vibration stretching of C=O in the carbonyl and ketones skeleton. Additionally, a phenolic O-H bending was observed at 1275 cm^{-1} coupled with an intense peak at 730 cm^{-1} attributable to the C=C benching of the aromatic ring due to a strong di-substitution.

Conversely, in strain *Tp*FLU12 products, a less intense peak was observed compared to strain *Tl*FLU1 products and the parent compound, anthracene. A slight shift to the left with an intense peak at 3100 cm^{-1} was observed due to the C-H vibration on the aromatic rings followed by C=O stretching of quinone carboxylic acid dimers 1675 cm^{-1}. Furthermore, an intense peak at 1275 cm^{-1} is linkable to phenolic O-H bending, while the intense peak at 730 cm^{-1} is attributable to the C=C benching of the aromatic ring due to a strong di-substitution.

Table 3: Assignment of the infrared spectra absorbance bands of anthracene degradation metabolites.

Code	Frequency (cm^{-1})		Assignment
	*Tl*FLU-1	*Tp*FLU-12	
i	3020 - 3170	3100 - 3170	C-H vibration stretch of the aromatic ring
ii	2800	ND	O-H stretch in carboxylic acid
iii	2000	ND	C-H bending overtone of the aromatic ring
iv	1740	ND	vibration stretching of C=O in carbonyl and ketones skeleton
v	1675		C=O stretching of quinone and carboxylic acid dimers
vi	1275		Phenolic O-H bending
vii	1000	ND	C-H bending of the aromatic ring
viii	730		C=C benching of the aromatic ring due to a strong di-substitution

ND:Not detected

3.4. Intracellular and extracellular ligninolytic enzymes profiles during the mycotransformation of anthracene:

The profiles of intracellular and extracellular ligninolytic enzymes produced by the isolates during the mycotransformation of anthracene are illustrated in Fig. 5. In control experiments, where *Tl*FLU1 was inoculated into flasks containing the culture medium (BSM without anthracene), maximum production of 0.0001 U/L was recorded for catechol 1,2 dioxygenase (C12D) which was constant throughout the incubation period and 0.00013 U/L for catechol 2,3 dioxygenase (C23D) on day 12 while for the ligninolytic enzymes, Lac and MnP-like exhibited a maximum activity of 0.05 U/L and 0.001 U/L, respectively, for on day 8. However, no LiP-like activity was observed throughout the incubation period (Fig. 5a). In contrast, in the *Tp*FLU12 flask, there were no intracellular C12D, C23D, Lac, LiP -like and MnP -like activities observed, except for a brief spike in C12D activity on day 16 with maximum activity of 0.0001 U/L and C23D on day 20 with maximum activity of 0.0001 U/L while LiP-like activity reached 0.0010 U/L on day 20 (Fig. 5b). In *Tl*FLU1 inoculated flasks with anthracene, a substantial increase in extracellaur ligninolytic enzymes activity was observed compared to the very low intracellular enzymes activities. Lac, LiP-like and MnP-like reached activity levels of 585 U/L, 49.8 U/L, and 40.3 U/L, respectively, on day 24, with maximum activities achieved on day 12 for Lac and LiP-like and on day 8 for MnP-like while C12D activity reached 7.1 U/L on day 4 and C23D showed a maximum activity of 8.0 U/L on day 8 (Fig. 5c). Similarly, in the *Tp*FLU12 flask, the activities of all ligninolytic enzymes increased steadily over time, culminating at day 24 with maximum activity levels of 97.7 U/L, 55.0 U/L, and 84.1 U/L for Lac, LiP-like, and MnP-like, respectively compared with intracellular enzymes which was so low with maximum activity of 5.3 U/L on day 2 and 3.2 U/L on day 4 for C12D and C23D activities respectively (Fig. 5d).

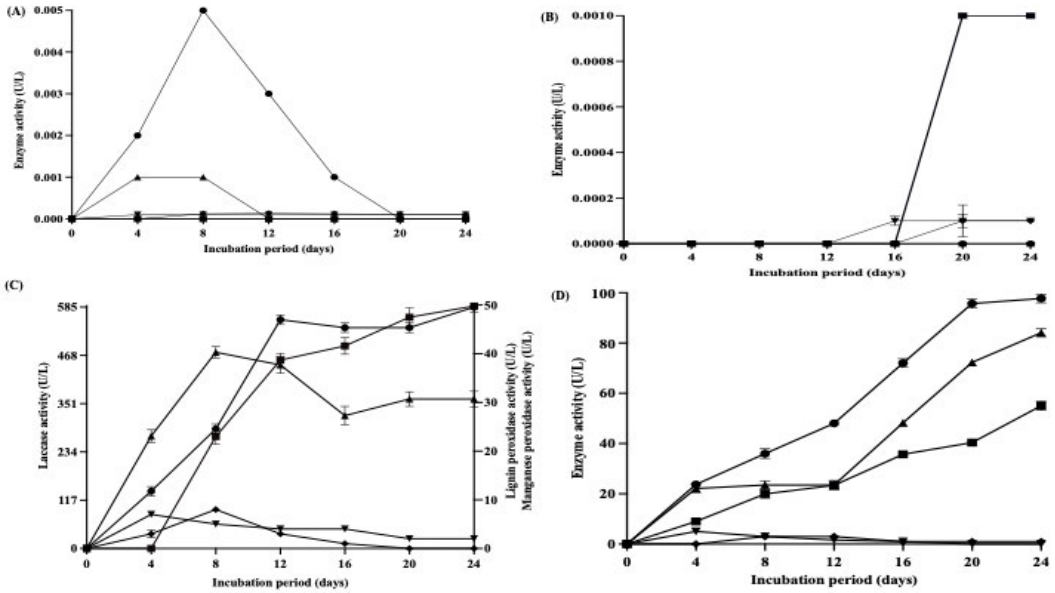

Figure 5. Ligninolytic enzyme activities in response to anthracene degradation by *Tl*FLU1+BSM (A), *Tp*FLU12+BSM (B), *Tl*FLU1+BSM+anthracene (C) and *Tp*FLU12+BSM+anthracene (D). Curves shown are activity of Catechol 1,2 dioxygenase (▼), Catechol 2,3 dioxygenase (◆) Lac (●), LiP-like (■) and MnP-like (▲).

3.5. Ecotoxicity of culture broth following mycotransformation of anthracene:

The profiles of the surviving population of *V. parahaemolyticus* following exposure to culture extracts collected at different incubation periods are shown in Fig. 6. An increase in *V. parahaemolyticus* survival was observed with an increase in daily anthracene degradation products except for *Tl*FLU1 at day 12 while the maximum survival value of 5.72 Log (CFU/mL) was recorded on day 24. In comparison, a value of 6.82 Log (CFU/mL) was observed on day 24 in *Tp*FLU12 inoculated medium, compared to the positive control (No biotransformation product) with a survival population value of 7.90 Log (CFU/mL) (Fig. 6a). Also, *V. parahaemolyticus* surviving population in all samples collected from *Tl*FLU1 and *Tp*FLU12 inoculated medium is statistically significant ($p \leq 0.05$). Effective concentration (EC_{50}) and toxicity unit (TU) of 266.1 mg/L and 0.4% were recorded for *Tl*FLU1 inoculated medium, while 262.3 mg/L and TU 0.4% were obtained for *Tp*FLU12 inoculated medium (Fig. 6b).

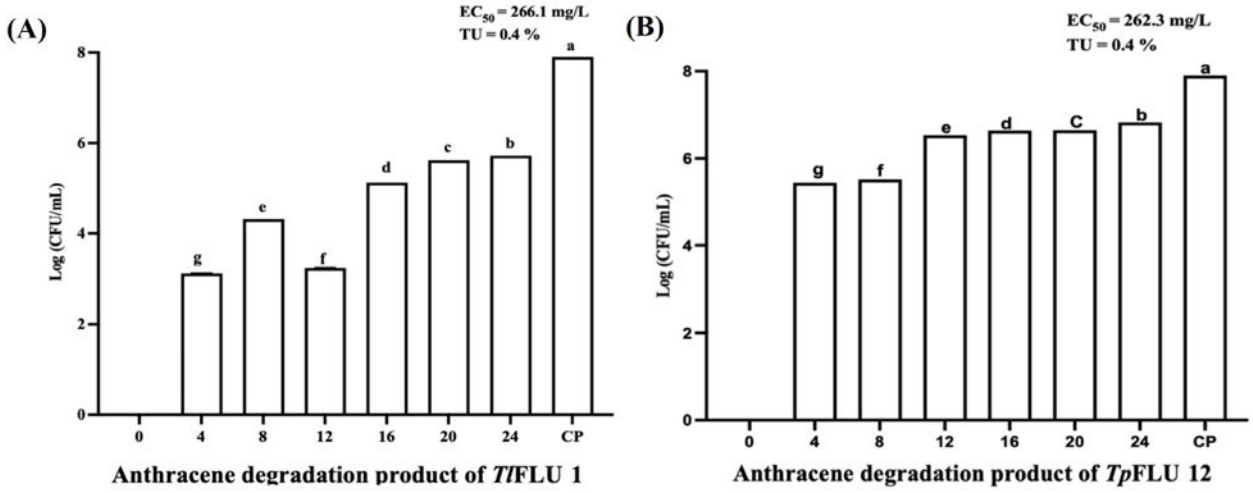

Figure 6. Effective concentration (EC_{50}) and toxicity unit (TU) of daily anthracene toxicants to *V. parahaemolyticus* (log CFU/mL) by *Tl*FLU1 (a) and *Tp*FLU12 (b) after 6 h exposure period. Values with different alphabetic superscripts are statistically significant at $p \leq 0.05$. Key: very toxic (EC50<1mg/L); toxic (1mg/L<EC50≤10mg/L); harmful (10mg/L<EC50≤100mg/L); non-toxic (≥ 100mg/L), CP (positive control: 400 mg/L anthracene). The data was evaluated using nonlinear regression (log (agonist) vs response model) of colony-forming unit (CFU/mL). Additionally, the bacterium survival data (log CFU/mL) was subjected to analysis of variance (ANOVA) while its means were ranked with Bonferroni's multiple comparisons test (BMCT) at $p \leq 0.05$.

4. Discussion

Fungi, being the most abundant free-living ubiquitous microorganism, are a significant determinant of PAHs fate in both terrestrial and aquatic ecosystems through mycotransformation process [39]. Mycotransformation of PAHs often commences with high PAHs concentration tolerance and low inhibition rate [40]. Factors like molecular weight, benzene rings count, concentrations, pH and temperature play a major role during PAHs degradation by fungi in the natural environment which then leads to unprecedented acute and chronic environmental toxicity[41,42].

The indigenous fungal strains *Tl*FLU1 and *Tp*FLU12 used here could utilize anthracene as carbon and energy sources and have been documented as ascomycetes strains with a strong affinity for PAHs [30]. Although it is known that complete mineralization of PAHs by fungi starts from their tolerance levels. The data from solid plating assay (Table S1) revealed that fungi tolerance to high anthracene concentrations is not directly proportional to their degradation efficiency but rather a function of ligninolytic enzyme secretion as shown in Figures 1 and 4. This observation is consistent with a recent report where tolerance to complex hydrocarbons by fungi was linked to the production of ligninolytic enzymes [43]. The efficiency of anthracene transformation varies among the two fungal strains where *Tp*FLU12 was found to be more efficient than *Tl*FLU1 by degrading 56% of anthracene with a dry biomass production of 645.6 mg/L and extracellular protein content of 760 mg/L. Similarly, other studies have reported high degradation rates of anthracene by various fungal strains, such as *Aspergillus fumigatus* (60% after 5 days) [44] *Pycnoporus sanguineus* H1 (67.5% under in vivo conditions after 14 days) [45], and *Armillaria* sp. F022 (92% within 30 days) [46]. Moreover, pH was observed to play a significant role during anthracene mycotransformation with a slight reduction in the pH medium of *Tl*FLU1 inoculated flask (Fig. 2). This observation could be attributed to the production of some

acidic metabolites, such as benzoic acid during the degradation process [44], Similarly, a recent study [47], demonstrates the ability of ascomycetes fungi to optimally degrade PAHs such as fluorene, pyrene, BaP effectively at a pH of 5 and 7 which corroborate the results from the present study. Additionally, the increase in media pH recorded in *Tp*FLU12 could be ascribed to anthracene metabolism linked to the production of a ligninolytic enzyme [48]. The complete metabolism of a PAH compound at a pH close to the current study (pH 7) due to the induction of ligninolytic enzymes during the optimization process is also documented [17]. Also, a previous study revealed that the metabolism of polyaromatic compounds by fungi is best enhanced at a pH range between 7 and 9 [49].

The degradation kinetics is a highly imperative tool for assessing total pollutant removal [33]. The observed zero and first-order kinetics fitting during the anthracene degradation by these indigenous fungi attest to the general proposition for microbial metabolism of PAHs, especially fungi [50,51]. The low rate constant (K) and high half-life ($t_{1/2}$) recorded in the first-order kinetics indicate that anthracene degradation by these fungi is both concentration and time-dependent [52]. Likewise, a report [51] showed that the degradation rate constant is $1/\propto$ to the low half-life period ($t_{1/2}$ = 4.2 d) of the substrate.

The GC-MS analysis established that anthracene mycotransformation proceed through an initial attack at the C-9 and C-10 position of anthracene *via* oxygenation to form either anthrone or 9,10-anthracenedione before undergoing a spontaneous tautomeric benzoic acid formation due to the hydroxylation and ring cleavage at the C-9 and C-10 position (Table 2). This novel metabolic pathway has been identified during anthracene degradation by marine fungi *Cladosporium sp*. CBMAI 1237 [53]. A similar observation [18], where anthracene degradation pathways in fungi were initiated at C-9 and C-10 to form anthraquinone and end with the formation of phthalic acid is available. However, the appearance of benzoic acid in pathway described in the present study (Fig. 3.) is not uncommon because phthalic acid and benzoic acid are known as a gateway to the TCA cycle during anthracene metabolism [54]. Also, the appearance of a quinone derivative (9,10-anthracenedione) as a dead-end product during anthracene degradation by isolate *Tp*FLU-12 is not unusual in the anthracene metabolic pathway [48].

The FTIR spectrum results (Table 3, Fig. S2) further strengthen the proposed anthracene degradation pathways, with products consisting of quinones derivatives, C-H stretch and bending of the aromatic ring, stretching O-H in carboxylic acid to form benzoic acid, expansion of C=O in carboxylic acids, O-H stretching of the carboxylic acid, C=O in carbonyl and ketones skeleton, bending of phenol O-H, C-C expansion in aromatic rings, C-H vibration of the aromatic rings and C = C-H: C-H bend in alkanes. The appearance of these functional groups has been attributed to features of PAHs metabolic pathway during the degradation of pyrene by *C. byrsina* strain APC5 [37]. A similar functional group has been documented while yeast mediated degradation of BaP using a 3-level Box-Behnken design [55]. Also, the presence of O-H dimer is indicative of the complete degradation of anthracene into less toxic products [56].

Recent studies have confirmed that fungi specifically from the ascomycota phylum often employ a variety of enzymes, including LiP, versatile peroxidase, MnP, Lac, cytochrome P450 monooxygenases, and epoxide hydrolases to degrade PAHs [57-60]. This study observed that interplay between intracellular (C12D and C23D) and extracellular enzymes (Lac, LiP-like and MnP-like) produced by ascomycetes fungi (*Tl*FLU1 and *Tp*FLU12) play a crucial role in the mycotransformation process of anthracene. This observation is consistent with previous studies which linked these enzymes to the mechanism used by yeast consortia during the breakdown of perylene and benzo[ghi]perylene individually when used a sole carbon source (Mandal and Das, 2018). Similar enzymes have been reported in *Trichoderma* sp. 109, a strain akin to *Tl*FLU1 in the degradation of phenanthrene as a

sole carbon source [61]. The role of intracellular enzymes C12D and C23D are of significant interest because they seem to be produced at their highest levels in the whole fungi at different stages (4 and 8-d respectively). This suggests they might be the first step in how anthracene is transformed. However, it was not entirely clear how involved these intracellular enzymes were because they were found in much lower amounts compared to the extracellular ligninolytic enzymes (Lac, LiP-like, and MnP-like) in both the whole fungi and the broth, regardless of whether anthracene was present. The most probable explanation for the detection of these intracellular enzymes in the early stage of the transformation process could be linked to the fungal strains defense system against oxidative stress, reactive oxygen species and ATP synthesis. This opinion aligns with a previous report [62] where MnP-like peroxidase activity was detected during the early stage of PAHs degradation which was linked to response against oxidative stress rather than been involved in the degradation of PAHs by *T. asperellum* H15. Therefore, the role of intracellular enzymes C12D and C23D in fungi, particularly in the early stages of anthracene transformation, is likely linked to the fungal strain's defense system against oxidative stress and ATP synthesis [63,64]. These enzymes are part of the fungal cell wall integrity signaling pathway, which is involved in the production of secondary metabolites [65]. Additionally, the structural analysis of anthracene derivatives like anthraquinone-fused enediynes sheds light on their biosynthetic pathways and their potential defense system mechanisms interactions with reactive oxygen species due to production of intracellular enzymes like C12D and C23 [66,67]. However, another potential intracellular enzyme, cytochrome P450, might be responsible for the initial transformation mechanism used by these fungi since they have been reported in *Penicillium oxalicum* when anthracene was used as a carbon source during its transformation process [48]. Further, overexpression of lac, LiP-like and MnP-like genes was observed in PAH-contaminated marine sediments belonging to Eurotiales, specifically *Talaromyces helices* and *Trichoderma* sp. during PAHs biotransformation [68]. An account of the induction of Lac, LP-like and MnP-like during the removal of manganese and phenanthrene with a removal efficiency of 92.17 and 93.85 % respectively by *P. eryngii* also reported [69]. Similarly, some authors [32], implicated the secretion of LP-like, MnP-like and Lac by *T. polyzona* RYNF13 in the degradation of fluorene, phenanthrene and pyrene. In addition, LiP-like, MnP-like and Lac have been linked to ring cleavage via oxidation, carboxylation and decarboxylation in various PAHs degradation pathways [17]. The significant role played by ligninolytic enzymes in the degradation of complex hydrocarbons such as aliphatic and PAH by ascomycete fungus, *Penicillium* sp. CHY-2 was demonstrated for the degradation of decane (49.0%), butylbenzene (42.0%) and dodecane (33.0%) and naphthalene (15.0%), acenaphthene (10.0%), octane (8.0%), ethylbenzene (4.0%) and benzo[a]pyrene (2.0%) [70].

Studies on PAHs' mycotransformation should not be limited to its complete disappearance alone or transient product formation, but the assessment of toxic intermediate products formed to evaluate its actual environmental impact. The ecotoxicity assays data revealed metabolites formed induced acute toxicity despite a significant reduction in parent compound concentration. A similar report [71] also available where metabolites of bisphenol degradation showed higher toxicity than bisphenol. The low survival of marine bacteria exposed to the toxicant (degradation products), in contrast to the high survival in the positive control group (No PAHs), could be attributed to the formation of oxygen-containing PAHs, specifically quinone derivatives. Quinone derivatives are recognized for their role as direct-acting mutagens, as noted in previous studies [72,73] further underscores their capacity to induce toxicity. Although an increase in the surviving population of the marine bacterium after the exposure to the anthracene-containing medium undergoing myco-degradation demonstrated a reduction in acute toxicity of the parent compound over treatment time, the observed reduced population on day 12 of *Tl*FLU1 inoculated medium (Fig. 5) revealed that toxicity level is not a function of contaminants concentration [74]. In addition, the recorded high EC_{50} and low TU values indicate metabolic

products accumulate during the mycotransformation process as a non-toxic product [56]. The observed reduction in the population of the marine bacterium on day 12 toxicant from *Tl*FLU1 could be attributed to the toxicity due to aromatic structure with *ortho-substituted* C=O and -OH groups formed during the degradation process [75]. Also, the observed reduction in toxicity suggest marine bacterium can be used as cheap bioassay protocol in the environmental risk assessment of organo-pollutant like anthracene and its metabolites because of their sensitivity to toxicants [76].

5. Conclusions

The study ascertained the tolerance levels of the fungal strains to varying anthracene concentrations on a solid agar plate, the role of ligninolytic enzymes in response to anthracene tolerance and its mycotransformation efficiency, kinetics and the detection of intermediates formed along with the effects on *Vibrio parahaemolyticus* survival. Both isolates under study, *Tl*FLU1 *and Tp*FLU12, could tolerate anthracene concentration up to 1000 mg/L, with ligninolytic enzymes linked to the tolerance rate and degradation efficiency. Intracellular enzymes could be involved in the initial mechanism employed by these fungi for the transformation process or may have been produced as a defense system against oxidative stress, reactive oxygen species and ATP synthesis. However, further genomics and secretome studies are required to confirm this observation. Both isolates best fitted zero and first order kinetics leading to accumulation of non-toxic transient products. The high EC_{50} and low TU values suggest that the accumulated toxicants in the anthracene degradation pathway are toxic. Additionally, the presence of aromatic structures featuring *ortho-substituted* C=O and -OH groups was linked to a noteworthy decrease in the marine bacteria survival when exposed to anthracene mycotransformation toxicants compared to the positive control (no anthracene or mycotransformation products present). Thus, this observation highlights the possible use of these fungal strains in the amelioration of PAHs contaminated sites and supports the notion of using solid plate techniques as a cheap, fast and sustainable procedure in selecting a high PAHs tolerance strain which are effective in degrading PAHs to non-toxic bye-products.

Supplementary Materials: The following supporting information can be downloaded at: www.mdpi.com/xxx/s1, Figure S1: Anthracene degradation kinetic modelling (A) zero order, (B) first order, (C) second order. Key: *Tl*FLU1 (●), *Tp*FLU12 (■), d = days. Figure S2: FTIR spectra of anthracene myco-transformation metabolites.

Author Contributions: Conceptualization, S.O.E. and A.O.O.; methodology, S.O.E. and A.K.; validation, S.O.E., A.K., and A.O.O.; formal analysis, S.O.E. and A.K.; investigation, S.O.E. and A.O.O.; resources, M.P.M. and A.O.O.; data curation, S.O.E. and A.K.; writing-S.O.E.; writing-A.K. and A.O.O.; visualization, S.O.E.; supervision, M.P.M. and A.O.O.; project administration, A.O.O.; funding acquisition, A.O.O. and M.P.M. All authors have read and agreed to the published version of the manuscript. All authors have read and agreed to the published version of the manuscript." P

Funding: National Research Foundation, South Africa. (Dr. Mduduzi P. Mokoena: 94036, Prof. Ademola Olaniran: 92803).

Institutional Review Board Statement: "Not applicable".

Informed Consent Statement: "Not applicable."

Data Availability Statement: Data is contained within the article or supplementary material.

Acknowledgments: S.O.E. Thanks University of KwaZulu Natal, Durban, South Africa for Ph.D. scholarship.

Conflicts of Interest: The authors declare no conflict of interest.

References:

1. Nacher-Mestre, J.; Serrano, R.; Portoles, T.; Berntssen, M.H.G.; Perez-Sanchez, J.; Hernandez, F. Screening of pesticides and polycyclic aromatic hydrocarbons in feeds and fish tissues by gas chromatography coupled to high-resolution mass spectrometry using atmospheric pressure chemical ionization. *J Agric Food Chem* **2014**, *62*, 2165-2174, doi:10.1021/jf405366n.
2. Baran, A.; Tarnawski, M.; Urbański, K.; Klimkowicz-Pawlas, A.; Spałek, I. Concentration, sources and risk assessment of PAHs in bottom sediments. *Environ. Sci Pollut Res* **2017**, *24*, 23180-23195, doi:10.1007/s11356-017-9944-y.
3. Souza, H.M.L.; Taniguchi, S.; Bícego, M.C.; Oliveira, L.A.; Oliveira, T.C.S.; Barroso, H.S.; Zanotto, S.P. Polycyclic aromatic hydrocarbons in superficial sediments of the Negro river in the Amazon region of Brazil. *J Braz Chem Soc* **2015**, *26*, 1438-1449, doi:10.5935/0103-5053.20150112.
4. Yang, S.Y.N.; Connell, D.W.; Hawker, D.W.; Kayal, S.I. Polycyclic aromatic hydrocarbons in air, soil and vegetation in the vicinity of an urban roadway. *Sci Total Environ* **1991**, *102*, 229-240, doi:https://doi.org/10.1016/0048-9697(91)90317-8.
5. Gao, J.P.; Maguhn, J.; Spitzauer, P.; Kettrup, A. Distribution of Polycyclic Aromatic Hydrocarbons (PAHs) in Pore Water and Sediment of a Small Aquatic Ecosystem. *Int J Environ Anal Chem* **1998**, *69*, 227-242, doi:10.1080/03067319808032589.
6. Terzi, E.; Samara, C. Gas-particle partitioning of polycyclic aromatic hydrocarbons in urban, adjacent coastal, and continental background sites of western Greece. *Environ Sci Technol* **2004**, *38*, 4973-4978, doi:10.1021/es040042d.
7. Wilcke, W.; Bandowe, B.A.M.; Lueso, M.G.; Ruppenthal, M.; del Valle, H.; Oelmann, Y. Polycyclic aromatic hydrocarbons (PAHs) and their polar derivatives (oxygenated PAHs, azaarenes) in soils along a climosequence in Argentina. *Sci Total Environ* **2014**, *473-474*, 317-325, doi:https://doi.org/10.1016/j.scitotenv.2013.12.037.
8. Childerns's environment health: Chemicals of special concern to children's health. **2019**, doi:https://www.health.state.mn.us/communities/environment/childenvhealth/chemicals.html#:~:text=Arsenic%2C%20Mercury%2C%20Lead%2C%20Cadmium.
9. Rengarajan, T.; Rajendran, P.; Nandakumar, N.; Lokeshkumar, B.; Rajendran, P.; Nishigaki, I. Exposure to polycyclic aromatic hydrocarbons with special focus on cancer. *Asian Pac J Trop Biomed* **2015**, *5*, 182-189, doi:10.1016/S2221-1691(15)30003-4.
10. Ellickson, K.M.; Herbrandson, C.; Krause, M.J.; Pratt, G.C.; Kellock, K.A. Comparative risk estimates of an expanded list of PAHs from community and source-influenced air sampling. *Chemosphere* **2020**, *253*, 126680-126680, doi:10.1016/j.chemosphere.2020.126680.
11. Jajoo, A.; Mekala, N.R.; Tomar, R.S.; Grieco, M.; Tikkanen, M.; Aro, E.M. Inhibitory effects of polycyclic aromatic hydrocarbons (PAHs) on photosynthetic performance are not related to their aromaticity. *J Photochem Photobiol B, Biol* **2014**, *137*, 151-155, doi:10.1016/j.jphotobiol.2014.03.011.
12. Eeshwarasinghe, D.; Loganathan, P.; Vigneswaran, S. Simultaneous removal of polycyclic aromatic hydrocarbons and heavy metals from water using granular activated carbon. *Chemosphere* **2019**, *223*, 616-627, doi:10.1016/j.chemosphere.2019.02.033.
13. Adnan, L.A.; Sathishkumar, P.; Yusoff, A.R.M.; Hadibarata, T.; Ameen, F.; Rahim, A.; Yusoff, M. Rapid bioremediation of Alizarin Red S and Quinizarine Green SS dyes using *Trichoderma lixii* F21 mediated by biosorption and enzymatic processes. *Bioprocess Biosyst Eng* **2016**, *40*, 85-97, doi:10.1007/s00449-016-1677-7.
14. Adenipekun, C.O.; Ipeaiyeda, A.R.; Olayonwa, A.J.; Egbewale, S.O. Biodegradation of polycyclic aromatic hydrocarbons (PAHs) in spent and fresh cutting fluids contaminated soils by *Pleurotus pulmonarius* (Fries). Quelet and *Pleurotus ostreatus* (Jacq .) Fr . P . Kumm. *Afr J Biotechnol* **2015**, *14*, 661-667, doi:10.5897/AJB2014.14187.
15. Bilal, M.; Adeel, M.; Rasheed, T.; Zhao, Y.; Iqbal, H.M.N. Emerging contaminants of high concern and their enzyme-assisted biodegradation – a review. *Environ Int* **2019**, *124*, 336-353, doi:10.1016/j.envint.2019.01.011.
16. Hadibarata, T.; Kristanti, R.A. Identification of metabolites from benzo[a]pyrene oxidation by ligninolytic enzymes of *Polyporus* sp. S133. *J Environ Manage* **2012**, *111*, 115-119, doi:10.1016/j.jenvman.2012.06.044.
17. Bankole, P.O.; Semple, K.T.; Jeon, B.H.; Govindwar, S.P. Biodegradation of fluorene by the newly isolated marine-derived fungus, *Mucor irregularis* strain bpo1 using response surface methodology. *Ecotoxicol Environ Saf* **2021**, *208*, 111619-111619, doi:10.1016/j.ecoenv.2020.111619.
18. Jove, P.; Olivella, M.A.; Camarero, S.; Caixach, J.; Planas, C.; Cano, L.; De Las Heras, F.X. Fungal biodegradation of anthracene-polluted cork: A comparative study. *J Environ Sci Health - Toxic/Hazard Subst. Environ Eng* **2016**, *51*, 70-77, doi:10.1080/10934529.2015.1079114.
19. Mtibaà, R.; Barriuso, J.; de Eugenio, L.; Aranda, E.; Belbahri, L.; Nasri, M.; Martínez, M.J.; Mechichi, T. Purification and characterization of a fungal laccase from the ascomycete *Thielavia* sp. and its role in the decolorization of a recalcitrant dye. *Int Biodeteriorat Biodegrad* **2018**, *120*, 1744-1751, doi:10.1016/j.ijbiomac.2018.09.175.
20. Asemoloye, M.D.; Ahmad, R.; Jonathan, S.G. Transcriptomic responses of catalase, peroxidase and laccase encoding genes and enzymatic activities of oil spill inhabiting rhizospheric fungal strains. *Environ Pollut* **2018**, *235*, 55-64, doi:10.1016/j.envpol.2017.12.042.

21. Hammel, K.E.; Green, B.; Gai, W.Z. Ring fission of anthracene by a eukaryote. *PNAS USA* **1991**, *88*, 10605-10608, doi:10.1073/pnas.88.23.106.
22. Kimani, V.; Ullrich, R.; Büttner, E.; Herzog, R.; Kellner, H.; Jehmlich, N.; Hofrichter, M.; Liers, C. First dye-decolorizing peroxidase from an ascomycetous fungus secreted by *Xylaria grammica*. *Biomolecules* **2021**, *11*, 1391, doi:0.3390/biom11091391.
23. Morgenstern, I.; Klopman, S.; Hibbett, D.S. Molecular evolution and diversity of lignin degrading heme peroxidases in the Agaricomycetes. *J Mol Evol* **2008**, *66*, 243-257, doi:10.1007/s00239-008-9079-3.
24. Zámocký, M.; Tafer, H.; Chovanová, K.; Lopandic, K.; Kamlárová, A.; Obinger, C. Genome sequence of the filamentous soil fungus *Chaetomium cochliodes* reveals abundance of genes for heme enzymes from all peroxidase and catalase superfamilies. *BMC genomics* **2016**, *17*, 1-15, doi:10.1186/s12864-016-3111-6.
25. Zeiner, C.A.; Purvine, S.O.; Zink, E.M.; Paša-Tolić, L.; Chaput, D.L.; Haridas, S.; Wu, S.; LaButti, K.; Grigoriev, I.V.; Henrissat, B. Comparative analysis of secretome profiles of manganese (II)-oxidizing Ascomycete fungi. *PloS One* **2016**, *11*, e0157844, doi:10.1371/journal.pone.0157844.
26. Turek, A.; Wieczorek, K.; Wolf, W.M. Digestion procedure and determination of heavy metals in sewage sludge-an analytical problem. *Sustainability* **2019**, *11*, 4-10, doi:10.3390/su11061753.
27. Jarque, S.; Masner, P.; Klánová, J.; Prokeš, R.; Bláha, L. Bioluminescent *Vibrio fischeri* assays in the assessment of seasonal and spatial patterns in toxicity of contaminated river sediments. *Front Microbiol* **2016**, *7*, 1-11, doi:10.3389/fmicb.2016.01738.
28. Rotini, A.; Manfra, L.; Spanu, F.; Pisapia, M.; Cicero, A.M.; Migliore, L. Ecotoxicological method with marine bacteria *Vibrio anguillarum* to evaluate the acute toxicity of environmental contaminants. *J Vis Exp* **2017**, 55211-55211, doi:10.3791/55211.
29. Saraswathy, A.; Hallberg, R. Degradation of pyrene by indigenous fungi from a former gasworks site. *FEMS Microbiol Lett* **2002**, *210*, 227-232, doi:10.1111/j.1574-6968.2002.tb11185.x.
30. Egbewale, S.O.; Kumar, A.; Mokoena, M.P.; Olaniran, A.O. Metabolic biodegradation pathway of fluoranthene by indigenous *Trichoderma lixii* and *Talaromyces pinophilus* spp. *Catalysts* **2023**, *13*, 791, doi:10.3390/catal13050791.
31. Argumedo-Delira, R.; Alarcón, A.; Ferrera-Cerrato, R.; Almaraz, J.J.; Peña-Cabriales, J.J. Tolerance and growth of 11 Trichoderma strains to crude oil, naphthalene, phenanthrene and benzo[a]pyrene. *J Environ Manage* **2012**, *95*, S291-S299, doi:https://doi.org/10.1016/j.jenvman.2010.08.011.
32. Teerapatsakul, C.; Pothiratana, C.; Chitradon, L.; Thachepan, S. Biodegradation of polycyclic aromatic hydrocarbons by a thermotolerant white rot fungus *Trametes polyzona* RYNF13. *J Gen Appl Microbiol* **2016**, *62*, 303-312, doi:10.2323/jgam.2016.06.001.
33. Ortega-González, D.K.; Cristiani-Urbina, E.; Flores-Ortíz, C.M.; Cruz-Maya, J.A.; Cancino-Díaz, J.C.; Jan-Roblero, J. Evaluation of the removal of pyrene and fluoranthene by *Ochrobactrum anthropi*, *Fusarium* sp. and their coculture. *Appl Biochem Biotechnol* **2015**, *175*, 1123-1138, doi:10.1007/s12010-014-1336-x.
34. Teh, Z.C.; Hadibarata, T. Enhanced degradation of pyrene and metabolite identification by *Pleurotus eryngii* F032. *Water Air Soil Pollut* **2014**, *225*, 1-8, doi:10.1007/s11270-014-1909-x.
35. Mandal, S.K.; Das, N. Biodegradation of perylene and benzo [ghi] perylene (5-6 rings) using yeast consortium: Kinetic study, enzyme analysis and degradation pathway. *J Environ Biol* **2018**, *39*, 5-15, doi:10.22438/jeb/39/1/MRN-540.
36. Patel, H.; Gupte, A.; Gupte, S. Biodegradation of fluoranthene by basidiomycetes fungal isolate *Pleurotus ostreatus* HP-1. *Appl Biochem Biotechnol* **2009**, *157*, 367-376, doi:10.1007/s12010-008-8286-0.
37. Agrawal, N.; Shahi, S.K. Degradation of polycyclic aromatic hydrocarbon (pyrene) using novel fungal strain *Coriolopsis byrsina* strain APC5. *International Biodeterioration and Biodegradation* **2017**, *122*, 69-81, doi:10.1016/j.ibiod.2017.04.024.
38. Lin, Z.; Du, J.; Yin, K.; Wang, L.; Yu, H. Mechanism of concentration addition toxicity: they are different for nonpolar narcotic chemicals, polar narcotic chemicals and reactive chemicals. *Chemosphere* **2004**, *54*, 1691-1701, doi:10.1016/J.CHEMOSPHERE.2003.09.031.
39. Ghosal, D.; Ghosh, S.; Dutta, T.K.; Ahn, Y. Current state of knowledge in microbial degradation of polycyclic aromatic hydrocarbons (PAHs): A review. *Front Microbiol* **2016**, *7*, 1369, doi:10.3389/fmicb.2016.01369.
40. de Lima Souza, H.M.; Sette, L.D.e.; da Mota, A.J.; do Nascimento Neto, J.F.; Rodrigues, A.; de Oliveira, T.s.B.; de Oliveira, F.M.; de Oliveira, L.A.n.; dos Santos Barroso, H.; Zanotto, S.P. Filamentous fungi isolates of contaminated sediment in the amazon region with the potential for benzo(a)pyrene degradation. *Water Air Soil Pollut* **2016**, *227*, 431, doi:10.1007/s11270-016-3101-y.
41. Lahkar, J.; Deka, H. Isolation of polycyclic aromatic hydrocarbons (pahs) degrading fungal candidate from oil-contaminated soil and degradation potentiality study on anthracene. *Polycycl Aromat Compd* **2017**, *37*, 141-147, doi:10.1080/10406638.2016.1220957.
42. Daccò, C.; Nicola, L.; Temporiti, M.E.E.; Mannucci, B.; Corana, F.; Carpani, G.; Tosi, S. Trichoderma: Evaluation of its degrading abilities for the bioremediation of hydrocarbon complex mixtures. *Appl Sci* **2020**, *10*, 3152-3152, doi:10.3390/APP10093152.
43. Asemoloye, M.D.; Tosi, S.; Daccò, C.; Wang, X.; Xu, S.; Marchisio, M.A.; Gao, W.; Jonathan, S.G.; Pecoraro, L. Hydrocarbon degradation and enzyme activities of *Aspergillus oryzae* and *Mucor irregularis* isolated from nigerian crude oil-polluted sites. *Microorganisms* **2020**, *8*, 1-19, doi:10.3390/microorganisms8121912.

44. Ye, J.-s.; Yin, H.; Qiang, J.; Peng, H.; Qin, H.-m. Biodegradation of anthracene by *Aspergillus fumigatus*. *J Hazard Mater* **2011**, *185*, 174-181, doi:10.1016/j.jhazmat.2010.09.015.
45. Zhang, S.; Ning, Y.; Zhang, X.; Zhao, Y.; Yang, X.; Wu, K.; Yang, S.; La, G.; Sun, X.; Li, X. Contrasting characteristics of anthracene and pyrene degradation by wood rot fungus Pycnoporus sanguineus H1. *Int Biodeterior Biodegrad* **2015**, *105*, 228-232, doi:https://doi.org/10.1016/j.ibiod.2015.09.012.
46. Hadibarata, T.; Zubir, M.M.F.A.; Rubiyatno; Chuang, T.Z.; Yusoff, A.R.M.; Salim, M.R.; Fulazzaky, M.A.; Seng, B.; Nugroho, A.E. Degradation and transformation of anthracene by white-rot fungus Armillaria sp. F022. *Folia Microbiol* **2013**, *58*, 385-391, doi:10.1007/s12223-013-0221-2.
47. Vipotnik, Z.; Michelin, M.; Tavares, T. Ligninolytic enzymes production during polycyclic aromatic hydrocarbons degradation: effect of soil pH, soil amendments and fungal co-cultivation. *Biodegradation* **2021**, *32*, 193-215, doi:10.1007/S10532-021-09933-2/METRICS.
48. Aranda, E.; Godoy, P.; Reina, R.; Badia-Fabregat, M.; Rosell, M.; Marco-Urrea, E.; García-Romera, I. Isolation of Ascomycota fungi with capability to transform PAHs: Insights into the biodegradation mechanisms of *Penicillium oxalicum*. *International Biodeterioration and Biodegradation* **2017**, *122*, 141-150, doi:10.1016/j.ibiod.2017.05.015.
49. Batista-garcía, A.; Vinoth, V.; Ariste, A.; Tovar-herrera, O.E.; Savary, O.; Peidro-guzm, H.; Jackson, S.A.; Dobson, A.D.W.; Gonz, D.; Folch-mallol, J.L.; et al. Simple screening protocol for identification of potential mycoremediation tools for the elimination of polycyclic aromatic hydrocarbons and phenols from hyperalkalophile industrial effluents. *J Environ Manage* **2017**, *198*, 1-11, doi:10.1016/j.jenvman.2017.05.010.
50. Mishra, S.; Singh, S.N.; Pande, V. Bacteria induced degradation of fluoranthene in minimal salt medium mediated by catabolic enzymes in vitro condition. *Bioresour Technol* **2014**, *164*, 299-308, doi:10.1016/j.biortech.2014.04.076.
51. Jauhari, N.; Mishra, S.; Kumari, B.; Singh, S.N.; Chauhan, P.S.; Upreti, D.K. Bacteria induced degradation of anthracene mediated by catabolic enzymes. *Polycycl Aromat Compd* **2020**, *40*, 313-325, doi:10.1080/10406638.2017.1420667.
52. Mandal, S.K.; Ojha, N.; Das, N. Process optimization of benzo [ghi] perylene biodegradation by yeast consortium in presence of ZnO nanoparticles and produced biosurfactant using Box-Behnken design. *Frontiers in Biology* **2018**, 418–424, doi:https://doi.org/10.1007/s11515-018-1523-1.
53. Birolli, W.G.; de A. Santos, D.; Alvarenga, N.; Garcia, A.C.F.S.; Romão, L.P.C.; Porto, A.L.M. Biodegradation of anthracene and several PAHs by the marine-derived fungus *Cladosporium* sp. CBMAI 1237. *Mar Pollut Bull* **2018**, *129*, 525-533, doi:10.1016/j.marpolbul.2017.10.023.
54. Hadibarata, T.; Khudhair, A.B.; Salim, M.R. Breakdown products in the metabolic pathway of anthracene degradation by a ligninolytic fungus *Polyporus* sp. S133. *Water Air Soil Pollut* **2012**, *223*, 2201-2208, doi:10.1007/s11270-011-1016-1.
55. Mandal, S.K.; Ojha, N.; Das, N. Optimization of process parameters for the yeast mediated degradation of benzo[a]pyrene in presence of ZnO nanoparticles and produced biosurfactant using 3-level Box-Behnken design. *Ecol Eng* **2018**, *120*, 497-503, doi:10.1016/j.ecoleng.2018.07.006.
56. Arunprasath, T.; Sudalai, S.; Meenatchi, R.; Jeyavishnu, K.; Arumugam, A. Biodegradation of triphenylmethane dye malachite green by a newly isolated fungus strain. *Biocatal Agric Biotechnol* **2019**, *17*, 672-679, doi:10.1016/j.bcab.2019.01.030.
57. Kadri, T.; Rouissi, T.; Brar, S.K.; Cledon, M.; Sarma, S.; Verma, M. Biodegradation of polycyclic aromatic hydrocarbons (PAHs) by fungal enzymes: A review. *J Environ Sci* **2017**, *51*, 52-74, doi: 10.1016/j.jes.2016.08.023.
58. Balaji, V.; Arulazhagan, P.; Ebenezer, P. Enzymatic bioremediation of polyaromatic hydrocarbons by fungal consortia enriched from petroleum contaminated soil and oil seeds. *Journal of Environmental Biology* **2014**, *35*, 521-529.
59. Aranda, E. Promising approaches towards biotransformation of polycyclic aromatic hydrocarbons with Ascomycota fungi. *Current Opinion in Biotechnology* **2016**, *38*, 1-8, doi:10.1016/j.copbio.2015.12.002.
60. Pozdnyakova, N.N. Involvement of the ligninolytic system of White-Rot and litter-decomposing fungi in the degradation of polycyclic aromatic hydrocarbons. *Biotechnol Res Int* **2012**, *2012*, 20-20, doi:doi:10.1155/2012/243217.
61. Hadibarata, T.; Tachibana, S.; Itoh, K. Biodegradation of phenanthrene by fungi screened from nature. *Pakistan Journal of Biological Sciences* **2007**, *10*, 2535-2543, doi: 10.3923/pjbs.2007.2535.2543.
62. Zafra, G.; Moreno-Montaño, A.; Absalón, Á.E.; Cortés-Espinosa, D.V. Degradation of polycyclic aromatic hydrocarbons in soil by a tolerant strain of *Trichoderma asperellum*. *Environmental Science and Pollution Research* **2015**, *22*, 1034-1042, doi:10.1007/s11356-014-3357-y.
63. Lebeda, A.; Luhová, L.; Sedlářová, M.; Jančová, D. The role of enzymes in plant-fungal pathogens interactions. *J Plant Diseases Protect* **2001**, 89-111, doi:https://www.jstor.org/stable/43215387.
64. Camacho-Morales, R.L.; García-Fontana, C.; Fernández-Irigoyen, J.; Santamaría, E.; González-López, J.; Manzanera, M.; Aranda, E. Anthracene drives sub-cellular proteome-wide alterations in the degradative system of *Penicillium oxalicum*. *Ecotoxicol Environ Saf* **2018**, *159*, 127-135, doi:10.1016/j.ecoenv.2018.04.051.
65. Valiante, V. The cell wall integrity signaling pathway and its involvement in secondary metabolite production. *J Fungi* **2017**, *3*, 68, doi:10.3390/jof3040068.
66. Kharlamova, T. Anti-fungal activity of anthraquinone derivatives. *Chemical Journal of Kazakhstan* **2022**, *2*, 26-47, doi:https://doi.org/10.51580/2022-2/2710-1185.63.

67. Hall, K.R.; Robins, K.J.; Williams, E.M.; Rich, M.H.; Calcott, M.J.; Copp, J.N.; Little, R.F.; Schwörer, R.; Evans, G.B.; Patrick, W.M. Intracellular complexities of acquiring a new enzymatic function revealed by mass-randomisation of active-site residues. *Elife* **2020**, *9*, e59081, doi:10.7554/eLife.59081.
68. Álvarez-Barragán, J.; Cravo-Laureau, C.; Wick, L.Y.; Duran, R. Fungi in PAH-contaminated marine sediments: cultivable diversity and tolerance capacity towards PAH. *Mar Pollut Bull* **2021**, *164*, 112082, doi:https://doi.org/10.1016/j.marpolbul.2021.112082.
69. Wu, M.; Xu, Y.; Ding, W.; Li, Y.; Xu, H. Mycoremediation of manganese and phenanthrene by *Pleurotus eryngii* mycelium enhanced by Tween 80 and saponin. *A Microbiol Biotechnol* **2016**, *100*, 7249-7261, doi:10.1007/S00253-016-7551-3/FIGURES/6.
70. Govarthanan, M.; Fuzisawa, S.; Hosogai, T.; Chang, Y.-C. Biodegradation of aliphatic and aromatic hydrocarbons using the filamentous fungus *Penicillium* sp. CHY-2 and characterization of its Manganese peroxidase activity. *RSC Advances* **2017**, *7*, 20716-20723, doi:10.1039/C6RA28687A.
71. Mtibaà, R.; Olicón-Hernández, D.R.; Pozo, C.; Nasri, M.; Mechichi, T.; González, J.; Aranda, E. Degradation of bisphenol A and acute toxicity reduction by different thermo-tolerant ascomycete strains isolated from arid soils. *Ecotoxicol Environ Saf* **2018**, *156*, 87-96, doi:10.1016/j.ecoenv.2018.02.077.
72. Chibwe, L.; Davie-Martin, C.L.; Aitken, M.D.; Hoh, E.; Massey Simonich, S.L. Identification of polar transformation products and high molecular weight polycyclic aromatic hydrocarbons (PAHs) in contaminated soil following bioremediation. *Sci Total Environ* **2017**, *599-600*, 1099-1107, doi:10.1016/j.scitotenv.2017.04.190.
73. Menzie, C.A.; Potocki, B.B.; Santodonato, J. Exposure to carcinogenic PAHs in the environment. *Environ Sci Technol* **1992**, *26*, 1278-1284, doi:https://doi.org/10.1021/es00031a002.
74. Lukić, B.; Panico, A.; Huguenot, D.; Fabbricino, M.; van Hullebusch, E.D.; Esposito, G. Evaluation of PAH removal efficiency in an artificial soil amended with different types of organic wastes. *Euro-Mediterr J Environ Integr* **2016**, *1*, doi:10.1007/s41207-016-0001-x.
75. Kamaya, Y.; Fukaya, Y.; Suzuki, K. Acute toxicity of benzoic acids to the crustacean *Daphnia magna*. *Chemosphere* **2005**, *59*, 255-261, doi:10.1016/j.chemosphere.2004.11.003.
76. Strotmann, U.; Flores, D.P.; Konrad, O.; Gendig, C. Bacterial toxicity testing: modification and evaluation of the luminescent bacteria test and the respiration inhibition test. *Processes* **2020**, *8*, 1-18, doi:10.3390/pr8111349.

Supplementary Materials

Mycotransformation of Anthracene by Indigenous *Trichoderma lixii* and *Talaromyces pinophilus* isolates: Insights into the Metabolic Pathways, Enzyme Profiles and Acute Toxicity

Samson O. Egbewale[1], Ajit Kumar[1], Mduduzi P. Mokoena[2] and Ademola O. Olaniran[1*]

[1]Discipline of Microbiology, University of KwaZulu-Natal (Westville Campus), Durban 4000, South Africa

[2]Department of Pathology, School of Medicine, University of Limpopo, Private Bag X1106, Sovenga-0727, South Africa.

* Corresponding author. Tel. +27 31 260 7400/7401.
Fax: +27 31 260 7809
Email address: olanirana@ukzn.ac.za

Fig. S1. Anthracene degradation kinetic modelling (A) Zero Order, (B) First Order, (C) Second Order. Key: *Tl*FLU1 (●), *Tp*FLU12 (■), d = days.

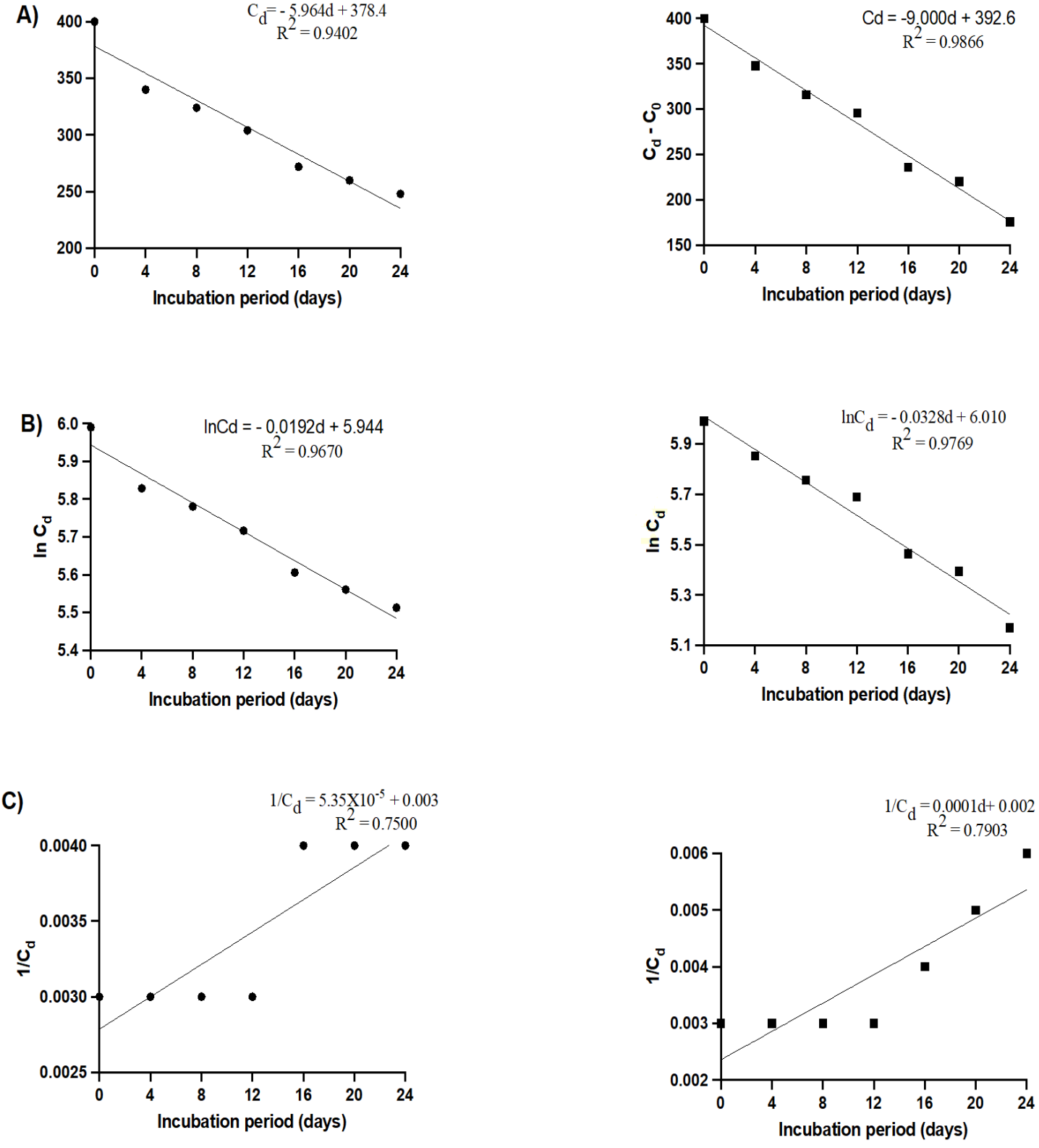

Fig. S2. FTIR spectra of anthracene myco-transformation metabolites.

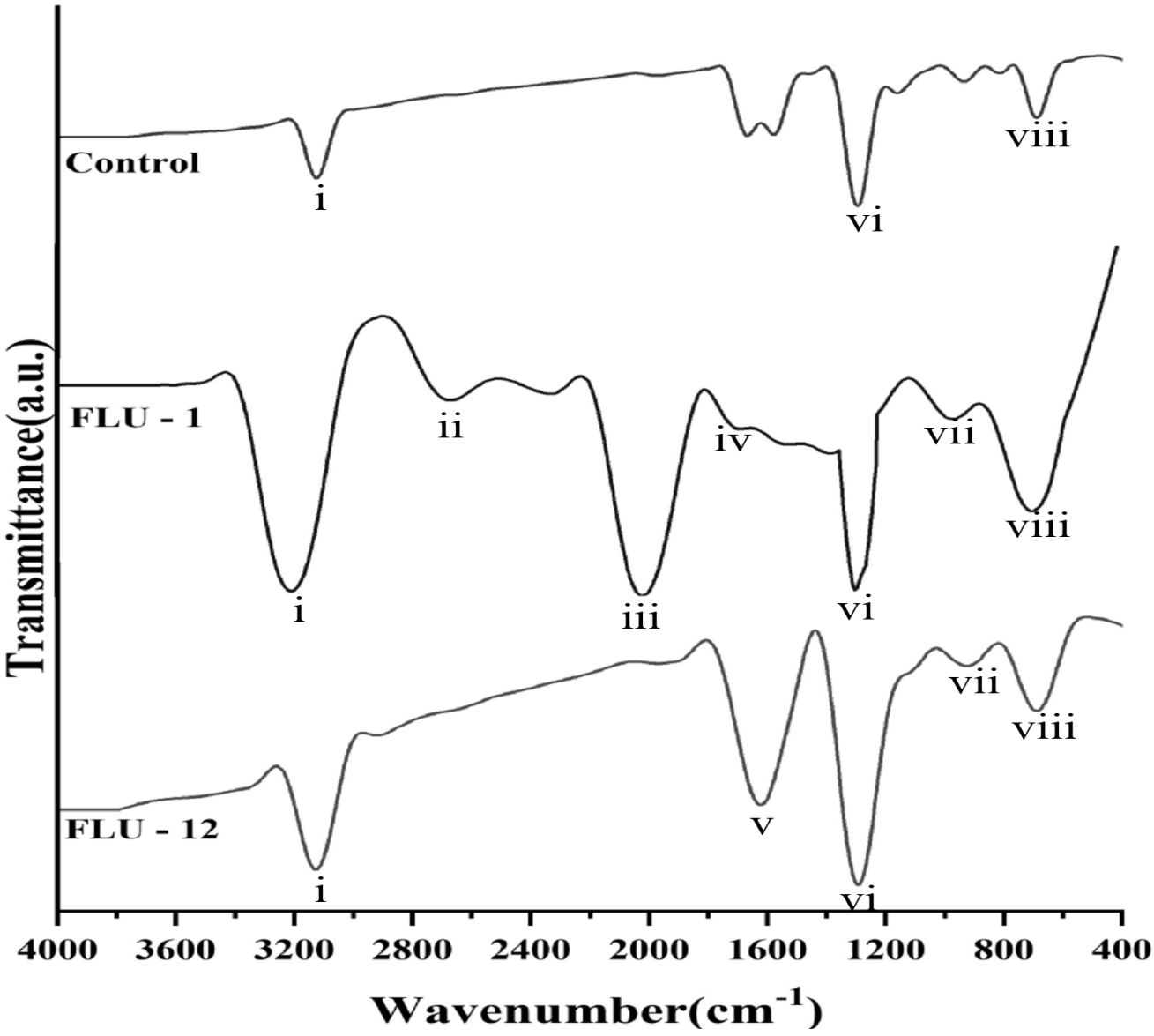

Table S1. Radial extension rate and growth inhibition of fungal strains *Tl*FLU1 and *Tp*FLU12 in response to anthracene concentrations

Concentration	Radial mycelial extension (mm/d)		Growth Inhibition (%)	
(mg/L)	*Tl*FLU1	*Tp*FLU12	*Tl*FLU1	*Tp*FLU12
0	4.50 ± 0.787^{a}	4.40 ± 0.719^{a}	0	0
50	4.50 ± 1.035^{a}	4.40 ± 1.154^{a}	0	0
100	4.50 ± 1.069^{a}	4.40 ± 1.175^{a}	0	0
200	4.50 ± 0.805^{a}	4.39 ± 0.189^{a}	0	0
400	4.49 ± 0.432^{a}	4.30 ± 0.303^{a}	0	2.27 ± 0.381^{d}
600	3.80 ± 0.361^{a}	3.70 ± 0.830^{a}	15.6 ± 0.499^{c}	15.9 ± 0.436^{c}
800	3.10 ± 0.771^{a}	3.50 ± 1.011^{a}	31.1 ± 0.023^{b}	20.5 ± 0.252^{b}
1000	2.70 ± 0.027^{a}	3.30 ± 0.642^{a}	40.0 ± 1.079^{a}	25.0 ± 0.0252^{a}

Each value is the means± standard error of four replicates. Values in the same column with different letters as superscripts are significantly different ($p \leq$ _0.05). The radial mycelial extension rate (mm/d) and growth inhibition of fungal strains *Tl*FLU-1 and *Tp*FLU12 in response to varying anthracene concentrations are shown in Table 1. The results revealed distinct responses to anthracene exposure between both strains. For strain *Tl*FLU-1, the highest radial mycelial extension rate of 4.50 mm/d was recorded at anthracene concentrations of 0 to 400 mg/L. However, at higher concentrations (600, 800 and 1000 mg/L), the radial mycelia rate decreased significantly to 3.80, 3.10 and 2.70 mm/d, respectively, when compared to the control. Conversely, strain *Tp*FLU-12 reveals a different pattern. The highest radial mycelial extension rate of 4.40 mm/d was recorded in concentrations 0 – 200 mg/L, while a gradual decrease in radial mycelia rate of 4.30, 3.70, 3.50 and 3.30 mm/d were recorded at concentrations 400, 600, 800 and 1000 mg/L respectively. Similar to *Tl*FLU1, these results indicate a significant reduction compared to the control as anthracene concentration increased. Also, no significant differences were observed among the radial mycelial extension rates at concentrations 0 – 100 mg/L at p ≤0.05 for strains *Tl*FLU1 and *Tp*FLU-12 respectively. Furthermore, the growth inhibition percentages differed between the two strains. *Tl*FLU1 exhibited the highest inhibition at 40%, while *Tp*FLU12 showed a maximum inhibition of 25%. Interestingly, *Tl*FLU1 showed no growth inhibition at concentrations ranging from 0 to 400 mg/L, whereas *Tp*FLU12 only exhibited 0% growth inhibition at concentrations ranging from 0 to 200 mg/L.

Table S2. Qualitative assay for Ligninolytic enzyme production (mm).

Concentration	Oxidation for laccase production		Oxidation for lignin peroxidase production		Oxidation for manganese peroxidase activities	
(mg/L)	*Tl*FLU1	*Tp*FLU12	*Tl*FLU1	*Tp*FLU12	*Tl*FLU1	*Tp*FLU12
0	58. 5 ± 0.761^{bc}	52.8 ± 2.107^{c}	40.9 ± 4.961^{bc}	15.8 ± 3.780^{a}	5.871 ± 11.18^{b}	42.3 ± 8.310^{c}
50	90.0 ± 10.71^{a}	88.0 ± 0.856^{a}	63.0 ± 1.641^{a}	26.4 ± 12.08^{a}	27.0 ± 6.883^{a}	70.4 ± 1.804^{a}
100	90.0 ± 2.720^{a}	88.0 ± 11.21^{a}	63.0 ± 0.660^{a}	26.4 ± 7.863^{a}	27.0 ± 11.43^{a}	70.4 ± 3.150^{a}
200	90.0 ± 0.891^{a}	88.0 ± 0.322^{a}	63.0 ± 2.450^{a}	26.4 ± 6.571^{a}	27.0 ± 0.666^{a}	70.4 ± 3.890^{a}
400	87.0 ± 2.030^{a}	79.2 ± 7.091^{ab}	60.0 ± 1.704^{a}	25.4 ± 8.037^{a}	32.4 ± 2.018^{a}	63.4 ± 5.66^{ab}
600	67.5 ± 1.311^{b}	66.0 ± 6.930^{bc}	47.2 ± 1.234^{b}	19.8 ± 1.172^{a}	20.3 ± 6.290^{ab}	52.8±12.15^{abc}
800	49.5 ± 3.964^{cd}	57.2 ± 10.66^{c}	34.7 ± 8.950^{c}	17.1 ± 12.09^{a}	14.8 ± 0.808^{ab}	45.8±6.23^{bc}
1000	43.2 ± 0.953^{d}	48.4 ± 10.95^{c}	30.2 ± 6.180^{c}	14.5 ± 11.23^{a}	12.9 ± 8.837^{ab}	38.7±11.35^{c}

Each value is the means±standard error of four replicates. Values in the same column with different letters as superscripts are significantly different ($p \leq 0.05$). The qualitative assay for ligninolytic enzyme production of fungal strains *Tl*FLU1 and *Tp*FLU12 in response to exposure to varying anthracene concentrations is shown in Table S2. For laccase production, *Tl*FLU1 exhibited a maximum oxidation diameter of 90.0 mm recorded for 50 to 200 mg/L anthracene concentration, followed by 400 mg/L anthracene concentration with an oxidation diameter of 87.0 mm, *Tl*FLU1 exhibited an oxidation rate of 43.2 ± 0.954 units while 600 to 1000 mg/L concentrations yielded oxidation diameters of 67.5, 49.5, and 43.2 mm, respectively, compared to the control with a 58.5 mm oxidation diameter. A similar trend was observed for strain *Tp*FLU12, with a maximum oxidation diameter of 88.0 mm at 50 to 200 mg/L, followed by 79.2 mm at 400 mg/L. Concentrations of 600 to 1000 mg/L resulted in oxidation diameters of 66.0, 57.2, and 48.4 mm, respectively, compared to the control with a 58.5 mm oxidation diameter. No significant differences were observed among oxidation diameters of anthracene concentrations of 50 – 400 mg/L for *Tl*FLU1 while *Tp*FLU12 showed no significant difference among oxidation diameters of anthracene concentrations of 50 – 200 mg/L at $p \leq 0.05$. Also, both strains exhibited decreasing oxidation diameters with increasing anthracene concentrations for lignin peroxidase production. *Tl*FLU1 displayed a maximum oxidation diameter of 63.0 mm at anthracene concentrations of 50–200 mg/L, followed by 60.0 mm at 400 mg/L, while concentrations of 600 to 1000 mg/L yielded oxidation diameters of 47.2, 34.7, and 30.2 mm, respectively, compared to the control's 40.9 mm oxidation diameter. Conversely, lignin peroxidase production was lower in *Tp*FLU12 than in *Tl*FLU1. For manganese peroxidase activities, both strains exhibited a decrease in oxidation rates with increasing anthracene concentrations, similar to lignin peroxidase production. However, in contrast to lignin peroxidase in *Tl*FLU1, manganese peroxidase was observed to be highly produced in *Tp*FLU-12, with a maximum oxidation diameter of 70.4 mm at 50–200 mg/L, followed by 63.4 mm at 400 mg/L. Concentrations of 600 to 1000 mg/L resulted in oxidation diameters of 52.8, 45.8, and 38.7 mm, respectively, compared to the control with a 42.3 mm oxidation diameter.

CHAPTER FIVE

Optimization of anthracene biodegradation by indigenous *Trichoderma lixii* and *Talaromyces pinophilus* strains using response surface methodology

This chapter is currently under review in the journal: *Ecotoxicology and Environmental Safety*.

The manuscript is presented in the following pages.

Optimization of anthracene biodegradation by indigenous *Trichoderma lixii* and *Talaromyces pinophilus* strains using response surface methodology

Samson O. Egbewale[1], Ajit Kumar[1], Mduduzi P. Mokoena[2] and Ademola O. Olaniran[1*]

[1]Discipline of Microbiology, University of KwaZulu-Natal (Westville Campus), Durban 4000, South Africa

[2]Department of Pathology, School of Medicine, University of Limpopo, Private Bag X1106, Sovenga-0727, South Africa.

*Correspondence: olanirana@ukzn.ac.za; Tel.: +27-31-260-7400

Abstract

Two indigenous fungal strains, *Trichoderma lixii* FLU1 (*Tl*FLU1) and *Talaromyces pinophilus* FLU12 (*Tp*FLU12) showed potential to biodegrade anthracene. Response Surface Methodology (RSM) employing Box-Behnken Design (BBD) and Central Composite Design (CCD) methods optimized crucial physicochemical parameters like pH, temperature, biomass, substrate concentration and media composition. BBD maximized anthracene biodegradation efficiency by predicting 98.7% to 103.2%. Analysis of Variance confirmed the model's accuracy with a significant F-value of 51.0 at $p < 0.0001$ while the quadratic regression model showed a high R^2 value 0.9808. CCD predicted 100% degradation efficiency which were validated for *Tl*FLU1 and *Tp*FLU12 respectively on day 8 and 12 at pH 4 and 5, temperatures 30°C and 25°C, with 20 mm biomass size and 200 mg/L anthracene. Acute toxicity tests showed that the degradation media toxicity reduced as evidenced by increased in survival rate (log CFU/mL) of *Vibrio parahaemolyticus* after 6 h exposure. Despite reduced toxicity, both strains were classified as harmful based on effective concentration (EC_{50}) and toxicity unit (TU) (20.92 ± 1.32 mg/L and 4.78% for *Tl*FLU1 and 35.29 ± 1.55 mg/L and 2.83% for *Tp*FLU12). This systematic optimization approach supported by robust statistical analyses and a deep exploration of biodegradation mechanisms holds the promise of more efficient and sustainable methods for remediating PAH-contaminated environments.

Keywords: Anthracene, Biodegradation, RSM, *Trichoderma lixii*, *Talaromyces pinophilus*, ligninolytic enzymes.

Introduction

Anthracene is classified as a priority pollutant by the US Environmental Protection Agency (EPA) due to its high toxicity and persistence in the environment (Dutta et al., 2022). It is a component of coal tar and is used in producing red dye alizarin and other dyes, wood preservatives, insecticides, and coating materials (Rani and Shanker, 2018). Anthracene is mutagenic, carcinogenic, teratogenic, and neurotoxic, which can adversely affect the reproductive, developmental, and metabolic processes of plants and animals (Ojha and Tiwary, 2021). The presence of anthracene in soil, water, and sediments can result in serious contamination, making it essential to develop efficient and cost-effective remediation strategies (Kumar et al., 2021). Biodegradation of this hazardous pollutant by microorganisms has emerged as a promising approach to remove this from the environment (Stoyanova et al., 2022). Micro fungi have shown promising potential for the biodegradation of anthracene (Kumar et al., 2021). Several studies have reported using different micro fungi strains, including *Aspergillus flavus, A. niger, A. glaucus, Paecilomyces sp., Fusarium oxysporum, Penicillium freii, Cadophora* sp. *and Trichoderma viride*, due to their capability to use anthracene as a carbon source and convert it into harmless compounds (González-Abradelo et al., 2019; Shourie and Vijayalakshmi, 2022; Singh and Roy, 2021; Stoyanova et al., 2022; Velmurugan et al., 2017). However, due to the low solubility and the impact of pH, temperature, and concentrations on the biodegradation process, further research focussing modelling the biodegradation efficiency is required to predict and optimize anthracene biodegradation.

Response Surface Methodology (RSM) is a multivariate statistical approach which aids in identifying optimum conditions for a process by analysing the interactions among the variables involved. Box-Benhken design (BBD) and central composite design (CCD) are the most used approaches during the optimization process for PAHs biodegradation (Ikrang and Umani, 2019). However, compared with CCD, BBD is more efficient in terms of the number of experiments, time, and costs needed to establish the quadratic model equation that connects variables and response, making it one of the most desirable approaches for RSM design (Wang et al., 2022). Several researchers have well-documented the use of RSM to optimize the biodegradation of anthracene by micro fungi. In a study conducted previously (Kashyap et al., 2020), RSM was used to optimize the biodegradation of phenanthrene by a strain of *Candida tropicalis*, with the optimum conditions obtained being pH 6.2, temperature of 33.4°C, mechanical shaking at 190 rpm, inoculum of 9.26 % v/v and an initial concentration of anthracene of 100 mg/L. Under these conditions, RSM effectively enhanced phenanthrene removal from the contaminated water samples by 25%. RSM was used to optimize the

biodegradation of fluorene by a strain of *Mucor irregularis,* where the interactions between the variables, including pH, temperature and initial fluorene concentration, were analysed. The results indicated that the optimum conditions for anthracene degradation were pH 7, temperature of 32.5°C, and an initial concentration of anthracene of 200 mg/L, which resulted in 81.5% removal of fluorene with 5 days (Bankole et al., 2021). Thus, since information with regards to degradation of anthracene by micro fungi is relatively scanty, this paper seeks to enhance anthracene degradation by optimizing physico-chemical parameters and culture media constituents using Response Surface Methodology- BBD and CCD. Additionally, the study intends to determine the influence of extracellular enzyme activities on the degradation and acute toxicity of the anthracene and its transient intermediate products.

Materials and methods

Chemicals and media

Anthracene, ethyl acetate, methanol, n-Hexane, ABTS, azure B, $(NH_4)_2SO_4$, K_2HPO_4, $NaH_2PO_4.2H_2O$, NaCl, $MgSO_4.7H_2O$, Nitrilotriacetic acid, $Al_2(SO_4)_3.H_2O$ and potato dextrose agar were procured from Merck (NJ, USA). All solvents and reagents are of HPLC grade with ≥ 98 % purity.

Preparation of standard solutions

A stock solution of anthracene was prepared by dissolving 500 mg of anthracene in 10 mL of methanol. The solution was sterilized using a 0.22 µm membrane filter (Millipore, Merck, NJ, USA) and stored at 4°C. Basal salt medium (BSM, pH5) was prepare as described previously (Saraswathy and Hallberg, 2002).

Fungal cultures and maintenance:

Trichoderma lixii isolate FLU1 (*Tl*FLU1; GenBank accession no. MK208694) and *Talaromyces pinophilus* isolate FLU12 (GenBank accession no. MK208704) have been characterized and reported earlier (Egbewale et al., 2023). The strains were maintained on the potato dextrose agar media before usage.

Anthracene biodegradation kinetics using response surface methodology (RSM)

The Box-Behnken factorial experimental design (BBD) was employed in the optimization of four independent variables, namely, pH (4 - 10), temperature (25 - 35ºC), fungal biomass (10 - 30 mm) and anthracene concentration (200 - 600 mg/L). Each independent variable was analysed at three levels (1, 0, and +1), encompassing 26 experimental runs along with one control (no fungus). All the experiments were performed in a total volume of 100 mL within

250 ml Erlenmeyer flasks. The effect of independent factors on the dependent factors was analysed using a quadratic equation:

$$Y=b_0+b_1A+b_2B+b_3C+b_4D+b_{12}AB+b_{13}BC+b_{23}AC+b_{34}AD+b_{23}BC+b_{34}BD+b_{14}CD+b_{11}A^2+b_{22}B^2+b_{33}C^2+b_{44}D^2 \quad \text{Equation 1.}$$

In this model, Y represents the predicted response. The variables A, B, C, and D are the independent factors. The term b0 is the intercept, while term b1, b_2, b_3, and b_4 denote the linear effects. The coefficients b11, b22, b33, and b44 are the squared terms, and b_{12}, b_{13}, b_{23}, b_{34}, b_{23}, b_{34} and b_{14} represent the interaction terms.

Central Composite Design (CCD) was utilized to assess the impacts of culture media components on the efficiency of anthracene biodegradation by *Tl*FLU1 and *Tp*FLU12 using RSM. To do this, the impact of various independent variables, namely $(NH_4)_2SO_4$, K_2HPO_4, $NaH_2PO_4.2H_2O$, NaCl, and $MgSO_4.7H_2O$ were investigated at three distinct levels: low (-1), intermediate (0), and high (1), leading in a total of 50 experimental runs. Additionally, three central point repetitions were used to assess the reliability and consistency of their analysis. A confidence level of 95% was considered to analyze the variable effect, while a polynomial equation was constructed for each response surface analysis. Also, an ANOVA analysis with a student's t-test was used to validate the statistical significance of the regression coefficients and to help confirm whether the variables had a meaningful impact on the efficiency of anthracene biodegradation.

Validation of the optimization process

Validation experiments for all the optimized variables were carried out in triplicate to assess the reproducibility of the results *via* the evaluation of the residual anthracene concentration, detection of metabolic intermediates by GC-MS and assessment of activities of enzymes involved during the biodegradation process. Also, a control (no fungus) was set up to monitor the abiotic influence.

Estimating the biomass of fungal strains

The biomass of the fungal strains was assessed using a method described previously (Egbewale et al., 2023). The procedure involved collecting 4 mL of culture broth at periodic intervals and centrifuging it at 10,000 rpm for 15 minutes. The supernatant was then used for quantifying the residual anthracene, while the pellets were washed three times with ethyl acetate to recover any anthracene that may have been absorbed by the fungi mycelia pellets. The washing process was necessary to avoid underestimating the residual anthracene concentration, as anthracene is known to be hydrophobic nature which hinders PAH biosorption by the fungi mycelia pellets. Afterwards, the pellets were dried at 80°C until a constant weight was achieved, and the

biomass's dry weight was measured using a Whatman filter paper no. 1 that has been pre-dried and pre-weighed

Extraction, quantification of residual anthracene concentration

The extraction and quantification of the residual anthracene concentration in the culture medium was carried out using the UV-Vis spectrometer method, which was described previously by (Egbewale et al., 2023; Teerapatsakul et al., 2016). The residual anthracene concentration was determined using a standard curve derived from known concentrations of anthracene which had an R^2 value of 0.972. A recovery study was done in a sterile BSM broth to verify analytical quantification accuracy, resulting in an average anthracene recovery of 98.7±2.53 %.

Quantitative estimation of ligninolytic enzymes activities

Laccase, Manganese peroxidase and Lignin peroxidase assays were performed as described previously (Egbewale et al., 2023; Patel et al., 2009). One unit of enzyme is defined as the oxidation of 1 µmol of respective substrate per min.

Ecotoxicity Test

In this study, the ecotoxicity of the culture medium during degradation was assessed utilizing a bacterial survival assay employing a liquid-to-plate micro-counting technique as outlined in a previous study (Egbewale et al., 2023). In brief, *Vibrio parahaemolyticus* (ATCC 17802) sourced from a standardized overnight culture broth with an initial inoculum size (1.0×10^8 CFU/mL), exhibiting an absorbance of 0.14 at 600 nm, was subjected to each degradation product (h) in marine broth (9:1 v/v) to achieve a final volume of 1 mL in a 15 mL centrifuge tube. To prevent settling, the degradation product (h) in marine broth was homogenized utilizing an MRC Lab suspension mixer (SM-3600) at 180 rpm and then incubated at 30°C for 6 hours in a 15 mL centrifuge tube in complete darkness. The suspensions were serially diluted at the beginning and end of exposure times, followed by spreading 10 µL of each sample on 45 mm TCBS agar plates. These plates were then placed in triplicates and incubated at 30°C for 96 hours. Bacterial survival was quantified by log-transforming the colony-forming unit (CFU/mL) using GraphPad Prism software (v. 7.05). A control experiment (CN) devoid of degradation products or PAHs was established to compare bacterial survival under standard conditions. The toxicity unit (TU) at the 50% effect endpoint of each toxicant was computed as the reciprocal of EC_{50} multiplied by 100.

Quality control measures

Reagent purity and storage: All chemicals used were of analytical or HPLC grade (≥ 98% purity) as specified in the methodology. Stock solutions were prepared fresh or stored

according to recommended conditions such as temperature and light exposure to minimize degradation.

Instrument calibration: Regular calibration of the UV-Vis spectrophotometer and GC-MS was performed to ensure accurate quantification of anthracene and its potential metabolites.

Blank controls: Blank controls were included in the anthracene quantification process using sterile BSM broth to assess potential background interference from the culture medium or extraction process.

Contamination monitoring: Fungal cultures were regularly monitored for contamination by physical observation and under microscope. Any contaminated cultures were discarded to prevent compromising the experiments.

Passage and strain purity: Fungal strains were routinely passaged on fresh potato dextrose agar (PDA) plates to maintain their viability and genetic stability. This practice ensured consistent performance in the biodegradation assays.

Aseptic technique: Strict aseptic technique was employed throughout the experiments to minimize microbial contamination that could potentially influence anthracene degradation.

Experimental replicates: All experiments were conducted in replicates (triplicates) as described in the methodology. This approach allowed for statistical analysis of the data and improved the reliability of the results.

Data analysis validation: Established statistical software (design expert) was used to analyse the RSM data. The significance of the obtained results was evaluated using appropriate statistical tests to ensure the validity of the model generated.

Fresh media preparation: Fresh culture media were prepared for each experiment to minimize degradation or nutrient depletion that could affect fungal growth and biodegradation activity.

pH monitoring: The pH of the culture media was monitored throughout the experiment, and adjustments were made if necessary to maintain optimal conditions for fungal growth and anthracene degradation.

Abiotic controls: Control experiments without fungi were included to assess abiotic degradation of anthracene, allowing for the differentiation between fungal and non-biological degradation processes.

Validation replicates: Validation experiments were conducted in triplicates to confirm the reproducibility of the results obtained during optimization.

Standardized harvesting: Consistent harvesting time points were used for fungal biomass estimation across all experiments to ensure accurate comparisons.

Alternative methods: Exploring alternative methods for biomass estimation, such as dry cell weight measurement, was considered to validate the chosen method and provide a more comprehensive picture of fungal growth.

Optimization of extraction: The extraction process (solvent selection and extraction time) was optimized to ensure maximum anthracene recovery as described in the methodology.

Recovery studies: Regular recovery studies were performed using sterile BSM broth spiked with known anthracene concentrations. This allowed us to determine the efficiency of the extraction procedure and account for potential losses during the process.

Standard curve preparation: A standard curve for anthracene quantification was prepared using a known concentrations in the specified solvent (ethyl acetate) to ensure accurate determination of residual anthracene.

Bacterial culture maintenance for ecotoxicity test: Consistent bacterial culture conditions (growth medium and temperature) were maintained for all experiments to ensure consistent bacterial activity in the ecotoxicity test.

Bacterial strain selection: A well-established bacterial strain with known sensitivity to PAHs (*Vibrio parahaemolyticus*) was employed for the ecotoxicity test as described in the methodology. This choice ensured sensitivity to potential toxic effects of anthracene or its degradation products.

Test controls: Positive and negative controls were included in the ecotoxicity test. The positive control used a known toxicant (parent compound degradation products) to verify the test's effectiveness, while the negative control used only bacterial culture medium to assess background effects.

Multiple ecotoxicity organisms: Consideration was given to using multiple ecotoxicity test organisms in future studies. This would provide a more comprehensive picture of the potential environmental impact of anthracene and its degradation products on a broader range of organisms.

Data analysis

The optimization response surface methodology design was performed using the statistical software Design-Expert version 11.1.0.1. Validations of the optimized conditions set up were lay in a completely randomized design (CRD) (Egbewale et al., 2023). Data presented as mean values and error bars and plotted in GraphPad Prism (San Diego, CA, USA). The EC_{50} and TU determination and further analysis were conducted as described previously (Egbewale et al., 2023).

Results

Optimization of anthracene biodegradation with response surface methodology

Physicochemical parameters

The effect of pH, temperature, biomass and substrate concentration on maximum anthracene biodegradation efficiency using the Box-Behnken Design (BBD) is shown in Table 1. Maximum anthracene biodegradation efficiency was predicted at runs 8, 20, 21 and 22 with prediction values at 103.2%, 98.7%, 101.6% and 101.1% respectively, while run 14 was predicted to have the lowest percentage of anthracene biodegradation efficiency with 53.3 %. However, the experimental values obtained closely matched the model's predicted values except for runs 21 and 22 which significantly deviated from the predicted values with biodegradation efficiency of 66.9% and 68.3% for strain *Tp*FLU12. Also, the ANOVA of the model and fitness significance (Table S1 and S2) reveals the accuracy of the model with an F-value of 51.0 at $p<0.0001$.

The regression model for anthracene biodegradation efficiency according to the quadratic model was highly significant ($p<0.01$) with a correlation coefficient of (R^2) value of 0.9808 (Table S3), indicating that 98.08% variability in the response factors, which was further be explained by a second-order polynomial equation in equation 1.

$$Y = 79.12 - 16.99A – 10.75B + 0.3067C – 7.53D + 3.19AB + 7.13AC - 0.2425AD - 2.80BC + 5.24BD + 1.74CD - 2.58A^2 – 6.38B^2 + 1.20C^2 + 2.42\ D^2 \quad \text{Equation 2}$$

Where Y is anthracene biodegradation efficiency (%), A is pH, B is the temperature (°C), C is biomass (mm), and D is substrate concentration (mg/L). The predicted R^2 value of 0.9144 is in reasonable agreement with the adjusted R^2 of 0.9615. Thus, the high R^2 values give a good estimate of the response within the studied range. The Cook's distance analysis (Fig. S1) further strengthens the model's goodness of fit for the experimental results with no outlier points (D) above 1. In contrast, the studentized residuals (Fig. S1) analysis shows none had a value higher than two and falls within an acceptable range between −3 and +3, which attests to the model's accuracy.

The interactive effect among the predicted optimized variables on the maximum anthracene biodegradation efficiency is presented in 3-dimensional response surface (3D) plots (Fig. 1A-F). Among all the regression model variables, variables AB, AC, AD, BC, BD and CD were found to be significant model terms ($p<0.05$). The interaction between variables pH and temperature showed that the percentage of anthracene biodegradation efficiency decreases as the pH increases with temperature. In contrast, the maximum anthracene biodegradation of 98.6 % was predicted at pH 4 and temperature 25°C with biomass of 20 mm and anthracene

concentration of 400 mg/L, as shown in Fig. 1A. The interaction between the variable AC (pH vs Biomass), depicted a significant decrease in maximum percentage anthracene biodegradation of 103.3 % with a pH 4 and Biomass 10 mm at a temperature of 30°C and anthracene concentration of 400 mg/L (Fig. 1B). Variable AD (pH and anthracene concentration) showed a linear increase in maximum anthracene biodegradation of 101.3 % was predicted for pH 4 and substrate concentration of 200 mg/L (Fig. 1C). Variable BC (temperature vs Biomass) predicted a decrease in percentage anthracene biodegradation efficiency as the temperature increases with biomass, while the maximum anthracene biodegradation efficiency of 90.85 % at a temperature of 25°C and Biomass of 30 mm (Fig. 1D). A similar trend of percentage anthracene biodegradation efficiency was predicted for variable CD (biomass vs substrate (anthracene concentration)) (Fig 1E), Where biomass of 10 mm and substrate 200 mg/L yielded a maximum anthracene biodegradation efficiency (92.93 %). Additionally, the interaction between the variable BD (Temperature vs substrate) reveals a significant decrease in maximum percentage anthracene biodegradation efficiency as temperature and anthracene concentration increased. At a temperature of 25°C and 200 mg/L of anthracene, the biodegradation efficiency was 100 % while at the maximum temperature of 35°C and anthracene concentration of 600 mg/L, the biodegradation efficiency decreased to 60 % (Fig. 1F).

Culture media

The effect of media composition on anthracene biodegradation efficiency using a central composite design is shown in Table 2. Maximum anthracene biodegradation efficiency was predicted at run 44 with a value of 89.74 % under the following media conditions (gL^{-1}); $(NH_4)_2SO_4$ 3.4; K_2HPO_4 2.1; $NaH_2PO_4.H_2O$ 0.65; Nacl 0.7; $MgSO_4$ $.7H_2O$ 0.16 while the experimental values closely matched the model's predicted values. Quadratic regression of the ANOVA, contour and 3D plots (Fig. S2) of the anthracene transformation design depict the significance of the model conditions (Table S4). Quadratic regression of the anthracene transformation model was significant, with an F-value of 29.44 at $p<0.0001$. In addition, the predicted R^2 (0.8571) and adjusted R^2 (0.9207) were in good agreement with one another with a difference of less than 0.2 and thus demonstrated a strong relationship between the designed model under investigation (Table S5). The obtained coefficient of the regression equation of the model was calculated as follows.

$$Y= 80.40+2.27A+0.7694B-1.08C-0.0012D-0.4293E+3.82AB+0.2512AC+0.0275AD+0.8037AE+0.4162BC+0.0737BD-0.0700BE-1.71CD-0.0638CE-0.3100DE+0.0111A^2-0.1126B^2-39C^2+0.2021D^2-0.7923E^2 \quad \text{Equation 3.}$$

Where A is $(NH_4)_2SO_4$, B is K_2HPO_4, C is $NaH_2PO_4.H_2O$, D is NaCl, and E is $MgSO_4.7H_2O$. The interactive effect among the optimized variables on the maximum anthracene transformation by *Tl*FLU1 and *Tp*FLU12 is presented in the 3D response surface (Fig. S2A-J). The interaction between the variables AB ($(NH_4)_2SO_4$, and K_2HPO_4) showed a linear increase with an increase in their concentrations with maximum anthracene transformation of 86.3% at $(NH_4)_2SO_4$ of 3.29 g/L and K_2HPO_4 of 2.06 g/L as shown in Fig. S2A. The interaction between the variable AC ($(NH_4)_2SO_4$ vs. $NaH_2PO_4.H_2O$), showed an increase in the concentration of $(NH_4)_2SO_4$ with a simultaneous decrease in $NaH_2PO_4.H_2O$ concentration are directly proportional to percentage anthracene transformation with maximum anthracene transformation of 82.01 % at a pH 4 $(NH_4)_2SO_4$ concentration of 3.07 g/L and $NaH_2PO_4.H_2O$ of 0.84 g/L. Similar trend was predicted for variable AE ($(NH_4)_2SO_4$ vs $MgSO_4.7H_2O$), variable BC ($NaH_2PO_4.H_2O$ vs K_2HPO_4), variable BE (K_2HPO_4 vs $MgSO_4.7H_2O$), variable CD ($NaH_2PO_4.H_2O$ vs NaCl), variable CE ($NaH_2PO_4.H_2O$ vs $MgSO_4.7H_2O$) and variable DE (NaCl vs $MgSO_4.7H_2O$).

Validation of the predicted model conditions of BBD and fungi growth.

The experimental values for runs 8 and 20 which exhibited the maximum anthracene degradation efficiency within a short incubation period, demonstrated that the optimized conditions for *Tl*FLU1 achieved 100 % (below instrumental detection limit) maximum anthracene degradation efficiency on 8 d after the incubation period under the following conditions: pH of 4, the temperature of 30°C, biomass 20 mm and substrate concentration of 200 mg/L while that of *Tp*FLU12 was obtained 100 % at 12 d after incubation period under the following conditions: pH 5, the temperature of 25°C, biomass of 20 mm and substrate concentration of 200 mg/L. Furthermore, anthracene biodegradation efficiency increased with an increase in the incubation period. Additionally, it was observed that the fungi increased with a longer incubation period by reaching a maximum value of 91.9 mg/L and 79.2 mg/L for *Tl*FLU1 and *Tp*FLU12 at 10 d and 12 d, presented in Fig. 2 A and 2B, respectively.

Enzymes involved in the biodegradation

The enzymes involved in the biodegradation of anthracene by *Tl*FLU1 and *Tp*FLU12 is presented in Fig. 3A-C. Laccase production was observed to be the most abundant reaching a maximum of 4448 U/L at 8 d and 2512.6 U/L at 10 d for *Tl*FLU1 and *Tp*FLU12, respectively (Fig. 3A). Following Laccase, Manganese peroxidase was the second most abundant enzyme produced enzyme with a maximum production concentration of 1903.7 U/L at 10 d for *Tp*FLU12 while *Tl*FLU1 was 110 U/L at 2 d (Fig. 3B). Also, Lignin peroxidase maximum

production concentration of 1213.6 U/L at 10 d and 47.4 U/L at 6 d for *Tp*FLU12 and *Tl*FLU1 (Fig. 3C).

Ecotoxicity Test

The time-course changes in *Vibrio parahaemolyticus* survival, effective concentration (EC_{50}), and toxicity unit (TU) after 6 h exposure to anthracene degradation products from *Tl*FLU1 and *Tp*FLU12 is presented in Fig. 4A, 4B and Table 3. Initially, both *Tl*FLU1 and *Tp*FLU12 showed 0 Log CFU/mL on 0 d, indicating no detectable bacterial growth with the parent compound, anthracene. For *Tl*FLU1 degradation product, bacterial survival increased significantly with time. On 2 d, *Tl*FLU1 showed a substantial increase to 4.4 Log CFU/mL, followed by further growth to 6.5 Log CFU/mL on 4 d. The bacterial survival count remained stable at 6.5 Log CFU/mL on 6 d, suggesting an initial adaptation phase. The count then increased to 7.6 Log CFU/mL on 8 d and reached its peak at 7.9 Log CFU/mL on 10 d by matching the positive control (CP). Statistically, the bacterial counts from 4 d to 6 d and 10 d with the CP were not significantly different ($p \leq 0.05$) (Fig. 4A). For *Tp*FLU12 degradation products, the survival pattern showed a rapid increase to 5.4 Log CFU/mL by 2 d, followed by a slight increase to 6.2 Log CFU/mL on 4 d. The count then increased to 6.6 Log CFU/mL on 6 d and further to 7.0 Log CFU/mL on 8 d. By 10 d, the survival count reached 7.6 Log CFU/mL, with the highest survival of 7.9 Log CFU/mL observed on 12 d and the CP. The bacterial counts on 12 d and CP were statistically similar ($p \leq 0.05$) (Fig. 4B). Additionally, the EC_{50} and TU for *Tl*FLU1 degradation product was 20.92 mg/L and 4.78%, respectively, with a toxicity class of harmful. In contrast, *Tp*FLU12 had an EC_{50} of 35.29 mg/L and a TU of 2.83%, also classified as harmful. Significant differences ($p \leq 0.05$) were observed in EC_{50} and TU between the degradation products of *Tl*FLU1 and *Tp*FLU12.

Discussion

During bioremediation processes, fungi play a crucial role in breaking down polycyclic aromatic hydrocarbons (PAHs) due to their enzymes. However, PAH degradation faces several challenges such as complex compounds, PAH concentration, pH, temperature, fungal tolerance, benzene rings, and molecular weight (Dhar et al., 2022; Sakshi and Haritash, 2020). To address these obstacles and optimize PAH biodegradation, researchers employ Response Surface Methodology (RSM) (Bhatt et al., 2014; Sachaniya et al., 2020). RSM systematically explores hindrances, focusing on pH, temperature, and nutrients, helping identify optimal conditions for fungi-driven PAH degradation (Moria et al., 2022; Sachaniya et al., 2020).

This study has underscored the importance of meticulous and precise optimization of physico-chemical parameters such as temperature, pH, fungal biomass, substrate concentration, and culture media composition in advancing the efficiency of anthracene biodegradation. This observation aligns with the findings of previous study (Bonatti et al., 2023), where precise optimization of physico-chemical parameters (temperature at 22°C, pH of 9.0, and substrate concentration of 50 mg/L) was linked to enhancing anthracene biodegradation efficiency to 90±11% by an endophytic fungus, *Didymellaceae* sp. LaBioMMi 155 in comparison with unoptimized condition with 48±7% biodegradation efficiency. Similarly, a study (Behera et al., 2023) attributed the pivotal significance of physico-chemical parameters at specific optimized conditions in the efficiency degradation of phenanthrene (50 mg/L) by *Trichoderma* sp. CNSC-2 to 79.9 ± 1.67 % at pH 6 in the presence of CU^{2+} compared with the unoptimized conditions at efficiency degradation of 64.05±0.75 %. Also, the high significance of the model in this study, as indicated by analysis of variance (ANOVA) and the robust regression model with an R^2 value of 0.9808 provide confidence in the accuracy and practical applicability of the optimization approach (Bankole et al., 2022). The 3D response surface plots in this study further lend credence to this accretion where significant interactions between the optimized variables (pH vs temperature, pH vs biomass, pH vs substrate concentration, temperature vs biomass, temperature vs substrate concentration and biomass vs substrate concentration) illustrated the intricating relationships between these variables in enhancing anthracene biodegradation efficiencies. Notably, the observed inversely interaction between pH and temperature during anthracene degradation by *Tp*FLU12 suggests that maximum biodegradation efficiency could only occur when the pH increases at a low temperature. This corroborates with the general hypothesis that an increase in metabolite accumulation during the biodegradation process could be attributed to the increase in the pH (Birolli et al., 2018). An increase from the initial pH of 5 to 7.5 triggered a 60% degradation efficiency of anthracene by *Aspergillus fumigatus* at a low temperature of 30 °C (Ye et al., 2011). Similarly, a previous study (Pawar, 2015) identifies a pH of 7 -7.5 and a temperature of 30℃ as optimal conditions for enhancing the biodegradation of PAHs by fungi. Likewise, the study using 3D response surface plots under BBD illustrated how pH 7 and temperature at 30 ℃ enhances the biodegradation efficiency of benzo[ghi]perylene by yeast consortium to 63.83±0.01% (Mandal and Das, 2018).

Culture media were observed to play a pivotal role in providing essential nutrients and conditions for fungi growth and metabolism. The utilization of the CCD methodology proved effective in pinpointing the optimal conditions for anthracene biodegradation, yielding an

impressive maximum biodegradation efficiency of 89.74% at run 44 under specific media composition conditions, including $(NH_4)_2SO_4$ at 3.4 g/L, K_2HPO_4 at 2.1 g/L, $NaH_2PO_4.H_2O$ at 0.65 g/L, NaCl at 0.7 g/L, and $MgSO_4.7H_2O$ at 0.16 g/L is not an unusual observation because metal ions like Mg^{2+} serve as enzyme co-factors, facilitating the growth of microbial mycelia cells and consequently improving degradation efficiency (Santos et al., 2008). Na^{2+} have been reported to play a pivotal role in membrane mechanisms and fungal cultures involved in PAH degradation while CU^{2+} as a trace element is known as a laccase enzyme inducer during PAHs aromatic ring oxidation (Ma et al., 2014). It is revealed that the optimal media process conditions, pinpointing KH_2PO_4 at 5.0 g/L, Na_2SO_4 at 1.00 g/L, $MgSO_4$ at 0.20 g/L, yeast at 0.05 g/L, and glucose at 0.1 g/L as the most effective combination in achieving a maximum fluorene degradation efficiency of 79.80% in comparison with maximum fluorene degradation efficiency of 11%, under media composition of KH_2PO_4 at 8 g/L, Na_2SO_4 at 3 g/L, $MgSO_4$ at 0.6 g/L, yeast at 0.15g/L, and glucose 0.3 g/L, respectively (Bankole et al., 2021). Interestingly, supplementing the culture media composition with carbon sources like glucose, lactose, and starch has no significant impact on PAHs degradation since fungi can utilize PAH as their sole carbon and energy source, as revealed in our study (Behera et al., 2023). Remarkably, the interaction between variables $(NH_4)_2SO_4$ and K_2HPO_4 illustrates a linear increase in anthracene degradation efficiency as their concentrations rise could be attributed to the interactions between NH^{4+} and $SO_4^{(2-)}$ which are known to be always at supersaturated states with implication of influencing the solubility and availability of anthracene in the medium for easy biodegradation by fungi (Dong et al., 2007). Also, the interaction between $(NH_4)_2SO_4$ and K_2HPO_4 concentrations influencing the anthracene degradation efficiency supports the idea that mechanisms such as enzyme production, sorption, and aeration are responsible for maximum PAHs degradation efficiency owing to the interactions between culture media such as $(NH_4)_2SO_4$ and K_2HPO_4 (Hadibarata et al., 2012; Kotterman et al., 1994; Weigand et al., 1999). The statistical analysis of the quadratic regression model complemented by the ANOVA results further provides robust evidence of the model's reliability and significance with a high F-value of 29.44 at $p<0.0001$ predicted R^2 (0.8571) and adjusted R^2 (0.9207) in predicting anthracene biodegradation outcomes similar to previous study (Sourav Bhattacharya, 2013) where the CCD ANOVA results showed R^2 (0.8420) and adjusted R^2 (0.7030) respectively. These values were linked with the 91.6 % degradation efficiency of benzo[a]pyrene by *Phanerochaete chrysosporium*, which was considered suitable for

biological experiments involving soil due to the challenges of mass transfer and PAH extraction in a complex matrix.

The validation of the BBD model conditions for anthracene biodegradation revealed the robustness of the predictive model through the close alignment between experimental and predicted values. In this study, the achieved 100 % anthracene biodegradation efficiency under specific optimized conditions for both *Tl*FLU1 (pH 5, temperature 25ºC, biomass 20 mm and substrate concentration 200 mg/L) and *Tp*FLU12 (pH 7, temperature 30 ºC, biomass 20 mm and substrate concentration 200 mg/L) align with the report (Bhatt et al., 2014) where pH ranges from 2-11 was demonstrated to enhanced biodegradation of chrysene, a PAHs by *Cochliobolus lunatus* Strain CHR4D. Similarly, pH 7 has been documented as considerable importance in the physiological development of fungi in fluoranthene breakdown by *Aspergillus aculeatus* and *Mucor irregularis* (Bankole et al., 2022). Also, the extension of incubation periods was found to enhance biodegradation efficiency which aligns with established biodegradation kinetics principles of PAH (perylene and benzo [ghi] perylene) by the yeast consortium (Mandal and Das, 2018). Similarly, the previous study (Agrawal and Shahi, 2017) findings demonstrated how the extension of incubation periods influenced pyrene biodegradation by *Coriolopsis byrsina* strain APC5. Notably, the observation of increased fungal biomass with incubation time underscores the correlation between growth dynamics and anthracene biodegradation efficiency which informs our understanding of the physiological response of the fungal strains *Tl*FLU1 and *Tp*FLU12 during anthracene biodegradation. Similarly, these fungi strains have demonstrated the same pattern of increased biomass over time while effectively degrading the fluoranthene (Egbewale et al., 2023). Previously, it was observed that an increase in biomass over time influenced the biodegradation efficiencies of pyrene and phenanthrene by *Podoscypha elegans* strain FTG4 (Agrawal et al., 2021).

This study highlights the pivotal role of ligninolytic enzymes in anthracene biodegradation efficiency with Laccase (Lac) production being the most abundant, followed by Lignin Peroxidase (LP) and Manganese Peroxidase (MnP). This finding suggests that the biodegradation rate depends on the production and concentration of these enzymes and growth substrate since existing literature has documented that the choice of growth substrate has the ability to trigger organism growth and promote the synthesis of catabolic enzymes (Cao et al., 2020; Cerniglia, 1992; Providenti et al., 1993). Furthermore, it is worth noting that the production of these ligninolytic enzymes has been linked with their mechanistic and catalytic contributions to the biodegradation efficiencies of other PAHs such as fluorene, pyrene,

chrysene, and benzo[a]pyrene by *T. viride* (EXF8977), *P. chrysogenum* (EXF1818) and *A. aegerita* (EXF3253) (Vipotnik et al., 2021).

In the food chain, using marine bacterial as a test organism to monitor the survival and ecological impact of anthracene and its intermediates on the ecosystem is crucial. Integrating toxicity assessments and multidisciplinary approaches offers an insight into how the primary producer in the food chain adapt and evolve in the presence of pollutants like anthracene by ensuring robust, sustainable mitigation of PAH pollution. The observed increase in bacterial survival over the time course on anthracene degradation products from *Tl*FLU1 and *Tp*FLU12 further lends credence to the efficiency of these strains in metabolizing anthracene to less toxic state. A previous study (Egbewale et al., 2023), highlighted the efficiency of fungal strains like *Tp*FLU-12 in degrading PAH compound (fluoranthene) to non-toxic states and thereby demonstrating their effective potential in bioremediation. Similarly, fungi such as *Polyporus sp.* S133, *A. fumigatus* and *A. sydowii* BPOI have shown high anthracene degradation efficiencies ranging from 71 % to 99.8 % by employing enzymes such as MnP, LP, and Lac (Bankole et al., 2020; Hadibarata et al., 2013; Ye et al., 2011). However, initial assessments show no detectable bacterial growth at Day 0 degradation product which could be attributed to the parent compound (anthracene) recalcitrant nature and toxic properties. This finding aligns with a previous report (Kottuparambil and Park, 2019), where an exposure to anthracene led to a reduction in growth rate and photosynthetic pigment production with an implication of anthracene inhibitory effects on biological systems of *Euglena agilis*. Additionally, a study (Takeda et al., 2023) highlights the chronic toxicity of anthracene with a carcinogenic effect in rats and mice after prolonged exposure. The significant increase in the bacterial count for degradation product of *Tl*FLU1 by d 2 indicates an adaptive response where the *V. parahaemolyticus* starts to utilize the degradation products as a carbon source by overcoming the initial inhibitory effects of anthracene due to different metabolites in the degradation products (Mahour, 2016; Wang et al., 2023). Also, the increase in bacterial count for *Tl*FLU1 degradation product by d 2 could be attributed to non-toxic metabolite accumulated during this period which then enhanced the marine bacterial to adapt, utilize them as its carbon and develop its novel metabolic activities in response to degradation products (Dell'Anno et al., 2021; Panigrahy et al., 2022).The plateau in bacterial counts observed in degradation products from Day 6 to Day 12 suggests that the bacterial population reaches a steady state, where the rate of cell growth balances the rate of cell death (Shi et al., 2021). This is consistent with the model proposed previously (Goldschmidt et al., 2018), which suggests that proliferation of harmful metabolites or the exhaustion of essential substrates hinders the growth process. Further

supporting this theory, an author (Theorell and Stelling, 2023), discuss bacterial population dynamics and reliance on complex compounds for growth by highlighting the significance of steady-state growth in microbial communities. For degradation product of *Tp*FLU-12, the initial rapid increase in bacterial survival from 5.4 Log CFU/mL on d 2 degradation product to 6.2 Log CFU/mL on d 4 degradation product suggests an effective utilization of anthracene degradation intermediates due to accumulation of non-toxic intermediates in these products. This is supported by a review (Ahmad, 2022), which reveals that the interactive effects of metabolic products of polycyclic aromatic hydrocarbons (PAHs) and bacteria can influence increase the rate of the products utilization when less toxic. Furthermore, the absence of PAHs derivatives such as quinones, phenolics, epoxides and diol in the degradation products can promote efficient bioremediation by allowing microbes in the ecosystem to effectively carries out their cellular activities such as cell division, regulation of cell cycle, and formation of biofilm (Mohapatra and Phale, 2021). The convergence in final bacterial counts for both CP and *Tl*FLU1 and *Tp*FLU-12 with 7.9 Log CFU/mL on degradation products of d 10 and d 12, respectively suggests eventual similar adaptation levels despite different initial growth patterns. This alignment in bacterial survival counts implies that degradation pathways and intermediates become more favourable over time due to non-toxic state of these degradation products by supporting sustained bacterial growth (Amin et al., 2020; Conde-Avila et al., 2021; Mishra et al., 2020). Also, these findings resonate with a previous study (Gross et al., 2020), which observed an increase change in *E. coli* population during stationary phase in culture medium. However, the differences in toxicity assessments between *Tl*FLU1 (EC_{50} 20.92 mg/L) and *Tp*FLU12 (EC_{50} 35.29 mg/L) degradation products can be attributed to the metabolites formed during the degradation process which then explains why the degradation product from *Tp*FLU12 is less toxic than *Tl*FLU1. This observation aligns with previous findings that established variability in toxicity levels throughout the biodegradation of aromatic hydrocarbons (Oberoi and Philip, 2017). The distinct sets of metabolites produced during degradation contribute to the differences in toxicity of *Tl*FLU1 degradation product and *Tp*FLU12 products (Egbewale et al., 2023; Mtibaà et al., 2018). Interestingly, both *Tl*FLU1 degradation products (TU of 4.78%) and *Tp*FLU12 products (TU of 2.83%) are considered harmful but less toxic than pure *Tl*FLU1. These variations suggest unique metabolite profiles resulting from the degradation processes which stems from more toxic intermediates like hydroxylated or carboxylated derivatives of anthracene accumulated in *Tl*FLU1 degradation product to be specific which can generate reactive oxygen species causing cellular damage during degradation (Agrawal and Shahi, 2017).

Conclusion

Polycyclic aromatic hydrocarbons (PAHs) like anthracene are environmental pollutants with significant ecological and health implications which necessitate its effective remediation strategies. This study reveals the potential of indigenous fungal isolates, *Tl*FLU1 and *Tp*FLU12 in the effective biodegradation of anthracene. Through the optimization of physicochemical parameters and culture media using RSM, it provides valuable insights into the mechanisms underlying biodegradation efficiency. The critical role of ligninolytic enzymes (Lac, LP and MnP) in anthracene degradation was elucidated. Validation of the predicted model conditions further corroborates the success of this approach, leading to 100% biodegradation under specific optimized conditions. Bacterial survival assays using *Vibrio parahaemolyticus* demonstrated that the degradation products from *Tl*FLU1 and *Tp*FLU12 resulted in different survival rates. *Tl*FLU1 degradation product showed a higher initial bacterial survival that stabilized over time, indicating a potentially higher initial toxicity that decreased as degradation progressed. Conversely, *Tp*FLU12 degradation products exhibited a rapid initial increase in bacterial survival, suggesting lower initial toxicity and a more consistent degradation process. The ecotoxicity tests demonstrated significant differences in effective concentration (EC_{50}) and toxicity unit (TU) between the degradation products of *Tl*FLU1 and *Tp*FLU12. *Tl*FLU1 showed higher toxicity with lower EC_{50} and higher TU values compared to *Tp*FLU12, indicating that although both fungal strains effectively degrade anthracene, *Tl*FLU1 may result in higher initial toxicity which reduces over time. Thus, these findings contribute to our understanding of bioremediation processes and offer promise for addressing environmental pollution challenges through eco-friendly remediation approaches. Additionally, future studies should explore the molecular mechanisms and genetic regulation of ligninolytic enzymes in fungal strains and their interactions with other microorganisms and environmental factors.

Acknowledgements:

S.O.E. Thanks University of KwaZulu Natal, Durban, South Africa for Ph.D. scholarship.

Funding:

National Research Foundation, South Africa (Grant No: 94036 and 92803).

Data Availability Statement:

Data are contained within the article or Supplementary Material.

Conflicts of Interest:

The authors declare no conflicts of interest.

REFERENCES

Agrawal, N., et al., 2021. Biodegradation pathway of polycyclic aromatic hydrocarbons by ligninolytic fungus *Podoscypha elegans* strain ftg4 and phytotoxicity evaluation of their metabolites. Environmental Processes. 8**,** 1307-1335.

Agrawal, N., Shahi, S. K., 2017. Degradation of polycyclic aromatic hydrocarbon (pyrene) using novel fungal strain *Coriolopsis byrsina* strain APC5. International Biodeterioration and Biodegradation. 122**,** 69-81.

Ahmad, I., 2022. Microalgae–Bacteria consortia: a review on the degradation of polycyclic aromatic hydrocarbons (PAHs). Arabian Journal for Science and Engineering. 47**,** 19-43.

Amin, S., et al., 2020. Degradation and toxicity analysis of a reactive textile diazo dye-Direct Red 81 by newly isolated *Bacillus* sp. DMS2. Frontiers in Microbiology. 11**,** 576680.

Bankole, P. O., et al., 2020. Enhanced enzymatic removal of anthracene by the mangrove soil-derived fungus, *Aspergillus sydowii* BPOI. Frontiers of Environmental Science and Engineering. 14**,** 1-13.

Bankole, P. O., et al., 2021. Biodegradation of fluorene by the newly isolated marine-derived fungus, *Mucor irregularis* strain bpo1 using response surface methodology. Ecotoxicology and Environmental Safety. 208**,** 111619-111619.

Bankole, P. O., et al., 2022. Co-biomass degradation of fluoranthene by marine-derived fungi; *Aspergillus aculeatus* and *Mucor irregularis:* Comprehensive process optimization, enzyme induction and metabolic analyses. Arabian Journal of Chemistry. 15**,** 104036-104036.

Behera, A. D., et al., 2023. Enzymatic degradation and metabolic pathway of phenanthrene by manglicolous filamentous fungus *Trichoderma* sp. CNSC-2. Microbiological Research. 276**,** 127483.

Bhatt, J. K., et al., 2014. Application of response surface methodology for rapid chrysene biodegradation by newly isolated marine-derived fungus *Cochliobolus lunatus* strain CHR4D. Journal of Microbiology. 52**,** 908-17.

Birolli, W. G., et al., 2018. Biodegradation of anthracene and several PAHs by the marine-derived fungus *Cladosporium* sp. CBMAI 1237. Marine Pollution Bulletin. 129**,** 525-533.

Bonatti, E., et al., 2023. Endophytic, extremophilic and entomophilic fungi strains biodegrade anthracene showing potential for bioremediation. World Journal of Microbiology and Biotechnology. 39**,** 152.

Cao, H., et al., 2020. Enzyme activities during Benzo[a]pyrene degradation by the fungus *Lasiodiplodia theobromae* isolated from a polluted soil. Scientific Reports 10**,** 1-11.

640 Cerniglia, C. E., 1992. Biodegradation of polycyclic aromatic hydrocarbons. Biodegradation.
641 3**,** 351-368.
642 Conde-Avila, V., et al., 2021. Pesticides degradation by immobilised microorganisms.
643 International Journal of Environmental Analytical Chemistry. 101**,** 2975-3005.
644 Dell'Anno, F., et al., 2021. Bacteria, fungi and microalgae for the bioremediation of marine
645 sediments contaminated by petroleum hydrocarbons in the omics era. Microorganisms. 9**,**
646 1695.
647 Dhar, K., et al., 2022. Efficient bioremediation of PAHs-contaminated soils by a
648 methylotrophic enrichment culture. Biodegradation. 33**,** 575-591.
649 Dong, J.-L., et al., 2007. Raman observation of the interactions between NH_4^+, SO_4^{2-}, and H_2O
650 in supersaturated $(NH_4)_2SO_4$ droplets. The Journal of Physical Chemistry B. 111**,** 12170-
651 12176.
652 Dutta, V., et al., 2022. Photocatalytic nanomaterials: applications for remediation of toxic
653 polycyclic aromatic hydrocarbons and green management. Chemical Engineering Journal
654 Advances. 11**,** 100353-100353.
655 Egbewale, S. O., et al., 2023. Metabolic biodegradation pathway of fluoranthene by indigenous
656 *Trichoderma lixii* and *Talaromyces pinophilus* spp. Catalysts. 13**,** 791.
657 Goldschmidt, F., et al., 2018. Metabolite toxicity slows local diversity loss during expansion
658 of a microbial cross-feeding community. The ISME journal. 12**,** 136-144.
659 González-Abradelo, D., et al., 2019. First demonstration that ascomycetous halophilic fungi
660 (*Aspergillus sydowii* and *Aspergillus destruens*) are useful in xenobiotic mycoremediation
661 under high salinity conditions. Bioresource Technology. 279**,** 287-296.
662 Gross, J., et al., 2020. Culture volume influences the dynamics of adaptation under long-term
663 stationary phase. Genome Biology and Evolution. 12**,** 2292-2301.
664 Hadibarata, T., et al., 2012. Breakdown products in the metabolic pathway of anthracene
665 degradation by a ligninolytic fungus *Polyporus* sp. S133. Water Air and Soil Pollution. 223**,**
666 2201-2208.
667 Hadibarata, T., et al., 2013. Degradation and transformation of anthracene by white rot fungus
668 *Armillaria* sp. F022. Folia Microbiology. 58**,** 385-391.
669 Ikrang, E. G., Umani, K. C., 2019. Optimization of process conditions for drying of catfish
670 *(Clarias gariepinus*) using Response Surface Methodology (RSM). Food Science and
671 Human Wellness. 8**,** 46-52.
672 Kashyap, N., et al., 2020. Mechanistic investigations in ultrasound-assisted biodegradation of
673 phenanthrene. Ultrasonics Sonochemistry. 62**,** 104890-104890.

Kotterman, M. J. J., et al., 1994. The physiology of anthracene biodegradation by the white-rot fungus *Bjerkandera* sp. strain BOS55. Applied Microbiology and Biotechnology. 42**,** 179-186.

Kottuparambil, S., Park, J., 2019. Anthracene phytotoxicity in the freshwater flagellate alga *Euglena agilis* Carter. Scientific Reports. 9**,** 15323.

Kumar, V., et al., Application of omics technologies for microbial community structure and function analysis in contaminated environment. In: A. S. a. S. M. Maulin P. Shah, (Ed.), Wastewater Treatment

Cutting Edge Molecular Tools, Techniques and Applied Aspects. Elsevier, 2021, pp. 1-40.

Mahour, R., Chemical and biological oxidation of naphthenic acids-where stoichiometry, kinetics and thermodynamics meet. Civil and Environmental Engineering Vol. Master of Science in Environmental Engineering University of Alberta, 2016, pp. 237.

Mandal, S. K., Das, N., 2018. Biodegradation of perylene and benzo [ghi] perylene (5-6 rings) using yeast consortium : Kinetic study, enzyme analysis and degradation pathway. Journal of Environmental Biology. 39**,** 5-15.

Mishra, S., et al., 2020. Carbofuran toxicity and its microbial degradation in contaminated environments. Chemosphere. 259**,** 127419.

Mohapatra, B., Phale, P. S., 2021. Microbial degradation of naphthalene and substituted naphthalenes: metabolic diversity and genomic insight for bioremediation. Frontiers in Bioengineering and Biotechnology. 9**,** 602445.

Moria, K. M., et al., 2022. Application of the response surface methodology (rsm) in the optimization of acenaphthene (acn) removal from wastewater by activated carbon. Sustainability. 14**,** 8581.

Mtibaà, R., et al., 2018. Degradation of bisphenol A and acute toxicity reduction by different thermo-tolerant ascomycete strains isolated from arid soils. Ecotoxicology and environmental safety. 156**,** 87-96.

Oberoi, A. S., Philip, L., 2017. Variation in toxicity during the biodegradation of various heterocyclic and homocyclic aromatic hydrocarbons in single and multi-substrate systems. Ecotoxicology and Environmental Safety. 135**,** 337-346.

Ojha, A., Tiwary, D., Organic pollutants in water and its health risk assessment through consumption. In: S. I. S. Arif Ahamad, Pardeep Singh, (Ed.), Contamination of Water: Health Risk Assessment and Treatment Strategies. Academic Press, 2021, pp. 237-250.

706 Panigrahy, N., et al., 2022. A comprehensive review on eco-toxicity and biodegradation of
707 phenolics: Recent progress and future outlook. Environmental Technology and Innovation.
708 27**,** 102423.
709 Patel, H., et al., 2009. Biodegradation of fluoranthene by basidiomycetes fungal isolate
710 *Pleurotus ostreatus* HP-1. Applied Biochemistry and Biotechnology. 157**,** 367-376.
711 Pawar, R. M., 2015. The effect of soil pH on bioremediation of polycyclic aromatic
712 hydrocarbons (PAHS). Journal of Bioremediation and Biodegradation. 06.
713 Providenti, M. A., et al., 1993. Selected factors limiting the microbial degradation of
714 recalcitrant compounds. Journal of Industrial Microbiology. 12**,** 379-395.
715 Rani, M., Shanker, U., Remediation of polycyclic aromatic hydrocarbons using nanomaterials.
716 In: G. Crini, E. Lichtfouse, Eds.), Green Adsorbents for Pollutant Removal. Springer
717 International Publishing, Cham, 2018, pp. 343-387.
718 Sachaniya, B. K., et al., 2020. Bioengineering for multiple PAHs degradation for contaminated
719 sediments: response surface methodology (RSM) and artificial neural network (ANN).
720 Chemometrics and Intelligent Laboratory Systems. 202.
721 Sakshi, Haritash, A. K., 2020. A comprehensive review of metabolic and genomic aspects of
722 PAH-degradation. Archives of Microbiology. 202**,** 2033-2058.
723 Santos, E. C., et al., 2008. Anthracene biodegradation and surface activity by an iron-stimulated
724 *Pseudomonas* sp. Bioresource Technology. 99**,** 2644-2649.
725 Shi, H., et al., 2021. Precise regulation of the relative rates of surface area and volume synthesis
726 in bacterial cells growing in dynamic environments. Nature Communications. 12**,** 1975.
727 Shourie, A., Vijayalakshmi, U., 2022. Fungal diversity and its role in mycoremediation.
728 Geomicrobiology Journal. 39**,** 426-444.
729 Singh, A., Roy, A., Fungal communities for the remediation of environmental pollutants. In:
730 A. N. Yadav, (Ed.), Recent Trends in Mycological Research. Springer, Cham, 2021, pp.
731 127-165.
732 Sourav Bhattacharya, A. D., Kuruvalli Prashanthi, Muthusamy Palaniswam, Jayaraman
733 Angayarkanni 2013. Mycoremediation of Benzo [a] pyrene by *Pleurotus ostreatus* in the
734 presence of heavy metals and mediators. 3 Biotech. 4**,** 205-211.
735 Stoyanova, K., et al., 2022. Biodegradation of naphthalene and anthracene by *Aspergillus*
736 *glaucus* strain isolated from antarctic soil. Processes. 10**,** 873-873.
737 Takeda, T., et al., 2023. Clear evidence of the carcinogenic potential of anthracene: A 2-year
738 feeding study in rats and mice. Environmental Toxicology. 38**,** 709-726.

739 Teerapatsakul, C., et al., 2016. Biodegradation of polycyclic aromatic hydrocarbons by a
740 thermotolerant white rot fungus *Trametes polyzona* RYNF13. The Journal of General and
741 Applied Microbiology. 62**,** 303-312.
742 Theorell, A., Stelling, J., 2023. Assumptions on decision making and environment can yield
743 multiple steady states in microbial community models. BMC Bioinformatics. 24**,** 262.
744 Velmurugan, N., et al., 2017. Proteomic analysis of the marine-derived fungus *Paecilomyces*
745 sp. Strain SF-8 in response to polycyclic aromatic hydrocarbons. Botanica Marina. 60**,** 381-
746 392.
747 Vipotnik, Z., et al., 2021. Ligninolytic enzymes production during polycyclic aromatic
748 hydrocarbons degradation: effect of soil pH, soil amendments and fungal co-cultivation.
749 Biodegradation. 32**,** 193-215.
750 Wang, H., et al., 2023. Marine micro (nano) plastics determination and its environmental
751 toxicity evaluation. TrAC Trends in Analytical Chemistry. 168**,** 117332.
752 Wang, L., et al., 2022. Degradation of bisphenol a by ozonation in a rotating packed bed:
753 Modeling by response surface methodology and artificial neural network. Chemosphere.
754 286**,** 131702.
755 Weigand, H., et al., 1999. Desorption controlled mobility and intrinsic biodegradation of
756 anthracene in unsaturated soil. Physics and Chemistry of the Earth, Part B: Hydrology,
757 Oceans and Atmosphere. 24**,** 549-555.
758 Ye, J.-s., et al., 2011. Biodegradation of anthracene by *Aspergillus fumigatus*. Journal of
759 Hazardous Materials. 185**,** 174-181.
760
761 **Figure Legends:**
762 **Figure 1.** The interactive effect among the predicted optimized variables on the maximum
763 anthracene biodegradation. pH vs temperature (A), pH vs Biomass (B), pH and anthracene
764 concentration (C), temperature vs Biomass (D), biomass vs anthracene concentration (E) and
765 Temperature vs anthracene concentration (F).
766 **Figure 2.** The biodegradation of anthracene by *Tl*FLU1 (A) and *Tp*FLU12 (B).
767 **Figure 3.** Ligninolytic enzymes Laccase (A), Manganese peroxidase (B) and Lignin peroxidase
768 (C) involved in anthracene biodegradation by *Tl*FLU1 and *Tp*FLU12.
769 **Figure 4.** The time-course changes in *Vibrio parahaemolyticus* survival (Log CFU/mL) after
770 6 h exposure to anthracene degradation products from *Tl*FLU1 (A) and *Tp*FLU12 (B).
771
772

Tables:

Table 1: The effect of pH, temperature, biomass and substrate concentration on anthracene biodegradation by *Tl*FLU1 and *Tp*FLU12.

Run	pH	Temperature ˚C	Biomass (mm)	Substrate (mg/L)	Degradation (%)		
					Predicted	*Tl*FLU1	*Tp*FLU12
1	10	30	30	400	68.2	53.4	60.3
2	7	35	20	200	66.7	68.4	67.7
3	7	25	10	400	81.6	71.7	87.5
4	7	30	10	600	73.2	75.1	74.1
5	7	30	30	200	88.8	76.1	80.8
6	7	35	20	600	62.1	58.9	62.5
7	4	30	30	400	87.9	94.3	62.2
8	4	30	20	200	103.2	LDL	73.4
9	4	30	20	600	88.7	70.5	59.5
10	10	30	20	200	69.7	55.9	52.1
11	10	30	20	600	54.2	51.6	47.7
12	7	25	20	600	73.1	71.6	74.4
13	7	30	20	400	79.1	78.5	80.4
14	10	30	10	400	53.3	52.1	59.5
15	7	25	30	400	87.8	73.8	95.7
16	10	25	20	400	60.7	60.6	59.7
17	7	30	10	200	91.7	79.2	91.6
18	7	30	20	400	79.1	86.2	88.1
19	7	30	30	600	77.3	86.3	81.6
20	7	25	20	200	98.7	74.4	LDL
21	4	30	10	400	101.6	90.2	66.9
22	4	25	20	400	101.1	96.2	68.3
23	10	35	20	400	45.6	48.2	53.5
24	7	35	30	400	60.7	65.8	65.7
25	4	35	20	400	73.2	69.5	70.1
26	7	35	10	400	65.7	68.2	61.3

LDL: laboratory detection limit.

793 Table 2: Central composite rotatable design (CCRD) for anthracene biodegradation by *Tl*FLU1
794 and *Tp*FLU12.

Run	$(NH_4)_2SO_4$	K_2HPO_4	$NaH_2PO_4.2H_2O$	NaCl	$MgSO_4$	Degradation (%)		
						Predicted	*Tl*FLU1	*Tp*FLU12
1	1.40	2.10	1.05	0.30	0.16	75.7	73.6	74.4
2	3.40	2.10	1.05	0.30	0.16	86.7	86.6	86.1
3	1.40	2.10	0.65	0.30	0.36	72.1	69.3	70.4
4	1.40	2.10	0.65	0.70	0.16	78.1	76.8	77.7
5	3.40	1.00	1.05	0.30	0.16	76.7	75.9	75.4
6	3.40	2.10	1.05	0.30	0.36	87.8	87.3	87.7
7	2.40	1.55	1.33	0.50	0.26	74.8	74.7	75.5
8	2.40	1.55	0.85	0.50	0.26	80.4	80.3	81.4
9	3.40	1.00	1.05	0.30	0.36	78.1	75.9	75.5
10	2.40	1.55	0.85	0.50	0.26	80.4	82.1	82.2
11	3.40	1.00	0.65	0.30	0.36	77.3	75.2	76.8
12	4.78	1.55	0.85	0.50	0.26	85.9	85.6	86.2
13	1.40	1.00	1.05	0.30	0.36	79.1	78.2	78.8
14	3.40	1.00	0.65	0.30	0.16	75.6	74.8	74.5
15	3.40	1.00	0.65	0.70	0.36	80.0	79.8	80.0
16	2.40	1.55	0.85	0.02	0.26	81.6	82.9	82.3
17	1.40	1.00	0.65	0.70	0.36	81.9	81.9	82.5
18	2.40	1.55	0.85	0.50	0.26	80.4	78.8	78.5
19	1.40	2.10	1.05	0.70	0.16	72.9	74.1	73.7
20	2.40	1.55	0.85	0.50	0.02	76.9	76.6	76.9
21	1.40	1.00	1.05	0.70	0.36	74.9	74.6	74.4
22	2.40	1.55	0.85	0.98	0.26	81.5	79.8	80.0
23	3.40	1.00	1.05	0.70	0.36	73.9	73.4	73.9
24	2.40	1.55	0.85	0.50	0.26	80.4	77.9	78.8
25	2.40	2.86	0.85	0.50	0.26	81.6	81.3	80.6
26	2.40	1.55	0.85	0.50	0.26	80.4	81.1	81.6
27	1.40	1.00	0.65	0.30	0.16	80.9	81.9	82.0
28	1.40	2.10	1.05	0.30	0.36	73.5	71.8	73.0
29	1.40	2.10	0.65	0.70	0.36	75.0	74.7	74.8
30	1.40	1.00	1.05	0.70	0.16	77.9	75.9	76.3
31	3.40	1.00	1.05	0.70	0.16	73.8	73.7	74.9
32	1.40	2.10	0.65	0.30	0.16	73.9	72.6	73.4
33	0.02	1.55	0.85	0.50	0.26	75.1	74.6	75.2
34	2.40	1.55	0.85	0.50	0.26	80.4	78.9	79.4
35	3.40	2.10	0.65	0.30	0.36	85.3	85.5	86.0
36	3.40	1.00	0.65	0.70	0.16	79.6	78.0	78.3
37	3.40	2.10	1.05	0.70	0.16	84.1	82.1	81.5
38	2.40	1.55	0.85	0.50	0.50	74.9	74.4	74.5
39	1.40	1.00	1.05	0.30	0.16	80.9	79.0	78.6
40	2.40	1.55	0.37	0.50	0.26	79.9	79.0	78.9
41	1.40	2.10	1.05	0.70	0.36	69.6	67.6	69.0
42	3.40	2.10	1.05	0.70	0.36	83.9	82.1	83.0
43	2.40	1.55	0.85	0.50	0.26	80.4	79.0	78.7
44	3.40	2.10	0.65	0.70	0.16	88.2	88.8	89.4
45	3.40	2.10	0.65	0.70	0.36	88.3	88.2	87.8
46	3.40	2.10	0.65	0.30	0.16	84.0	81.1	82.0
47	2.40	0.24	0.85	0.50	0.26	77.9	77.7	78.1
48	1.40	1.00	0.65	0.70	0.16	84.7	82.8	82.6
49	1.40	1.00	0.65	0.30	0.36	79.3	78.0	77.8
50	2.40	1.55	0.85	0.50	0.26	80.4	80.3	79.4

795 Table 3. Acute toxicity (EC_{50}) of the anthracene degradation products of *Tl*FLU1 and
796 *Tp*FLU12.

Acute Toxicity Profile	Strain	
	*Tl*FLU1	*Tp*FLU12
EC_{50} (mg/L)	20.92^{b}	35.29^{a}
TU (%)	4.78^{a}	2.83^{b}
Class	Harmful	

797
798 Key: Very toxic (EC_{50} < 1 mg/L); Toxic (1 mg/L < EC_{50} ≤ 10 mg/L); Harmful (10 mg/L < EC_{50} ≤ 100 mg/L);
799 Non-toxic (≥ 100 mg/L). Values with the same alphabet as superscripts are not statistically different ($p \leq 0.05$
800

Figure 1A

Click here to access/download;Figure;Fig. 1A.JPG

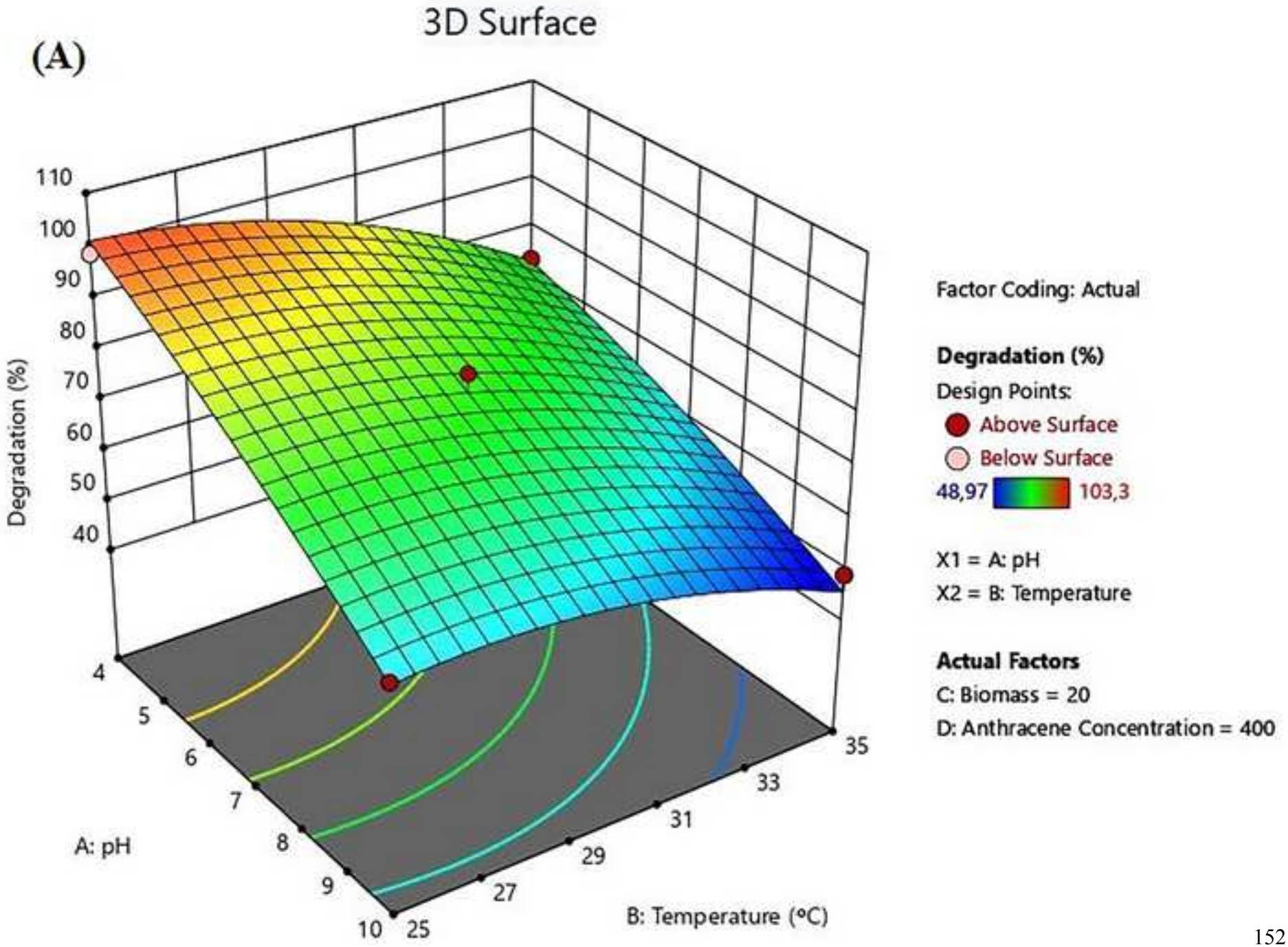

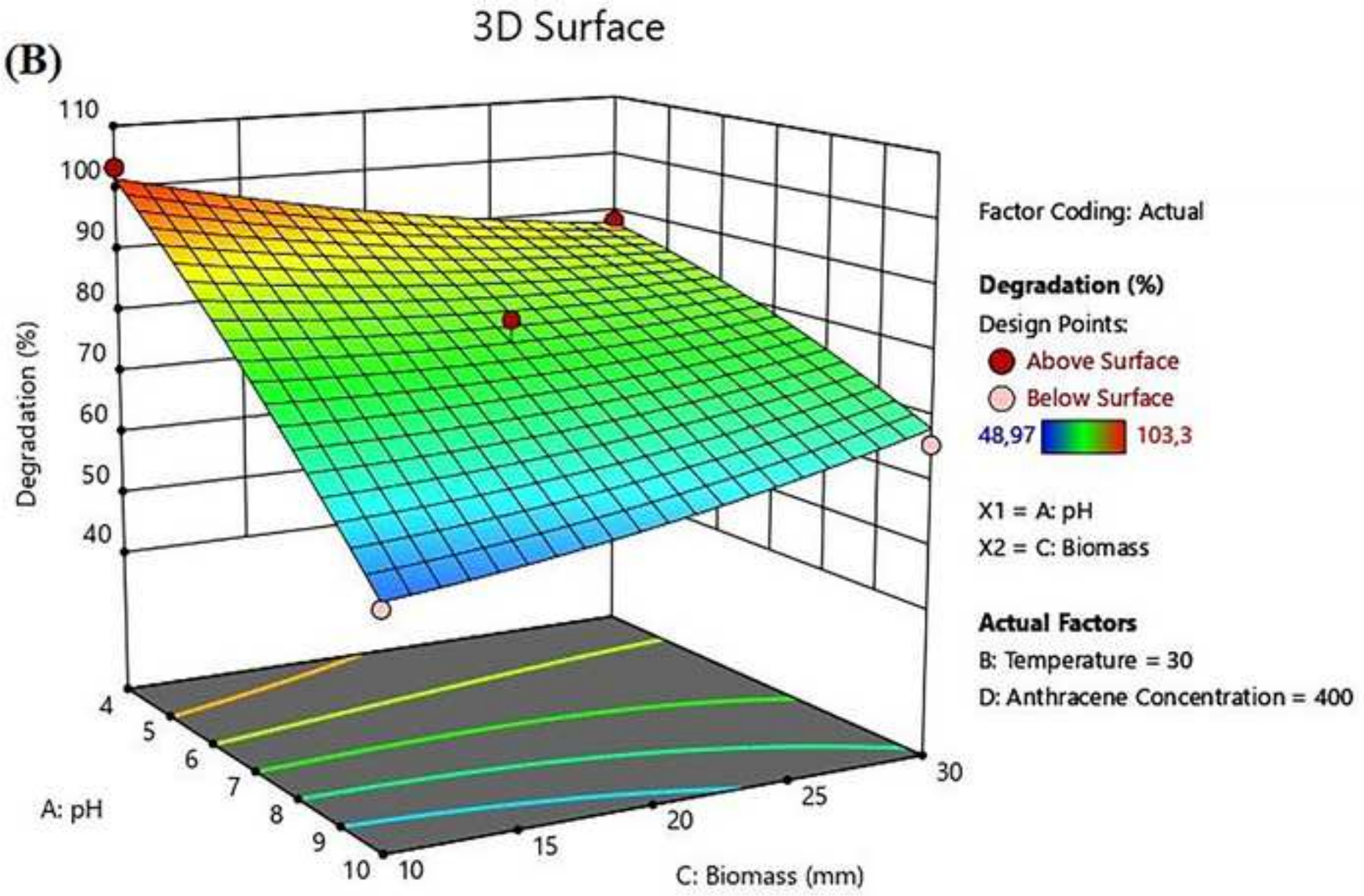

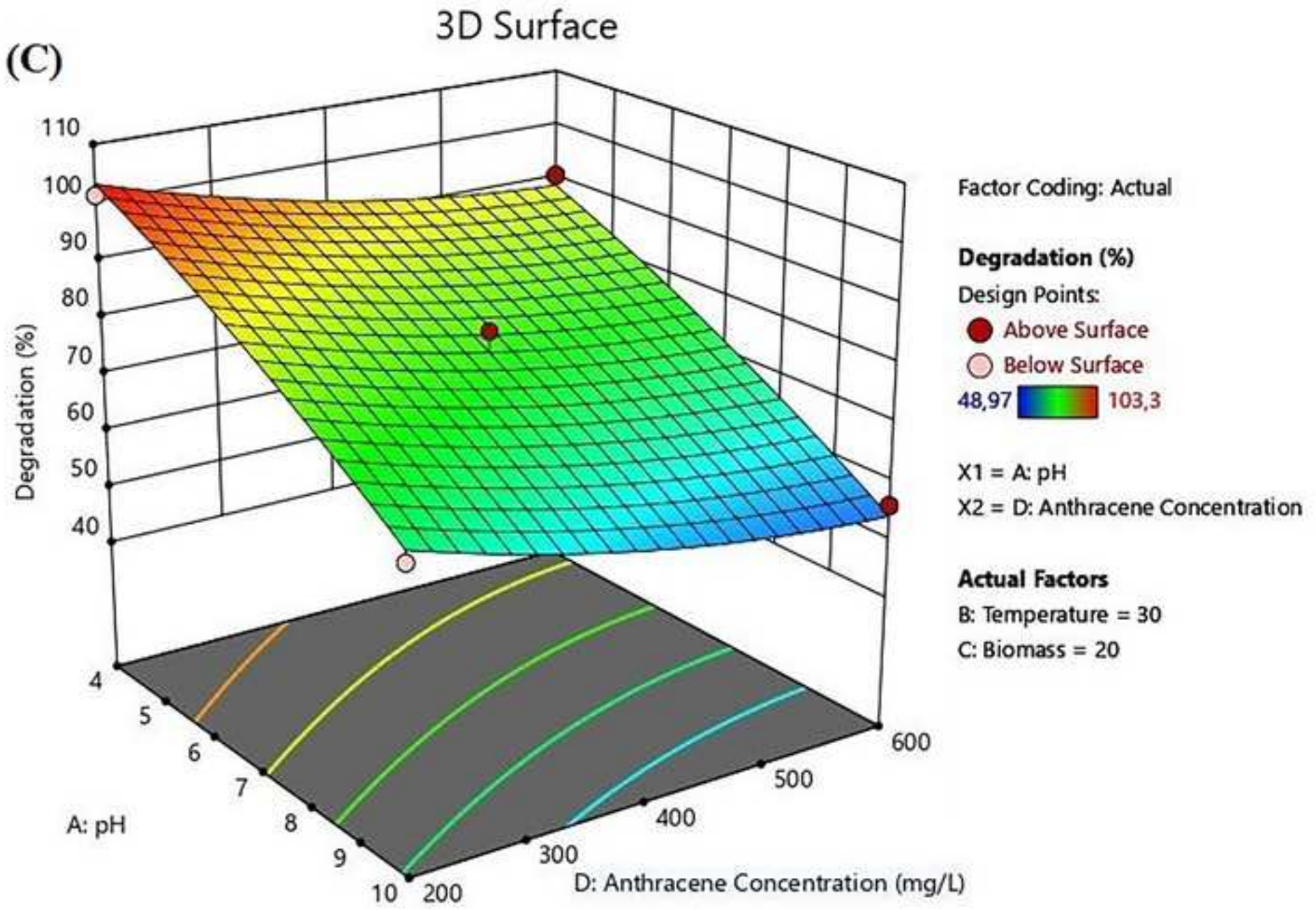

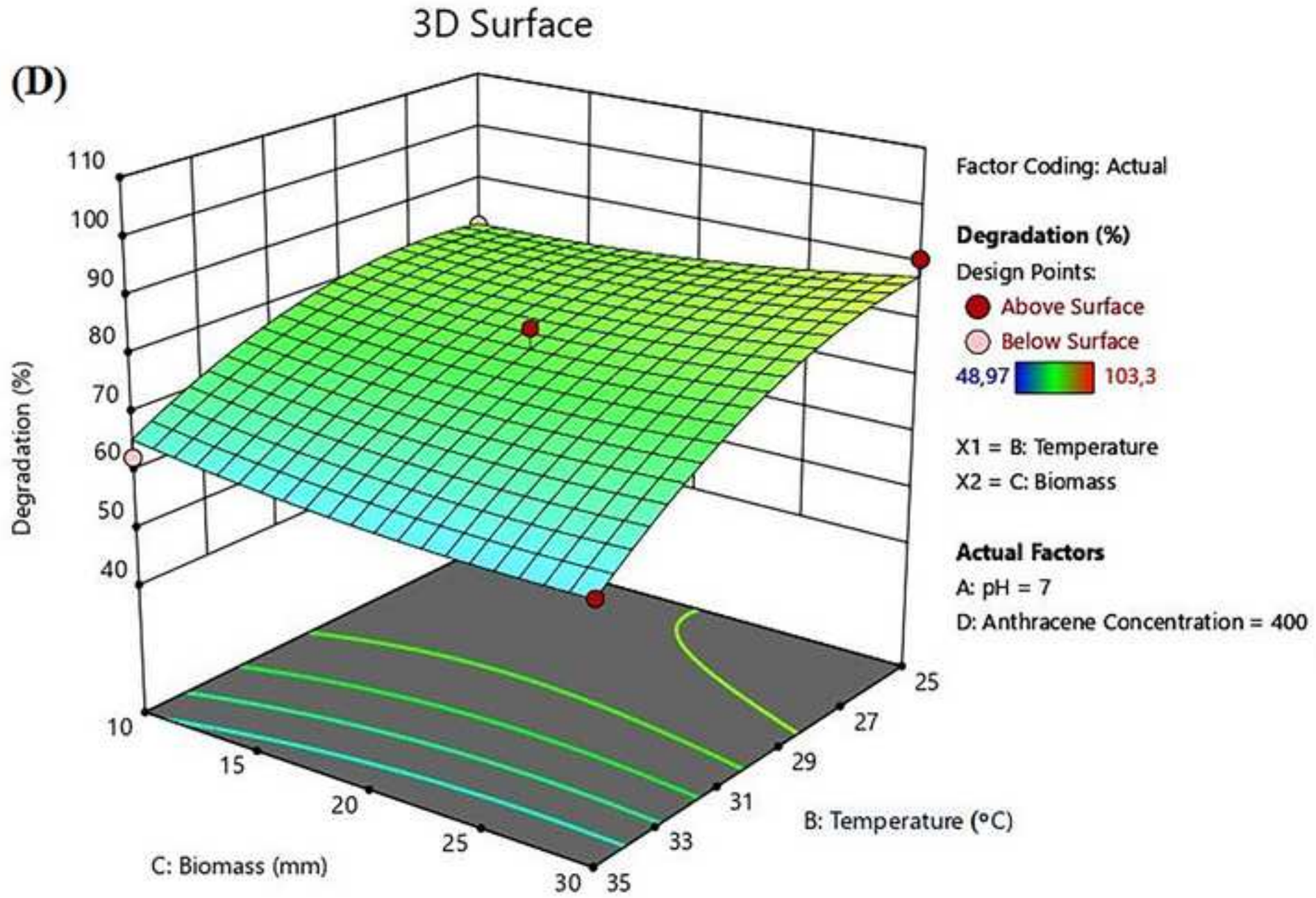

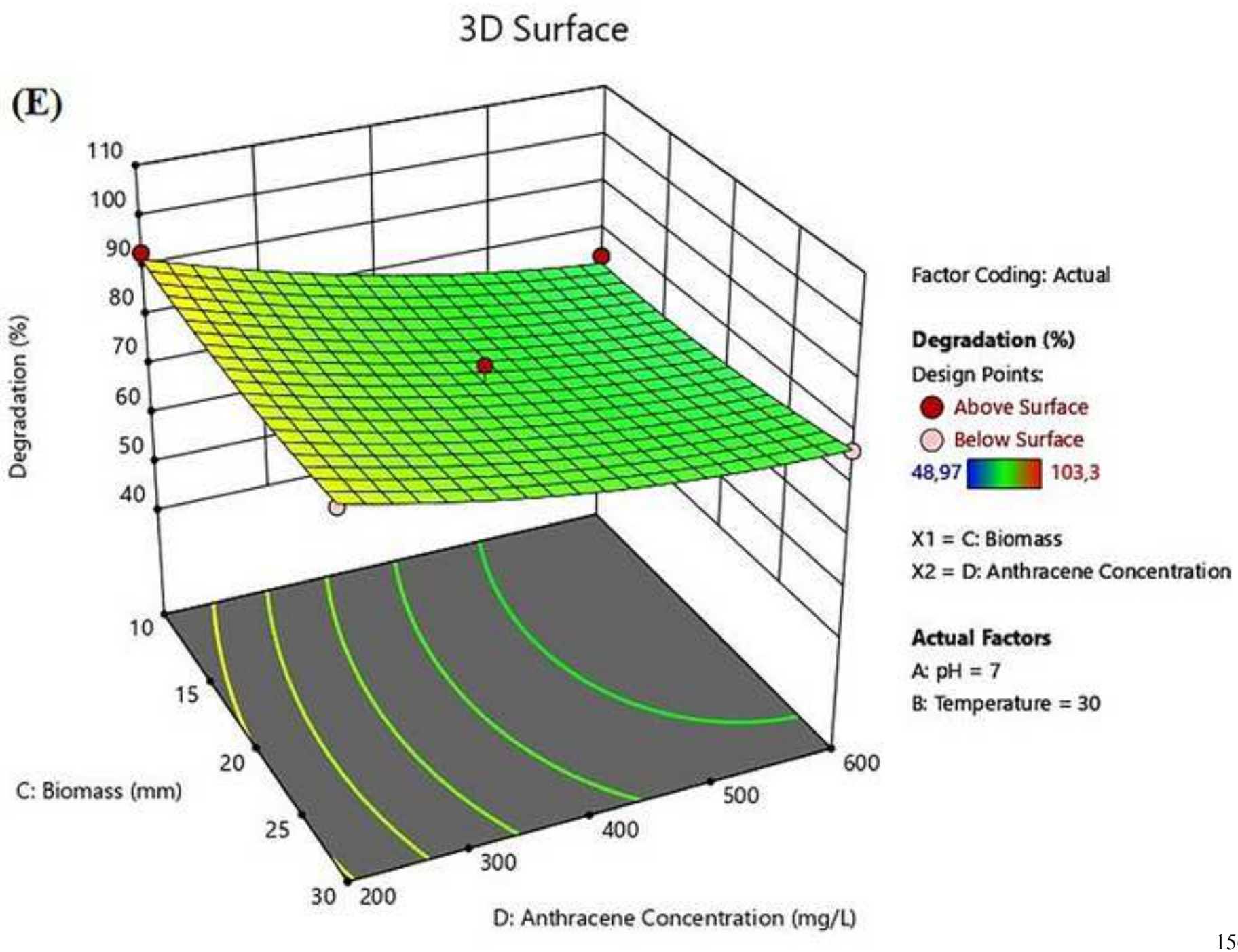

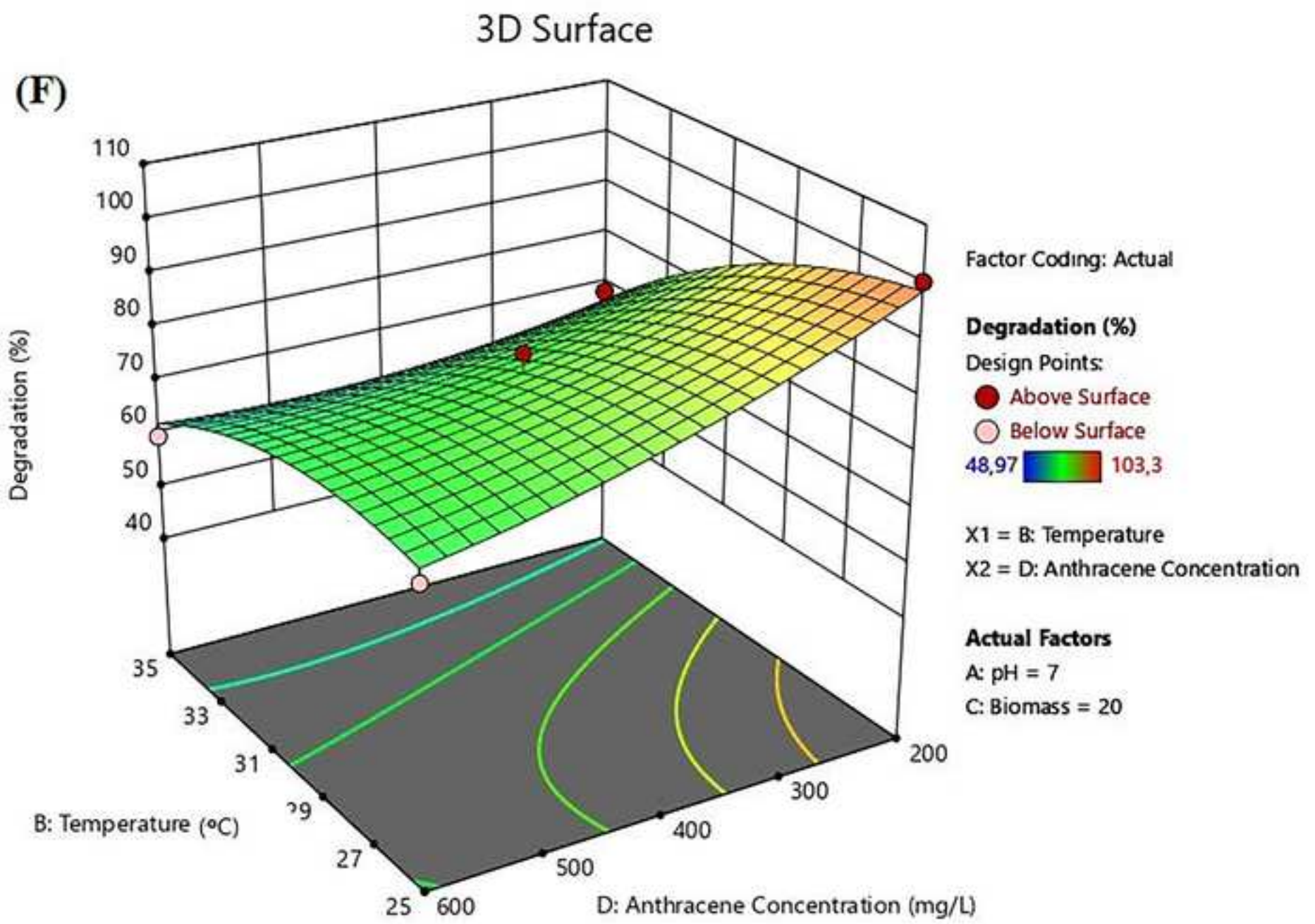

Figure 2A

Click here to access/download;Figure;Fig 2A.jpg

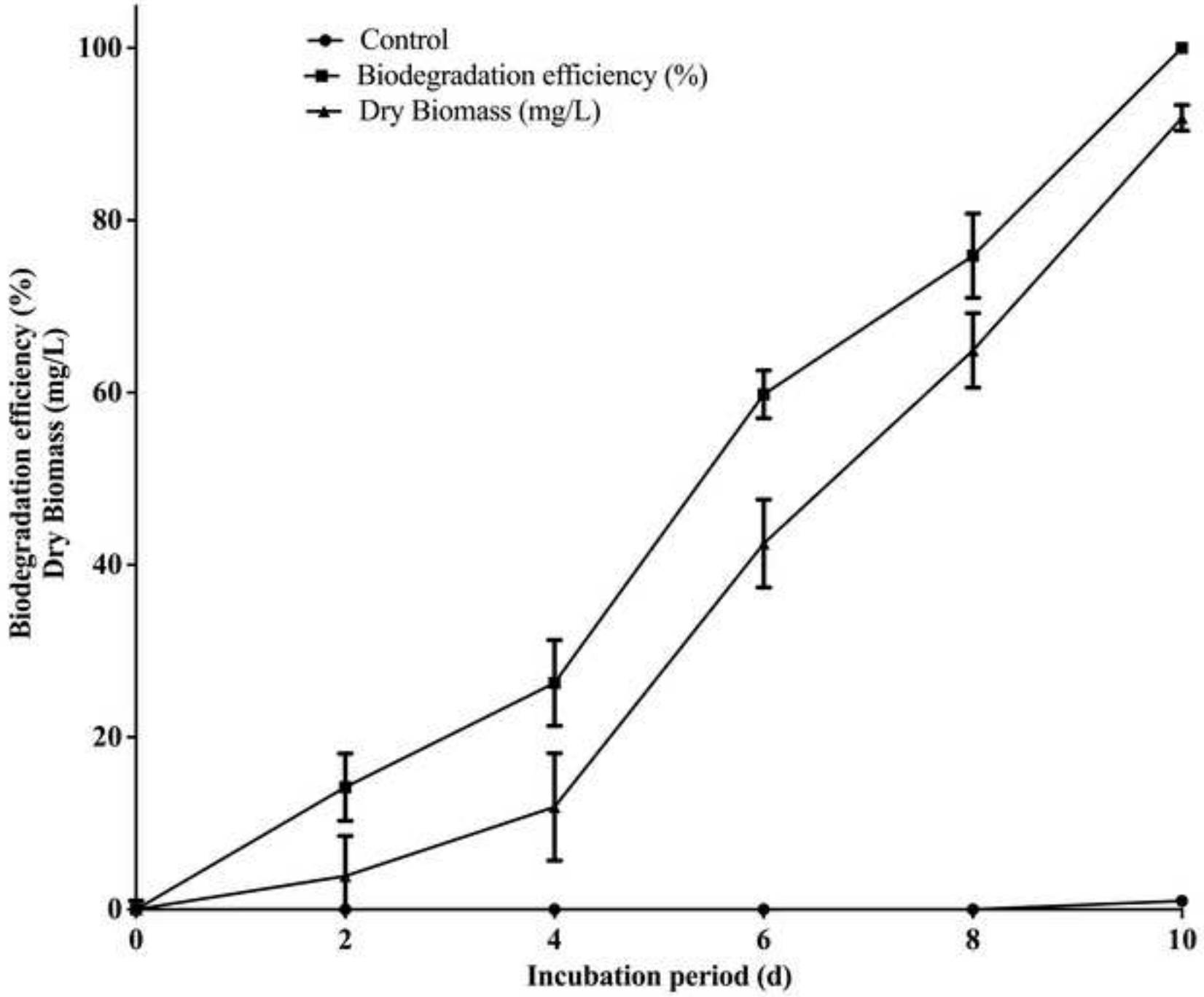

Figure 2B

Click here to access/download;Figure;Fig 2B.jpg

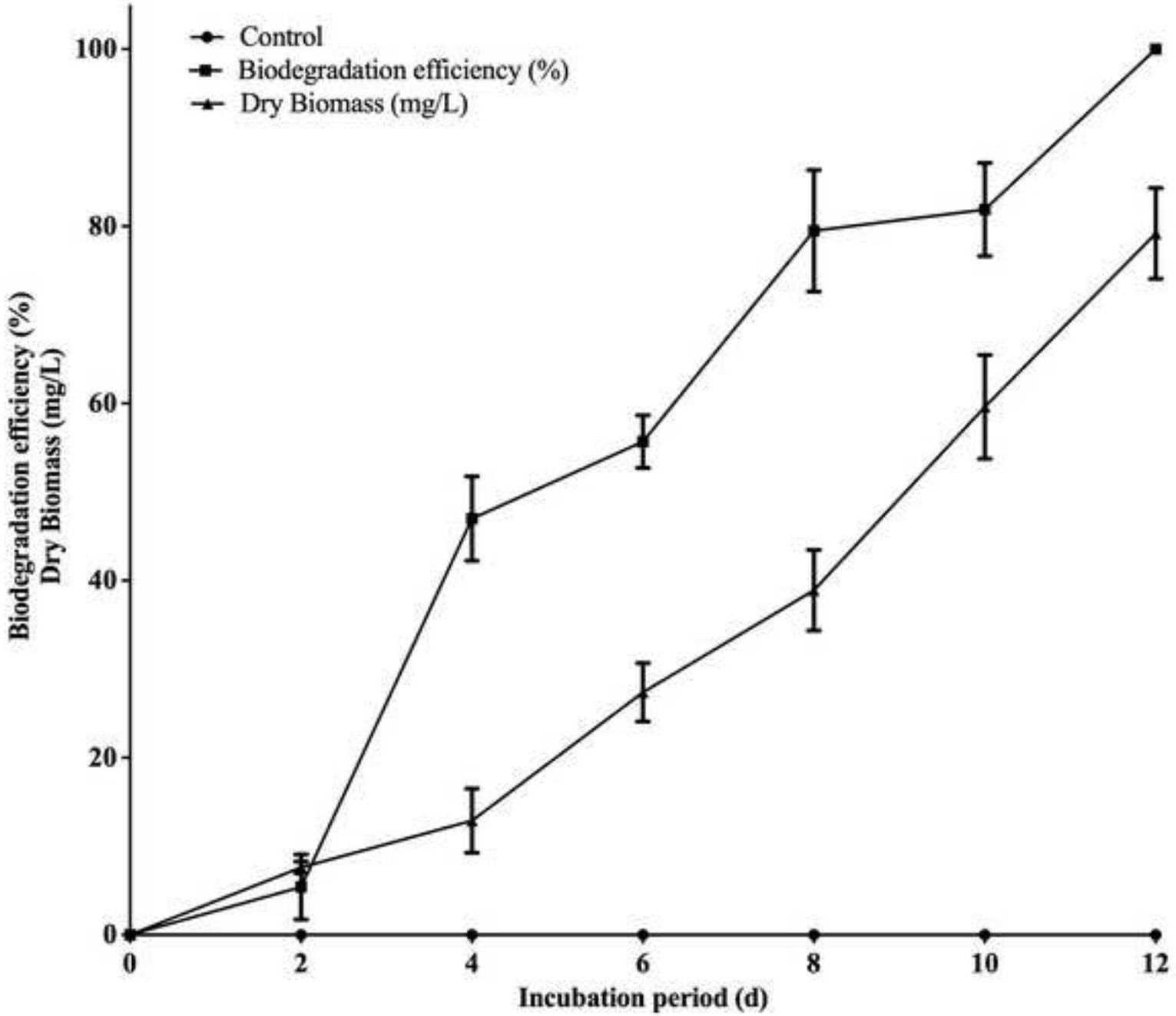

Figure 3A

Click here to access/download;Figure;Fig 3A.jpg

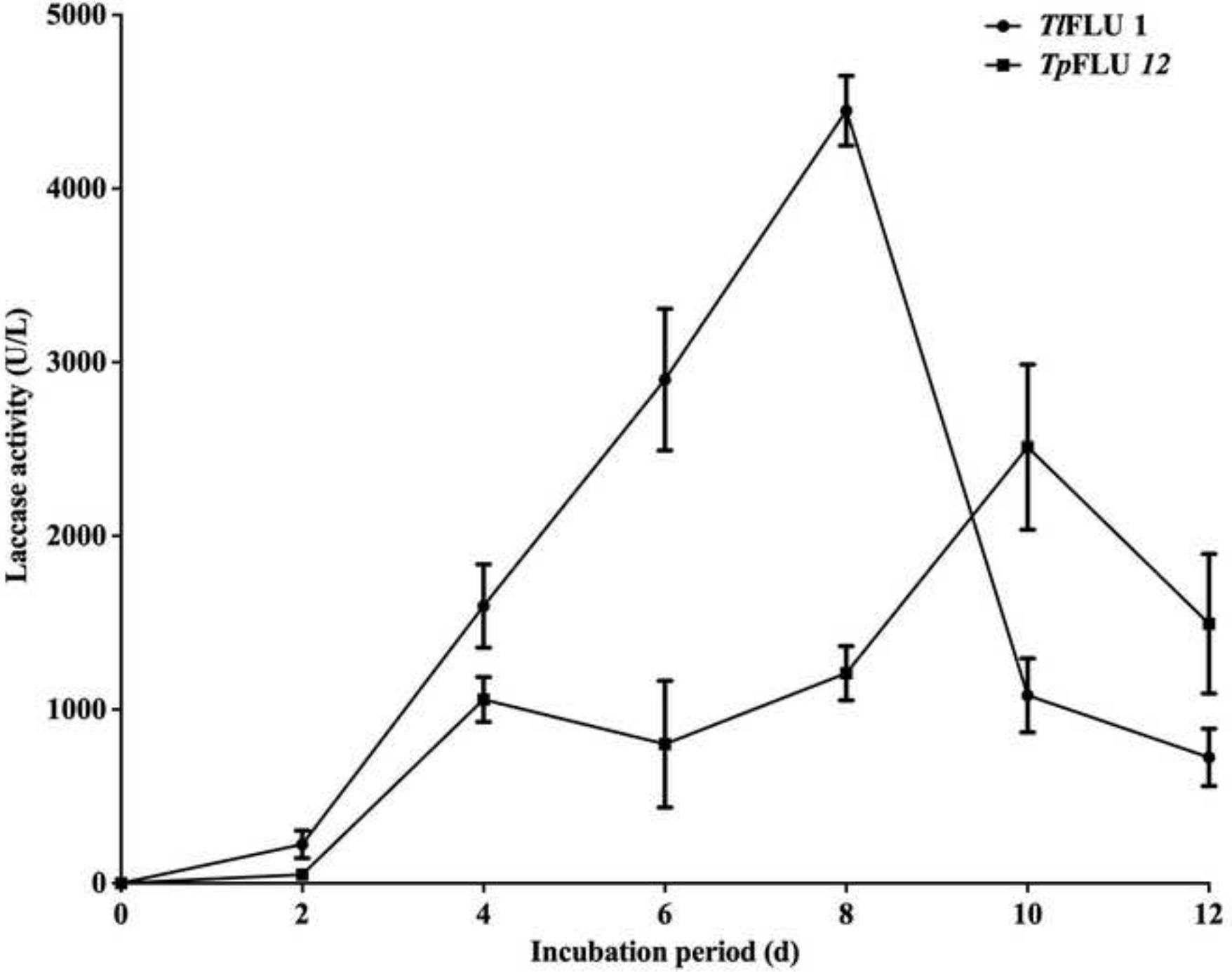

Figure 3B

Click here to access/download;Figure;Fig 3B.jpg

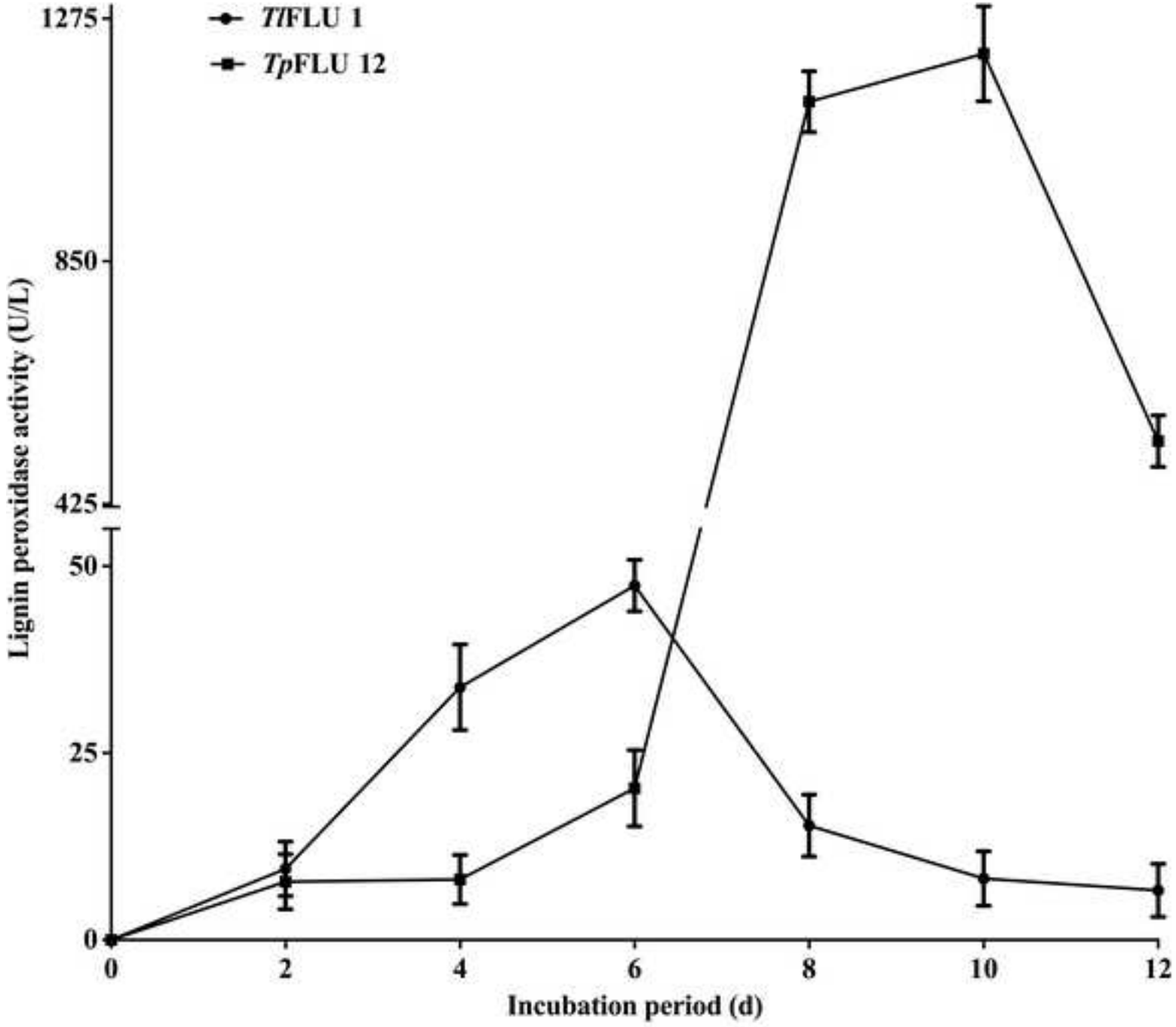

Figure 3C

Click here to access/download;Figure;Fig 3C.jpg

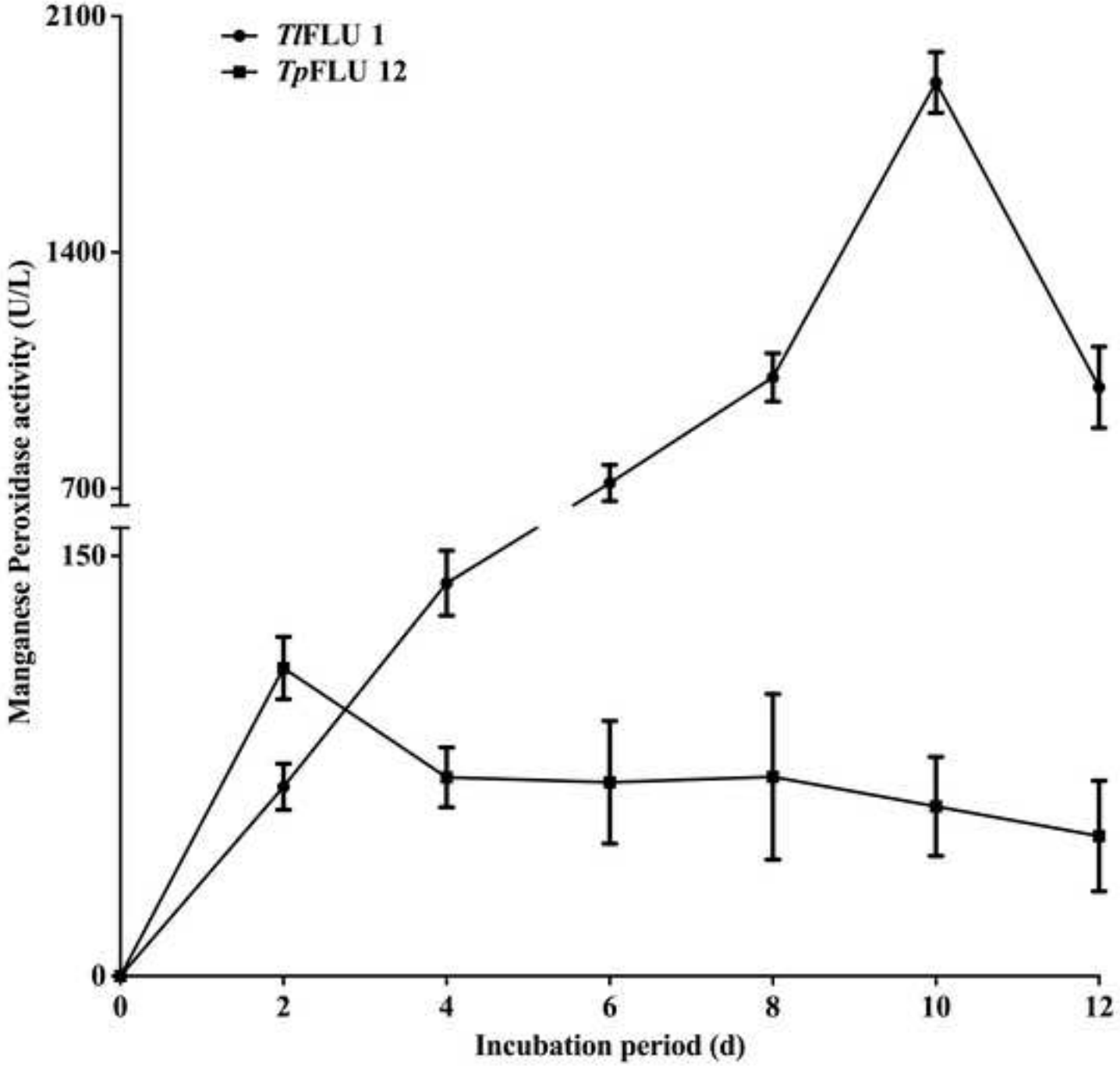

Figure 4A

Click here to access/download;Figure;Fig 4A.jpg

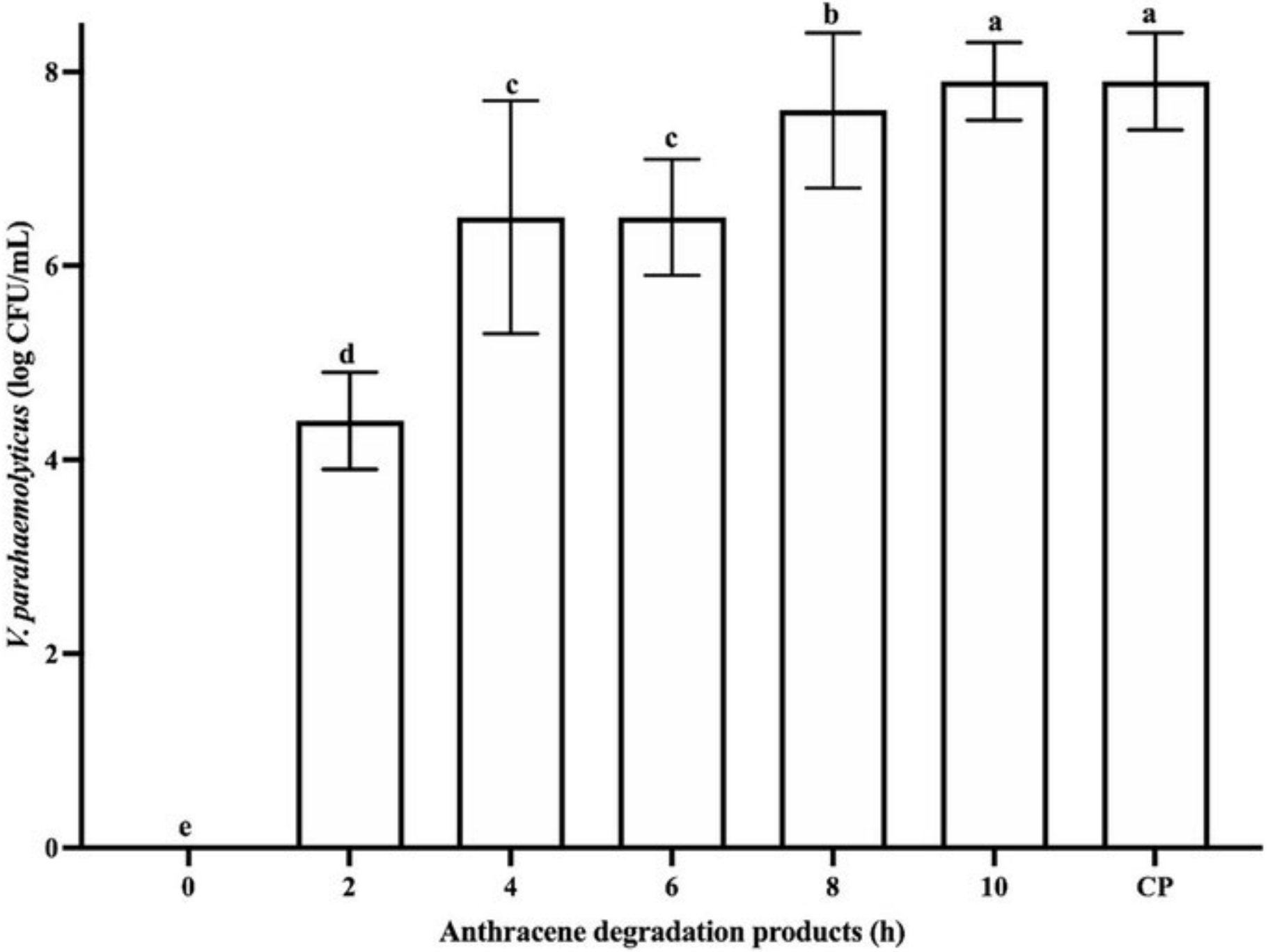

Figure 4B

Click here to access/download;Figure;Fig 4B.jpg

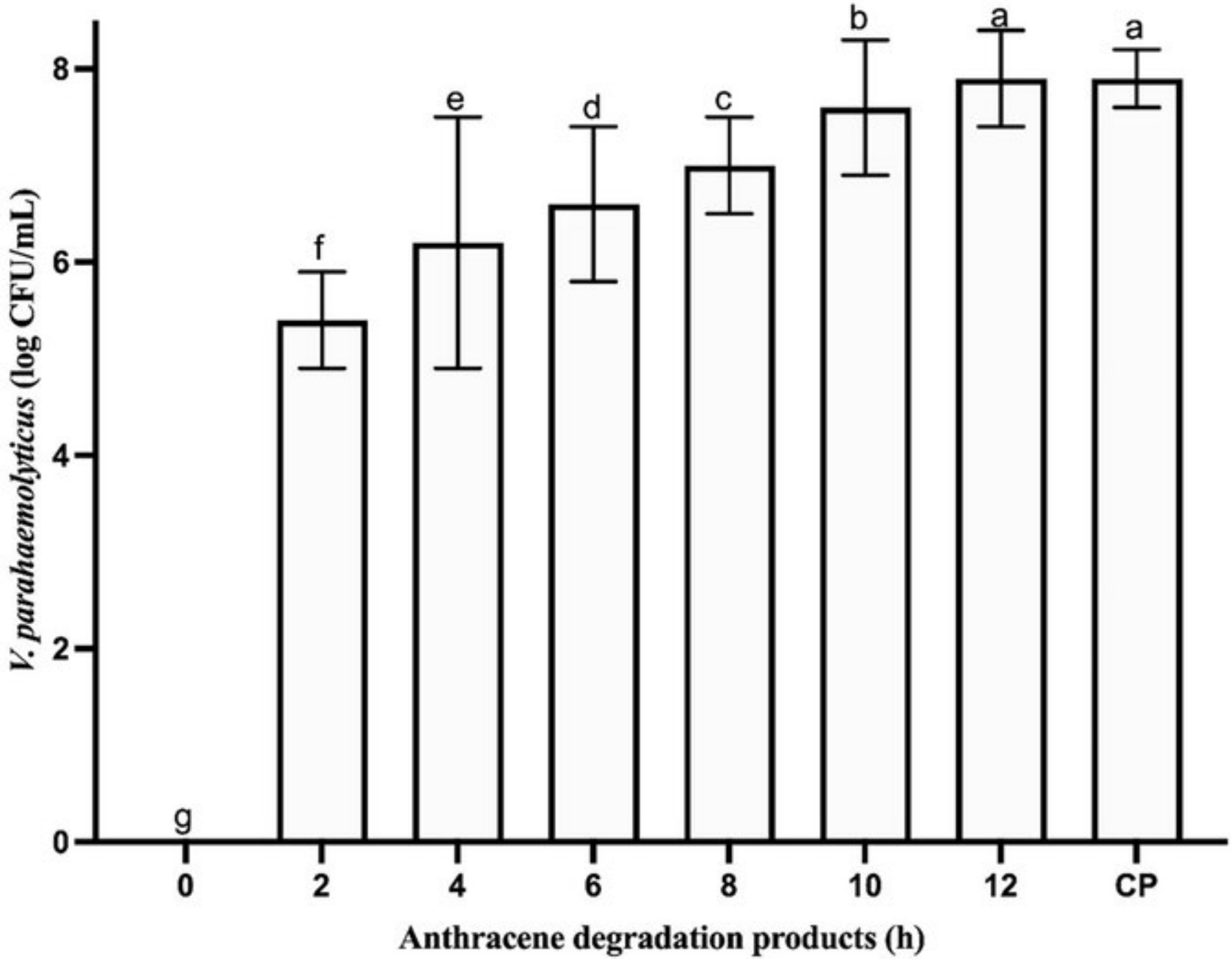

Supplementary Materials

Journal: Ecotoxicology and Environmental Safety

Optimization of anthracene biodegradation by indigenous *Trichoderma lixii* and *Talaromyces pinophilus* strains using response surface methodology

Samson O. Egbewale[1], Ajit Kumar[1], Tosin A. Olasehinde[1], Mduduzi P. Mokoena[2] and Ademola O. Olaniran[1*]

[1]Discipline of Microbiology, University of KwaZulu-Natal (Westville Campus), Durban 4000, South Africa

[2]Department of Pathology, School of Medicine, University of Limpopo, Private Bag X1106, Sovenga-0727, South Africa.

*Correspondence: olanirana@ukzn.ac.za; Tel.: +27-31-260-7400

Figure S1. Cook's distance (A), Residual vs predicted (B), leverage vs run (C), box-cox plot for power transformation (D) and predicted vs actual (E).

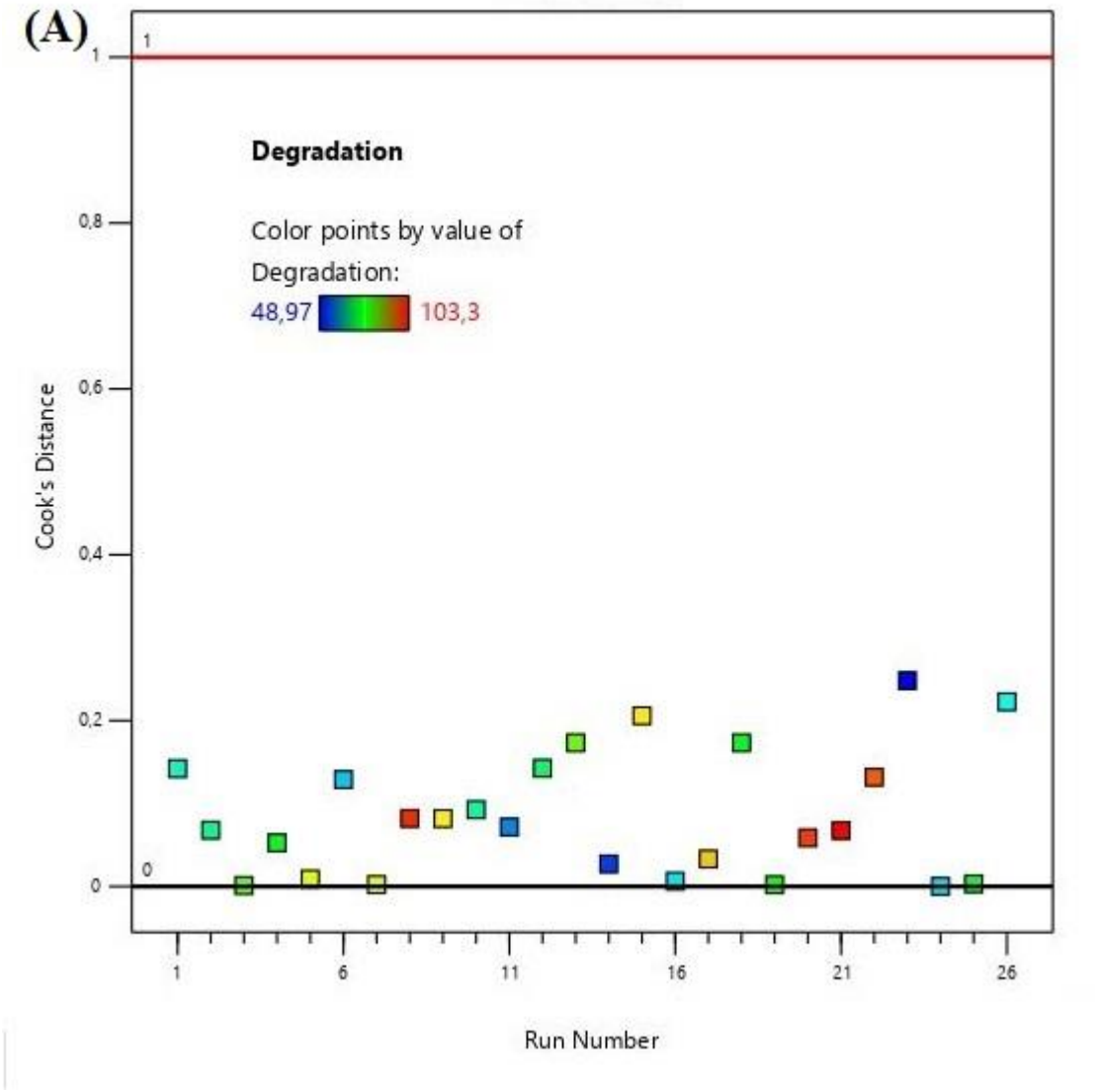

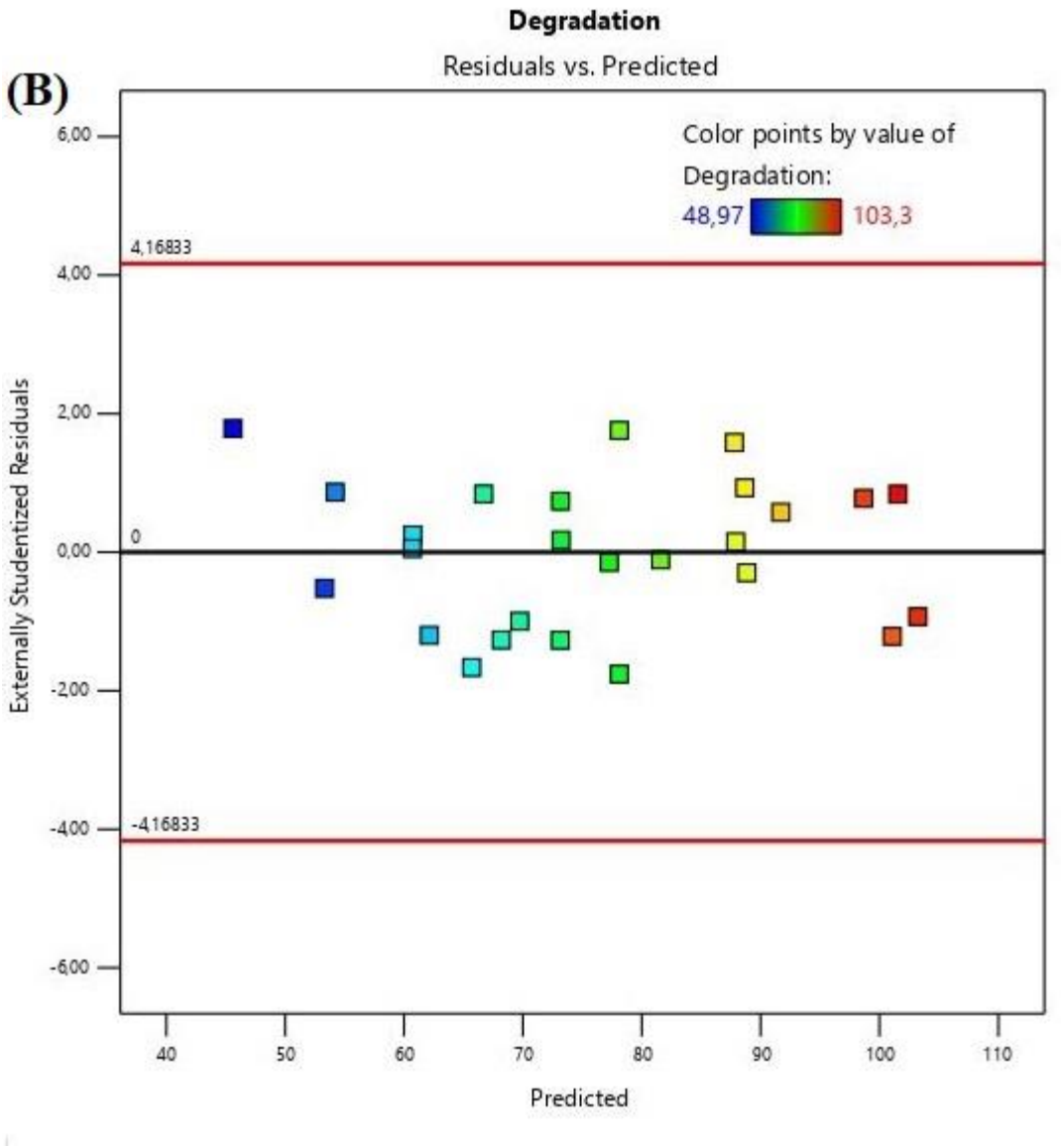
(B)
Degradation
Residuals vs. Predicted
Color points by value of
Degradation:
48,97
103,3
4,16833
-4,16833
0
Externally Studentized Residuals
Predicted
6,00
4,00
2,00
0,00
-2,00
-4,00
-6,00
40
50
60
70
80
90
100
110

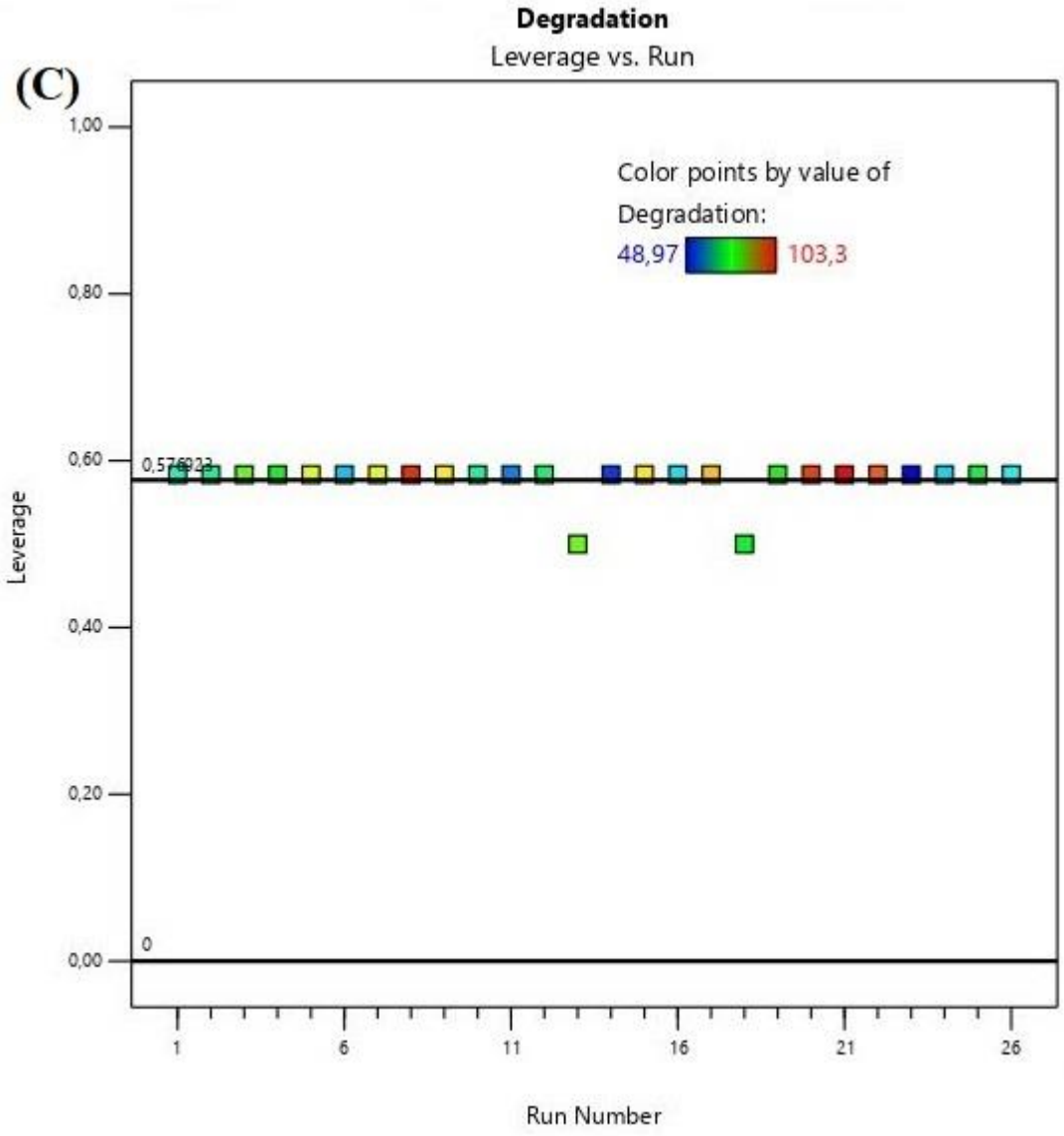
(C)
Degradation
Leverage vs. Run
Color points by value of
Degradation:
48,97
103,3
1,00
0,80
0,60
0,40
0,20
0,00
0,576923
0
Leverage
1
6
11
16
21
26
Run Number

(D)

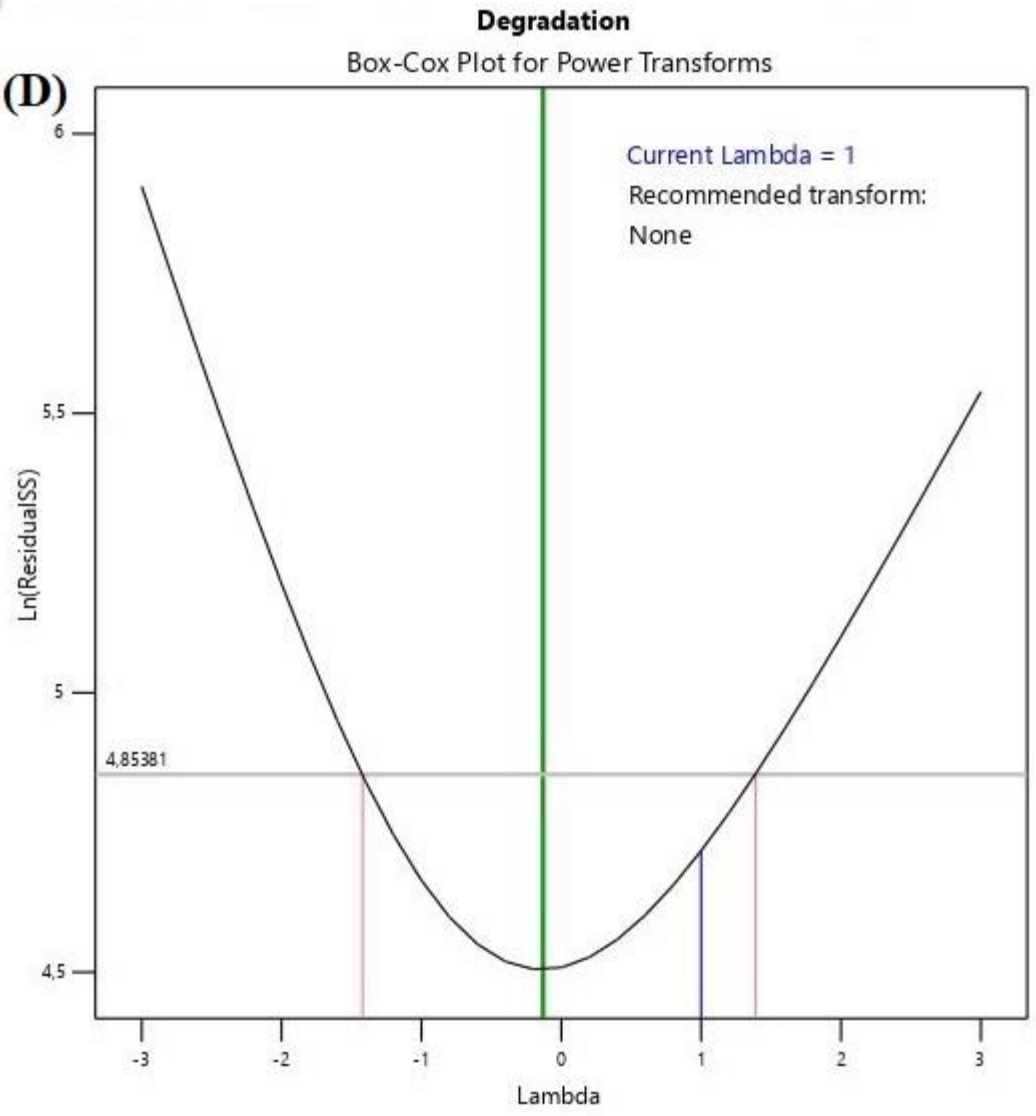
Degradation
Box-Cox Plot for Power Transforms
Current Lambda = 1
Recommended transform:
None
Ln(ResidualSS)
6
5,5
5
4,5
4,85381
-3
-2
-1
0
1
2
3
Lambda

(E)

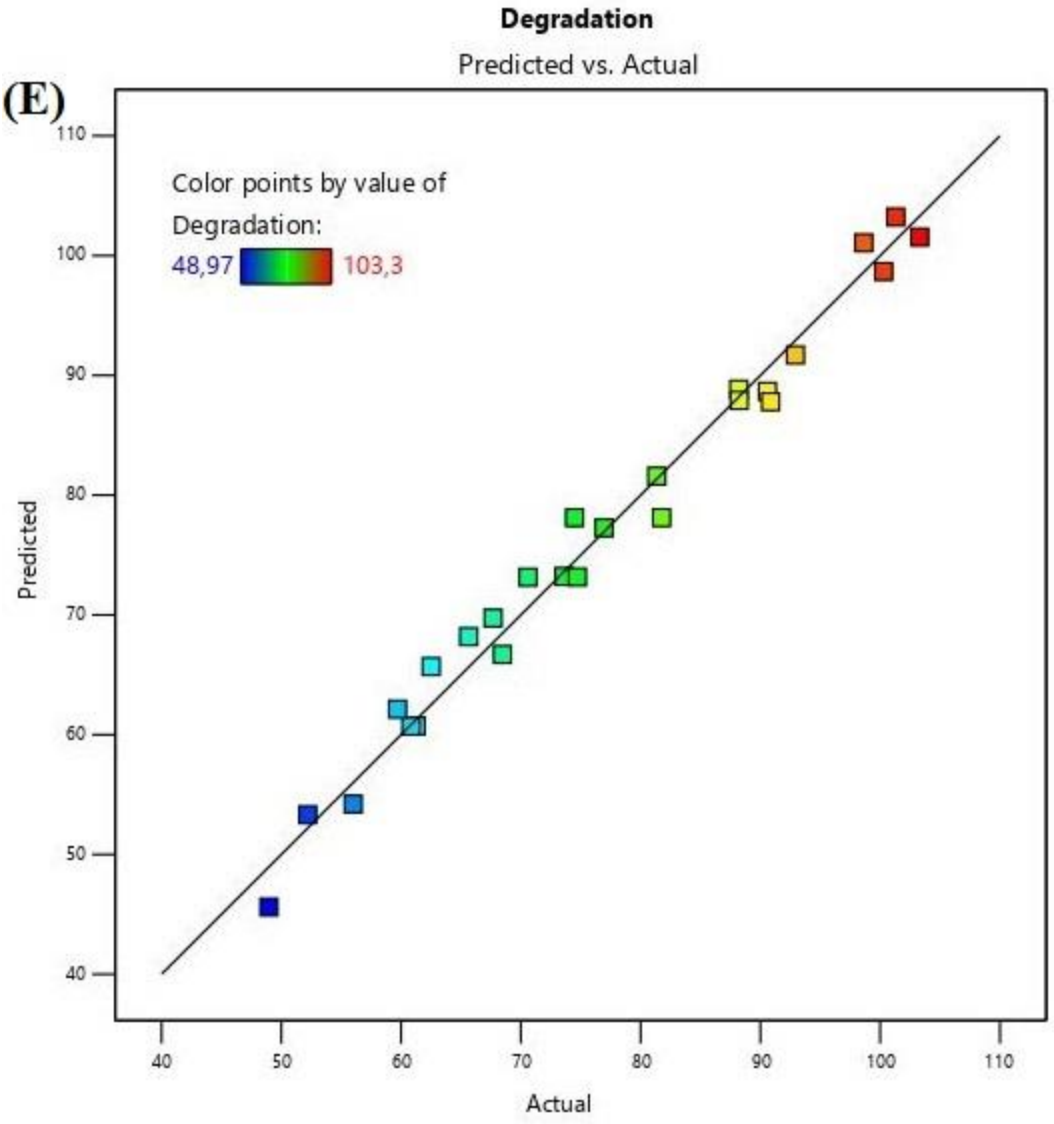
Degradation
Predicted vs. Actual
Color points by value of
Degradation:
48,97
103,3
Predicted
Actual
40
50
60
70
80
90
100
110

Figure S2. The 3D interactive effect among the predicted optimized variables on the maximum anthracene transformation using central composite rotatable design (CCRD).

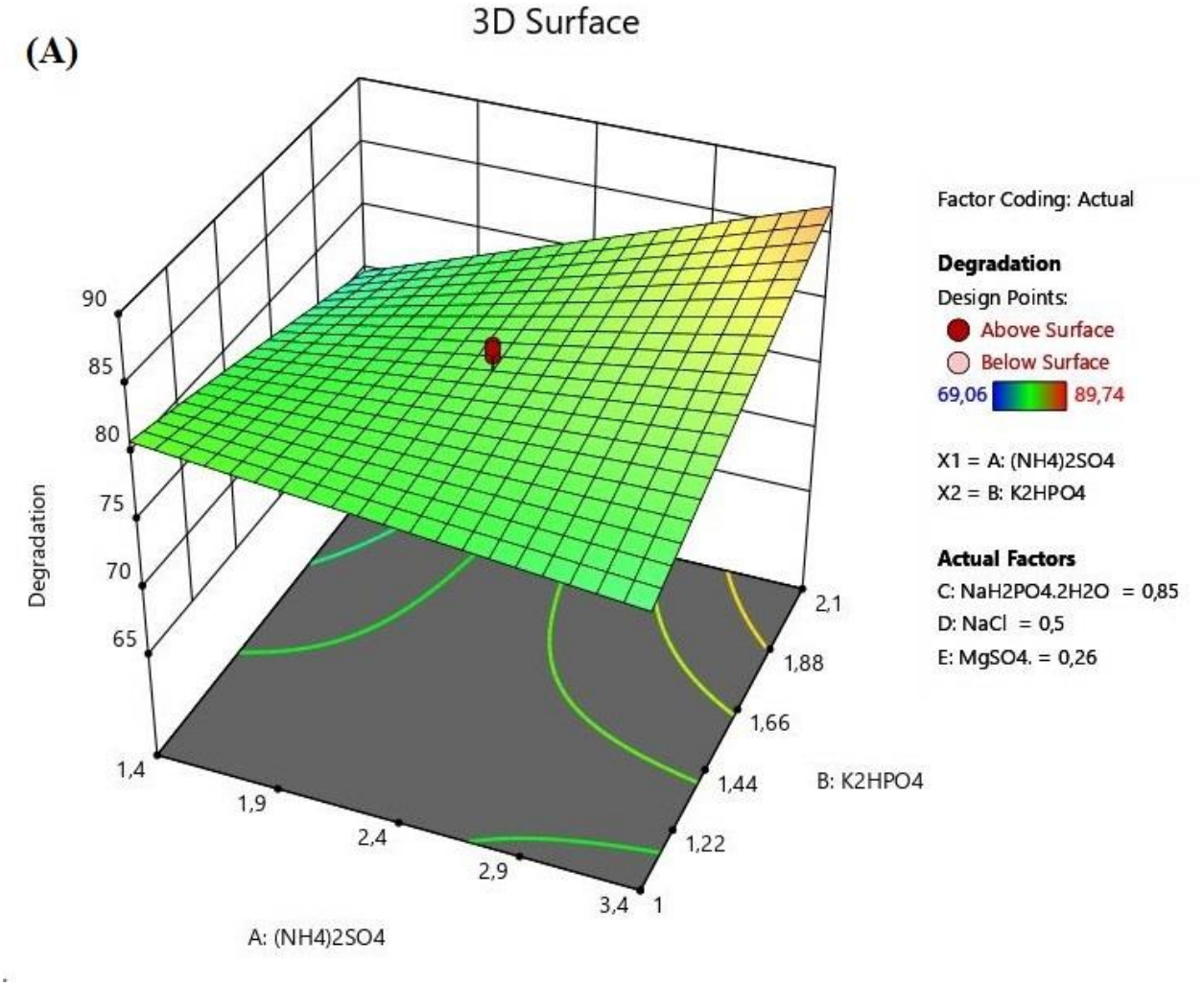

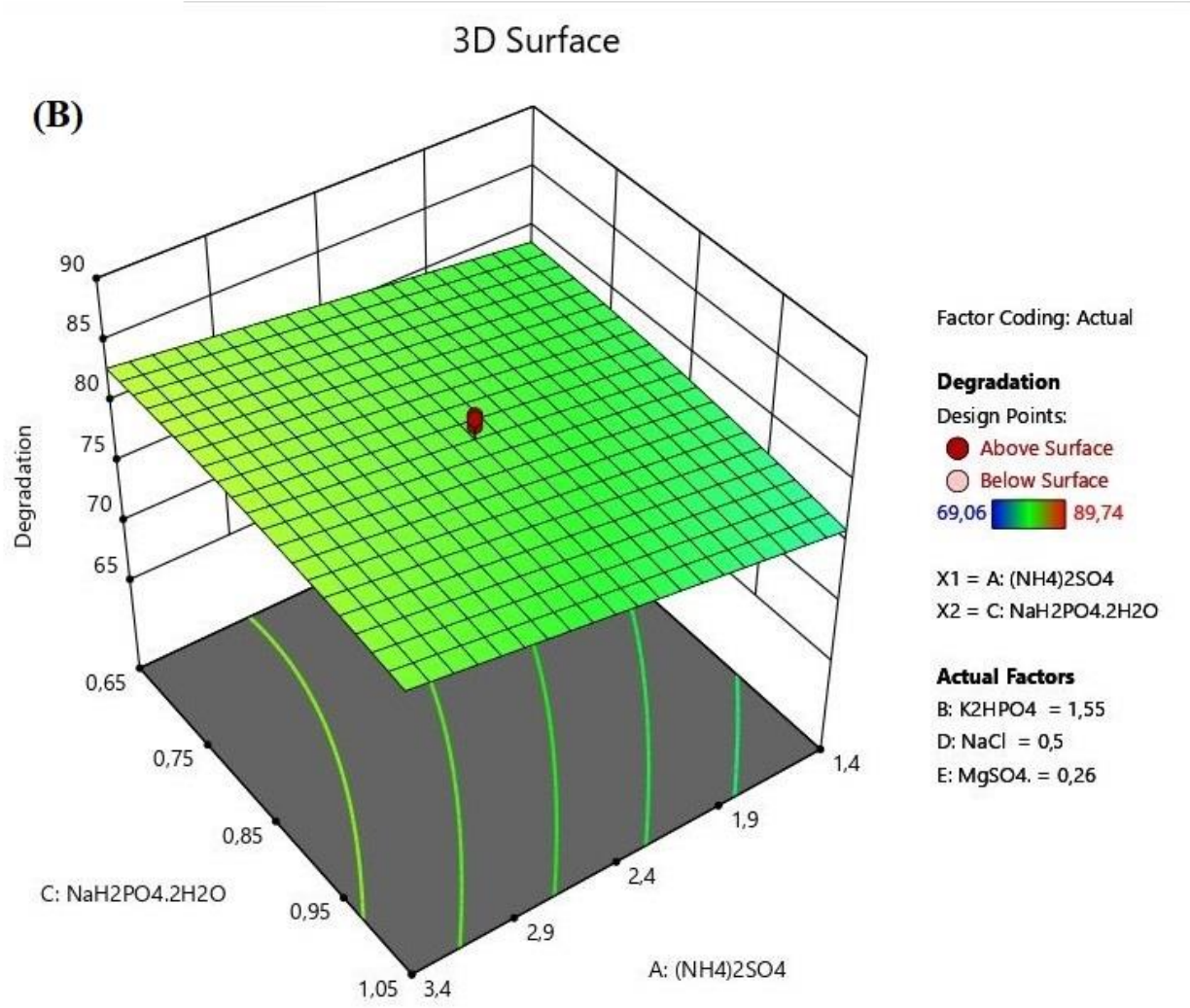
3D Surface
(B)
Degradation
90
85
80
75
70
65
0,65
0,75
0,85
0,95
1,05
C: NaH2PO4.2H2O
3,4
2,9
2,4
1,9
1,4
A: (NH4)2SO4
Factor Coding: Actual
Degradation
Design Points:
Above Surface
Below Surface
69,06
89,74
X1 = A: (NH4)2SO4
X2 = C: NaH2PO4.2H2O
Actual Factors
B: K2HPO4 = 1,55
D: NaCl = 0,5
E: MgSO4. = 0,26

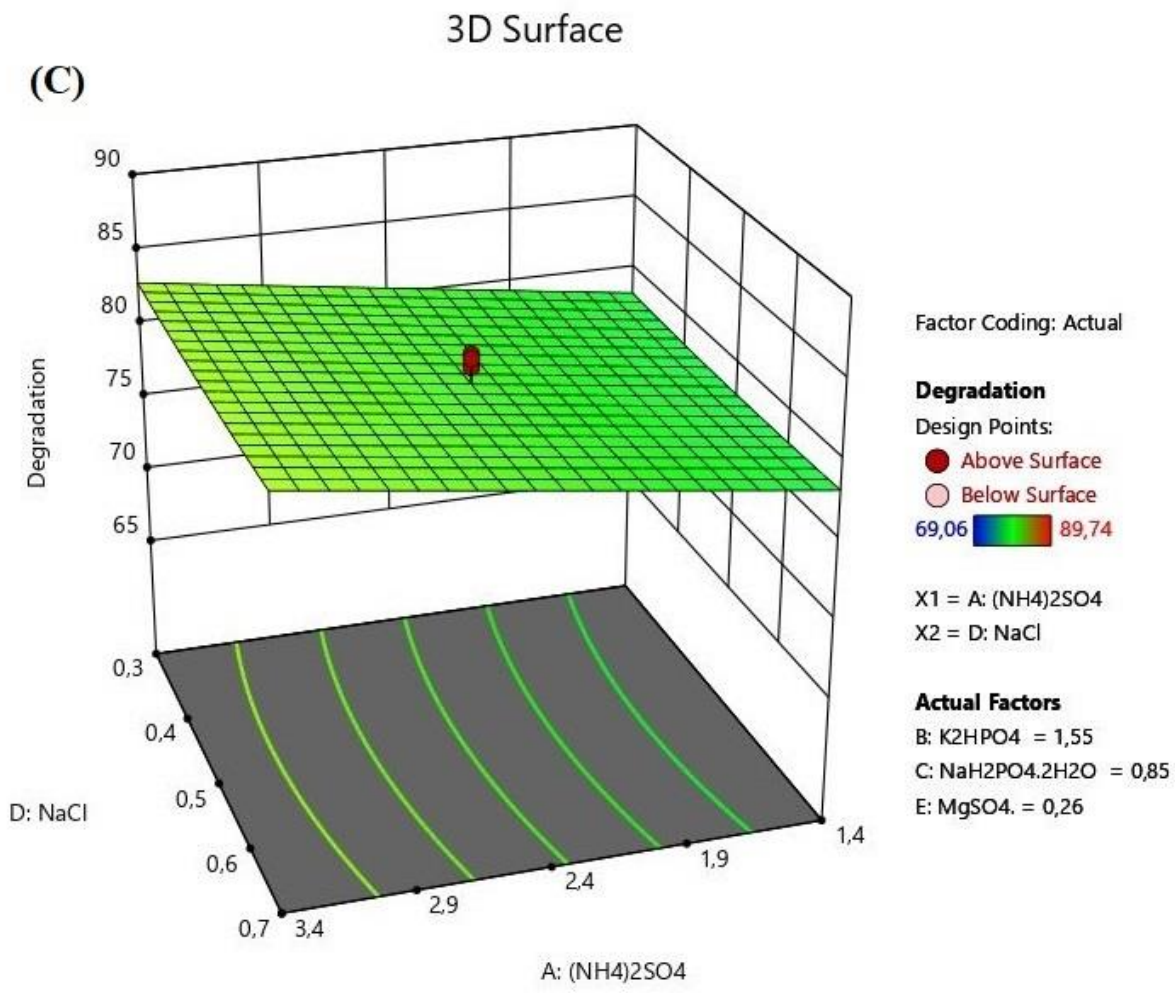
3D Surface
(C)
Degradation
90
85
80
75
70
65
D: NaCl
0,3
0,4
0,5
0,6
0,7
A: (NH4)2SO4
3,4
2,9
2,4
1,9
1,4
Factor Coding: Actual
Degradation
Design Points:
Above Surface
Below Surface
69,06
89,74
X1 = A: (NH4)2SO4
X2 = D: NaCl
Actual Factors
B: K2HPO4 = 1,55
C: NaH2PO4.2H2O = 0,85
E: MgSO4. = 0,26

(D)

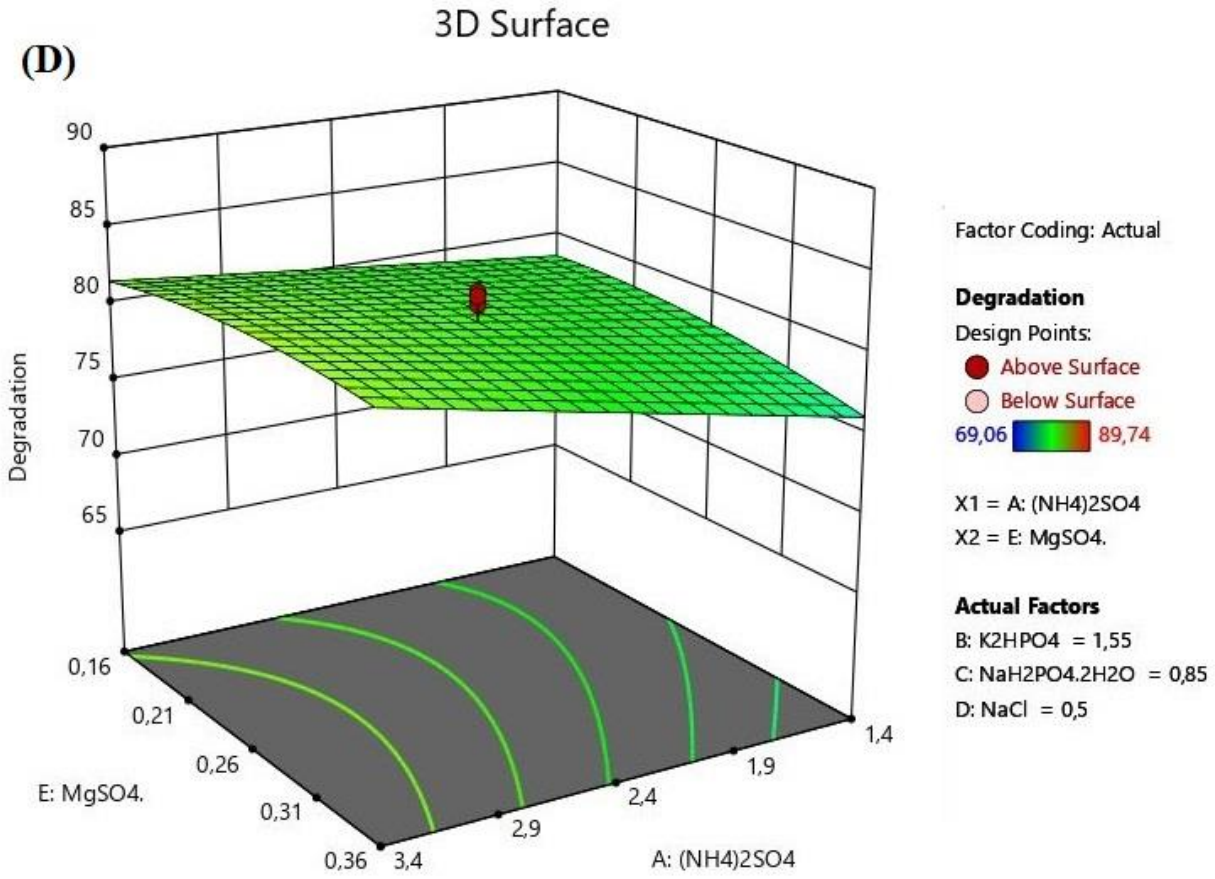
3D Surface
Degradation
90
85
80
75
70
65
0,16
0,21
0,26
0,31
0,36
E: MgSO4.
3,4
2,9
2,4
1,9
1,4
A: (NH4)2SO4
Factor Coding: Actual
Degradation
Design Points:
Above Surface
Below Surface
69,06
89,74
X1 = A: (NH4)2SO4
X2 = E: MgSO4.
Actual Factors
B: K2HPO4 = 1,55
C: NaH2PO4.2H2O = 0,85
D: NaCl = 0,5

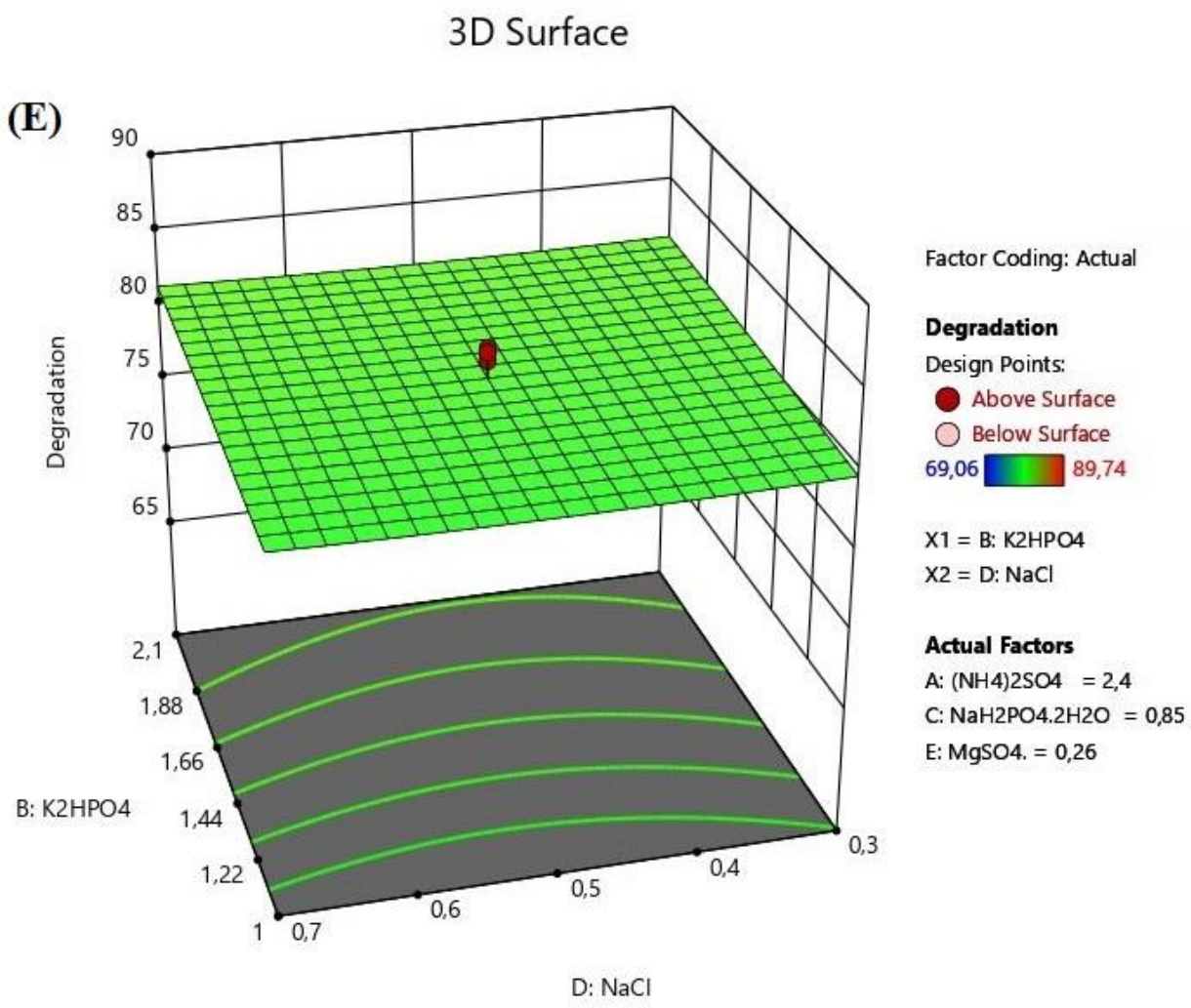
3D Surface
(E)
90
85
80
75
70
65
Degradation
2,1
1,88
1,66
1,44
1,22
1
B: K2HPO4
0,7
0,6
0,5
0,4
0,3
D: NaCl
Factor Coding: Actual
Degradation
Design Points:
Above Surface
Below Surface
69,06
89,74
X1 = B: K2HPO4
X2 = D: NaCl
Actual Factors
A: (NH4)2SO4 = 2,4
C: NaH2PO4.2H2O = 0,85
E: MgSO4. = 0,26

(F)

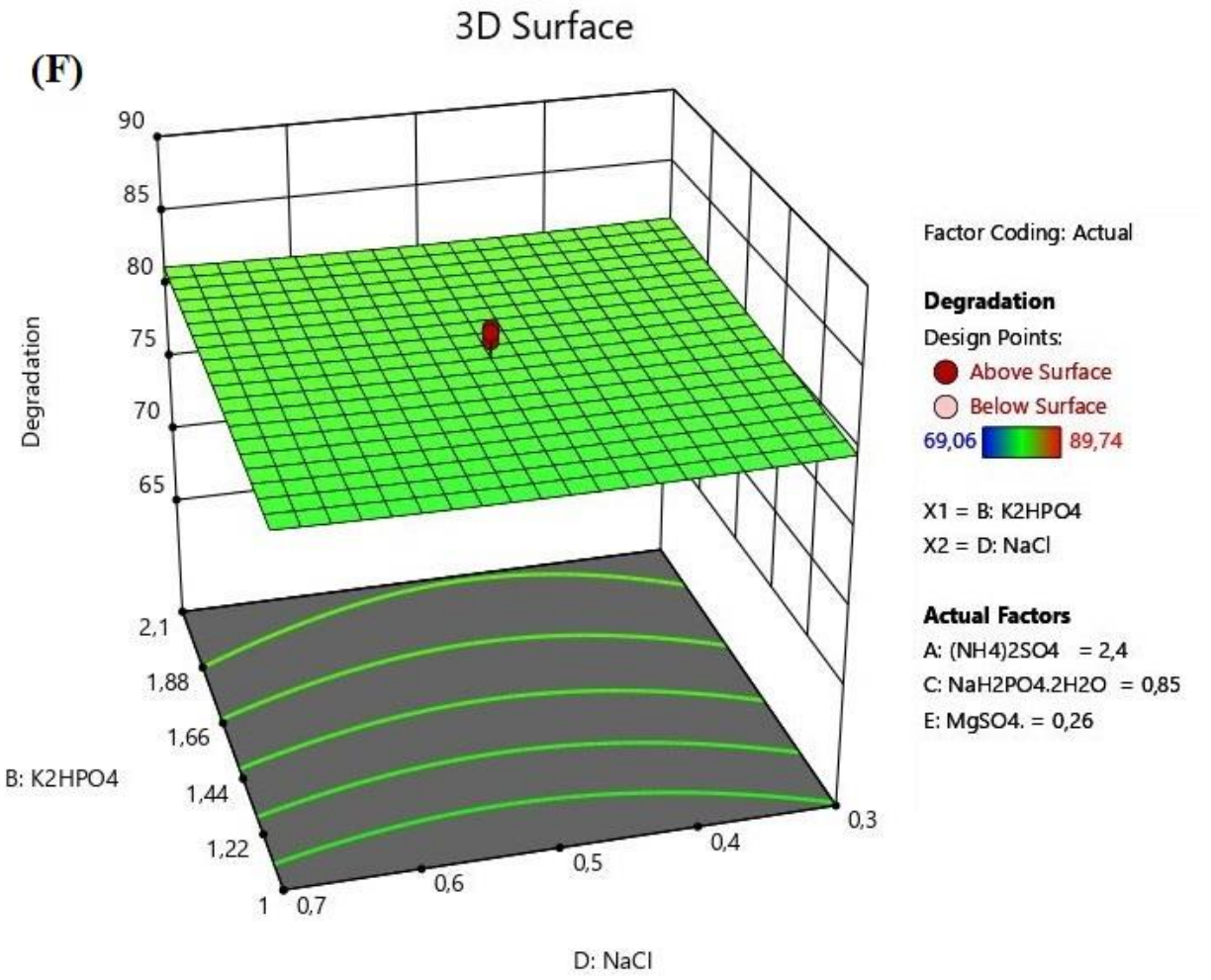
3D Surface
Degradation
90
85
80
75
70
65
B: K2HPO4
2,1
1,88
1,66
1,44
1,22
1
D: NaCl
0,7
0,6
0,5
0,4
0,3
Factor Coding: Actual
Degradation
Design Points:
Above Surface
Below Surface
69,06
89,74
X1 = B: K2HPO4
X2 = D: NaCl
Actual Factors
A: (NH4)2SO4 = 2,4
C: NaH2PO4.2H2O = 0,85
E: MgSO4. = 0,26

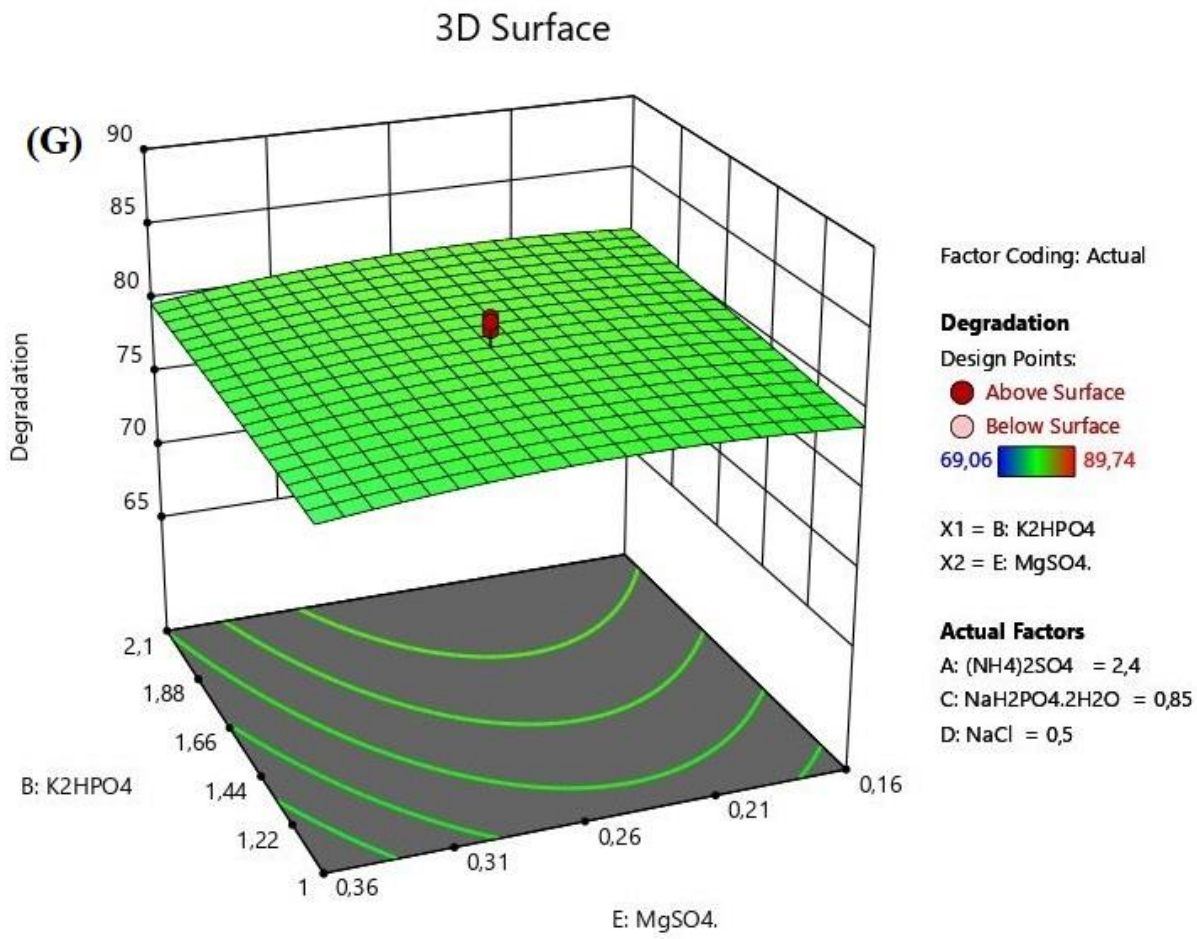
3D Surface
(G)
Degradation
90
85
80
75
70
65
B: K2HPO4
2,1
1,88
1,66
1,44
1,22
1
E: MgSO4.
0,36
0,31
0,26
0,21
0,16
Factor Coding: Actual
Degradation
Design Points:
Above Surface
Below Surface
69,06
89,74
X1 = B: K2HPO4
X2 = E: MgSO4.
Actual Factors
A: (NH4)2SO4 = 2,4
C: NaH2PO4.2H2O = 0,85
D: NaCl = 0,5

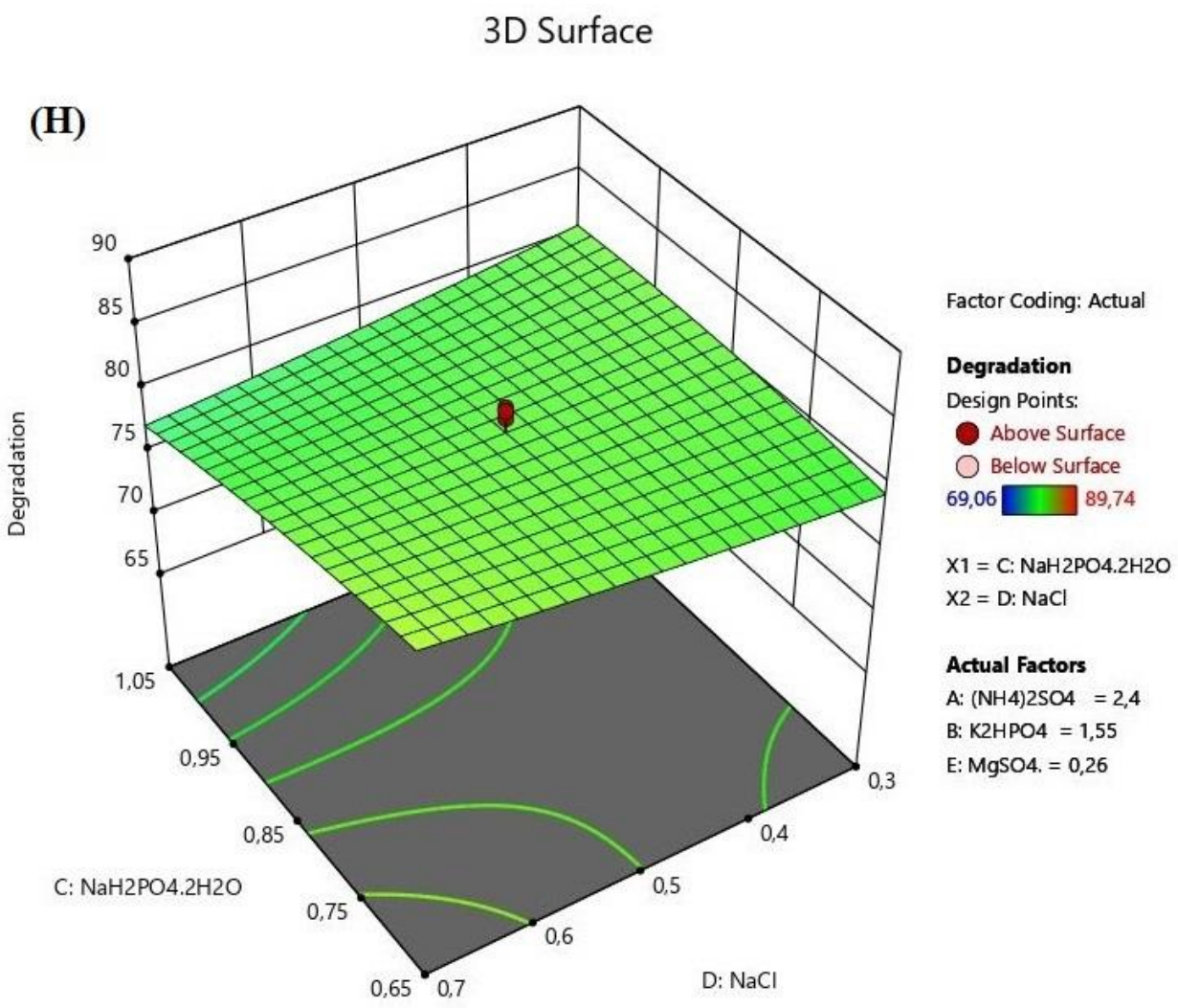
3D Surface
(H)
90
85
80
75
70
65
Degradation
1,05
0,95
0,85
0,75
0,65
C: NaH2PO4.2H2O
0,7
0,6
0,5
0,4
0,3
D: NaCl
Factor Coding: Actual
Degradation
Design Points:
Above Surface
Below Surface
69,06
89,74
X1 = C: NaH2PO4.2H2O
X2 = D: NaCl
Actual Factors
A: (NH4)2SO4 = 2,4
B: K2HPO4 = 1,55
E: MgSO4. = 0,26

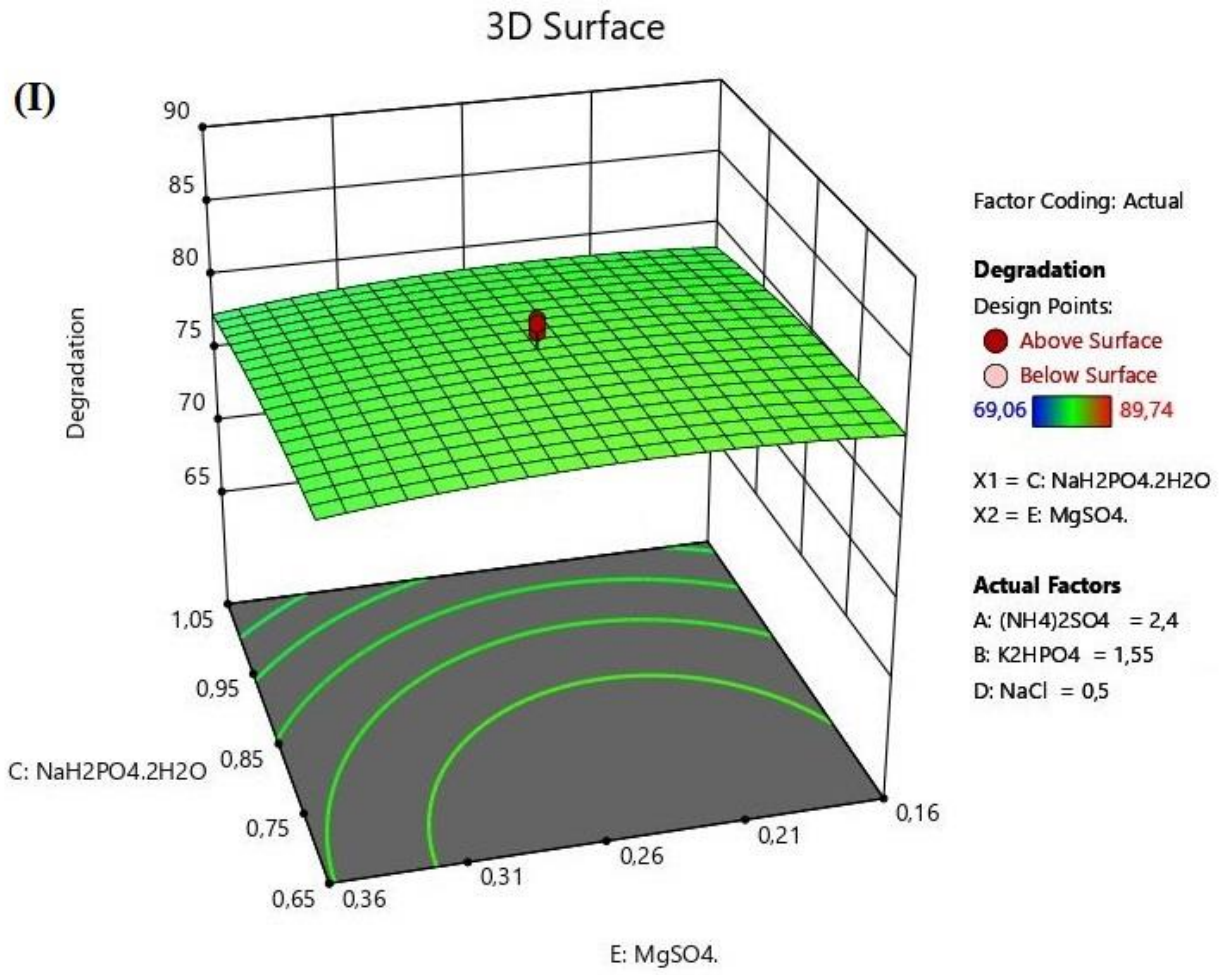
(I)
3D Surface
Degradation
90
85
80
75
70
65
C: NaH2PO4.2H2O
1,05
0,95
0,85
0,75
0,65
E: MgSO4.
0,36
0,31
0,26
0,21
0,16
Factor Coding: Actual
Degradation
Design Points:
Above Surface
Below Surface
69,06
89,74
X1 = C: NaH2PO4.2H2O
X2 = E: MgSO4.
Actual Factors
A: (NH4)2SO4 = 2,4
B: K2HPO4 = 1,55
D: NaCl = 0,5

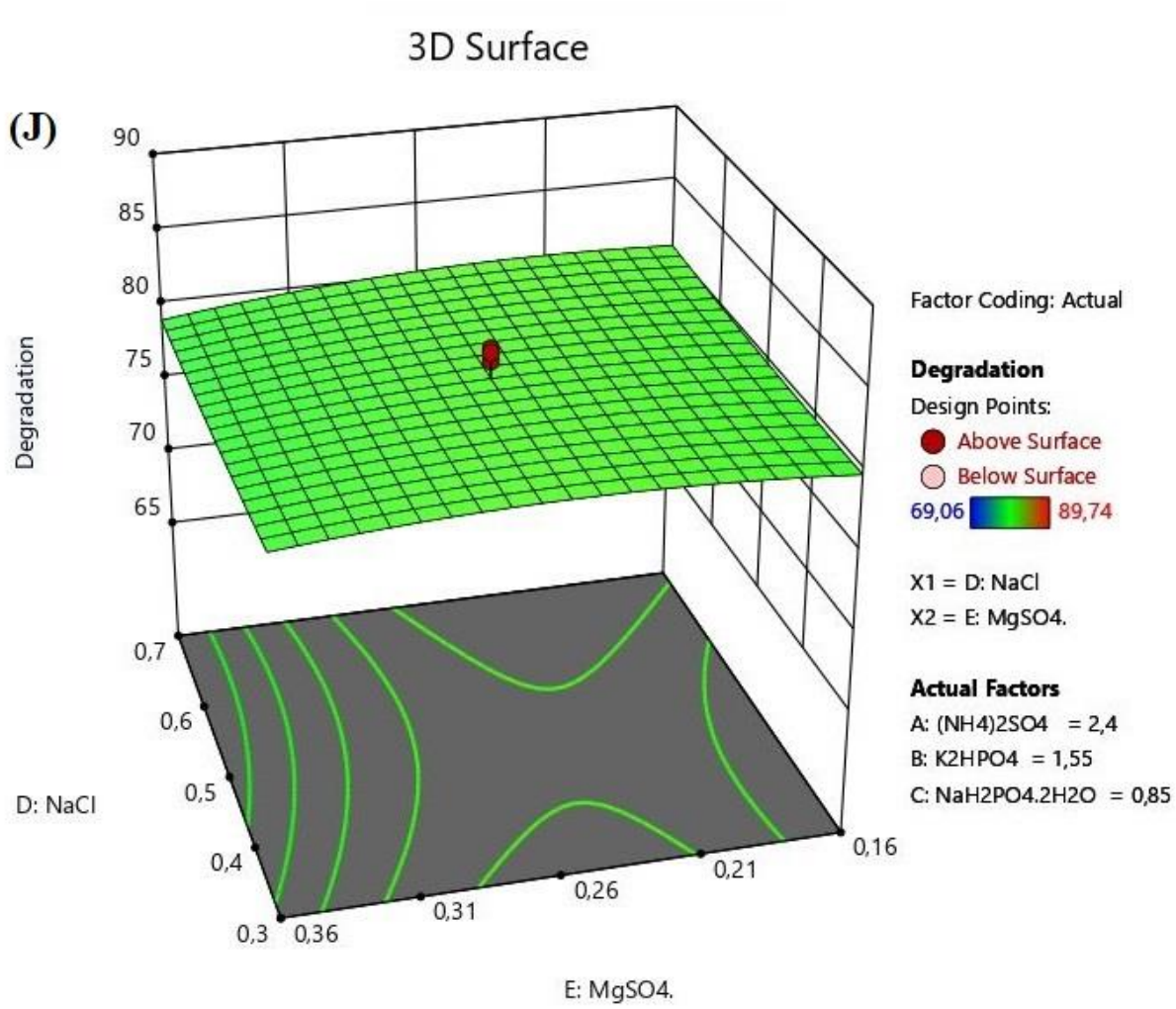
3D Surface
(J)
90
85
80
75
70
65
Degradation
0,7
0,6
0,5
0,4
0,3
D: NaCl
0,36
0,31
0,26
0,21
0,16
E: MgSO4.
Factor Coding: Actual
Degradation
Design Points:
Above Surface
Below Surface
69,06
89,74
X1 = D: NaCl
X2 = E: MgSO4.
Actual Factors
A: (NH4)2SO4 = 2,4
B: K2HPO4 = 1,55
C: NaH2PO4.2H2O = 0,85

(K)

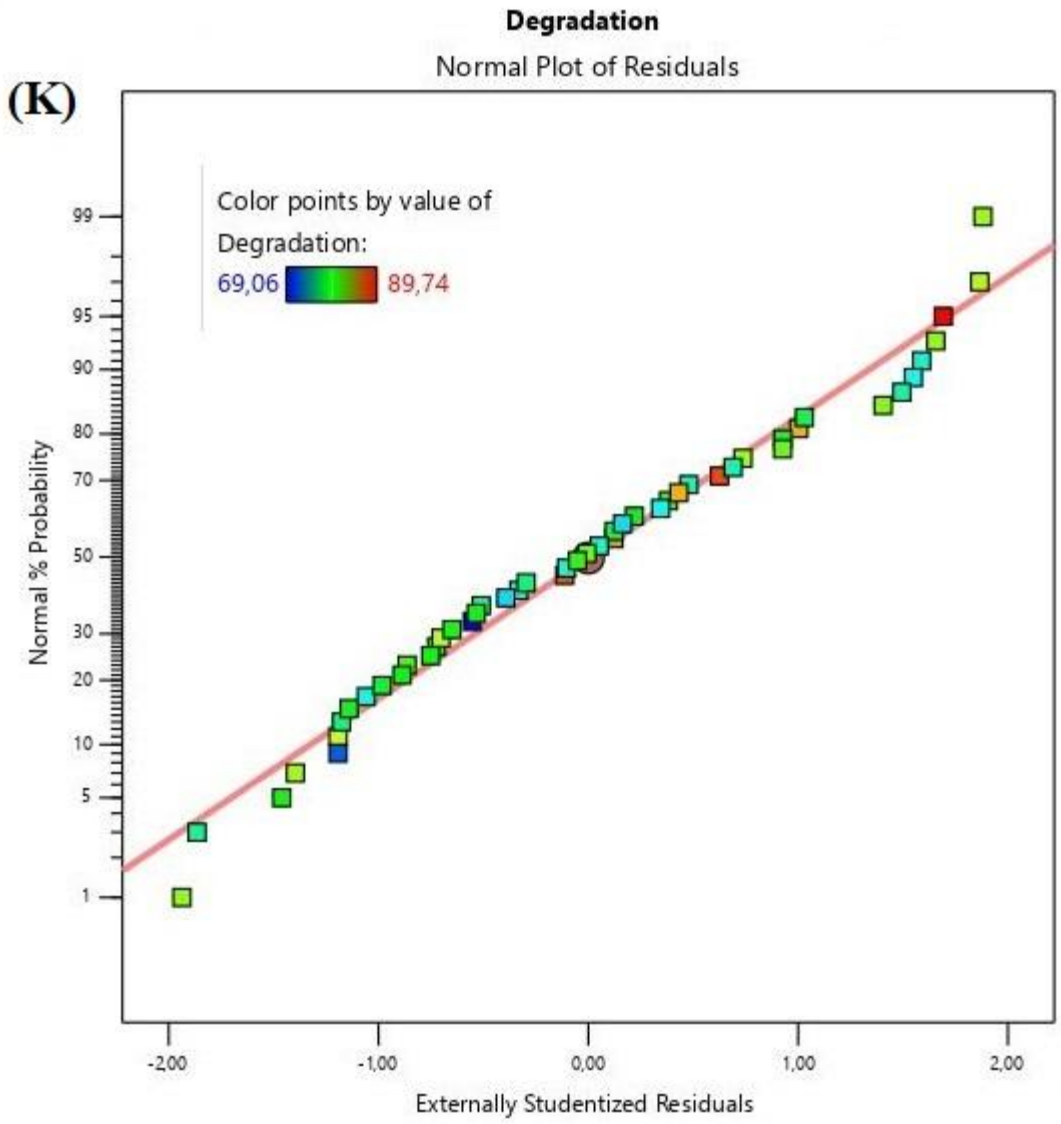
Degradation
Normal Plot of Residuals
Color points by value of
Degradation:
69,06
89,74
Normal % Probability
99
95
90
80
70
50
30
20
10
5
1
-2,00
-1,00
0,00
1,00
2,00
Externally Studentized Residuals

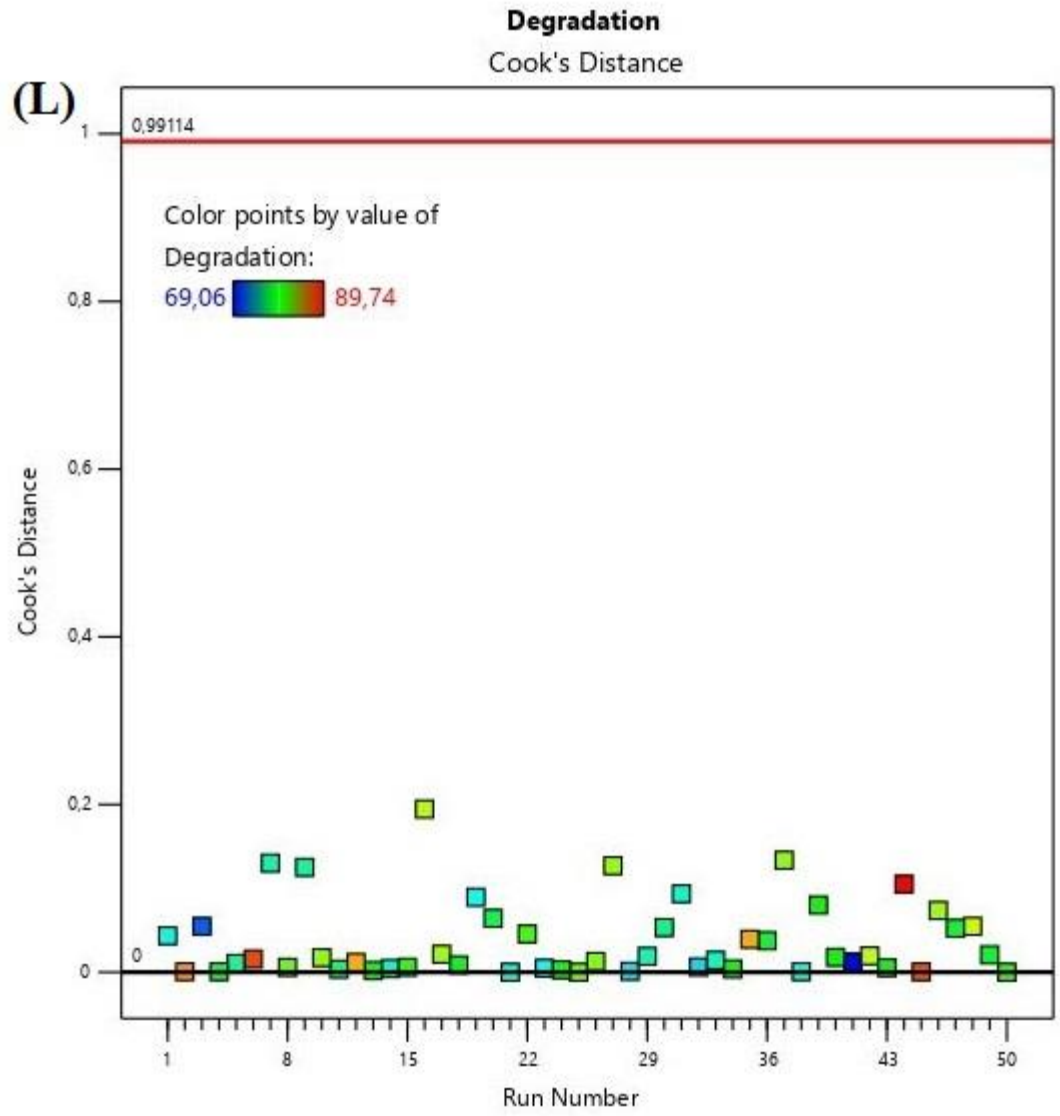
(L)
Degradation
Cook's Distance
0,99114
Color points by value of
Degradation:
69,06
89,74
Cook's Distance
1
0,8
0,6
0,4
0,2
0
1
8
15
22
29
36
43
50
Run Number

(M)

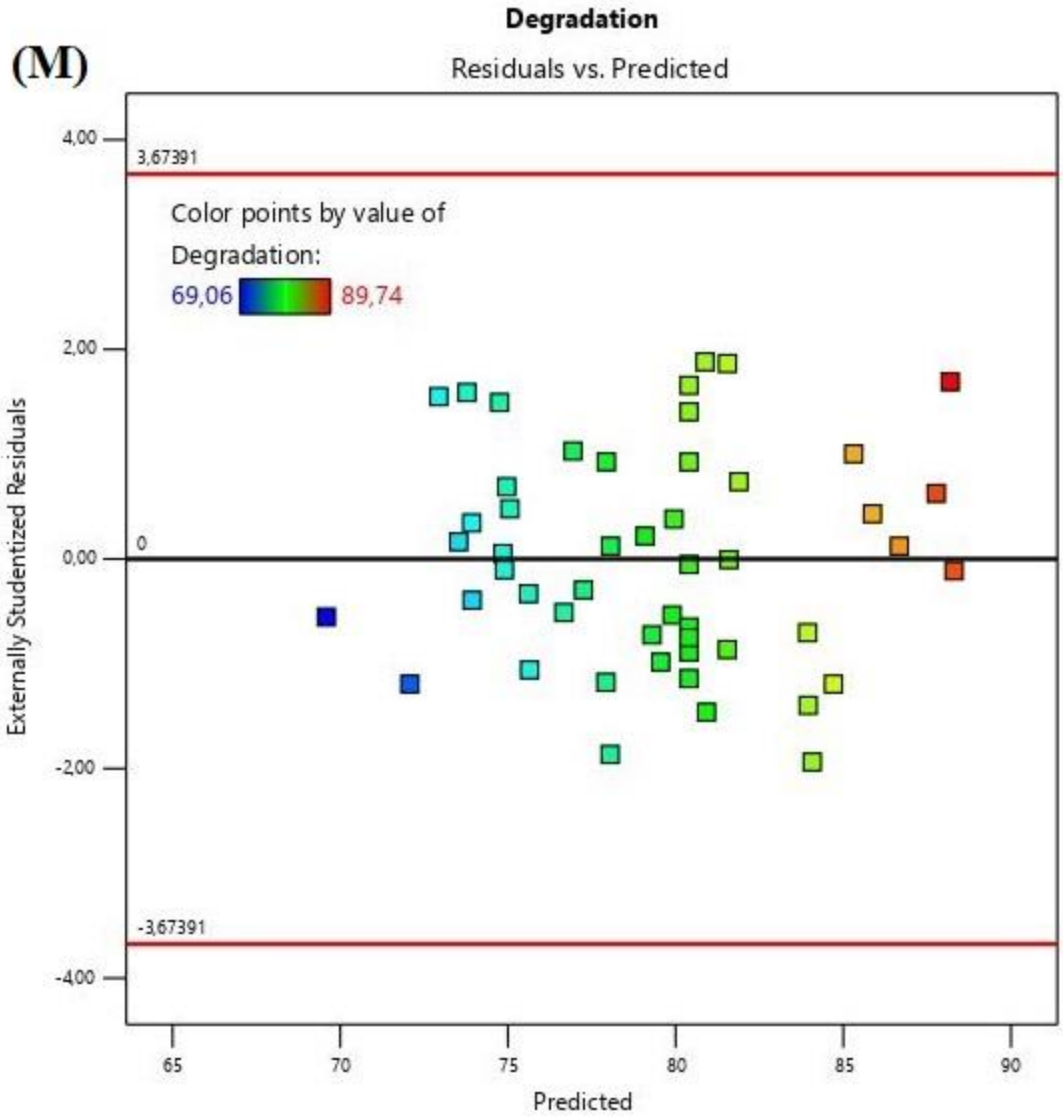
Degradation
Residuals vs. Predicted
4,00
3,67391
Color points by value of
Degradation:
69,06
89,74
2,00
0
0,00
-2,00
-3,67391
-4,00
Externally Studentized Residuals
65
70
75
80
85
90
Predicted

(N)

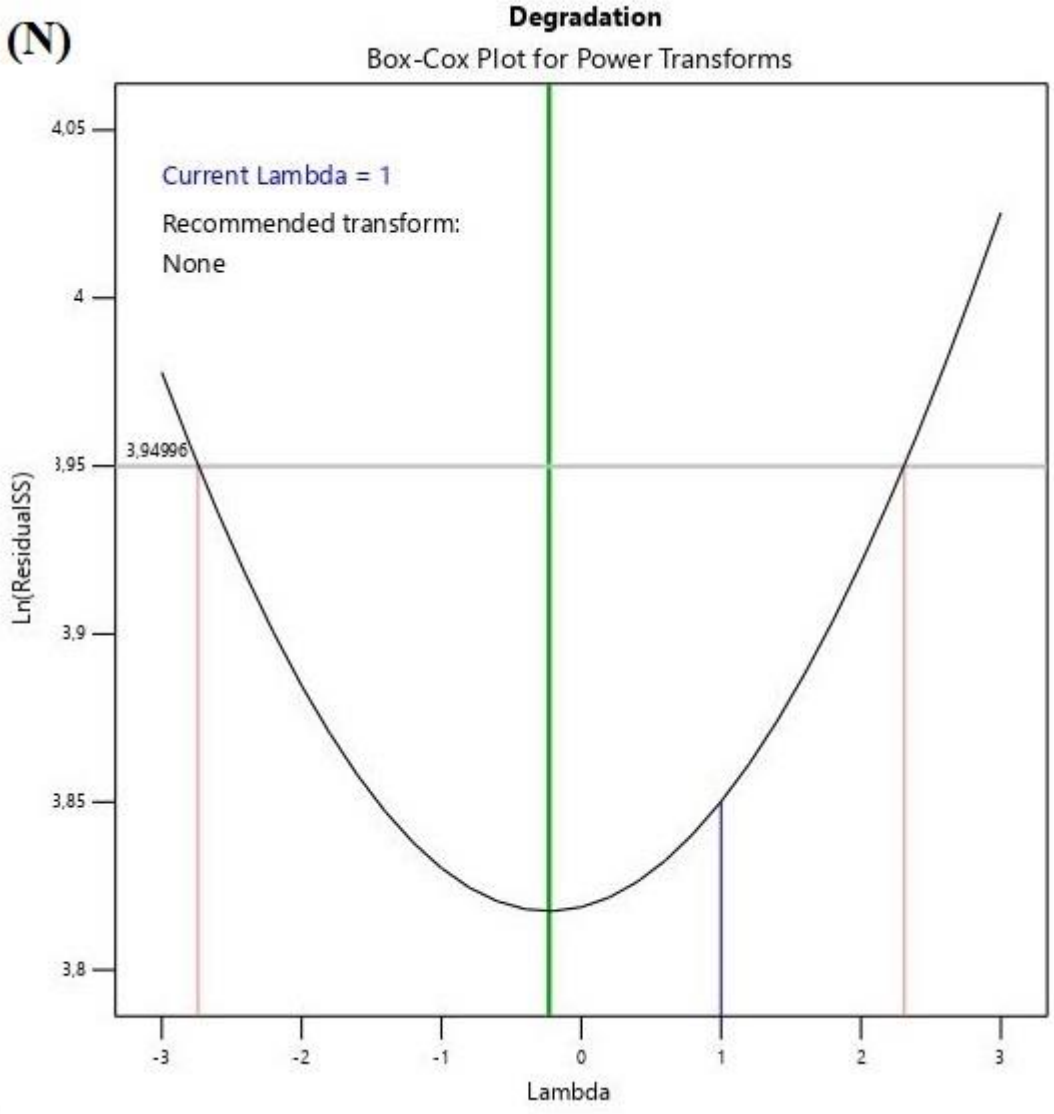
Degradation
Box-Cox Plot for Power Transforms
Current Lambda = 1
Recommended transform:
None
3,94996
Ln(ResidualSS)
4,05
4
3,95
3,9
3,85
3,8
-3
-2
-1
0
1
2
3
Lambda

(O)

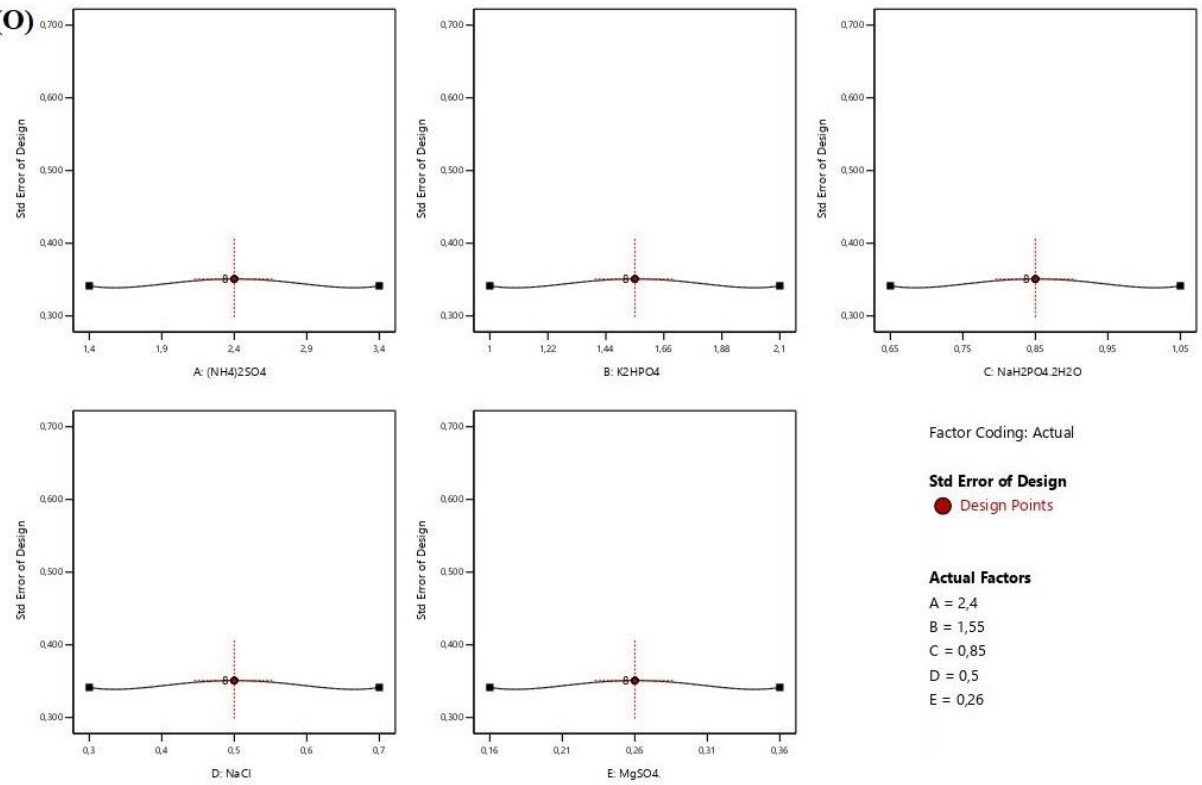
Std Error of Design
A: (NH4)2SO4
B: K2HPO4
C: NaH2PO4.2H2O
D: NaCl
E: MgSO4
Factor Coding: Actual
Std Error of Design
Design Points
Actual Factors
A = 2,4
B = 1,55
C = 0,85
D = 0,5
E = 0,26

Table S1: ANOVA for the Box-Behnken Design.

Source	Sum of Squares	df	Mean Square	F-value	p-value	
Model	6311.30	14	450.81	44.34	< 0.0001	significant
A-pH	3462.56	1	3462.56	340.53	< 0.0001	
B-Temperature	1385.46	1	1385.46	136.26	< 0.0001	
C-Biomass	1.13	1	1.13	0.1110	0.7453	
D-Anthracene Concentration	679.51	1	679.51	66.83	< 0.0001	
AB	40.58	1	40.58	3.99	0.0711	
AC	203.21	1	203.21	19.98	0.0009	
AD	0.2352	1	0.2352	0.0231	0.8819	
BC	31.30	1	31.30	3.08	0.1071	
BD	109.73	1	109.73	10.79	0.0073	
CD	12.11	1	12.11	1.19	0.2985	
A^2	18.86	1	18.86	1.86	0.2004	
B^2	150.70	1	150.70	14.82	0.0027	
C^2	12.70	1	12.70	1.25	0.2876	
D^2	37.29	1	37.29	3.67	0.0818	
Residual	111.85	11	10.17			
Lack of Fit	85.42	10	8.54	0.3232	0.8909	not significant
Pure Error	26.43	1	26.43			
Cor Total	6423.15	25				

Factor coding is Coded. Sum of squares is Type III – Partial. The Model F-value of 44.34 implies the model is significant. There is only a 0.01% chance that an F-value this large could occur due to noise. P-values less than 0.0500 indicate model terms are significant. In this case A, B, D, AC, BD, B^2 are significant model terms. Values greater than 0.1000 indicate the model terms are not significant. If there are many insignificant model terms (not counting those required to support hierarchy), model reduction may improve your model. The Lack of Fit F-value of 0.32 implies the Lack of Fit is not significant relative to the pure error. There is 89.09% chance that a Lack of Fit F-value this large could occur due to noise. Non-significant lack of fit is good -- we want the model to fit.

Table S2: The fit summary for Box-Behnken Design.

Source	Sequential p-value	Lack of Fit p-value	Adjusted R^2	Predicted R^2	
Linear	< 0.0001	0.5556	0.8342	0.7820	
2FI	0.1300	0.6096	0.8710	0.7503	
Quadratic	0.0014	0.8909	0.9604	0.9069	Suggested
Cubic	0.5385	0.9487	0.9619	0.9177	Aliased

Table S3. Regression model for Box-Behnken Design.

Std. Dev.	3.19	R^2	0.9826
Mean	76.58	Adjusted R^2	0.9604
C.V. %	4.16	Predicted R^2	0.9069
		Adeq Precision	23.7883

The Predicted R^2 of 0.9069 is in reasonable agreement with the Adjusted R^2 of 0.9604; i.e. the difference is less than 0.2. Adeq Precision measures the signal to noise ratio. A ratio greater than 4 is desirable. Your ratio of 23.788 indicates an adequate signal. This model can be used to navigate the design space.

Table S4: ANOVA for central composite rotatable design (CCRD).

Source	Sum of Squares	df	Mean Square	F-value	p-value	
Model	954.12	20	47.71	29.44	< 0.0001	significant
A-(NH4)2SO4	223.71	1	223.71	138.04	< 0.0001	
B-K2HPO4	25.64	1	25.64	15.82	0.0004	
C-NaH2PO4.2H2O	50.62	1	50.62	31.24	< 0.0001	
D-NaCl	0.0001	1	0.0001	0.0000	0.9951	
E-MgSO4.	7.98	1	7.98	4.93	0.0344	
AB	466.96	1	466.96	288.13	< 0.0001	
AC	2.02	1	2.02	1.25	0.2734	
AD	0.0242	1	0.0242	0.0149	0.9036	
AE	20.67	1	20.67	12.76	0.0013	
BC	5.54	1	5.54	3.42	0.0746	
BD	0.1740	1	0.1740	0.1074	0.7455	
BE	0.1568	1	0.1568	0.0968	0.7580	
CD	93.30	1	93.30	57.57	< 0.0001	
CE	0.1300	1	0.1300	0.0802	0.7790	
DE	3.08	1	3.08	1.90	0.1789	
A^2	0.0069	1	0.0069	0.0043	0.9485	
B^2	0.7047	1	0.7047	0.4348	0.5148	
C^2	16.44	1	16.44	10.15	0.0034	
D^2	2.27	1	2.27	1.40	0.2464	
E^2	34.88	1	34.88	21.52	< 0.0001	
Residual	47.00	29	1.62			
Lack of Fit	35.02	22	1.59	0.9307	0.5880	not significant
Pure Error	11.97	7	1.71			
Cor Total	1001.12	49				

Factor coding is Coded. Sum of squares is Type III – Partial. The Model F-value of 29.44 implies the model is significant. There is only a 0.01% chance that an F-value this large could occur due to noise. P-values less than 0.0500 indicate model terms are significant. In this case A, B, C, E, AB, AE, CD, C^2, E^2 are significant model terms. Values greater than 0.1000 indicate the model terms are not significant. If there are many insignificant model terms (not counting those required to support hierarchy), model reduction may improve your model. The Lack of Fit F-value of 0.93 implies the Lack of Fit is not significant relative to the pure error. There is a 58.80% chance that a Lack of Fit F-value this large could occur due to noise. TA non-significant lack of fit is good -- we want the model to fit.

Table S5: Fit Statistics for central composite rotatable design (CCRD).

Std. Dev.	1.27	R^2	0.9531
Mean	79.33	Adjusted R^2	0.9207
C.V. %	1.60	Predicted R^2	0.8571
		Adeq Precision	22.6900

The Predicted R^2 of 0.8571 is in reasonable agreement with the Adjusted R^2 of 0.9207; i.e. the difference is less than 0.2. Adeq Precision measures the signal to noise ratio. A ratio greater than 4 is desirable. Your ratio of 22.690 indicates an adequate signal. This model can be used to navigate the design space.

CHAPTER SIX

Anthracene detoxification by Laccases from indigenous fungal strains *Trichoderma lixii* FLU1 and *Talaromyces pinophilus* FLU12

This chapter has been published in current format in the journal: *Biodegradation, 35(5), 769-787. https://doi.org/10.1007/s10532-024-10084.*

The published paper is presented in the following pages.

Biodegradation
https://doi.org/10.1007/s10532-024-10084-3

ORIGINAL PAPER

Anthracene detoxification by Laccases from indigenous fungal strains *Trichoderma lixii* FLU1 and *Talaromyces pinophilus* FLU12

Samson O. Egbewale · Ajit Kumar · Tosin A. Olasehinde · Mduduzi P. Mokoena · Ademola O. Olaniran

Received: 12 September 2023 / Accepted: 13 April 2024

Abstract The persistence and ubiquity of polycyclic aromatic hydrocarbons (PAHs) in the environment necessitate effective remediation strategies. Hence, this study investigated the potential of purified Laccases, *Tl*FLU1L and *Tp*FLU12L, from two indigenous fungi *Trichoderma lixii* FLU1 (*Tl*FLU1) and *Talaromyces pinophilus* FLU12 (*Tp*FLU12), respectively for the oxidation and detoxification of anthracene. Anthracene was degraded with v_{max} values of 3.51 ± 0.06 mg/L/h and 3.44 ± 0.06 mg/L/h, and K_m values of 173.2 ± 0.06 mg/L and 73.3 ± 0.07 mg/L by *Tl*FLU1L and *Tp*FLU12L, respectively. The addition of a mediator compound 2,2-azino-bis (3-ethylbenzothiazoline-6-sulfonic acid) (ABTS) to the reaction system significantly increased the degradation of anthracene, with up to a 2.9-fold increase in v_{max} value and up to threefold decrease in K_m values of *Tl*FLU1L and *Tp*FLU12L. The GC–MS analysis of the metabolites suggests that anthracene degradation follows one new pathway unique to the ABTS system—hydroxylation and carboxylation of C-1 and C-2 position of anthracene to form 3-hydroxy-2-naphthoic acid, before undergoing dioxygenation and side chain removal to form chromone which was later converted into benzoic acid and CO_2. This pathway contrasts with the common dioxygenation route observed in the free Laccase system, which is observed in the second degradation pathways. Furthermore, toxicity tests using *V. parahaemolyticus* and HT-22 cells, respectively, demonstrated the non-toxic nature of Laccase-ABTS-mediated metabolites. Intriguingly, analysis of the expression level of Alzheimer's related genes in HT-22 cells exposed to degradation products revealed no induction of neurotoxicity unlike untreated cells. These findings propose a paradigm shift for bioremediation by highlighting the Laccase-ABTS system as a promising green technology due to its efficiency with the discovery of a potentially less harmful degradation pathway, and the production of non-toxic metabolites.

Keywords Alzheimer · Anthracene · ABTS · Laccase

Supplementary Information The online version contains supplementary material available at https://doi.org/10.1007/s10532-024-10084-3.

S. O. Egbewale · A. Kumar · T. A. Olasehinde · A. O. Olaniran (✉)
Discipline of Microbiology, University of KwaZulu-Natal (Westville Campus), Durban 4000, South Africa
e-mail: olanirana@ukzn.ac.za

M. P. Mokoena
Department of Pathology, School of Medicine, University of Limpopo, Private Bag X1106, Sovenga 0727, South Africa

Introduction

Polycyclic aromatic hydrocarbons (PAHs) are a ubiquitous class of persistent organo-pollutants consisting

Published online: 01 June 2024

of two or more fused aromatic rings with a varying degree of carcinogenicity, genotoxicity, and mutagenicity (Slámová et al. 2017). They are formed during incomplete combustion, pyrolysis processes and from anthropogenic sources such as industrial food processing methods (heating, drying and smoking processes), home food preparation (grilling and roasting processes), municipal seep and oils spillages (Singh et al. 2016). Anthracene is considered a marker in the environmental assessment of PAHs, owing to its frequent detection in indoor suspended particles (air), surface water and groundwater that receive wastewater effluent (Adeniji et al. 2018). Primary target for anthracene includes the skin, hematopoietic system, lymphoid system, and gastrointestinal tract with varying degrees of toxicity and carcinogenicity (Hu et al. 2009). Also, its metabolites (quinones) have been implicated in acute and chronic toxicity of aquatic organisms, such as reduction in photosynthesis rate and population growth repression (Othman et al. 2012; Šepič et al. 2003).

Despite efforts from regulatory agencies like the United States Environmental Protection Agency, the European Union Scientific Committee on Food, the Joint FAO/WHO Expert Committee on Food Additives (JECFA) and the International Programme on Chemical Safety (IPCS), PAHs persist in the environment, necessitating new strategies to mitigate their acute and chronic effects (Zelinkova and Wenzl 2015). Several treatment methods, including physical, chemical, and biological methods or their combinations have been developed (Forján et al. 2020; Haneef et al. 2020). Among these, biological methods which relies on the use of microorganisms for enzymatic breakdown of PAHs offer many advantages such as low-cost, safety, reduced energy requirements, operation under milder conditions, and avoid generation of toxic compounds (Asemoloye et al. 2020). However, these methods have drawbacks, such as the need for long incubation times, mycelia ageing in the case of fungi, generation of a waste stream and possible formation of more toxic compounds (Ali et al. 2017).

To overcome these limitations, purified ligninolytic enzymes (Laccase, Manganese peroxidase and Lignin peroxidase) have been proposed as alternatives to whole cells owing to their low energy input requirement, moderate operational conditions, the specificity in the minimization of the undesirable products, ability to retain extremophilic property and stability under harsh conditions (Kumar and Chandra 2020).

Laccase (EC 1.10.3.2, benzenediol: dioxygen oxidoreductase) belonging to a multicopper oxidase family has become an attractive candidate for an eco-friendly degradation of persistent organo-pollutants into an innocuous state (Janusz et al. 2020) due to its stability, low cost, feasible production, broad substrate range and low substrate specificity (Agrawal et al. 2018). Compared to commercially available Laccases, isolated enzymes from whole cells offer several potential advantages. They are eco-friendly, utilizing molecular oxygen and yielding water as the sole by-product (Mayolo-Deloisa et al. 2020). Furthermore, the immobilization of Laccase enhances its stability and reusability, making it a more efficient and cost-effective option (Brandi et al. 2006; Fernández-Fernández et al. 2013; Ren et al. 2020). These factors, combined with its ability to oxidize a wide range of substrates, make isolated Laccase a superior choice for various industrial and environmental applications. However, recent studies highlight a critical challenge of the low degradation efficiency of Laccases towards PAHs due to their specific molecular structure (Xu et al. 2020). Redox mediators like 2,2′-azino-bis(3-ethyl-benzothiazoline-6-sulfonic acid) (ABTS) have shown promise in improving this degradation efficiency (Grassi et al. 2011; Wu et al. 2008).

According to available literature, a crucial gap in our understanding lies in the impact of these Laccase-mediated degradation products on living organisms. This lack of knowledge hinders a complete picture of the environmental safety of Laccase-based bioremediation. This study addresses this critical gap by investigating the oxidation and detoxification of anthracene by purified Laccases from two specific fungal strains: *Trichoderma lixii* FLU1 and *Talaromyces pinophilus* FLU12. We explore the significance of the Laccase-mediator ABTS system in enhancing anthracene degradation and elucidate degradation kinetics and pathways through metabolite profiling. Furthermore, to assess the environmental safety of this approach, we evaluate the acute toxicity of the resulting degradation products on a marine bacterium, *Vibrio parahaemolyticus*, which represents a potential ecological recipient of PAH contamination. Additionally, we investigate the cytotoxicity of these products on a mouse hippocampal neuronal cell line

(HT-22) to explore potential neurotoxic effects, linking back to the established connection between PAHs and neurodegenerative diseases (Tang et al. 2003). Also, we analyze the effects on genes associated with Alzheimer's disease, providing further insight into potential neurotoxicity. By investigating these aspects, this study aims to comprehensively evaluate the environmental safety of Laccase-mediated PAH degradation, providing valuable insights for its potential application in bioremediation strategies.

Material and methods

Reagents

ABTS (2,2-azino-bis-(3-ethyl-benzothiazoline-6-sulphonic acid)), anthracene and ethyl acetate of analytical grade with ≥ 98% purity were purchased from Merck (St. Louis, MI, USA). The mouse hippocampal neuronal cell line was a gift from Salk Institute for Biological Studies, La Jolla, CA, USA. The PAH anthracene was selected for this study based on its toxicological profile as a known or reasonably anticipated human carcinogen on the US EPA's priority pollutants list (Zelinkova and Wenzl 2015).

Enzyme production and purification

Laccase production was carried out in cotton-plugged Erlenmeyer flasks (250 mL) containing basal salt medium (BSM) supplemented with anthracene (200 mg/L) as an inducer to a final volume of 150 mL prior to the set-up. The media were sterilized by autoclaving at 121 °C for 15 min. Inoculation was done directly into individual Erlenmeyer flasks using two 20 mm mycelial disks of each strain before incubating at 30 ℃ and shaking at 180 rpm for 10 days in complete darkness (MRC laboratory instrument, Essex, U.K). The pH of the flask containing strain *Tl*FLU1 was adjusted to 4 using 1 M HCl while that of *Tp*FLU12 was adjusted to 7 using 1 M NaOH. The rationale behind the variation in the culture media pH values was due to its optimized condition during anthracene degradation with 100% degradation at 12 days during our previous study. Also, the fungal strains whole cell showed tolerance to fluoranthene (Egbewale et al. 2023) and anthracene (data not shown) with zero growth inhibition at 400 mg/L of fluoranthene and 400 mg/L of anthracene for *Tl*FLU1 except for *Tp*FLU12 with no growth inhibition at 600 mg/L of anthracene. The detailed composition of the BSM media, including specific components and their concentrations, is provided in Table S1.

The purification was done according to the previously described method (Othman et al. 2018) with some modifications. Briefly, crude extract from *Tl*FLU1 (*Tl*FLU1L abbreviated for Laccase from *Tl*FLU1) and *Tp*FLU12 (*Tp*FLU12L abbreviated for Laccase from *Tp*FLU12) was individually centrifuged at 5000×*g* for 20 min at 4 ℃ to obtain a clear supernatant. Protein from each supernatant was sequentially precipitated to saturation with 60% $(NH_4)_2SO_4$ under a gentle continuous stirring at 4 ℃ overnight. The protein pellets were recovered by centrifugation at 10,000×*g* for 20 min, dissolved in sodium acetate buffer (50 mM, pH 5) and dialyzed against a large volume of the same buffer using 30 kDa cut off size dialysis tubing cellulose membrane (Merck, Burlington, MA, USA). The protein was further purified using DEAE liquid chromatography column (1.5 × 9 cm) at room temperature before eluting with 100 mM NaCl in 50 mM sodium acetate buffer (pH 7) at a flow rate of 0.5 mL/min. Six fractions showing Laccase enzymes activity of substrate ABTS were pooled and applied on Sephadex G-100 column (2.0 × 9 cm) size exclusion column before elution with 50 mM sodium acetate buffer (pH 7). All fractions with Laccase activity were pooled, desalted, filter-sterilized, and stored at 4℃ until further usage.

The Laccase purity and molecular mass was visualized with SDS-PAGE using a 12% resolving gel and a 5% stacking gel. At the end of electrophoresis, the gel was stained with Coomassie brilliant blue (Laemmli 1970). The Laccases were purified to homogeneity with a specific activity of 34 U/mg protein. *Tl*FLU1L was characterized as a yellow Laccase while *Tp*FLU12L was a blue Laccase with a molecular mass of 44 kDa and 68.7 kDa, respectively. Both showing remarkable stability in various organic solvents, detergents, inhibitors, and metal ions with excellent residual activity.

Assay for laccase activity

Laccase activity was measured as described previously (Zungu et al. 2020). Briefly, Laccase (370 µg) was mixed with 800 µL of 20 mM Na-Acetate buffer

(pH 5) and 100 µL of 5 mM ABTS. After 15 min incubation period at 30 °C, the reaction was terminated with 50 µL of 20% (v/v) trichloroacetic acid (TCA) solution. One unit of Laccase is the amount of enzyme that produces 1 µM of oxidized product per minute (ε_{420nm} = 36,000 /M/cm for oxidized product).

Degradation of anthracene by Laccases

Anthracene degradation was determined as previously described (Cambria et al. 2008) with some modifications. The reaction mixture (10 mL) consisted of anthracene (200 mg/L) and Laccase (2 U/mL, pH 5) in Na–Acetate buffer (50 mM, pH 5). Tween 80 (1%) was added to the mixture to enhance anthracene bioavailability and incubated at 30 °C in the dark for 96 h, with continuous shaking at 80 rpm to avoid precipitation. The pH of 5 was adopted for this study due to the observed 100% residual activity after 24 h reaction during the enzyme characterization assays in our previous study. The sample aliquots (1 mL) were drawn every 24 h and 50 µL of a 20% (v/v) TCA solution added to stop further enzymatic oxidation. All the experiments were performed in triplicates and a control (heat-denatured Laccase) set-up was carried out under the same experimental condition. The concentration of residual anthracene in the reaction mixture was measured as described previously (Mot et al. 2020) with slight modifications. Briefly, the reaction mixture aliquots were mixed with ethyl-acetate (1:4 v/v) in a separating funnel, vigorously shaken for 5 min and allowed to stand for 20 min to enhance the separation of aqueous and organic phases. The organic phase was collected, dried over 10 g anhydrous Na_2SO_4 and evaporated to dryness at 40 °C under reduced pressure. The dried fractions were then re-dissolved with the same extraction solvent and diluted tenfold with ethyl-acetate before quantifying the anthracene by measuring optical density at scanning mode from wavelength 200–400 nm as well as at wavelength 265 nm using Agilent Cary60 UV–Vis spectrophotometer (Santa Clara, CA, USA).

Detection of the metabolites by GC–MS analysis

The extracted fractions from the aliquots collected were pooled together, dried at 40 °C under reduced pressure and redissolved to a final volume of 1 mL with *n*-hexane. 1 µL of samples were injected into Rxi-PAH capillary GC column (GCMS-QP2010 SE Shimadzu scientific, Kyoto, Japan) for metabolite detection under the following conditions: split injection (injector temperature 330 °C, split 1/8 for samples and 1/20 for standard samples); oven temperature programmed from 60 °C (held for 2 min) to 300 °C (15 min) at 10 °C/min. The carrier gas used was helium at a flow rate of 1 mL/min. The metabolites were analyzed at a full scanning mode at 10–220 m/z using the NIST library (National Institute of standard technology, USA) (Teh and Hadibarata 2014).

Influence of Laccase-mediator system on anthracene degradation

The influence of ABTS as a mediator on anthracene oxidation was determined by adding ABTS at a varying concentration (200 µM to 10 mM) to the Laccase solution (2 U/mL). Subsequently, anthracene (200 mg/L) was correspondingly added into the Laccase-mediator solutions in a final volume of 10 mL containing Na-Acetate buffer (50 mM) and Tween 80 (1%). Each reaction mixture solution was adjusted to pH 5 and incubated in the dark at 30 °C, with shaking at 80 rpm for 96 h. Aliquots (1 mL) were drawn from each reaction every 24 h and residual anthracene concentration, metabolite detection and change in the functional group of the detected metabolite were determined as described above. All the experiments were performed in triplicates and a control (heat denatured enzyme) set-up was carried out under the same experimental condition. It is worth noting that the choice for ABTS as a mediator, concentration (200 µM to 10 mM and pH 5 condition were based on the higher binding activity of the Laccases towards ABTS in comparison to other mediators during the enzyme characterization study, which aligns with previous studies Camarero et al. 2008; Liu et al. 2017), where optimum pH for oxidation of ABTS was reported to range between 4 and 7 with the highest activity with ABTS. The stability and reusability of ABTS@MIL-100(Fe) as a Laccase mediator make it a promising tool for dye removal (Liu et al. 2017).

Determination of kinetic parameters of the Laccase-mediator system

The kinetic parameters of the Laccase and Laccase-mediator were determined using anthracene

concentrations ranging from 50 to 400 mg/L, following the assays described above (de Freitas et al. 2017). A non-linear regression model was used to estimate the Michaelis–Menten constant K_m and v_{max} for the substrate disappearance. The changes in the anthracene concentrations were monitored over a 96-h period immediately after reaction initiation by the addition of 3 U Laccase and 10 mM ABTs (for Laccase-mediator set-up) at 30 °C. Anthracene concentrations above 400 mg/L could not be used due to the solubility issue.

Ecotoxicity analysis

Ecotoxicity analysis of the anthracene degradation products (metabolites) was carried out to assess the potential risk on biota using time-course acute toxicity effects on a marine bacterium, *Vibrio parahaemolyticus* (ATCC 17802) as a model organism, being the primary consumer in the food web. The acute toxicity of pure anthracene (control), Laccase degraded and Laccase-mediator (degradation products/h) on *V. parahaemolyticus* (100 µL of diluted standardized overnight culture broth) was monitored based on a modified liquid-to-plate micro-counting method as described previously (Egbewale et al. 2023; Rotini et al. 2018).

Cytotoxicity assay

The cytotoxicity assay was performed using mouse hippocampal neuronal (HT-22) cell line as the secondary consumer. The time course cytotoxic effect of the degradation product on HT-22 cells was carried out using an MTT assay. The MTT assay was based on the colorimetric test of cell proliferation and percentage cell viability of the degradation product/h. Briefly, cells maintained in DMEM supplemented with 10% FBS and 100 mg/L streptomycin and 100 IU/mL penicillin at 37 °C in a humidified atmosphere of 5% CO_2 were plated at a density of 1.28×10^5 cells/mL in 96 well plates. The cells were exposed to each degradation product (1:4 v/v) of 400 mg/L anthracene concentration in a 96-well plate and allowed to incubate for 48 h. Metabolites from the degradation of anthracene at an initial concentration of 400 mg/L were used due to the presence of residual anthracene at the end of the reaction period.

Cell morphology evaluation

The evaluation of HT-22 cells for viability, morphology and overall health was done by capturing multiple field views for each experimental condition to ensure representative analysis using a high-resolution microscope, Invitrogen EVOS™ Floid EN61326 equipped with phase contrast or fluorescence capabilities (Thermos-Fisher Scientific, Waltham, MA, USA).

Alzheimer's related gene expression analysis

Alzheimer's related gene expression analysis in HT-22 cells incubated with control (pure anthracene), oxidation products of 72 h (anthracene 37 mg/L and 32 mg/L incubated with 3 U of *Tl*FLU1L and *Tp*FLU12L, respectively) and 96 h (anthracene 139 mg/L and 58 mg/L incubated with 3 U of *Tl*FLU1L and *Tp*FLU12L, respectively) was performed using RT-qPCR (CFX Connect Real-Time PCR System, Bio-Rad CFX 976, Hercules, CA, USA). Total RNA from HT-22 cells was extracted using GeneJET RNA purification Kit (Thermos-Fisher Scientific, Waltham, MA, USA). cDNA was synthesized from 100 ng of total RNA using the Maxima First-strand cDNA Synthesis Kit (Thermos-Fisher Scientific, Waltham, MA, USA). RT-qPCR conditions were as follows: 40 cycles of 95 °C for 30 s, 95 °C for 0.05 s, 60 °C for 30 s, and 72 °C for 20 s. Melting curve analysis was performed from 65 to 95 °C. The primer pairs used are shown in Table 1. Triplicate analyses were carried out for each cDNA sample along with the 'no reverse transcriptase' and 'no template' controls. The specificity of the amplicons was confirmed through melting curve analysis and size determination on 2% agarose gels. Gene expression was quantified using the relative standard curve method. Different dilutions of cDNA synthesized from RNA extracted from untreated HT-22 cells were used to plot the standard curves for each gene. BACE-1, ADAM-10, TAU, PPARγ and APP mRNA expression were presented as fold regulation (negative inverse of fold change).

Quality control measures

Recovery study

We have included a recovery study using sterile Na-acetate buffer with heat-denatured Laccase spiked with a known concentration of anthracene

Table 1 Primers sequences to amplify genes associated with Alzheimer's disease in HT-22 cells

Genes		Primers (5′–3′)	Size (bp)	References
Housekeeping gene β-actin (ACTB)	F	ATCTGGCACCACACCTTCTACAATGAG CTGCG	120	Hu et al. (2022)
	R	CGTCATACTCCTGCTTGCTGATCCACA TCTGC		
ADAM-10 (a disintegrin and metalloproteinase)	F	GCCAGTTCTGATGGCAAAGATG	90	Ao et al. (2022)
	R	AGACCCTGTACTGCCACAAGTTGA		
TAU (microtubule-associated protein tau)	F	CAAGTGTGGCTCAAAGGACAATATC	55	Yi et al. (2019)
	R	TCAATCTTCTTATTCCCTCCTCCAG		
PPARγ (peroxisome proliferator-activator recepter gamma)	F	CTCCCAGCTGTCGCAAGGTGC	174	Pesantet al.(2006)
	R	GCAATCGATAGAAGGAACACT		
APP (amyloid precursor protein)	F	AATGTGGATTCTGCTGATGCGGAG-	657	Ko et al. (2004)
	R	CCCATTCTCTCATGACCTGGGA		
BACE-1 (beta-secretase 1)	F	CATTGGAGGTATCGACCACTCGCT	624	Tamagno et al. (2006)
	R	CCACAGTCTTCCATGTCCAAGGTG		

F = Forward, R = Reverse

as standard. This step assesses potential losses during sample preparation and extraction. The average recovery of anthracene in our study was 98.7 ± 3.53%.

Standard curve

A standard curve was generated using known anthracene concentrations (with an R^2 value of 0.972) to ensure accurate quantification of residual anthracene in the reaction mixtures.

Triplicate experiments

All experiments were performed in triplicates to account for experimental variability and enhance data reliability.

Control experiment

A control experiment using heat-denatured Laccase was included under the same conditions as the treatment groups to account for non-enzymatic degradation of anthracene.

Blank control

Blank controls included a well containing all reaction components except the enzyme sample. This controls for background absorbance at the measurement wavelength.

Substrate controls

Substrate controls included wells with only substrate and buffer (no enzyme) and only enzyme and buffer (no substrate) to assess potential non-enzymatic conversion of the substrate and background enzyme activity, respectively.

Serial dilution of enzyme

A serial dilution of the enzyme sample was carried out to ensure the measured activity falls within the linear range of the assay.

Cell viability assay

Cell viability assay alongside the ecotoxicity test was conducted to distinguish between growth inhibition and cell death caused by the degradation products.

No template control (NTC)

NTV included a reaction mixture containing all components except the cDNA template. This controls for

potential contamination from reagents or amplification of nonspecific products.

Positive control

A reference gene (β-actin) with known stable expression in the HT-22 cell line was used to verify the functionality of reverse transcription and PCR steps.

Melt curve analysis

Melt curve analysis after amplification was carried out to ensure the generation of a single specific product for each gene of interest.

Efficiency testing

The amplification efficiency of each primer was measured using a standard curve to ensure accurate quantification of gene expression levels.

Anthracene and ABTS treatments after studies

The anthracene and ABTS used in the experiment were treated according to the South African Department of Water and Forestry (DWAF 1996; Pillay and Olaniran 2016) waste treatment protocol and standards. After the reaction with Laccase, the anthracene and ABTS were neutralized and safely disposed of per environmental regulations to prevent potential environmental issues. Although the degradation products of ABTS were not found to pose a risk to the environment yet we took care of it to ensure that all waste generated during the experiment was properly managed to minimize any adverse impact on the environment.

Statistics analysis

All measurements were carried out in triplicates. The data were expressed as the means ± standard deviations. Statistics was performed using the Graph-Pad Prism v3.0 (Boston, MA, USA). To determine the K_m and v_{max}, experimental data was fitted to reciprocal form of the Michaelis–Menten equation ($v = v_{max}[S]/(K_m + [S])$) using Graph-Pad Prism v3.0.

Results

Oxidation of anthracene by Laccases

The residual anthracene (%) after oxidation by purified Laccase from *Trichoderma lixii* FLU1 (*Tl*FLU1L) and *Talaromyces pinophilus* FLU12 (*Tp*FLU12L) is shown in Fig. 1A and Table S2. Both

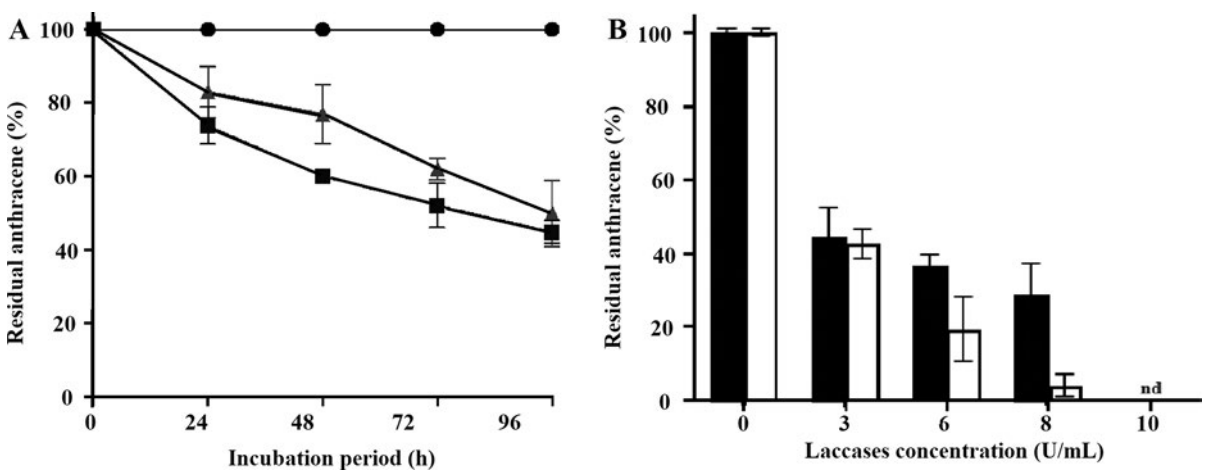

Fig. 1 **A** The percentage of residual anthracene concentration after the oxidation by *Tl*FLU1L (filled square) and *Tp*FLU12L (filled triangle) and no enzyme controls (filled circle); **B** Effect of *Tl*FLU1L (filled square) and *Tp*FLU12L (open square) concentrations on oxidation of anthracene (200 mg/L), at pH 5, temperature 30 °C, after 96 h incubation period

enzymes reduced the anthracene concentration during the 96-h incubation period. *Tl*FLU1L (2 U/mL) and *Tp*FLU12L (2 U/mL) could oxidise 55.1% and 49.9% of anthracene (200 mg/L) as 44.9% and 50.1% of anthracene concentration was recorded after 96 h incubation, respectively. As the concentration of Laccases increases, a significant reduction in the concentration of anthracene was observed after 96 h incubation period (Fig. 1B, Table S3). 3 U/mL of *Tl*FLU1L and *Tp*FLU12L could oxidise 55.7% and 57.5% while 8 U/mL of respective enzyme oxidized about 71.3% and 96.1% of anthracene, respectively, after 96 h incubation period. No residual anthracene was detected when 10 U/mL concentration of Laccases was used, indicating 100% anthracene oxidation.

Oxidation of anthracene by Laccases in the presence of ABTS

The in vitro oxidation of anthracene in the presence of varying concentration of mediator (ABTS) by purified *Tl*FLU1L and *Tp*FLU12L is shown in Fig. 2A, B. 2 U/mL of purified *Tl*FLU1L (Fig. 2A, Table S4) and *Tp*FLU12L (Fig. 2B, Table S5) incubated with ABTS concentration (10 mM) before adding to 200 mg/L of anthracene showed higher

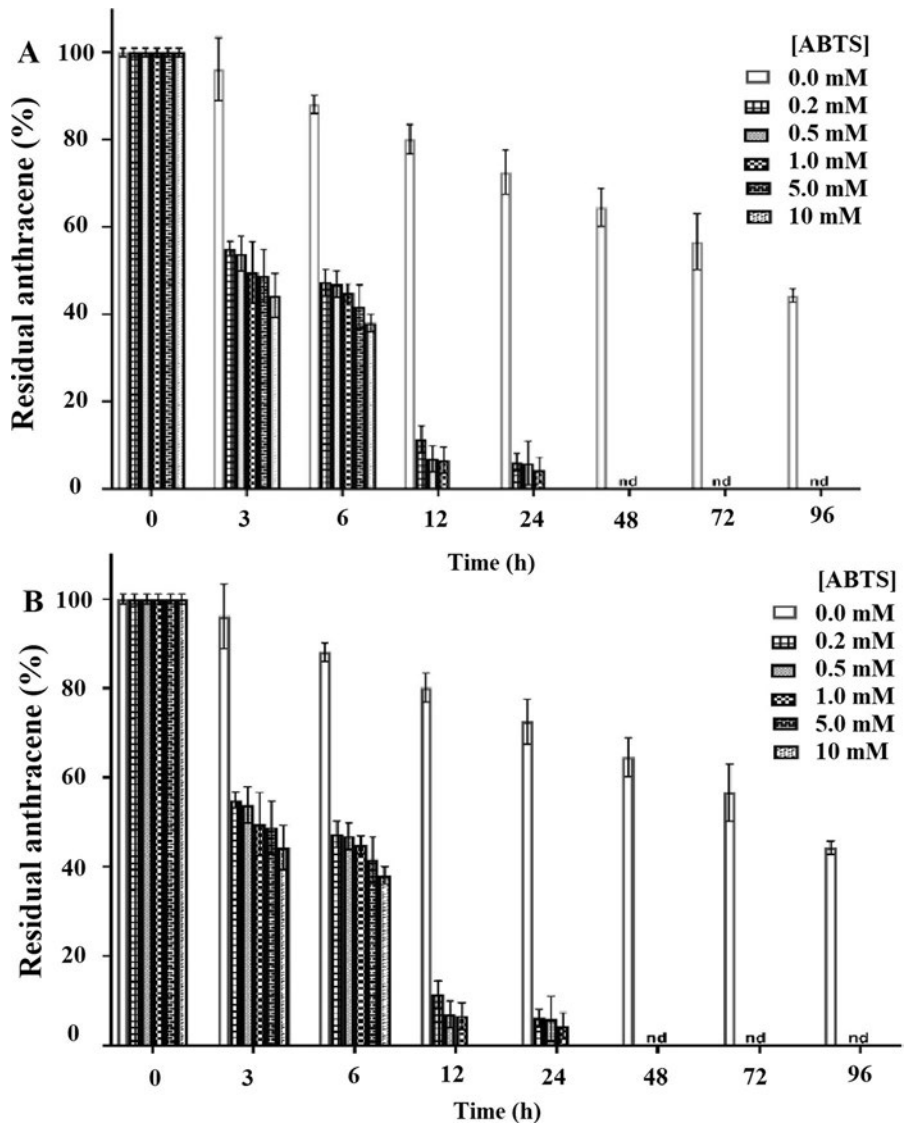

Fig. 2 The influence of mediator (ABTS) concentration on *invitro* oxidation of anthracene by *Tl*FLU1L (**A**) and *Tp*FLU12L (**B**)

reduction in the anthracene as compared to when only enzymes was added to the reaction. Addition of 200 µM ABTS drastically increased the anthracene degradation by both enzymes just after 3–24 h of incubation period. There was no residual anthracene concentration observed after 6 h when 5–10 mM of ABTS were added to the reactions. *Tp*FLU12L could reduce anthracene concentrations to 4.1% and 6.0% after 24 h of incubation when 5 or 10 mM of ABTS was added, respectively. The results indicate that just after 3 h of incubation, 200 µM of ABTS enhances anthracene degradation by 41% and by 100% after 12 h in presence of 5–10 mM of ATBS in case of *Tl*FLU1L.

The degradation kinetics analysis

The degradation kinetics of anthracene mediated by *Tl*FLU1L and *Tp*FLU12L in the absence and presence of mediator (ABTS) is presented in Fig. 3 and Table 2. In the absence of ABTS, v_{max} values of 3.51 ± 0.06 mg/L/h and 3.44 ± 0.06 mg/L/h with K_m 173.2 ± 0.06 mg/L and 73.3 ± 0.07 mg/L were recorded for *Tl*FLU1L and *Tp*FLU12L, respectively, during in vitro degradation of anthracene. Interestingly, in the presence of a mediator (ABTS), v_{max} values increased to 8.63 ± 0.16 mg/L/h and 9.89 ± 0.22 mg/L/h while K_m values decreased to 58.5 ± 0.19 mg/L and 54.6 ± 0.25 mg/L, respectively, for *Tl*FLU1L and *Tp*FLU12L (Fig. 3, Table 2).

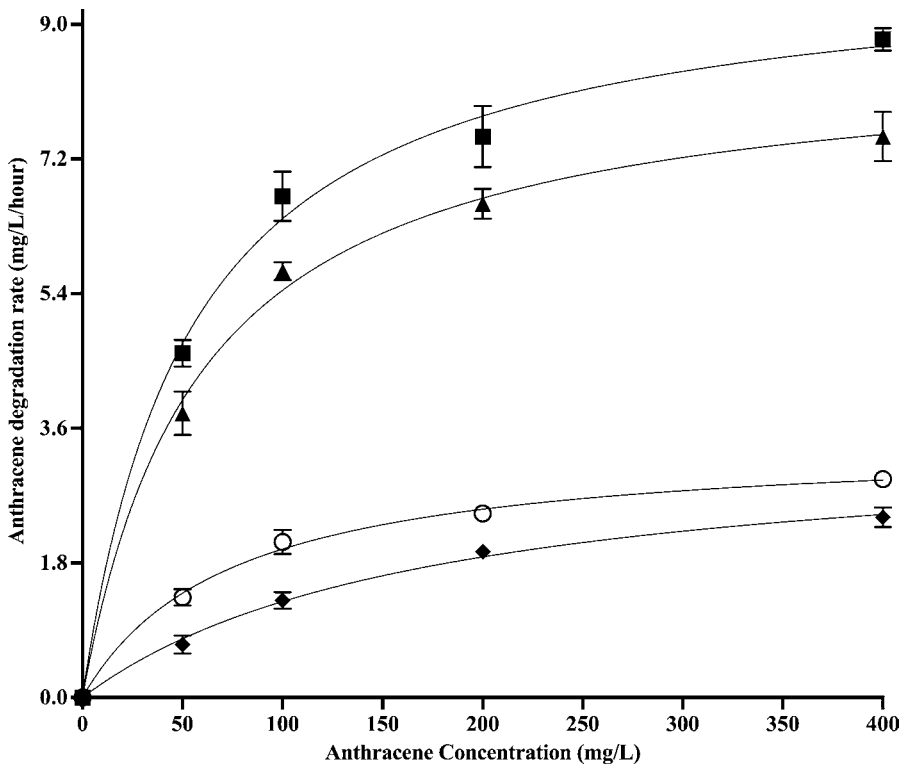

Fig. 3 Laccase-ABTS kinetics of anthracene (200 mg/L) oxidation by *Tl*FLU1L (filled diamond), *Tp*FLU12L (open circle), *Tl*FLU1L + ABTS (filled triangle) and *Tp*FLU12L + ABTS (filled square). Conditions: pH 5, temperature 30 °C, Laccases concentration (3 U/mL), ABTS concentration (10 mM) and incubation period 96 h

Table 2 Michaelis–Menten kinetic parameters of the in vitro degradation of anthracene by *Tl*FLU1L and *Tp*FLU12L

	v_{max} (mg/L/h)		K_m (mg/L)		R^2	
	*Tl*FLU1	*Tp*FLU12	*Tl*FLU1	*Tp*FLU12	*Tl*FLU1	*Tp*FLU12
Anthra	3.51 ± 0.06	3.44 ± 0.06	173.2 ± 0.06	73.3 ± 0.07	0.997	0.997
Anthra + ABTS	8.63 ± 0.16	9.89 ± 0.22	58.5 ± 0.19	54.6 ± 0.25	0.997	0.996

Value in each column is the mean ± standard error. Anthra: Anthracene

The proposed degradation pathway depicted by GC–MS

The GC–MS data analysis proposed that during anthracene degradation, five metabolites were detected which are anthracene-9,10-quinone at a retention time (RT): 16.1 min and m/z: 180) and benzoic acid (RT: 9.3 min and m/z: 105), respectively, in *Tl*FLU1L incubated tube and 3-hydroxy-2- naphthoic acid (RT: 17.5 min and m/z: 170), anthrone (RT: 11.8 min and m/z: 194), chromone (RT: 11.1 min and m/z: 146), benzoic acid (RT: 9.3 min and m/z: 9.3) in *Tp*FLU12L incubated tube. Based on the theoretical arrangement of the detected transient products, anthracene degradation was proposed to undergo two metabolic pathways, namely hydroxylation and carboxylation of C-1 and C-2 position of anthracene to form 3-hydroxy-2-naphthoic acid, before undergoing dioxygenation and side chain removal to form chromone which was later converted into Benzoic acid and CO_2 release as a dead-end product. In addition, the second route was only observed in the absence of the mediator (ABTS) and proceeded via dioxygenation at C9–C10 position to form anthracene-9,10-quinone before its further conversion to anthrone via oxygenation which is broken down into chromone through dioxygenation and undergo carboxylation to form benzoic acid as a dead-end product (Fig. 4).

Ecotoxicity and cytotoxicity analysis of the metabolites of anthracene degradation

Time-course changes in toxicity of anthracene degradation metabolites on *V. parahaemolyticus* (log CFU/mL) are presented in Fig. 5A, B. In the absence of a mediator (ABTS), the marine bacterium survival was recorded at 53.8% and 44.3%, in assays containing *Tl*FLU1L and *Tp*FLU12L, respectively, and the percentage survival increased with an increase in the number of days when the degradation products were collected. However, a significantly high survival of *V. parahaemolyticus* (7.9 log CFU/mL) was obtained with metabolites collected from the degradation assay in presence mediator (ABTS) after 24 h of incubation.

The time-course changes in the cytotoxic effect of anthracene degradation metabolites on HT-22 cells are presented in Fig. 6A, B. Without the mediator ABTS, a slight reduction in the cell viability (10% and 13% for metabolites collected after 24 h and 48 h, respectively) during anthracene degradation by *Tl*FLU1L, while metabolite from *Tp*FLU12L degradation resulted in 86% cell viability (for 24 h degradation product) and 70% cell viability (for 48 h degradation product). However, cell viability of 100% and 93% were obtained after 72-h degradation with *Tl*FLU1L and *Tp*FLU12L, respectively. In the presence of the ABTS mediator, up to 115% and 106% cell viability was obtained when treated with metabolites obtained after 24 h degradation by *Tl*FLU1L and *Tp*FLU12L, respectively.

Micrograph analysis of HT-22 cells treated with fluoranthene oxidation product from *Tl*FLU1L and *Tp*FLU12L is shown Fig. 7A, B. A distinct difference was noted between the control (blank) and HT-22 cells treated with anthracene oxidation product. In the control group and HT-22 cells treated with anthracene + ABTS oxidation product from *Tl*FLU1L and *Tp*FLU12L, cells exhibited a healthy morphology with a characteristic neuronal-like appearance with elongated, spindle-shaped bodies, well-defined nuclei, and uniform neurite processes. In contrast, the treated cells with anthracene only (positive control) and anthracene oxidation product from *Tl*FLU1L and *Tp*FLU12L, exhibited cytotoxic effects with cellular shrinkage, increased membrane blebbing, and loss of neurite extensions. The cells appeared smaller, with disrupted cell membranes and fragmented neurites, indicating impaired connectivity and reduced cell viability. Overall, the treated cells displayed decreased density, suggesting cell death caused by oxidation products.

The effect of anthracene degradation metabolites on genes associated with Alzheimer's disease in HT-22 cells is presented in Fig. 8. The expression of genes BACE-1 (1.7-fold), ADAM-10 (3.6-fold), TAU (1.5-fold), PPARγ (4.7-fold) and APP (2.8-fold) genes were upregulated in cells treated with degradation products of *Tl*FLU1L 1 in comparison with the cell treated with degradation product of control group (Uncatalyzed anthracene). Conversely, in the degradation products of *Tp*FLU12L, *Tl*FLU1L + ABTS and *Tp*FLU12L + ABTS, down-regulation of BACE-1, ADAM-10, TAU, PPARγ and APP was observed.

Discussion

The results of in-vitro enzymatic degradation of anthracene lend credence to the report that purified

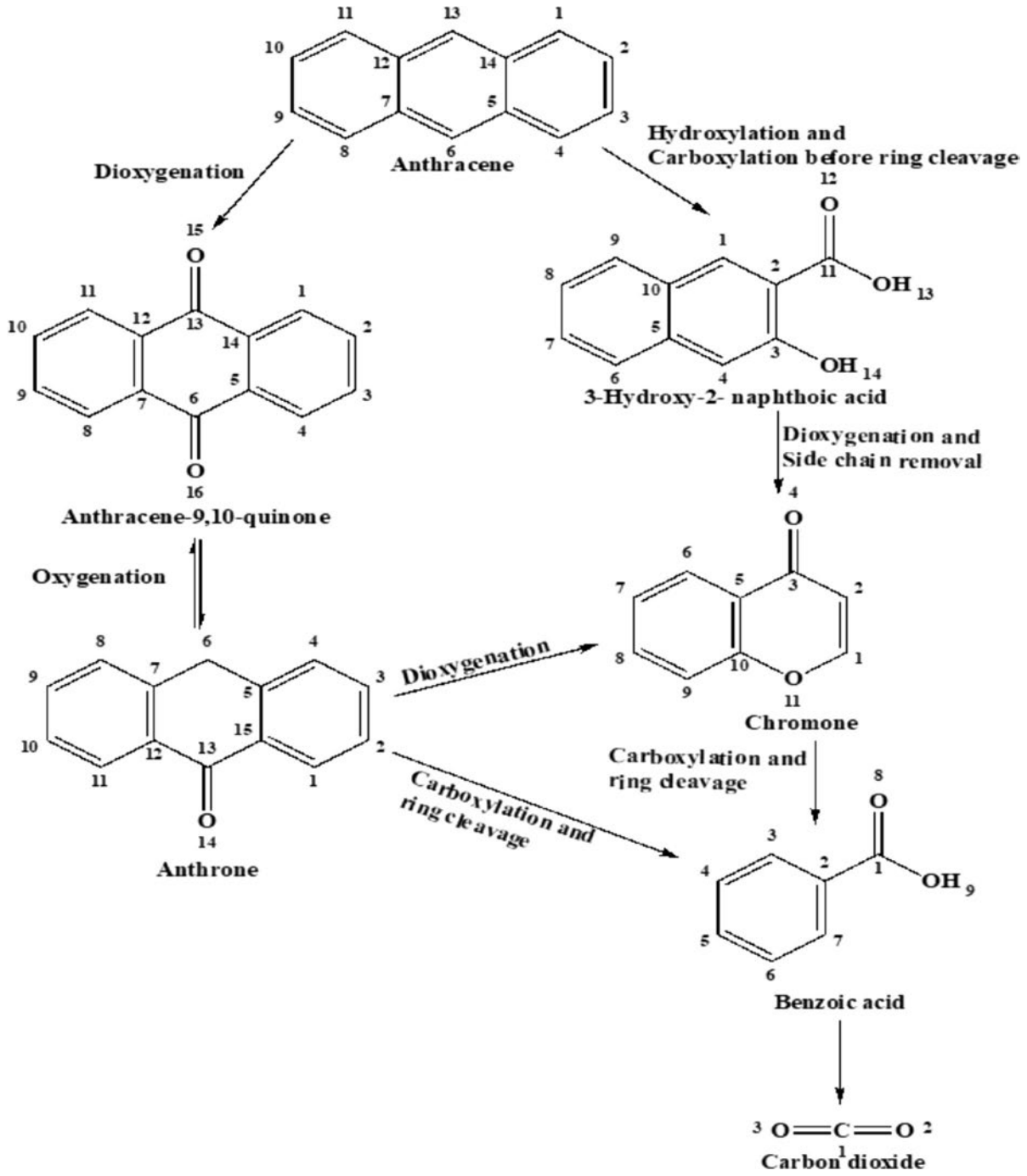

Fig. 4 A proposed pathway for anthracene degradation by *Tl*FLU1L and *Tp*FLU12L

Laccase has broad substrate specificity due to its ability to degrade a wide range of aromatic compounds like PAHs (Ezike et al. 2021; Wu et al. 2010). The obtained low residual anthracene concentration in the tube incubated with purified Laccase from *Tl*FLU1 (*Tl*FLU1L) compared to that of purified laccase from *Tp*FLU12 (*Tp*FLU12L) can be linked to the intrinsic properties of the yellow Laccase from *Tl*FLU1

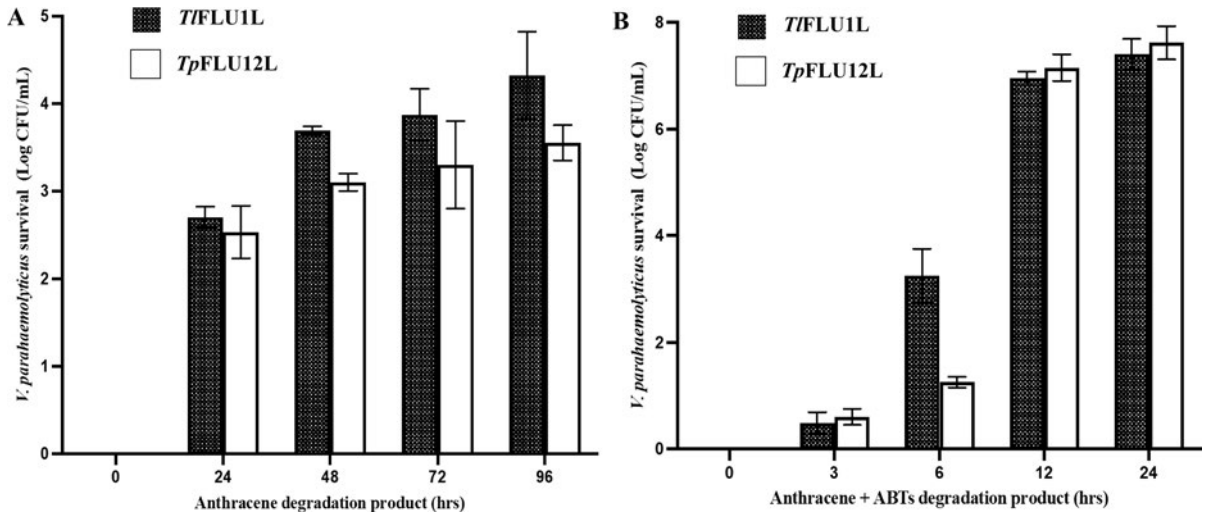

Fig. 5 Time-course changes in toxicity of anthracene degradation products of *Tl*FLU1L, *Tp*FLU12L, *Tl*FLU1L + ABTS and *Tp*FLU12L + ABTS on *V. parahaemolyticus* (log CFU/mL)

(*Tl*FLU1L) such as its structure/specific amino acid composition which could render it to be more efficient in catalyzing the oxidation of anthracene's aromatic rings than their blue counterpart. Pozdniakova et al. (2006) opined that the yellow Laccase is superior in degradation efficiency compare to its blue counterparts leading to into an innocuous state in the absence of mediators. Likewise, the low residual anthracene concentration in the tube incubated with *Tl*FLU1L could be attributed to its enigmatic preference for radical-forming aromatic substrate like PAHs which in return boosts its enzyme activity and stability during the catalytic reaction (Fig. 1A) (Mot et al. 2020).

Laccase concentration played a significant role in the degradation process as evident by the observed low residual anthracene concentration with an increase in *Tl*FLU1L concentrations (Fig. 1B) aligns with the expected enzyme–substrate kinetics. Higher Laccase concentration provides more catalytic sites available for anthracene oxidation, leading to faster degradation rates. This observation is consistent with previous studies on Laccase-mediated PAH degradation where efficient degradation of several PAHs increase with an increase in pure Laccase concentration during an aged soil amendment (Wu et al. 2008). Some authors have demonstrated that PAHs degradation in water is proportional to Laccase concentration in the beads of a Laccase-loading spider-type reactor (LSTR) (Niu et al. 2013). Also, the removal of PAHs is known to be influenced by low ionization potentials (IPs) (Kadri et al. 2017) while anthracene having an IP of 7.43 eV (Kukhta et al. 2009) could explain the rapid degradation of anthracene. Furthermore, PAHs with IP ≤ 7.55 eV are more susceptible to enzymatic degradation by fungi to quinonic metabolites, a substrate easily mineralized to CO_2 by microbial populations and could naturally undergo polymerization to become part of the humus pool (Pozdnyakova 2012). The mechanism for PAHs degradation by Laccase could be attributed to Ips and Laccase can effectively degrade PAHs with IP below 7.45 eV (Li et al. 2010b).

Although several purified Laccase from fungi have been reported to degrade PAHs, its high production cost is a major challenge for commercial application. Hence, it becomes imperative to assess the influence of mediators on low Laccase concentration as an alternative to reduce high Laccase concentration usage. The observed low residual anthracene concentrations at 3 U of *Tl*FLU1L and *Tp*FLU12L in the presence of high mediator (ABTs) concentration suggests a synergistic effect between Laccase and mediator leading to a rapid generation of ABTS radicals due to high Laccase activity which then promote an attack at the PAHs benzene rings. This observation is consistent with the report of Naghdi et al. (2018) where ABTS was demonstrated to acts as a redox

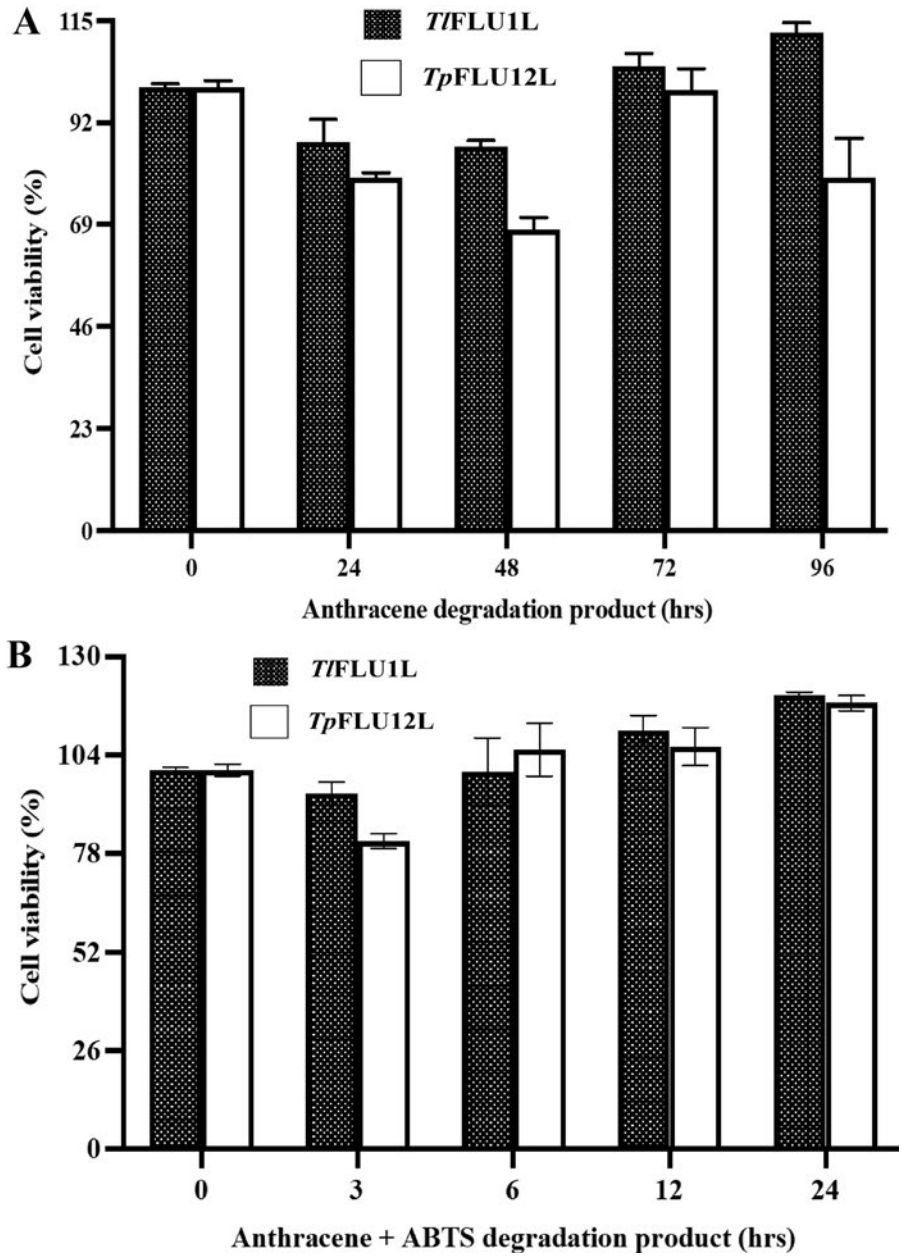

Fig. 6 Time-course changes in toxicity of anthracene degradation products of *Tl*FLU1L, *Tp*FLU12L, *Tl*FLU1L + ABTS and *Tp*FLU12L + ABTS on on HT-22 cell-line

mediator by readily accepting electrons from laccase and transferring them to xenobiotics, facilitating its oxidation and subsequent degradation. Another possible explanation for this observation is that ABTS could function as an "electron shuttle" between the free enzyme and the substrate. This aligns with the report of (Dodor et al. 2004), where the mechanism of overall catalytic efficiency of Laccase in degrading anthracene was linked to ABTS acting as an "electron shuttle" between Laccase and the substrate (anthracene).

The degradation kinetics reaction of anthracene and *Tl*FLU1L under free- and mediator system revealed that the reaction undergoes first-order kinetics, where the rate of the reaction was independent of the substrate concentration but dependent on the amount of the enzyme used. This observation is in accordance with a previous report

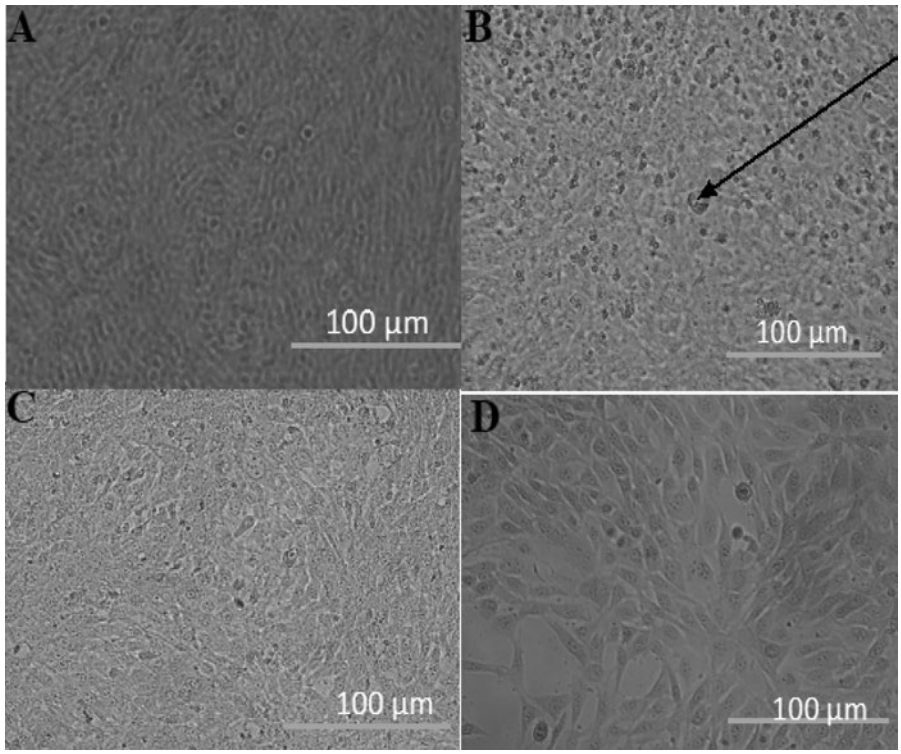

Fig. 7 The micrograph of the HT-22 cell-line grown on anthracene degradation products. **A** Control (Blank), **B** Control (Anthracene), **C** *Tl*FLU1L treated cell line and **D** *Tp*FLU12L treated cell line. Arrow shows dead cells

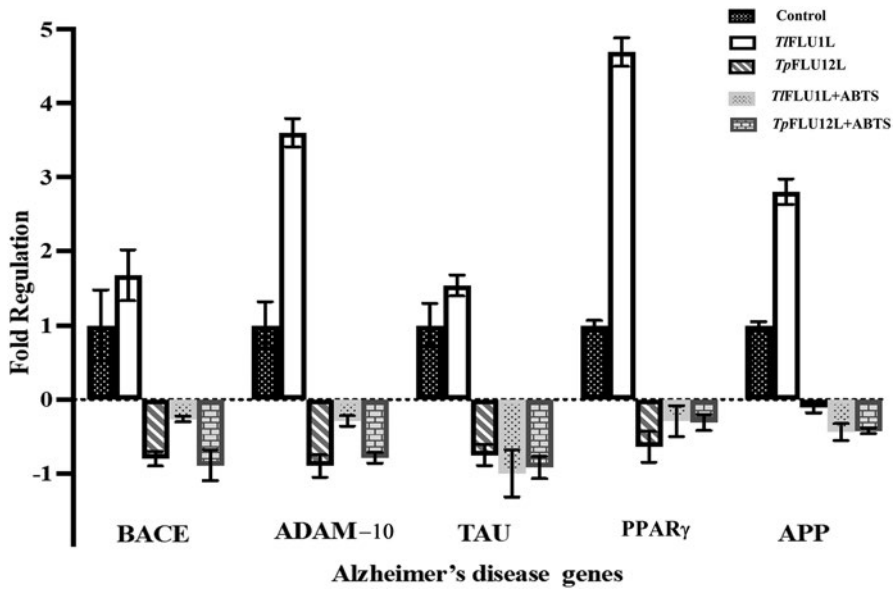

Fig. 8 Effect of anthracene degradation products on expression of genes linked with Alzheimer's in HT-22 cells

(Dodor et al. 2020) where PAHs degradation by fungi Laccase obeys first-order kinetics. The relatively lower K_m values of the mediator immobilized Laccases compared to the free enzyme indicate a potential conformational change of the enzyme due to mediator immobilization, leading to a higher affinity for ABTS used as a substrate for the enzyme activity assay. Likewise, the oxidization state(s) of ABTS and the pH of the reaction medium (acidic)

can be considered as major factors which influenced the anthracene degradation (Li et al. 2010a).

Interestingly, two possible pathways were proposed for anthracene degradation by the Laccases investigated in this study. The first degradation route is initiated in the presence of the mediator alone (Table 3) with hydroxylation and carboxylation with ring cleavage at the C-1 and C-2 position of anthracene to form 3-hydroxy-2-naphthoic acid, before undergoing decarboxylation and side chain removal to form chromone which is later converted to benzoic acid and carbon dioxide through carboxylation and ring cleavage as a dead-end product. This same degradation product in our proposed pathway has been documented during anthracene metabolism in a halophilic bacterium, *Martelella* sp. AD-3, suggesting that it is a common metabolic pathway for anthracene (Cui et al. 2014). Conversely, the second degradation pathway was mainly observed during the free Laccase degradation of anthracene which proceeded through dioxygenation of C-9, and the C-10 position of the anthracene ring to form anthracene-9,10-quinone which is later converted to anthrone via oxygenation before yielding benzoic acid as a dead-end degradation product. This same degradation pathway has been identified during anthracene degradation by marine fungi *Cladosporium sp*. CBMAI 1237 (Birolli et al. 2018). Also, the appearance of only anthracene-9,10-quinone in the *Tl*FLU1L tube and anthrone alone in the *Tp*FLU12L tube suggest that those products are not stable and agree with various researchers who have well-confirmed anthraquinone/anthrone as a dead-end metabolite of anthracene (Aranda et al. 2017). The observation in the *Tp*FLU12L tube is consistent with a previous report (Jove et al. 2016) where fungi ligninolytic enzymes initiate anthracene degradation at C-9 and C-10 positions to form anthrone, which was later converted to benzoic acid.

Ecotoxicity tests are rapid tests commonly used to determine the impact of contaminants on living organisms (Clasen and Lisbôa 2019). The obtained data on ecotoxicity revealed that the formation of one or more metabolites could induce acute toxicity despite a significant reduction in parent compound concentration. A similar observation was reported where biodegradation of bisphenol by fungi produces metabolites of higher toxicity than the parent compound (Mtibaà et al. 2018). Since quinone derivatives such as chromones are known toxicity inducers which act as a direct-acting mutagen, this could explain the low survival of *V. parahaemolyticus* (log CFU/mL) when exposed to anthracene degradation product of *Tp*FLU12L-mediator (Fig. 5B) within 6 h degradation period (Chibwe et al. 2017; Menzie et al. 1992). Also, the slight reduction in *V. parahaemolyticus* survival (log CFU/mL) as the primary decomposer in the ecosystem and the percentage cell viability of HT-22 cell line as a tertiary consumer could be attributed to the presence of 9-oxo-9*H*-fluorene-1-carboxylic acid. This observation corroborate previous finding which demonstrated that carboxylation on C-1 of fluorene which yielded fluorene-1-carboxylic acid as a metabolite increased acute toxicity in zebrafish than its parent compound (fluorene) (Kim et al. 2020). It is worth noting that the variation in log CFU/mL of

Table 3 GC–MS profile of the metabolites accumulated during anthracene degradation by *Tl*FLU1L and *Tp*FLU12L

M	Retention Time (min)	Major m/z of fragment ions (% relative abundance)	Tentative metabolite Identification	Laccase source	
				*Tl*FLU1L	*Tp*FLU12
1	19.8	76 (6, **M**$^+$), 88 (4), 89 (8), 150 (4), 151 (6), 152 (7), 176 (14),177 (8),**178** (100), 179 (16)	Anthracene	xx	
2	17.5	63 (14, M$^+$), 71 (25), 88 (12), 113 (18), 115 (16), 142 (80), **170** (100), 171 (13), 188 (46)	3-Hydroxy-2-naphthoic acid	x	xxxA
3	16.1	50 (19, **M**$^+$), 75 (17), 76 (44), 150 (15), 151 (78), 152 (78), **180** (100), 181 (14), 208 (98), 209 (15)	Anthracene-9,10-quinone	xx	x
4	11.8	63 (3, **M**$^+$), 82 (7), 139 (4), 163 (7), 164 (6), 165 (53),166 (10),193 (9), **194** (100), 195 (15)	Anthrone	x	xx
5	11.1	50 (11, **M**$^+$), 63 (20), 64 (14), 89 (11), 90 (12), 92 (40), 118 (62), 120 (24), **146** (100), 147(10)	Chromone	x	xxxA

M = metabolite

the primary decomposer and the tertiary consumer percentage cell viability per each PAHs degradation product has revealed that toxicity is not a function of contaminant concentrations but its molecular structure and exposure time-dependent (Lukić et al. 2016). Also, the most probable explanation for the observed cell viability exceeding 100% in the ABTS degradation products exposed cells further attests to the non-toxic nature of these degradation products with the possibility of the cell line utilizing one or more metabolites, leading to the enhanced metabolic activity of the cell line. This phenomenon is well-documented in various studies, such as those investigating the effects of X-ray irradiation on human lens epithelial cells (Dehankar et al. 2015), the viability of human melanoma cells following drug and proton irradiation treatments (Petrović et al. 2007), and the relationship between cell viability and treatment outcomes in acute myeloid leukaemia (Maha et al. 2008) where no toxic product increased cell viability. Furthermore, a review (Stoddart 2011) highlighted that cell viability could exceed 100% under certain circumstances, often due to enhanced metabolic activities resulting from cell line treatments. This situation commonly arises when calculating the ratio between treated and non-treated cells' optical density (OD) values. For example, if the OD value of treated cells is 0.9 and the OD value of non-treated cells is 0.8, then the cell viability percentage is calculated as $0.9/0.8 \times 100 = 112.5\%$. This indicates an increase in metabolic activity or cell numbers in treated cells compared to non-treated cells.

There is a relatively limited number of existing studies that utilize transcriptomic analysis to investigate the toxicity of metabolic products of polycyclic aromatic hydrocarbons (PAHs). This scarcity of research has prompted us to employ HT-22 cells as a model system to gain further insights into the ecological implications of fluoranthene degradation products. This decision was made based on the low survival rate of bacteria observed and the perceived decrease in cell viability. The observed increase in the expression level of BACE-1, ADAM-10, TAU, PPARγ, and APP genes in the positive control group (uncatalyzed, anthracene only), as well as in cells treated with *Tl*FLU1L degradation product, suggests that these products are neurotoxic and capable of inducing neurodegeneration like Alzheimer's disease (AD). This observation lends credence to the previous report where these genes were attributed to the production and aggregation of amyloid beta peptides and neurofibrillary tangles, which are the primary causes of neuronal damage and death in AD (Hardy and Selkoe 2002). However, the degradation products of *Tp*FLU12L, *Tl*FLU1L + ABTS, and *Tp*FLU12L + ABTS showed decreased expression of these genes, indicating lower neurotoxicity and a potential for neuroprotection (Fig. 8). These compounds might prevent or reduce the formation and accumulation of amyloid beta peptides and neurofibrillary tangles by modulating the activity or expression of BACE-1 and ADAM-10, which are critical enzymes in the processing of amyloid precursor protein (APP) (Vassar et al. 2014). Also, the exhibited healthy morphological characteristics such as neuronal-like appearance with elongated, spindle-shaped bodies, well-defined nuclei, and uniform neurite processes (Fig. 7C, D) further attest to the lower neurotoxicity of the degradation product from *Tp*FLU12L, *Tl*FLU1L + ABTS, and *Tp*FLU12L + ABTS. The exhibited cytotoxic effects with cellular shrinkage, increased membrane blebbing, and loss of neurite extensions in HT-22 treated cells with positive control (anthracene only) and anthracene oxidation products from *Tl*FLU1L and *Tp*FLU12L can be linked to the neurodegeneration potential of these products due to decrease in cell viability because of swelling and decrease in the microvilli content, varying degrees damages to the cellular membrane integrity, sparse chromatin, very wide gap mitochondria ridge gap and scarcity of the microfilament and microtubule density (Chen et al. 2023).

Conclusion

This study explored the potential of Laccases from *Tl*FLU1 (*Tl*FLU1L) and *Tp*FLU12L for the biodegradation of anthracene. Our findings demonstrate the superior efficiency of *Tl*FLU1L, particularly when coupled with a Laccase-mediator system. This combined approach enhanced degradation and displayed greater stability compared to the free Laccase system. However, GC–MS analysis revealed a crucial finding: the degradation pathways differed between methods. The mediator system produced benzoic acid through a potentially less harmful route involving hydroxylation and carboxylation, while the free Laccase system utilized a dioxygenation pathway. Significantly, ecotoxicity tests suggest that some degradation products might be more toxic than anthracene. This underscores the importance

of evaluating not only degradation efficiency but also the environmental and health impacts of the resulting metabolites. Overall, this study establishes *Tl*FLU1L with its Laccase-mediator system as a promising candidate for eco-friendly bioremediation of anthracene-contaminated environments. The observed differences in degradation pathways highlight the need for further research to fully understand the enzymatic mechanisms and the fate of these metabolites in real-world ecosystems. Additionally, in-vivo studies are crucial to assess the potential risks and benefits of these Laccases for practical environmental clean-up applications. By elucidating the structure–activity relationship of the degradation products, we can develop more sustainable strategies that maximize contaminant removal while minimizing the generation of harmful byproducts. This knowledge is essential for ensuring the safe and effective implementation of enzymatic bioremediation in the field.

Acknowledgements S.O.E. Thanks University of KwaZulu Natal, Durban, South Africa for Ph.D. scholarship.

Author contributions Conceptualization, S.O.E. and A.O.O.; methodology, S.O.E., T.A.O. and A.K.; validation, S.O.E., A.K., and A.O.O.; formal analysis, S.O.E., T.A.O. and A.K.; investigation, S.O.E. and A.O.O.; resources, M.P.M. and A.O.O.; data curation, S.O.E. and A.K.; writing-S.O.E.; writing-A.K. and A.O.O.; visualization, S.O.E.; supervision, M.P.M. and A.O.O.; project administration, A.O.O.; funding acquisition, A.O.O. and M.P.M. All authors have read and agreed to the published version of the manuscript.

Funding Open access funding provided by University of KwaZulu-Natal. National Research Foundation, South Africa (Grant No: 94036 and 92803).

Data availability Data are contained within the article or Supplementary Material.

Declarations

Competing interests The authors declare no competing interests.

Conflict of interest The authors declare no conflicts of interest.

References

Adeniji AO, Okoh OO, Okoh AI (2018) Analytical methods for polycyclic aromatic hydrocarbons and their global trend of distribution in water and sediment: a review. In: Mansoor Z (ed) Recent insights in petroleum science and engineering. IntechOpen Limited, London, pp 393–428

Agrawal K, Chaturvedi V, Verma P (2018) Fungal Laccase discovered but yet undiscovered. Bioresour Bioprocess 5:1–1

Ali A, Guo D, Mahar A, Wang P, Shen F, Li R, Zhang Z (2017) Mycoremediation of potentially toxic trace elements—a biological tool for soil cleanup: a review. Pedosphere 27:205–222

Ao T, Mochizuki S, Kajiwara Y, Yonemura K, Shiraishi T, Nagata K, Shinto E, Okamoto K, Nearchou IP, Shimazaki H (2022) Cancer-associated fibroblasts at the unfavorable desmoplastic stroma promote colorectal cancer aggressiveness: potential role of ADAM9. Int J Cancer 150:1706–1721

Aranda E, Godoy P, Reina R, Badia-Fabregat M, Rosell M, Marco-Urrea E, García-Romera I (2017) Isolation of *Ascomycota* fungi with capability to transform PAHs: insights into the biodegradation mechanisms of *Penicillium oxalicum*. Int Biodeterior Biodegrad 122:141–150

Asemoloye MD, Tosi S, Daccò C, Wang X, Xu S, Marchisio MA, Gao W, Jonathan SG, Pecoraro L (2020) Hydrocarbon degradation and enzyme activities of *Aspergillus oryzae* and *Mucor irregularis* isolated from nigerian crude oil-polluted sites. Microorganisms 8:1–19

Birolli WG, Santos DA, Alvarenga N, Garcia ACFS, Romão LPC, Porto ALM (2018) Biodegradation of anthracene and several PAHs by the marine-derived fungus *Cladosporium* sp. CBMAI 1237. Mar Pollut Bull 129:525–533

Brandi P, D'Annibale A, Galli C, Gentili P, Pontes ASN (2006) In search for practical advantages from the immobilisation of an enzyme: the case of Laccase. J Mol Catal B Enzym 41:61–69

Camarero S, Cañas AI, Nousiainen P, Record E, Lomascolo A, MaJ MartÍnez, MartÍnez ÁT (2008) p-Hydroxycinnamic acids as natural mediators for laccase oxidation of recalcitrant compounds. Environ Sci Technol 42:6703–6709

Cambria MT, Minniti Z, Librando V, Cambria A (2008) Degradation of polycyclic aromatic hydrocarbons by rigidoporus lignosus and its laccase in the presence of redox mediators. Appl Biochem Biotechnol 149:1–8

Chen L, Jia P, Liu Y, Wang R, Yin Z, Hu D, Ning H, Ge Y (2023) Fluoride exposure disrupts the cytoskeletal arrangement and ATP synthesis of HT-22 cell by activating the RhoA/ROCK signaling pathway. Ecotoxicol Environ Saf 254:114718

Chibwe L, Davie-Martin CL, Aitken MD, Hoh E, Massey Simonich SL (2017) Identification of polar transformation products and high molecular weight polycyclic aromatic hydrocarbons (PAHs) in contaminated soil following bioremediation. Sci Total Environ 599–600:1099–1107

Clasen B, Lisbôa RM (2019) Ecotoxicological tests as a tool to assess the quality of the soil. In: Vázquez-Luna D, Cuevas-Díaz MC (eds) Soil contamination and alternatives for sustainable development. IntechOpen, London, pp 13–33

Cui C, Ma L, Shi J, Lin K, Luo Q, Liu Y (2014) Metabolic pathway for degradation of anthracene by halophilic *Martelella* sp. AD-3. Int Biodeterior Biodegrad 89:67–73

de Freitas EN, Bubna GA, Brugnari T, Kato CG, Nolli M, Rauen TG, Peralta Muniz Moreira RF, Peralta RA, Bracht A, de Souza CGM, Peralta RM (2017) Removal of bisphenol A by laccases from *Pleurotus ostreatus* and *Pleurotus pulmonarius* and evaluation of ecotoxicity of degradation products. Chem Eng J 330:1361–1369

Dehankar R, Bapat S, Ksheersagar DD, Paikrao V (2015) Cell viability in X-ray irradiated human lens epithelial cell (HLEC) culture by using trypan blue dye exclusion test. J Evid Based Med Healthc 2:9003–9008

Dodor DE, Hwang HM, Ekunwe SIN (2004) Oxidation of anthracene and benzo[a]pyrene by immobilized Laccase from *Trametes versicolor*. Enz Microb Technol 35:210–217

Dodor DE, Miyittah M, Ahiabor BDK (2020) Immobilized Laccase mediator-catalyzed oxidation of aqueous mixtures of polycyclic aromatic hydrocarbons. Polycycl Aromat Compd 40:563–573

DWAF (1996) South African water quality guidelines, Domestic Use. In Department of Water Affairs and Forestry, Vol. 1, Issue 2

Egbewale SO, Kumar A, Mokoena MP, Olaniran AO (2023) Metabolic biodegradation pathway of fluoranthene by indigenous *Trichoderma lixii* and *Talaromyces pinophilus* spp. Catalysts 13:791

Ezike TC, Udeh JO, Joshua PE, Ezugwu AL, Isiwu CV, Eze SOO, Chilaka FC (2021) Substrate specificity of a new Laccase from *Trametes polyzona* WRF03. Heliyon 7:e06080–e06080

Fernández-Fernández M, Sanromán MÁ, Moldes D (2013) Recent developments and applications of immobilized laccase. Biotechnol Adv 31:1808–1825

Forján R, Lores I, Sierra C, Baragaño D, Gallego JLR, Peláez AI (2020) Bioaugmentation treatment of a PAH-polluted soil in a slurry bioreactor. Appl Sci 10:2837

Grassi E, Scodeller P, Filiel N, Carballo R, Levin L (2011) Potential of *Trametes trogii* culture fluids and its purified Laccase for the decolorization of different types of recalcitrant dyes without the addition of redox mediators. Int Biodeterior Biodegrad 65:635–643

Haneef T, Ul Mustafa MR, Yusof KW, Isa MH, Bashir MJK, Ahmad M, Zafar M (2020) Removal of polycyclic aromatic hydrocarbons (PAHs) from produced water by ferrate(VI) oxidation. Water 12:1–17

Hardy J, Selkoe DJ (2002) The amyloid hypothesis of Alzheimer's disease: progress and problems on the road to therapeutics. Science 297:353–356

Hu X, Wang P, Hm H (2009) Oxidation of anthracene by immobilized Laccase from *Trametes versicolor*. Bioresour Technol 100:4963–4968

Hu Y, Pan Q, Zhou K, Ling Y, Wang H, Li Y (2022) RUNX1 inhibits the antiviral immune response against influenza A virus through attenuating type I interferon signaling. Virology J 19:39

Janusz G, Pawlik A, Świderska-Burek U, Polak J, Sulej J, Jarosz-Wilkołazka A, Paszczyński A (2020) Laccase properties, physiological functions, and evolution. Int J Mol Sci 21:966–966

Jove P, Olivella MA, Camarero S, Caixach J, Planas C, Cano L, De Las Heras FX (2016) Fungal biodegradation of anthracene-polluted cork: a comparative study. J Environ Sci Health Tox Hazard Subst Environ Eng 51:70–77

Kadri T, Rouissi T, Kaur Brar S, Cledon M, Sarma S, Verma M (2017) Biodegradation of polycyclic aromatic hydrocarbons (PAHs) by fungal enzymes: a review. J Environ Sci 51:52–74

Kim YC, Lee SR, Jeon HJ, Kim K, Kim MJ, Choi SD, Lee SE (2020) Acute toxicities of fluorene, fluorene-1-carboxylic acid, and fluorene-9-carboxylic acid on zebrafish embryos (*Danio rerio*): molecular mechanisms of developmental toxicities of fluorene-1-carboxylic acid. Chemosphere 260:127622–127622

Ko SY, Lin SC, Chang KW, Wong YK, Liu CJ, Chi CW, Liu TY (2004) Increased expression of amyloid precursor protein in oral squamous cell carcinoma. Int J Cancer 111:727–732

Kukhta AV, Kukhta IN, Zavilopulo AN, Agafonova AS, Shpenik OB (2009) Ionization of 4,4′-bis(Phenylethynyl)-anthracene by electron impact. Eur J Mass Spectrom 15:563–570

Kumar A, Chandra R (2020) Ligninolytic enzymes and its mechanisms for degradation of lignocellulosic waste in environment. Heliyon 6:e03170–e03170

Laemmli UK (1970) Cleavage of structural proteins during the assembly of the head of bacteriophage T4. Nature 227:680–685

Li X, Lin X, Yin R, Wu Y, Chu H, Zeng J, Yang T (2010) Optimization of Laccase-mediated benzo[a]pyrene oxidation and the bioremedial application in aged polycyclic aromatic hydrocarbons-contaminated soil. J Health Sci 56:534–540

Li X, Lin X, Zhang J, Wu Y, Yin R, Feng Y, Wang Y (2010) Degradation of polycyclic aromatic hydrocarbons by crude extracts from spent mushroom substrate and its possible mechanisms. Curr Microbiol 60:336–342

Liu Y, Geng Y, Yan M, Huang J (2017) Stable ABTS immobilized in the MIL-100 (Fe) metal-organic framework as an efficient mediator for laccase-catalyzed decolorization. Molecules 22:920

Lukić B, Panico A, Huguenot D, Fabbricino M, van Hullebusch ED, Esposito G (2016) Evaluation of PAH removal efficiency in an artificial soil amended with different types of organic wastes. Euro Mediterr J Environ Integr 1:5. https://doi.org/10.1007/s41207-016-0001-x

Maha A, Cheong S-K, Leong C-F, Seow H-F (2008) Cell viability of acute myeloid leukaemia blasts in culture correlates with treatment outcome. Hematology 13:13–20

Mayolo-Deloisa K, González-González M, Rito-Palomares M (2020) Laccases in food industry: bioprocessing, potential industrial and biotechnological applications. Front Bioeng Biotechnol 8:222

Menzie CA, Potocki BB, Santodonato J (1992) Exposure to carcinogenic PAHs in the environment. Environ Sci Technol 26:1278–1284

Mot AC, Coman C, Hadade N, Damian G, Silaghi-Dumitrescu R, Heering H (2020) "Yellow" Laccase from *Sclerotinia sclerotiorum* is a blue laccase that enhances its substrate affinity by forming a reversible tyrosyl-product adduct. PLoS ONE 15:e0225530

Mtibaà R, Olicón-Hernández DR, Pozo C, Nasri M, Mechichi T, González J, Aranda E (2018) Degradation of bisphenol A and acute toxicity reduction by different thermo-tolerant ascomycete strains isolated from arid soils. Ecotoxicol Environ Saf 156:87–96

Niu J, Dai Y, Guo H, Xu J, Shen Z (2013) Adsorption and transformation of PAHs from water by a laccase-loading spider-type reactor. J Hazard Mater 248–249:254–260

Othman HB, Leboulanger C, Le Floc'h E, Hadj Mabrouk H, Sakka Hlaili A (2012) Toxicity of benz(a)anthracene and fluoranthene to marine phytoplankton in culture: does cell size really matter? J Hazard Mater 243:204–211

Othman AM, Elsayed MA, Elshafei AM, Hassan MM (2018) Purification and biochemical characterization of two isolated laccase isoforms from *Agaricus bisporus* CU13 and their potency in dye decolorization. Int J Biol Macromol 113:1142–1148

Pesant M, Sueur S, Dutartre P, Tallandier M, Grimaldi PA, Rochette L, Connat JL (2006) Peroxisome proliferator-activated receptor δ (PPARδ) activation protects H9c2 cardiomyoblasts from oxidative stress-induced apoptosis. Cardiovasc Res 69(2):440–449

Petrović IM, Korićanac LB, Todorović DV, RistiĆ-Fira AM, Valastro LM, Privitera G, Cuttone G (2007) Viability of a human melanoma cell after single and combined treatment with fotemustine, dacarbazine, and proton irradiation. Ann N Y Acad Sci 1095:154–164

Pillay L, Olaniran AO (2016) Assessment of physicochemical parameters and prevalence of virulent and multiple-antibiotic-resistant *Escherichia coli* in treated effluent of two wastewater treatment plants and receiving aquatic milieu in Durban, South Africa. Environ Monit Assess 188:260

Pozdniakova NN, Turkovskaia OV, Iudina EN, Rodakiewicz-Nowak Y (2006) Yellow Laccase from the fungus *Pleurotus ostreatus* D1: purification and characterization. Appl Biochem Microbiol 42:56–61

Pozdnyakova NN (2012) Involvement of the ligninolytic system of White-Rot and litter-decomposing fungi in the degradation of polycyclic aromatic hydrocarbons. Biotechnol Res Int 2012:20–20

Ren D, Wang Z, Jiang S, Yu H, Zhang S, Zhang X (2020) Recent environmental applications of and development prospects for immobilized laccase: a review. Biotechnol Genet Eng Rev 36:81–131

Rotini A, Gallo A, Parlapiano I, Berducci MT, Boni R, Tosti E, Prato E, Maggi C, Cicero AM, Migliore L, Manfra L (2018) Insights into the CuO nanoparticle ecotoxicity with suitable marine model species. Ecotoxicol Environ Saf 147:852–860

Šepič E, Bricelj M, Leskovšek H (2003) Toxicity of fluoranthene and its biodegradation metabolites to aquatic organisms. Chemosphere 52:1125–1133

Singh L, Varshney JG, Agarwal T (2016) Polycyclic aromatic hydrocarbons' formation and occurrence in processed food. Food Chem 199:768–781

Slámová T, Fraňková A, Hubáčková A, Banout J (2017) Polycyclic aromatic hydrocarbons in Cambodian smoked fish. Food Addit Contam Part B Surveill 10:248–255

Stoddart MJ (2011) Cell viability assays: introduction. In: Stoddart M (ed) Mammalian cell viability: methods in molecular biology. Humana Press, Totowa, pp 1–6

Tamagno E, Bardini P, Guglielmotto M, Danni O, Tabaton M (2006) The various aggregation states of β-amyloid 1–42 mediate different effects on oxidative stress, neurodegeneration, and BACE-1 expression. Free Radic Biol Med 41:202–212

Tang Y, Donnelly KC, Tiffany-Castiglioni E, Mumtaz MM (2003) Neurotoxicity of polycyclic aromatic hydrocarbons and simple chemical mixtures. J Toxicol Environ Health A 66:919–940

Teh ZC, Hadibarata T (2014) Enhanced degradation of pyrene and metabolite identification by *Pleurotus eryngii* F032. Water Air Soil Pollut 225:1–8

Vassar R, Kuhn PH, Haass C, Kennedy ME, Rajendran L, Wong PC, Lichtenthaler SF (2014) Function, therapeutic potential and cell biology of BACE proteases: current status and future prospects. J Neurochem 130:4–28

Wu Y, Teng Y, Li Z, Liao X, Luo Y (2008) Potential role of polycyclic aromatic hydrocarbons (PAHs) oxidation by fungal Laccase in the remediation of an aged contaminated soil. Soil Biol Biochem 40:789–796

Wu YR, Luo ZH, Kwok-Kei Chow R, Vrijmoed LLP (2010) Purification and characterization of an extracellular laccase from the anthracene-degrading fungus *Fusarium solani* MAS2. Bioresour Technol 101:9772–9777

Xu P, Du H, Peng X, Tang Y, Zhou Y, Chen X, Fei J, Meng Y, Yuan L (2020) Degradation of several polycyclic aromatic hydrocarbons by Laccase in reverse micelle system. Sci Total Environ 708:134970

Yi S, Liu Q, Wang X, Qian T, Wang H, Zha G, Yu J, Wang P, Gu X, Chu D (2019) Tau modulates Schwann cell proliferation, migration and differentiation following peripheral nerve injury. J Cell Sci 132:jcs222059

Zelinkova Z, Wenzl T (2015) The occurrence of 16 EPA PAHs in food—a review. Polycycl Aromat Compd 35:248–284

Zungu NS, Egbewale SO, Olaniran AO, Pérez-Fernández M, Magadlela A (2020) Soil nutrition, microbial composition and associated soil enzyme activities in KwaZulu-Natal grasslands and savannah ecosystems soils. Appl Soil Ecol 155:103663–103663

SUPPLEMENTARY MATERIALS

Anthracene Detoxification by Laccases from Indigenous strains *Trichoderma lixii* FLU1 and *Talaromyces pinophilus* FLU12

Samson O. Egbewale[1], Ajit Kumar[1], Tosin A. Olasehinde[a], Mduduzi P. Mokoena[1,2] and Ademola O. Olaniran [1,*]

[1]Discipline of Microbiology, University of KwaZulu-Natal (Westville Campus), Durban-4001, South Africa

[2]Department of Pathology, School of Medicine, University of Limpopo, Private Bag X1106, Sovenga-0727, South Africa.

*Correspondence: olanirana@ukzn.ac.za; Tel.: +27-31-260-7400

Table S1. The percentage of residual Anthracene concentration after the degradation by *Tl*FLU1L and *Tp*FLU12L (2U).

Time (h)	Control	*Tl*FLU-1	*Tp*FLU-12
0	99.9±0.2	99.9±0.2	99.9±0.2
24	99.9±0.2	73.9±5.1	83.1±7.2
48	99.9±0.2	60.1±1.3	77.3±8.4
72	99.9±0.2	52.1±6.1	62.0±3.1
96	99.9±0.2	44.9±3.0	50.1±9.2

Table S2. The influence of *Tl*FLU1L and *Tp*FLU12L concentrations on *in vitro* degradation of anthracene (96 h).

U/mL	*Tl*FLU-1	*Tp*FLU-12
0	99.9±0.2	99.9±0.2
3	44.3±8.1	42.5±4.1
6	36.5±3.1	19.3±8.8
8	28.7±8.5	3.9±3.1
10	nd	nd

nd=not detected

Table S3. The influence of mediator (ABTS) concentration on *invitro* oxidation of anthracene by *Tl*FLU1L and *Tp*FLU12L (2U).

Time (h)	0 mM	200 µM	500 µM	1 mM	5 mM	10 mM
0	99.9±0.2	99.9±0.2	99.9±0.2	99.9±0.2	99.9±0.2	99.9±0.2
3	96.1±7.2	55±1.7	53.9±4	49.6±7	48.8±6	44.3±5
6	88.1±2.1	47.3±3	46.9±3	44.9±2	41.7±5	38±2
12	80.1±3.3	11.4±3	6.9±3	6.6±3	nd	nd
24	72.5±5.1	6.1±2	5.9±5	4.3±3	nd	nd
48	64.5±4.3	nd	nd	nd	nd	nd
72	56.6±6.4	nd	nd	nd	nd	nd
96	44.3±1.5	nd	nd	nd	nd	nd

nd=not detected

Table S4. The influence of mediator (ABTS) concentration on *invitro* oxidation of anthracene by *Tl*FLU1L and *Tp*FLU12L (2U).

Time (h)	0 mM	200 µM	500 µM	1 mM	5 mM	10 mM
0	99.9±0.2	99.9±0.2	99.9±0.2	99.9±0.2	99.9±0.2	99.9±0.2
3	96.8±4.2	57.1±5.6	56.8±1	55.3±3.3	53.9±2.5	53.4±5.4
6	93.6±5.8	50.2±4.6	49.1±7.5	48.8±1.2	48.2±1.7	47.2±6
12	84±3.5	10.3±5.5	9.3±3.2	8.7±6.4	8.4±7.2	7.3±5.4
24	71.3±3.7	8.5±3.9	8.8±1.7	6.6±2	4.1±1.2	6±3.8
48	64.9±2.2	nd	nd	nd	nd	nd
72	48.9±9.2	nd	nd	nd	nd	nd
96	42.5±3.1	nd	nd	nd	nd	nd

nd=not detected

CHAPTER SEVEN

Synergistic biotransformation of fluoranthene by Laccases from indigenous fungal strains *Trichoderma lixii* and *Talaromyces pinophilus* and ABTS mediator

This chapter is currently under review in the journal: *International Biodeterioration & Biodegradation.*

The manuscript is presented in the following pages.

Synergistic Biotransformation of Fluoranthene by Laccases from Indigenous Fungal strains *Trichoderma lixii* FLU1 and *Talaromyces pinophilus* FLU12 and ABTS Mediator

Samson O. Egbewale[1], Ajit Kumar[1], Tosin A. Olasehinde[1], Mduduzi P. Mokoena[2] and Ademola O. Olaniran[1*]

[1]Discipline of Microbiology, University of KwaZulu-Natal (Westville Campus), Durban 4000, South Africa

[2]Department of Pathology, School of Medicine, University of Limpopo, Private Bag X1106, Sovenga-0727, South Africa.

*Correspondence: olanirana@ukzn.ac.za; Tel.: +27-31-260-7400

Abstract

Polycyclic aromatic hydrocarbons (PAHs) like fluoranthene poses a significant environmental threat due to their persistence and toxicity. The Laccases from *Trichoderma lixii* FLU1 (*Tl*FLU1L) and *Talaromyces pinophilus* FLU12 (*Tp*FLU12L) are shown to act as biocatalysts for fluoranthene degradation in this study. Both Laccases effectively reduced residual fluoranthene concentration with reductions of 46.1% and 38.6% for *T*lFLU1L and *Tp*FLU12L respectively, at 3 U/mL after 96 h. Higher enzyme concentrations further improved degradation with residual fluoranthene concentration reaching 33.1% and 37.4% for *T*lFLU1L and *Tp*FLU12L at 8 U/mL. Complete elimination of residual fluoranthene occurred in some cases with 10 U/mL of either enzyme, while the addition of the mediator (ABTS) significantly enhanced degradation by virtually eliminating residual fluoranthene within 3-24 hours at 200 µM ABTS. Degradation kinetics analysis revealed similar v_{max} values for *Tl*FLU1L (7.73 ± 0.23 mg/L/h) and *Tp*FLU12L (7.97 ± 0.18 mg/L/h), but *Tp*FLU12L exhibited higher affinity with a lower K_m value of 26.6 ± 0.21 mg/L compared to *Tl*FLU1L (54.8 ± 0.27 mg/L) in the presence of ABTS. Without ABTS, v_{max} values were 1.35 ± 0.02 mg/L/h and 1.29 ± 0.02 mg/L/h for *Tl*FLU1Land *Tp*FLU12L, respectively, with K_m values of 119.2 ± 0.02 mg/L and 170.8 ± 0.03 mg/L for *Tl*FLU1L and *Tp*FLU12L, respectively. GC-MS analysis revealed two distinct degradation pathways. *Tl*FLU1L generated a broad spectrum of products including 9-oxo-fluorene-1-carboxylic acid, 9H-fluoren-9-one, and phthalic acid. In contrast, *Tp*FLU12L favoured simpler transformations by producing 9,10-phenanthrenedione and benzene-1,2,3-tricarboxylic acid as metabolites. However, *Tl*FLU1L initiated the degradation pathway with dioxygenation at the C1-C2 carbon bond of fluoranthene, leading to the formation of 9-oxo-fluorene-1-carboxylic acid before undergoing decarboxylation to form 9H-fluoren-9-one and phthalic acid as the dead-end product. *Tp*FLU12L followed a second pathway with dioxygenation and ring cleavage at the C2-C3 carbon bond of fluoranthene to form 9,10-phenanthrenedione which later underwent hydrolysis to generate benzene-1,2,3-tricarboxylic acid as the dead-end product. Ecotoxicity and cytotoxicity analysis indicate a potential toxicity from *Tl*FLU1L degradation products towards marine bacteria, while those of *Tp*FLU12L which are primarily benzene derivatives were found to be harmless.

Keywords: Laccase, Biocatalytic pathways, fluoranthene, ABTS-mediated bioremediation, Sustainability

Introduction

Polycyclic aromatic hydrocarbons (PAHs) constitute a class of organic pollutants that have gained significant attention due to their environmental persistence and detrimental effects on ecosystems and human health (Robin and Marchand, 2022). Among these compounds, fluoranthene, a four-ring PAH, is of particular concern due to its widespread occurrence in contaminated sites, resistance to degradation, and potential carcinogenicity (Ahmed and Ahmed, 2014). Fluoranthene contamination arises from anthropogenic activities like industrial processes, incomplete combustion of fossil fuels and waste disposal (Mojiri et al., 2019). Traditional remediation methods, including physical and chemical techniques, often need to improve in effectively mitigating PAH pollution due to their high cost, limited efficacy, and potential generation of harmful by-products (Egbewale et al., 2023).

Bioremediation, an eco-friendly approach that exploits the metabolic capabilities of microorganisms, has emerged as a promising alternative for remediating PAH-contaminated environments (Sangwan and Dukare, 2018). Enzymatic degradation has shown immense potential among the bioremediation strategies, with Laccases being pivotal enzymes in this context (Kumar et al., 2021). Laccases also known as multicopper oxidases, oxidise wide range of substrates by reducing molecular oxygen to water (Salas and Camarero, 2021). Their ability to oxidize various aromatic and non-aromatic compounds, including PAHs, makes them valuable candidates for bioremediation applications (Agrawal et al., 2019). However, Laccases' inherently low substrate specificity and limited stability often impede their practical use in environmental cleanup (Adamian et al., 2021).

To overcome these challenges, the ABTS (2,2'-azino-bis(3-ethylbenzothiazoline-6-sulfonic acid)) mediator system has emerged as a promising strategy to enhance Laccase activity (García-Morales et al., 2018). This mediator system facilitates electron transfer from the enzyme to the recalcitrant pollutant, effectively expanding the substrate range of Laccases and improving their degradation efficiency (Bhardwaj et al., 2022). By harnessing the synergy between indigenous fungal isolates, Laccases, and the ABTS mediator system, this research aims to develop an innovative and sustainable approach for enhanced bioremediation of fluoranthene-contaminated environments. This multidisciplinary study at the intersection of microbiology, enzymology, and environmental chemistry holds great promise for advancing our understanding of enzyme-mediated degradation and providing a practical solution to address the pressing issue of PAH pollution more efficiently and environmentally friendly.

The link between toxicity and carcinogenicity in polycyclic aromatic hydrocarbons (PAHs) underscores the need to comprehend the effects of Laccase-mediated degradation pathways on

ecosystems for accurate environmental risk assessment. PAHs and their breakdown products are linked to brain-related issues like tumorigenesis, neurotransmitter enzyme inhibition, and nervous system dysfunction (Mesnil et al., 2020). This study employs cell lines to investigate PAH mechanisms and degraded product cytotoxicity to explore these concerns. The research aims to analyze the influence of ABTS in enhancing the biodegradation of fluoranthene by Laccases from *Trichoderma lixii* FLU1L (*Tl*FLU1L) and *Talaromyces pinophilus* FLU12L (*Tp*FLU12L). Moreover, the study assesses the Laccase-mediator ABTS system's potential in degrading fluoranthene, outlining degradation kinetics and biocatalytic pathways by profiling metabolites. Additionally, the investigation presents empirical data on metabolite acute toxicity to *Vibrio parahaemolyticus* marine bacteria and cytotoxicity to rat hippocampal neurons (HT-22 cell line).

Material and methods

Reagents

ABTS, fluoranthene, ethyl acetate (≥ 98% purity) procured from Merck (St. Louis, MI, USA). All the reagents used were of analytical grade. Fluoranthene was selected as listed as human carcinogen on the US EPA's list (Zelinkova and Wenzl, 2015).

Laccases production, purification and activity assay

The blue and yellow Laccase (Mr. 44 kDa and 68.7 kDa) were produce by *Tl*FLU1 and *Tp*FLU12, respectively, and purified to homogeneity (Egbewale et al., 2024a; Egbewale et al., 2024b). To measure enzyme activity, Laccase (370 µg) was mixed in Na-Acetate buffer (800 µl of, 20 mM, pH 5) with ABTS (100 µl, 5 mM) for 15-minute at 30 °C followed by reaction termination with 50 µl of a 20% (v/v) trichloroacetic acid (Zungu et al., 2020). 1 µM of oxidized product (ε420 nm =36,000 $M^{-1}cm^{-1}$) produced per minute was defined as 1 unit of Laccase. The Laccases showed a specific activity of 34 U/mg protein. Both the enzymes exhibited excellent residual activity in various metal ions, organic solvents, detergents and inhibitors (Egbewale et al., 2024a; Egbewale et al., 2024b)

Degradation of fluoranthene by Laccases

The degradation studies were conducted by mixing 200 mg/L fluoranthene with 2 U/ml Laccase in 10 mL Na-Acetate buffer (50 mM, pH 5, 1% Tween 80) (Cambria et al., 2008; Egbewale et al., 2024b) at 30°C in darkness for 96 h and shaking at 80 rpm. Further experimental procedures were explained elsewhere (Egbewale et al., 2024b; Teerapatsakul et al., 2016). The average recovery of 97.9±7.17 % fluoranthene was considered. The GC-MS analysis and specific conditions used are described previously (Teerapatsakul et al., 2016; Teh

and Hadibarata, 2014). The effect of ABTS (200 µM to 10 mM) on the fluoranthene oxidation by the Laccase solution (2 U/mL) was studied as described previously (Egbewale et al., 2024b). To determine kinetic parameters, 50 to 400 mg/L of fluoranthene was used (de Freitas et al., 2017). K_m and v_{max} were determined by using non-linear regression model and applying Michaelis-Menten equation ($v=v_{max}[S]/(K_m+[S])$) (Egbewale et al., 2024b).

Ecotoxicity and cytotoxicity analysis

To address the risk assessment on biota, ecotoxicity analysis of the fluoranthene degradation metabolites was conducted on *Vibrio parahaemolyticus* (ATCC 17802) and the cytotoxicity assay was performed using rat hippocampal neuronal cell line (HT-22 cell line) as described previously (Egbewale et al., 2023; Egbewale et al., 2024b; Rotini et al., 2018). All the data were carried out in triplicates and expressed as the means ± standard deviations. Throughout the manuscript, *Tl*FLU1L and *Tp*FLU12L stands for purified enzymes unless otherwise stated.

RESULTS

Fluoranthene Degradation by Laccases

The percentage of residual fluoranthene after the degradation by *Tl*FLU1L and *Tp*FLU12L) is shown in Fig. 1 and Table S1. Throughout the 96-h reaction period, both enzymes consistently reduced residual fluoranthene concentration. At 3 U/mL of *Tl*FLU1L and *Tp*FLU12L, the residual concentration was recorded at 49.5% and 61.0% respectively. However, as the concentration increased to 8 U/mL, the residual fluoranthene concentration dropped further to 33.1% and 37.4% for *Tl*FLU1L and *Tp*FLU12L while at a concentration of 10 U/mL, the residual fluoranthene concentration reached its lowest concentration with 19.2% for *Tl*FLU1L and 28.7% for *Tp*FLU12L.

Degradation of Fluoranthene by Laccases in the Presence of ABTS

The influence of ABTS concentration on the degradation of fluoranthene by *Tl*FLU1L and *Tp*FLU12L is shown in Fig. 2 (A-B). At 3 U/mL *Tl*FLU1L (Fig. 2A, Table S2) and *Tp*FLU12L (Fig. 2B, Table S3), reaction with 10 mM ABTS and 200 mg/L of fluoranthene resulted in a significant reduction in residual fluoranthene with no residual concentration for both enzymes at 24 h compared to 49.5±8.68% and 61.0±0.95% residual concentration for *Tl*FLU1L and *Tp*FLU12L when only the enzymes (without ABTS) was added. Interestingly, the addition of 200 µM ABTS to 3 U/mL of the enzymes drastically increased fluoranthene degradation within 24 h with residual concentrations of 28.0±0.39% for *Tl*FLU1L and 21.8±0.46% for *Tp*FLU12L. This trend continued by revealing a further decrease in residual fluoranthene at higher ABTS concentrations over subsequent time intervals.

The degradation kinetics analysis

Fig. 3, Table 1 and Table S4 presents degradation kinetics data. In the absence of ABTS, K_m values of 119.2 ± 0.02 mg/L and 170.8 ± 0.15 mg/L and v_{max} values of 1.35 ± 0.02mg/L/h and 1.29 ± 0.15 mg/L/h were recorded for *Tl*FLU1L and *Tp*FLU12L, respectively, while, in the presence of a mediator (ABTS), K_m values decreased to 54.8 ± 0.23 mg/L and 26.6 ± 0.28 mg/L and v_{max} values increased to 7.73 ± 0.23 mg/L/h and 7. 97 ± 0.28 mg/L/h while for *Tl*FLU1L and *Tp*FLU12L, respectively.

The degradation pathway proposed by GC-MS

The GC-MS data has shown that during fluoranthene degradation, five different intermediate products apart from the parent compound (fluoranthene with retention time (RT): 28.2 with molecular ion (M^+) m/z: 202) were detected in *Tl*FLU1L and *Tp*FLU12L Laccase incubated tubes. In the *Tl*FLU-1L tube, 9-oxo-fluorene-1-carboxylic acid (RT: 14.8 min and m/z: 224), and Phthalic acid (RT: 17.5 min and m/z: 104), while 9,10-phenanthrenedione, Benzene-1,2,3-tricarboxylic acid (RT: 12.7 min and m/z: 148) and Benzoic acid (RT: 9.3 mins and m/z: 105) was observed in *Tp*FLU-12L (Fig. 4 and Table 2). However, based on the theoretical arrangement of these detected intermediate products, fluoranthene degradation is proposed to occur through two main pathways. The first route, as observed in the *Tl*FLU1L route, begins with dioxygenation at the C1-C2 carbon bond of fluoranthene, leading to the formation of 9-oxo-fluorene-1-carboxylic acid before undergoing decarboxylation which then yields 9*H*-fluoren-9-one. Subsequently, this intermediate undergoes ring cleavage in one of the aromatic rings to form phthalic acid before entering the protocatechuate pathway. However, the second pathway, which is observed in *Tp*FLU12L, begins with dioxygenation and ring cleavage at the C2-C3 carbon bond of fluoranthene to form 9,10-phenanthrenedione and subsequently undergoes hydrolysis to generate benzene-1,2,3-tricarboxylic acid which later then enters the protocatechuate pathway. Noteworthy, the 9*H*-fluoren-9-one was not detected in our GC-MS analysis

Ecotoxicity and cytotoxicity analysis of fluoranthene degradation metabolites

Fig. 5 (A-B) shows the toxicity of fluoranthene degradation metabolites on *V. parahaemolyticus* survival (log CFU/mL). Overall, in the absence ABTS, each degradation products from *Tl*FLU1L and *Tp*FLU12L support the marine bacterium survival. Notably, *Tp*FLU12 displayed a more pronounced *V. parahaemolyticus* survival particularly at 72 and 96 h with log CFU/mL value of 5.49 and 7.79, respectively, when compared to *Tl*FLU1 which shows 3.95 log CFU/mL at 72 h and a slight decrease to 2.86 log CFU/mL at 96 h (Fig. 5 A). However, when the degradation

products obtained in the presence mediator (ABTS) and tested on *V. parahaemolyticus,* a significant increase in the bacterium survival was obtained with the growth reaching 7.3 and 7.9 log CFU/mL at 24 h degradation products (Fig. 5B).

Fig. 6 (A - B) and Fig. S1 shows the cytotoxic effect of fluoranthene degradation metabolites on HT-22 cells. Without ABTS, cell viability reduction observed during the exposure to *Tl*FLU1L degradation product from 97.2 % at 72 h degradation product to 87.3 % at 96 h degradation product was obtained (Fig. 6 A) while that of *Tp*FLU12L was increasing with from 49.2 % cell viability at 24 h degradation product to 93.9 % at 96 h degradation product (Fig. 6 B). In the presence of a mediator, cell viability was increased on each degradation product per h with maximum cell viability of 100 % for both *Tl*FLU1L and *Tp*FLU12L, respectively.

Discussion

Laccase enzymes, particularly those from *Trichoderma*, *Fusarium*, and *Pleurotus* fungi, have shown potential in degrading PAHs, but their efficiency is limited (Behera et al., 2024; Cañas and Camarero, 2010). Immobilization of Laccase can enhance its storage and operational stabilities, but further improvements are needed (Fernández-Fernández et al., 2013; Xia et al., 2023). The use of high-potential Laccases, particularly those from non-mushroom-forming fungi, could address this issue (Senthivelan et al., 2016). Additionally, the Laccase-mediator system, which uses natural mediators like phenolic compounds, has been proposed as a more efficient approach for PAH degradation because it capitalizes on electron shuttles between the Laccase and the substrate in degrading the PAHs into an innocuous state (Bueno-Nieto et al., 2023; Cañas and Camarero, 2010). These advancements highlight the potential of Laccase enzymes in bioremediation, but further research is needed to optimize their performance for efficacy.

In this study, Laccase enzymes from *Tl*FLU1L and *Tp*FLU12L displayed promising results in degrading fluoranthene with a significant reduction in its residual concentration at varying Laccase concentrations within a 96-hour reaction period. This observation can be attributed to the supplementation of the reaction buffer with Tween 80, which has been documented to enhance fluoranthene solubility and promote its degradation, as well as to improve Laccase stability and protect it from oxidative damage (Arca-Ramos et al., 2012; Yang et al., 2021). Also, the addition of Tween 80 has been found to enhance the biodegradation and detoxification of anthraquinone dye, an anthracene derivative by Laccase from an electron beam irradiated endophytic fungus (Navada et al., 2018).

Fungi-derived Laccases are known to degrade PAHs efficiently but face cost barriers and labour intensiveness, but exploring mediators at lower concentrations and low enzyme concentrations could aid in reducing expenses for commercial viability. The substantial decrease in residual fluoranthene concentrations across various levels of the mediator (ABTS) underscores the pivotal role of the mediator in augmenting Laccase activity and enhancing the biodegradability of fluoranthene. This observation aligns with the findings of (Kumar et al., 2022), who demonstrated that Laccase derived from *Pleurotus ostreatus*, cultivated on cassava waste remarkably improved the degradation of 91% of PAHs, particularly the low molecular weight variants, and facilitated a 65% reduction in phenolic compounds concurrently. Similarly, (Daniel E Dodor, 2004) established the enhanced efficacy of Laccases sourced from *Trametes versicolor* in catalyzing the in vitro oxidation of anthracene and benzo[a]pyrene when co-oxidized with ABTS.

The kinetic degradation of fluoranthene by free Laccases from *Tl*FLU1L and *Tp*FLU12L reveals insights into their biocatalytic dynamics, with both Laccases demonstrating similar Vmax values and a great affinity for fluoranthene as a substrate with an implication of breaking down into different compound potentials. This observation is not a usual observation since fungal Laccases are known to have broad substrate affinities (Xia et al., 2023). Similarly, this same enzyme has been reported to be involved in the biotransformation and degradation of pyrene by *Trichoderma* sp. F03 (Al Farraj et al., 2020). Also, the observation of how *Tp*FLU12L displays a significantly higher affinity for the substrate (fluoranthene) at lower Km suggests that there are subtle structural differences impacting its active site (Liu et al., 2006). However, the presence of the mediator ABTS facilitates electron transfer between the enzyme and the substrate (fluoranthene), leading to efficient fluoranthene degradation (Saha and Mukhopadhyay, 2021). This interaction also leads to improved substrate binding, potentially due to conformational changes optimizing the active site for fluoranthene interaction (Zhou et al., 2021). The role of the mediator-enzyme-substrate interactions in fluoranthene degradation kinetics is further highlighted with *Tp*FLU12L, which demonstrates higher intrinsic affinity (Humel et al., 2023).

The GC-MS data analysis revealing transient products during fluoranthene degradation presents intriguing insights into the process. Apart from the parent compound, fluoranthene, five distinct transient products, namely of 9-oxo-fluorene-1-carboxylic acid, 9,10-phenanthrenedione, Benzene-1,2,3-tricarboxylic acid, Phthalic acid, and Benzoic acid emerged during the reaction period with Laccases *Tl*FLU-1L and *Tp*FLU-12L. These products indicate diverse pathways in fluoranthene degradation, with *Tp*FLU-12 generating a broader spectrum

of products and *Tl*FLU-1L favouring a simpler transformation which has been reported as part of fluoranthene degradation pathways (Weissenfels et al., 1990). Similarly, these same products have been reported in the biocatalytic pathways of fluoranthene, where Laccase was one of the major mechanisms (Hadibarata and Kristanti, 2015). Also, the observation of two distinct pathways based on C1-C2 and C2-C3 dioxygenation aligns with our past findings, such as the initial cleavage at C1-C2 leading to 9-oxo-fluorene-1-carboxylic acid followed by decarboxylation and ring cleavage has been reported in the metabolic biodegradation of fluoranthene by *Trichoderma lixii* and *Talaromycess pinophillus* (Egbewale et al., 2023) and formation of 9,10-phenanthrenedione *via* C2-C3 cleavage followed by hydrolysis and benzoic acid generation have been observed in *Celeribacter indicus* P73^{T} (Cao et al., 2015). Notably, the non-appearance of 9H-fluoren-9-one in our GC-MS analysis could be attributed to factors like rapid conversion to subsequent metabolites or limitations of the detection method.

The time-dependent effects of fluoranthene degradation products from *Tl*FLU1L and *Tp*FLU12L, respectively on ecotoxicity and cytotoxicity give an insight into their potential threat to human health and ecosystems. The obtained data on reduction in *V. parahaemolyticus* survival (log CFU/mL) and cell viability mainly in degradation products from *Tl*FLU1L without a mediator (ABTS) revealed that metabolites induce acute toxicity despite a significant reduction in parent compound concentration. This similar observation aligns with the report by (Diniz et al., 2015; Eom et al., 2007), where they demonstrated how the formation of metabolites during the degradation of contaminants leads to increased toxicity. Also, the report of (Kim et al., 2020) further strengthened the reason for the slight reduction in *V. parahaemolyticus* survival (log CFU/mL) and the cell viability. Conversely, the notable increase in the *V. parahaemolyticus* survival *Tl*flu-1 in the presence of ABTS, *V. parahaemolyticus* survival and cell viability of the HT-22 cell lines of degradation products from *Tp*FLU12L both without ABTS and in the presence of ABTS suggests that the fluoranthene degradation products intermediates do not possess any environmental and health risks due to the presence of benzene derivatives (Benzene-1,2,3-tricarboxylic acid and Phthalic acid) as the end products. (Amorim et al., 2013; Zhou et al., 2011) both similarly highlight that the degradation products of various pollutants, including PAHs and benzene derivatives, do not pose significant environmental or health risks. Also, studies by (Bankole et al., 2022; Nembudani and Chirwa, 2019; Sheng and Lyu, 2023; Yao et al., 2023) confirm that fluoranthene degradation produces harmless benzene derivatives resulting in the elimination of environmental/health concerns. Similarly, the dead-end metabolites of PAHs, after degradation

by *Mycobacterium* sp. strain SNP11, showed a significant reduction in their toxic potential (Pagnout et al., 2006).

Conclusion

This study underscores the promising potential of *Tl*FLU1L and *Tp*FLU12L particularly in conjunction with mediator (ABTS), for environmentally friendly and efficient bioremediation of fluoranthene-contaminated environments. Both enzymes exhibited efficient fluoranthene reduction with higher concentrations leading to further degradation and complete removal achievable at optimized levels. The kinetic degradation analysis revealed the improved binding and catalytic efficiency of Laccases in the presence of ABTS, highlighting its crucial role in facilitating fluoranthene biotransformation. Also, the GC-MS analysis provided insights into the degradation pathways by identifying two distinct routes employed by the enzymes: C1-C2 dioxygenation and C2-C3 dioxygenation. Interestingly, while some intermediate products exhibited negligible toxicity towards *Vibrio parahaemolyticus* and human HT-22 cells, others displayed slight acute toxicity. However, the complete detoxification achieved in the presence of ABTS suggests the formation of nontoxic end products such as benzene derivatives.

Acknowledgements:

S.O.E. Thanks University of KwaZulu Natal, Durban, South Africa for Ph.D. scholarship.

Funding: National Research Foundation, South Africa (Grant No: 94036 and 92803).

Data Availability Statement: Data are contained within the article or Supplementary Material.

Conflicts of Interest: The authors declare no conflicts of interest.

References

Adamian, Y., Lonappan, L., Alokpa, K., Agathos, S.N., Cabana, H., 2021. Recent developments in the immobilization of laccase on carbonaceous supports for environmental applications-a critical review. Front Bioeng Biotechnol 9, 778239.

Agrawal, P.K., Shrivastava, R., Verma, J., 2019. Bioremediation approaches for degradation and detoxification of polycyclic aromatic hydrocarbons, In: Ram Naresh Bharagava, P.C. (Ed.), Emerging and eco-friendly approaches for waste management. Springer, pp. 99-119.

Ahmed, R.Z., Ahmed, N., 2014. Effect of yeast extract on fluoranthene degradation and aromatic ring dioxygenase expressing bacterial community structure of a fluoranthene degrading bacterial consortium. Int Biodeteriorat Biodegrad 88, 56-61.

Al Farraj, D.A., Hadibarata, T., Elshikh, M.S., Al Khulaifi, M.M., Kristanti, R.A., 2020. Biotransformation and degradation pathway of pyrene by filamentous soil fungus *Trichoderma* sp. F03. Water Air Soil Pollut 231, 1-9.

Amorim, C.L., Carvalho, M.F., Afonso, C.M.M., Castro, P.M.L., 2013. Biodegradation of fluoroanilines by the wild strain *Labrys portucalensis*. Int Biodeteriorat Biodegrad 80, 10-15.

Arca-Ramos, A., Eibes, G., Moreira, M.T., Feijoo, G., Lema, J.M., 2012. Surfactant-assisted two phase partitioning bioreactors for laccase-catalyzed degradation of anthracene. Process Biochem 47, 1115-1121.

Bankole, P.O., Omoni, V.T., Mulla, S.I., Adebajo, S.O., Adekunle, A.A., 2022. Co-biomass degradation of fluoranthene by marine-derived fungi; *Aspergillus aculeatus* and *Mucor irregularis*: Comprehensive process optimization, enzyme induction and metabolic analyses. Arab J Chem 15, 104036.

Behera, A.D., Chittoria, N., Kumari, S., Chatterjee, S., Das, S., 2024. Homology modeling of laccase enzyme of filamentous fungus *Trichoderma* sp. CNSC-2 and its role in pyrene degradation. Geomicrobiol J 41, 404-416.

Bhardwaj, P., Kaur, N., Selvaraj, M., Ghramh, H.A., Al-Shehri, B.M., Singh, G., Arya, S.K., Bhatt, K., Ghotekar, S., Mani, R., 2022. Laccase-assisted degradation of emerging recalcitrant compounds–a review. Bioresour Technol 364, 128031.

Bueno-Nieto, C., Cortés-Antiquera, R., Espina, G., Atalah, J., Villanueva, J., Aliaga, C., Zuñiga, G.E., Blamey, J.M., 2023. Biochemical and spectroscopic characterization of a recombinant laccase from thermoalkaliphilic *Bacillus* sp. FNT with potential for degradation of polycyclic aromatic hydrocarbons (PAHs). Catalysts 13, 763.

Cambria, M.T., Minniti, Z., Librando, V., Cambria, A., 2008. Degradation of polycyclic aromatic hydrocarbons by rigidoporus lignosus and its laccase in the presence of redox mediators. Appl Biochem Biotechnol 149, 1-8.

Cañas, A.I., Camarero, S., 2010. Laccases and their natural mediators: biotechnological tools for sustainable eco-friendly processes. Biotechnol Adv 28, 694-705.

Cao, J., Lai, Q., Yuan, J., Shao, Z., 2015. Genomic and metabolic analysis of fluoranthene degradation pathway in *Celeribacter indicus* P73T. Sci Rep 5, 7741.

Daniel E Dodor, H.-M.H., Stephen I.N Ekunwe, 2004. Oxidation of anthracene and benzo [a] pyrene by laccases from *Trametes versicolor*. Enzyme Microb Technol 35, 210-217.

de Freitas, E.N., Bubna, G.A., Brugnari, T., Kato, C.G., Nolli, M., Rauen, T.G., Peralta Muniz Moreira, R.d.F., Peralta, R.A., Bracht, A., de Souza, C.G.M., Peralta, R.M., 2017. Removal of bisphenol A by laccases from *Pleurotus ostreatus* and *Pleurotus pulmonarius* and evaluation of ecotoxicity of degradation products. Chem Eng J 330, 1361-1369.

Diniz, M.S., Salgado, R., Pereira, V.J., Carvalho, G., Oehmen, A., Reis, M.A.M., Noronha, J.P., 2015. Ecotoxicity of ketoprofen, diclofenac, atenolol and their photolysis byproducts in zebrafish (*Danio rerio*). Sci Total Environ 505, 282-289.

Egbewale, S.O., Kumar, A., Mokoena, M.P., Olaniran, A.O., 2023. Metabolic biodegradation pathway of fluoranthene by indigenous *Trichoderma lixii* and *Talaromyces pinophilus* spp. Catalysts 13.

Egbewale, S.O., Kumar, A., Mokoena, M.P., Olaniran, A.O., 2024a. Purification, characterization and three-dimensional structure prediction of multicopper oxidase Laccases from *Trichoderma lixii* FLU1 and *Talaromyces pinophilus* FLU12. Sci Rep 14, 13371.

Egbewale, S.O., Kumar, A., Olasehinde, T.A., Mokoena, M.P., Olaniran, A.O., 2024b. Anthracene detoxification by Laccases from indigenous fungal strains *Trichoderma lixii* FLU1 and *Talaromyces pinophilus* FLU12. Biodegradation 35, 769-787.

Eom, I.C., Rast, C., Veber, A.M., Vasseur, P., 2007. Ecotoxicity of a polycyclic aromatic hydrocarbon (PAH)-contaminated soil. Ecotoxicol Environ Saf 67, 190-205.

Fernández-Fernández, M., Sanromán, M.Á., Moldes, D., 2013. Recent developments and applications of immobilized laccase. Biotechnol Adv 31, 1808-1825.

García-Morales, R., García-García, A., Orona-Navar, C., Osma, J.F., Nigam, K.D.P., Ornelas-Soto, N., 2018. Biotransformation of emerging pollutants in groundwater by laccase from *P. sanguineus* CS43 immobilized onto titania nanoparticles. J Environ Chem Eng 6, 710-717.

Hadibarata, T., Kristanti, R.A., 2015. Biotransformation studies on fluoranthene, a four-ring polycylic aromatic hydrocarbon, by white-rot fungus *Armillaria* sp. F022. Agric Agric Sci Procedia 3, 45-50.

Humel, S., Führer, B., Svetitsch, M., Mayer, P., Loibner, A.P., 2023. Targeting sorbed PAHs in historically contaminated soil–Can laccase mediator systems or Fenton's reagent remove inaccessible PAHs? J Hazard Mater 443, 130286.

Kim, Y.-C., Lee, S.-R., Jeon, H.-J., Kim, K., Kim, M.-J., Choi, S.-D., Lee, S.-E., 2020. Acute toxicities of fluorene, fluorene-1-carboxylic acid, and fluorene-9-carboxylic acid on zebrafish embryos (*Danio rerio*): Molecular mechanisms of developmental toxicities of fluorene-1-carboxylic acid. Chemosphere 260, 127622.

Kumar, M., Vivekanand, V., Pareek, N., 2021. Enzymatic degradation of lignocellulosic waste: bioremediation and industrial implementation, Bioremediation for Environmental Sustainability. Elsevier, pp. 163-191.

Kumar, V.V., Venkataraman, S., Kumar, P.S., George, J., Rajendran, D.S., Shaji, A., Lawrence, N., Saikia, K., Rathankumar, A.K., 2022. Laccase production by Pleurotus ostreatus using cassava waste and its application in remediation of phenolic and polycyclic aromatic hydrocarbon-contaminated lignocellulosic biorefinery wastewater. Environ Pollut 309, 119729.

Liu, Z.-h., Shao, M., Cai, R.-x., Shen, P., 2006. Online kinetic studies on intermediates of laccase-catalyzed reaction in reversed micelle. J Colloid Interface Sci 294, 122-128.

Mesnil, M., Defamie, N., Naus, C., Sarrouilhe, D., 2020. Brain disorders and chemical pollutants: A gap junction link? Biomolecules 11, 51.

Mojiri, A., Zhou, J.L., Ohashi, A., Ozaki, N., Kindaichi, T., 2019. Comprehensive review of polycyclic aromatic hydrocarbons in water sources, their effects and treatments. Sci Total Environ 696, 133971.

Navada, K.K., Sanjeev, G., Kulal, A., 2018. Enhanced biodegradation and kinetics of anthraquinone dye by laccase from an electron beam irradiated endophytic fungus. Int Biodeteriorat Biodegrad 132, 241-250.

Nembudani, T.B.L., Chirwa, E.M.N., 2019. Biodegradation of fluoranthene in an aerated biofilm reactor with biosurfactant producing CSTR staged in series. Chem Eng Trans 76, 1273-1278.

Pagnout, C., Rast, C., Veber, A.-M., Poupin, P., Férard, J.-F., 2006. Ecotoxicological assessment of PAHs and their dead-end metabolites after degradation by *Mycobacterium* sp. strain SNP11. Ecotoxicol Environ Saf 65, 151-158.

436 Robin, S.L., Marchand, C., 2022. Polycyclic aromatic hydrocarbons (PAHs) in mangrove
437 ecosystems: A review. Environ Pollut 311, 119959.
438 Rotini, A., Gallo, A., Parlapiano, I., Berducci, M.T., Boni, R., Tosti, E., Prato, E., Maggi, C.,
439 Cicero, A.M., Migliore, L., Manfra, L., 2018. Insights into the CuO nanoparticle ecotoxicity
440 with suitable marine model species. Ecotoxicol Environ Saf 147, 852-860.
441 Saha, R., Mukhopadhyay, M., 2021. Electrochemical analysis of catechol polymerization in
442 presence of *Trametes versicolor* laccase and the mediator ABTS. Enzyme Microb Technol 152,
443 109934.
444 Salas, F.d., Camarero, S., 2021. Fungal laccases as biocatalysts for wide range applications.
445 Ency Mycol 2, 233-246.
446 Sangwan, S., Dukare, A., 2018. Microbe-mediated bioremediation: an eco-friendly sustainable
447 approach for environmental clean-up, In: Pardeep Singh, A.K., Anwesha Borthakur (Ed.),
448 Advances in soil microbiology: Recent trends and future prospects: Volume 1: Soil-microbe
449 interaction. Springer, pp. 145-163.
450 Senthivelan, T., Kanagaraj, J., Panda, R.C., 2016. Recent trends in fungal laccase for various
451 industrial applications: an eco-friendly approach-a review. Biotechnol Bioprocess Eng 21, 19-
452 38.
453 Sheng, X., Lyu, S., 2023. Insights into enhanced removal of fluoranthene by sulfidated
454 nanoscale zero-valent iron: In aqueous solution and soil slurry. Chemosphere 312, 137172.
455 Teerapatsakul, C., Pothiratana, C., Chitradon, L., Thachepan, S., 2016. Biodegradation of
456 polycyclic aromatic hydrocarbons by a thermotolerant white rot fungus *Trametes polyzona*
457 RYNF13. J Gen Appl Microbiol 62, 303-312.
458 Teh, Z.C., Hadibarata, T., 2014. Enhanced degradation of pyrene and metabolite identification
459 by *Pleurotus eryngii* F032. Water Air Soil Pollut 225, 1-8.
460 Weissenfels, W.D., Beyer, M., Klein, J., 1990. Degradation of phenanthrene, fluorene and
461 fluoranthene by pure bacterial cultures. Appl Microbiol Biotechnol 32, 479-484.
462 Xia, Y., Xia, L., Lin, X., 2023. Laccase-based self-amplifying catalytic system enables efficient
463 antibiotic degradation for sustainable environmental remediation. Adv Sci 10, 2300210.
464 Yang, Z., Mao, X., Cui, J., Wang, Y., Zhang, Y., 2021. Enhancement and analysis of
465 anthracene degradation by Tween 80 in LMS-HOBt. Sci Rep 11, 13121.
466 Yao, Z., He, X., Yin, M., Han, H., Zhang, Q., 2023. Mechanochemical remediation of
467 fluoranthene contaminated soil and biotoxicity evaluation. Environ Technol 44, 2104-2112.
468 Zelinkova, Z., Wenzl, T., 2015. The occurrence of 16 EPA PAHs in food – A review. Polycycl
469 Aromat Compd 35, 248-284.

Zhou, F., Mu, X., Nie, Y., Xu, Y., 2021. Enhanced catalytic efficiency and coenzyme affinity of leucine dehydrogenase by comprehensive screening strategy for L-tert-leucine synthesis. Appl Microbiol Biotechnol 105, 3625-3634.

Zhou, Y.-Y., Chen, D.-Z., Zhu, R.-Y., Chen, J.-M., 2011. Substrate interactions during the biodegradation of BTEX and THF mixtures by *Pseudomonas oleovorans* DT4. Bioresour Technol 102, 6644-6649.

Zungu, N.S., Egbewale, S.O., Olaniran, A.O., Pérez-Fernández, M., Magadlela, A., 2020. Soil nutrition, microbial composition and associated soil enzyme activities in KwaZulu-Natal grasslands and savannah ecosystems soils. Appl Soil Ecol 155, 103663-103663.

Figure Legends:

Figure 1. The percentage of residual fluoranthene concentration after the degradation by different concentrations of purified Laccase from *Tl*FLU1L and *Tp*FLU12L at 96 h.

Figure 2. The influence of mediator (ABTS) concentration on the degradation of fluoranthene by purified *Tl*FLU1L (A) and *Tp*FLU12L (B) at 96 h.

Figure 3. The degradation kinetics of fluoranthene mediated by *Tl*FLU1L and *Tp*FLU12L in the absence and presence of a mediator (ABTS).

Figure 4. The proposed fluoranthene degradation pathway by *Tl*FLU1L and *Tp*FLU12L.

Figure 5. Time-course changes in toxicity of fluoranthene degradation products from *Tl*FLU1L (A) and *Tp*FLU12L (B) on *V. parahaemolyticus* survival (log CFU/mL).

Figure 6. Time-course changes in the cytotoxicity effect of fluoranthene degradation products from *Tl*FLU1L (A) and *Tp*FLU12L (B) on HT-22 cells.

Tables:

Table 1. The degradation kinetics of fluoranthene mediated by *Tl*FLU1L and *Tp*FLU12L in the absence and presence of a mediator (ABTS)

	v_{max} (mg/L/h)		K_m (mg/L)		R^2	
	*Tl*FLU1	*Tp*FLU12	*Tl*FLU1	*Tp*FLU12	*Tl*FLU1	*Tp*FLU12
Fluoranthene	1.35±0.02	1.29±0.15	119.2±0.02	170.8±0.15	0.999	0.996
Fluoranthene + ABTS	7.73±0.23	7.97±0.28	54.8±0.23	26.6±0.28	0.993	0.996

Value in each column is the mean ± standard error

531 Table 2: GC-MS profile of the metabolites accumulated during PAHs degradation by purified from *Trichoderma lixii* FLU1 and *Talaromyces*
532 *pinophilus* FLU12.

PAH Compounds	Metabolites	Retention time(min)	Major m/z of fragment ions (% relative abundance)	Tentative metabolite identification	Laccase source	
					*Tl*FLU1L	*Tp*FLU12L
Fluoranthene	1	28.2	88 (3, M^+), 100 (5), 101 (9), 174 (2), 175 (2), 199 (2), 200 (15), 201 (12), 202 (100), 203 (17)	Fluoranthene		✓
	2	14.8	75 (6, M^+), 76 (5), 126 (5), 150 (15), 151 (22), 152 (37), 153 (5),180 (100), 181 (14), 224 (18)	9-oxo-9*H*-fluorene-1-carboxylic acid	✓	×
	3	10.8	39 (2, M^+), 50 (3), 63 (8), 76 (17), 87(20), 98(2) 126 (7), 152 (38), 180 (100), 208 (22)	9,10-phenanthrenedione	×	✓
	3	12.7	18 (15, M^+), 44 (11), 50 (15), 64 (13), 74 (19), 75 (23), 76 (31),92 (25), 104 (44), 148 (100),	Benzene-1,2,3-tricarboxylic acid	×	✓
	4	17.5	17 (14, M^+), 18 (63), 37 (11), 38 (19), 50 (44), 74 (17), 75 (10), 76 (86), 104 (100), 148 (37)	Phthalic acid	✓	×
	5	9.3	50(19, M^+), 51 (3), 74 (8), 76 (6), 77 (66), 78(6), 105(100), 106 (7),122 (83),123 (7)	Benzoic acid	×	✓

533
534

Figure 1

Click here to access/download;Figure;Fig 1.jpg

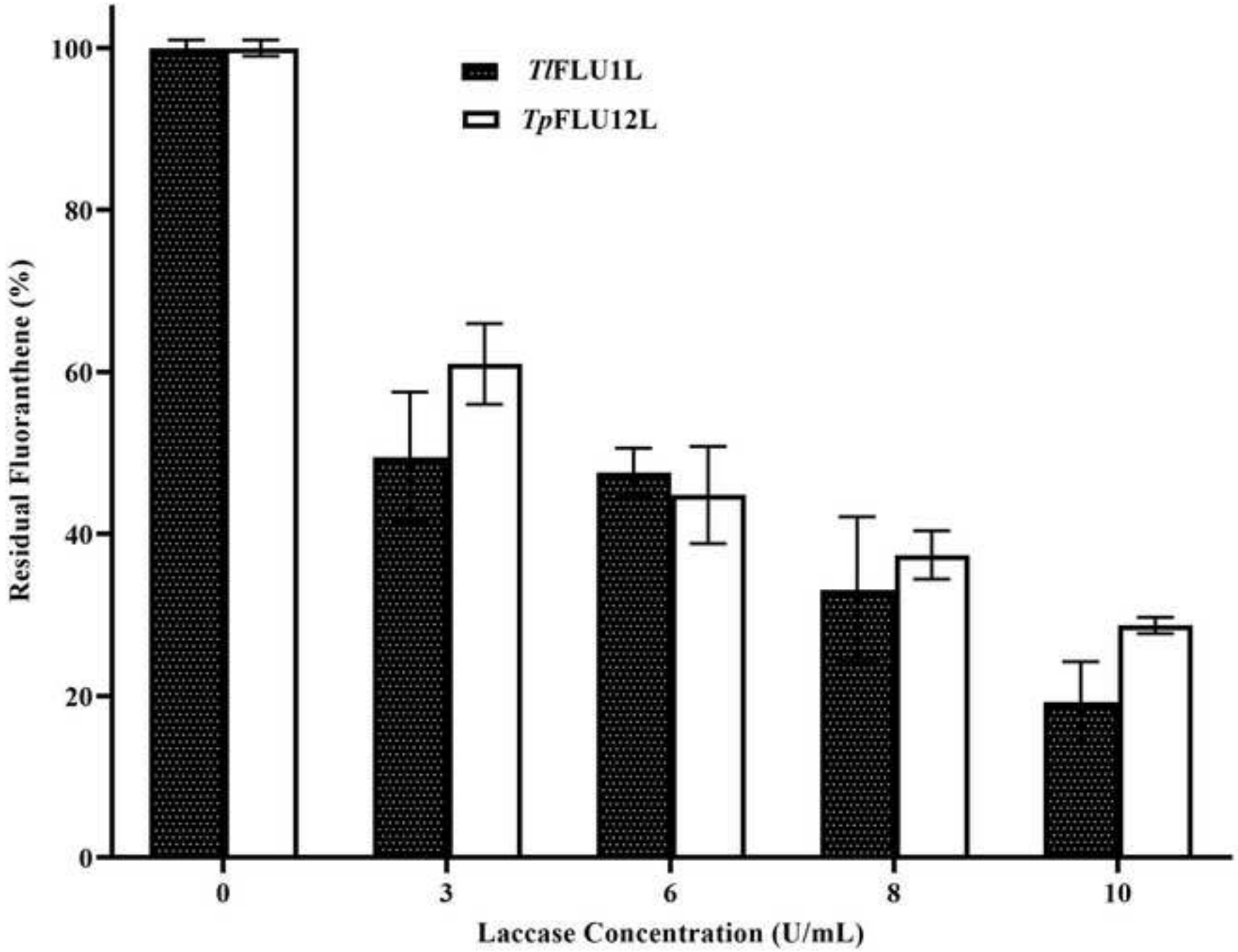

Figure 2A

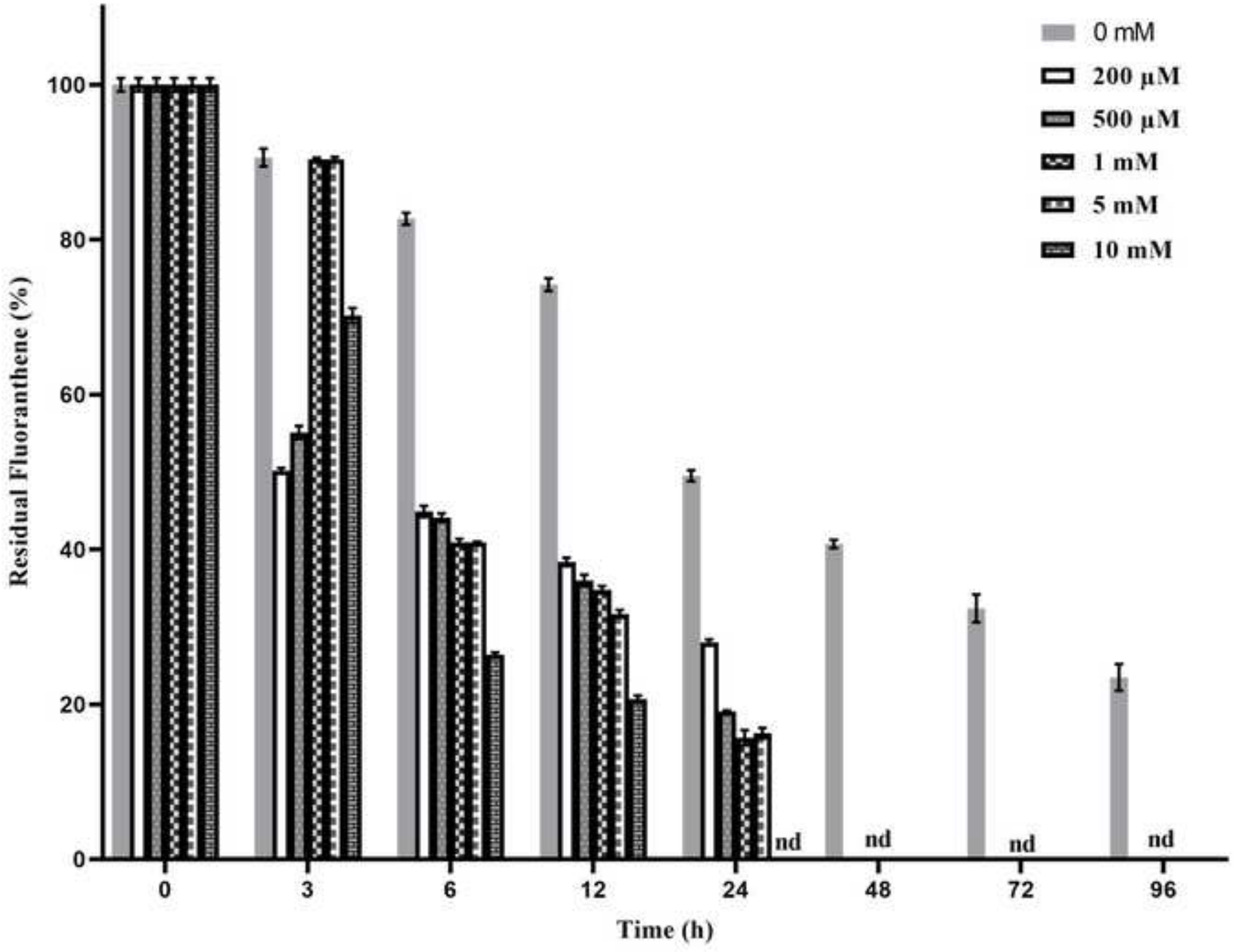

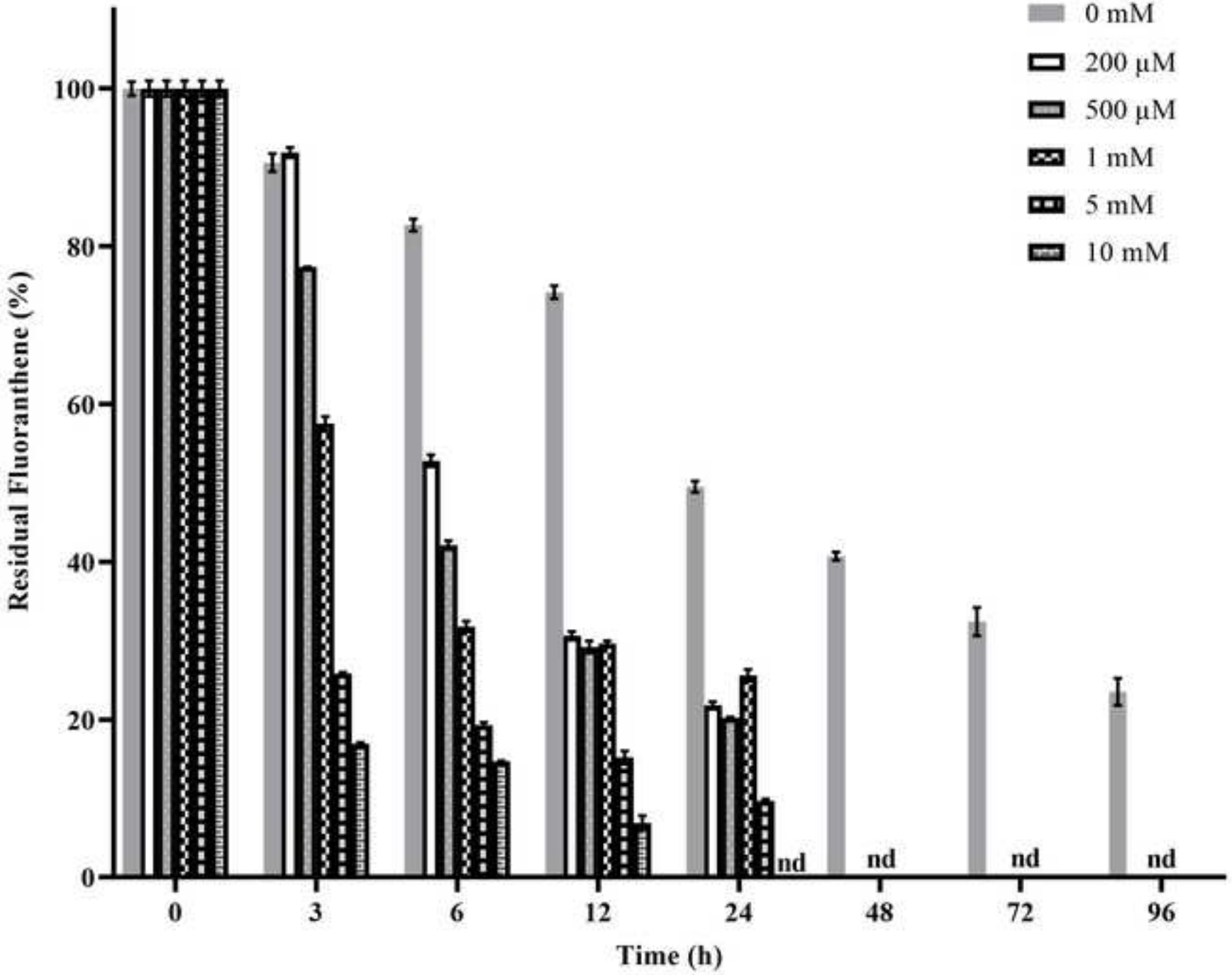

Figure 3

Click here to access/download;Figure;Fig 3.jpg

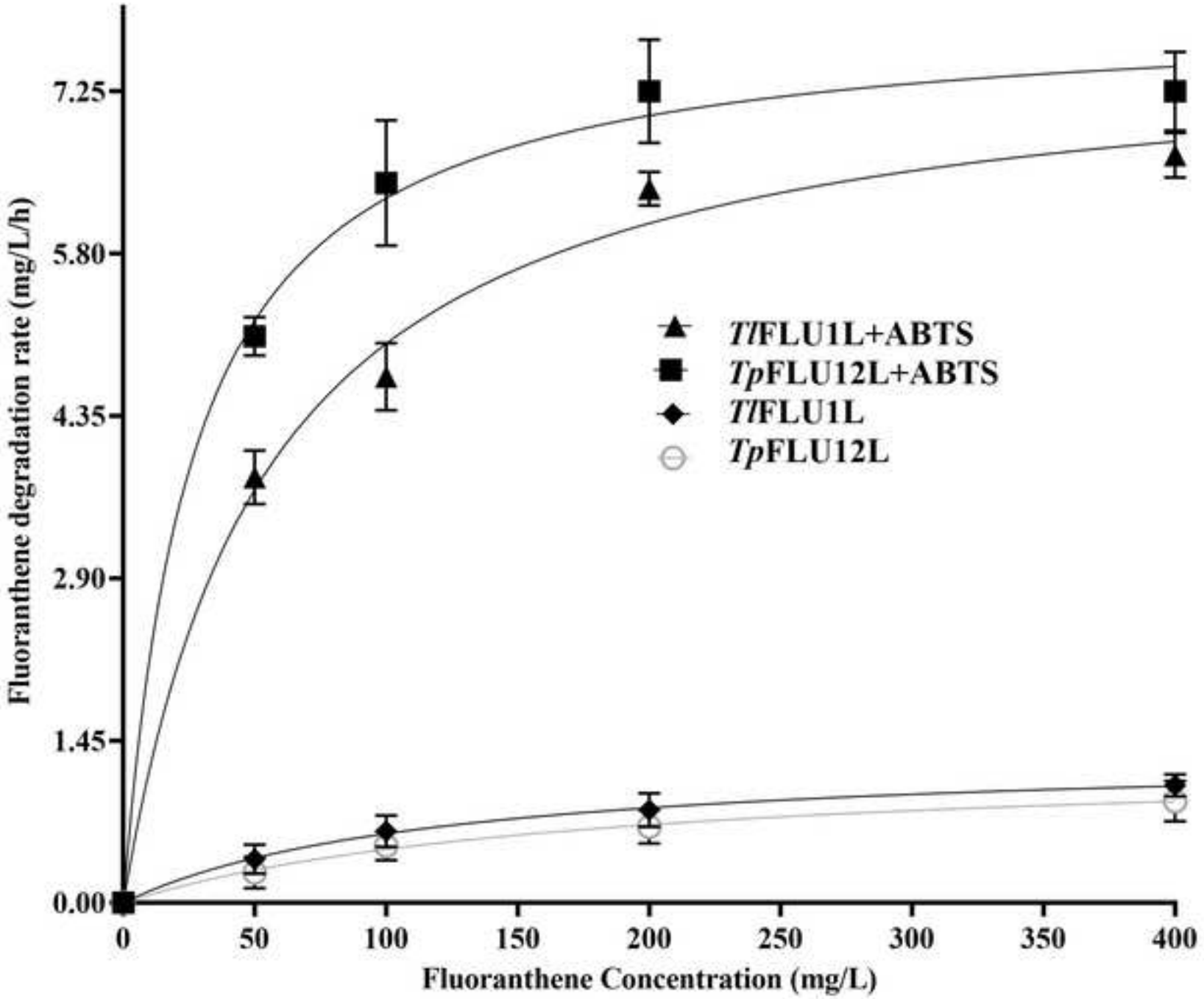

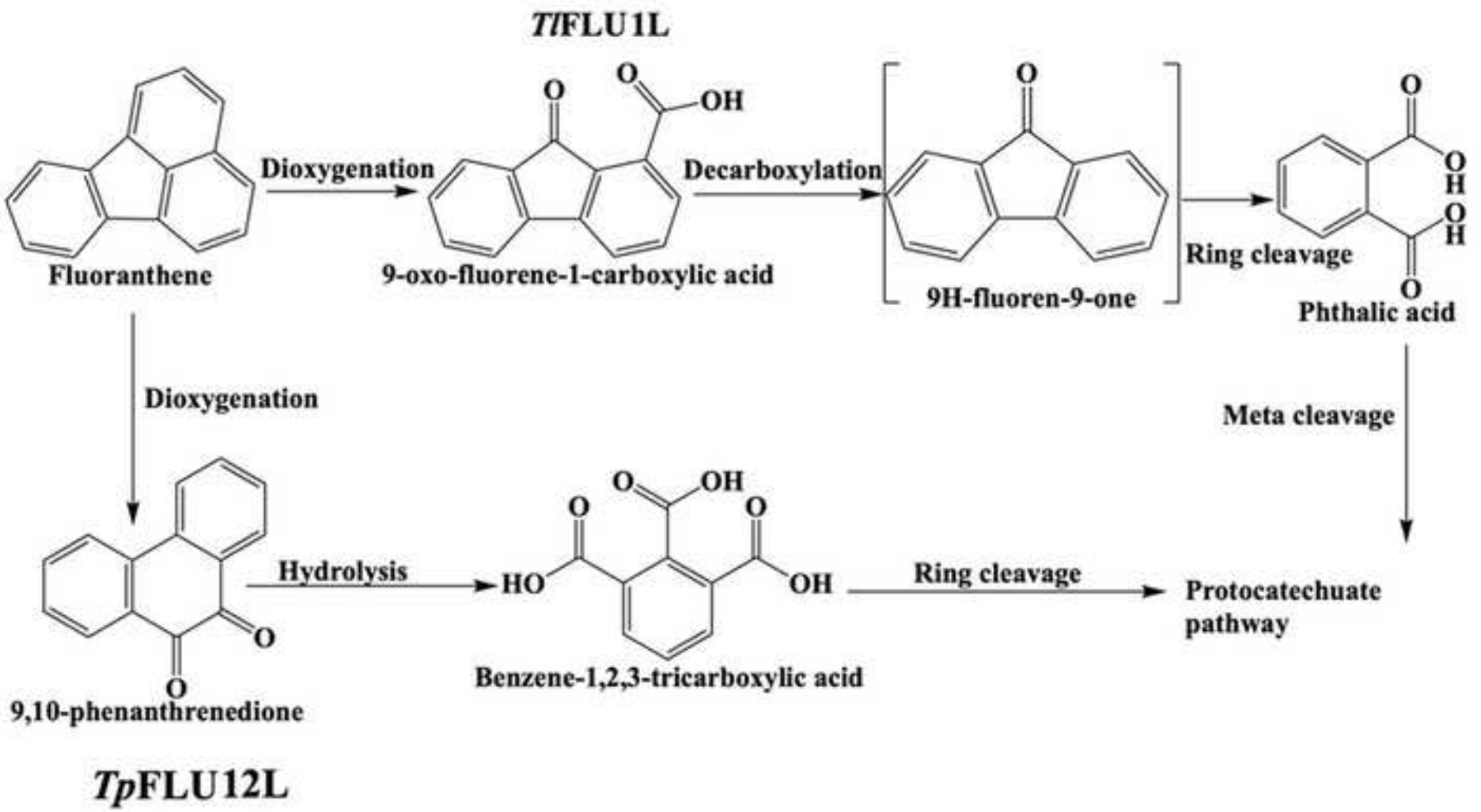

Figure 5A

Click here to access/download;Figure;Fig 5A.jpg

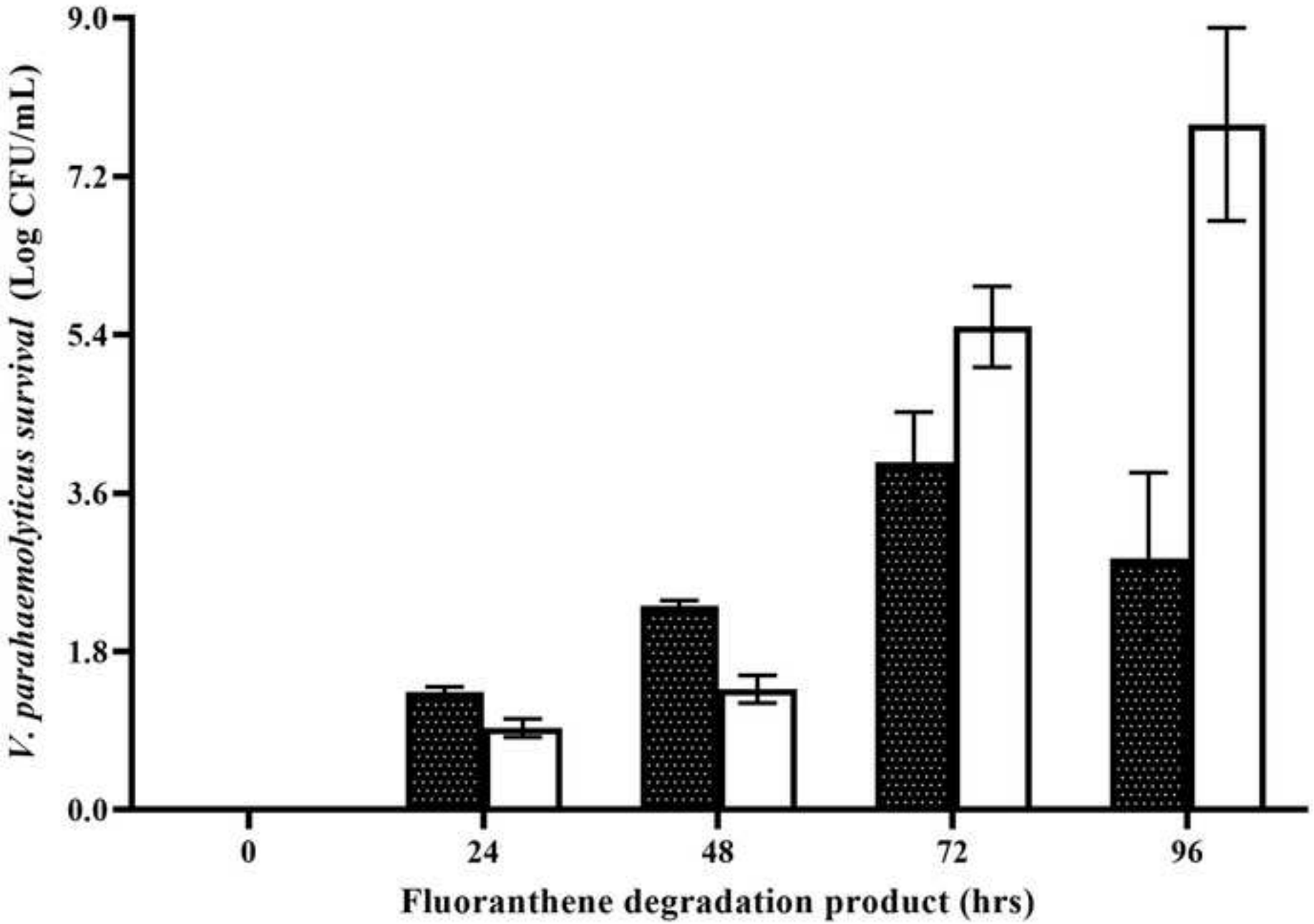

Figure 5B

Click here to access/download;Figure;Fig 5B.jpg

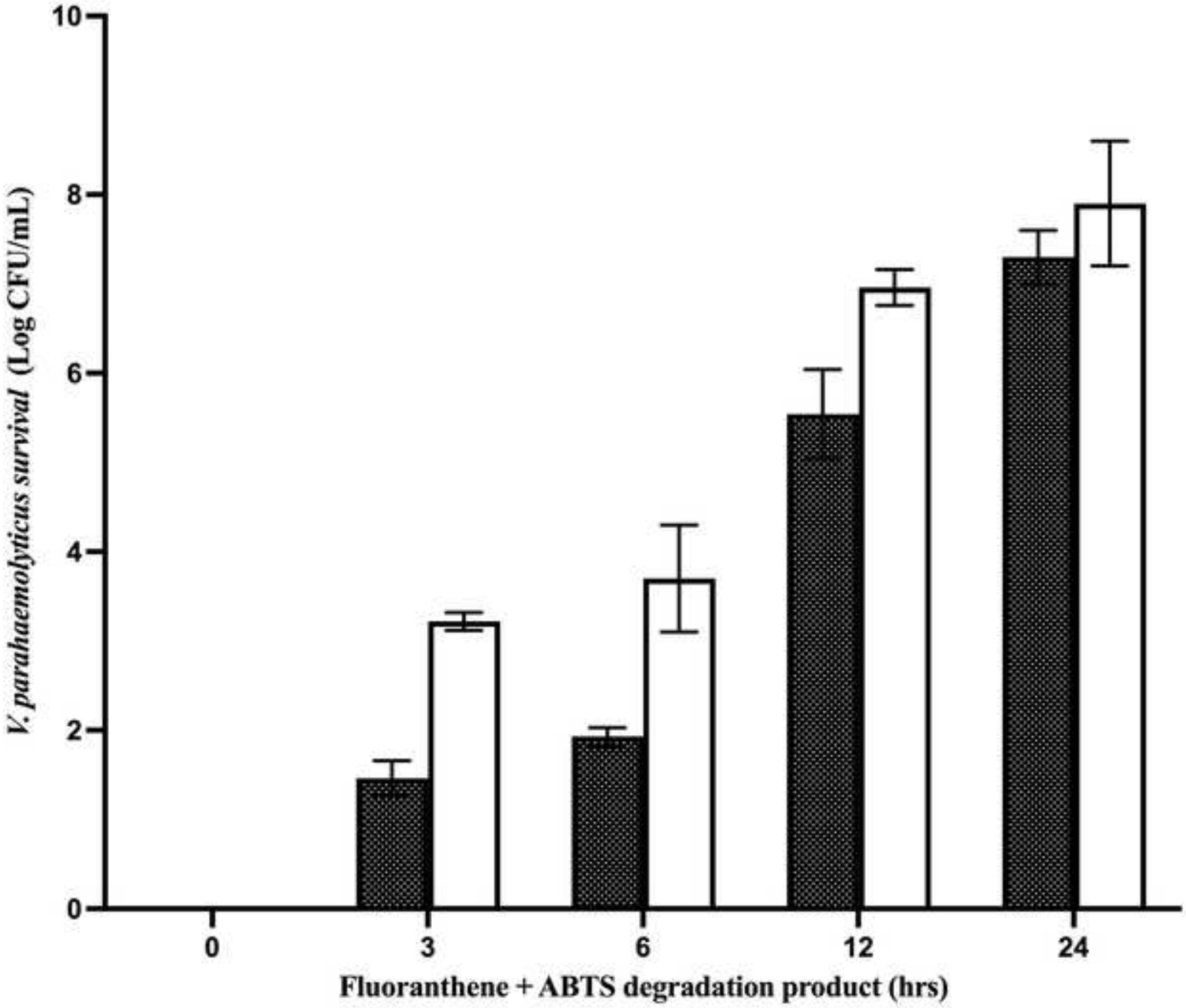

Figure 6A

Click here to access/download;Figure;Fig 6A.jpg

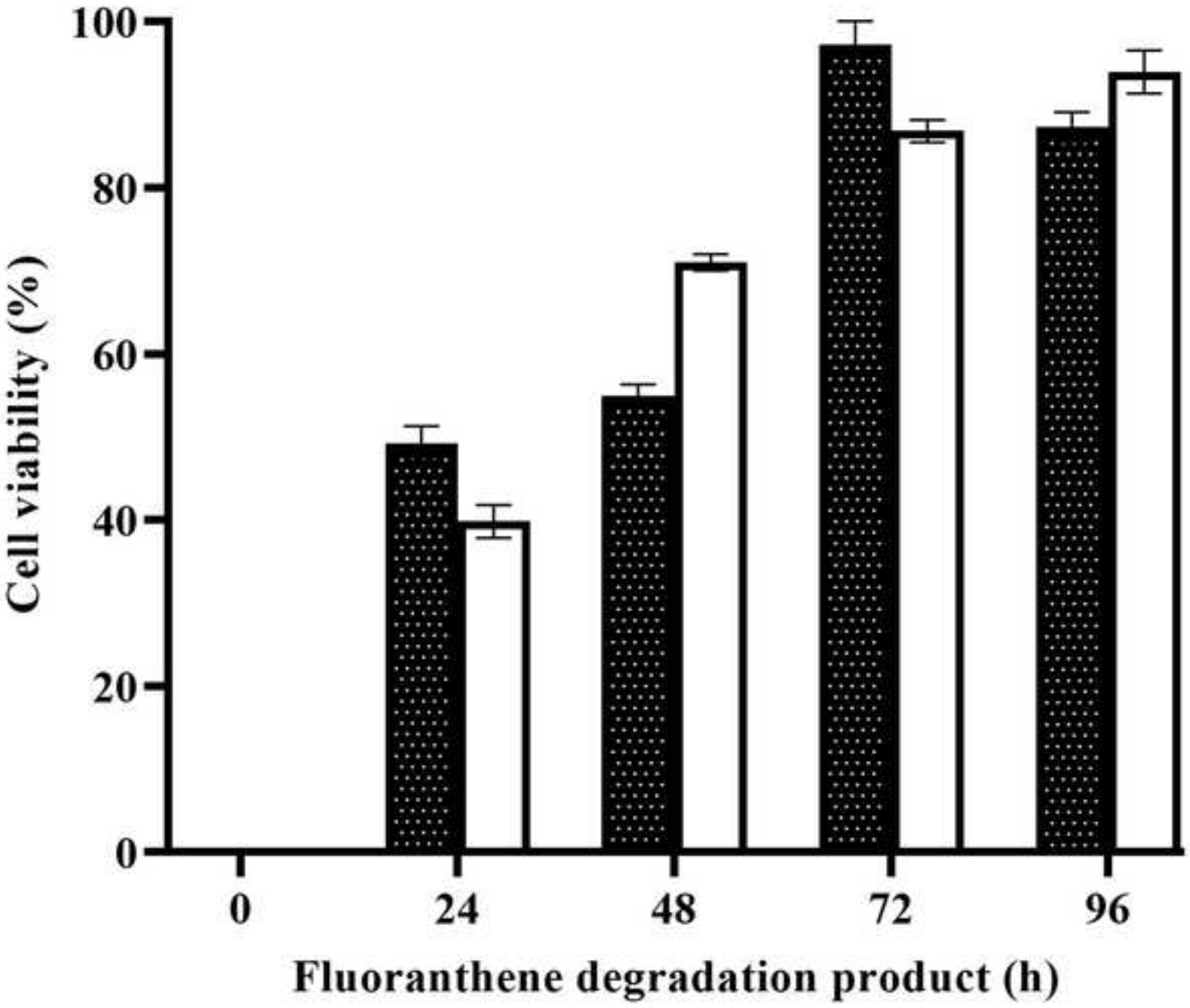

Figure 6B

Click here to access/download;Figure;Fig 6B.jpg

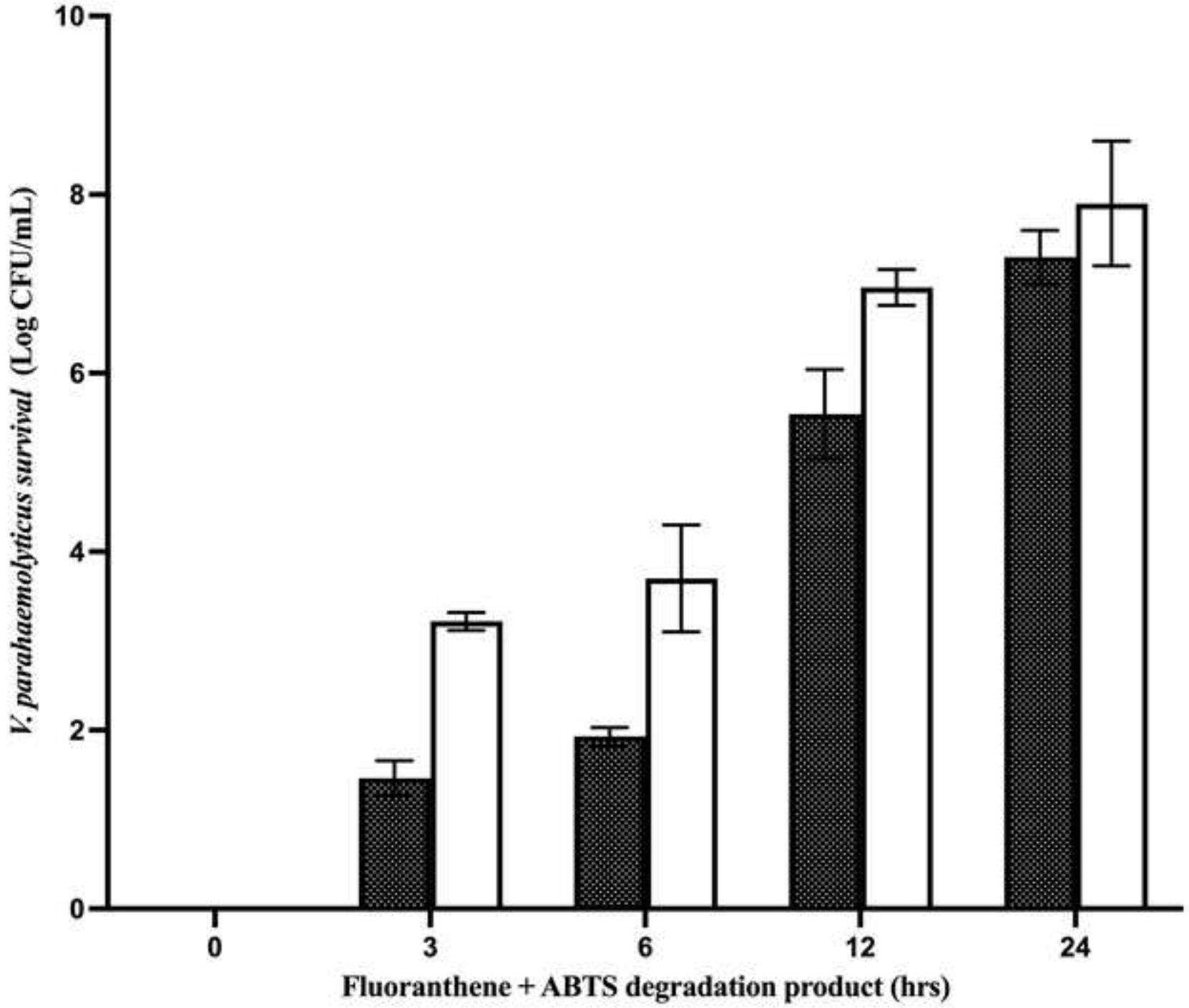

Supplementary Materials

Journal: International Biodeterioration & Biodegradation

Synergistic Biotransformation of Fluoranthene by Laccases from Indigenous Fungal strains *Trichoderma lixii* FLU1 and *Talaromyces pinophilus* FLU12 and ABTS Mediator

Samson O. Egbewale[1], Ajit Kumar[1], Tosin A. Olasehinde[1], Mduduzi P. Mokoena[2] and Ademola O. Olaniran[1*]

[1]Discipline of Microbiology, University of KwaZulu-Natal (Westville Campus), Durban 4000, South Africa

[2]Department of Pathology, School of Medicine, University of Limpopo, Private Bag X1106, Sovenga-0727, South Africa.

*Correspondence: olanirana@ukzn.ac.za; Tel.: +27-31-260-7400

Table S1. The influence of purified Laccase concentration on *in vitro* degradation of fluoranthene

U/mL	*Tl*FLU1	*Tp*FLU12
0	98.4±1.61	98.4±1.61
3	49.5±8.68	61.0±5.66
6	47.6±3.19	44.8±6.09
8	33.1±9.02	37.4±3.60
10	19.2±5.95	28.7±1.25

Table S2. The influence of mediator (ABTS) concentration on *invitro* oxidation of fluoranthene by purified Laccase from *Tl*FLU1

Time (h)	0 mM	200 µM	500 µM	1 mM	5 mM	10 mM
0	98.4±1.61	98.4±1.61	98.4±1.61	98.4±1.61	98.4±1.61	98.4±1.61
3	90.6±1.15	50.2±0.33	55.1±0.84	90.4±0.2	90.4±0.28	70.2±0.98
6	82.7±0.76	44.9±0.72	44.1±0.56	40.9±0.47	40.9±0.12	26.4±0.30
12	74.2±0.82	38.4±0.54	36.0±0.74	34.8±0.49	31.7±0.53	20.7±0.46
24	49.5±0.72	28±0.39	19.1±0.1	15.7±0.99	16.3±0.68	nd
48	40.7±0.53	nd	nd	nd	nd	nd
72	32.4±1.79	nd	nd	nd	nd	nd
96	23.5±1.72	nd	nd	nd	nd	nd

Table S3. The influence of mediator (ABTS) concentration on *invitro* oxidation of fluoranthene by purified Laccase from *Tp*FLU12

Time (h)	0 mM	200 µM	500 µM	1 mM	5 mM	10 mM
0	98.4±1.61	98.4±1.61	98.4±1.61	98.4±1.61	98.4±1.61	98.4±1.61
3	94.2±0.78	91.9±0.64	77.4±0.02	57.5±0.92	25.8±0.17	16.9±0.2
6	88.3±0.99	52.8±0.75	42.1±0.55	31.8±0.69	19.3±0.34	14.7±0.05
12	82.9±0.13	30.6±0.54	29.2±0.77	29.6±0.36	15.2±0.82	6.9±0.9
24	61.0±0.95	21.8±0.46	20.2±0.1	25.6±0.73	9.7±0.23	nd
48	54.8±0.74	nd	nd	nd	nd	nd
72	49.7±0.84	nd	nd	nd	nd	nd
96	43.7±0.78	nd	nd	nd	nd	nd

Table S4. The degradation kinetics of fluoranthene mediated by purified Laccase from *Tl*FLU1 and *Tp*FLU12 in the presence and absence of mediator (ABTS)

Concentration (mg/L)	*Tl*FLU1+ABTS	*Tp*FLU12+ABTS	*Tl*FLU1	*Tp*FLU12
50	3.8±0.24	5.06±0.17	0.39±0.13	0.27±0.14
100	4.7±0.3	6.43±0.56	0.64±0.14	0.51±0.13
200	6.38±0.15	7.25±0.46	0.83±0.15	0.68±0.15
400	6.68±0.2	7.25±0.35	1.05±0.1	0.91±0.18

CHAPTER EIGTH

Purification, characterization and three-dimensional structure prediction of multicopper oxidase Laccases from *Trichoderma lixii* FLU1 and *Talaromyces pinophilus* FLU12

This chapter has been published in current format in the journal: *Scientific Reports, 4(1). https://doi.org/10.1038/s41598-024-63959-z*

The published paper is presented in the following pages.

scientific reports

Check for updates

OPEN

Purification, characterization and three-dimensional structure prediction of multicopper oxidase Laccases from *Trichoderma lixii* FLU1 and *Talaromyces pinophilus* FLU12

Samson O. Egbewale[1], Ajit Kumar[1], Mduduzi P. Mokoena[1,2] & Ademola O. Olaniran[1]✉

Broad-spectrum biocatalysts enzymes, Laccases, have been implicated in the complete degradation of harmful pollutants into less-toxic compounds. In this study, two extracellularly produced Laccases were purified to homogeneity from two different Ascomycetes spp. *Trichoderma lixii* FLU1 (*Tl*FLU1) and *Talaromyces pinophilus* FLU12 (*Tp*FLU12). The purified enzymes are monomeric units, with a molecular mass of 44 kDa and 68.7 kDa for *Tl*FLU1 and *Tp*FLU12, respectively, on SDS-PAGE and zymogram. It reveals distinct properties beyond classic protein absorption at 270–280 nm, with *Tl*FLU1's peak at 270 nm aligning with this typical range of type II Cu site (white Laccase), while *Tp*FLU12's unique 600 nm peak signifies a type I Cu^{2+} site (blue Laccase), highlighting the diverse spectral fingerprints within the Laccase family. The K_m and k_{cat} values revealed that ABTS is the most suitable substrate as compared to 2,6-dimethoxyphenol, caffeic acid and guaiacol for both Laccases. The bioinformatics analysis revealed critical His, Ile, and Arg residues for copper binding at active sites, deviating from the traditional two His and a Cys motif in some Laccases. The predicted biological functions of the Laccases include oxidation–reduction, lignin metabolism, cellular metal ion homeostasis, phenylpropanoid catabolism, aromatic compound metabolism, cellulose metabolism, and biological adhesion. Additionally, investigation of degradation of polycyclic aromatic hydrocarbons (PAHs) by purified Laccases show significant reductions in residual concentrations of fluoranthene and anthracene after a 96-h incubation period. *Tl*FLU1 Laccase achieved 39.0% and 44.9% transformation of fluoranthene and anthracene, respectively, while *Tp*FLU12 Laccase achieved 47.2% and 50.0% transformation, respectively. The enzyme structure–function relationship study provided insights into the catalytic mechanism of these Laccases for possible biotechnological and industrial applications.

Keywords *Trichoderma lixii*, *Talaromyces pinophilus*, Laccases, Polycyclic aromatic hydrocarbons (PAHs), Biodegradation

Fungi belonging to the phylum Ascomycota are well known for rapid growth, utilization of diverse substrate ranges, and degradation of the xenobiotics[1]. Among these fungi, the families *Hypocreaceae* and *Trichocomacea* are not only studied primarily for their role as biological control agents against numerous pathogens[2,3], but also for their versatile enzymatic system including Laccases, Peroxidases and Oxidases which are crucial for degrading lignin and other recalcitrant aromatic compounds of environmental concerns[4]. Among these groups of versatile extracellular enzymes, Laccases have continued to receive significant attention in the past decade because of high redox potentials, its metal tolerance properties[5,6] and industrial applications, such as polyaromatic hydrocarbons

[1]Discipline of Microbiology, School of Life Sciences, College of Agriculture, Engineering and Science, University of KwaZulu-Natal (Westville Campus), Durban 4001, South Africa. [2]Department of Pathology, School of Medicine, University of Limpopo, Private Bag X1106, Sovenga 0727, South Africa. ✉email: olanirana@ukzn.ac.za

(PAHs) bioremediation, delignification or second-generation ethanol production, pulp bleaching, dye decolorization and detoxification of xenobiotics[7–10].

Laccase (Benzenediol oxygen oxidoreductases, EC 1.10.3.2) belongs to the multi-copper class of enzymes with the potential of oxidizing aromatic and non-aromatic compounds to an innocuous state, unlike other lignin-olytic enzymes such as Manganese peroxidase (MnP) and Lignin peroxidase (LiP), which require hydrogen peroxide for activity[11]. Laccases ubiquitously found in fungi, higher plants, some insects, and a few bacteria[12]. The production of these enzymes is always triggered in response to environmental stress and nutrient depletion[7]. The physiological function of Laccase varies depending on the organisms; in plants these enzymes are involved in the lignification processes[13], in insects, it aids the formation of cuticles during the sclerotization process[14], in fungi, it helps the morphogenesis process (formation of spores, pigments of fruiting bodies)[15,16], pathogenesis[17], virulence[18], lignin degradation, monomer cross-linking, polymer degradation[19], and also the breakdown of aromatic rings[19]. The precise role of Laccase in bacteria remains unclear but few studies have shown its functions in industrial applications requiring activity at high pH and temperatures as robust biocatalysts[20]. Fungal Laccases are glycoproteins which exist as monomer, homodimer, heterodimer, and multimer forms, with four redox-active copper atoms used in oxidizing substrates using oxygen as electron acceptor and its subsequent reduction to form water molecule[21]. The molecular mass and isoelectric point (pl) of Laccases ranges from 50 to 100 kDa and 3–7, respectively[22]. Typical Laccase consists of three Cu centres (Type I, II and III) with UV–vis spectrum absorption between 280 to 610 nm and a shouldering at 330 nm[23]. Type I Cu is responsible for the intense blue colour with UV–vis absorption spectrum at 605 nm and detectable in electro paramagnetic resonance (EPR) spectrum with narrow hyperfine coupling characteristics due to an S-Cu LMCT transition (ligand-to-metal charge transfer)[24,25]. Type II, unlike type I, is colourless and EPR detectable, while Type III Cu, on the other hand, has a pair of Cu atoms which have weak absorbance in the UV–vis spectrum and lacks an EPR spectrum[24]. Both. Type II and III Cu, forms the trinuclear cluster of Laccases where dioxygen binds and four-electron reduction to water takes place[26]. Different fungal species with blue Laccase production characteristics and PAHs degradation potential includes *Trametes versicolor*[27], *Trichoderma viride* (EXF8977), *Penicillium chrysogenum* (EXF1818) and *Irpex lacteus* (MUM 04.98)[28], while the use of a monomeric yellow Laccase in *Leucoagaricus gongylophorus* (Lac1Lg) has been documented in the oxidization of anthracene[29].

Despite the wide distribution and importance of Laccases, detailed studies on different Laccases in ascomycetes and their potential application in transforming organo-pollutants like PAHs into an innocuous state are scanty. Additionally, systematic spectral studies and bioinformatic analyses of ascomycete Laccases remain limited. Hence, this study aims to fill these knowledge gaps and contribute to the development of more effective strategies for PAH bioremediation using ascomycete Laccases by purifying and characterizing from *Trichoderma lixii* FLU1 and *Talaromyces pinophilus* FLU12, two ascomycetes isolated from benzo(b)fluoranthene activated sludge and known for degrading anthracene and fluoranthene. Furthermore, the substrate binding mechanism, homology modelling and prediction of their three-dimensional structure were determined.

Materials and methods

Reagents

ABTS (2,2-azino-bis-(3-ethyl-benzothiazoline-6-sulphonic acid)), Basal Salt Medium (BSM), anthracene, benzo (b) fluoranthene (BbF), 2,6-dimethoxyphenol (DMP), $(NH_4)_2SO4$ DEAE-cellulose and Sephadex G-100 were purchased from Merck (Burlington, MA, USA). All other chemicals used were of the highest purity and analytical grade.

Fungal strains and molecular identification

The isolation and identification of the two fungal strains, *Trichoderma lixii* FLU1 (*Tl*FLU1) and *Talaromyces pinophilus* FLU12 (*Tp*FLU12), used in this study have been reported previously[30]. Briefly, the strains were isolated from benzo(b)fluoranthene-enriched activated sludge which was later serially diluted and plated on potato dextrose agar (PDA) medium containing 100 mg/L of benzo(b)fluoranthene. The plates were incubated at 30 °C for 7 days and observed for the appearance of fungal colonies. The colonies that showed clear zones were selected as potential benzo(b)fluoranthene-degrading fungi, purified by repeated subculturing on fresh PDA plates and maintained on PDA slants at 4 °C. Due to the hydrophobic nature of benzo(b)fluoranthene, a superficial concentration of 100 mg/L was achieved on a PDA agar plate by evenly spreading it across the surface using a sterile glass rod and then left in the laminar hood for 2 h to allow the solvent used to prepare benzo(b)fluoranthene to evaporate which ensures a strict adherence of benzo(b)fluoranthene to the agar surface.

Later, the purified fungal strains were identified by morphological and molecular methods. The morphological characteristics of the fungal strains were examined by light microscopy and compared with standard references. The molecular identification was performed by extracting the genomic DNA from the fungal strains and amplifying the internal transcribed spacer (ITS) region of the ribosomal RNA gene by PCR. The PCR products were sequenced and compared with the sequences available in the GenBank database. The phylogenetic analysis was conducted by using the MEGA software.

Culture conditions for Laccase production

Each fungal strain was separately cultured in cotton-plugged Erlenmeyer flasks (250 mL) containing BSM and anthracene (200 mg/L) as an inducer to a final volume of 150 mL prior to the set-up. The media were sterilized by autoclaving at 121 °C for 15 min. Inoculation was done directly into individual Erlenmeyer flasks using two 20 mm mycelial disks of each strain before incubating at 30℃ and shaking at 180 rpm for 10 days in complete darkness (MRC laboratory instrument, Essex, U.K). The pH of the flask containing strain *Tl*FLU1 was adjusted to 4 using 1 M HCl while that of *Tp*FLU12 was adjusted to 7 using 1 M NaOH. The details of the specific

components and concentration for the BSM media and PDA are presented in Table S1. The variation in the culture media pH was observed due to optimized condition during anthracene degradation with 100% degradation efficiency after 12 days.

Purification of Laccase

The purification was carried out according to the previously described method (Othman et al., 2018) with some modifications. Briefly, crude extract from *Tl*FLU1 and *Tp*FLU12 was individually centrifuged at 5,000 × *g* for 20 min at 4℃ to obtain a clear supernatant. Protein from each supernatant was sequentially precipitated to saturation with 60% $(NH_4)_2SO_4$ under a gentle continuous stirring at 4℃ overnight. The protein pellets were recovered by centrifugation at 10,000 × *g* for 20 min, dissolved in sodium acetate buffer (50 mM, pH 5) and dialyzed against a large volume of the same buffer using 30 kDa cut off size dialysis tubing cellulose membrane (Merck, Burlington, MA, USA). The protein was further purified using DEAE liquid chromatography column (1.5 × 9 cm) at room temperature before eluting with 100 mM NaCl in 50 mM sodium acetate buffer (pH 7) at a flow rate of 0.5 ml/min. Six fractions showing Laccase enzymes activity of substrate ABTS were pooled and applied on Sephadex G-100 column (2.0 × 9 cm) size exclusion column before elution with 50 mM sodium acetate buffer (pH 7). All fractions with Laccase activity were pooled, desalted, filter-sterilized, and stored at 4℃ until further usage.

Protein quantification and enzyme activity

The protein concentrations were determined as described previously[31] using bovine serum albumin (BSA) as standard. Laccase activity was determined according to previously described method[32] with slight modifications. Briefly, the reaction mixture contained 100 µL of 50 mM ABTS and 800 µL of 20 mM sodium acetate buffer (pH 5) and an appropriately diluted purified enzyme (370 µg). The mixture was incubated at 30℃ for 15 min and the reaction was terminated with 40 µL of 20% trichloroacetic acid. One unit of Laccase is the amount of enzyme that produces 1 µM of oxidized product per minute ($\varepsilon_{420\ nm} = 36{,}000\ M^{-1}\ cm^{-1}$ for oxidized product).

Zymogram analysis

Non-denaturing polyacrylamide gel electrophoreses (Zymogram) were used to confirm the protein purity and activity[33]. The sample loading buffer was prepared without the addition of β-mercaptoethanol (non-reducing condition), and the samples (100 µg for *Tl*FLU1 and 75 µg for *Tp*FLU12 of total protein) were not heated before loading into the wells. To detect the Laccase activity after the electrophoresis, the gel was washed once with a mixture of equal parts of isopropanol-sodium acetate buffer (50 mM, pH 5.0) for 30 min and once with sodium acetate buffer for 30 min, to remove the SDS, fix the proteins in the gel, and to reduce the pH to 5.0. The gel was then transferred onto a glass plate before layering with ABTS-agar (20 mg of ABTS, 400 mg of agar, 40 mL of water; heated to dissolve agar). These layers were incubated at 25 °C until the appearance of green bands.

UV–visible absorption spectrum and FTIR analysis

To study the copper active centre of purified enzymes, 1 mL of enzymes (370 µg of total protein) was added to a 10 mm optical path quartz cuvette and absorbance was measured in a scanning mode wavelength from 200–800 nm using Agilent Cary 60 UV–Vis spectrophotometer (Agilent, Santa Clara, CA, USA)[34]. To monitor functional groups of the purified proteins (370 µg of total protein), FTIR analysis was performed as described previously[30].

Catalytic properties of the purified Laccases

Laccase activity was assayed by using several substrates. Assays were performed in 50 mM of the appropriate buffer and pH, and the oxidized products were read at the appropriate wavelength, as follows: 5 mM ABTS ($\varepsilon_{420} = 36.00\ cm^{-1}\ mM^{-1}$), 5 mM 2,6-DMP ($\varepsilon_{469} = 49.60\ cm^{-1}\ mM^{-1}$), 5 mM guaiacol ($\varepsilon_{465} = 12.10\ cm^{-1}\ mM^{-1}$) and 5 mM caffeic acid ($\varepsilon_{312} = 11.20\ cm^{-1}\ mM^{-1}$). The optimum pH for Laccase activity was investigated by using purified enzyme prepared in a reaction mixture containing the appropriate substrate in buffers as follows: 50 mM citrate buffer pH 1–6, 50 mM acetate buffer pH 3–5, 50 mM phosphate buffer pH 6–8 and 50 mM Tris buffer at pH 7 and 11. The optimum temperature of Laccase activity was investigated by using each purified enzyme (370 µg of total protein) for *Tl*FLU1 and *Tp*FLU12, respectively) prepared separately in a reaction mixture containing 5 mM ABTS in 50 mM acetate buffer pH 5, which was incubated at different temperatures (5, 10, 20, 30, 40, 50, 60, 70, 80, 90 and 100 °C) for 1 h. Also, the pH stability and thermal stability of the purified Laccase were studied by determining the residual activity for each enzyme (370 µg of total protein) after 24 h incubation under the same assay conditions for the optimum pH and temperature in darkness using ABTS as substrate. The reaction was monitored at 420 nm using Agilent Cary 60 UV–Vis spectrophotometer (Agilent, Santa Clara, CA, USA). The effect of appropriate substrate concentration (ABTS, 2,6-DMP, guaiacol and caffeic acid) on initial reaction velocity catalysed by purified Laccase was also investigated at constant enzyme concentration (370 µg of total protein). Therefore, as described above, the purified enzyme was assayed using varying concentrations (1–5 mM) of each substrate in 50 mM acetate buffer pH 5 and 7 at 30 and 50 °C for Laccase from *Tl*FLU1 and *Tp*FLU12, respectively. Michaelis–Menten reciprocal plots were used to determine the kinetic constants (v_{max}, $K_{m,}$ k_{cat} and k_{cat}/K_m) for appropriate substrate using the Graph-Pad Prism 8.0 (San Diego, USA) software. The residual enzyme activity at varied concentrations of metal ions (10, 50 and 100 mM: Al^{3+}, As^{5+}, Ca^{2+}, Cd^{2+}, Co^{2+}, Cu^{2+}, Fe^{2+}, K^+, Li^+, Mg^{2+}, Mn^{2+}, Mo^+, Na^+, Ni^{2+} and Zn^{2+}), Organic solvent (10, 50 and 90%: 1,4 Dioxane, acetone, acetonitrile, butanol, DMSO, ethanol, ethyl-acetate, isopropanol, methanol and toluene) and inhibitors (DTT, 0.01 and 0.1 mM; EDTA, 1 and 10 mM; NaN_3, 0.05 and 0.1 mM, SDS 5 and 10 mM; Urea, 20, 50 and 100 mM) was investigated by pre-incubating the purified enzymes (370 µg of total protein) for 24 h.

In-gel trypsin digestion and identification of the purified Laccase in ESMS

Purified Laccase (100 µg) from *Tl*FLU1 and *Tp*FLU12 was loaded onto 10% SDS-PAGE and stained with Coomassie blue R250. Protein bands were excised, digested with trypsin and subjected to electrospray mass spectrometry (ES-MS) for amino acid fragment identification at the Central Analytical Facility of Stellenbosch University, Stellenbosch, South Africa. The raw files generated by the mass spectrometer were imported into Proteome Discoverer v1.4 and processed using the Sequest algorithm against the UniProt (www.uniprot.org) *Trichoderma* genus and *Talaromyces* genus database, limited to Laccases. The peptide sequences were inferred from these matches with validation using the Target-Decoy PSM validator node. The search results were further validated using Scaffold Q + [35].

Template-based structure prediction, homology modelling and Laccase ligand binding site prediction for Laccase

The three-dimensional structure of the protein was predicted by submitting the amino acid sequence to the I-TASSER servers[36]. LOMETS approach was used to search for templates of similar folds from the PDB library[37,38]. Ten templates were used to build homology models while the top model structure was selected to optimize using the PyMOL Molecular Graphics System program (Schrödinger LLC., USA). The model quality validation through the 3D protein structure assessment, Errat and Ramachandran plot was performed using the Schrödinger Maestro software (Schrödinger LLC., NY, USA). Structural homology alignment was constructed with Jalview 2.11.2.4[39]. Additionally, the Laccase ligand binding sites residues, their molecular function, biological process, and cellular components were predicted using I-TASSER servers in accordance with the ancestor chart of the EMBL's European Bioinformatics institute gene ontology (GO) terms.

Sequence alignment

Detection of Laccase amino acid sequences from *Tl*FLU1 and *Tp*FLU12 similarities with amino acid sequences of Laccase from *Trichoderma species* and *Talaromyces species* deposited at UniProtKB were analysed using the BLAST tool (http://uniprot.org/blast). A phylogenetic approach was used to determine the taxonomic classification while amino acid sequence alignment was performed using muscle (multiple sequence comparison by UMPGA) as implanted in MEGA 11. Alignments were examined manually and a phylogenetic tree was constructed with a neighbour-joining likelihood approach and bootstrap resampling of 1000 replicates using MEGA 11[40].

Degradation of PAHs by Laccase

The two PAHs (fluoranthene and anthracene) were selected based on their designated profile as known or reasonably anticipated human carcinogens on US EPA's priority pollutants list[41]. The assays were carried out as described previously[42] with some modifications. Briefly, 5 mL reaction mixture contained anthracene and fluoranthene (200 mg/L) individually in a 15 mL centrifuge tube, Laccase (2 U/ml) and sodium acetate buffer (50 mM, pH 5 and 7 for *Tl*FLU1 and *Tp*FLU12, respectively). Tween 80 (1%) was added to the mixture to enhance PAH bioavailability and shaken continuously at 80 rpm to avoid PAHs precipitation at 30 °C in darkness for 96 h (MRC Lab suspension mixer SM-3600, U.K). The set up was performed in triplicate while samples were drawn every 24 h for residual PAHs quantification. 50 µl of 20% (v/v) TCA solution was constantly added to each draw sample before quantifying residual PAHs to stop further enzymatic oxidation. A control set up was carried out under the same experimental condition except for the Laccase being heated denatured. However, extraction and quantification of the residual PAHs was carried out as previously[30]. The mixture was then vigorously shaken for 5 min and allowed to stand for 20 min to enhance the separation of aqueous and organic phases using the standard extraction method. The organic phase was collected, dried over 10 g anhydrous Na_2SO_4 and evaporated to dryness at 40 °C under reduced pressure. The dried fractions were then redissolved with the same extraction solvent and diluted tenfold with ethyl-acetate before quantifying the residual anthracene in a scanning spectrum mode using Agilent Cary 60 UV–Vis spectrophotometer from a wavelength of 200 to 400 nm. The absorption spectrum of anthracene and fluoranthene shows peaks at λ_{max} 286 and 265 nm respectively, using a quartz cuvette with an optical path of 10 mm. However, the reaction medium's anthracene and fluoranthene residual concentrations were determined through extrapolation from a standard curve with an R^2 value of 0.972 and 0.958 respectively. Also, a recovery study was carried out in triplicate with a sterile sodium acetate buffer with heated-denatured Laccase to an appropriate volume of known concentrations of each PAH compounds as standard, under static conditions and subjected to PAH determination with an average recovery of 98.7 ± 0.53% and 97.9 ± 7.17%, respectively, for anthracene and fluoranthene.

Statistics analysis

All data were collected in triplicates. Data were statistically analysed using the Graph-Pad Prism 8.0 (San Diego, USA) software and expressed as the means ± standard error. For determining K_m and v_{max}, the Michaelis–Menten equation was fitted directly to the experimental data using the nonlinear least-squares fitting procedure of the Graph-Pad Prism 8.0 software.

Results

Purification of Laccases

Table 1 shows the purification summary of Laccases from *Tl*FLU1 and *Tp*FLU12. Laccase from *Tl*FLU1 was purified to 25.3-fold showing specific activity of 4003 U/mg of protein and a total yield of 7.0% while Laccase from *Tp*FLU12 was purified to 5.6-fold showing specific activity of 790 U/mg of protein and a total yield of

Strains	Purification step	Volume (mL)	Total activity (U)	Total protein (mg)	Specific activity (U/mg)	Yield (%)	Purification (fold)
*Tl*FLU1	Crude enzyme	50	21,198.8	134	158	100	1
	$(NH_4)_2SO_4$ precipitation (80%)	10	12,389.2	6.53	1897	58.4	12.0
	Dialysis	20	8359.8	3.2	2612	39.4	16.5
	Ion-Exchange Chromatography (DEAE-Cellulose)	10	4121.7	1.4	2944	19.4	18.6
	Gel filtration on Sephadex G-100	5	1481	0.37	4003	7.0	25.3
*Tp*FLU12	Crude enzyme	50	17,271	123	140	100	1
	$(NH_4)_2SO_4$ precipitation (80%)	10	12,102	75.1	161	70.1	1.1
	Dialysis	20	7287	21.97	332	42.2	2.4
	Ion-Exchange Chromatography (DEAE – Cellulose)	7	1292	3.18	406	7.5	2.9
	Gel filtration on Sephadex G-100	5	948	1.2	790	5.5	5.6

Table 1. Purification summary of Laccases purified from *Tl*FLU1 and *Tp*FLU12. % Yield = relative to 21,198.8 considering 100%; Purification (fold) = relative to specific activity (U/mg) considering 1.

5.5%. The purified Laccase from *Tl*FLU1 showed a single band with molecular mass of 44 kDa (Fig. 1a, Fig. S1), while *Tp*FLU-12 showed a molecular mass of 68.7 kDa (Fig. 1b, Fig. S2). The activity staining zymogram gel corresponding to the Laccase's bands confirmed the nature of the enzymes (Fig. 1c, Fig. S3).

UV–visible and FTIR spectra of purified Laccases

The purified Laccases from *Tl*FLU1 and *Tp*FLU12 showed the absorption peak at wavelengths 270 nm and 600, respectively, measured by UV–visible spectrophotometer (Fig. 2). The FTIR spectra of Laccase from *Tl*FLU1 showed the intense peaks at 3270 cm^{-1}, 2148 cm^{-1}, 1652 cm^{-1}, 1066 cm^{-1} and 594 cm^{-1} attributing to $-NH_2$ and –OH of amides A and B, OH/NH of Amide II, C=O stretching of α helix, C=C and C–N stretching of Amides II, respectively (Fig. 3, curve A, Table 2). The FTIR spectra of Laccase from *Tp*FLU12 showed the peaks at 3260 cm^{-1}, 2148 cm^{-1}, 1646 cm^{-1} and 600 cm^{-1} attributing to $-NH_2$ and –OH of amides A, B, OH/NH of Amide II, ß-sheets of peptide and C=C stretching and C-N stretching of Amides II, respectively (Fig. 3, curve B, Table 2).

Optimum pH, optimum temperature and stabillity

Purified Laccases from *Tp*FLU1 and *Tp*FLU12 showed optimum activity at pH 5 and pH 7, respectively (Fig. 4a). *Tp*FLU1 Laccase showed 80–100% residual activity at pH 5–9 while *Tp*FLU12 showed 60–100% residual activity at pH 1–5 after 24 h of incubation period prior to the assay (Fig. 4b). Furthermore, Laccases from *Tp*FLU1 and

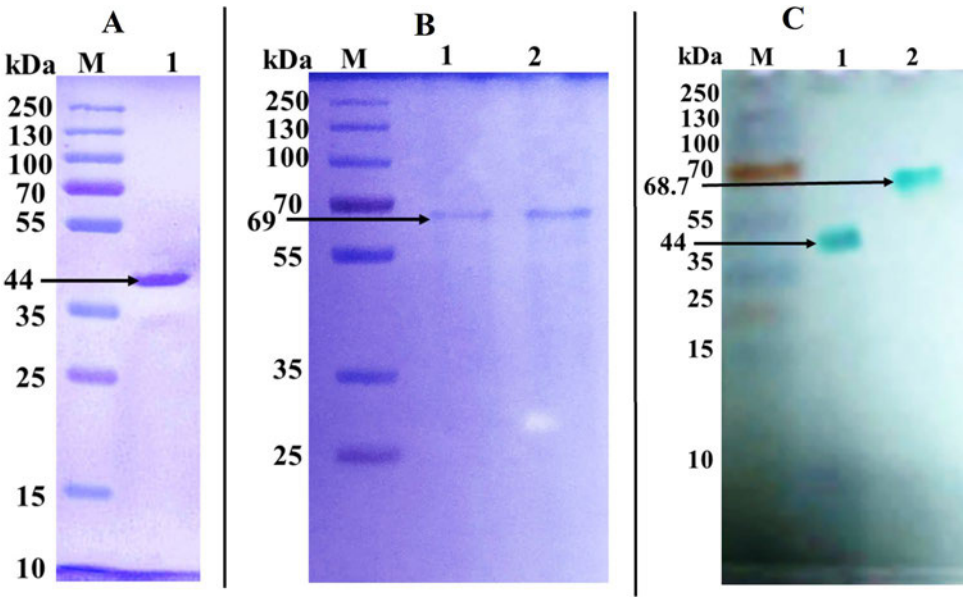

Figure 1. SDS-PAGE and native page showing single bands and in gel activity of Laccases. (**A**) Lane M: protein marker, Lane 1: purified Laccase from *Tl*FLU1; (**B**) Lane M: protein marker, Lane 1–2 purified Laccase from *Tp*FLU12; (**C**) Lane M: protein marker, Lane 1: In gel activity of purified Laccase from *Tl*FLU1, Lane 2: In gel activity of purified Laccase from *Tp*FLU12.

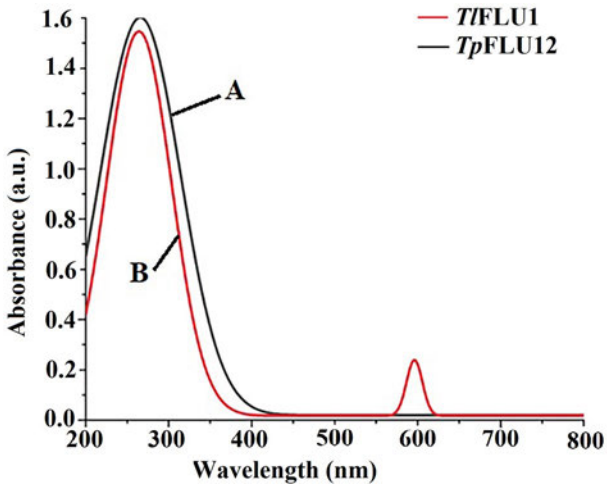

Figure 2. UV–vis spectrum of the purified Laccase from *Tl*FLU1 (curve A) and *Tp*FLU12 (curve B).

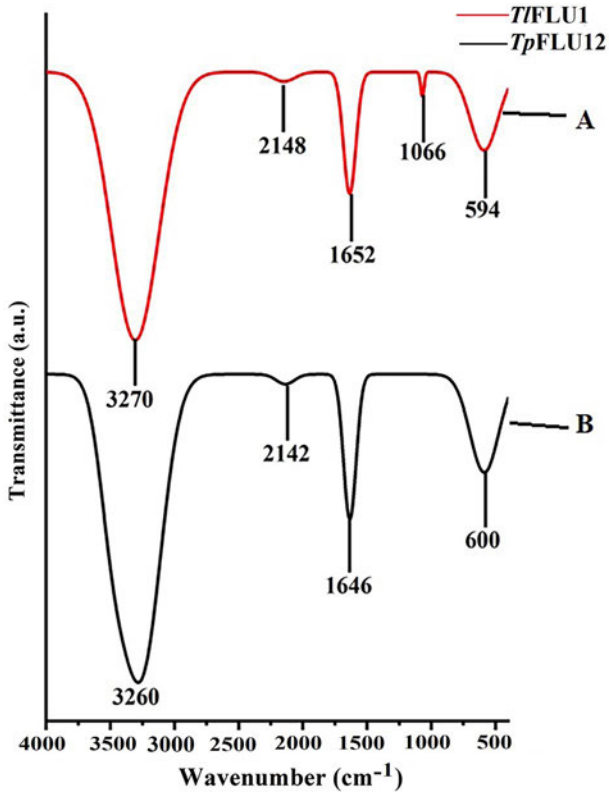

Figure 3. FTIR spectral of the purified Laccase from *Tl*FLU1 (curve A) and *Tp*FLU12 (curve B).

Frequency (cm^{-1})	Attribution
> 3000	$-NH_2$ and –OH of Amides A, B
2142–2148	OH/NH of Amide II
1600–1700	Amide I
1650–1658	C=O stretching of α helix
1620–1646	ß-sheets
594–1400	C=C stretching and C–N stretching of Amides II

Table 2. Attribution of the infrared spectra absorbance bands of purified Laccase from *Tl*FLU1 and *Tp*FLU12.

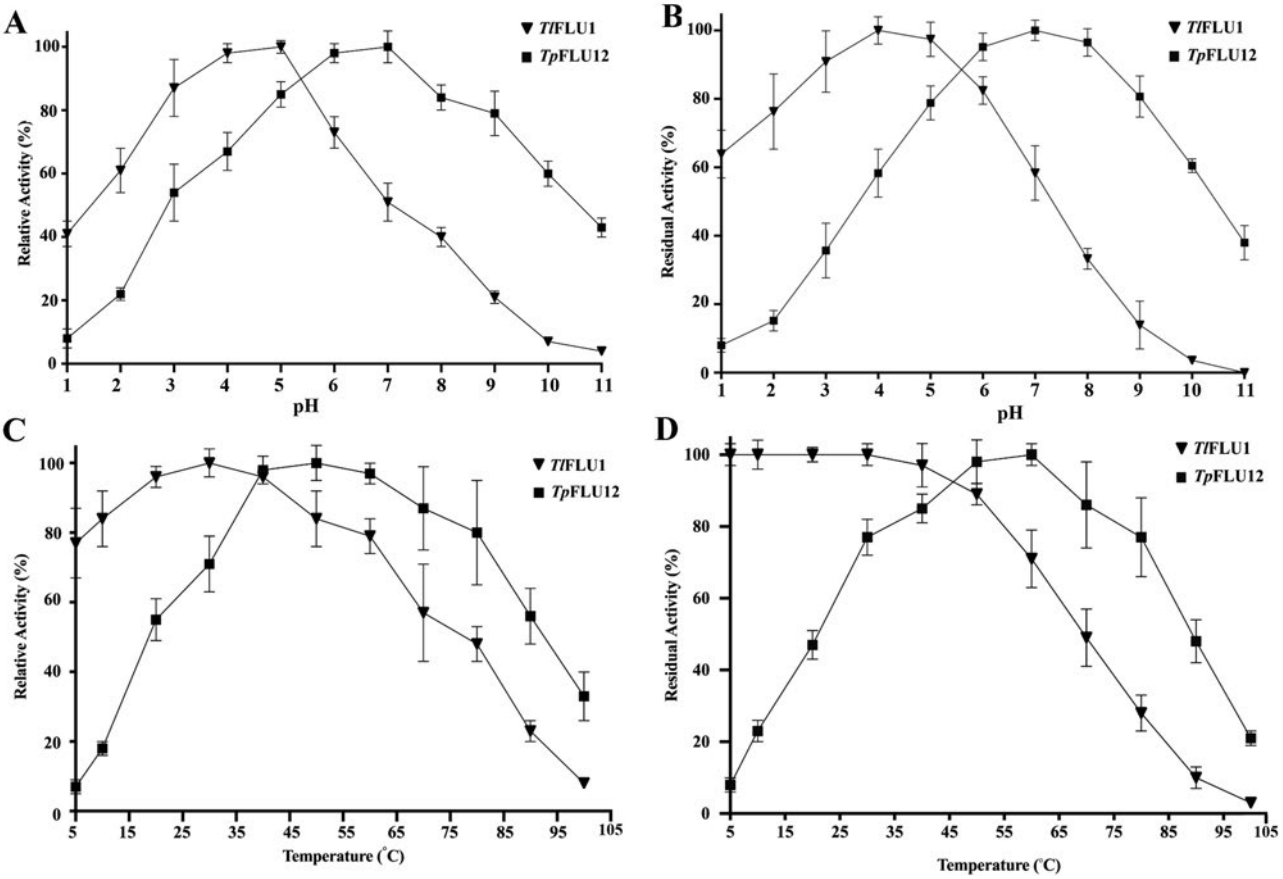

Figure 4. Optimum pH (**A**) and pH stability (**B**), optimum temperature (**C**) and temperature stability (**D**) of purified Laccase from *Tl*FLU1 and *Tp*FLU12.

*Tp*FLU12 showed optimum activity at temperatures 30 °C and 50 °C, respectively (Fig. 4c). After 24 h of incubation at 10–30 °C, Laccases from *Tp*FLU1 retained 100% activity and dropped to 90% at 50 °C, 70% at 60 °C, 50% at 70 °C and finally lost activity at 100 °C. *Tp*FLU12 Laccase residual activity was found to be very much stable between a temperature 50–60 °C. The enzyme showed 80% residual activity at temperatures 30 °C and 80 °C while retained 85% residual activity at 70 °C (Fig. 4d).

Effect of metal ions, organic solvents and inhibitors on activity

Table 3 summarises the activity of Laccases in the presence of metal ions, organic solvents, and inhibitors. Laccase from *Tl*FLU1 showed 100%, 121%, 100%, 100%, 102%, 98.0% and 107% relative activity in the presence of Ca^{2+}, Cu^{2+}, Fe^{2+}, Mg^{2+}, Mn^{2+}, Na^{+} and Zn^{2+}, respectively, at 10 mM concentration, however, the activity was decreased with increased metal ion concentrations. Laccase from *Tp*FLU12 showed 104%, 100%, 101%, 119% and 100% relative activity in presence of Ca^{2+}, Cd^{2+}, Co^{2+}, $Cu^{2+}$and Na^{+} at concentration of 10 mM, while a relative activity of 100% was recorded in the presence of 50 mM $Cu^{2+}$and Na^{+}.

The relative activity of Laccase enzyme from *Tl*FLU1 and *Tp*FLU12 in the presence of organic solvents is shown in Table 4. Enzyme from *Tl*FLU1 showed decreased relative activity with an increase in the organic solvents' concentrations. 100% relative activity was recorded in the presence of acetone, acetonitrile, and ethyl-acetate while a relative activity of 127% was recorded in the presence of toluene at a concentration of 10%. The purified Laccase from *Tp*FLU12 was more active in organic solvents up to 90% of concentration. Maximum relative activity of 100% was recorded in the presence of acetonitrile and ethyl-acetate at a concentration of 10%. Relative activity of 100% was recorded in the presence of acetone and ethyl-acetate at a 50 and 90% concentration, respectively.

The enzymatic acvity of Laccase from both the isolates, *Tl*FLU1 and *Tp*FLU12 were significantly inhibited by the tested inhibitors (Fig. 5). NaN_3 significantly inhibited Laccases from both strains showing 81% and 97% inhibition at a concentration of 0.05 and 0.1 mM for enzyme from *Tl*FLU1. In comparison, 97% and 100% inhibition were recorded at a concentration of 0.05 and 0.1 mM for enzyme from *Tp*FLU12.

Kinetic parameters analysis

Table 5 shows the kinetics parameters values for Laccase from *Tl*FLU1 and *Tp*FLU12 when assayed with various substrates. Among all the phenolic compounds used as substrates, Laccase from *Tl*FLU1 and *Tp*FLU12 showed lowest K_m values 10.8 µM and 8.20 µM, for substrate ABTs, followed by guaiacol with K_m values of 12.7 µM and

Strains	Relative activity (%)			
	Ions	10 mM	50 mM	100 mM
*Tl*FLU1	Control	100.0 ± 0.64	100.0 ± 0.64	100.0 ± 0.64
	Al^{3+}	37.0 ± 0.26	16.0 ± 0.15	10.0 ± 0.84
	As^{5+}	80.0 ± 0.02	83.0 ± 0.17	62.0 ± 0.21
	Ca^{2+}	100.0 ± 0.99	74.0 ± 0.77	22.7.0 ± 0.98
	Cd^{2+}	70.0 ± 0.47	64.0 ± 0.27	42.0 ± 0.81
	Co^{2+}	85.0 ± 0.64	87.0 ± 0.05	65.0 ± 0.16
	Cu^{2+}	121.0 ± 0.93	84.0 ± 0.46	63.0 ± 0.88
	Fe^{2+}	100.0 ± 0.15	33.0 ± 0.27	32.0 ± 0.97
	K^{+}	33.0 ± 0.61	33.0 ± 0.32	30.0 ± 0.62
	Li^{+}	46.0 ± 0.02	30.0 ± 0.18	25.0 ± 0.68
	Mg^{2+}	100.0 ± 0.32	61.0 ± 0.05	48.0 ± 0.23
	Mn^{2+}	102.0 ± 0.29	79.0 ± 0.54	18.0 ± 0.68
	Mo^{+}	72.0 ± 0.81	70.0 ± 0.33	61.0 ± 0.38
	Na^{+}	98.0 ± 0.36	96.0 ± 2.93	31.0 ± 4.95
	Ni^{2+}	67.0 ± 0.37	81.0 ± 0.55	54.0 ± 0.19
	Zn^{2+}	107.0 ± 0.21	89.0 ± 0.55	18.0 ± 0.79
*Tp*FLU12	Control	100.0 ± 0.66	100.0 ± 0.66	100.0 ± 0.66
	Al^{3+}	75.0 ± 0.35	46.0 ± 0.39	27.0 ± 0.56
	As^{5+}	83.0 ± 0.19	64.0 ± 0.41	79.0 ± 0.75
	Ca^{2+}	104.0 ± 0.93	89.0 ± 0.22	70.0 ± 0.81
	Cd^{2+}	100.0 ± 0.87	74.0 ± 2.17	41.0 ± 0.41
	Co^{2+}	101.0 ± 0.65	75.0 ± 0.91	82.0 ± 0.17
	Cu^{2+}	119.0 ± 076	100.0 ± 0.44	17.0 ± 0.58
	Fe^{2+}	84.0 ± 0.81	57.0 ± 0.89	39.0 ± 0.65
	K^{+}	73.0 ± 0.15	38.0 ± 0.53	16.0 ± 0.22
	Li^{+}	74.0 ± 0.04	46.0 ± 0.74	19.0 ± 0.35
	Mg^{2+}	82.0 ± 0.76	61.0 ± 0.27	49.0 ± 0.86
	Mn^{2+}	81.0 ± 0.67	53.0 ± 0.41	34.0 ± 0.70
	Mo^{+}	84.0 ± 0.49	76.0 ± 0.95	70.0 ± 0.13
	Na^{+}	100.0 ± 0.81	100.0 ± 0.68	73.0 ± 0.82
	Ni^{2+}	82.0 ± 0.25	66.0 ± 0.53	71.0 ± 0.18
	Zn^{2+}	85.0 ± 0.75	73.0 ± 0.23	65.0 ± 0.23

Table 3. Effect of metal ions on the activity of purified Laccase enzyme from *Tl*FLU1 and *Tp*FLU12. Each value in the same column are the mean ± standard error.

11.6 µM while 13.03 µM and 14.91 µM for 2,6-DMP, respectively. Caffeic acid showed the lowest affinity as a substrate for both the enzymes from *Tl*FLU1 and *Tp*FLU12 with the K_m values of 43 µM and 38.60 µM.

ES-MS analysis of tryptic digested proteins

ES-MS analysis of tryptic digested Laccase from *Tl*FLU1 and *Tp*FLU12 showed 12 and 18 protein clusters, respectively, when searched in UniProt Laccase database (Fig. S4a,b). The protein purified from *Tl*FLU1 showed 100% similarity with 386 amino acids long Laccase from *Trichoderma asperellum* strain OX with Uniprot accession number A0A6V8QJQ4 while protein purified from *Tp*FLU12 showed 100% similarity with 619 amino acids long Laccase from *Talaromyces marneffei* strain PM1 with Uniprot accession number A0A093UKS0 (Fig. S4c). Interestingly, no common proteins were detected between the Laccase from both strains at a 100% false discovery rate (FDR), and it quite raises concerns about relying soley on MS data sequence accuracy which might lead to unreliable models and inaccurate biophysical property predictions of the protein 3D structures. To address these limitations, a phylogenetic analysis using RSB PDB sequences of Laccases from both *Trichoderma* and *Talaromyces* families was conducted (Figs. S2 and S3). This approach provides a more robust understanding of the evolutionary relationships between the studied Laccases and their known counterparts, potentially offering a more reliable basis for modelling and prediction. Upon analysis, Laccase from *Tl*FLU1 was observed to share the same cluster with that of Laccase from *Trichoderma asperellum* with Uniprot accession number A0A6V8QJQ4 (Fig. S5), while Laccase from *Tp*FLU12 shared the same cluster with Laccase from *Talaromyces marneffei* PM1 with Uniprot accession number A0A093V1A3 (Fig. S6).

Strain	Organic solvent	Relative activity (%)		
		10%	50%	90%
*Tl*FLU1	Control	100.0 ± 0.71	100.0 ± 0.54	100.0 ± 0.49
	1,4-Dioxane	70.0 ± 0.34	69.0 ± 0.29	65.0 ± 0.24
	Acetone	100.0 ± 0.31	68.0 ± 0.53	43.6 ± 0.68
	Acetonitrile	100.0 ± 0.21	51.0 ± 0.24	19.0 ± 0.96
	Butanol	96.0 ± 0.85	88.0 ± 0.42	51.0 ± 0.25
	DMSO	66.0 ± 0.23	67.0 ± 0.83	41.7 ± 0.86
	Ethanol	73.0 ± 0.81	62.0 ± 0.14	51.5 ± 0.82
	Ethyl acetate	100.0 ± 0.42	73.0 ± 0.83	42.0 ± 0.67
	Isopropanol	89.0 ± 0.31	75.0 ± 0.27	61.3 ± 0.62
	Methanol	84.0 ± 0.63	77.0 ± 0.85	44.0 ± 0.77
	Toluene	127.0 ± 0.97	96.0 ± 0.5	53.4 ± 0.82
*Tp*FLU12	Control	100.0 ± 0.99	100.0 ± 0.65	100.0 ± 0.16
	1,4-Dioxane	93.0 ± 0.63	93.0 ± 0.13	44.1 ± 0.14
	Acetone	88.0 ± 0.20	100.0 ± 0.87	100.0 ± 0.45
	Acetonitrile	100.0 ± 0.03	97.0 ± 0.68	37.0 ± 0.68
	Butanol	70.0 ± 0.61	98.0 ± 0.79	82.0 ± 0.75
	DMSO	77.0 ± 0.93	99.0 ± 0.64	68.0 ± 0.92
	Ethanol	82.0 ± 0.61	89.0 ± 0.35	98.0 ± 0.77
	Ethyl acetate	100.0 ± 0.43	100.0 ± 0.82	100.0 ± 0.14
	Isopropanol	83.0 ± 0.51	97.0 ± 0.77	98.0 ± 0.17
	Methanol	76.0 ± 0.43	88.0 ± 0.52	97.0 ± 0.73
	Toluene	62.0 ± 0.71	83.0 ± 0.62	81.0 ± 0.63

Table 4. Effect of organic solvents on the relative activity of purified Laccase enzyme from *Tl*FLU1 and *Tp*FLU12. Each value in the same column is the mean ± standard error.

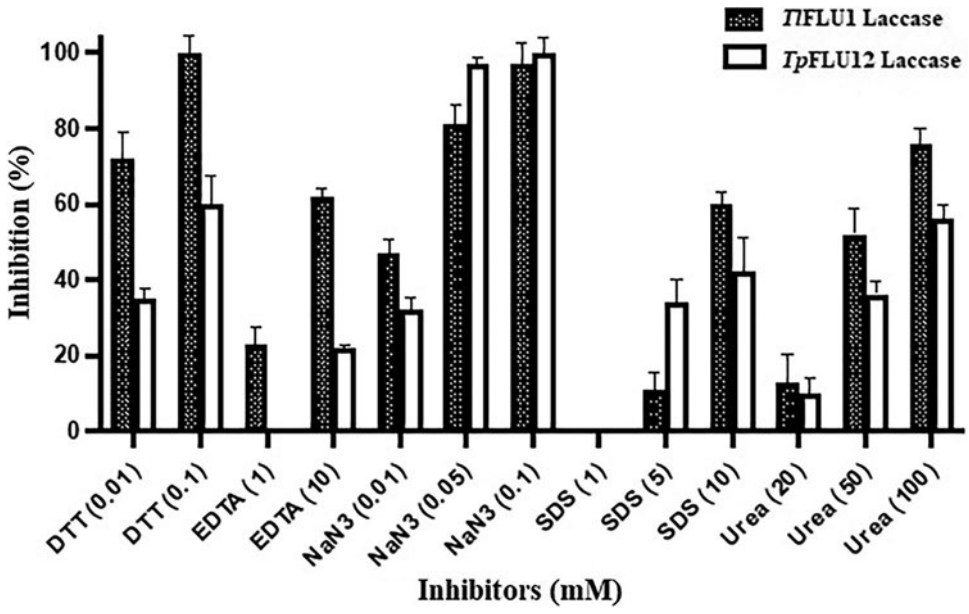

Figure 5. The percentage inhibition of inhibitors on Laccase activity from *Tl*FLU1 and *Tp*FLU12.

Homology sequence alignment

The homology sequence alignment of Laccases from *Tl*FLU1 and *Tp*FLU12 were constructed with PDB template IGW0 (Laccase from *Melanocarpus albomyces*) (Fig. S7) and 4X4KA (Laccase from *Botrytis aclada*) (Fig. S8), respectively, using LOMETS threading programs of the I-TASSER server. Laccases from *Tl*FLU1 shared 13% sequence identity with the template IGW0 in the threading aligned region with the query sequence, 24% sequence identity of the whole template chains with the query sequence, 81% coverage of the threading alignment and

Strain	Substrate	Absorbance (nm)	ε (cm^{-1} mM^{-1})	K_m (μM)	K_{cat} (S^{-1})	K_{cat}/K_m ($\mu M^{-1}S^{-1}$)
*Tl*FLU1	ABTS	420	36.00	10.80	88.25	8.17
	2,6-DMP	469	49.60	13.00	90.20	6.94
	Guaiacol	465	12.10	12.70	90.20	7.10
	Caffeic acid	312	11.20	43.00	116.20	2.70
*Tp*FLU12	ABTS	420	36.00	8.20	85.38	10.41
	2,6-DMP	469	12.10	11.60	89.17	7.69
	Guaiacol	465	49.60	14.90	92.20	6.19
	Caffeic acid	312	11.20	38.60	106.50	2.76

Table 5. Kinetic characterization of purified Laccase from *Tl*FLU1 and *Tp*FLU12. ε: Extinction coefficient.

1.78 normalized Z-score of the threading alignments. Amino acids sequence WADNLINGYRLLNYWFNPDN-PVNTLPNDPGVAVLNPRRWRHI (42 sequences) were observed as the consensus sequence between template IGW0. Laccase from *Tp*FLU12 shared 16% sequence identity with the template 4X4KA in the threading aligned region with the query sequence, 18% sequence identity of the whole template chains with the query sequence, 73% coverage of the threading alignment and 5.85 normalized Z-score of the threading alignments. Amino acids sequence DTGTHWHGQCPQPTCINLGDGFLINGFIDHLTVIANDVVARYTPPGSDNPLDDSKNNDNLNP-SEITG (67 sequences) were observed as the consensus sequence between template 4X4KA.

Template based structure prediction

Template-based structure modelling and ligand binding site residues of Laccases were predicted on iterative threading assembly refinement (I-TASSER) and shown in Fig. 6A–D and Table 6. The investigation revealed that the Laccase from *Tl*FLU1 shares 13% sequence identity with the IGW0 template within the threading-aligned

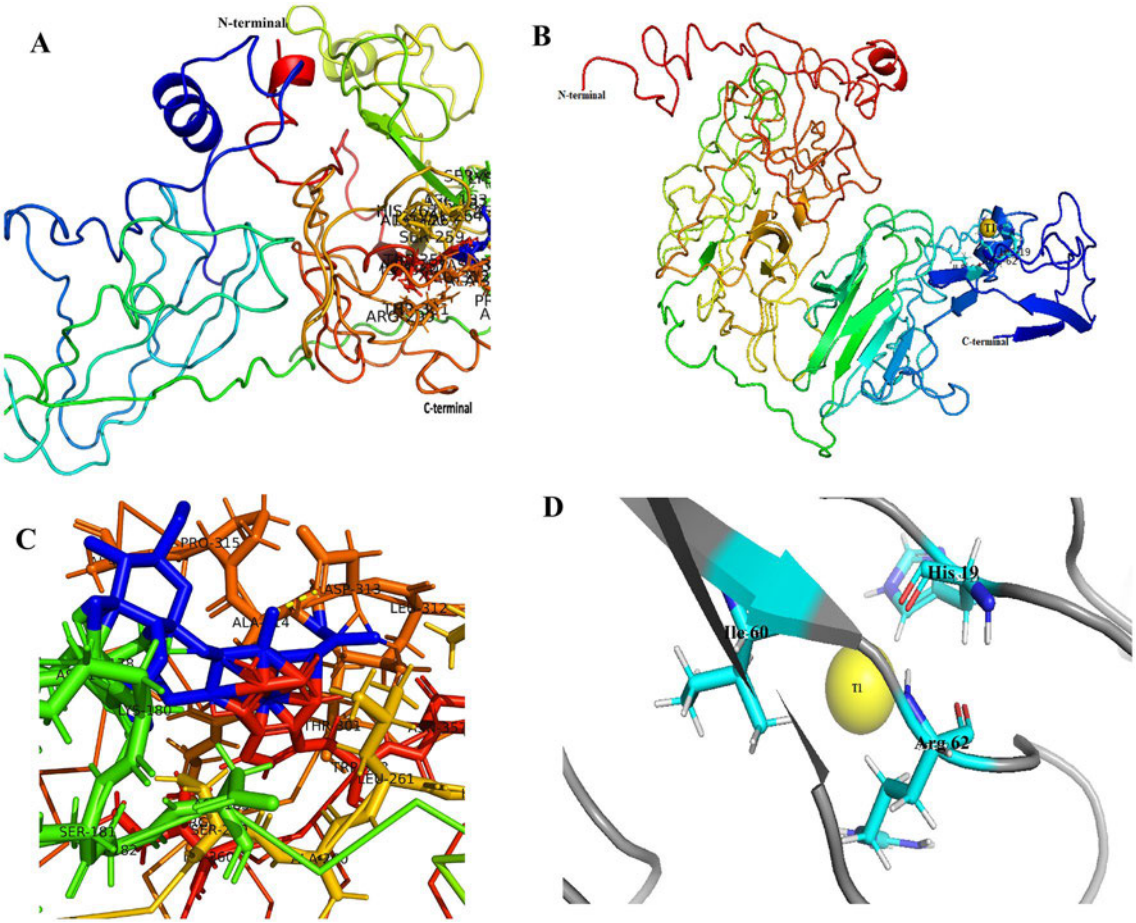

Figure 6. Structural models for Laccases from *Tl*FLU1 and *Tp*FLU12. Molecular surface structure with the binding sites (**A**) and (**B**); 3D cartoon (**C**) and (**D**); binding sites (**E**) and (**F**) of the Laccase from *Tl*FLU1 and *Tp*FLU12, respectively. The yellow ball colour (T1) is the Cu^{2+} of the protein.

Strain	Ligand binding Site residues	Consensus prediction of GO terms	GO terms code	GO terms functions	GO-score
*Tl*FLU1	Pro-177, Ala-178,	Molecular function	GO:0005507	Copper ion binding	0.65
	Asp-179, Lys-180,		GO:0016682	Oxidoreductase activity	0.36
	Lys-182, Asp-183,		GO:0008471	Laccase activity	0.34
	Ser-258, Ala-259,				
	Leu-260, His-261,	Biological process	GO:0055114	Oxidation—reduction	0.65
	Val-263, Arg-298,		GO:0009808	Lignin metabolism	0.4
	Thr-300, Leu-312,		GO:0046271	Phenylpropanoid catabolic	0.4
	Asp-313, Ala-314,		GO:0006725	Aromatic compound metabolism	0.4
	Pro-315, Als-316		GO:0030243	Cellulose metabolism	0.4
	Asn-355, Trp-356,				
	Ile-358	Cellular component	GO:0044421	Extracellular structure	0.4
*Tp*FLU12	His-19, Ile-60,	Molecular function	GO:0005507	Copper ion binding	0.44
	Arg-62		GO:0016724	Oxidoreductase activity	0.57
			GO:0052716	Oxygen oxidoreductase activity	0.46
		Biological process	GO:0055114	Oxidation—reduction	0.57
			GO:0022610	Biological adhesion	0.46
			GO:0044237	Cellular metabolism	0.44
			GO:0006875	Cellular metal ion homeostasis	0.44
			GO:0018955	Aromatic compound metabolism	0.44
		Cellular component	GO:0044421	Extracellular structure	0.4

Table 6. The Laccase ligand binding sites residues and predicted functions.

region and exhibits 24% sequence identity with the complete template chains. Furthermore, the threading alignment covers 81% of the sequence and the normalized Z-score amounts to 1.78 (Fig. 6A). Likewise, the Laccase derived from *Tp*FLU12 shares 16% sequence identity with the 4X4KA template within the threading-aligned region and shows 18% sequence identity with the entire template chains. The threading alignment coverage encompasses 73% of the sequence, with a normalized Z-score of 5.85. Employing Jalview workbench alignment, 3-D models that conform to spatial restraints were generated, exhibiting high precision as evidenced by minimal restraint violations (Fig. 6B). Further, The I-TASSER server-generated predicted protein structures for *Tl*FLU1 and *Tp*FLU12, manifest a moderate degree of structural similarity based on the TM-score (0.48 ± 0.15 and 0.53 ± 0.15, respectively). However, these models exhibited moderate structural deviation, as indicated by the root mean square deviation (RMSD) values of 1.13 ± 0.5 Å and 1.15 ± 0.5 Å, respectively. Notably, the aligned sequences display a relatively low sequence identity (24% and 18%, respectively), implying a limited proportion of identical residues. Nevertheless, the alignment covered a substantial portion of the hit structure, as indicated by the coverage (Cov) values of 81% and 73%, respectively.

To evaluate the quality of the models, verified 3D visualization using polymol was employed. The assessment revealed that the protein model derived from *Tl*FLU1 exhibited good 3D-1D scores for 43.95% of the total residues, while the model obtained for *Tp*FLU12 demonstrated good scores for 90% of the total residues. Structural analysis of the *Tl*FLU1 protein model unveiled the presence of four α-helices, with the absence of β-strands, β-α-β motifs, and β-hairpins. In contrast, the *Tp*FLU12 model displayed 104 α-helices, 60 β-sheets, one β-α-β motif, and two β-hairpins. Also, the Ramachandran plots (not shown) of the final minimized model suggested that the protein residues from *Tl*FLU1 was 9% most favourable, 12.11% additional allowed, 79% generously allowed and 0% disallowed, while that of *Tp*FLU12 had 72.7% most favourable regions, 17.3% additional allowed regions, 0% generously allowed regions and 0% disallowed regions. When compared with the template and results obtained from COACH and COFACTOR, 21 catalytic residues such as Pro-177, Ala-178, Aap-179, Lys-180, Lys-182, Asp-183, Ser-258, Ala-259, Leu-260, His-261, Val-263, Arg-298, Thr-300, Leu-312, Asp-313, Ala-314, Pro-315, Ala-316, Asn-355, Trp-356 and Ile-358 were obtained for Laccase from *Tl*FLU1 (Fig. 6C) while only Laccase from *Tp*FLU12 showed three combinations of catalytic residues namely His-19, Ile-60 and Arg-62 with Cu^{2+} (T1) residues at the binding site (Fig. 6D). The 21 ligands binding sites residues of Laccase from *Tl*FLU1 were shown to be associated with molecular functions related to copper ion binding, oxidoreductase activity and Laccase activity; biological process related to oxidation–reduction, lignin metabolism, phenylpropanoid catabolic, aromatic compound metabolism and cellulose metabolism; and cellular component related to extracellular structure; according to the gene ontology (GO). There were 3 binding residue sites (His-19, Ile-60 and Arg-62) of Laccase from *Tp*FLU12 were predicted with molecular functions related to copper ion binding, oxidoreductase activity and oxygen oxidoreductase activity; biological process related to oxidation–reduction, biological adhesion, cellular metabolism, cellular metal ion homeostasis, aromatic compound metabolism; and cellular component related to extracellular structure (Table 6).

Biophysical properties

The amino acid sequences (386 and 619 amino acids for Laccases from *Tl*FLU1 and *Tp*FLU12, respectively) were submitted to ProtParam to predict their biophysical properties (Table 7). Molecular mass of 43.8 and 68.6 kDa, theoretical pI value of 9.33 and 5.41 were predicted for Laccases from *Tl*FLU1 and *Tp*FLU12, respectively. The extinction coefficient values of 68,995 $M^{-1}cm^{-1}$ and 85,050 $M^{-1}cm^{-1}$ assuming all pairs of Cys residues form cystines while 68,870 $M^{-1}cm^{-1}$ and 84,800 $M^{-1}cm^{-1}$ when assuming all Cys residues are reduced were exhibited by Laccase from *Tl*FLU1 and *Tp*FLU12, respectively. However, Laccase from *Tl*FLU1 was predicted to have an estimated half-life of 4.4 h in mammalian reticulocytes (in vitro), > 20 h in yeast (in vivo) and > 10 h in *E. coli* (in vivo) while that of *Tp*FLU12 Laccase was estimated to have a half-life of 1.1 h in mammalian reticulocytes (in vitro), > 3 min in yeast (in vivo) and > 10 h in *E. coli* (in vivo), confirming their stability in eukaryotic and prokaryotic cells. The predicted instability, aliphatic index, and grand average of hydropathicity (GRAVY) values of 39.54, 33.43; 76.58, 77.50 and -0.508, -0.578 for Laccases from *Tl*FLU1 and *Tp*FLU12, respectively, classify them as stable, thermophilic, and non-polar.

Degradation of PAHs by purified Laccase

A general reduction in the residual PAHs (Fluoranthene and anthracene) concentrations were observed after 96 h incubation period (Fig. 7A,B). For fluoranthene, a residual concentration of 61.0% of 200 mg/L initial concentration was recorded in *Tl*FLU1 Laccase incubated tube while that of the *Tp*FLU12 Laccase incubated tube accounted for 52.8% residual fluoranthene concentration in comparison with the control tube (no Laccase addition) where no reduction was recorded in its initial concentration (100%). Therefore, 39.0% and 47.2% transformation of fluoranthene was recorded by Laccases from *Tl*FLU1 and *Tl*FLU12, respectively (Fig. 7A). Also, during anthracene degradation, a residual concentration of 44.9% was recorded at 96 h incubation period

Property	*Tl*FLU1	*Tp*FLU12
Number of amino acids	386	619
Molecular weight (kDa)	43.8	68.6
Theoretical pI	9.33	5.41
Extinction coefficients (M^{-1} cm^{-1})		
Cys residues from cystines	68,995	85,050
Cys residues are reduced	68,870	84,800
Estimated half-life		
Mammalian reticulocytes (In-vitro)	4.4 h	1.1 h
Yeast (In- vivo)	> 20 h	3 min
E. coli (In-vivo)	> 10 h	> 10 h
Instability index	39.54 (stable)	33.43 (stable)
Aliphatic index	76.58 (Thermophilic)	77.50 (Thermophilic)
Grand average of hydropathicity (GRAVY)	– 0.508 (hydrophilic)	– 0.578 (hydrophilic)

Table 7. The Biophysical and chemical properties of Laccase from *Tl*FLU1 and *Tp*FLU12.

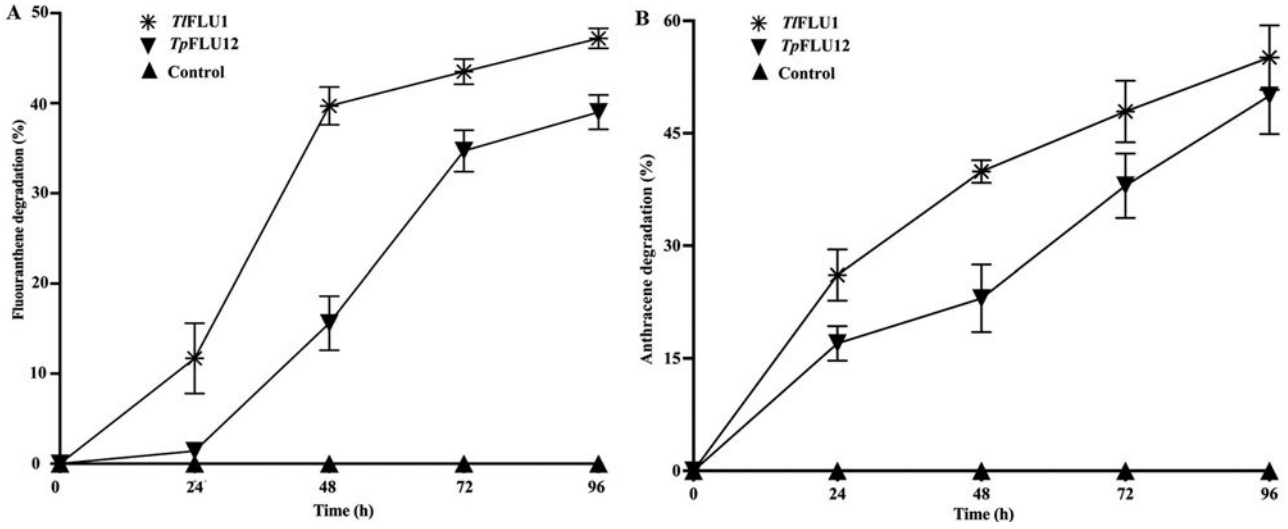

Figure 7. Biotransformation of PAHs fluoranthene (**A**) and anthracene (**B**) by purified Laccase from *Tl*FLU1 and *Tp*FLU12. The % transformation of fluoranthene and anthracene is 100% residual concentration. Control experiment curves are overlapping the x-axis.

in the *Tl*FLU1 Laccase incubated tube while that of the *Tp*FLU12 Laccase incubated tube showed a residual concentration of 50.0% at the same incubation period in comparison with the control tube (no Laccase addition) where no reduction was recorded in its initial concentration (100%). There was 55.1% and 50.0% transformation of fluoranthene was recorded by Laccases from *Tl*FLU1 and *Tl*FLU12, respectively (Fig. 7B).

Discussion

The capability of *Tl*FLU1 and *Tp*FLU12, investigated in this study, to produce active Laccases with a robust cold-adaptation and thermostability using anthracene as the sole carbon source corroborates previous study[33], where the use of anthracene as a sole carbon source for growth and production of Laccase with high pH stability and temperature stability in an ascomycete fungus, *Fusarium solani* MAS2.

In this study, the obtained low purification fold with high protein-specific activities of purified Laccases from both strains following adoption of chromatographic techniques like ion-exchange (DEAE-cellulose) and gel filtration (Sephadex G-100) in chronological order is an indication that Laccases were the most abundant among the extracellular enzymes released into the media[43]. Similarly, the purification fold falls within the range of a previously reported purified Laccase from *Ganoderma lucidum* with a purification fold of 25.4[44]. The absence of a peak near 600 nm in the UV–vis spectrum at 270 nm observed in Laccase from *Tl*FLU1 suggests the presence of a type 2 copper centre with unique Laccase peptide interactions, which is characteristic of white Laccase enzymes[45]. Also, the absence of type 1 spectrum (blue Laccase) could be due to incomplete oxidation of copper ions which then results in the formation of one copper atom at the catalytic site in combination with metal ions like zinc, iron or manganese, which give it four active reaction sites[46]. Similarly, the presence of white/yellow Laccase in ascomycete fungi might may be due to the quenching of the type 1 Laccase (blue Laccase) through an exogenous bond of aromatic group harnessed from the carbon source used during production, which then acts as a redox mediator in its high redox potential[25]. In addition, the UV–vis spectrum absorption at 600 nm by Laccase from *Tp*FLU12 is a characteristic of blue Laccase due to the type 1 spectrum peak[24]. Fourier-transform infrared spectroscopy (FTIR) analysis is an effective tool used in analysing proteins and polypeptides structures. In *Tp*FLU-12 Laccase, the observed vibrational bands at wavenumber 1646 cm^{-1} attributing to β-sheets, absorption at 600 cm^{-1} (amides II) and amide A, B (bands > 3000 cm^{-1}) is an indication of blue Laccase[24] while the peaks at 594–1066 cm^{-1}, 1652 cm^{-1} and > 3000 cm^{-1} in purified Laccase from *Tl*FLU1 could be linked to α helix, amides II and amide A, B of white Laccase structures[45]. It is important to note that the peaks at 2142 cm^{-1} and 2148 cm^{-1} observed in both purified Laccases represent the presence of O–H stretching due to water interaction with the protein and its polypeptide structures.

Under denaturing and native conditions, the single band of both Laccases with a molecular mass of 44 and 68.7 kDa from *Tl*FLU1 and *Tp*FLU12, respectively, is consistent with other documented fungal Laccases (40–66 kDa) (Kumar et al. 2017). A Laccase with molecular mass of 45 kDa have been previously reported to be produced by *Ceriporiopsis subvermispora* (Jung et al. 2002). Another Laccases showing a molecular mass of ~ 67kD[47] and with a molecular mass of 70 kDa from ascomycete fungus, *Thielavia sp.* HJ22[48] are also reported previously, very close to Laccase purified from *Tp*FLU12 (68.7 kDa) in this study.

In this study, the catalytic rate of Laccases and their stability were significantly influenced by pH and temperature which is of industrial advantage compared to previous reports. The optimum pH activity (5 and 7) and stability at a wide range of pH for both Laccases corroborate with the previous study[49] where optimum pH activity of white Laccase was reported at pH 4 and stable from pH 2–7. Similarly, relative activities of two Laccase isoforms (Lacc1 and Lacc2) from *Agaricus bisporus* CU13 were optimum at pH of 5 and 7, respectively, while the stability was reported at pH 7 and pH 9[50]. Here, optimum temperature of 30 °C and 50 °C were recorded for Laccase from *Tl*FLU1 and *Tp*FLU12, respectively, is corroborated with previous report[51] where a temperature of 30 °C best-enhanced Laccase activity of a Laccase from white-rot fungus *Trametes hirsute* and maintained its 80% activity at a temperature between 20 to 40 °C. Likewise, an optimum temperature of 50 °C has been implicated in enhancing the maximum activity for purified Laccase from *Lentinus tigrinus*[52]. The temperature stability of purified Laccase from *Tl*FLU1 (white Laccase), which is from 5 to 50 °C with over 90% residual activity after 24 h incubation period, is inconsonant with the previous report[53], where thermo-stability reported between 50 and 70 °C for Laccase from *Trichoderma harzianum* strain HZN10. Notably, the observed difference in Laccase activity between *Tl*FLU1 and *Tp*FLU12 at 5 °C could be attributed to the inherent genetic and physiological differences between the two strains[54–56]. *Tl*FLU1 might have a more robust cold-shock response mechanism that allows it to maintain higher Laccase activity at lower temperatures compared to *Tp*FLU12. This aligns with a previous report, where Laccase from *Thielavia terrastris* Co3Bag1 retains 86% of its activity after 12 d storage at 4 ˚C due to cold-shock response[57]. Similarly, it has been reported that Laccases from fungi can retain activity at low temperature (4–7 °C)[58]. Conversely, the substantial loss of activity in *Tp*FLU12 below 20 °C after 24 h of incubation could be since Laccase like many enzymes, has an optimal temperature range for activity[59]. At higher temperatures, fungi Laccases have been reported to possess characteristics of retaining more activity above 20 °C after 24 h[57]. Also, Psychrophilic Laccases, such as those produced by *Kabatiella bupleuri* G3 IBMiP which have been documented to have exhibit an optimal temperature range of 30–40 °C, with a significant decrease in activity below this ranges but still retains some activity even at 10 °C. This behaviour further attests to the substantial loss of activity in *Tp*FLU12 below 20 °C after 24 h of incubation period.

The effect of different metal ion concentrations on Laccase stability is highly imperative in assessing the enzyme's biotechnological applications. The significant low activity of Laccase from *Tl*FLU1 in the presence of metal ions (Al^{3+} and K^{+}) at a low concentration (10 mM) implies that these metal ions are activity inhibition stimulator which interferes with the electron transport system of Laccase activity. Similarly, a previous report linked Laccase inhibition with interaction of Fe^{2+} with the electron transport system of Laccase[60]. Laccase from *Ganoderma lucidum* showed complete activity inhibition in the presence of Fe^{2+} during the effect of metal ions

on reactive dye decolourization[61]. 1 mM K^+ reported to show 54% inhibition activity of Laccase from *Lentinula edodes*[62]. A detailed study on the inhibitory effect of metal ion concentration of 12.5 mM showed that Al^{3+} inhibit 55.9% and Mn^{2+} inhibit 63.5% Laccase activity on Laccase activity[63]. It is worth noting that the significant decrease in activity of Laccase from *Tl*FLU1 at concentrations above 10 mM suggests that Laccase activity is a function of the metal ions concentration[63]. Conversely, the increase in activity of Laccase from *Tp*FLU12 in the presence of high Ca^{2+}, Cd^{2+}, Co^{2+}, Cu^{2+} and Na^{2+} concentrations suggest them as a potent Laccase activity activator due to the oxidation state (divalent cations) of the metal ions. It is opined that divalent cations of metal ions enhance Laccase activity and stability which aided in its binding to the carboxylic group of aspartic and glutamic acid residues for better complete substrate consumption and catalytic effect activation[64]. Also, the stability of Laccase activity to a high concentration of Cu^{2+} (100 mM) might be due to the type-2 copper-binding sites filled by the copper ions[62].

The phenomenon of Laccase activity stability at a varying concentration of hydrophobic and hydrophilic organic solvents in this study could be ascribed to the stripping-off of the crucial bound-water monolayer from the enzyme molecule[64]. Also, the variability in the stability of purified Laccase from *Tp*FLU12 observed at high organic solvents concentrations could be linked to each solvent's physical and chemical properties, the mixture pH, log P of the solvent and thermodynamic activity of water in mixed systems[23,65]. Unlike Laccase from *Tp*FLU12, Laccase from *Tl*FLU1 could not tolerate low water content systems containing organic solvents, which explains why high organic solvent concentrations inhibited its stability. A similar observation has been reported previously[66], where Laccase stability was inhibited at high organic solvent concentrations after an hour incubation period which was credited to a low water content of the solvent.

The extent of the inhibitory effect of metalloenzymes and detergents varied greatly with their concentrations. The high inhibitory effect of NaN_3 in both strains is due to internal electron transfer obstruction at the types 2 and 3 Laccase copper atom binding sites[65]. The high inhibition rate of the chelating agent (EDTA), denaturing agents DDT and SDS at varying concentrations could be justified by their interactions between the substrate and the Laccase active site leading to the unfolding of the compact protein structure during the catalytic enzyme activity[48]. Likewise, the high inhibition by NaN_3 and EDTA is due to the chelating effect on the Cu atoms, which leads to inactivation of the Laccase[12], while high inhibition by DTT suggests the strong inhibitory effect on the di-sulphide bonds present at the Laccase active domain[33].

The obtained K_m and K_{cat} values established the superior affinity of the purified Laccases towards substrate ABTS as compared to other phenolic substrates (2,6 DMP, caffeic acid and guaiacol). This observation agrees with the previous reports[48], where strong affinity towards ABTS as substrate was documented during the characterization of Laccase from an ascomycetes fungi, *Thielavia sp.* In comparison with that of Laccase from *Tp*FLU12 (blue Laccase), the observed high K_m and v_{max} values for purified Laccase of *Tl*FLU1 (white Laccase) in the presence ABTS, 2,6 DMP, caffeic acid and guaiacol confirm the characteristics of a yellow Laccase of fungi origin[24,44].

The ES-MS generated unique Laccase peptides from Laccases from *Tl*FLU1 and *Tp*FLU12 and showed different numbers of protein clusters suggesting that these ascomycetes fungi produce two types of Laccases. The most likely explanation for this observation is that the number of Cys residues in the putative copper-binding site in the peptide sequence leads to the formation of two disulphide bridges which are known to be titratable in non-reducing conditions, a sole characteristic type-I copper (blue Laccase)[67]. Also, changes in the valence state of the Laccase Cu^{2+} residues and Fe^{2+} residues with a low spin electronic configuration account for the lack of blue colouration in white Laccase from *Tl*FLU1 could be attributed to the differences in the numbers of protein clusters and unique Laccase peptides[49]. The variation in ascomycetes amino acids sequence number and structural differences in sensu stricto Laccases is linked to variation in the number of their encoding genes[68].

Sequence homology analysis according to the LOMETS threading programs of the I-TASSER server revealed that variation in consensus sequence of Laccases from *Tl*FLU1 and *Tp*FLU12 which ranges between 42 and 67 suggests these sites as a major contributing factor to the protein stability due to non-covalent interactions[69]. Similarly, a previous report, demonstrated how 20 consensus mutation sequence cloned into *Saccharomyces cerevisiae* was linked to stabilizing Laccase with high-redox without compromising its catalytic activity[70].

Prediction of binding site residues such as Pro-177, Ala-178, Aap-179, Lys-180, Lys-182, Asp-183, Ser-258, Ala-259, Leu-260, His-261, Val-263, Arg-298, Thr-300, Leu-312, Asp-313, Ala-314, Pro-315, Ala-316, Asn-355, Trp-356 and Ile-358, His-19, Ile-60 and Arg-62 in Laccases from both strains further strengthen the result of this study that the purified enzyme is Laccase with high catalytic activity since their high conservation across the amino acid sequences have been linked in the stabilization of the protein secondary structure leading to correct formation of the copper-binding site[71]. Similarly, it is opined that positively charged amino acids like Arg), His and Lys are responsible for the favourable conformation changes in Laccase leading to an increase in its catalytic activity[69]. It is previously demonstrated how binding residues such as Ala191, Pro192, Glu235, Leu363, Phe371, Trp373, Phe427, Leu429, Trp507 and His508 are crucial in the oxidation of phenolics during the structure–function studies of *Melanocarpus albomyces* Laccase[72]. Additionally, the Laccase gene ontology predicted molecular functions such as copper ion binding, oxidoreductase activity and Laccase activity, biological processes such as oxidation–reduction, lignin metabolism, phenylpropanoid catabolic, biological adhesion, cellular metabolism, cellular metal ion homeostasis, aromatic compound metabolism and cellulose metabolism and cellular component such as extracellular structure is not surprising because Laccases are known as oxidoreductases[68], with Cu atoms in the active site, capable of lignin metabolism[73,74], phenylpropanoid[75], biological adhesion[74], aromatic compound metabolism like fluorene[76], cellular metal ion homeostasis[77] and cellulose metabolism[78].

The TM-score (0.48 ± 0.15 and 0.53 ± 0.15), and RMSD values (1.13 ± 0.5 Å and 1.15 ± 0.5 Å) observed in the model structure prediction for Laccases from *Tl*FLU1 and *Tp*FLU12, respectively, indicted a moderate degree of structural similarity with the PDB hit template used for model prediction since TM score close to 1 is classified as a perfect match with template structure, while a lower RMSD indicates a better structural alignment or match with template structure[36,37]. Despite covering a substantial portion of the hit structure, as indicated by

the coverage (Cov) values of 81% and 73% for Laccases from *Tl*FLU1 and *Tp*FLU12, respectively, the aligned sequences displayed a relatively low sequence identity (24% and 18%). The most probable explanation for this observation can be linked to evolutionary divergences between the taxa of the template used and that of Laccases from *Tl*FLU1 and *Tp*FLU12[79]. Similarly, a previous study opined further that as species diverge evolutionarily, the sequence identity between their protein-coding regions may decrease due to changes in selective pressures and the fixation of different alleles[80]. Further, verify3D is a commonly used method for evaluating the quality of protein models. It compares the 3D environment of each residue in the model with high-resolution structures, assigning a 3D-1D score based on compatibility[81]. The predicted protein structure model obtained a high 3D-1D score in this study, indicating its excellent quality and similarity in overall shape and active site with the template structure[82]. The underlying assumption of verify3D is that a good 3D-1D score implies a similar structural arrangement to well-established protein structures[83]. Therefore, if the model's residues exhibit comparable structural characteristics and environments to those in known high-quality structures, it suggests that the model itself is likely of good quality.

Bioinformatics analysis by ProtParam further lends credence to this study finding that the two strains possess two different Laccase types. The predicted molecular weight of 44 and 68.6 kDa and theoretical pI values 5.22 and 6.32 agree with previous studies, where Laccase amino acids sequence of 566–600 aa, a molecular weight of 61.83–66.84 KDa and pl of pH 4–6 have been documented in *Trichoderma* Laccases[68]. While an amino acids sequence of 594 and with a molecular weight of 66.6 kDa close to this study has been reported in *Talaromyces marneffei* (strain ATCC 18,224/CBS 334.59/QM 7333). The predicted low instability indices (39.54 for *Tl*FLU1 and 33.43 for *Tp*FLU12) further gave an insight that the enzyme could be stable under harsh conditions. This prediction agrees with the previous report[84] where low instability indices of 31.92 was linked to the Laccase from *Kurthia huakuii* stability under harsh conditions. Similarly, a report[85] documented how low Laccase instability indices of 34.70 close to this study's prediction gave 40% of the Laccase relative activity at 70 °C after 60 min incubation period. In addition, the predicted aliphatic index values of the Laccase proteins ranged from 76.58 to 77.50 with a GRAVY index values mostly negative suggesting this protein to be thermophilic and hydrophilic nature. This prediction is in corroborated with previous reports[86] where aliphatic index values of the Laccase proteins ranged from 74.44 to 90.4 with negative values of GRAVY index were attributed to the thermophilic and hydrophilic nature of Laccase during the comparative modelling and molecular docking analysis of white, brown and soft rot fungal Laccases using lignin model compounds for understanding the structural and functional properties of Laccases.

The findings of this study suggest that Laccase enzymes from *Tl*FLU1 and *Tp*FLU12 have the potential to degrade fluoranthene and anthracene, two commonly encountered PAHs of environmental concern. This observation is consistent with previous research highlighting the ability of fungi Laccase (50 U) purified from *Leucoagaricus gongylophorus* in degrading 10 ppm of anthracene (72 ± 1%), fluorene (40 ± 3%) and phenanthrene (25 ± 3%), respectively at pH 6 and 30 °C under 24 h incubation period[28]. Similarly, a previous study demonstrated the degradation of chrysene (75.8%) and Benzo[a]pyrene (35.6%), using a Laccase from *Trametes versicolor*[29].

Conclusion

The study demonstrated the utilization of anthracene as carbon and energy sources by *Tl*FLU1 and *Tp*FLU12, resulted in the production of Laccase enzymes with broad catalytic potentials. The enzymes with molecular mass of 44 kDa and 68.7 kDa respectively, exhibit different optimum pH and temperature ranges with an implication potential application across various conditions. Despite the differences, both enzymes showed an enhanced activity under diverse metal ions and organic solvents. Structural predictions suggest that the differing in the copper atoms in the active sites contribute to their varied optimal pH. Additionally, the functional analysis indicates their involvement in key biological processes such as oxidation–reduction, lignin metabolism and aromatic compounds metabolism. This study provides valuable insights into the potential of Laccase-based systems for PAH removal and highlighting the potential of these enzymes as eco-friendly alternative for xenobiotic degradation.

Data availability

Data is provided within the manuscript or supplementary information files.

Received: 4 March 2024; Accepted: 4 June 2024
Published online: 11 June 2024

References

1. Mishra, S. *et al.* Recent advanced technologies for the characterization of xenobiotic-degrading microorganisms and microbial communities. *Front. Bioeng. Biotechnol.* **9**, 1–26. https://doi.org/10.3389/fbioe.2021.632059 (2021).
2. Zafra, G. & Cortés-Espinosa, D. V. Biodegradation of polycyclic aromatic hydrocarbons by *Trichoderma species*: A mini review. *Environ. Sci. Pollut. Res.* **22**, 19426–19433. https://doi.org/10.1007/s11356-015-5602-4 (2015).
3. Frisvad, J. C. Taxonomy, chemodiversity, and chemoconsistency of Aspergillus, Penicillium, and Talaromyces species. *Front. Microbiol.* **5**, 1–7. https://doi.org/10.3389/fmicb.2014.00773 (2015).
4. Mate, D. M. & Alcalde, M. Laccase: A multi-purpose biocatalyst at the forefront of biotechnology. *Microb. Biotechnol.* **10**, 1457–1467. https://doi.org/10.1111/1751-7915.12422 (2017).
5. Zhuo, R. & Fan, F. A comprehensive insight into the application of white rot fungi and their lignocellulolytic enzymes in the removal of organic pollutants. *Sci. Total Environ.* **778**, 146132. https://doi.org/10.1016/j.scitotenv.2021.146132 (2021).
6. Chen, L., Zhang, X., Zhang, M., Zhu, Y. & Zhuo, R. Removal of heavy-metal pollutants by white rot fungi: Mechanisms, achievements, and perspectives. *J. Clean. Prod.* **354**, 131681. https://doi.org/10.1016/j.jclepro.2022.131681 (2022).
7. Kumar, A. & Chandra, R. Ligninolytic enzymes and its mechanisms for degradation of lignocellulosic waste in environment. *Heliyon* **6**, e03170. https://doi.org/10.1016/j.heliyon.2020.e03170 (2020).

8. Xu, P. *et al.* Degradation of several polycyclic aromatic hydrocarbons by Laccase in reverse micelle system. *Sci. Total Environ.* **708**, 134970–134970. https://doi.org/10.1016/j.scitotenv.2019.134970 (2020).
9. Chen, S., Zhu, M., Guo, X., Yang, B. & Zhuo, R. Coupling of Fenton reaction and white rot fungi for the degradation of organic pollutants. *Ecotoxicol. Environ. Saf.* **254**, 114697. https://doi.org/10.1016/j.ecoenv.2023.114697 (2023).
10. Gao, X. *et al.* Copper removal from aqueous solutions by white rot fungus Pleurotus ostreatus GEMB-PO1 and its potential in co-remediation of copper and organic pollutants. *Bioresour. Technol.* **395**, 130337. https://doi.org/10.1016/j.biortech.2024.130337 (2024).
11. Falade, A., Jaouani, A., Mabinya, L., Okoh, A. & Nwodo, U. Exoproduction and molecular characterization of peroxidase from *Ensifer adhaerens*. *Appl. Sci.* **9**, 1–15. https://doi.org/10.3390/app9153121 (2019).
12. Sondhi, S., Kaur, R. & Madan, J. Purification and characterization of a novel white highly thermo stable Laccase from a novel *Bacillus* sp. MSK-01 having potential to be used as anticancer agent. *Int. J. Biol. Macromol.* **170**, 232–238. https://doi.org/10.1016/j.ijbiomac.2020.12.082 (2021).
13. Zhu, Y. *et al.* Laccase directed lignification is one of the major processes associated with the defense response against pythium ultimum infection in apple roots. *Front. Plant Sci.* **12**, 1862–1862. https://doi.org/10.3389/FPLS.2021.629776/BIBTEX (2021).
14. Yang, C. H. *et al.* Involvement of Laccase2 in cuticle sclerotization of the whitefly, *Bemisia tabaci* middle East-Asia minor 1. *Insects* **13**, 471. https://doi.org/10.3390/insects13050471 (2022).
15. Sakamoto, Y. Influences of environmental factors on fruiting body induction, development and maturation in mushroom-forming fungi. *Fungal Biol. Rev.* **32**, 236–248. https://doi.org/10.1016/J.FBR.2018.02.003 (2018).
16. Yan, L., Xu, R., Bian, Y., Li, H. & Zhou, Y. Expression profile of Laccase gene family in white-rot basidiomycete *Lentinula edodes* under different environmental stresses. *Genes* **10**, 1045–1045. https://doi.org/10.3390/GENES10121045 (2019).
17. Zhu, X. & Williamson, P. R. Role of Laccase in the biology and virulence of *Cryptococcus neoformans*. *FEMS Yeast Res.* **5**, 1–10. https://doi.org/10.1016/J.FEMSYR.2004.04.004 (2004).
18. Williamson, P. R. Role of Laccase in the virulence of *Talaromyces marneffei*: A common link between AIDS-related fungal pathogens?. *Virulence* **7**, 627–629. https://doi.org/10.1080/21505594.2016.1198867 (2016).
19. Santo, M., Weitsman, R. & Sivan, A. The role of the copper-binding enzyme–Laccase–in the biodegradation of polyethylene by the actinomycete *Rhodococcus ruber*. *Int. Biodeteriorat. Biodegrad.* **84**, 204–210. https://doi.org/10.1016/j.ibiod.2012.03.001 (2013).
20. Chauhan, P. S., Goradia, B. & Saxena, A. Bacterial laccase: Recent update on production, properties and industrial applications. *3 Biotech* **7**, 323–323. https://doi.org/10.1007/s13205-017-0955-7 (2017).
21. Arregui, L. *et al.* Laccases: Structure, function, and potential application in water bioremediation. *Microb. Cell Fact.* https://doi.org/10.1186/s12934-019-1248-0 (2019).
22. Ali, W. B. *et al.* Enzyme properties of a laccase obtained from the transcriptome of the marine-derived fungus *Stemphylium lucomagnoense*. *Int. J. Mol. Sci.* **21**, 1–16. https://doi.org/10.3390/ijms21218402 (2020).
23. Radveikienė, I., Vidžiūnaitė, R., Meškienė, R., Meškys, R. & Časaitė, V. Characterization of a yellow Laccase from *Botrytis cinerea* 241. *J. Fungi* **7**, 1–16. https://doi.org/10.3390/jof7020143 (2021).
24. Agrawal, K. & Verma, P. Multicopper oxidase laccases with distinguished spectral properties: A new outlook. *Heliyon* **6**, e03972–e03972. https://doi.org/10.1016/j.heliyon.2020.e03972 (2020).
25. Mot, A. C. *et al.* "Yellow" Laccase from *Sclerotinia sclerotiorum* is a blue laccase that enhances its substrate affinity by forming a reversible tyrosyl-product adduct. *Plos One* **15**, e0225530. https://doi.org/10.1371/journal.pone.0225530 (2020).
26. Sekretaryova, A., Jones, S. M. & Solomon, E. I. O_2 Reduction to water by high potential multicopper Oxidases: Contributions of the T1 copper site potential and the local environment of the trinuclear copper cluster. *J. Am. Chem. Soc.* **141**, 11304–11314. https://doi.org/10.1021/jacs.9b05230 (2019).
27. Li, X. *et al.* Optimization of laccase-mediated benzo[a]pyrene oxidation and the bioremedial application in aged polycyclic aromatic hydrocarbons-contaminated soil. *J. Health Sci.* **56**, 534–540. https://doi.org/10.1248/jhs.56.534 (2010).
28. Vipotnik, Z., Michelin, M. & Tavares, T. Development of a packed bed reactor for the removal of aromatic hydrocarbons from soil using Laccase/mediator feeding system. *Microbiol. Res.* **245**, 126687–126687. https://doi.org/10.1016/j.micres.2020.126687 (2021).
29. Ike, P. T. L., Birolli, W. G., dos Santos, D. M., Porto, A. L. M. & Souza, D. H. F. Biodegradation of anthracene and different PAHs by a yellow laccase from *Leucoagaricus gongylophorus*. *Environ. Sci. Pollut. Res.* **26**, 8675–8684. https://doi.org/10.1007/s11356-019-04197-z (2019).
30. Egbewale, S. O., Kumar, A., Mokoena, M. P. & Olaniran, A. O. Metabolic biodegradation pathway of fluoranthene by indigenous *Trichoderma lixii* and *Talaromyces pinophilus* spp. *Catalysts* **13**, 791. https://doi.org/10.3390/catal13050791 (2023).
31. Lowry, O. H., Rosebrough, N. J., Farr, A. L. & Randall, R. J. Protein measurement with the Folin phenol reagent. *J. Gen. Microbiol.* **31**, 3017–3027. https://doi.org/10.1016/S0021-9258(19)52451-6 (1951).
32. Zungu, N. S., Egbewale, S. O., Olaniran, A. O., Pérez-Fernández, M. & Magadlela, A. Soil nutrition, microbial composition and associated soil enzyme activities in KwaZulu-Natal grasslands and savannah ecosystems soils. *Appl. Soil Ecol.* **155**, 103663–103663. https://doi.org/10.1016/j.apsoil.2020.103663 (2020).
33. Wu, Y. R., Luo, Z. H., Kwok-Kei Chow, R. & Vrijmoed, L. L. P. Purification and characterization of an extracellular Laccase from the anthracene-degrading fungus *Fusarium solani* MAS2. *Bioresour. Technol.* **101**, 9772–9777. https://doi.org/10.1016/j.biortech.2010.07.091 (2010).
34. Ning, Y.-J. *et al.* An extracellular yellow Laccase with potent dye decolorizing ability from the fungus *Leucoagaricus naucinus* LAC-04. *Int. J. Biol. Macromol.* **93**, 837–842. https://doi.org/10.1016/j.ijbiomac.2016.09.046 (2016).
35. Setlhare, B., Kumar, A., Mokoena, M. P., Pillay, B. & Olaniran, A. O. Phenol hydroxylase from *Pseudomonas* sp. KZNSA: Purification, characterization and prediction of three-dimensional structure. *Int. J. Biol. Macromol.* **146**, 1000–1008. https://doi.org/10.1016/j.ijbiomac.2019.09.224 (2020).
36. Wei, Z. *et al.* Folding non-homology proteins by coupling deep-learning contact maps with I-TASSER assembly simulations. *Cell Rep. Methods* **1**, 100014. https://doi.org/10.1016/j.crmeth.2021.100014 (2021).
37. Yang, J. & Zhang, Y. I-TASSER server: New development for protein structure and function predictions. *Nucleic Acids Res.* **43**, W174–W181. https://doi.org/10.1093/nar/gkv342 (2015).
38. Zhang, C., Freddolino, P. L. & Zhang, Y. COFACTOR: Improved protein function prediction by combining structure, sequence and protein–protein interaction information. *Nucleic Acids Res.* **45**, W291–W299. https://doi.org/10.1093/nar/gkx366 (2017).
39. Waterhouse, A. M., Procter, J. B., Martin, D. M. A., Clamp, M. & Barton, G. J. Jalview Version 2—A multiple sequence alignment editor and analysis workbench. *Bioinformatics* **25**, 1189–1191. https://doi.org/10.1093/bioinformatics/btp033 (2009).
40. Tamura, K., Stecher, G. & Kumar, S. MEGA11: Molecular evolutionary genetics analysis version 11. *Mol. Biol. Evol.* **38**, 3022–3027. https://doi.org/10.1093/molbev/msab120 (2021).
41. Zelinkova, Z. & Wenzl, T. The occurrence of 16 EPA PAHs in food—A review. *Polycycl. Aromat. Compd.* **35**, 248–284. https://doi.org/10.1080/10406638.2014.918550 (2015).
42. Cambria, M. T., Minniti, Z., Librando, V. & Cambria, A. Degradation of polycyclic aromatic hydrocarbons by *Rigidoporus* lignosus and its laccase in the presence of redox mediators. *Appl. Biochem. Biotechnol.* **149**, 1–8. https://doi.org/10.1007/s12010-007-8100-4 (2008).
43. Ezike, T. C., Ezugwu, A. L., Udeh, J. O., Eze, S. O. O. & Chilaka, F. C. Purification and characterisation of new laccase from *Trametes polyzona* WRF03. *Biotechnol. Rep.* **28**, e00566. https://doi.org/10.1016/j.btre.2020.e00566 (2020).

44. Mukhopadhyay, M. & Banerjee, R. Purification and biochemical characterization of a newly produced yellow Laccase from *Lentinus squarrosulus* MR13. *3 Biotech* **5**, 227–236. https://doi.org/10.1007/s13205-014-0219-8 (2015).
45. Agrawal, K., Bhardwaj, N., Kumar, B., Chaturvedi, V. & Verma, P. Process optimization, purification and characterization of alkaline stable white laccase from *Myrothecium verrucaria* ITCC-8447 and its application in delignification of agroresidues. *Int. J. Biol. Macromol.* **125**, 1042–1055. https://doi.org/10.1016/j.ijbiomac.2018.12.108 (2019).
46. Schückel, J., Matura, A. & van Pée, K. H. One-copper Laccase-related enzyme from *Marasmius* sp.: Purification, characterization and bleaching of textile dyes. *Enz. Microb. Technol.* **48**, 278–284. https://doi.org/10.1016/j.enzmictec.2010.12.002 (2011).
47. Jeon, S. J. & Lim, S. J. Purification and characterization of the laccase involved in dye decolorization by the white-rot fungus *Marasmius scorodonius*. *J. Microbiol. Biotechnol.* **27**, 1120–1127. https://doi.org/10.4014/jmb.1701.01004 (2017).
48. Mtibaà, R. *et al.* Purification and characterization of a fungal laccase from the ascomycete *Thielavia* sp. and its role in the decolorization of a recalcitrant dye. *Int. Biodeteriorat. Biodegrad.* **120**, 1744–1751. https://doi.org/10.1016/j.ijbiomac.2018.09.175 (2018).
49. Zhao, D., Zhang, X., Cui, D. & Zhao, M. Characterisation of a novel white laccase from the deuteromycete fungus *Myrothecium verrucaria* NF-05 and its decolourisation of dyes. *Plos One* **7**, e38817. https://doi.org/10.1371/journal.pone.0038817 (2012).
50. Othman, A. M., Elsayed, M. A., Elshafei, A. M. & Hassan, M. M. Purification and biochemical characterization of two isolated Laccase isoforms from *Agaricus bisporus* CU13 and their potency in dye decolorization. *Int. J. Biol. Macromol.* **113**, 1142–1148. https://doi.org/10.1016/j.ijbiomac.2018.03.043 (2018).
51. Navada, K. K. & Kulal, A. Kinetic characterization of purified Laccase from *Trametes hirsuta*: A study on Laccase catalyzed biotransformation of 1,4-dioxane. *Biotechnol. Lett.* **43**, 613–626. https://doi.org/10.1007/s10529-020-03038-1 (2021).
52. Sadeghian-Abadi, S., Rezaei, S., Yousefi-Mokri, M. & Faramarzi, M. A. Enhanced production, one-step affinity purification, and characterization of Laccase from solid-state culture of *Lentinus tigrinus* and delignification of pistachio shell by free and immobilized enzyme. *J. Environ. Manag.* **244**, 235–246. https://doi.org/10.1016/j.jenvman.2019.05.058 (2019).
53. Bagewadi, Z. K., Mulla, S. I. & Ninnekar, H. Z. Purification and immobilization of laccase from *Trichoderma harzianum* strain HZN10 and its application in dye decolorization. *J. Genet. Eng. Biotechnol.* **15**, 139–150. https://doi.org/10.1016/j.jgeb.2017.01.007 (2017).
54. Liu, X., Zain Ul Arifeen, M., Xue, Y. & Liu, C. Genome-wide characterization of laccase gene family in Schizophyllum commune 20R–7-F01, isolated from deep sediment 2 km below the seafloor. *Front. Microbiol.* **13**, 923451. https://doi.org/10.3389/fmicb.2022.923451 (2022).
55. Xu, X., Zhang, Y., Liang, M., Kong, W. & Liu, J. The citrus Laccase gene CsLAC18 contributes to cold tolerance. *Int. J. Mol. Sci.* **23**, 14509 (2022).
56. Sharma, V., Upadhyay, L. S. B. & Vasanth, D. Extracellular thermostable Laccase-like enzymes from *Bacillus licheniformis* strains: Production, purification and characterization. *Appl. Biochem. Microbiol.* **56**, 420–432. https://doi.org/10.1134/S000368382004014 6 (2020).
57. Gutiérrez-Antón, M. *et al.* Improvement of Laccase production by Thielavia terrestris Co3Bag1. Enhancing the bio-catalytic performance of the native thermophilic TtLacA via immobilization in copper alginate gel beads. *J. Fungi* **9**, 308 (2023).
58. Chatterjee, R., Johansson, K., Järnström, L. & Jönsson, L. J. Evaluation of the potential of fungal and plant Laccases for active-packaging applications. *J. Agric. Food Chem.* **59**, 5390–5395. https://doi.org/10.1021/jf103811g (2011).
59. Quynh, D. T., Hoang, N. H., Lan, N. N., Hoang, L. V. & Nghi, D. H. Cloning, experession, and characterization of a Laccase from the white rot fungi *Pleurotus pulmonarius* MPN18. *VNU J. Sci. Nat. Sci. Technol.* **39**, 59–67. https://doi.org/10.25073/2588-1140/vnunst.5312 (2023).
60. Lin, Y. *et al.* Purification and characterization of a novel Laccase from *Coprinus cinereus* and decolorization of different chemically dyes. *Mol. Biol. Rep.* **40**, 1487–1494. https://doi.org/10.1007/s11033-012-2191-x (2013).
61. Murugesan, K., Kim, Y. M., Jeon, J. R. & Chang, Y. S. Effect of metal ions on reactive dye decolorization by laccase from *Ganoderma lucidum*. *J. Hazard. Mater.* **168**, 523–529. https://doi.org/10.1016/j.jhazmat.2009.02.075 (2009).
62. Nagai, M. *et al.* Purification and characterization of an extracellular laccase from the edible mushroom *Lentinula edodes*, and decolorization of chemically different dyes. *Appl. Microbiol. Biotechnol.* **60**, 327–335. https://doi.org/10.1007/s00253-002-1109-2 (2002).
63. Zhang, G. Q., Wang, Y. F., Zhang, X. Q., Ng, T. B. & Wang, H. X. Purification and characterization of a novel Laccase from the edible mushroom *Clitocybe maxima*. *Process Biochem.* **45**, 627–633. https://doi.org/10.1016/j.procbio.2009.12.010 (2010).
64. Rezaei, S., Shahverdi, A. R. & Faramarzi, M. A. Isolation, one-step affinity purification, and characterization of a polyextremotolerant Laccase from the halophilic bacterium *Aquisalibacillus elongatus* and its application in the delignification of sugar beet pulp. *Bioresour. Technol.* **230**, 67–75. https://doi.org/10.1016/j.biortech.2017.01.036 (2017).
65. Sadhasivam, S., Savitha, S., Swaminathan, K. & Lin, F.-H. Production, purification and characterization of mid-redox potential Laccase from a newly isolated *Trichoderma harzianum* WL1. *Process Biochem.* **43**, 736–742. https://doi.org/10.1016/j.procbio.2008.02.017 (2008).
66. Lueangjaroenkit, P. *et al.* Two Manganese peroxidases and a Laccase of *Trametes polyzona* KU-RNW027 with novel properties for dye and pharmaceutical product degradation in redox mediator-free system. *Mycobiology* **47**, 217–229. https://doi.org/10.1080/12298093.2019.1589900 (2019).
67. Giardina, P. *et al.* Protein and gene structure of a blue laccase from *Pleurotus ostreatus*. *Biochem. J.* **341**, 655–663. https://doi.org/10.1042/BJ3410655 (1999).
68. Cázares-García, S. V., Vázquez-Garcidueñas, M. S. & Vázquez-Marrufo, G. Structural and phylogenetic analysis of Laccases from *Trichoderma*: A bioinformatic approach. *Plos One* **8**, e55295. https://doi.org/10.1371/journal.pone.0055295 (2013).
69. Nadar, S. S. & Rathod, V. K. Amino acid induced hyper activation of laccase and its application in dye degradation. *Biocatal. Agric. Biotechnol.* **18**, 101064. https://doi.org/10.1016/j.bcab.2019.101064 (2019).
70. Gomez-Fernandez, B. J., Risso, V. A., Sanchez-Ruiz, J. M. & Alcalde, M. Consensus design of an evolved high-redox potential Laccase. *Front. Bioeng. Biotechnol.* **8**, 354–354. https://doi.org/10.3389/FBIOE.2020.00354/BIBTEX (2020).
71. Mehra, R., Muschiol, J., Meyer, A. S. & Kepp, K. P. A structural-chemical explanation of fungal Laccase activity. *Sci. Rep.* **8**, 1–16. https://doi.org/10.1038/s41598-018-35633-8 (2018).
72. Kallio, J. P. *et al.* Structure-function studies of a *Melanocarpus albomyces* Laccase suggest a pathway for oxidation of phenolic compounds. *J. Mol. Biol.* **392**, 895–909. https://doi.org/10.1016/j.jmb.2009.06.053 (2009).
73. Fernández-Fueyo, E., Ruiz-Dueñas, F. J., MikiY, M. M. J., Hammel, K. E. & Martínez, A. T. Lignin-degrading peroxidases from genome of selective ligninolytic fungus *Ceriporiopsis subvermispora*. *J. Biol. Chem.* **287**, 16309–16916. https://doi.org/10.1074/jbc.M112.356378 (2012).
74. Fathi-Roudsari, M., Behmanesh, M., Salmanian, A.-H., Sadeghizadeh, M. & Khajeh, K. Iranian biomedical functional surface display of laccase in a phenol-inducible bacterial circuit for bioremediation purposes. *Iran Biomed. J.* **22**, 202–209. https://doi.org/10.22034/ibj.22.3.202 (2018).
75. Hu, Q. *et al.* Laccase GhLac1 modulates broad-spectrum biotic stress tolerance via manipulating phenylpropanoid pathway and jasmonic acid synthesis. *Plant Physiol.* **176**, 1808–1823. https://doi.org/10.1104/pp.17.01628 (2018).
76. Bankole, P. O., Semple, K. T., Jeon, B. H. & Govindwar, S. P. Biodegradation of fluorene by the newly isolated marine-derived fungus, *Mucor irregularis* strain bpo1 using response surface methodology. *Ecotoxicol. Environ. Saf.* **208**, 111619–111619. https://doi.org/10.1016/j.ecoenv.2020.111619 (2021).

77. Huang, W., Zhang, W., Gan, Y., Yang, J. & Zhang, S. Laccase immobilization with metal-organic frameworks: Current status, remaining challenges and future perspectives. *Crit. Rev. Environ. Sci. Technol.* **52**, 1282–1324. https://doi.org/10.1080/10643389.2020.1854565 (2022).
78. Oliva-Taravilla, A., Tomás-Pejó, E., Demuez, M., González-Fernández, C. & Ballesteros, M. Inhibition of cellulose enzymatic hydrolysis by Laccase-derived compounds from phenols. *Biotechnol. Prog.* **31**, 700–706. https://doi.org/10.1002/BTPR.2068 (2015).
79. Di Franco, A., Poujol, R., Baurain, D. & Philippe, H. Evaluating the usefulness of alignment filtering methods to reduce the impact of errors on evolutionary inferences. *BMV Evol. Biol.* **19**, 21. https://doi.org/10.1186/s12862-019-1350-2 (2019).
80. Malhis, N., Jones, S. J. M. & Gsponer, J. Improved measures for evolutionary conservation that exploit taxonomy distances. *Nat. Commun.* **10**, 1556. https://doi.org/10.1038/s41467-019-09583-2 (2019).
81. Singh, A. K., Katari, S. K., Umamaheswari, A. & Raj, A. In silico exploration of lignin peroxidase for unraveling the degradation mechanism employing lignin model compounds. *RCS Adv.* **11**, 14632–14653. https://doi.org/10.1039/D0RA10840E (2021).
82. Vanajothi, R. *et al.* In silico and in vitro analysis of *Nigella sativa* bioactives against Chorismate synthase of *Listeria monocytogenes*: A target protein for biofilm inhibition. *Appl. Biochem. Biotechnol.* **195**, 519–533. https://doi.org/10.1007/s12010-022-04157-3 (2023).
83. Nelapati, A. K., Meena, S., Singh, A. K., Bhakta, N. & PonnanEttiyappan, J. In silico structural and functional analysis of *Bacillus* uricases. *Curr. Prot.* **18**, 124–142. https://doi.org/10.2174/1570164617999200512081127 (2021).
84. Guo, X. *et al.* Characterization of a highly thermostable and organic solvent-tolerant copper-containing polyphenol Oxidase with dye-decolorizing ability from *Kurthia huakuii* LAM0618T. *Plos One* **11**, e0164810. https://doi.org/10.1371/JOURNAL.PONE.0164810 (2016).
85. Endo, K. *et al.* Enzymological characterization of EpoA, a laccase-like phenol oxidase produced by *Streptomyces griseus*. *J. Biochem.* **133**, 671–677. https://doi.org/10.1093/jb/mvg086 (2003).
86. Kumar, A., Kameshwar, S., Barber, R. & Qin, W. Comparative modeling and molecular docking analysis of white, brown and soft rot fungal Laccases using lignin model compounds for understanding the structural and functional properties of Laccases. *J. Mol. Graph Model* **79**, 15–26. https://doi.org/10.1016/j.jmgm.2017.10.019 (2018).

Acknowledgements

The authors appreciate Dr Mare Vlok of the central analytical facility, Stellenbosch, South Africa for the Liquid-Chromatography Mass-Spectrometry proteomics analysis of the protein.

Author contributions

Conceptualization, S.O.E. and A.O.O.; methodology, S.O.E. and A.K.; vali-dation, S.O.E., A.K., and A.O.O.; formal analysis, S.O.E. and A.K.; investigation, S.O.E. and A.O.O.; resources, M.P.M. and A.O.O.; data curation, S.O.E. and A.K.; writing-S.O.E.; writing-A.K. and A.O.O.; visualization, S.O.E.; supervision, M.P.M. and A.O.O.; project administration, A.O.O.; funding acquisition, A.O.O. and M.P.M. All authors have read and agreed to the published version of the manuscript.

Funding

National Research Foundation, South Africa (Grant No: 94036 and 92803).

Competing interests

The authors declare no competing interests.

Additional information

Supplementary Information The online version contains supplementary material available at https://doi.org/10.1038/s41598-024-63959-z.

Correspondence and requests for materials should be addressed to A.O.O.

SUPPLEMENTARY MATERIALS

Journal: Scientific Reports

Purification, Characterization and Three-Dimensional Structure Prediction of Multicopper Oxidase Laccases from *Trichoderma lixii* FLU1 and *Talaromyces pinophilus* FLU12

Samson O. Egbewale, Ajit Kumar, Mduduzi P. Mokena, Ademola O. Olaniran*

Discipline of Microbiology, University of KwaZulu- Natal (Westville Campus), Durban, Republic of South Africa.

* Corresponding author. Tel. +27 31 260 7400

Fax: +27 31 260 7809

Email address: olanirana@ukzn.ac.za

Figure S1: Raw gel for figure 1a. Area shown in the box was cropped and presented as Figure 1a.

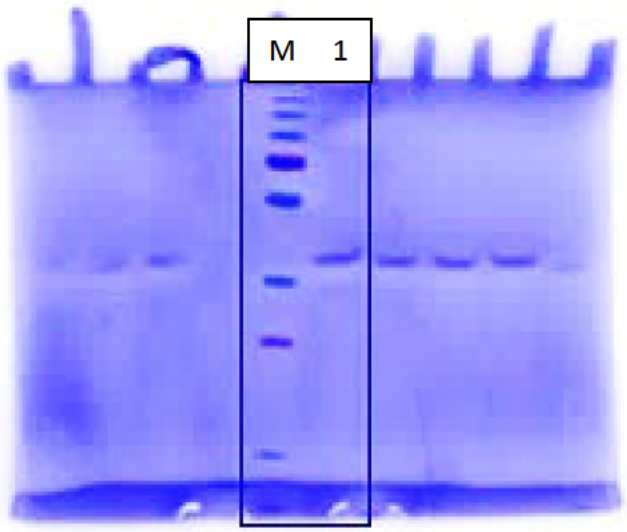

Figure S2: Raw gel for figure 1b. Area shown in the box was cropped and presented as Figure 1b.

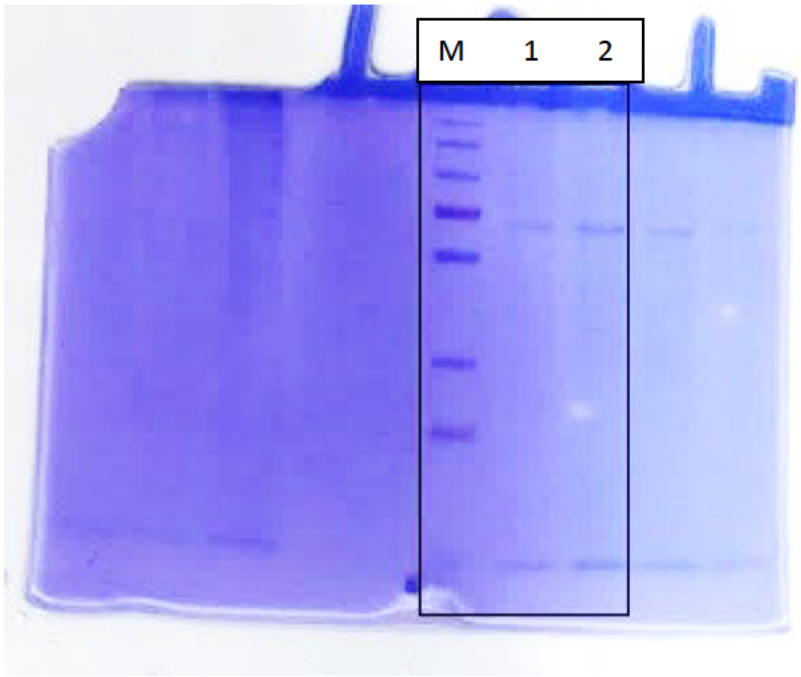

Figure S3: Raw gel for figure 1c. Area shown in the box was cropped and presented as Figure 1c.

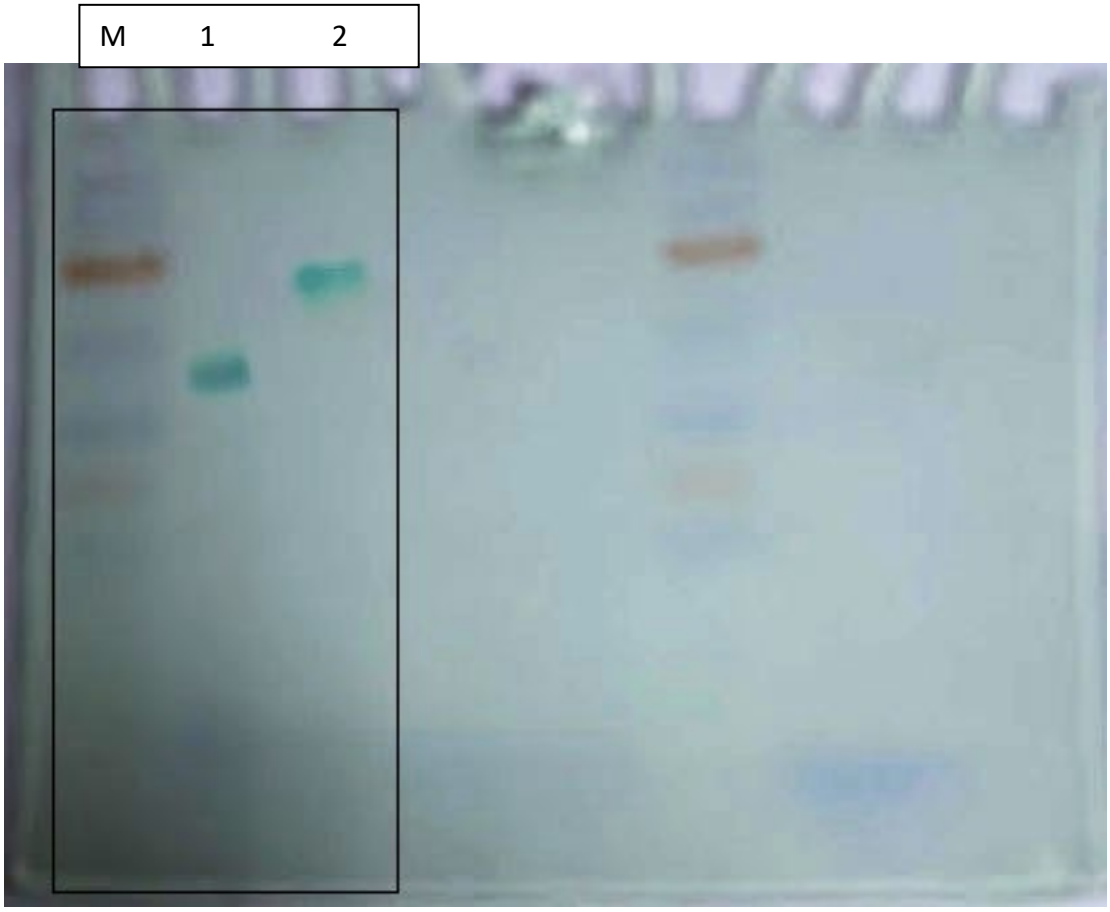

Figure S4: Venn diagram of the protein cluster (A), amino acid sequence (B) and scaffold view Laccases from *Tl*FLU1 and *Tp*FLU12 (C).

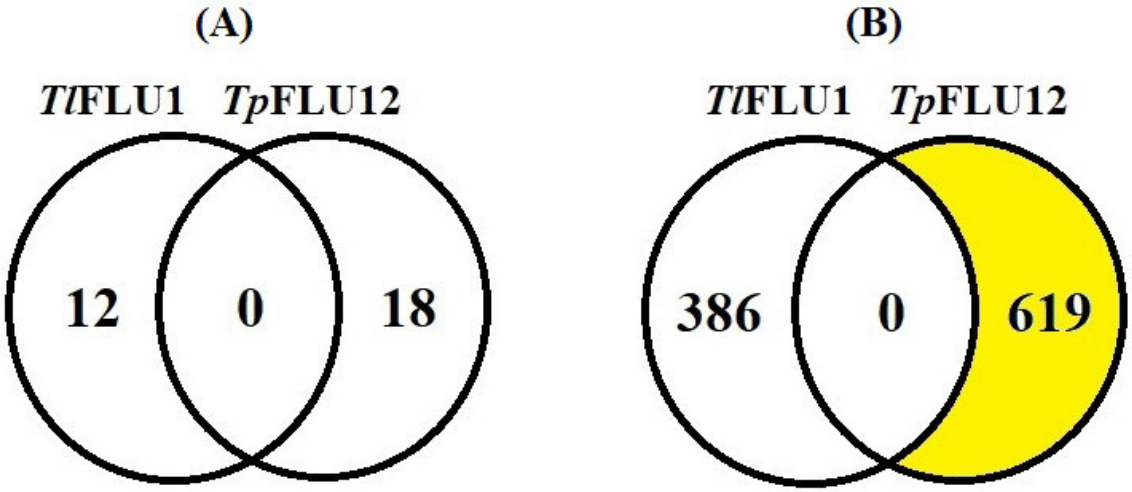

(C)

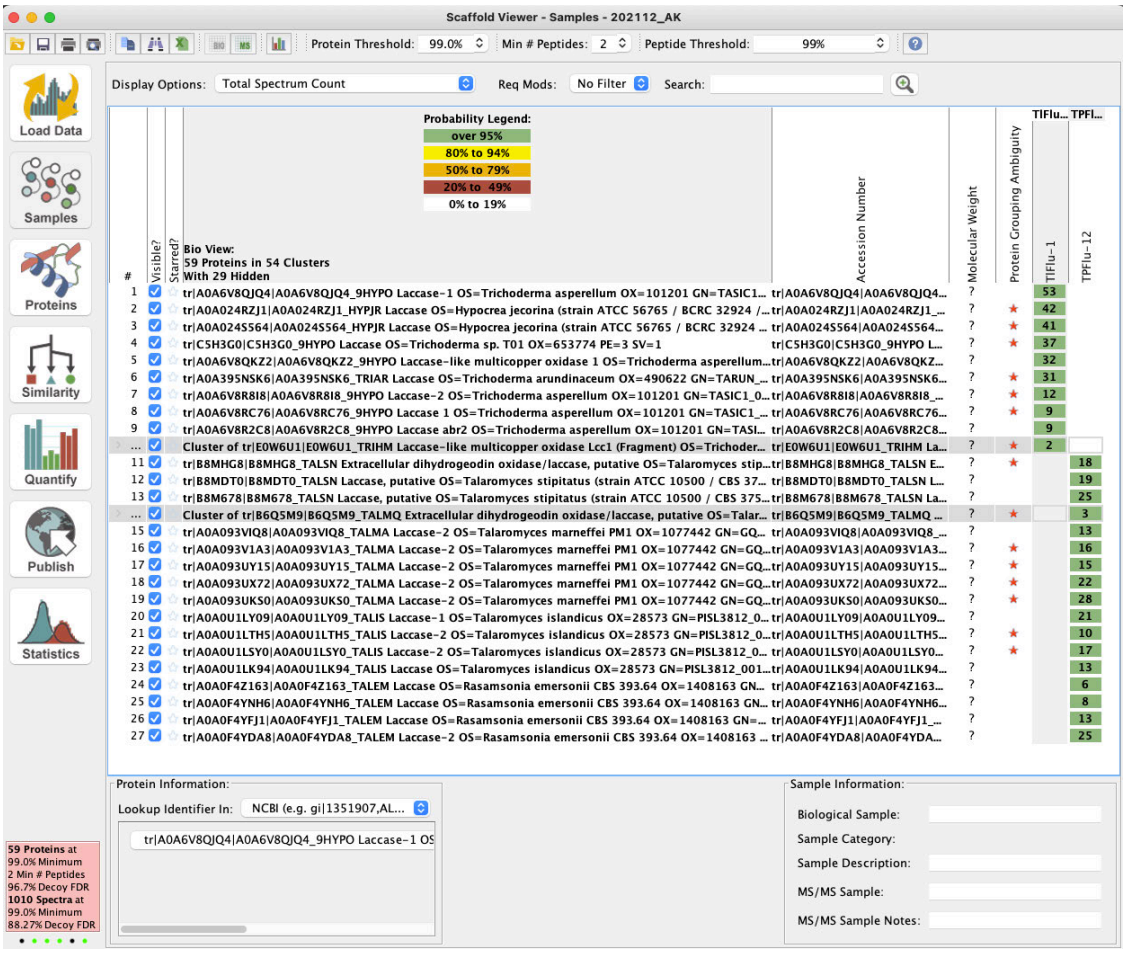

Figure S5. Neighbourhood-joining phylogenetic tree of 8 Laccases from the *Trichoderma* family and the reference RSB PDB sequence used as template for modelling the protein structure.

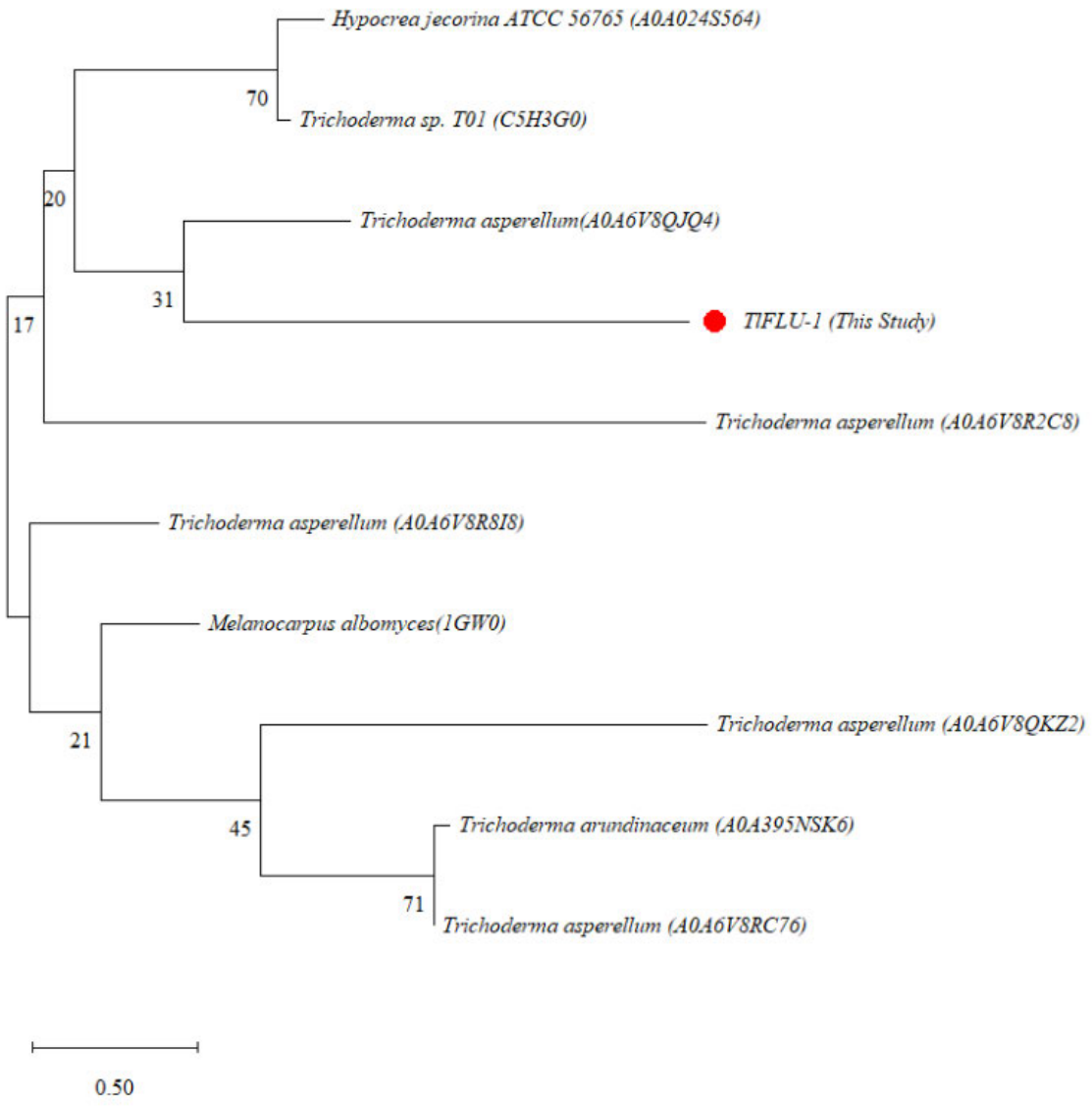

Figure S6. Neighbourhood-joining phylogenetic tree of 9 Laccases from the *Talaromyces* family and the reference RSB PDB sequence (4X4K) used as template for modelling the protein structure.

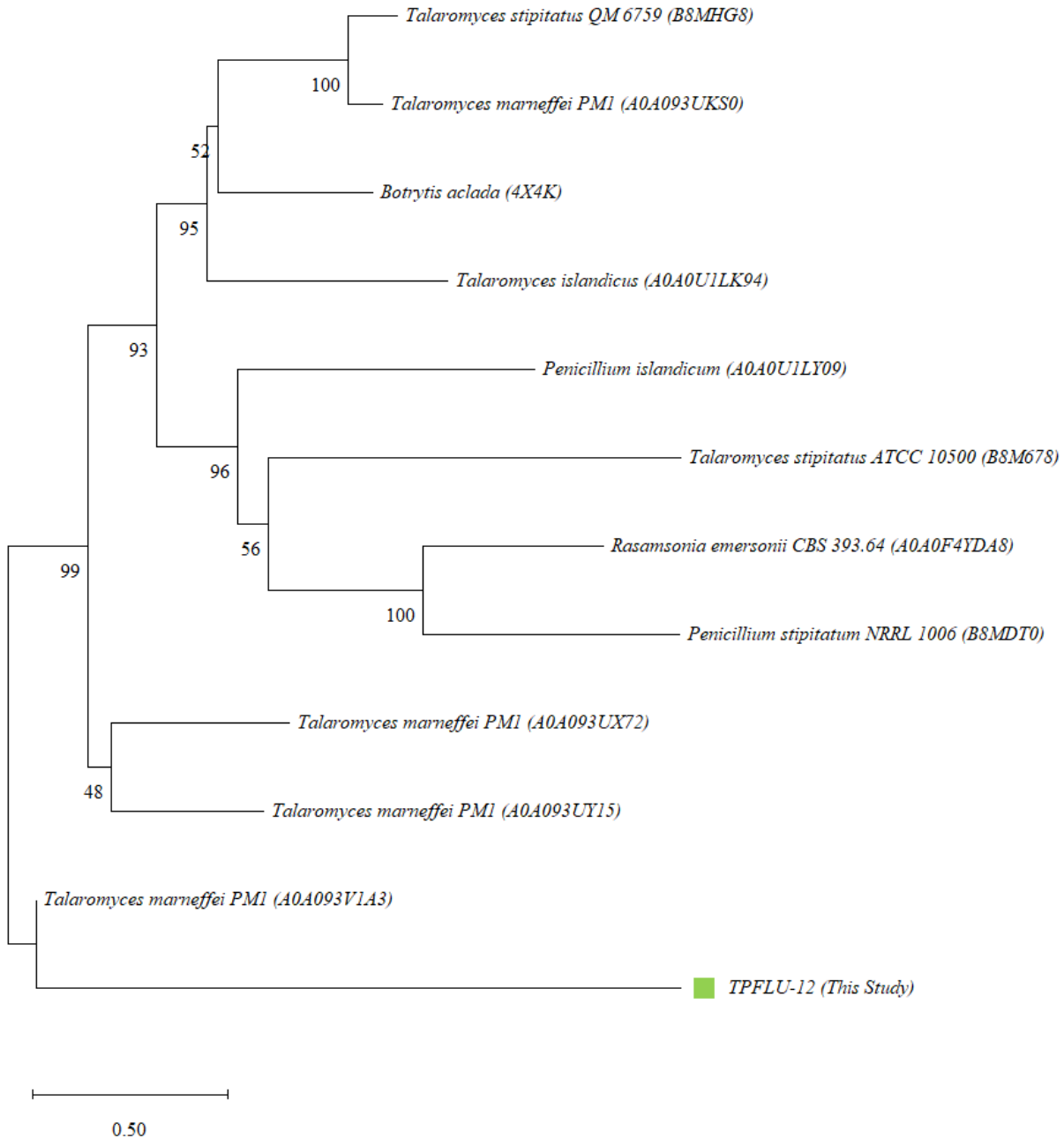

Figure S7. The homology sequence alignment of *Tl*FLU1 Laccase and IGW0 (*Melanocarpus albomyces*) template from the LOMETS threading programs of the I-TASSER server constructed with Jalview workbench.

a) Ident1 is the percentage sequence identity of the templates in the threading aligned region with the query sequence.
b) Ident2 is the percentage sequence identity of the whole template chains with query sequence.
c) Cov represents the coverage of the threading alignment and is equal to the number of aligned residues divided by the length of query protein.
d) Norm. Z-score is the normalized Z-score of the threading alignments. Alignment with a Normalized Z-score >1 mean a good alignment and vice versa.
e) The aligned sequence was selected in order of their ranking from the following threading programs: 1: FFAS-3D 2: SPARKS-X 3: HHSEARCH2 4: HHSEARCH I 5: Neff-PPAS 6: HHSEARCH 7: pGenTHREADER 8: wdPPAS 9: PROSPECT2 10: SP3.

In the consensus, '–' is a gap, '+' is an ambiguous position with no consensus while the most conserved residues are highlighted in a blue box.

Rank	PDB Hit	Iden1	Iden2	Cov	Norm. Z-score	Download Align.
1	1gw0A	0.13	0.24	0.81	1.78	Download

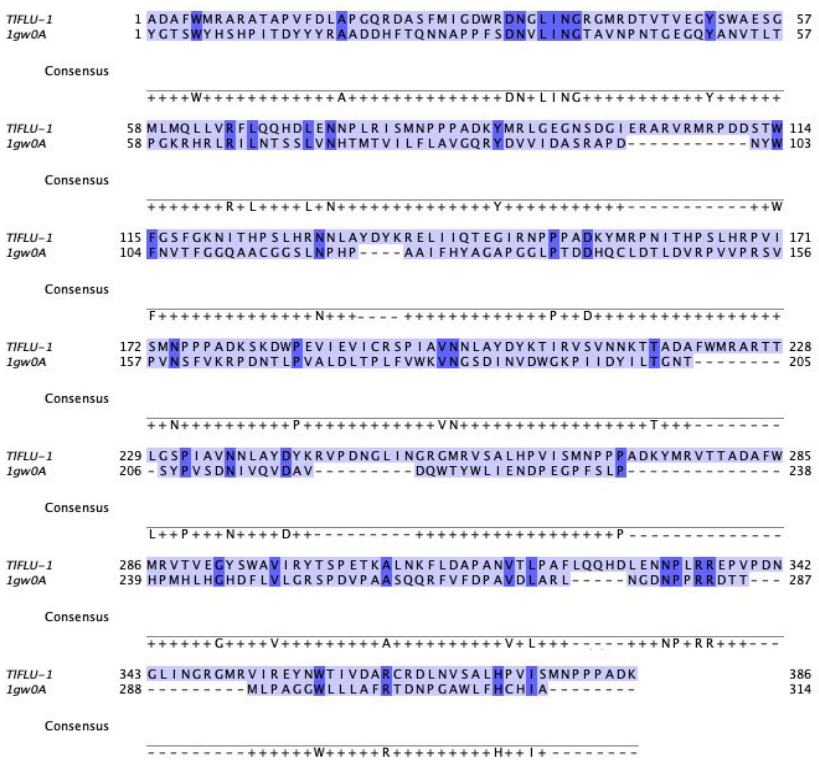

Figure S8. The homology sequence alignment of *Tp*FLU12 Laccase and 4x4kA (*Botrytis aclada*) template from the LOMETS threading programs of the I-TASSER server constructed with Jalview workbench.

a) Ident1 is the percentage sequence identity of the templates in the threading aligned region with the query sequence.
b) Ident2 is the percentage sequence identity of the whole template chains with query sequence.
c) Cov represents the coverage of the threading alignment and is equal to the number of aligned residues divided by the length of query protein.
d) Norm. Z-score is the normalized Z-score of the threading alignments. Alignment with a Normalized Z-score >1 mean a good alignment and vice versa.
e) The aligned sequence was selected in order of their ranking from the following threading programs: 1: FFAS-3D 2: SPARKS-X 3: HHSEARCH2 4: HHSEARCH I 5: Neff-PPAS 6: HHSEARCH 7: pGenTHREADER 8: wdPPAS 9: PROSPECT2 10: SP3.

In the consensus, '−' is a gap, while '+' is an ambiguous position with no consensus. The most conserved residues are highlighted.

Rank	PDB Hit	Iden1	Iden2	Cov	Norm. Z-score	Download Align.
1	4x4kA	0.16	0.18	0.73	5.85	Download

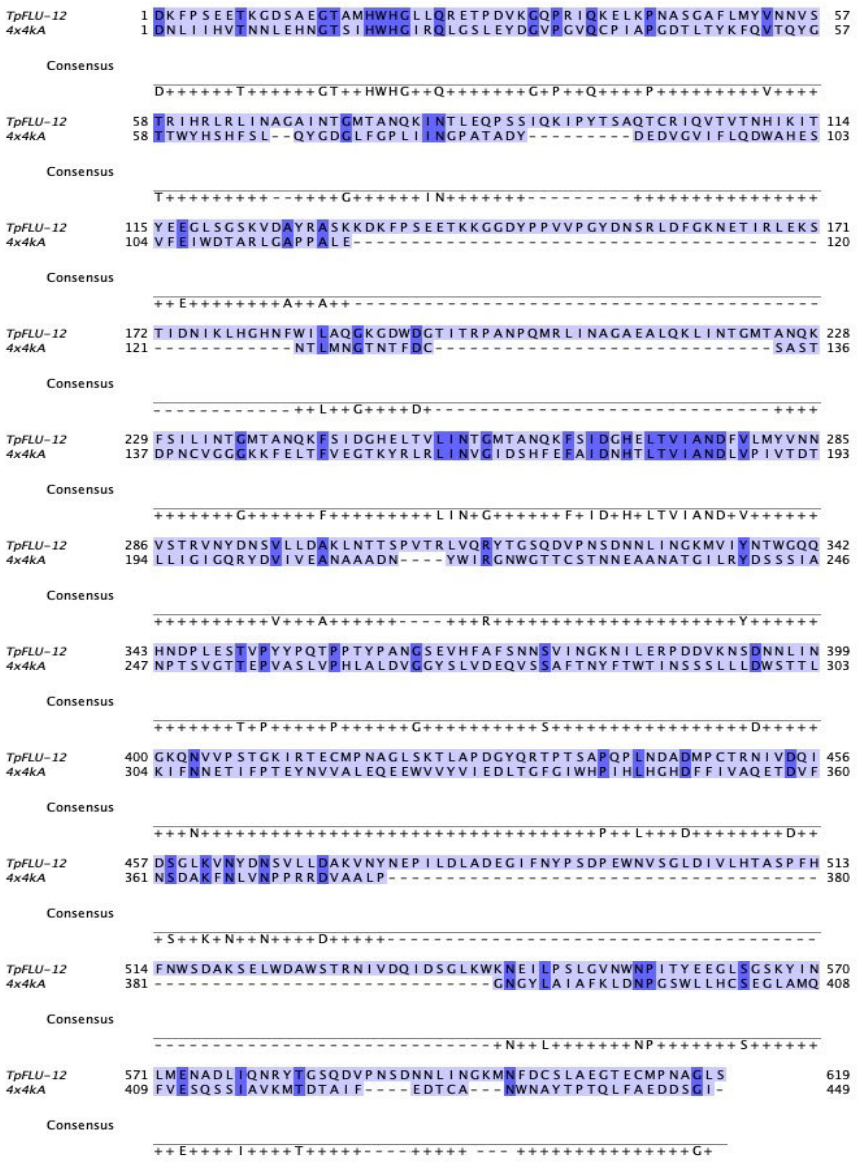

Table S1. The composition of the media used.

Media	Component	Amount (g/L)	Trace Elements	Amount (mg/L)
Basal salt media (BSM)	$(NH_4)_2SO_4$	2.4	Nitrilotriacetic acid	15
	$K2HPO_4$	1.55	$CaCl_2.2H_2O$	15
	$NaH2PO_4.2H_2O$	0.85	$MnCl_2.2H_2O$	6
	NaCl	0.5	$FeSO_4.7H_2O$	1
	$MgSO_4.7H_2O$	0.26	$Co(NO_3).6H_2O$	1
			$ZnSO_4$	1
			$CuSO_4$	0.1
			H_3BO_3	0.1
			Na_2MoO_4	0.1
			$Al_2(SO_4)_3.H_2O$	0.1
Potato Dextrose Agar PDA	Potato Infusion (infusion from 200g potatoes)	4		
	D(+)-Glucose (=Dextrose)	20		
	Agar	15		

CHAPTER NINE

General discussion and conclusion

9.1: The research in perspective

Although biodegradation shows promise for cleaning up PAHs-contaminated sites, there are several potential drawbacks to the process (Kaleem et al., 2023). Primarily, the process can be slow, taking months or even years to achieve desired results due to the hydrophobicity and recalcitrance of PAHs (Vaksmaa et al., 2023). Also, it may not be effective in treating all types of contamination, especially if the contaminants are highly toxic while the onsite indigenous fungi have low tolerance and degrading ability (Antón-Herrero et al., 2023). Likewise, the process can be expensive, especially if specialized equipment and trained personnel are required (Cotter, 2014). Furthermore, biodegradation can pose risks to human health and the environment if not properly managed (Kumar et al., 2021). In order to increase the chances of a successful biodegradation, priority should be given to the selection of fungi that are highly competent and able to adapt to contaminated sites, and that have the ability to mineralize PAHs of varying high concentrations (Shankhwar and Paliwal, 2021; Xiao and Li, 2022). In addition, it is essential to optimize the remediation conditions and understand the fate of the fungi diversity and populations during the remediation processes (Baker et al., 2019; Wang et al., 2022). Likewise, detailed knowledge of the mechanism employed by fungi for PAHs' degradation has to be explored by characterizing the most active enzymes involved for possible improvement of their functional activity (Kallio et al., 2011; Mehra et al., 2018).

The main objective of this thesis was to to assess the myco-remediation of two PAH compounds (low molecular weight and high molecular weight) by indigenous fungi inhabiting activated sludge.

Findings from this study suggests that activated sludge is a major reservoir of fungi with potential for PAHs' biodegradation. Chapter 3 and 4 highlights that *Trichoderma lixii* strain FLU1 (*Tl*FLU1) and *Talaromyces pinophilus* strain FLU12 (*Tp*FLU12) are highly tolerant to both high molecular weight (fluoranthene) and low molecular weight (anthracene) PAH compounds with the capacity to utilize these compounds as a sole carbon source. The high tolerance levels observed in *Tl*FLU1 and *Tp*FLU12 suggest that these fungi can adapt and survive in environments with high PAH contaminations due to their robust degradative capabilities. This resilience aligns with previous findings linking high PAH tolerance in fungi strains to enhanced biodegradation efficiency, as reported by Lee et al. (2014). Efficient PAH removal has been shown to correlate with high PAH concentration tolerance and low inhibition rates (Souza et al., 2017), supporting the adaptability of *Tl*FLU1 and *Tp*FLU12 in degrading

these compounds. Assessment of the metabolic pathway of two fungal strains during the PAHs removal showed that the main degradative pathway of non-mushroom-forming fungi is like that of mushroom-forming fungi but different from the bacteria. The biodegradation of fluoranthene and anthracene was found to be growth-associated, driven by the activity of ligninolytic enzymes (Lac, LiP, and MnP) in fluoranthene, resulting in its complete removal (100%) as documented in chapter 3. Also, fluoranthene degradation was found to primarily began at the C1-C2 position of the compound ring through oxygenation and ring cleavage to form 9-oxo-9*H*-fluorene-1-carboxylic acid and then underwent further ring cleavage to yield fluorenone which was subsequently transformed *via* oxygenation and side-chain removal into ß- Ketoadipate by passing through benzene-1,2,3-tricarboxylic acid as documented in mushroom fungi, *Armillaria* sp. F022 (Hadibarata and Ayu, 2015).

In the case of anthracene, the initial degradation mechanism involved intracellular enzymes catechol 1,2 dioxygenase (ortho-cleaving) and catechol 2,3 dioxygenase (meta-cleaving), followed by ligninolytic enzymes. This process led to anthracene degradation rates of up to 56% by *Tl*FLU1 and 38% by *Tp*FLU12 over a 24-d period as reported in chapter 4. This observation is consistent with the report of Bankole et al. (2021) for the biodegradation of fluorene *by Mucor irregularis* strain bpo1 where high PAH concentration was growth linked and correlated with extracellular enzymes activities (Lac, LiP and MnP) throughout the study period. Anthracene degradation was initiated through the attack at the C-9 and C-10 position of anthracene *via* oxygenation to form either anthrone or 9,10-anthracenedione before undergoing a spontaneous tautomeric benzoic acid formation due to the hydroxylation and ring cleavage at the C-9 and C-10 position as previously observed in marine fungi *Cladosporium* sp. CBMAI 1237 (Birolli et al., 2018) and mushroom-forming fungi, *Armillaria* sp. F022 (Hadibarata et al., 2013).

Also, overexpression of Lac, LiP and MnP coding genes observed in PAH-contaminated marine sediments fungi belonging to Eurotiales, specifically *Talaromyces helices* and *Trichoderma* sp. during PAHs biotransformation (Álvarez-Barragán et al., 2021), further attest to the efficient PAHs removal which is attributed to the biocatalytic roles played by these extracellular enzymes. The involvement of intracellular enzymes during anthracene myco-remediation could not be fully ascertained due to their low concentrations in both the whole fungi biomass of anthracene-culture broth and non-anthracene-culture broth in comparison with extracellular ligninolytic enzymes. The most probable explanation for the detection of

these intracellular enzymes in the early stage of the transformation process could be linked to the fungal strains defence system against oxidative stress, reactive oxygen species and ATP synthesis. This opinion aligns with a previous report by Zafra et al.(2015) where MnP-like peroxidase activity was detected during the early stage of PAHs degradation which was linked to response against oxidative stress rather than participating directly in the degradation of PAHs by *Trichoderma asperellum* H15. A comprehensive genomic and transcriptomic analysis of PAH degradation by *Dentipellis* sp. KUC8613 revealed that these dioxygenases enzymes were only involved in the translocation of PAHs as a defence system against reactive oxygen species and ATP synthesis (Park et al., 2019). However, another potential intracellular enzyme, cytochrome P450, might be responsible for the initial transformation mechanism used by these fungi since they have been reported in *Penicillium oxalicum* when anthracene was used as a carbon source during its myco-remediation process (Aranda et al., 2017). However, complete degradation of anthracene could not be achieved due to its acute toxicity, which further necessitated the use of response surface methodology (RSM) to optimize degradation conditions as presented in chapter 5. The Box-Behnken Design (BBD) identified optimal conditions for maximum anthracene biodegradation by *Tl*FLU1 and *Tp*FLU12, with pH levels of 4 and 7, temperatures of 30°C and 25°C, biomass sizes of 20 mm, and anthracene concentrations of 200 mg/L, achieving 100% degradation after 7 and 12 days, respectively. This observation perfectly aligns with the report of Bankole et al. (2021), where validation of BBD showed that degradation of PAH (fluorene) by an indigenous marine fungus (*Mucor irregularis*) is primarily regulated by temperature, PAH concentration, inoculum size (biomass size) and pH. Similarly, the report of Abo-State et al. (2018), identified optimum conditions for the growth of *P. chrysosporium* to maximally (100%) degrade 100 mg/L of each PAHs (fluoranthene, acenaphthene, phenanthrene, pyrene and anthracene) to be at a temperature of 25°C, pH 5 and inoculum size (10 mm of five mycelia discs) at 7 incubation period.

To establish whether the abundantly produced ligninolytic enzyme, laccase (Lac) can be used for *in vitro* degradation of PAHs in a cell-free system, a series of purification, characterization, structural analysis, catalytic efficiency and biological process functions were unravelled in this study as described in chapter 5. The obtained data shows that Lac purified from *Tl*FLU1 and *Tp*FLU12 have a molecular mass of 44 kDa and 68.7 kDa, respectively. These enzymes differ in their optimum pH and temperature, with that of *Tl*FLU1 being more active at lower pH and that of *Tp*FLU12 being more active at higher pH. Their activity was enhanced by a broad range of metal ion and organic solvents while sodium azide was a strong inhibitor of their activity.

Both Lacs have similar kinetic properties with a better affinity to ABTS as a substrate compared to other phenolic substrates. Based on the structural predictions, the difference in optimum pH is likely due to the different arrangements of the copper atoms in the active site. Also, the biological functions of these Lac were associated with oxidation-reduction, lignin metabolism, phenylpropanoid catabolism, biological adhesion, cellular metabolism, metal ion homeostasis, aromatic compound metabolism, and cellulose metabolism. Thus, these unusual properties suggest that Lac from *Tl*FLU1 and *Tp*FLU12 has potential for biotechnological and industrial applications. The enzyme's catalytic efficiency depends primarily on its structural conformation and stability. The Lac-amino acid conjugates were predicted to be stable, with an instability index ranging from 33.43 to 39.45, thermophilic with an aliphatic index of 76.58 to 77.50, and hydrophilic with a grand average of hydropathicity between -0.508 and -0.578. The predicted biological functions of the protein encompass oxidation-reduction, lignin metabolism, metal ion homeostasis, phenylpropanoid catabolism, aromatic compound metabolism, cellulose metabolism, and biological adhesion. These insights into the enzyme structure-function relationship enhance our understanding of its catalytic mechanism, paving the way for the possible use of this enzyme in biotechnological and industrial applications.

Following the characterization of the purified Lac from *Tl*FLU1 and *Tp*FLU12, it became necessary to understand the mechanisms by which these non-mushroom forming fungi degrade PAHs, and for advancing its application during the degradation process. Thus, this study assessed the potential of Lac produced during the degradation process for in vitro degradation of PAHs in a cell-free system and under a mediator system. It was evident that purified Lac from *Tl*FLU1 and *Tp*FLU12 are effective in the degradation of anthracene and fluoranthene but the Lac-mediator system yielded a high and relatively stable enzymatic activity during degradation process compared to the free Lac system as documented in chapters 6 and 7. GC-MS analysis of the fluoranthene and anthracene degradation products showed similarities to those observed in the fungi biomass degradation system. Two new anthracene degradation products were observed under the Lac-mediator degradation system and was used to propose new possible anthracene degradation pathways. It was presumed to have been initiated through the hydroxylation and carboxylation at the C-1 and C-2 position of anthracene, yielding 3-hydroxy-2-naphthoic acid, chromone and benzoic acid as a dead-end product.

A successful biodegradation study cannot be completed without an evaluation of potential risks posed by PAH metabolites to ensure the safety of the remediation process. Hence a time-course changes in the acute toxicity using a marine bacterium (*Vibrio parahaemolyticus*), cytotoxicity

test using mouse hippocampal neuronal cell lines (HT-22) and gene expression of Alzheimer's related disease (AD) genes in HT-22 cells line were also monitored and reported in chapters 6 and 7. During the whole fungi biomass biodegradation, metabolites from *Tl*FLU1 degradation media were toxic to *V. parahaemolyticus* after 6 h of exposure with effective concentration (EC_{50}) and toxicity unit (TU) values of 14.25 mg/L and 7.018%, respectively. In contract, metabolites from *Tp*FLU12 degradation media were non-toxic with EC_{50} and TU values of 197.1 mg/L and 0.507%, respectively. In the context of anthracene degradation EC_{50} and TU of 266.1 mg/L and 0.4% were recorded for *Tl*FLU1 inoculated medium, while 262.3 mg/L and TU 0.4% were obtained for *Tp*FLU12 inoculated medium with toxicity classification of non-toxic for both strains. However, under optimized anthracene degradation condition using RSM, acute toxicity tests of the degradation media showed significant toxicity reduction with *V. parahaemolyticus* survival increasing after 6-hour exposure, yielding effective concentration (EC_{50}) and toxicity unit (TU) values of 20.92 mg/L and 4.78% for *Tl*FLU1, and 35.29 mg/L and 2.83% for *Tp*FLU12 with toxicity classification for both strains being harmful. Furthermore, toxicity tests of anthracene degradation products from purified Lac with and without a mediator ABTS on *V. parahaemolyticus* and HT-22 cells respectively demonstrated the non-toxic nature of Lac-ABTS-mediated metabolites. Interestingly, examining the expression levels of Alzheimer's-related genes in HT-22 cells exposed to degradation products showed no signs of neurotoxicity, unlike the untreated cells. These results suggest that although *V. parahaemolyticu*s survival improved with degradation products, ecotoxicity and cytotoxicity assessments of fluoranthene degradation from purified Lac (with and without a mediator ABTS) indicated potential toxicity from *Tl*FLU1 degradation products towards marine bacteria whereas *Tp*FLU12 products were primarily non-toxic. This study supports the hypothesis that degradation products could be more toxic than the parent compounds (Lundstedt, 2003; Marquès et al., 2017; Gbeddy et al., 2020; Lee and Kwon, 2020). A similar observation was reported by Mtibaà et al. (2018) where biodegradation of bisphenol produces more toxic metabolites than the original compound. The formation of oxygen-containing PAHs (quinone derivatives) could be attributed to the high toxicity owing to the fact that they are direct-acting mutagens (Menzie et al., 1992; Chibwe et al., 2017). Although, the increase in the marine bacterium survival demonstrated the reduction in acute toxicity of the parent compound over treatment time but slight reduction in survival (CFU/mL) of the marine bacterium in this study, particularly that of *Tl*FLU1 degradation products has reveal that toxicity level is not solely a function of contaminants concentration (Lukić et al., 2016). The high EC_{50} value observed in strain *Tp*FLU-12 products confirms that less toxic metabolites

were accumulated during the transformation process due to the dimer OH auras (Arunprasath et al., 2019). Hence the choice of Lac from *Tl*FLU1 and *Tp*FLU12 as a potential tool for a green environmental clean-up method should be harnessed.

9.2: Limitations of the Current Study

Despite the promising findings of this research, yet several limitations should be noted.

i. **Limited scope of fungal strains:** The study focused on two specific fungal strains, *Tl*FLU1 and *Tp*FLU12. The results might not be generalizable to other fungal strains with potential biodegradation capabilities.
ii. **Controlled laboratory conditions:** The experiments were conducted under controlled laboratory conditions, which may not accurately reflect the complexities and variabilities of natural contaminated environments.
iii. **Incomplete metabolic pathway analysis:** While metabolic pathways for PAH degradation were proposed, the complete degradation pathway and all intermediate metabolites were not fully elucidated.
iv. **Optimization parameters:** The study optimized certain parameters (pH, temperature, biomass size, and PAH concentration) for maximum degradation. However, other potentially influential factors such as nutrient availability, moisture content, and microbial community interactions were not explored.
v. **Enzyme efficiency and stability:** While the study characterized the Lac enzymes from the fungal strains, the long-term stability and efficiency of these enzymes under different environmental conditions were not assessed.

9.3: Potential for future development of the study

The promising results of this study open multiple avenues for future research and practical applications in the field of myco-remediation and beyond. The following points outline potential directions for future development:

i. **Scaling up Myco-remediation processes:** While laboratory-scale experiments have demonstrated the efficiency of *Tl*FLU1 and *Tp*FLU12 in PAH degradation, scaling up these processes to field applications is crucial. Future studies should focus on developing pilot-scale bioreactors and in situ remediation strategies to evaluate the performance of these fungal strains in diverse environmental conditions and real-world

contaminations. Further detailed metabolomic, secretomic and transcriptomic analyses are required to comprehensively understand the degradation mechanisms.

ii. **Genetic and metabolic engineering:** Advances in genetic and metabolic engineering could allow for genetic modification of the fungal strains tested in this study to enhance their degradative capabilities. By introducing specific genes or pathways, these fungi could be tailored to target a broader range of PAHs and other persistent organic pollutants, increasing their versatility and effectiveness for use in bioremediation.

iii. **Optimization of enzyme production and activity:** Further research into optimizing the production and activity of ligninolytic enzymes, particularly Lac, is essential. Investigating alternative inducers, cultivation conditions, and immobilization techniques could improve enzyme yields and stability, making them more viable for industrial applications.

iv. **Development of enzyme-mediator systems:** The study has shown that Lac-mediator systems enhance PAH degradation. Future research should explore the development of novel, cost-effective mediators and their integration into bioremediation protocols. Additionally, understanding the interactions between enzymes and mediators at the molecular level could lead to more efficient degradation pathways.

v. **Application in mixed pollutant scenarios:** Environmental contamination often involves complex mixtures of pollutants. Future studies should investigate the performance of *Tl*FLU1 and *Tp*FLU12 in degrading mixed PAHs and other co-contaminants, evaluating their synergistic and/or antagonistic effects on biodegradation efficiency.

vi. **Economic and feasibility analysis**: Conducting a detailed economic analysis of the myco-remediation process is essential for its practical implementation. Assessing the costs associated with fungal cultivation, enzyme production, and large-scale application will provide a clearer understanding of the feasibility and commercial potential of this bioremediation approach.

vii. **Integrative approaches with other bioremediation techniques:** Combining myco-remediation with other bioremediation strategies, such as phytoremediation or microbial consortia, could yield synergistic effects. Integrative approaches may enhance the overall efficiency of pollutant removal and contribute to more sustainable environmental management practices.

9.4: References

Abo-State, M.A.M., Riad, B.Y., Bakr, A.A., Abdel Aziz, M.F., 2018. Biodegradation of naphthalene by *Bordetella avium* isolated from petroleum refinery wastewater in Egypt and its pathway. *Journal of Radiation Research and Applied Sciences* 11, 1–9. https://doi.org/10.1016/J.JRRAS.2017.10.001

Álvarez-Barragán, J., Cravo-Laureau, C., Wick, L.Y., Duran, R., 2021. Fungi in PAH-contaminated marine sediments: cultivable diversity and tolerance capacity towards PAH. *Marine Pollution Bulletin* 164, 112082. https://doi.org/10.1016/j.marpolbul.2021.112082

Antón-Herrero, R., Chicca, I., García-Delgado, C., Crognale, S., Lelli, D., Gargarello, R.M., Herrero, J., Fischer, A., Thannberger, L., Eymar, E., Petruccioli, M., D'Annibale, A., 2023. Main factors determining the scale-up effectiveness of mycoremediation for the decontamination of aliphatic hydrocarbons in soil. *JoF* 9, 1205. https://doi.org/10.3390/jof9121205

Aranda, E., Godoy, P., Reina, R., Badia-Fabregat, M., Rosell, M., Marco-Urrea, E., García-Romera, I., 2017. Isolation of Ascomycota fungi with capability to transform PAHs: Insights into the biodegradation mechanisms of *Penicillium oxalicum*. *International Biodeterioration and Biodegradation* 122, 141–150. https://doi.org/10.1016/j.ibiod.2017.05.015

Arunprasath, T., Sudalai, S., Meenatchi, R., others, 2019. Biodegradation of triphenylmethane dye malachite green by a newly isolated fungus strain. *Biocatalysis and Agricultural Biotechnology* 17, 672–679. https://doi.org/10.1016/j.bcab.2019.01.030

Baker, P., Tiroumalechetty, A., Mohan, R., 2019. Fungal Enzymes for Bioremediation of Xenobiotic Compounds, in: Yadav, A.N., Singh, S., Mishra, S., Gupta, A. (Eds.), Recent Advancement in White Biotechnology Through Fungi, Fungal Biology. Springer International Publishing, Cham, pp. 463–489. https://doi.org/10.1007/978-3-030-25506-0_19

Bankole, P.O., Semple, K.T., Jeon, B.H., Govindwar, S.P., 2021. Biodegradation of fluorene by the newly isolated marine-derived fungus, *Mucor irregularis* strain bpo1 using response surface methodology. Ecotoxicology and Environmental Safety 208, 111619–111619. https://doi.org/10.1016/j.ecoenv.2020.111619

Birolli, W.G., de A. Santos, D., Alvarenga, N., others, 2018. Biodegradation of anthracene and several PAHs by the marine-derived fungus *Cladosporium sp*. CBMAI 1237. *Marine Pollution Bulletin* 129, 525–533. https://doi.org/10.1016/j.marpolbul.2017.10.023

Chibwe, L., Davie-Martin, C.L., Aitken, M.D., others, 2017. Identification of polar transformation products and high molecular weight polycyclic aromatic hydrocarbons (PAHs) in contaminated soil following bioremediation. *Science of The Total Environment* 599–600, 1099–1107. https://doi.org/10.1016/j.scitotenv.2017.04.190

Cotter, T., 2014. Organic mushroom farming and mycoremediation: Simple to advanced and experimental techniques for indoor and outdoor cultivation. Chelsea Green Publishing.

Gbeddy, G., Goonetilleke, A., Ayoko, G.A., Egodawatta, P., 2020. Transformation and degradation of polycyclic aromatic hydrocarbons (PAHs) in urban road surfaces: Influential factors, implications and recommendations. *Environmental Pollution* 257, 113510. https://doi.org/10.1016/j.envpol.2019.113510

Hadibarata, T., Ayu, R., 2015. Biotransformation Studies on fluoranthene, a four-ring polycylic aromatic hydrocarbon, by White-Rot *Fungus Armillaria* sp. F022. *Italian Oral Surgery* 3, 45–50. https://doi.org/10.1016/j.aaspro.2015.01.011

Hadibarata, T., Zubir, M.M., Rubiyatno, Chuang, T.Z., Yusoff, A.R., Salim, M.R., Fulazzaky, M.A., Seng, B., Nugroho, A.E., 2013. Degradation and transformation of anthracene by white-rot fungus armillaria Sp. F022. Folia Microbiologica 58, 385–391.

Kaleem, M., Mumtaz, A.S., Hashmi, M.Z., Saeed, A., Inam, F., Waqar, R., Jabeen, A., 2023. Myco- and phyco-remediation of polychlorinated biphenyls in the environment: a review. *Environ Sci Pollut Res* 30, 13994–14007. https://doi.org/10.1007/s11356-022-24902-9

Kallio, J.P., Gasparetti, C., Andberg, M., Boer, H., Koivula, A., Kruus, K., Rouvinen, J., Hakulinen, N., 2011. Crystal structure of an ascomycete fungal Laccase from *Thielavia arenaria* - Common structural features of asco-Laccases. *FEBS Journal* 278, 2283–2295. https://doi.org/10.1111/j.1742-4658.2011.08146.x

Kumar, A., Yadav, A.N., Mondal, R., Kour, D., Subrahmanyam, G., Shabnam, A.A., Khan, S.A., Yadav, K.K., Sharma, G.K., Cabral-Pinto, M., Fagodiya, R.K., Gupta, D.K., Hota, S., Malyan, S.K., 2021. Myco-remediation: a mechanistic understanding of contaminants alleviation from natural environment and future prospect. *Chemosphere* 284, 131325. https://doi.org/10.1016/j.chemosphere.2021.131325

Lee, Hwanhwi, Jang, Y., Choi, Y.S., Kim, M.J., Lee, J., Lee, Hanbyul, Hong, J.H., Lee, Y.M., Kim, G.H., Kim, J.J., 2014. Biotechnological procedures to select white rot fungi for the degradation of PAHs. *Journal of Microbiological Methods* 97, 56–62. https://doi.org/10.1016/j.mimet.2013.12.007

Lee, S.Y., Kwon, J.H., 2020. Enhancement of toxic efficacy of alkylated polycyclic aromatic hydrocarbons transformed by *sphingobium quisquiliarum*. *International Journal of*

Environmental Research and Public Health 17, 1–13. https://doi.org/10.3390/ijerph17176416

Lukić, B., Panico, A., Huguenot, D., Fabbricino, M., van Hullebusch, E.D., Esposito, G., 2016. Evaluation of PAH removal efficiency in an artificial soil amended with different types of organic wastes. *Euro-Mediterranean Journal for Environmental Integration* 1, 1-11 https://doi.org/10.1007/s41207-016-0001-x

Lundstedt, S., 2003. Analysis of PAHs and their transformation products in contaminated soil and remedial processes. (Doctoral dissertation, Kemi).

Marquès, M., Mari, M., Sierra, J., Nadal, M., Domingo, J.L., 2017. Solar radiation as a swift pathway for PAH photodegradation: A field study. *Science of The Total Environment* 581–582, 530–540. https://doi.org/10.1016/j.scitotenv.2016.12.161

Mehra, R., Muschiol, J., Meyer, A.S., Kepp, K.P., 2018. A structural-chemical explanation of fungal Laccase activity. *Scientific Reports* 8, 1–16. https://doi.org/10.1038/s41598-018-35633-8

Menzie, C.A., Potocki, B.B., Santodonato, J., 1992. Exposure to carcinogenic PAHs in the environment. *Environ. Health Perspect*. 26, 1166-1170.-1166-1170.

Mtibaà, R., Olicón-Hernández, D.R., Pozo, C., Nasri, M., Mechichi, T., González, J., Aranda, E., 2018. Degradation of bisphenol A and acute toxicity reduction by different thermo-tolerant ascomycete strains isolated from arid soils. *Ecotoxicology and Environmental Safety* 156, 87–96. https://doi.org/10.1016/j.ecoenv.2018.02.077

Park, H., Min, B., Jang, Y., Kim, J., Lipzen, A., Sharma, A., Andreopoulos, B., Johnson, J., Riley, R., Spatafora, J.W., Henrissat, B., Kim, K.H., Grigoriev, I.V., Kim, J.J., Choi, I.G., 2019. Comprehensive genomic and transcriptomic analysis of polycyclic aromatic hydrocarbon degradation by a mycoremediation fungus, *Dentipellis* sp. KUC8613. *Applied Microbiology and Biotechnology* 103, 8145–8155. https://doi.org/10.1007/s00253-019-10089-6

Shankhwar, A.K., Paliwal, R., 2021. Fungi in bioremediation of soil: mycoremediation of PAHs compounds, in: Fungi Bio-Prospects in Sustainable Agriculture, Environment and Nanotechnology. Elsevier, pp. 157–170. https://doi.org/10.1016/B978-0-12-821925-6.00008-3

Vaksmaa, A., Guerrero-Cruz, S., Ghosh, P., Zeghal, E., Hernando-Morales, V., Niemann, H., 2023. Role of fungi in bioremediation of emerging pollutants. *Front Mar Sci* 10. https://doi.org/10.3389/fmars.2023.1070905

Wang, Y., Pan, F., Wang, Q., Luo, J., Zhang, Q., Pan, Y., Wu, C., Liu, W., 2022. The effect of different remediation treatments on soil fungal communities in rare earth tailings soil. *Forests* 13, 1987. https://doi.org/10.3390/f13121987

Xiao, Y., Li, Y., 2022. Advances in fungal removal of polycyclic aromatic hydrocarbons. AJST 3(2), 45–47. https://doi.org/10.54097/ajst.v3i2.2088

Zafra, G., Moreno-montaño, A., Absalón, Á.E., Cortés-espinosa, D.V., 2015. Degradation of polycyclic aromatic hydrocarbons in soil by a tolerant strain of *Trichoderma asperellum*. *Environ Sci Pollut Res* 22, 1034–1042. https://doi.org/10.1007/s11356-014-3357-y